(NASA-CR-120193) TURBOPUMPS FOR CRYOGENIC UPPER STAGE ENGINES Final Report, Jul. 1971 - Sep. 1973 (Rocketdyne) 360 p HC $22.00 CSCL 13K

N74-21070

Unclas

G3/15 16518

Rocketdyne Division
Rockwell International

R-9367

FINAL REPORT

TURBOPUMPS FOR CRYOGENIC UPPER-STAGE ENGINES

(July 1971 through September 1973)

by

A. T. Zachary, A. Csomor, and

L. L. Tignac

Rocketdyne, A Division of Rockwell International
6633 Canoga Avenue
Canoga Park, California 91304

December 1973

Contract NAS8-27794

Prepared for

George C. Marshall Space Flight Center
Marshall Space Flight Center
Alabama 35812

FOREWORD

This report was prepared by the Rocketdyne Division/Rockwell International in fulfillment of the requirements under NAS8-27794, "Turbopumps for Cryogenic, Upper-Stage Engines". The program was conducted for George C. Marshall Space Flight Center of the National Aeronautics and Space Administration under the direction of Charles D. Miller, Contracting Officer's Representative.

The principal Rocketdyne participants were:

LO_2 Project Engineer	A.T. Zachary
LH_2 Project Engineer	J.R. Lauffer
LO_2 Turbopump Principal Engineer	J.E. Wolf
LH_2 Turbopump Principal Engineer	A. Csomor
Development and Acceptance Testing	L.L. Tignac

ABSTRACT

Small, high-performance LO_2 and LH_2 turbopump assembly configurations were selected, detail designs were prepared and two of each unit were fabricated with each unit consisting of pump, turbine gas generator, and appropriate controls. Following fabrication, development testing was conducted on each type to demonstrate performance, durability, transient characteristics, and heat transfer under simulated altitude conditions. Following successful completion of development effort, the two LO_2 turbopump units and one LH_2 turbopump unit were acceptance tested as specified. A weld failure in the turbine manifold of one LH_2 turbopump unit prevented its acceptance. Other than the weld failure, detail inspection of the units following development testing revealed no deleterious effects of testing. The test results of LO_2 turbopump assembly testing correlated well with predicted performance while the LH_2 turbopump test results, though generally consistant with predicted values, did show lower than anticipated developed head at the design point and in the high flow range of operation. The lower developed head is attributed to higher than anticipated pump flow passage resistance from effects typical of small multistage pumps. The results of this program have established a sound technology base for future development of small, high performance turbopumps and gas generators.

CONTENTS

ILLUSTRATIONS

TABLES

INTRODUCTION

To provide optimum performance of the Space Shuttle as originally conceived, it was determined that a Hydrogen-Oxygen Auxiliary Propulsion Subsystem (APS) would be required. The APS would provide attitude control and maneuvering propulsion for the orbiter stage and attitude control for the booster. Definition studies conducted had shown that turbopump-fed systems were optimum, and although a large portion of the components could be designed, utilizing existing knowledge, some new technology was required. To meet this need, this program was initiated to design, fabricate, development test, acceptance test, and deliver two each LO_2 and LH_2 turbopump assemblies. With the changes to the Space Shuttle to utilize a storable propellant APS, the program emphasis was shifted to provide broad-range, small turbopump system technology applicable to high-energy, upper-stage engines and to other cryogenic system applications.

SUMMARY

The turbopump program for cryogenic upper-stage engines was initiated in July 1971 with a one and one-half month preliminary design phase during which the baseline component and assembly configurations were identified. Thereafter a five and one-half month detail design phase was conducted with release of the fabrication drawings on schedule.

Some stretch out of the program schedule resulted from vendor delays. However, assembly of the units was accomplished and testing was conducted with completion of all testing on July 1, 1973.

During the Task I - Preliminary Design effort the key factors in determining the component configurations were identified and preliminary designs selected. The turbopump configurations selected are presented in Table 1.

TABLE 1. SELECTED TURBOPUMP CONFIGURATIONS

Oxidizer Turbopump	
• Pump	Single stage centrifugal
• Turbine	Single row, impulse, 49 percent admission Inlet pressure 1,861,584 N/m^2 (270 psia) Inlet temperature 1117 K (2010 R)
• Nominal Shaft Speed	3142 rad/s (30,000 rpm)
LH_2 Turbopump	
• Pump	Two-stage centrifugal
• Turbine	Two row axial impulse, 100 percent admission Inlet pressure 1,861,584 N/m^2 (270 psia) Inlet temperature 1117 K (2010 R)
• Shaft Speed	6283 rad/s, nominal (60,000 rpm)

The determining factors in the final configuration selections were identified as bearing life and turbine flowrate for the LH_2 turbopump and net positive suction pressure (NPSP), start time, and turbine flowrate for the LO_2 turbopump. The start time and NPSP for the LH_2 turbopump did not vary sufficiently for the configurations under consideration to significantly influence the final selection. Similarly, bearing life was considered adequate for all the LO_2 pump configurations. Start time was a primary factor in the selection of the LO_2 TP configuration and the bypass flow during start was also another factor affecting start time among the competing configurations. The heat transfer analysis outlined the difficulty in maintaining the pumps cold when kept dry between cycles thus emphasizing the need for wet pumps during periods when rapid start is required.

In addition, gas generator configuration alternates were identified, valves to be used were selected from available units, and analysis of the PCA system and dynamic characteristics as related to the LO_2 and LH_2 TPA's were conducted.

The detail drawings of the components and system were prepared and released during the Phase II - Detail Analyses and Design task. Isometric presentations of the LH_2 and LO_2 turbopump/gas generator assemblies are shown in Fig. 1 and 2 respectively. The Phase II detail design of the LH_2 turbopump resulted in some minor changes from the Phase I Conceptual Design. To reduce heat transfer from the LH_2 turbine to pump pin connections were provided. Also, increased bearing span and turbine manifold isolation by means of a bellows was also included. The turbine diameter was reduced to 15.24 cm (6 inches), from 16.51 cm (6.5 inches), to reduce tip speed (stress), which also resulted in reduced start time and heat soakback.

The Phase II detailed design effort of the LO_2 turbopump resulted in increasing the shaft length by 2.54 cm (1 inch) and incorporating pin joints and turbine manifold isolation by means of a bellows to reduce heat transfer from the turbine to the pump. The turbine diameter was reduced to 15.24 cm (6 inches), from 18.42 cm (7.25 inches), to arrive at common LH_2 and LO_2 first-stage wheels. This also resulted in reduced start time and heat soakback from the turbine to pump.

9AY24-11/23/71-S1B*

Figure 1. Liquid Hydrogen Turbopump Assembly

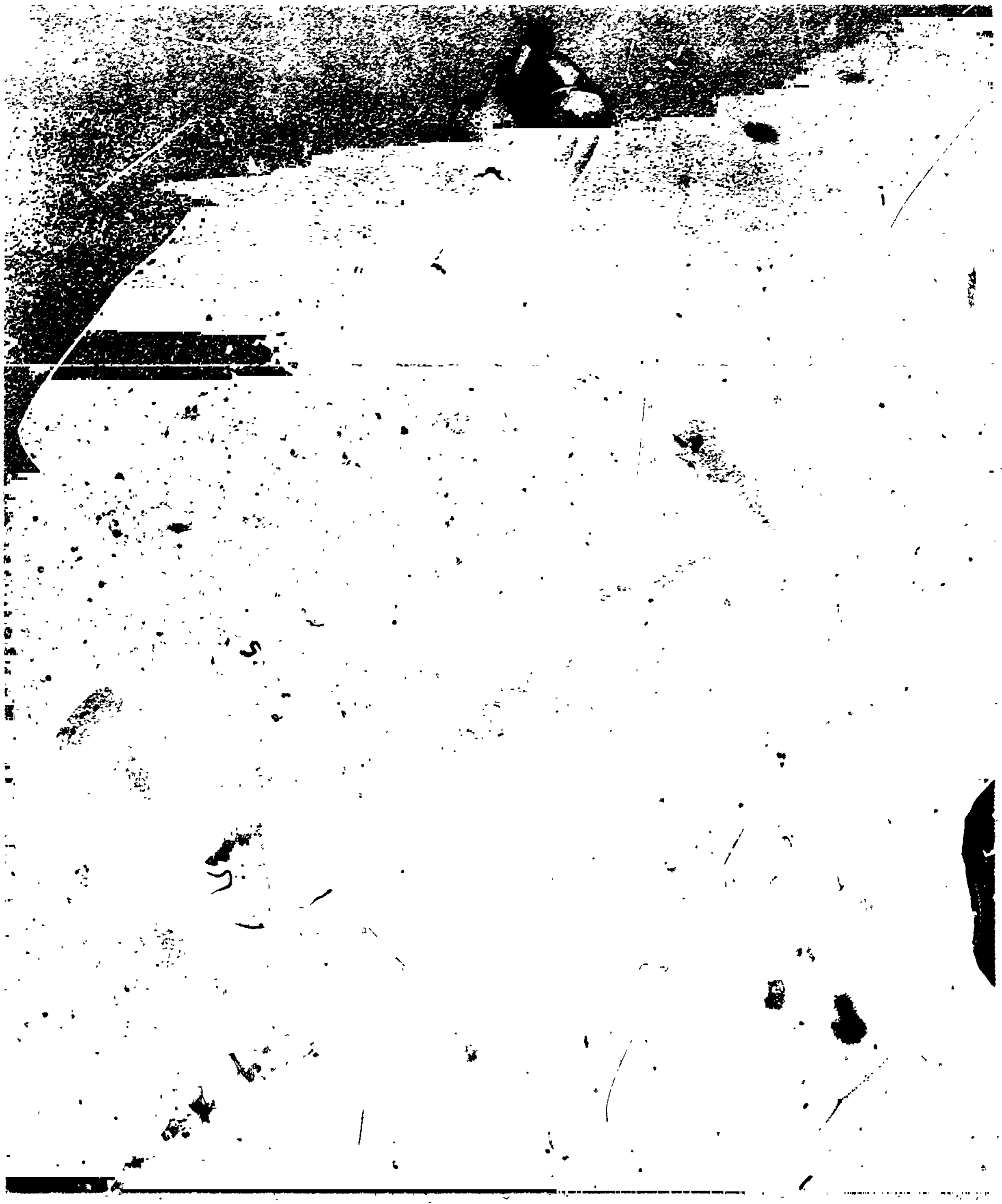

9AY24-11/23/71-S1D*

Figure 2. Liquid Oxygen Turbopump Assembly

The Failure Modes and Effects analysis was conducted for each turbopump design and Potential Failure Modes were eliminated by redesign or instrumentation was incorporated to monitor and provide for a safe shutdown.

Concurrent with the completion of the detail design effort, component fabrication was initiated. Because of component vendor delays the program was extended approximately 4 months. However, satisfactory fabrication of all components and spares was accomplished and the test units assembled as shown in Fig. 3 and 4.

The test effort was conducted at the Rocketdyne Propulsion Field Laboratory in test cells 26A and 26B of the CTL 4 test area. The testing consisted of development test effort to demonstrate performance, physical integrity and heat transfer characteristics and acceptance testing to verify unit integrity prior to delivery.

The development testing of the LO_2 turbopump assembly was initiated with gas generator checkout followed by assembly testing for a total of 55 tests and 6580 seconds of accumulated duration.

The development testing of the LH_2 turbopump assembly was essentially completed on the Unit #1 with an accumulated duration of 5,091 seconds and 57 tests when a weld failure in the turbine manifold interrupted the effort. The development test effort was completed on Unit #2.

Acceptance testing of both LO_2 turbopump assemblies and Unit #2 LH_2 assembly was conducted. This effort in conjunction with the development effort resulted in a total of 78 tests and 8,579 seconds of duration on the LO_2 units and 70 tests for a total duration of 6,351 seconds on the LH_2 units.

Following completion of the test program the units were usually inspected and prepared for delivery. Delivery of the units to the Government will be conducted in place at Rocketdyne.

Figure 3. LO_2 Turbopump Assembly

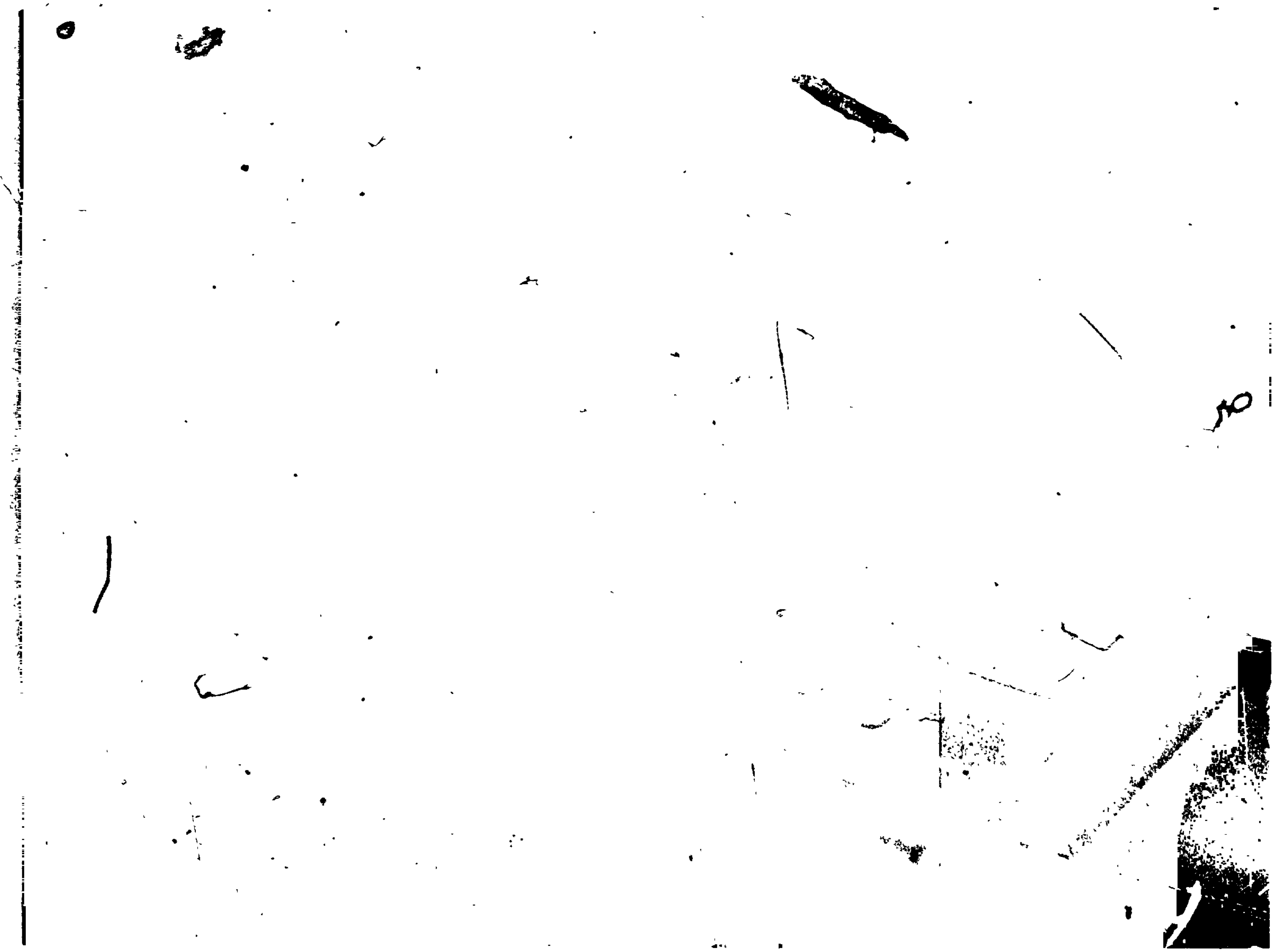

Figure 4. LH_2 Turbopump Assembly

PHASE I - GENERAL SCREENING ANALYSIS

Tradeoff studies were conducted to select the baseline configurations of the major components for the LO_2 and LH_2 turbopump assemblies. The alternative configuration of pumps, turbines, gas generators, and propellant valves were evaluated and recommendations made. The results of the analysis were presented at the Preliminary Design Review and approval received from the NASA Contracting Officers Representative for initiating the Phase II effort. The studies conducted and the results of the Phase I - General Screening Analysis are subsequently presented.

TURBOPUMP SELECTION

In the general screening analysis of the APS O_2/H_2 turbopumps, both steady-state and transient operating requirements were evaluated. Turbopump configurations were analyzed for the following transient operating performances: NPSP, start time, deadhead start, useful life and operating cycles.

The region within the operating envelope at which zero NPSP can be met by the H_2 pump, and minimum NPSP (27,579 N/m or 4 psi) can be met by the O_2 pump, was defined. The effect of startup operating line (ϕ/ϕ_{des}) on inertial NPSP and on deadhead start was also defined. The ability of the turbine to meet the useful life requirement of 10 hours (creep rupture) and the operating cycle requirement of 10,000 cycles (thermal fatigue) were evaluated. The turbopump critical speeds within the operating envelope were also defined and the ability of the bearings to meet both life and starts was assessed.

Based on the results of the screening analysis, the APS O_2/H_2 turbopump configurations were selected for the breadboard APS system. A quantitative evaluation of the turbopump designs and a qualitative evaluation of the turbopump development and operational requirements were made.

The results of the screening analysis indicated the following selection of optimum O_2 and H_2 turbopump configurations for the breadboard APS system:

O_2: Single-stage, centrifugal pump and a single-stage, partial admission, impulse turbine with inboard ball bearings.

H_2: Two-stage, centrifugal pump and a two-stage, full admission turbine (two-row, velocity compound) with inboard ball bearings.

The configurations selected are high-speed, lightweight designs that meet low NPSP, bearing DN, start time and turbine mass flowrate requirements.

O_2/H_2 Turbopump Configuration Study

In the APS O_2/H_2 turbopump configuration study, the effects of number of pump and turbine stages and turbopump speeds were evaluated. The speed range was selected to cover parametrically the O_2 pump NPSP range of 13,790, 27,579, 41,369 N/m^2 (2, 4, 6 psi) and the N_2 pump NPSP range of 6895, 13,790, 20,684, 27,579 N/m^2 (0, 1, 2, 3, 4 psi). Configuration layouts were made to establish design and operational requirements.

The approach used in the screening and selection of the APS O_2/H_2 turbopump is illustrated in the logic diagram (Fig. 5). Although two-stage pumps and turbines were considered for both turbopumps, a one-stage pump and turbine was considered only for the O_2 turbopump. The merits of using different turbine types such as pressure compound, reentry, and radial turbines were also evaluated.

LO_2 Turbopump Configuration. The configuration layout of the 3142 rad/s (30,000 rpm) O_2 turbopump is shown in Fig. 5. Overall envelope dimensions are: 24.38 cm (9.60 inches) in length and 24.77 cm (9.75 inches) in diameter. The weight is estimated to be 16.33 kg (36 pounds). To meet long operating life and large number of starting cycles, static liftoff seal, floating ring seals and preloaded ball bearings are used. To minimize heat soak-back, a thermal short is used between the turbine manifold and pump housing.

The configuration layout for the 2094 rad/s (20,000 rpm) O_2 turbopump is shown in Fig. 6 and 7 compared with the 3142 rad/s (30,000 rpm) configuration. The overall envelope dimensions are 28.96 cm (11.4 inches) in length and 24.77 cm (9.75 inches)

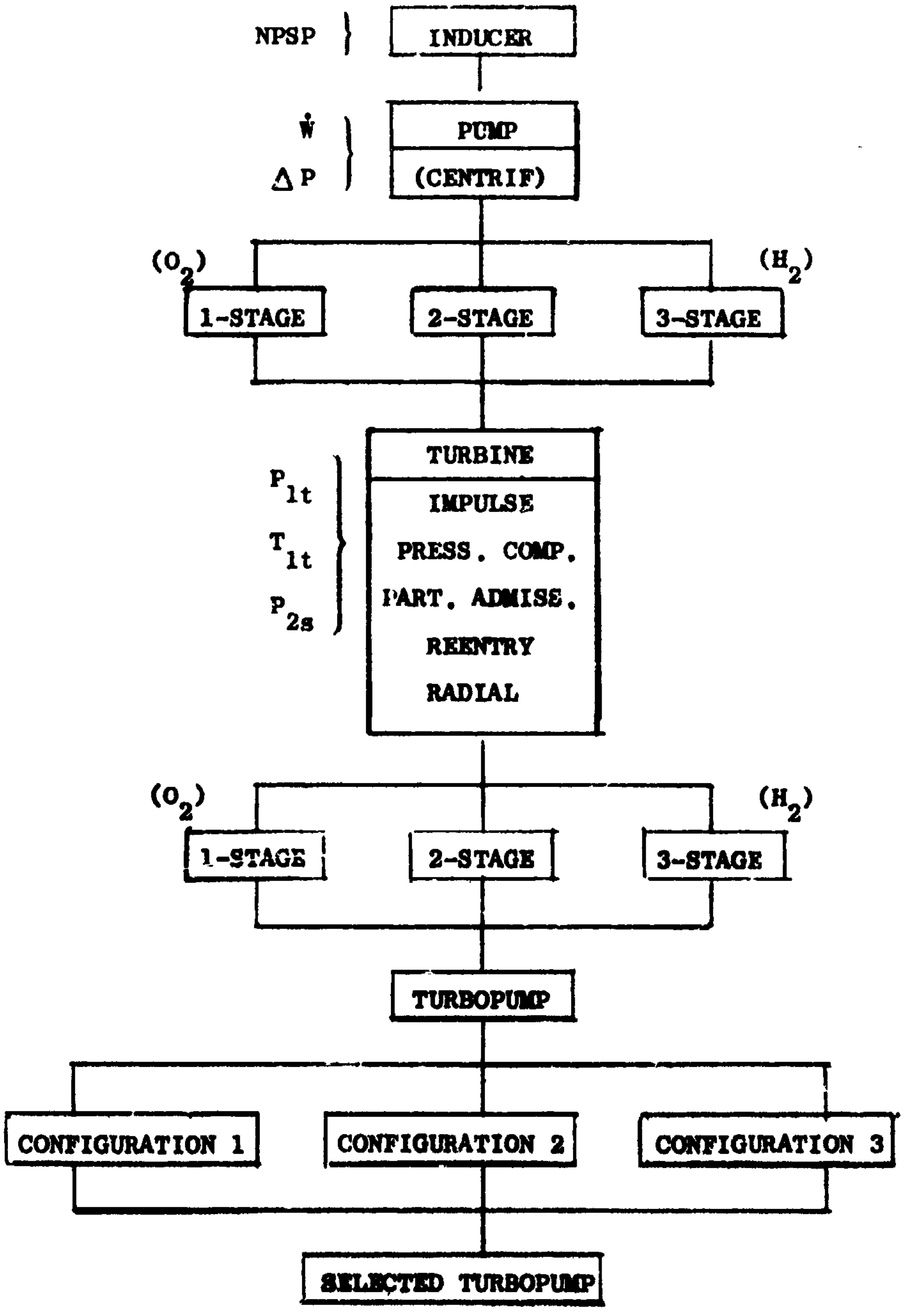

Figure 5. APS-O_2/H_2 Turbopump Selection Approach

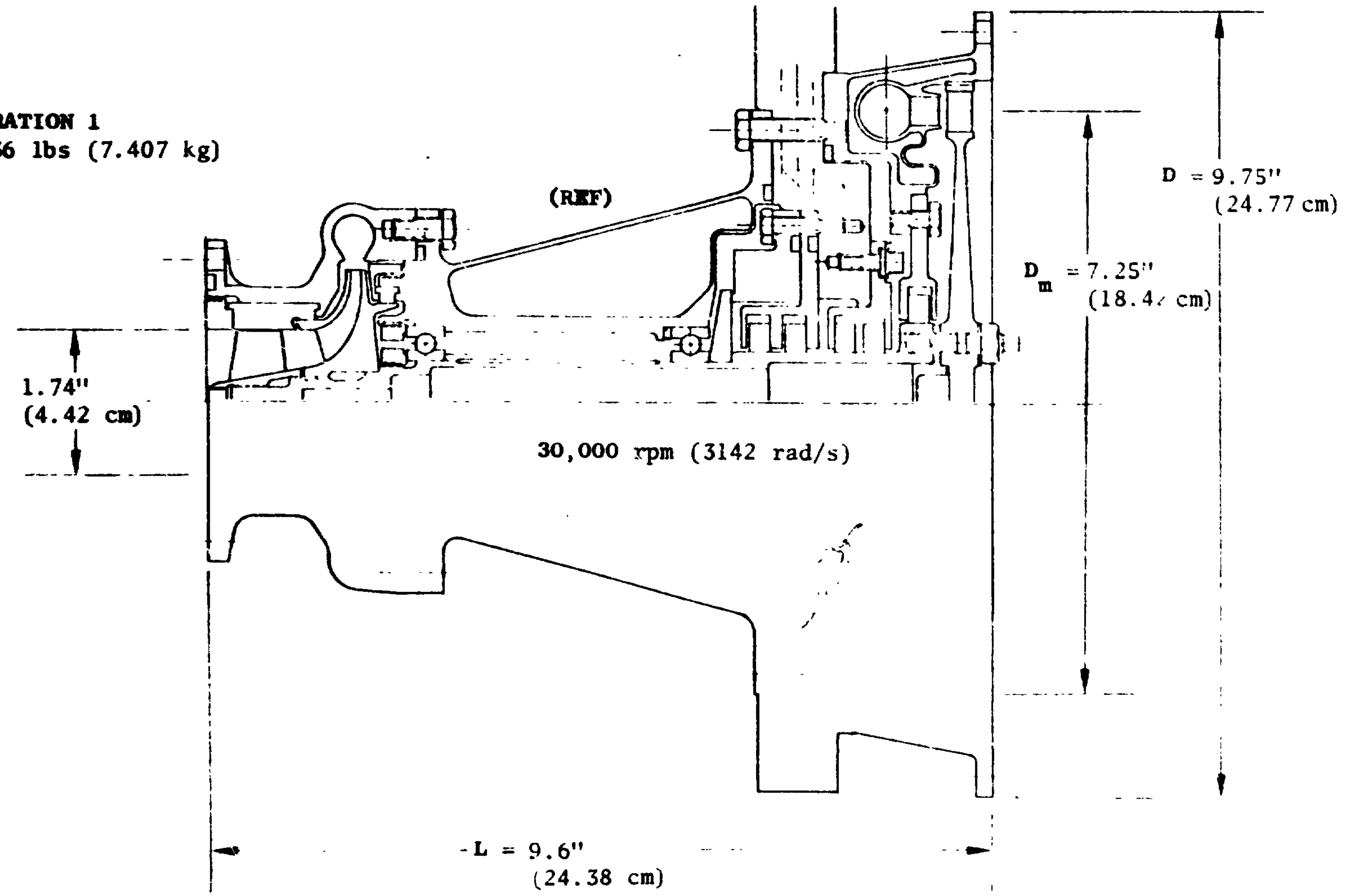

Figure 6. APS LO_2-Turbopump N_{DES} = 3142 rad/s (30,000 rpm), Ref.; $NPSH_S$ = 27,579 N/m^2 (4.0 psi) Max

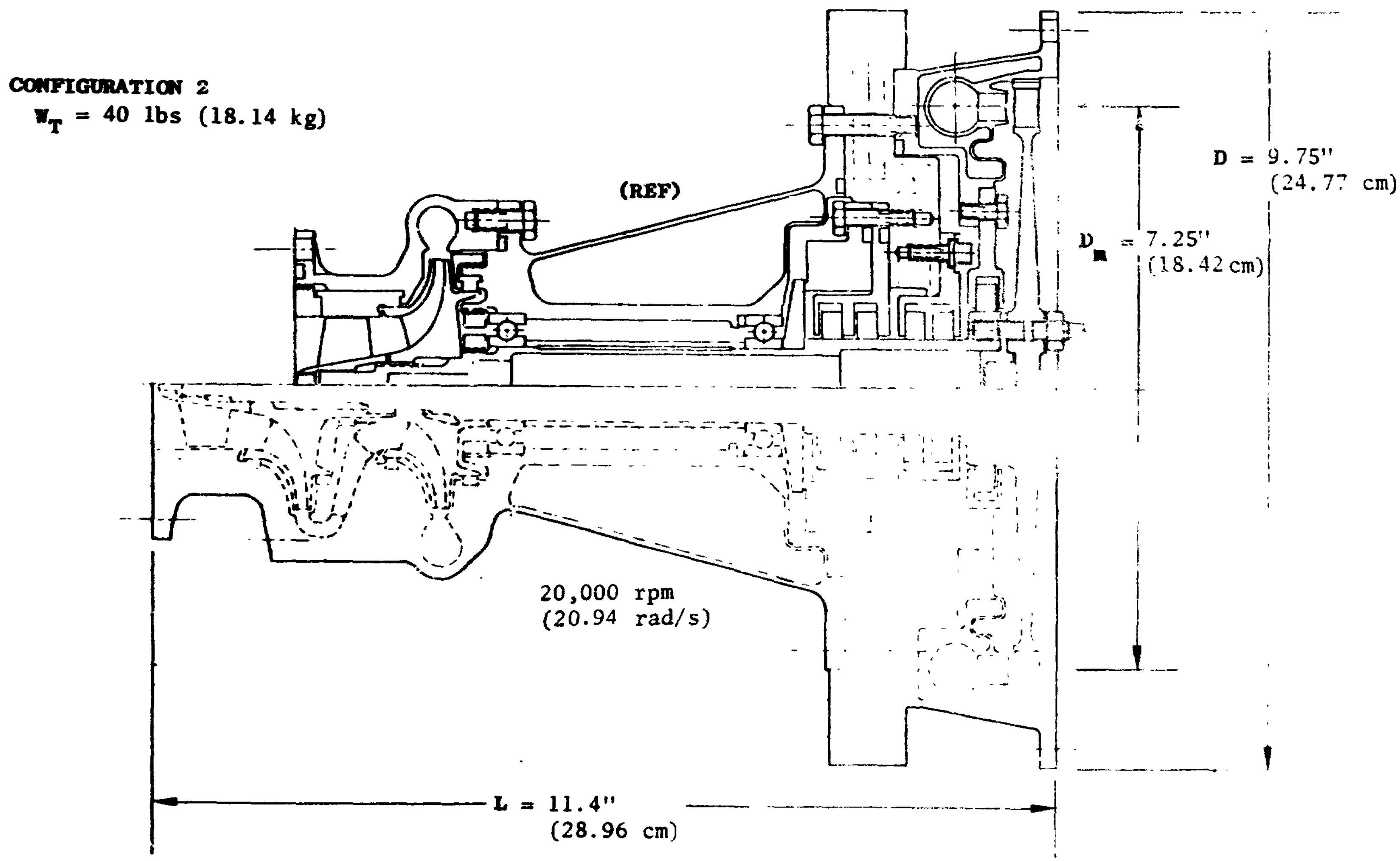

Figure 7. APS LO_2-Turbopump N_{DES} = 2,094 rad/s (20,000 rpm), $NPSP_S$ = 11,032 N/m^2 (1.60 psi), Max

in diameter. The weight is approximately 18.14 kg (40 pounds) The identical 3142 rad/s (30,000 rpm) turbine is used for this configuration with good performance. A two-stage pump is used to increase pump efficiency since a reduction in pump efficiency occurs with a lowering of pump design speed. The mechanical design is similar to the 3142 rad/s (30,000 rpm) configuration in the arrangement of the bearings and seals.

The configuration layout for the 1047 rad/s (10,000 rpm) O_2 turbopump is shown in Fig. 8 and 9 compared with the 3142 rad/s (30,000 rpm) configuration. The overall envelope dimensions are 37.59 cm (14.8 inches) in length and 28.45 cm (11.2 inches) in diameter. The weight is approximately 45.36 kg (100 pounds). Because both pump and turbine efficiencies are reduced at low design speeds, two stages are used in both the pump and turbine to improve component efficiencies. The pump diameter must still increase to meet tip speed required to develop the pressure and the turbine diameter must be larger to maintain velocity ratios for good efficiency. The mechanical arrangement of bearings and seals is similar to the 3142 rad/s (30,000 rpm) configuration, except the pump bearing is located between the stages to avoid critical speed problems.

Based on the configuration layouts of the O_2 turbopumps, the critical speeds of these designs are predicted. A comparison of nominal operating speeds and critical speeds is shown in Fig. 10. The low-speed design at 1047 rad/s (10,000 rpm) is seen to operate below the first critical speed while the 2094 and 3142 rad/s (20,000 and 30,000 rpm) designs are operating between the first and second critical speeds.

The predicted critical speeds of the O_2 turbopump configurations are superimposed onto the required operating envelope, as shown in Fig. 11. In each configuration, the critical speeds are spread apart as much as possible to allow operation over a large region of the envelope without encountering critical speeds. This is done by appropriate distribution of masses and adjustment of spring rates. While both the 2094 rad/s and 3142 rad/s (20,000 and 30,000 rpm) configurations are not expected to encounter the second critical speed, the 3142 rad/s (30,000 rpm) configuration is seen to allow the largest region of operation within the envelope before encountering the first critical speed.

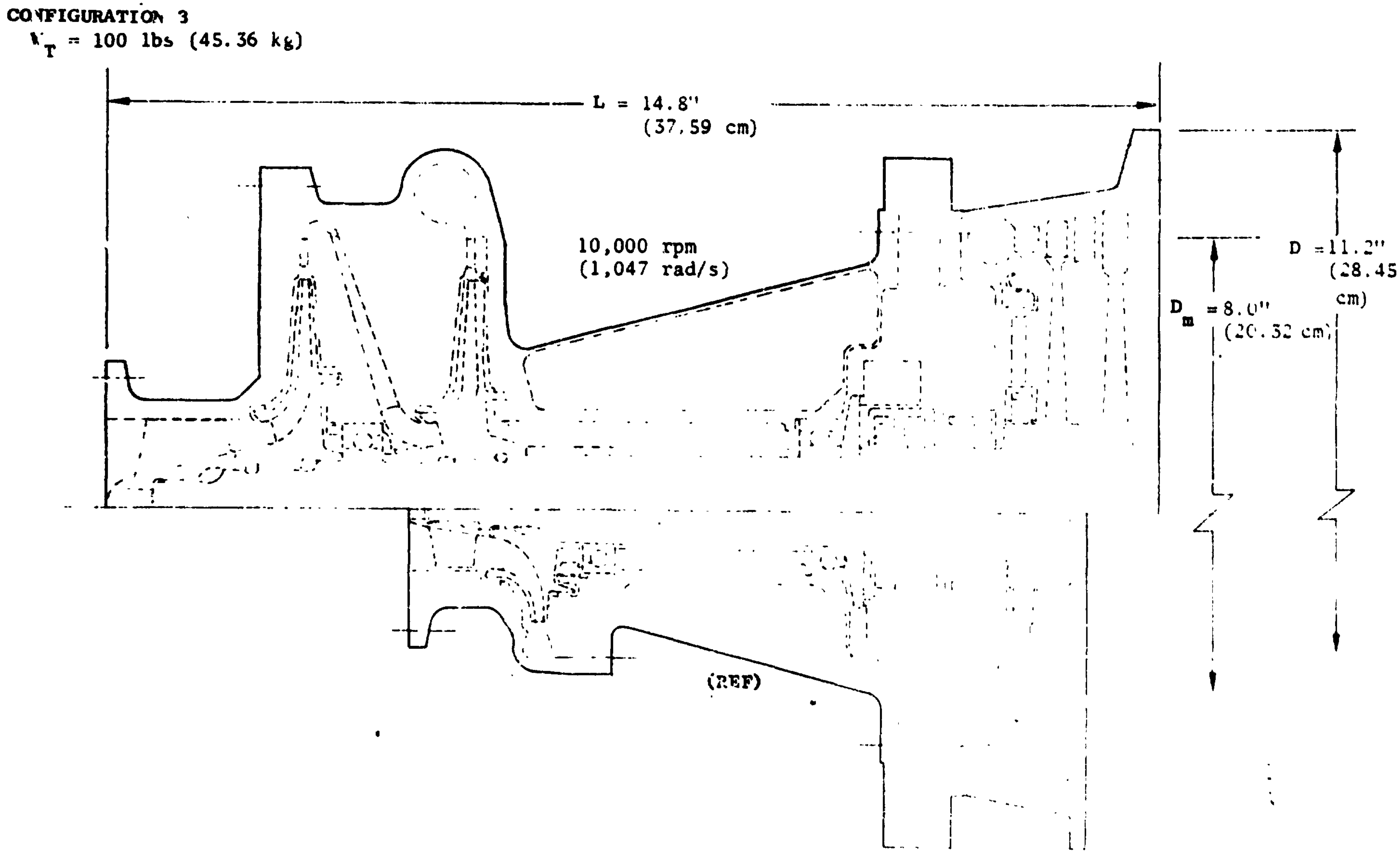

Figure 8. APS LO_2-Turbopump N_{DES} = 1,047 Rad/s (10,000 rpm), $NPSP_S$ = 2,068 N/m^2 (0.30 psi), Max

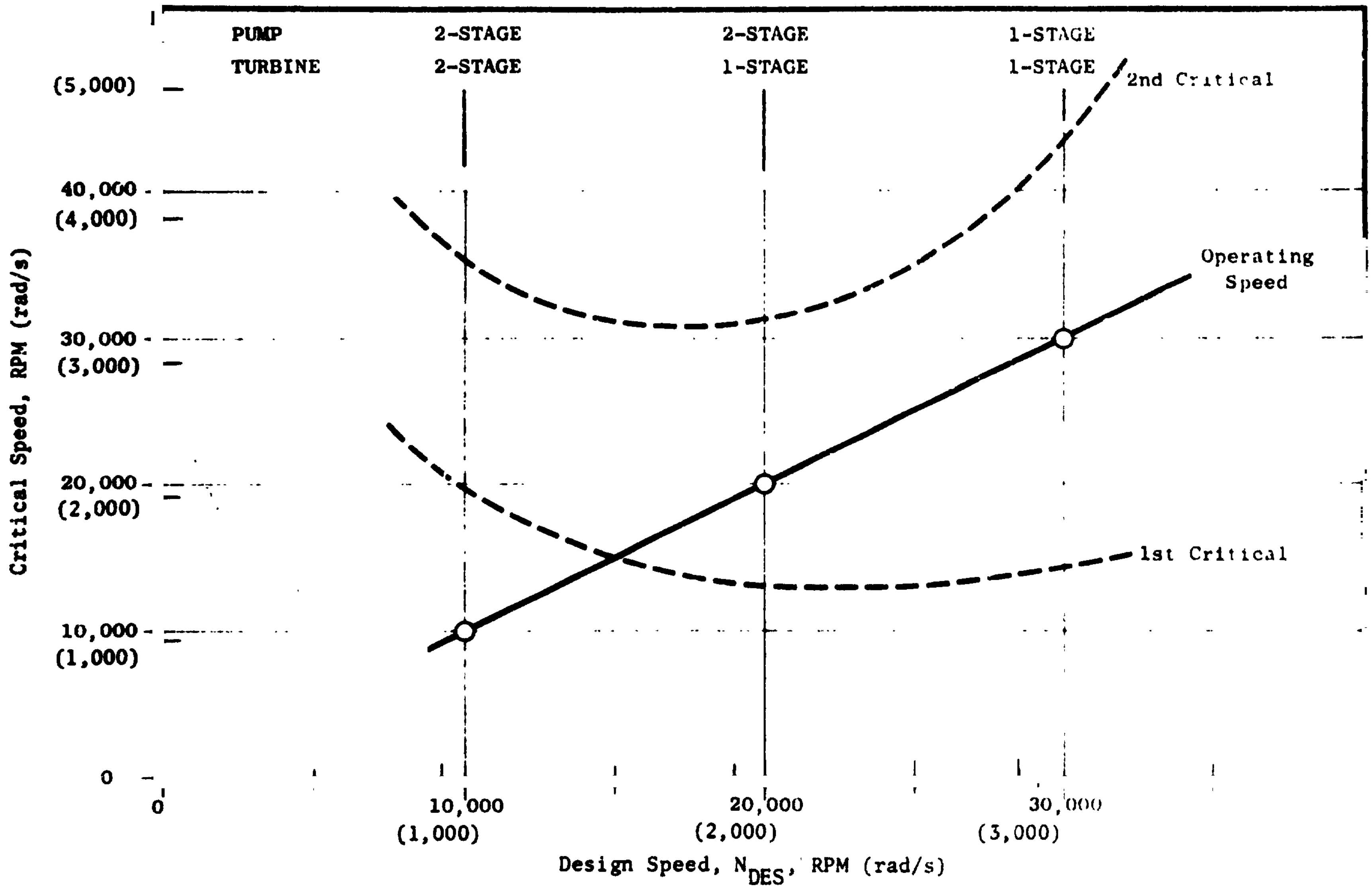

Figure 9. Critical Speeds of O_2 Turbopumps

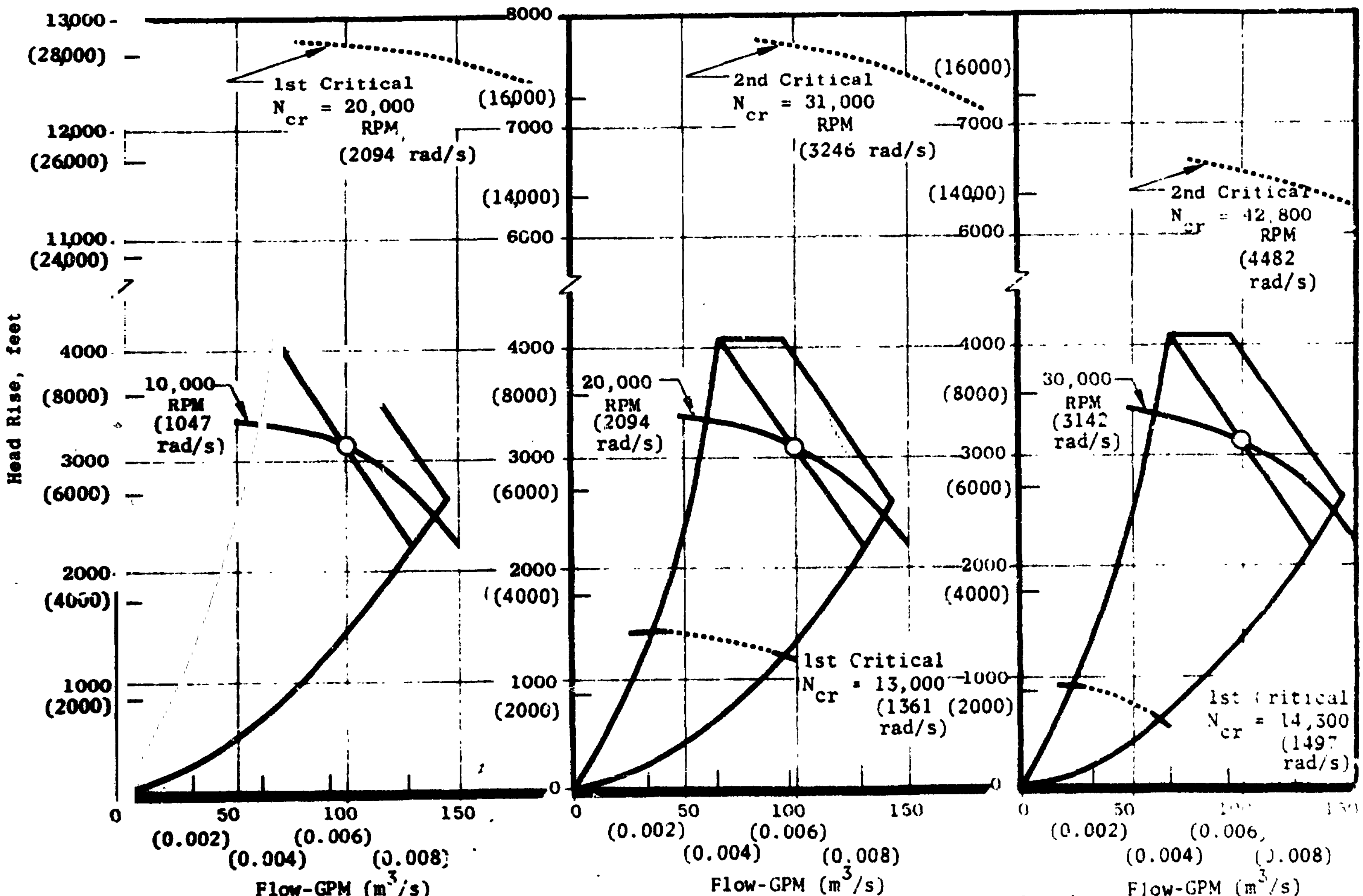

Figure 10. Effect of O_2 Pump Configurations on Critical Speed

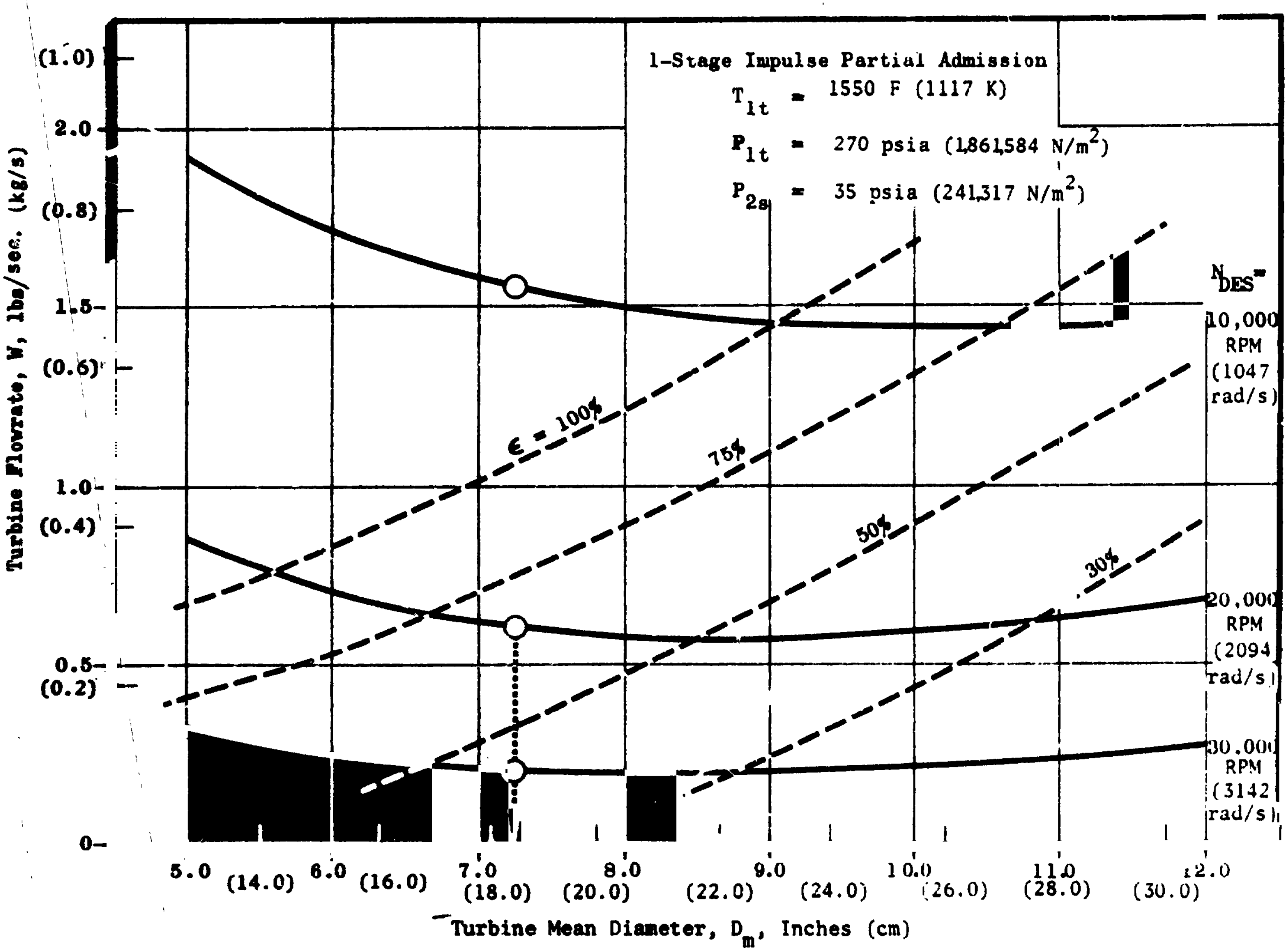

Figure 11. APS O_2-Turbine

The bearing size and speed (DN) for the O_2 turbopump configurations are estimated from a relationship of design speed and torque required to drive the pump. The bearing DNs for the O_2 turbopump configurations are not high, all being below 0.70 million.

An estimate of turbine performance for each O_2 turbopump configuration is obtained from the parametric curves shown in Fig. 11. The turbine mass flowrate required for each configuration is indicated. The turbine pitch diameter is selected at the largest value to give minimum mass flowrate without exceeding the allowable stresses of the turbine blades. The 1047 rad/s (10,000 rpm) configuration is seen to be over twice the mass flowrate required by the higher speed configurations.

A summary of the O_2 turbopump configurations is presented in Table 2. The high-speed designs are the lightest and smallest with moderately low bearing DN. The ratio of the pump mass to the turbine mass, which is a relative indication of this turbine heat soakback rate, is also listed. If the 1047 rad/s (10,000 rpm) configuration were a one-stage pump design, the mass ratio would be 1.25 rather than 1.0.

TABLE 2. SUMMARY APS O_2-TURBOPUMP CONFIGURATION

N_{DES} rad/s (rpm)	Pump Stages	Turbine Stages	L cm (inches)	D cm (inches)	Bearing DN 10^6	Weight Kg (pounds)	Weight/Ratio Pump/Turbine
1047 (10,000)	2(1)	2	37.59 (14.8)	28.45 (11.2)	0.28	45.36 (100)	1.0(1.25)
2094 (20,000)	2	1	28.96 (11.4)	24.77 (9.75)	0.41	18.14 (40)	1.22
3142 (30,000)	1	1	24.38 (9.6)	24.77 (9.75)	0.57	16.33 (36)	1.0
4189 (40,000)	1	1	--	--	0.68	13.61 (30)	1.0

$\underline{LH_2}$ Turbopump Configuration. The configuration layout of the 8378 rad/s (80,000 rpm) H_2 turbopump is shown in Fig. 12 Overall envelope dimensions are 21.59 cm (8.5 inches) in length and 14.73 cm (5.8 inches) in diameter. The weight is approximately 20.41 kg (45 pounds). Similar to the O_2 turbopump, static liftoff seals, floating ring seals, and preloaded ball bearings are used to meet the requirements of long operating life and large number starting cycles. To minimize heat soakback, a thermal short is used between the turbine manifold and pump housing. The mechanical arrangement of bearings and seals are identical to the 5236 rad/s (50,000 rpm) configuration shown for comparison (above the centerline).

The configuration layout for the 5236 rad/s (50,000 rpm) H_2 turbopump is shown in Fig. 13. Overall envelope dimensions are 34.67 cm (13.65 inches) in length and 23.62 cm (9.3 inches) in diameter. The weight is 29.03 kg (64 pounds). The mechanical design was briefly described in the previous figure (Fig. 12).

The configuration layout for the 4189 rad/s (40,000 rpm) H_2 turbopump is shown in Fig. 14. Overall envelope dimensions are 34.8 cm (13.7 inches) in length and 27.69 cm (10.9 inches) in diameter. The weight is approximately 38.56 kg (85 pounds). A three-stage pump is used to increase pump efficiencies since a reduction in pump efficiency occurs with a lowering of pump design speed. To avoid a large overhang, the pump bearing is located between the inducer and first pump stage. As a result, the pump is in closer proximity to the turbine than the higher speed configurations.

Based on the configuration layouts of the H_2 turbopumps, the critical speeds for these designs were predicted. A comparison of nominal operating speeds and critical speeds is shown in Fig. 15. All configurations are found to operate between the second and third critical speeds. For the parametric evaluation, a 6283 rad/s (60,000 rpm) configuration is used in the configuration study.

The predicted critical speeds of the H_2 turbopump configurations are superimposed onto the required operating envelope, as shown in Fig. 16. In each configuration, the critical speeds are spread apart as much as possible to allow operation over

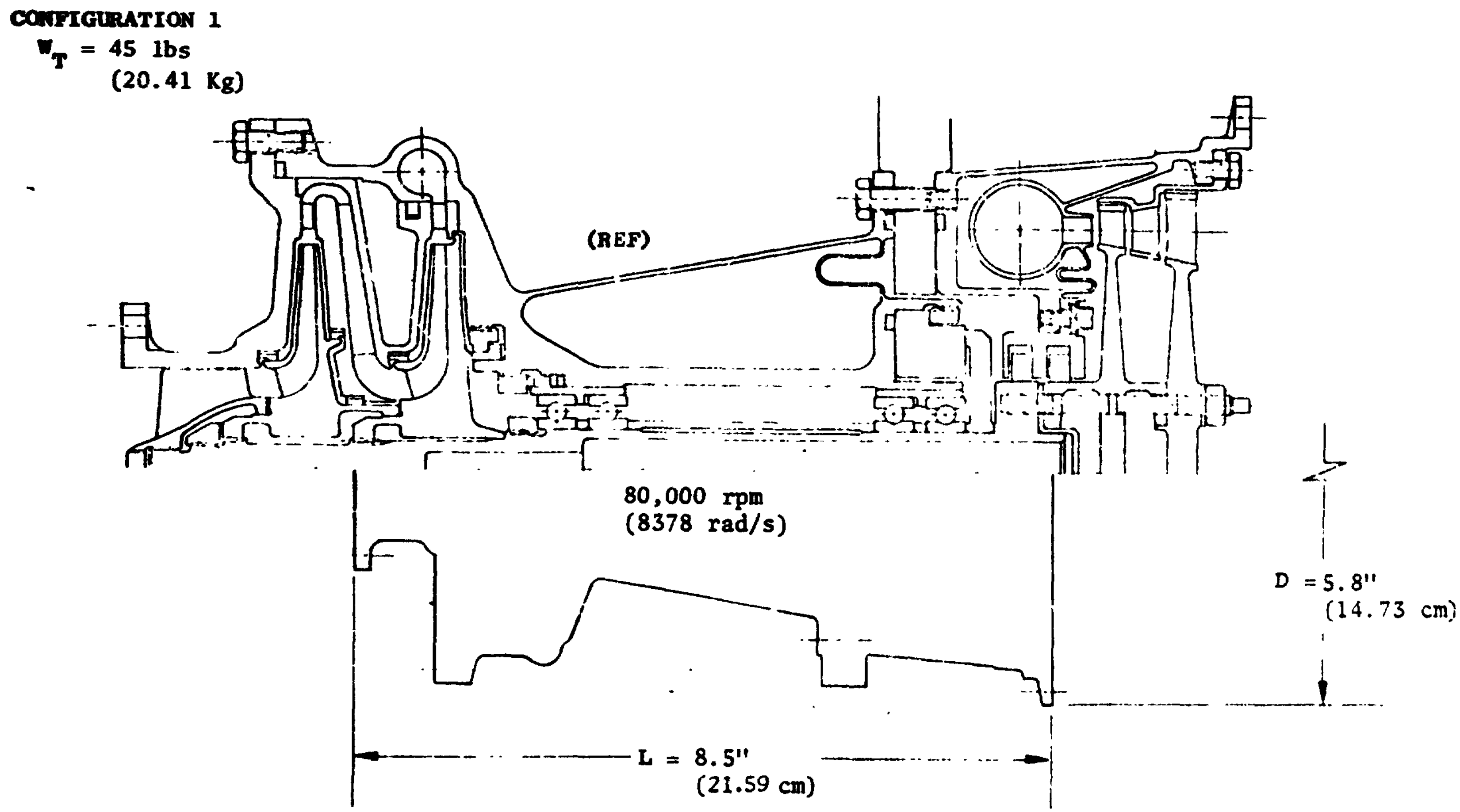

Figure 12. APS LH_2-Turbopump N_{DES} = 80,000 rpm (8378 rad/s); $NPSP_S$ = 1.2 psi, (8273 N/m^2) Max

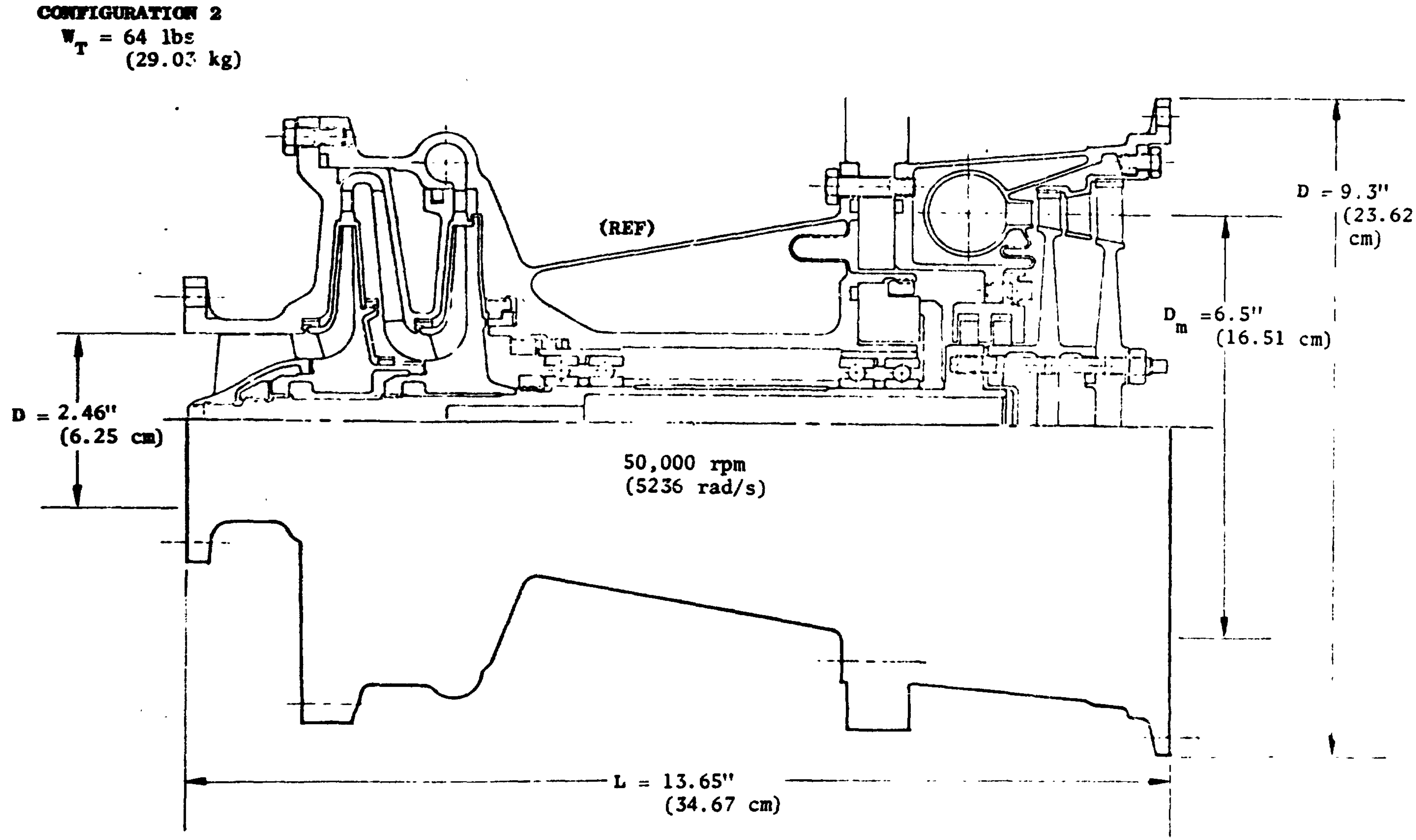

Figure 13. APS LH_2-Turbopump N_{DES} = 50,000 rpm (5236 rad/s) (Ref) $NPSP_S$ = 0.60 psi (4137 N/m^2) max

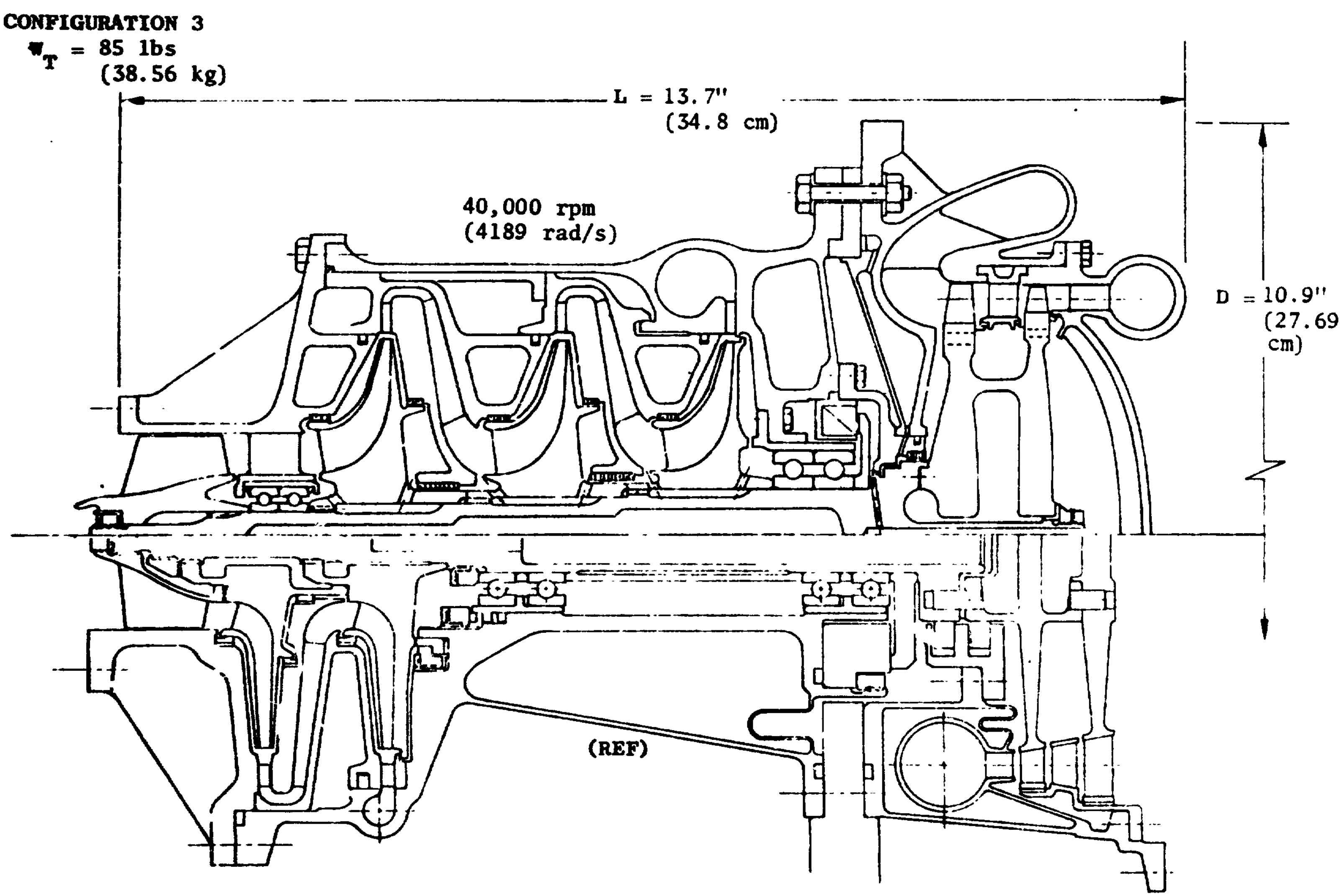

Figure 14. APS LH_2-Turbopump N_{DES} = 40,000 rpm (4189 rad/s), $NPSP_S$ = 0.35 psi, (2413 N/m^2) max

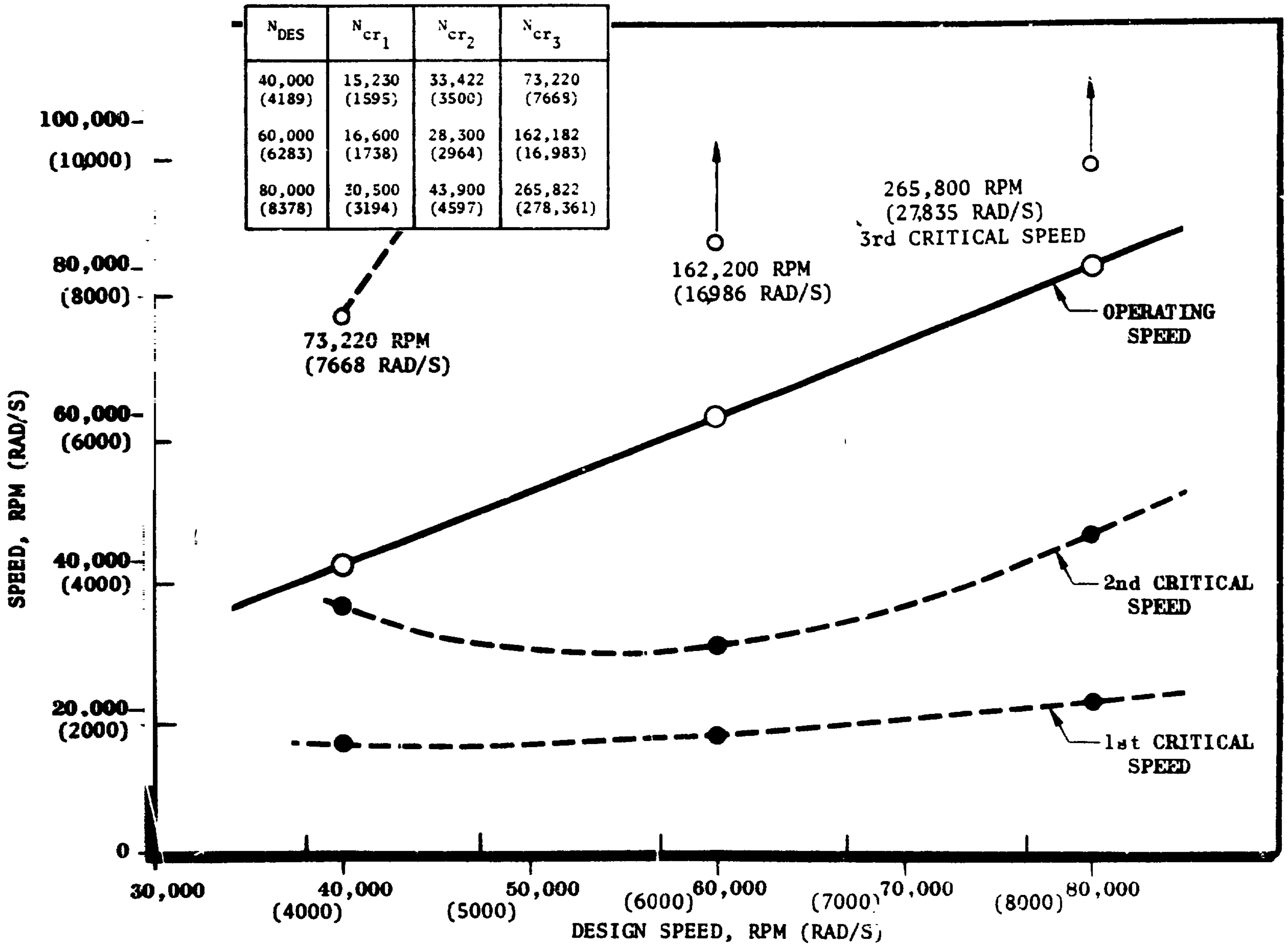

N_{DES}	N_{cr_1}	N_{cr_2}	N_{cr_3}
40,000 (4189)	15,230 (1595)	33,422 (3500)	73,220 (7669)
60,000 (6283)	16,600 (1738)	28,300 (2964)	162,182 (16,983)
80,000 (8378)	30,500 (3194)	43,900 (4597)	265,822 (278,361)

Figure 15. Critical Speeds of H_2-Turbopump Configurations

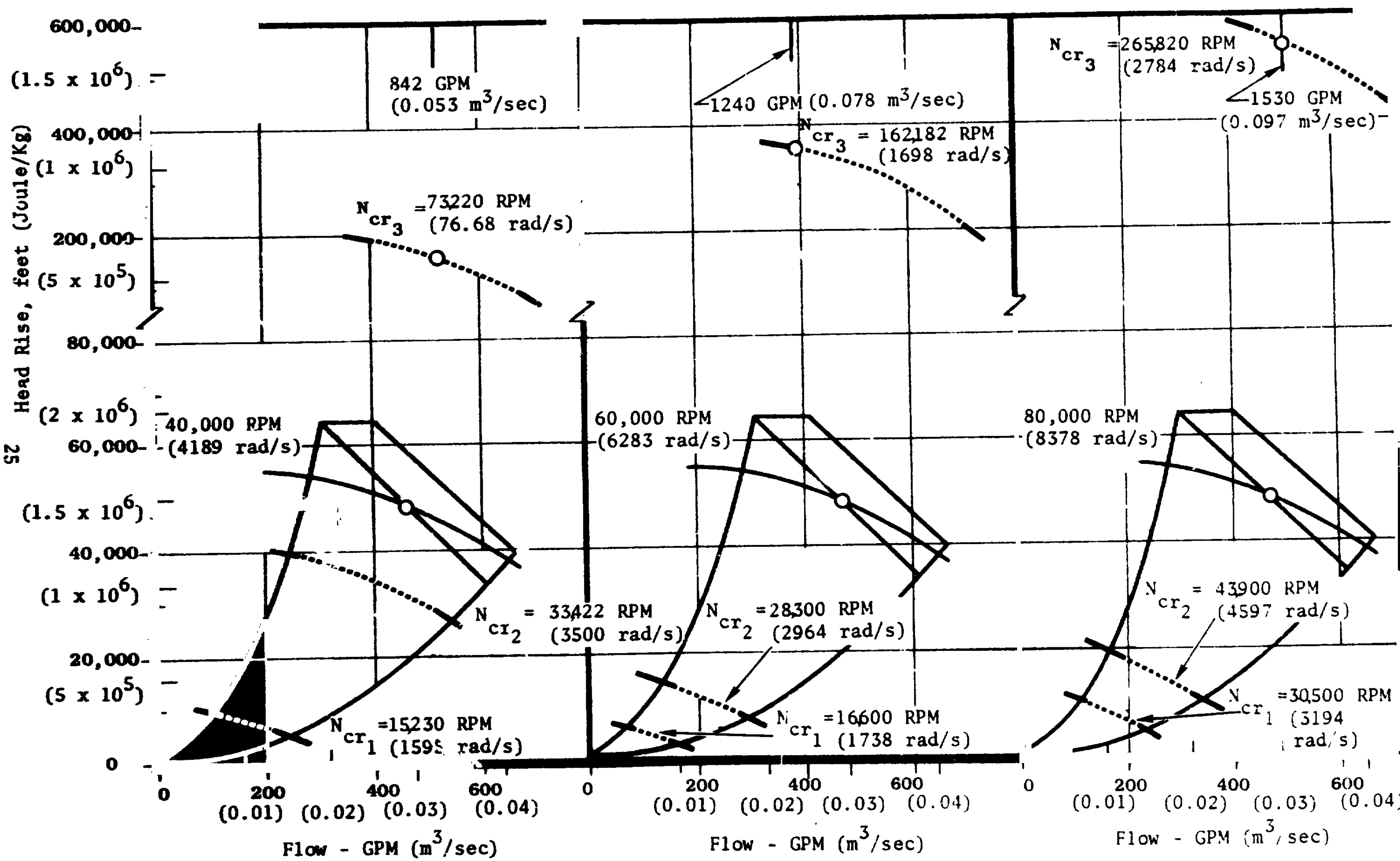

Figure 16. Operating Speed Range of H_2-Turbopump Configurations

a large region of the envelope without encountering critical speeds. (This is done by using an appropriate bearing span and spring rates.) The 6283 rad/s (60,000 rpm) configuration is seen to allow the largest region of operation within the envelope.

The bearing size and speed (DN) for the H_2 turbopump configurations are estimated from a relationship of design speed and torque required to drive the pump. The estimated bearing DN for each configuration is shown in Fig. 17 . Above 5236 rad/s (50,000 rpm), the two-stage pump curve is used and below 5236 rad/s (50,000 rpm), the three-stage pump curve is used. For turbopumps designed about 6283 rad/s (60,000 rpm), the bearing DN will be near 1.5 million.

The technology for designing cryogenic bearings to meet 10-hour life and 10,000 cycles is not clearly established. It is reasonable to assume some tradeoff exists between bearing DN and the number of start cycles for a given life requirement. Similarly, a tradeoff probably exists between bearing life and number of starts for a given bearing DN. Successful operation of bearings has been demonstrated for up to three hours with no indication of failure. The potential for meeting the 10,000-cycle, 10-hour life exists but requires demonstration. Existing criteria were utilized in the selection of configurations.

An estimate of turbine performance for each H_2 turbopump configuration is obtained from the parametric curves, shown in Fig. 17. The turbine mass flowrate required for each configuration is indicated. The turbine pitch diameter is selected to give minimum mass flowrate without exceeding the allowable stresses of the turbine blades. The 4189 rad/s (40,000 rpm) configuration is seen to be over twice the mass flowrate required by the 6283 rad/s (60,000 rpm) configuration and the difference is nearly twice the total mass flowrate of the O_2 turbopump.

A summary of the H_2 turbopump configurations is presented in Table 3. The high-speed designs are the lightest and smallest with moderately low bearing DN. The ratio of the pump mass to the turbine mass, which is a relative indication of the turbine heat soakback rate, is also listed. Because of the added third pump stage, the mass ratio of the 4189 rad/s (40,000 rpm) configuration is significantly greater than the higher speed configurations.

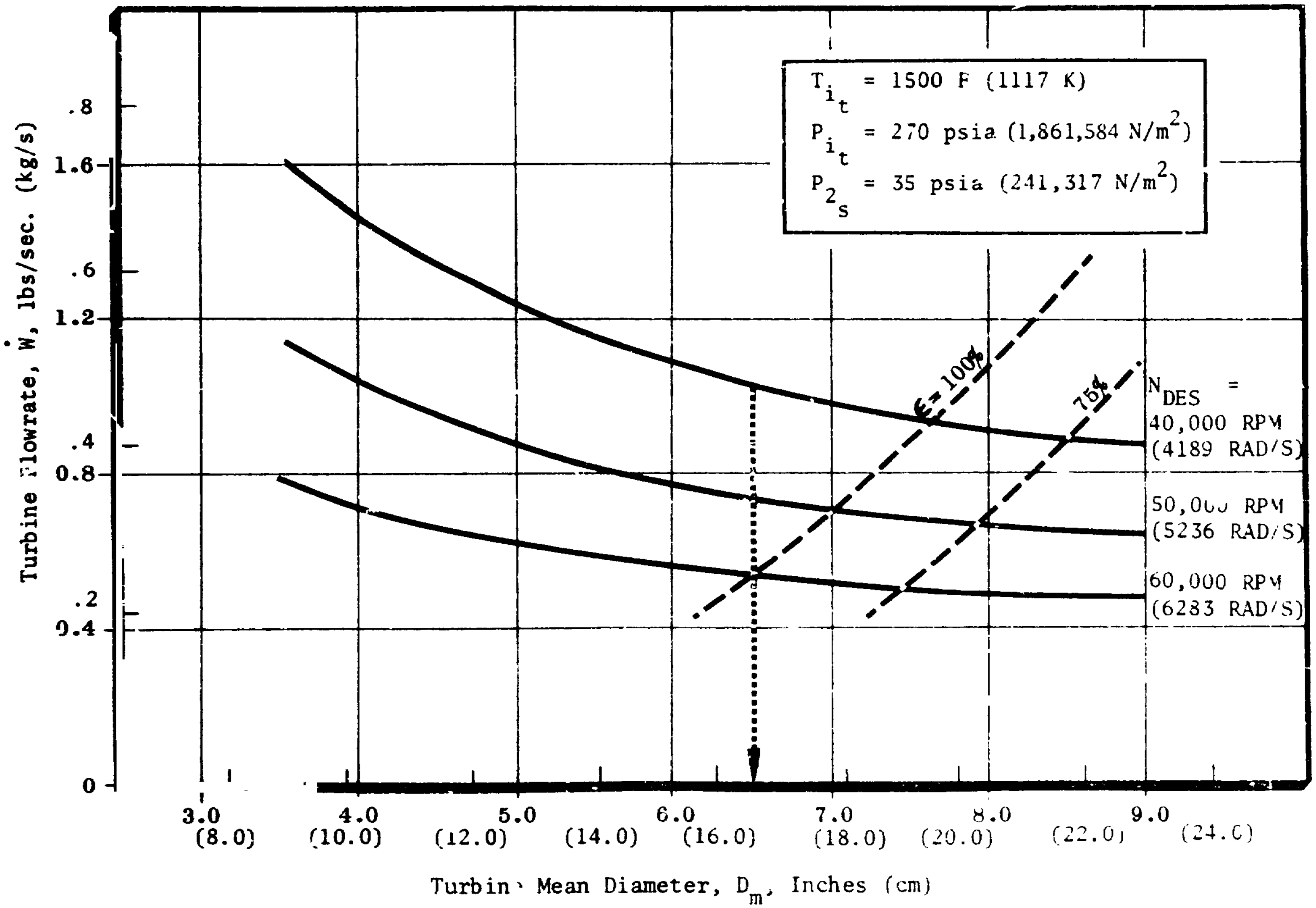

Figure 17. APS-LH_2 Turbine (Two-Stage Impulse)

TABLE 3. APS H_2-TURBOPUMP CONFIGURATION

N_{DES} rad/s (rpm)	Stages	Turbine Stages	L cm (inches)	D cm (inches)	Bearing DN 10^6	Weight Kg (pounds)	Weight/Ratio Pump/Turbine
4,189 (40,000)	3	2	34.8 (13.7)	27.7 (10.9)	1.05	38.6 (85)	3.05
5,236 (50,000)	2	2	34.7 (13.65)	23.6 (9.3)	1.25	29.0 (64)	1.78
6,283 (60,000)	2	2	--	--	1.40	24.9 (55)	1.10
8,378 (80,000)	2	2	21.6 (8.5)	14.7 (5.8)	1.68	20.4 (45)	1.0

NPSP and Start Ramp. The range over which the required NPSP is less than 27,579 N/m^2 (4 psi) during startup is illustrated in Fig. 18 for the O_2 turbopump configurations studied. The lower limit of $\bar{\Phi}$ is defined at which NPSP is equal to 27,579 N/m^2 (4 psi). Startup along $\bar{\Phi}$ less than the lower limit will require excessive NPSP. The 1047 rad/s (10,000 rpm) configuration is seen to be capable of a deadhead start without requiring an NPSP above 27,579 N/m^2 (4 psi).

The effect of startup on inertial NPSP required, as a result of pressure drop caused by accelerating the liquid in the inlet line, was studied for the O_2 turbopump configurations. A line 3.048 m (10 feet) long and 10.2 cm (4 inches) in diameter was assumed. Generally, the low-speed configuration has large inertial NPSP requirement and short start time and the high-speed configuration has low inertial NPSP requirement and long start time.

The tradeoff between NPSP and start time for the O_2 turbopump configurations is shown in Fig. 19. Using the start transient along $\bar{\Phi} = 0.5$, the maximum NPSP required during start and start time are plotted for each O_2 turbopump configuration. The 3142 rad/s (30,000 rpm) configuration is seen to be optimum with low NPSP requirement and low start time.

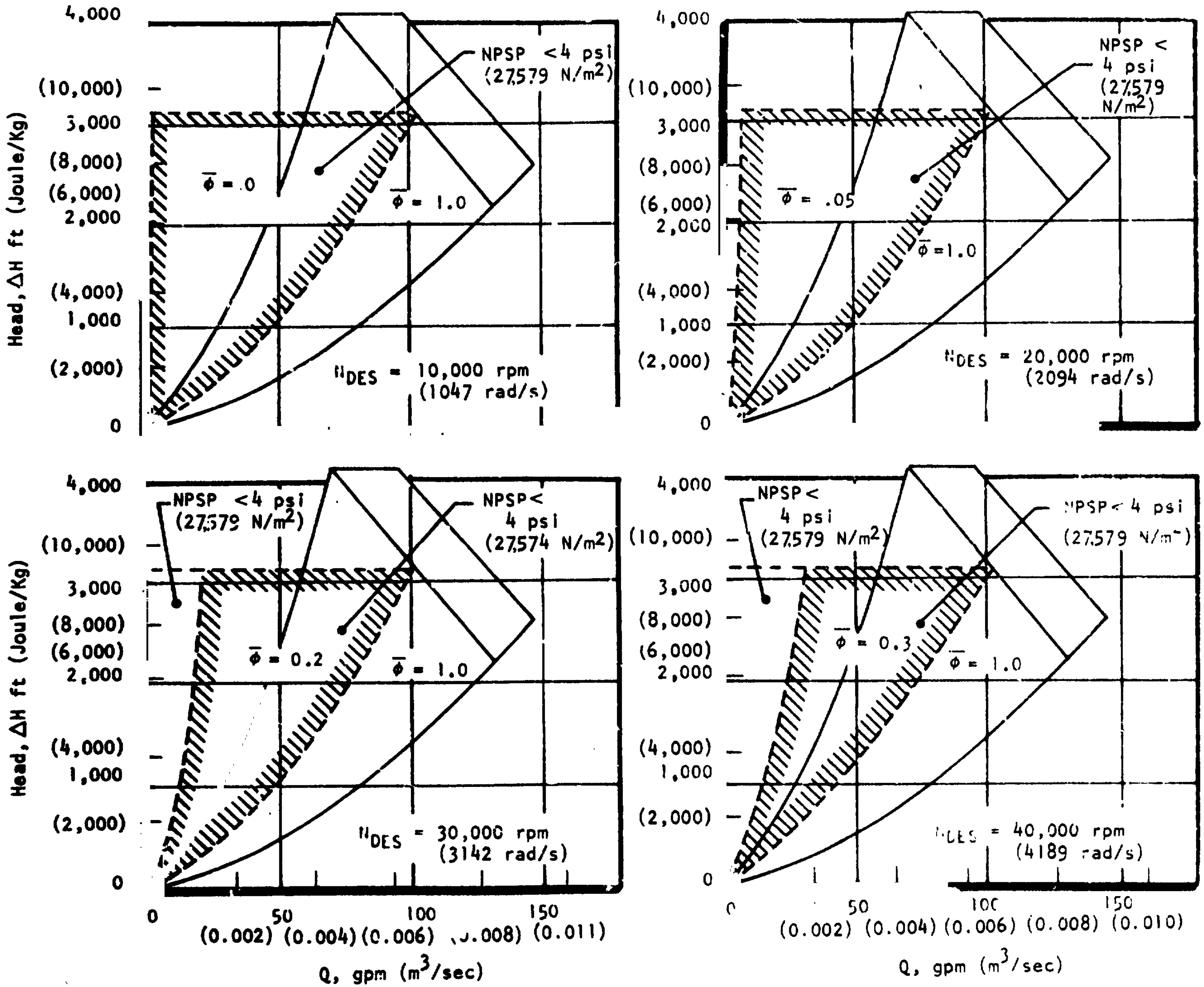

Figure 18. APS-O_2 Turbopump NPSP Requirement and Start Transient Range

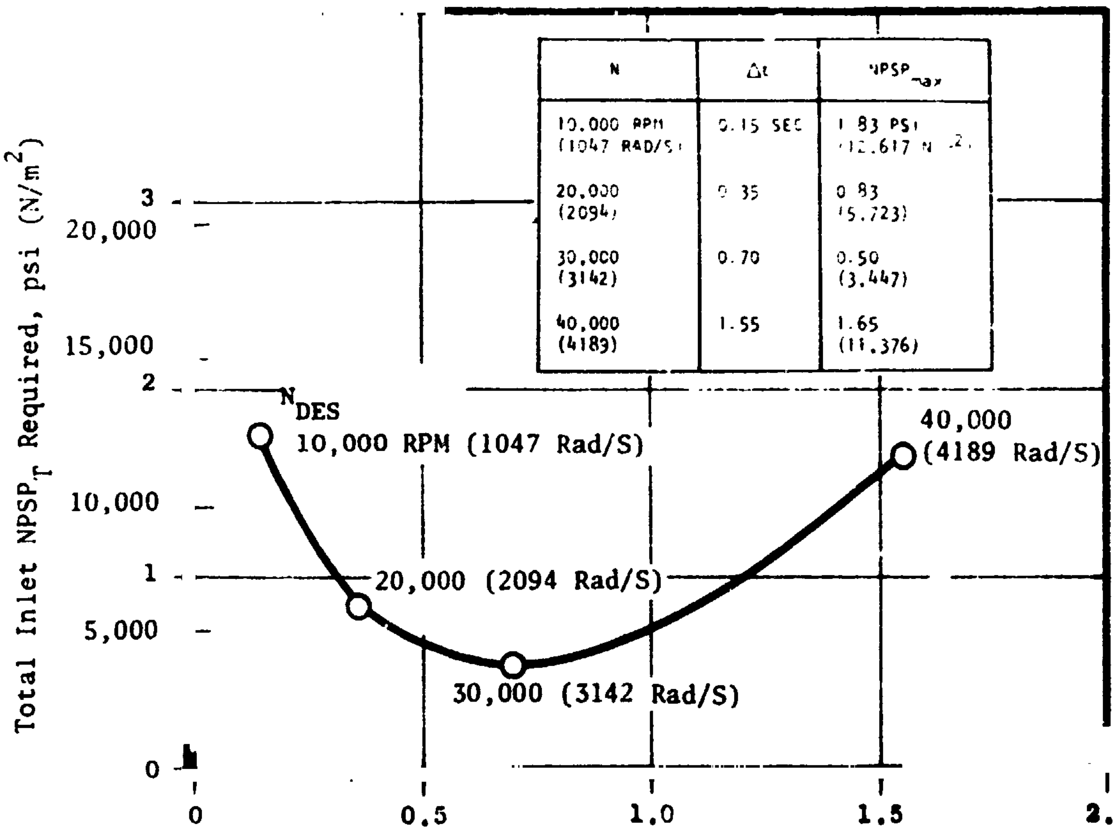

N	Δt	$NPSP_{max}$
10,000 RPM (1047 RAD/S)	0.15 SEC	1.83 PSI (12,617 N/m^2)
20,000 (2094)	0.35	0.83 (5,723)
30,000 (3142)	0.70	0.50 (3,447)
40,000 (4189)	1.55	1.65 (11,376)

Figure 19. Tradeoff of NPSP and Start Time O_2-Turbopump

Deadhead Start, LO_2 Pump. The ability of the O_2 turbopump configurations to start under deadhead conditions (downstream valve closed and flow through the pump is zero) on a $\bar{\Phi} = 0$ startup line is illustrated in Fig. 20. The following assumptions are made: (a) chilled pump, (b) mass of trapped propellant in pump is constant, (c) head rise (ft) will be developed according to the square of pump speed, (d) the deadhead horsepower will correspond to the power at the shutoff head of the pump characteristic curve at any given speed (approximately one-half of the horsepower at $\bar{\Phi} = 1.0$), and (e) all the power transmitted by the pump will go into heating up (enthalpy rise) of the trapped propellant and decreasing its density. The 1047 and 2094 rad/s (10,000 and 20,000 rpm) configurations are able to develop 11,552,289 N/m^2 (1600 psi) despite some propellant heating; however, the 3142 rad/s (30,000 rpm) configuration is able to produce only 5,054,120 N/m^2 (700 psi)

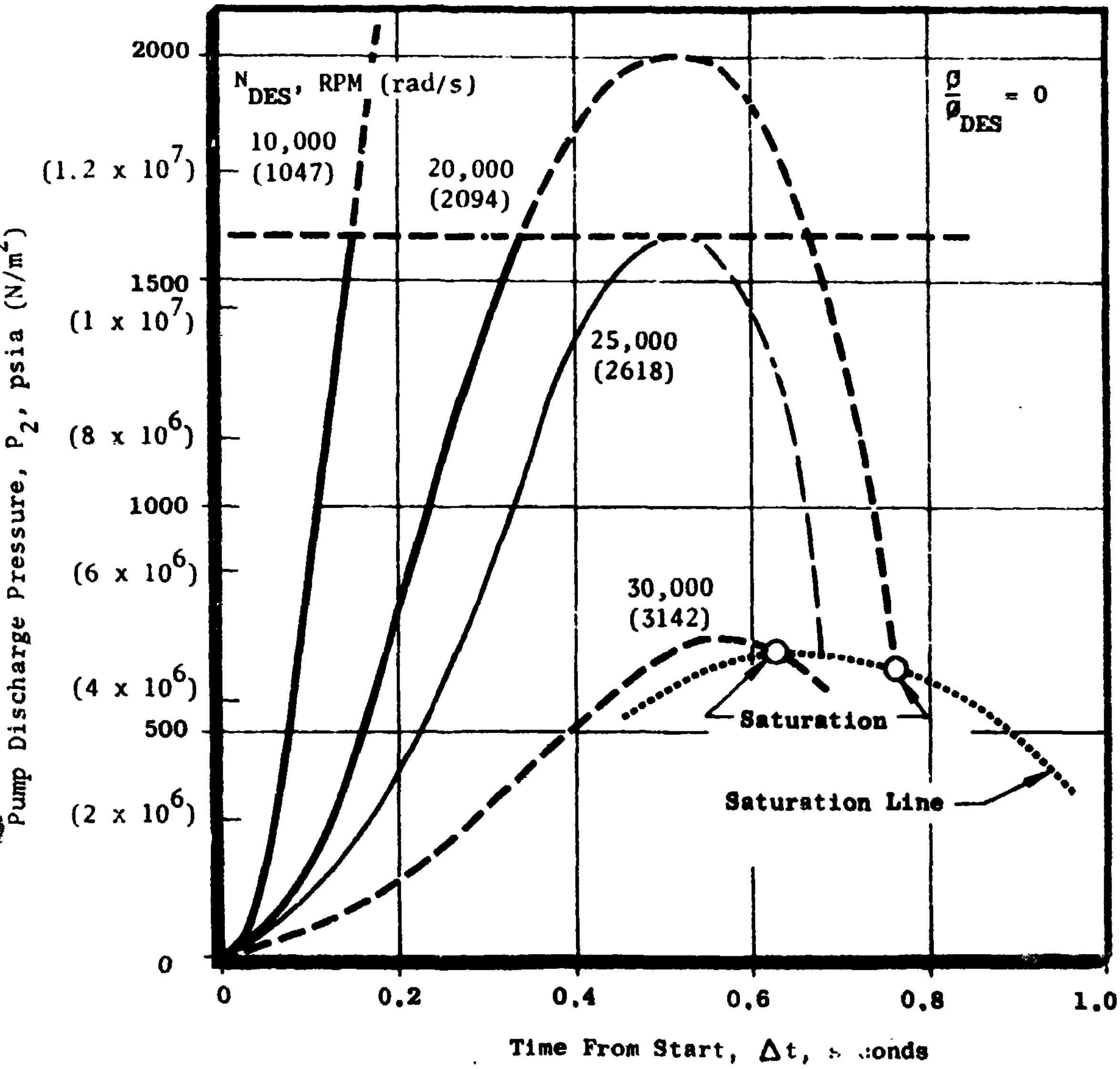

Figure 20. Deadhead Start Transient O_2-Turbopumps

because of the reduced propellant density due to heating. Because of the faster starts obtained with the low-speed configurations, there is less time for the propellants to accumulate heat.

The amount of propellant used during a start transient along a $\bar{\Phi} = 0.50$ startup line (there is throughflow in the pump) for the O_2 turbopump configurations studied is shown in Fig. 21. The propellant consumption is assumed to be equivalent to

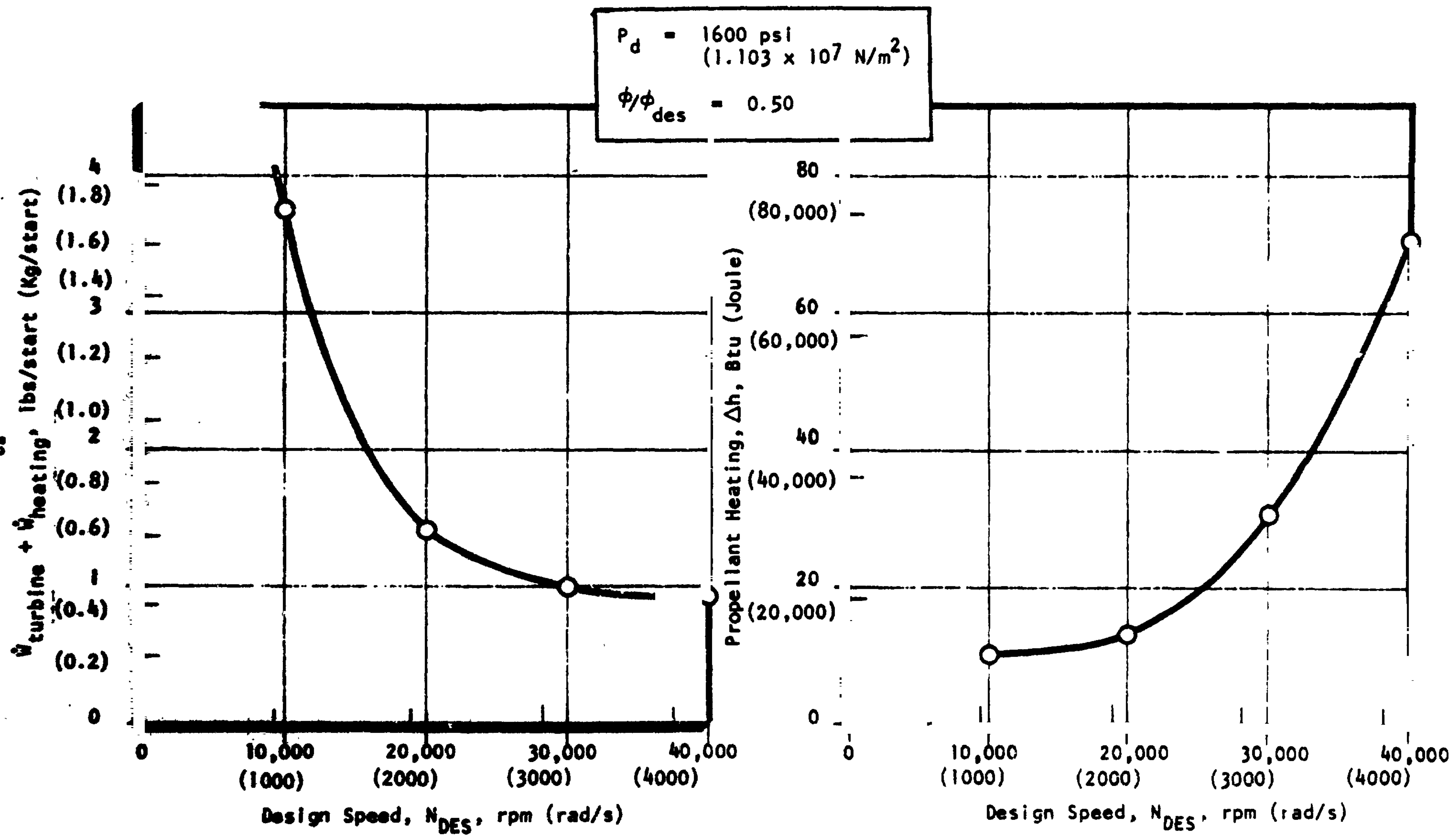

Figure 21. Effect of Design Speed on Propellant Consumption O_2-Turbopump

the sum of the total turbine mass flow used during the start transient and an amount of propellant which would be vaporized due to heating at saturation pressure. The 1047 rad/s (10,000 rpm) configuration is seen to have nearly four times the amount of propellant consumption per start over the 3142 rad/s (30,000 rpm) configuration. (A similar difference exists for a deadhead start along $\bar{\Phi} = 0$.)

<u>Conclusions of LO_2 Pump Start Analysis.</u> A summary of O_2 turbopump transient performance in terms of total NPSP requirement, start time, and turbine mass flowrate is presented in Table 4. The 1047 rad/s (10,000 rpm) configuration has a fast start time; however, it also has a high NPSP and high turbine mass flowrate. The 3142 rad/s (30,000 rpm) configuration has a relatively fast start and will require only low NPSP and low turbine mass flowrate. This configuration is found to be optimum with respect to start requirements.

TABLE 4. APS LO_2-TURBOPUMP NPSP SUMMARY

Configuration	Data				
N_{DES} rad/s (rpm)	$NPSP_S$ N/m^2 (psi) Max.	Nom.	Start Time ΔT (secs)	$NPSP_T$ Req. N/m^2 (psi)	Turbine W Kg/s (lb/sec)
1,047 (10,000)	2,068 (0.3)	1,034 (0.15)	0.20	12,411 (1.8)	0.770 (1.700)
2,094 (20,000)	11,032 (1.6)	6,895 (1.0)	0.40	4,826 (0.7)	0.372 (0.820)
3,142 (30,000)	27,579 (4.0)	11,721 (1.7)	0.70	3,447 (0.5)	0.1397 (0.308)
4,189 (40,000)	50,332 (7.3)	24,132 (3.5)	1.0	11,721 (1.7)	0.1134 (0.250)
			$\phi/\phi_{DES} = 0.50$ $P_d = 1.103 \times 10^7\ N/m^2$ (1600 psi)		

NPSP and Start LH_2 Pump. Based on hydrodynamic and two-phase flow data and analysis, the criterion for predicting off-design suction performance of hydrogen inducers is illustrated in Fig. 22. Within the two-phase flow capability of the inducer, the required NPSP (defined at 2 percent head loss) can be less than one velocity head (where inlet line equilibrium flow Mach number is less than one) or even zero (where area contraction and choking within the blades are avoided). For low $\bar{\Phi}$ at which the incidence-to-blade angle is greater than 0.60, the required NPSP will be greater than one velocity head. At high $\bar{\Phi}$ where two-phase Mach number is greater than one, the required NPSP must be at least one velocity head to ensure liquid flow and avoid choking. At even higher $\bar{\Phi}$, the minimum flow area will be within the inducer blades rather than upstream, and the required NPSP will be substantially greater than one velocity head. Based on system considerations, a margin to the predicted NPSP may be applied.

The maximum pump NPSP required (maximum flowrate point of operating envelope) as a function of design speed for H_2 turbopump configurations for different vapor pressure is shown in Fig. 23. For a given NPSP required, increasing vapor pressure will lower the NPSP required by the pump. At the nominal operating point and a vapor pressure of 117,211 N/m^2 (17 psia), zero-NPSP (saturated propellants) operation up to a design speed of 12,566 rad/s (120,000 rpm) is indicated.

A summary of zero-NPSP capability of H_2 turbopumps is shown in Fig. 24. The range ($\Delta\bar{\Phi}$) and the minimum ($\bar{\Phi}$ min.) and the maximum off design flow limits ($\bar{\Phi}$ max.) of the range are tabulated for each configuration.

The effect of inlet line inertance on NPSP for the H_2 turbopump configurations studied is shown in Fig. 25. A line 3.048 m (10 feet) long and 10.16 cm (4 inches) in diameter is assumed. Because there is closer similarity of size and performance of the H_2 configurations considered (relative to O_2 turbopump configurations) and because H_2 pumps are capable of low NPSP operation, the effect of inertial NPSP and the start time of all the configurations are found to be about the same.

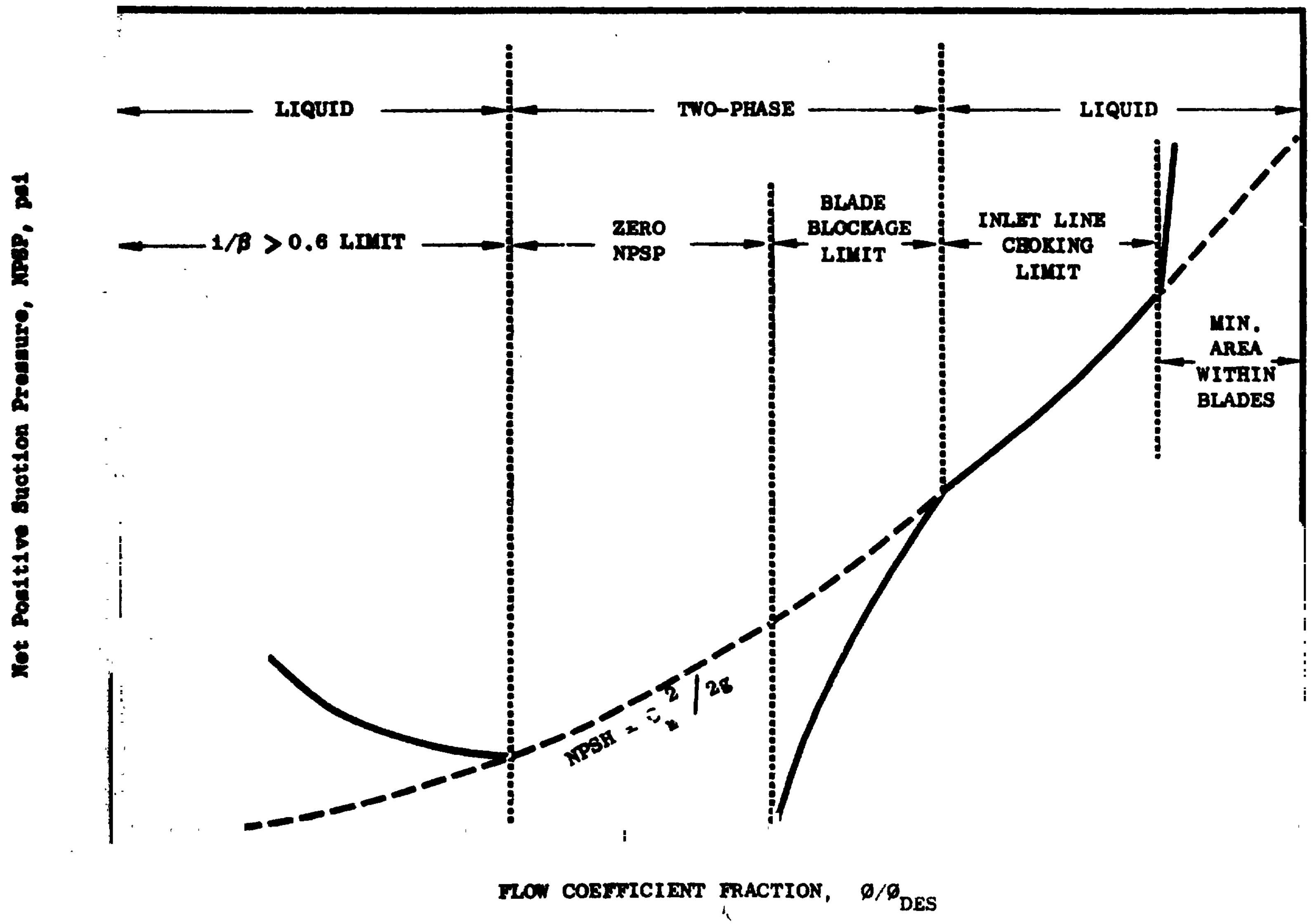

Figure 22. Schematic of LH_2 Inducer Suction Characteristics

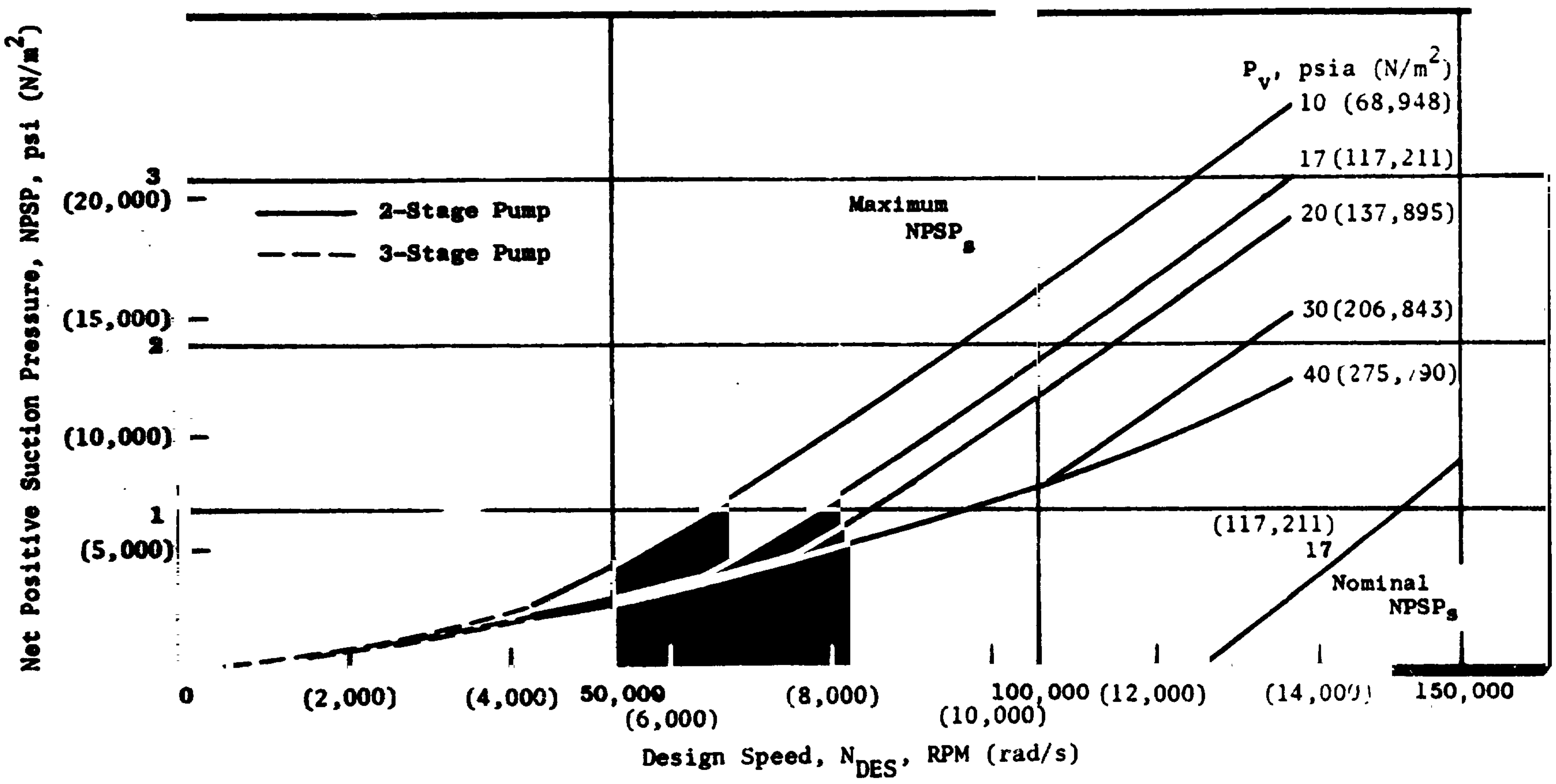

Figure 23. Effect of Design Speed on Maximum and Nominal NPSP H_2-Pump

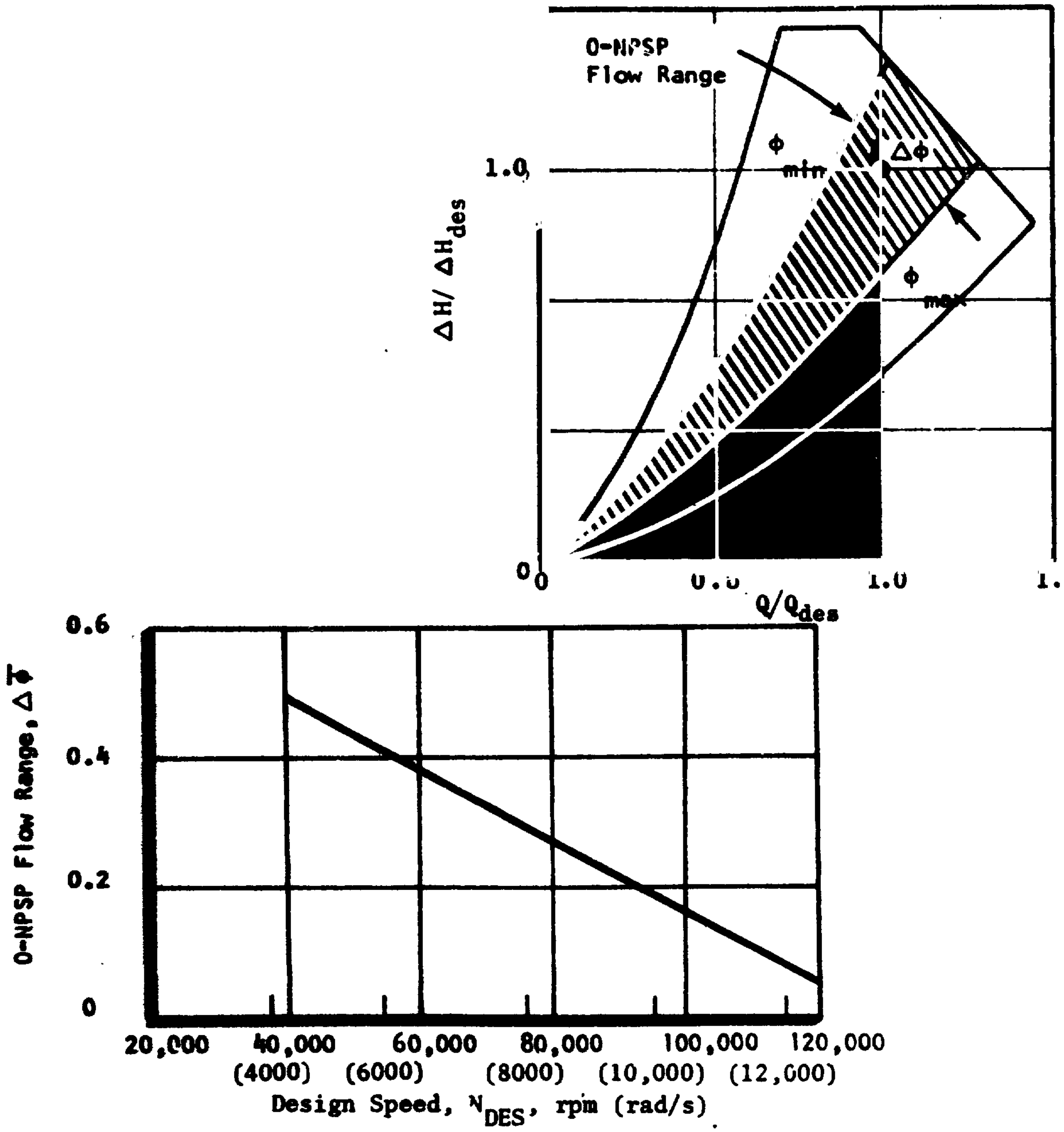

$\bar{\phi} = \phi/\phi_{des}$

N_{des} rpm Rad/s	$\bar{\phi}_{min}$	$\bar{\phi}_{max}$	$\Delta\bar{\phi}$
40,000 (4189)	0.88	1.37	0.49
50,000 (5236)	0.86	1.37	0.44
60,000 (6283)	0.86	1.24	0.38
80,000 (8378)	0.84	1.11	0.27
100,000 (10,472)	0.84	0.99	0.16
120,000 (12,566)	0.84	0.89	0.05

Figure 24. Summary of Zero NPSP Capability of H_2 Turbopump

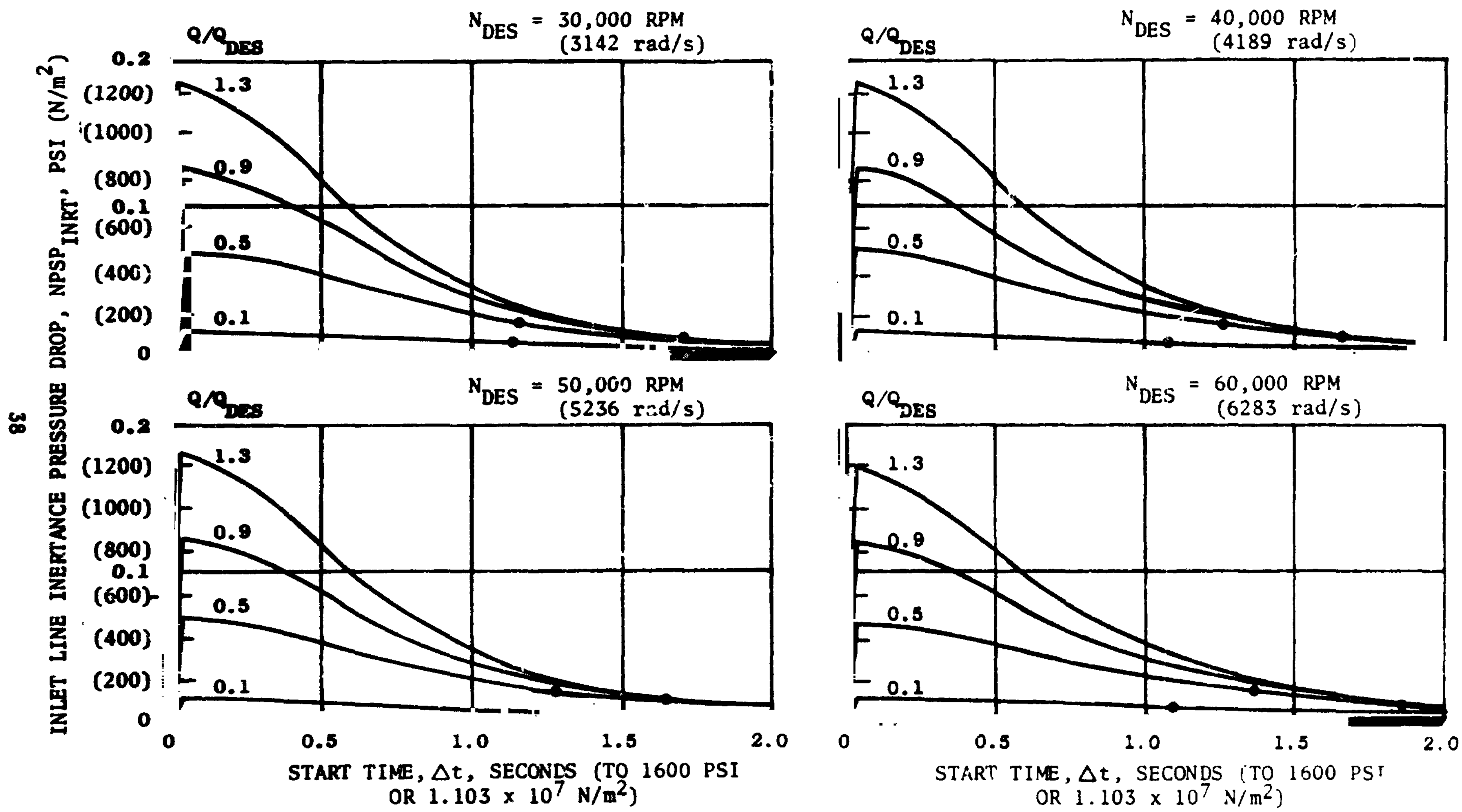

Figure 25. Effect of Line Inertance on NPSP H_2-Turbopump Configurations

A tradeoff does not exist for the H_2 turbopump configurations. The effect of design speed on total NPSP required and start time, along a start transient of $\phi = 0.50$, is shown in Fig. 26. The difference between the 4189 and 6283 rad/s (40,000 and 60,000 rpm) configurations is a start time of approximately one-tenth of a second and a quarter of a psi.

Deadhead Start, H_2 Pump. The same assumptions used for evaluating the effects of deadhead start of O_2 turbopump configurations were used for the H_2 turbopumps. Because of the longer start time and smaller propellant mass (low density), little pressure can be developed by H_2 turbopump configurations above 3142 rad/s (30,000 rpm) during a deadhead start due to propellant heating. Propellant heating is approximately the same for all the configurations; however, the propellant consumption (based on similar assumptions used for O_2 turbopump configurations) for the 3142 rad/s (30,000 rpm) configuration is approximately twice that for the 6283 rad/s (60,000 rpm) configuration. This is particularly significant because the H_2-turbine mass flowrate constitutes over two-thirds of the total turbine flowrate.

Conclusions of LH_2 Start Analysis

A summary of H_2-turbopump start times ($\phi = 0.5$), required total NPSP, turbine mass flowrate and bearing DN is presented in Table 5. With little significant difference in NPSP and start time between configurations, the 6283 rad/s (60,000 rpm) configuration has low turbine mass flowrate requirement and has a bearing DN potentially capable of meeting 10 hours life and 10,000 starts.

O_2/H_2 Turbine Design Comparison. Both impulse and pressure-compound turbine designs were evaluated for O_2 and H_2 turbines. Since the O_2 turbine will be partial admission and because of low horsepower requirement, a reentry turbine was also evaluated. A comparison of turbine performances for an approximately 3142 rad/s (30,000 rpm) O_2 turbopump and a 5236 rad/s (50,000 rpm) H_2 turbopump is presented in Table 6. The pressure compound turbine is seen to require approximately 5 percent less mass flowrate than the impulse turbine.

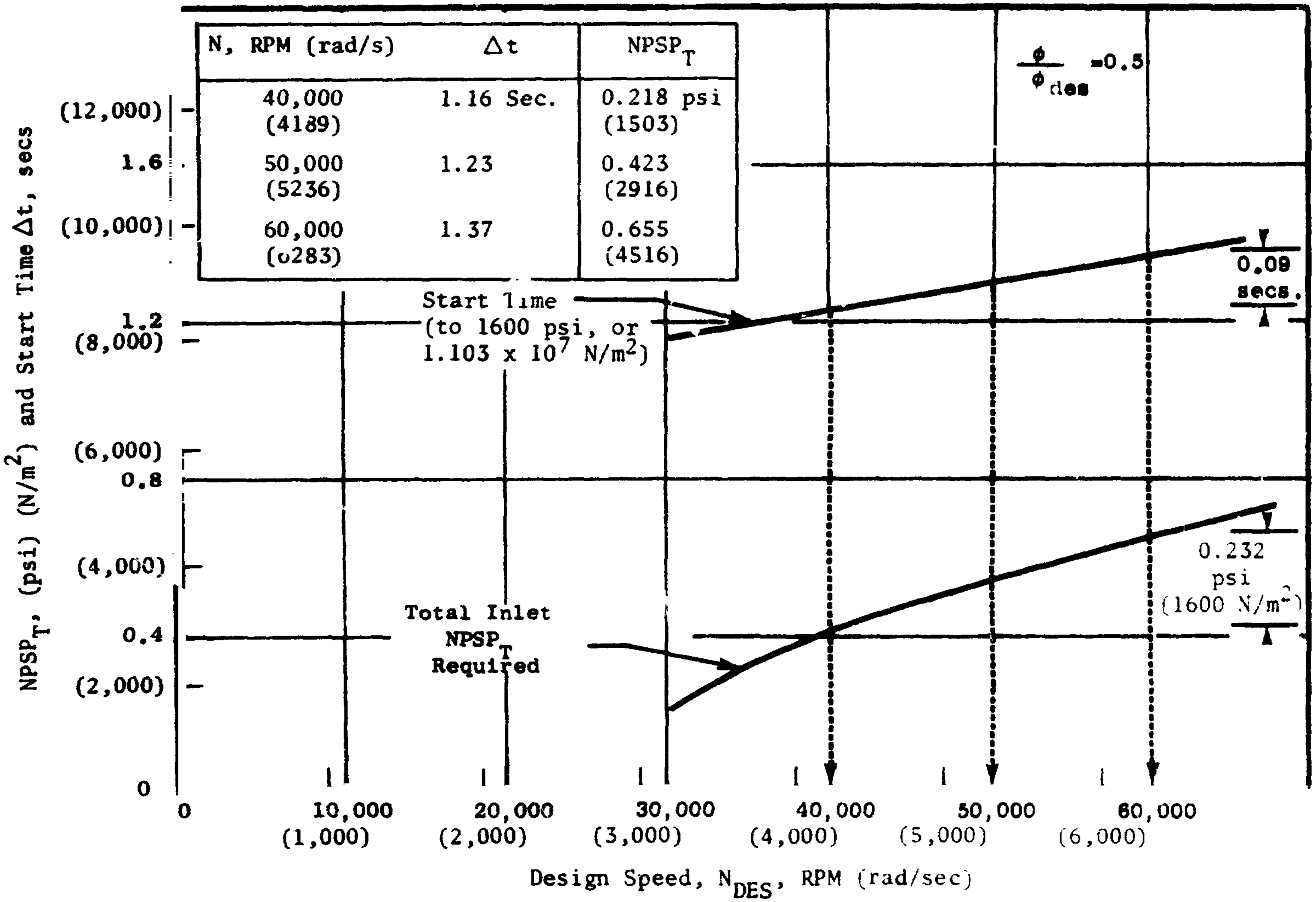

Figure 26. Effect of Design Speed on Start Time and Total NPSP H_2-Turbopump

TABLE 5. APS LH_2-TURBOPUMP NPSP SUMMARY

Configuration		Data					
N_{DES} rad/s (rpm)	O-NPSP Range $\Delta\left\{\frac{\delta\theta}{\theta}\right\}_{DES}$	$NPSP_S$ N/m^2 (psi) Max.	Nom.	Start Time Δt (secs)	$NPSP_T$ Required N/m^2 (psi)	Turbine $\dot{W}$ (lb/sec)	Bearing DN 10^6
4,189 (40,000)	0.49	2,413 (0.35)	0	1.23	2,896 (0.42)	0.590 (1.30)	1.05
5,236 (50,000)	0.45	3,309 (0.48)	0	1.28	3,723 (0.54)	0.431 (0.95)	1.25
6,283 (60,000)	0.38	4,137 (0.6)	0	1.37	4,551 (0.66)	0.340 (0.75)	1.4
8,378 (80,000)	0.27	8,274 (1.2)	0	1.60	8,618 (1.25)	0.249 (0.55)	1.68
14,661 (140,000)	0	20,684 (3.0)	6,205 (0.9)	-	-	-	2.55

[illegible]

TABLE 6. APS O_2 AND H_2 TURBINE DESIGN COMPARISONS

		O_2 Turbine			H_2 Turbine	
		1-Stage Impulse	2-Stage Pressure Compound	2-Stage Re-entry	2-Stage Impulse	2-Stage Pressure Compound
Inlet Temperature, K (R)	T_{1t}	1,117 (2,010)	1,117 (2,010)	1,117 (2,010)	1,117 (2,010)	1,117 (2,010)
Inlet Pressure, N/m^2 (psia)	P_{1t}	1,861,584 (270)	1,861,584 (270)	1,861,584 (270)	1,861,584 (270)	1,861,584 (270)
Pressure Ratio	PR	7.72	7.72	7.72	7.72	7.72
Exhaust Pressure, N/m^2 (psia)	P_{2s}	241,317 (35)	241,317 (35)	241,317 (35)	241,317 (35)	241,317 (35)
Speed, rad/s (RPM)	N	3,204 (30,600)	3,204 (30,600)	3,204 (30,600)	5,039 (48,600)	5,039 (48,600)
Mean Diameter, cm (inch)	D_m	18.4 (7.25)	18.4 (7.25)	18.4 (7.25)	16.5 (6.5)	16.5 (6.5)
Blade Speed, m/s (f/s)	U_m	295.7 (970)	295.7 (970)	295.7 (970)	420.6 (1,380)	420.6 (1,380)
Power watt (HP)	HP	159,580 (214)	159,580 (214)	159,580 (214)	848,606 (1,138)	848,606 (1,138)
Efficiency, percent	η_{T-S}	30.7	32.5	31.5	57.9	61.0
Flowrate, Kg/s (lb/s)	$\dot{W}$	0.1397 (0.308)	0.1324 (0.292)	0.1370 (0.302)	0.4064 (0.896)	0.3856 (0.850)
Admission, percent	ϵ	33	25	20	100	100

A radial turbine, typically with good efficiency at high velocity ratios (U/C_o of 0.50), does not meet the performance required by the APS turbopumps. Its starting torque characteristic (important to rapid acceleration) is also poorer than axial turbines.

A comparison of mechanical design, blade temperature, fabrication complexity, and cost of the turbine candidates was made. Based on simplicity in design (no interstage sealing, thrust balance, and balde shroud requirements), lower blade temperatures, simple fabrication requirements, and lower cost, the impulse turbine is the best candidate for both the O_2 and H_2 turbopumps.

A summary of design parameters for the optimum O_2 turbine is listed in Table 7 for both nominal and maximum horsepower conditions. Maximum horsepower occurs at the maximum flowrate point of the operating envelope. This turbine, with a pitch diameter of 18.4 cm (7.25 inches), is shown in the configuration layout for the 3142 rad/s (30,000 rpm) O_2 turbopump (Configuration 1).

A summary of design parameters for the optimum H_2 turbine is listed in the table for both nominal and maximum horsepower conditions. Maximum horsepower occurs at the maximum flowrate point of the operating envelope. This turbine, with a pitch diameter of 16.51 cm (6.5 inches), is similar to the one shown in the configuration layout for the 5236 rad/s (50,000 rpm) H_2 turbopump (Configuration 2).

Using a common turbine for both the O_2 and H_2 turbopumps offers the advantage of saving time and cost. A comparison of turbine performance, as a result of using a common turbine, is shown in Table 8 for 15.24, 16.51 and 18.42 cm (6.0, 6.5 and 7.25 inches) pitch diameters. In using a 16.51 cm (6.5 inches) diameter common turbine, the H_2 turbine will be an optimum design and the O_2 turbine mass flowrate will increase by only 0.0104 Kg/sec (0.023 lb/sec).

Life and Operating Cycles. The turbine operating life is estimated on the basis of stress-rupture characteristics at elevated temperatures, based on a Larson-Miller diagram. The operating blade temperature and stress for both O_2 and H_2 turbines are shown in Table 9 for nominal operating conditions. The turbine

TABLE 7. APS-O_2 TURBINE DESIGN D_m = 7.25 INCH (OPTIMUM)

Parameters	Power (Nom)	Power (Max)
Inlet Temperature, T_{1t}, K (F)	1,117 (1,550)	1,117 (1,550)
Inlet Pressure, P_{1t}, N/m^2 (psia)	1,861,584 (270)	2,240,796 (325)
Exhaust Pressure, P_{2s}, N/m^2 (psia)	241,317 (35)	241,317 (35)
Pressure Ratio, PR --	7.72	9.3
• Speed, N, rad/s (rpm)	3,142 (30,000)	3,173 (30,300)
• Flowrate, $\dot{W}$, Kg/sec (lb/sec)	0.100 (0.221)	0.147 (0.325)
• Power, watt (HP)	113,346 (152)	159,580 (214)
• Efficiency, η_{t-s} Percent	30.7	29.5
• Admission, ϵ, Percent	50	50

operating life is seen to be in the thousands of hours and in excess of the 10 hour life requirement of the turbopumps. The effect of ±311 K (±100 F) on turbine life is also illustrated in Fig. 27.

A typical APS duty cycle assumed for evaluating the low cycle thermal fatigue life of the O_2 and H_2 turbines is shown in Fig. 28. The total start per mission and the type of start cycle (frequency, blade material, temperature gradient, and shutdown time between starts) are listed. The blade thermal strain is based on an estimated blade temperature profile. The typical duty cycle described in the previous chart is illustrated in Fig. 29 to show the sequence of types of starts encountered by the turbine. The level of temperature reached during cooldown period is also shown.

TABLE 8. APS-H_2 TURBINE DESIGN D_m = 6.5 INCH (OPTIMUM)

Parameters	Power (Nom)	Power (Max)
Inlet Temperature, T_{1t}, K (F)	1,117 (1,550)	1,117 (1,550)
Inlet Pressure, P_{1t}, N/m^2 (psia)	1,861,584 (270)	2,137,375 (310)
Exhaust Pressure, P_{2s}, N/m^2 (psia)	241,317 (35)	241,317 (35)
Pressure Ratio, PR	7.72	8.88
• Speed, N, rad/s (rpm)	6,283 (60,000)	6,346 (60,600)
• Flowrate, $\dot{W}$, Kg/sec (lb/sec)	0.223 (0.492)	0.297 (0.654)
• Power, watt (HP)	518,261 (695)	736,006 (987)
• Efficiency, η_{t-s}, Percent	64.0	63.5
• Admission, ϵ, Percent	100	100

The Universal Slope method for predicting cycles to failure for thermal fatigue of Waspoloy is illustrated in Fig. 30. The points plotted indicate the cyclic life obtainable for the temperature gradient shown. The number of cycles per mission and for 300 missions (to approximate 10,000 total start requirement) are also indicated along side the plotted points. As a conservative approach, all starts with temperature gradients below 422 K (300 F) are assumed at 422 K (300 F) (these constitute 8700 starts over 300 missions).

An accumulative damage analysis which combines effects of stress rupture, high cycle fatigue, and low cycle fatigue of Waspoloy (with appropriate fatigue factor criteria) is shown in Fig. 31. The major contributor to damage fraction is low

TABLE 9. COMMON APS-O_2 AND H_2 TURBINES COMMON D_m = 16.51 CM (6.50 INCH)

T_{1t} = 1117 K (1550 F)
P_{1t} = 1,861,584 N/m^2 (270 psia)
P_{2s} = 241,317 N/m^2 (35 psia)
PR = 7.72

		O_2 - Turbine			H_2 - Turbine		
Speed N_{DES}, rad/s (rpm)		3,142 (30,000)			6,283 (60,000)		
Power, watt (HP)		113,346 (152)			518,261 (695)		
		Optimum	Common	Common	Common	Optimum	Common
Mean Diameter, cm (inch)	D_m	18.42 (7.25)	16.51 (6.5)	15.24 (6.0)	15.24 (6.0)	16.51 (6.5)	18.42 (7.25)
Velocity Ratio	U/C_o	0.108	0.097	0.089	0.174	0.189	0.211
Mean Blade Speed, m/s (ft/sec)	U_m	295.7 (970)	265.2 (870)	243.8 (800)	478.5 (1,570)	518.2 (1,700)	579.1 (1,900)
Efficiency, percent	η_{T-S}	30.7	27.8	25.9	61	64	65.5
Admission, percent	ϵ	50	50	50	100	100	100
Flowrate, Kg/sec (lb/sec)	$\dot{W}$	0.1002 (0.221)	0.1107 (0.244)	0.1188 (0.262)	0.2341 (0.516)	0.2232 (0.492)	0.2223 (0.490)
Common, cm (inch)	D_m	16.51 (6.5)			16.51 (6.5)		
$\Delta\dot{W}$ Kg/sec (lb/sec)		+0.01043 (+0.023)			0		

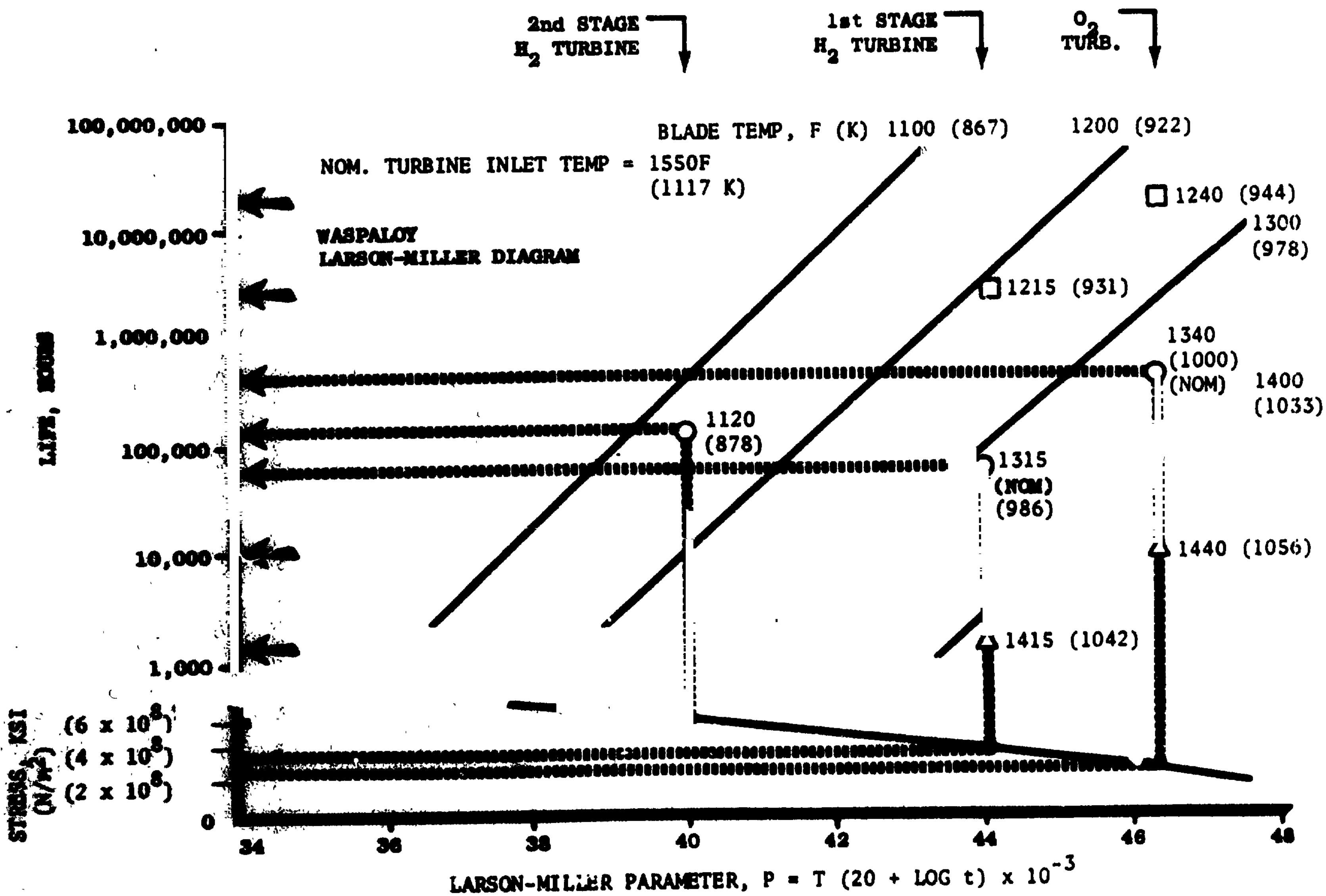

Figure 27. Turbine Operating Life

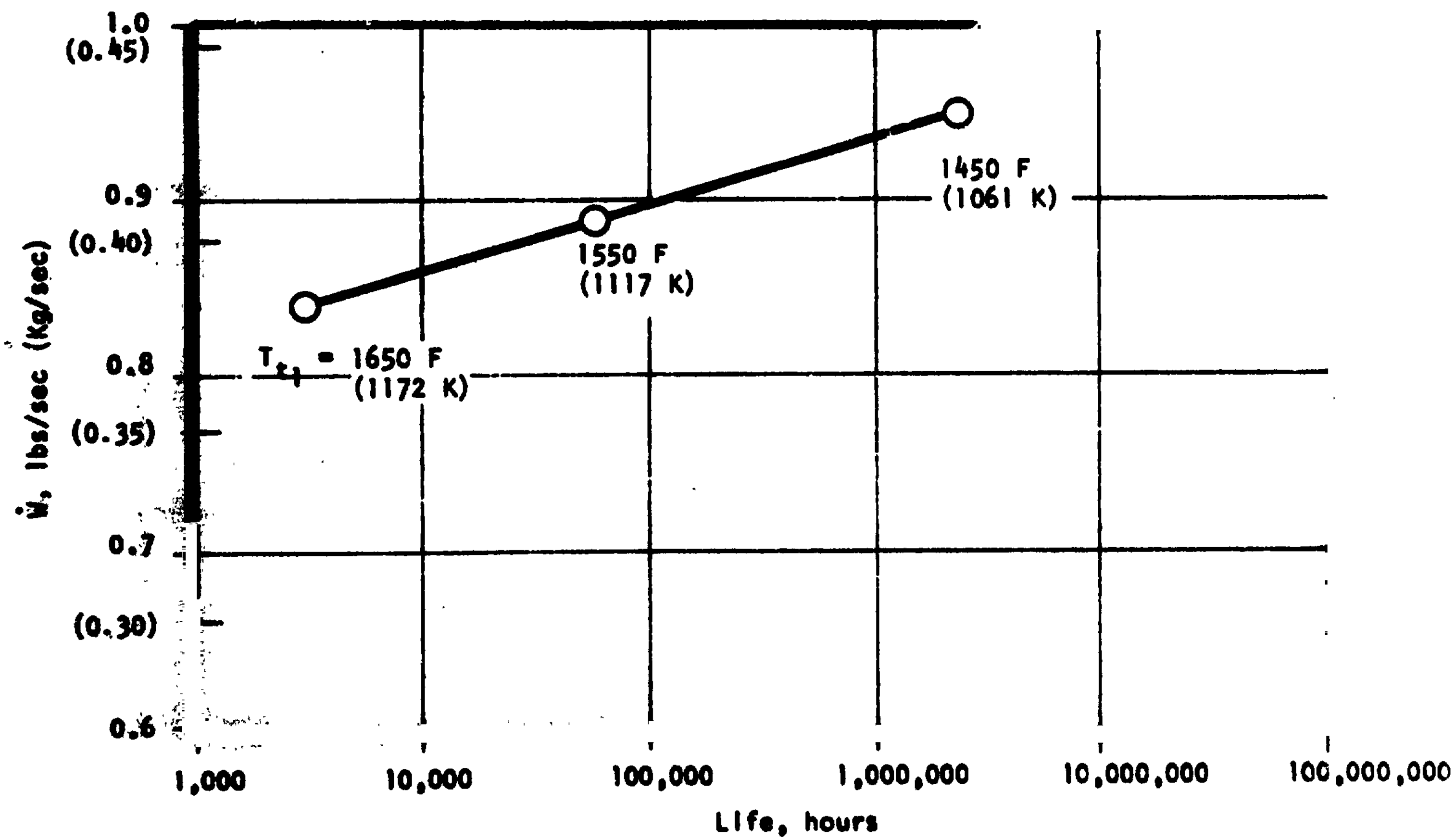

Figure 28. Tradeoff of Turbine Operating Life and Temperature

Number of Cycles per Mission	ΔT R (K)	Down Time sec
3	453 (815)	>3600
3	235 (423)	2700
2	163 (293)	1450
1	127 (228)	950
4	99.4 (179)	500
4	81.1 (146)	300
5	36.1 (	80
13	18.3 (33)	10
Total 35		

Figure 29. Typical APS Duty Cycle

cycle fatigue. Using the cyclic life results obtained from the previous figure, and the worse case where 29 starts (per mission) will only have a life of 1,000,000 cycles, the accumulative damage fraction is found to be less than one (fatigue criteria) for 300 missions. Thus, the turbine thermal fatigue life is found to meet the 10,000 start requirement for the turbopumps.

Recommended Turbopump Configurations

Based on an evaluation of O_2 turbopump configurations for steady-state and transient operation, which includes NPSP, start time, deadhead start turbine mass flowrate,and thermal fatigue (starts), the 3142 rad/s (30,000 rpm) configuration is recommended as the optimum O_2 turbopump. A comparison of design parameters for all configurations studies is shown in Table 10.

An evaluation of development, operation and service requirements for O_2 turbopump configurations is shown in Table 11. Development Cost and Risk: increase with speed and bearing DN; Maintenance: increase with size and number of parts;

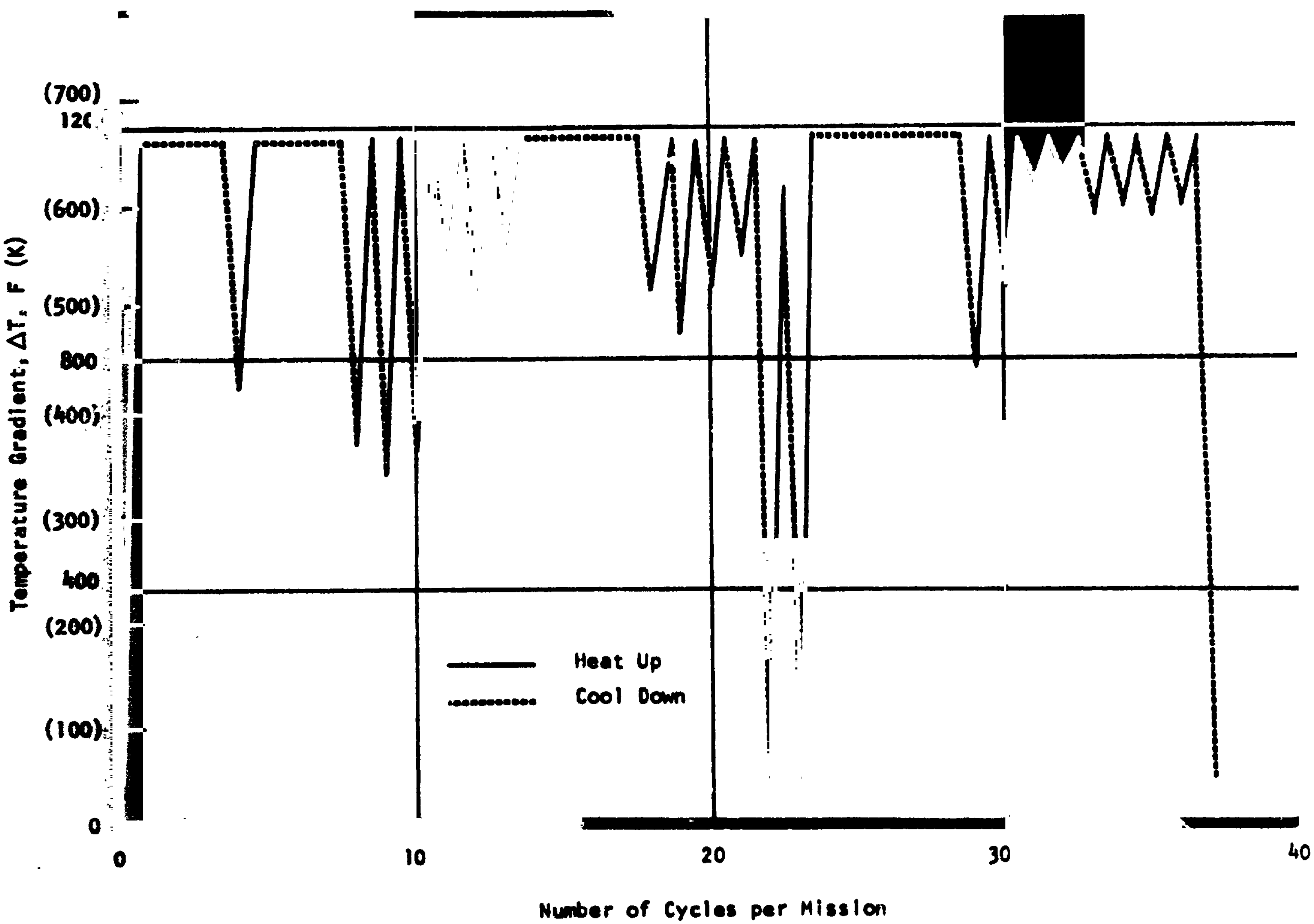

Figure 30. Typical APS Duty Cycle Heatup and Cooldown Transients

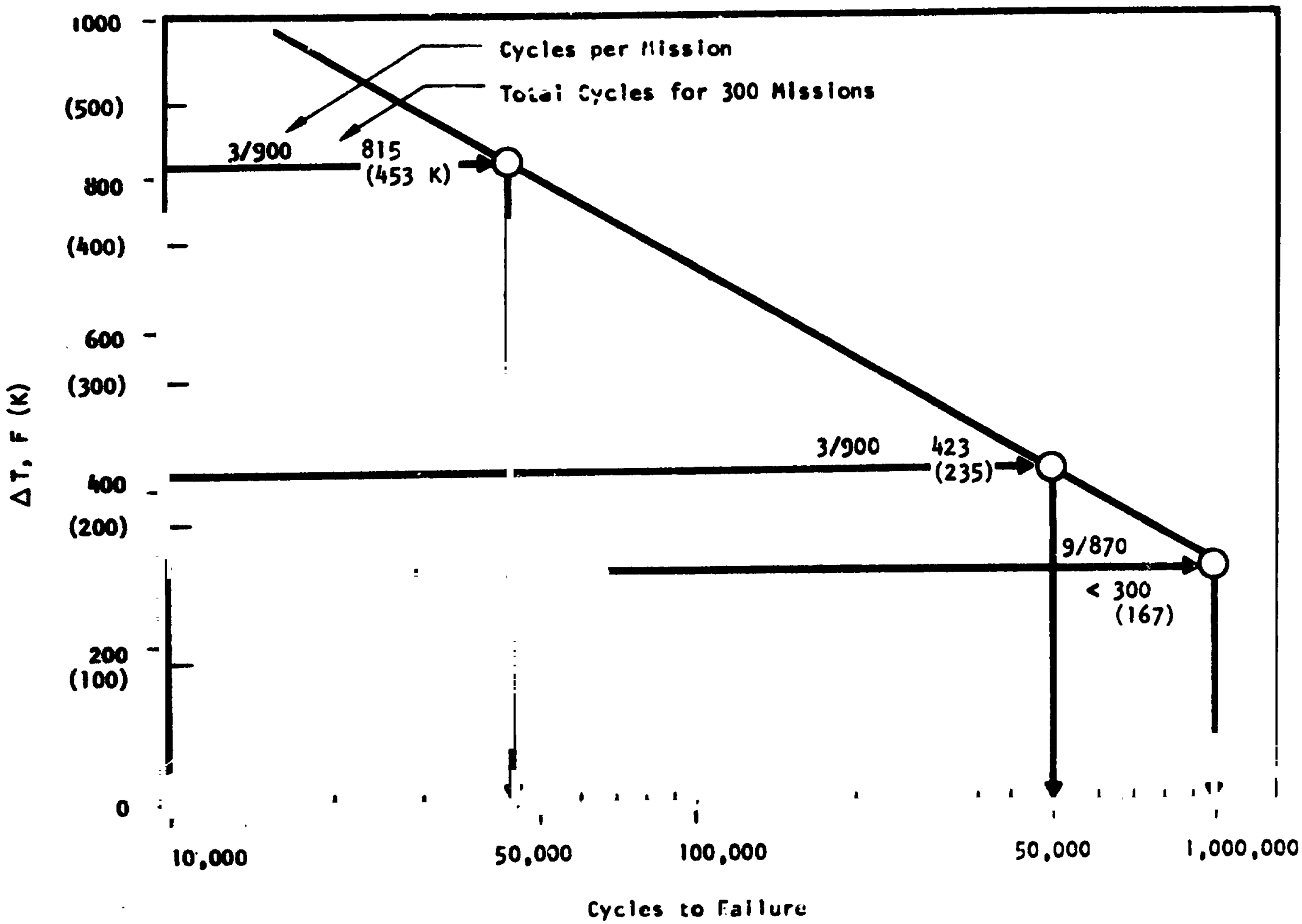

Figure 31. First-Stage H_2-Turbine Blade Waspaloy (Universal Slope)

TABLE 10. APS LO_2-TURBOPUMP CONFIGURATION COMPARISON

	Configuration			Data					
N_{DES} rad/s (rpm)	Pump Stages	Turbine Stages	Bearing DN 10^6	$NPSP_S$ N/m^2 (psi) Max.	$NPSP_S$ N/m^2 (psi) Nom.	Start Time Δt (secs)	$NPSP_T$ Req. N/m^2 (psi)	Turbine $\dot{W}$ Kg/sec (lb/sec)	Weight Kg (lbs)
1,047 (10,000)	2	2	0.28	2,068 (0.3)	1,034 (0.15)	0.20	12,411 (1.8)	0.771 (1.700)	45.4 (100)
2,094 (20,000)	2	1	0.41	11,032 (1.6)	6,895 (1.0)	0.40	4,826 (0.7)	0.372 (0.820)	18.1 (40)
3,142 (30,000)	1	1	0.57	27,579 (4.0)	11,721 (1.7)	0.70	3,447 (0.5)	0.140 (0.308)	16.3 (36)
4,189 (40,000)	1	1	0.68	50,332 (7.3)	24,132 (3.5)	1.0	11,721 (1.7)	0.109 (0.240)	13.6 (30)

$\phi/\phi_{DES} = 0.50$

$P_d = 1.103 \times 10^7 \ N/m^2$ (1600 psi)

TABLE 11. APS LO_2-TURBOPUMP CONFIGURATION COMPARISON

Configuration	Ranking						
N_{DES} rad/s (rpm)	Development Cost/Risk	Life	Maintenance and Service	Manufacturing Cost	Insensitive to Duty Cycle	Safety	Heat Soakback
1,047 (10,000)	1	1	3	3	3	2	3
2,094 (20,000)	3	2	2	2	1	2	2
3,142 (30,000)	2	3	1	1	1	1	1
4,189 (40,000)	4	4	1	1	2	2	1

- TOTAL DAMAGE FRACTION

$$\phi_{TOT} = 4\,\phi_{LOW\ CYCLE} + \cancelto{0}{10\,\phi_{HIGH\ CYCLE}} + \cancelto{0}{4\,\phi_{RUPTURE}}$$

- PER MISSION

$$\phi_{TOT} = \Sigma\,\phi_{LOW\ CYCLE} = \frac{3}{45,000} + \frac{3}{500,000} + \frac{29}{1,000,000}$$

$$= 0.0000668 + 0.000006 + 0.000029$$

$$= 0.0001018$$

- APPROXIMATELY 300 MISSIONS

$$\phi_{TOT} = \frac{10,000}{35} \times 0.0001018 = 0.0292$$

- WITH SAFETY FACTOR OF 4

$$4 \times \phi_{TOTAL} = < 1.0$$

$$4 \times 0.0292 = 0.117 < 1.0$$

Figure 32. Turbine Blade Thermal Fatigue Accumulative Damage Analysis

Manufacturing Cost: increase with size and number of parts; Duty Cycle Sensitivity: high for low performance and long start time; Safety: low for high speed and large number of parts; Heat Soakback: high for large turbine size. The 3142 rad/s (30,000 rpm) configuration is found to be the optimum O_2 turbopump based on the above criteria.

Based on an evaluation of H_2 turbopump configurations for steady-state and transient operation, which includes NPSP, start time, deadhead start turbine mass flowrate, and thermal fatigue (starts), the 6283 rad/s (60,000 rpm) configuration is recommended as the optimum H_2 turbopump. A comparison of design parameters for all configurations studies is shown in Table 12.

An evaluation of development, operation and service requirements for H_2 turbopump configurations is shown in Table 13. Development Cost and Risk: increase with speed, size, and number of parts; Life: risk increase with speed and bearing DN;

TABLE 12. APS LH_2-TURBOPUMP CONFIGURATION COMPARISON

Configuration					Data					
N_{DES} rad/s (rpm)	0-NPSP Range $\left\{\delta \frac{\theta}{\theta}\right\}_{DES}$	Pump Stages	Turbine Stages	Bearing DN 10^6	$NPSP_S$ N/m^2 (psi) Max.	Nom.	Start Time Δt (secs)	$NPSP_T$ Req. N/m^2 (psi)	Turbine $\dot{W}$ Kg/sec (lb/sec)	Weight Kg (lbs)
4,189 (40,000)	0.49	3	2	1.05	2,413 (0.35)	6 0	1.23	2,896 (0.42)	0.590 (1.30)	38.6 (85)
5,236 (50,000)	0.45	2	2	1.25	3,309 (0.48)	0	1.28	3,723 (0.54)	0.431 (0.95)	29.0 (64)
6,283 (60,000)	0.38	2	2	1.4	4,137 (0.6)	0	1.37	4,551 (0.66)	0.340 (0.75)	24.9 (55)
8,378 (80,000)	0.27	2	2	1.68	8,274 (1.2)	0	1.60	8,618 (1.25)	0.249 (0.55)	20.4 (45)
1,456 (140,000)	0	1	2	2.55	206,343 (3.0)	6,205 (0.9)	-	-	-	-

$\phi/\phi_{DES} = 0.50$
$P_d = 1.103 \times 10^7 \ N/m^2$
(1600 psi)

TABLE 13. APS LH_2-TURBOPUMP CONFIGURATION COMPARISON

Configuration	Ranking						
N_{DES} rad/s (rpm)	Development Cost/Risk	Life	Maintenance and Service	Manufacturing Cost	Insensitive to Duty Cycle	Safety	Heat Soakback
4,189 (40,000)	3	1	3	3	3	2	4
5,236 (50,000)	1	2	1	1	2	1	3
6,283 (60,000)	2	3	1	1	1	2	2
8,378 (80,000)	4	4	2	2	2	3	1

Maintenance: increase with size, speed and number of parts; Manufacturing Cost: increase with size, speed and number of parts; Duty Cycle Sensitivity: high for low performance and long start time; Safety: low for high speed and large number of parts; Heat Soakback: high for large pump and turbine sizes. The 6283 rad/s (60,000 rpm) configuration is found to be the optimum H_2 turbopump based on the above criteria.

HEAT TRANSFER ANALYSIS

Thermal analyses were conducted in support of Phase 1 design selection in three major areas. Evaluation of (1) pump start thermal conditioning, (2) turbine to pump thermal isolation and (3) turbine blade thermal cycling has been compiled and results are presented.

Thermal Conditioning

Start characteristics for both a dry pump and wet pump were determined with respect to rapid start requirements, propellant usage minimization and system impact. Four alternate thermal conditioning systems were included in this investigation: (1) dump vent valve, (2) recirculation, with the small recirculation pump wet and upstream of the TPA isolation valve, (3) recirculation, with a dry pump downstream of TPA pump exit and (4) refrigeration.

Chilldown of a warm (70 F) LH_2 turbopump requires 30 to 900 seconds for initial chilldown and rapid start (specified 1.5 seconds start requirement), resulting in an initial pre-operation chilldown requirement. Initial thermal preoperation methods: (1) vent valve dump, 30 seconds, (2) recirculation; small liquid pump, 80 seconds, (3) recirculation, small liquid filled pump, 80 seconds, (3) recirculation; small vapor filled pump, 600 seconds, and (4) refrigeration, 870 seconds.

Design Criteria

1. Thermal preparation: pump wetted surfaces including second-stage impeller within 13.9 K (25 R) of tanked saturated liquid temperature.

2. Dump vent valve flows choked GH_2 to vacuum from tanked pressure.

3. Small recirculation pumps upstream of TPA will develop 104.6 Joule/Kg (35 ft) head of liquid and vapor respectively.

4. Refrigeration with 4.44 K (8 R) subcooled liquid hydrogen flow applied in intimate contact with both bearings and pump casing.

Initial chilldown of the liquid oxygen TPA will require (1) 28 seconds utilizing a dump vent valve, (2) 75 seconds for recirculation generating 104.6 Joule/Kg (35 ft) of liquid oxygen head, (3) 800 seconds for recirculation of boil-off oxygen vapor, and (4) 480 seconds refrigeration of bearings and pump casing with 36.1 K (65 R) hydrogen vapor.

Propellant usage for the LH_2 and LO_2 TPA's are tabulated for the four thermal conditioning methods in Table 14. Based upon these results, the LH_2 and LO_2 TPA's at ambient temperatures will not meet rapid start requirements.

Succeeding analysis was conducted assuming that (1) the isolation valve was open and tanked cryogen communication to the pump wetted paths was possible, (2) rapid start must be possible at any time in the mission, and (3) rapid start specification could be met if the inducer, first-stage impeller, second-stage impeller and associated stationary wetted flow path was within 139 K (25 R) of tanked saturated liquid temperature.

The proposed LH_2 TPA is predicted to transfer less than 52,752 Joule/hr (50 Btu/hr) from the turbine to the pump during non-operating standby in accordance with the contract work statement. The 52,752 Joule/hr (50 Btu/hr) non-operating heat transfer is based upon the favorable, start criteria discussed previously and is not valid for a refrigeration system or for an entire pump maintained at saturated liquid temperature, such as a buried pump.

<u>Thermal Isolation</u>. The proposed LO_2 TPA will be maintained in start readiness, with the pump absorbing less than 158,256 Joule/hr (150 Btu/hr) operating and less than 52,752 Joule/hr (50 Btu/hr) non-operating from the turbine.

TABLE 14. SS APS TPA DRY PUMP INITIAL CHILLDOWN PROPELLANT LOSS

LH_2 TPA		
• Dump Vent Valve	2.95 Kg (6.5 lb)	(LH_2)
• Recirculation		
• Wet Pump Upstream	2.72 Kg (6.0 lb)	(LH_2)
• Dry Pump Downstream	3.08 Kg (6.8 lb)	(LH_2)
• Refrigeration	4.99 Kg (11.0 lb)	(LH_2)
LO_2		
• Dump Vent Valve	3.22 Kg (7.1 lb)	(LO_2)
• Recirculation		
• Wet Pump	2.18 Kg (4.8 lb)	(LO_2)
• Dry Pump	2.95 Kg (6.5 lb)	(LO_2)
• Refrigeration	3.86 Kg (8.5 lb)	(H_2 Vapor)

To reduce the turbine to pump heat transfer, the key thermal isolation features considered for the LH_2 TPA illustrated in Fig. 33 are (1) titanium dog-bone shaped ring with contact Kel-F sealing surface; (2) titanium hat, shaft isolation link; (3) remote turbine volute-to-case design; (4) glass batting volute cavity fill; and (5) aluminum disc thermal shunt. A 400 series CRES, dog-bone shaped, cross section ring with Kel-F coating for sealing at the contact surfaces was successfully used in the F-1 LO_2 T/P (NASw-16). Turbine-to-pump thermal resistances are increased by milled relief of contact areas wherever structurally feasible. Holes will be used in the turbine-to-pump stiffness webs to reduce weight and increase axial thermal resistance, and circular line contact washers will be used under casing connecting bolts. The TPA shaft is hollow, and filled with liquid during operation which reduced adjacent pump and turbine hardware temperatures. Less than 0.0907 Kg (0.2 lb) total liquid is trapped in all pump cavities. This liquid vaporizes during the first hour of soakback absorbing approximately 21,101 Joule/hr (20 Btu/hr). Thereafter, the vapor has almost no effect on the TPA temperature during long periods of non-operation.

Key thermal isolation features also shown in Fig. 33 for the LO_2 TPA are: (1) titanium ring with relief-milled contact surfaces; (2) titanium hat, shaft isolation line; (3) remote turbine volute-to-case design; (4) glass batting volute cavity fill; and (5) aluminum disk thermal shunt. Turbine-to-pump thermal resistances were increased by milled relief of contact areas wherever structurally feasible. Holes are to be used in the turbine-to-pump stiffning webs to reduce weight and increase axial thermal resistance, and circular line contact washers will be used under casing connecting bolts. The TPA shaft is hollow, decreasing the thermal transfer path. Less than 0.272 Kg (0.6 pound) liquid is trapped in all pump cavities. This liquid vaporizes during the first hour of soakback absorbing approximately 52,752 Joule/hr (50 Btu/hr). Thereafter, the vapor has almost no effect on the TPA temperature during long non-operating periods.

Where a three TPA system is utilized for reliability and after the th[illegible] TPAs have been chilled following a long duration operation on one of the pumps, t[illegible] maximum liquid hydrogen required to maintain start readiness for the system was determined to be 0.544 kg/hr (1.2 lb/hr) for refrigeration cooling, 0.227 kg/hr (0.5 lb/hr) for recirculation and 0.163 kg/hr (0.36 lb/hr) for a combined system. The heat transfer from the turbine to the pump was assumed to be 52,752 Joule/hr (50 Btu/hr) for the hot TPA and 26,376 Joule/hr (25 Btu/hr) for the two standby TPAs if the wetted path was maintained 13.9 K (25 R) or less above the tanked saturated liquid temperature for the recirculation systems. Refrigeration will further reduce the casing temperature and the heat transfer for this conditioning method was allowed to increase above 52,752 Joule/hr (50 Btu/hr) to meet the start requirement.

FOLDOUT FRAME

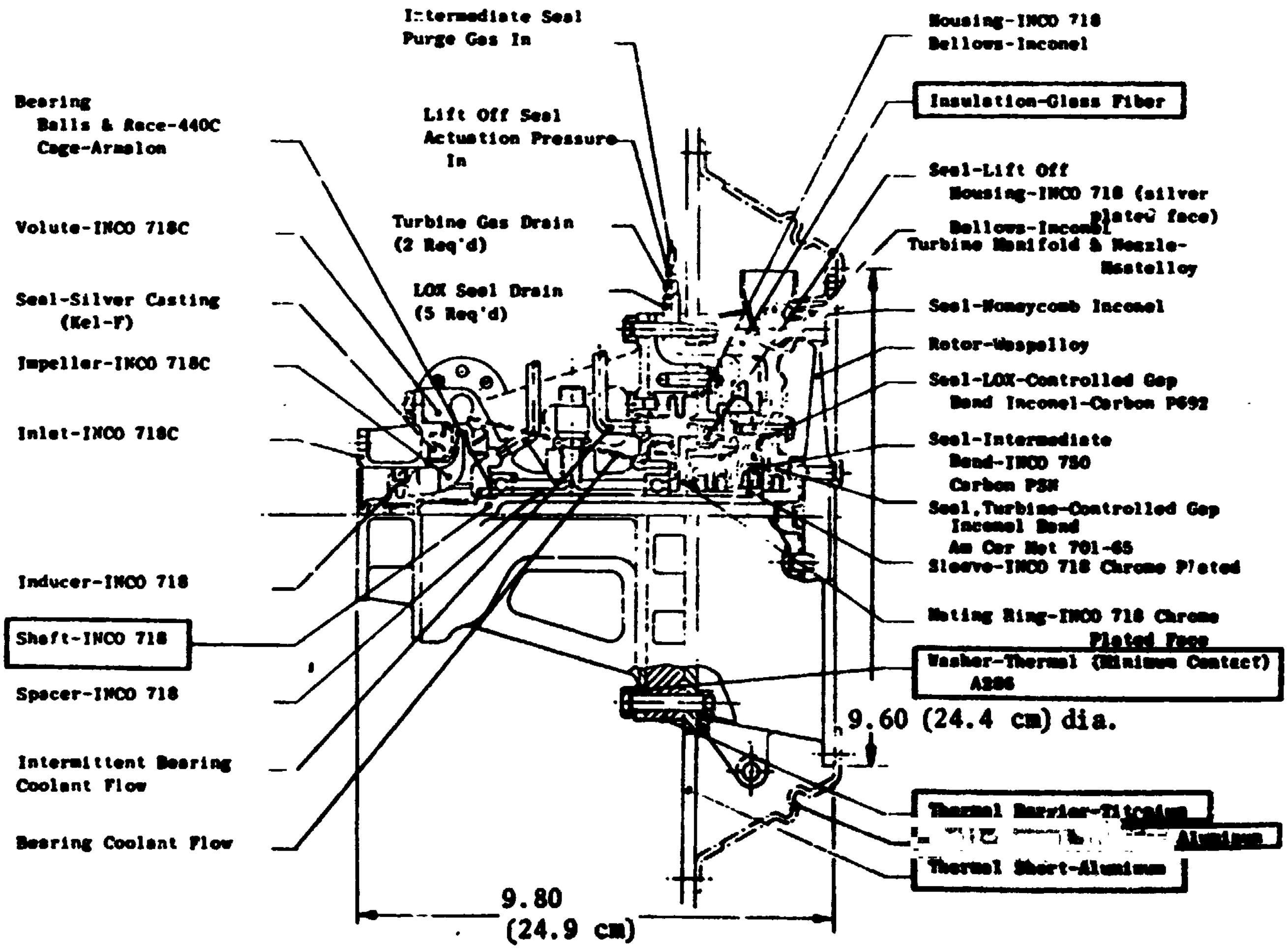

LO_2 Turbopump Assembly

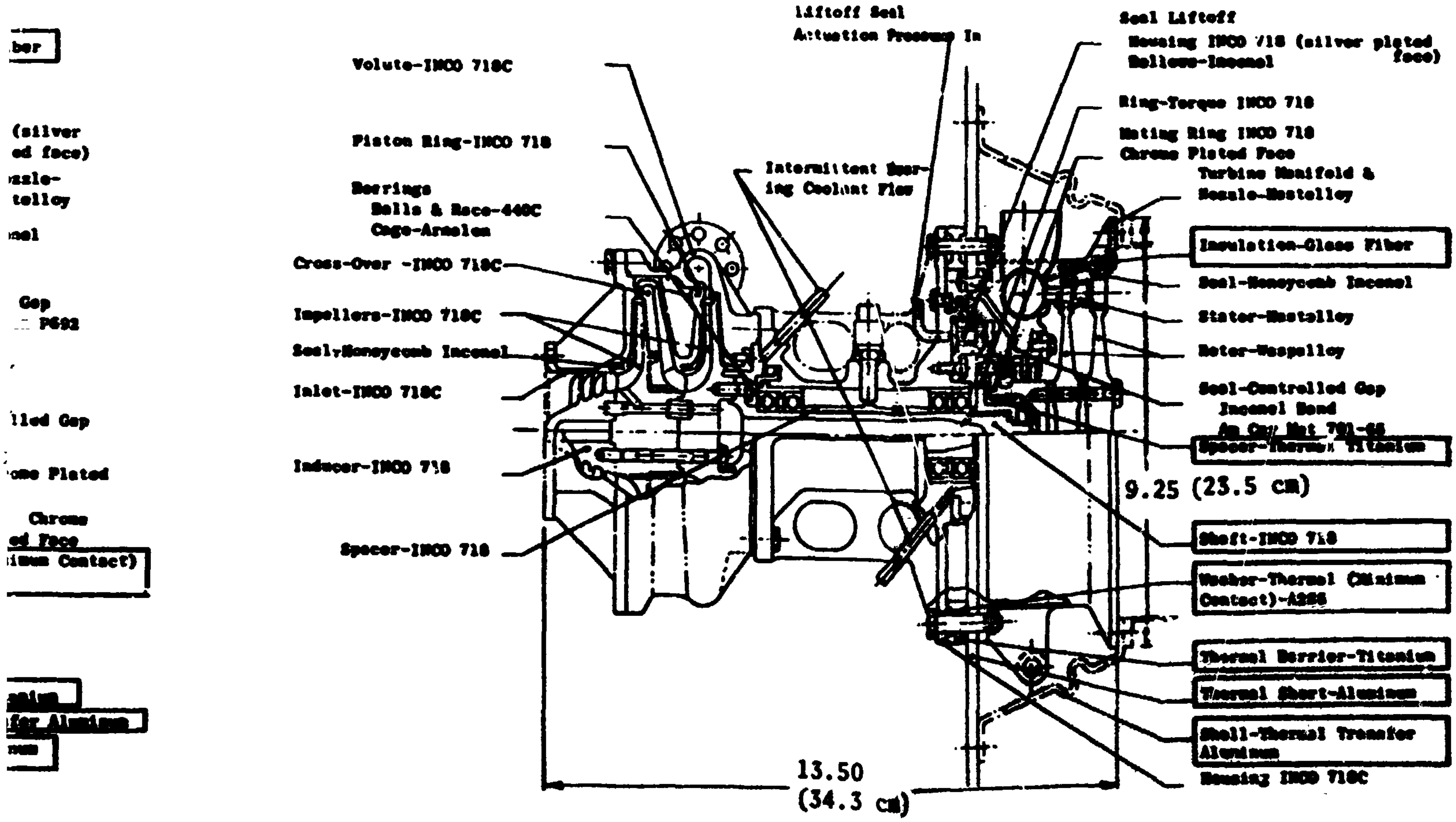

LH$_2$ Turbopump Assembly

Figure 33. Typical LO$_2$ and LH$_2$ Turbopump Assembly Thermal Insulation

The combined recirculation refrigeration system utilizes the H_2 vapor superheat and full tank pressure prior to dumping and represents a practical minimum conditioning propellant usage.

Turbine Analysis

To support turbine blade design, the proposed LH_2 TPA was subjected to various operating and soakback conditions which were representative of predicted mission duty cycles.

The turbine blade of any proposed design is predicted to remain above 88.9 K (160 R) at all times during even the most severe duty cycle.

Turbine blade transient bulk temperature (average temperature) is predicted to be as shown in Fig. 34 during initial exposure to hot GG gases. The LH_2 TPA first and second-stage turbine blade transient temperatures for 294 K (530 R) and 88.9 K (160 R) initial temperatures are superimposed on this figure.

Both the initial system temperature and operational durations affect the soakback (non-operation) transient temperature.

Figure 35 indicates the transient temperature of the LH_2 TPA turbine blade during 10 hour soakback following 20 seconds of operation from an initial turbine wheel and blade temperature of 294 K (530 R). Turbine blade temperatures remain above 333 K (600 R) for the full 10 hours.

Turbine blade temperatures below ambient 294 K (530 R) will require off times in the order of days such as during docking. Extreme thermal cycles will be experienced only once or twice during a complete mission.

The LH_2 TPA turbine blade soakback temperature varies markedly following operation durations of 5, 20, and 100 seconds and an initial temperature of 88.9 K (160 R).

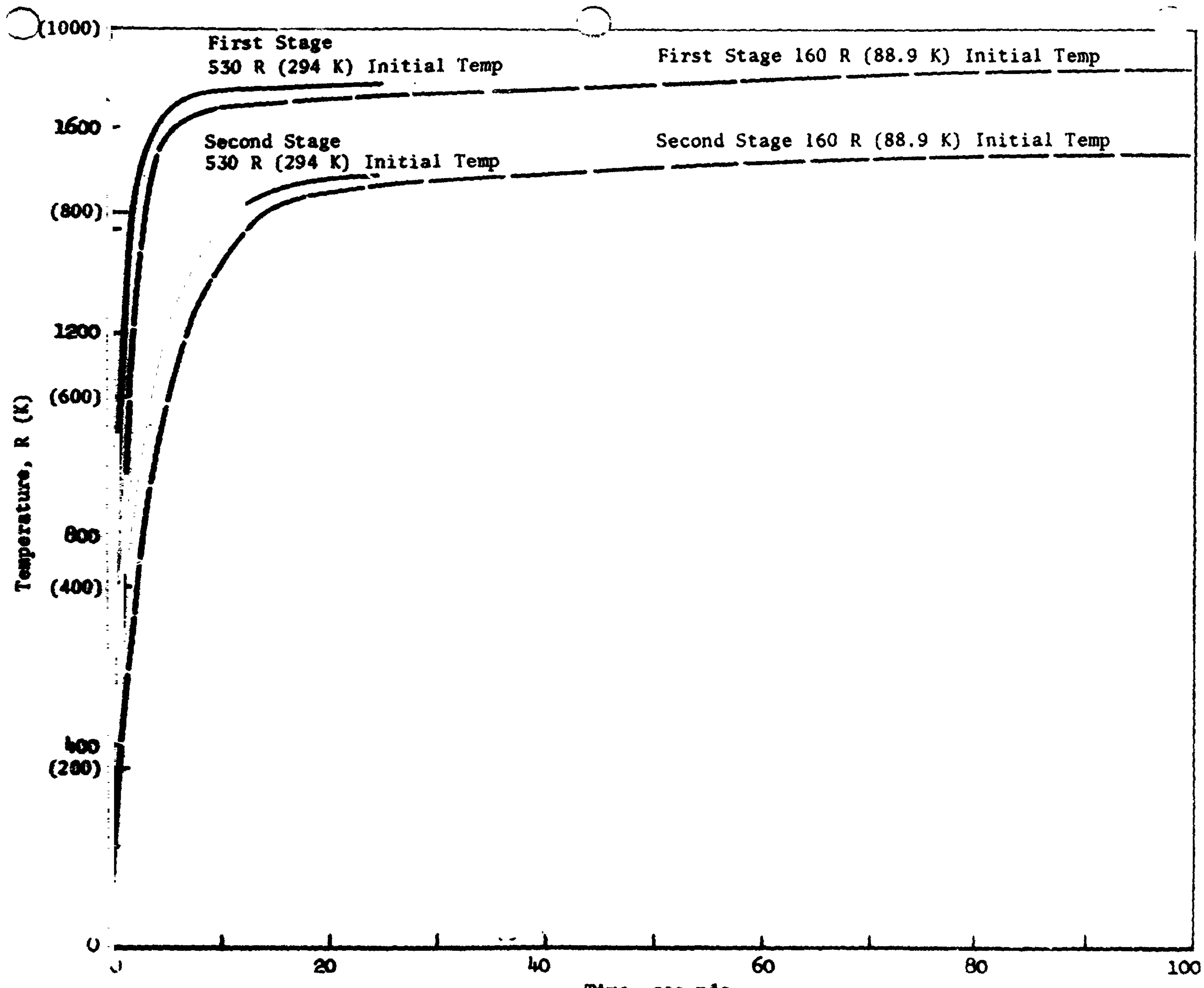

Figure 34. LH_2 Turbine Blades Start Temperature Transients

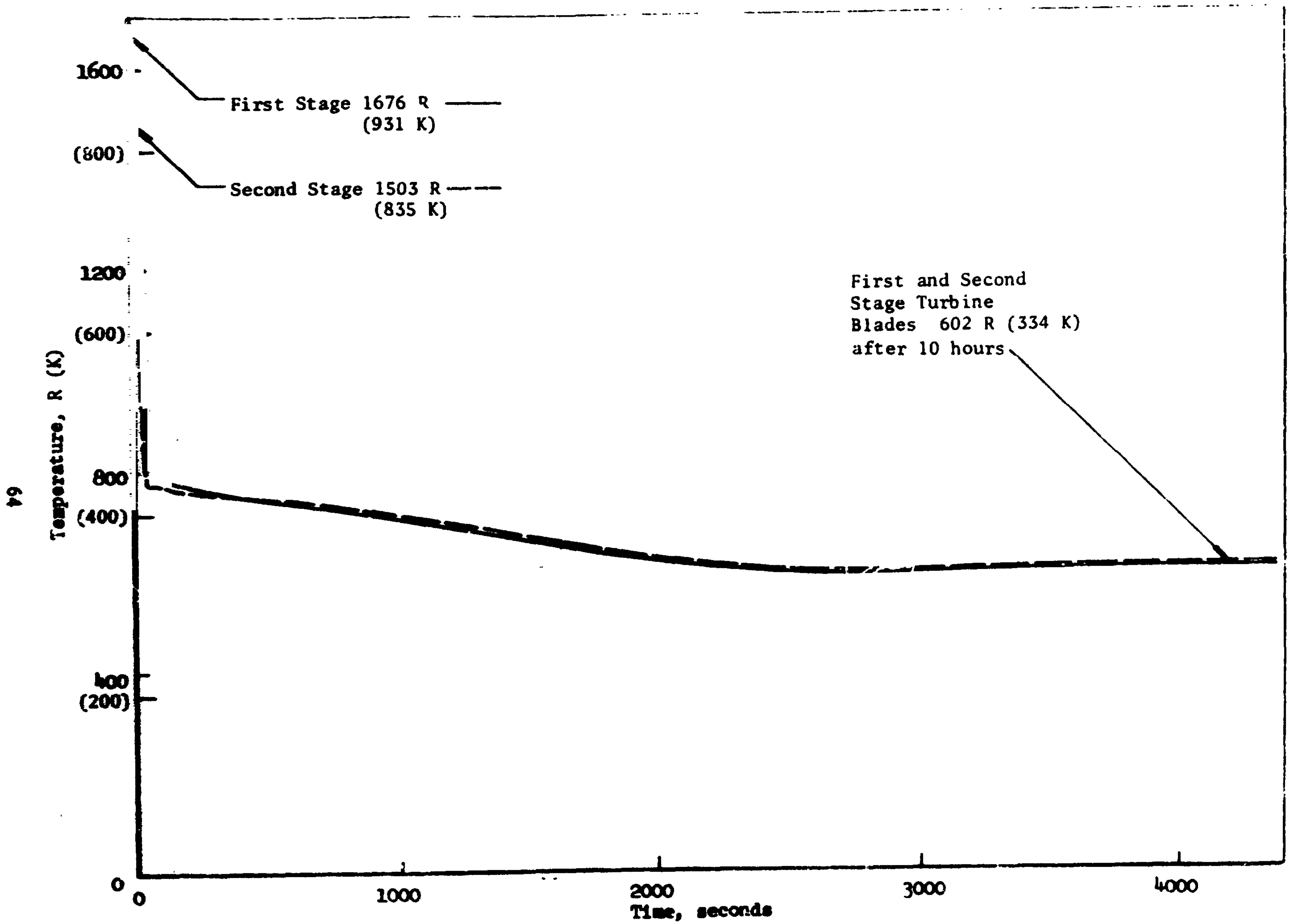

Figure 35. LH_2 Turbine Blade Soakback Following 20 Seconds Operation and 70 F Initial Temp

The short 5 second operation heats the blade to near maximum blade temperature but the turbine wheel remains relatively cool and acts as a heat sink reducing the rate of blade cooling below the temperature of the wheel.

GAS GENERATOR SELECTION

Alternate ignition methods, injector configurations, and combustor designs were evaluated for selection of the gas generator configuration.

The gas generator utilizes GO_2 and GH_2 propellants from the SS/APS accumulator storage. The function of the gas generator is to mix the propellants, ignite the mixture, combust the mixture with high efficiency and provide a uniform high pressure hot gas as a working fluid for the turbine. For the Phase I screening study the "proposal" turbine flowrates were utilized. (The maximum flowrates of the selected configurations are: (1) LH_2 TPA turbine flowrate, -0.340 kg/sec or -0.75 lb/sec, and (2) LO_2 TPA turbine flowrate, -0.140 kg/sec or -0.308 lb/sec.

The gas generator design parameters are given in Table 15 for both the LH_2 and LO_2 TPA. The nominal chamber pressure of 270 psia was selected based upon analyses considering the requirements for providing nominal power with the maximum temperature propellant 333 K (600 R) at the minimum inlet pressure 2,344,217 N/m^2 (340 psia), and providing reasonable GG injector pressure drop when propellant inlet temperatures were a minimum.

A large number of alternate concepts was evaluated; however, only the most applicable alternates (sufficient technology status for breadboard hardware fabrication) were considered.

The gas generator igniter evaluation was limited to electrical techniques (contract work statement limitation). Direct spark and indirect spark or augmented spark igniters (ASI) were evaluated. A gas generator with direct spark ignition is shown in Fig. 36.

TABLE 15. GAS GENERATOR DESIGN REQUIREMENTS

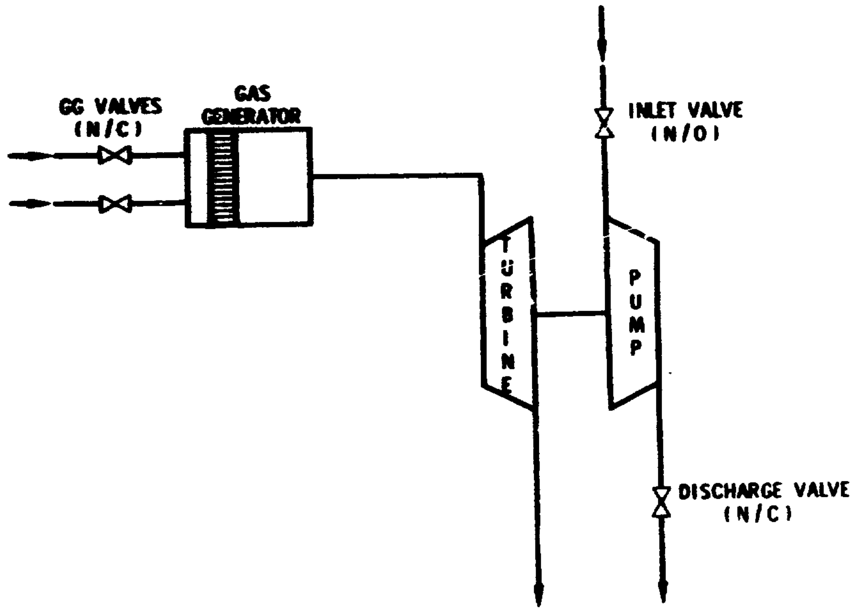

Parameter			LH_2	LO_2
$\dot{W}_T$ Kg	Max.	Kg (lb)	0.4853 (1.07)	0.166 (0.365)
	Nom.	Kg (lb)	0.374 (0.825)	0.127 (0.280)
P_C N/m^2	Nom.	N/m^2 (psia)	1,861,584 (270)	1,861,584 (270)
MR	Nom.		0.97	0.97

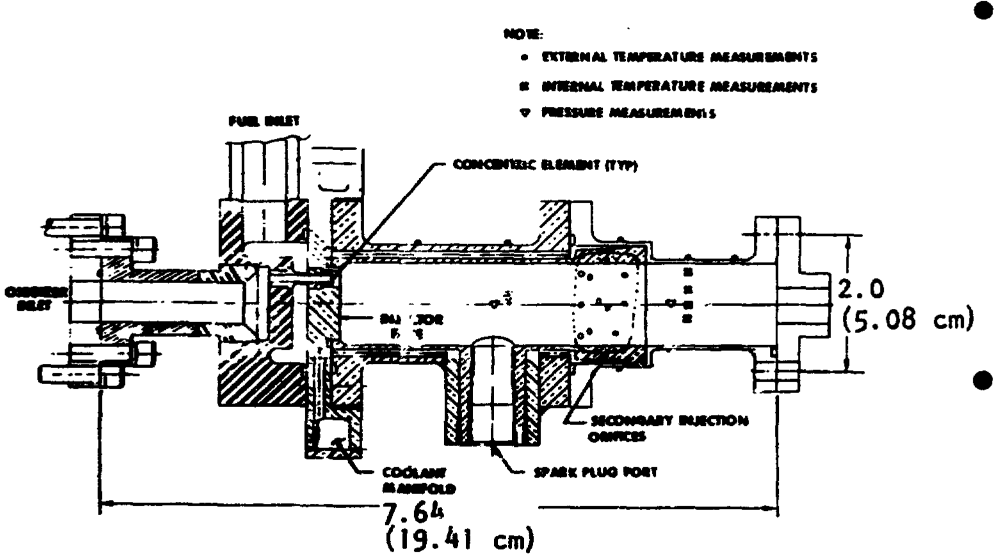

- **ADVANTAGES**
  - SIMPLE
  - IR & D EXPERIENCE
- **DISADVANTAGES**
  - SENSITIVE TO LOCATION
  - SCALING QUESTIONS
  - SENSITIVE TO SEQUENCING
  - REQUIRES HIGH M.R. AREA ($\geq$ 1.3 O/F)

Figure 36. Gas Generator Ignition (Direct Spark)

The advantages of direct spark ignition are simplicity and experience. The drawing shown is a cross-section of an IR&D configuration which has been evaluated during hot-fire testing.

Indirect spark ignition of the gas generator is also being evaluated experimentally at Rocketdyne under IR&D funding. The primary ignition is initiated in a precombustor and the actual gas generator ignition is accomplished with the hot-gas torch emanating from the precombustor. This technique has been used successfully on thrust chambers (J-2 and SS/APS) and on gas generators (NASA PCA breadboard). The advantages of this technique include the use of a common well-developed igniter head (preburner) in which the flow conditions are well controlled and reliable ignition can be contained. The torch then provides a relatively high energy source for ignition of the low mixture ratio gas generator propellants.

Alternate methods of injecting and mixing the GO_2 and GH_2 propellants were also evaluated. Coaxial elements have been evaluated experimentally by cold flow and hot-firing tests.

The tri-slot injector element in which two rectangular fuel streams are impinged into a rectangular oxidizer stream has also been evaluated.

Uncooled and cooled gas generator combustors were evaluated. For the cooled configurations dump cooled and regeneratively cooled designs were considered. The cooled configurations offer the advantages of additional cooling margin in the upper combustion zone and added heat sink capability during coast periods (turbine heat soakback can be absorbed before reaching gas generator valves).

The dump cooled design utilizes an injector mixture ratio of 1.3 o/f and provides the desired mixture ratio for the side mounted direct spark ignition. The excess fuel (overall MR ~0.8 to 1.0) is passed through the combustor walls for cooling and is injected through a series of orifices normal to the flow of the main combustion gases. This combustor configuration has been successfully tested during recent testing at Rocketdyne.

The gas generator body can also be cooled by regenerative methods. Cooling is accomplished with a single uppass flow of all the fuel. In this configuration all the fuel and oxidizer are injected at the injector and a more uniform exhaust mixture ratio and temperature can be obtained. However, this cooling technique is not directly applicable to direct spark ignition (no high mixture ratio zone).

An important consideration in the evaluation of alternate gas generator igniter, injector and combustor designs was the actual hot-firing test experience. The most experience has been obtained with a direct spark igniter, a coaxial injector, in a dump cooled gas generator body.

The configuration selected for fabrication is shown in Fig. 37 incorporating a coaxial injector, direct spark igniter, dump cooled combustor body with capability for incorporating baffles if required to ensure uniform exhaust temperatures. The overriding consideration in this selection was experience.

VALVE SELECTION

Available valves were selected for the turbopump inlet, turbopump discharge and gas generator propellant inlet lines. However, as a result of discussions during the Phase I [illegible] the pump inlet line diameter and therefore valve selection was reevaluated.

As part of the deliverable turbopump assembly, pump inlet, pump outlet, and gas generator propellant valves were required. During Phase I various valve configurations and available valve hardware were evaluated. The primary consideration was to provide valves which simulated flight-type valve pressure drop and dynamic response; of course availability of hardware, flexibility, and penumatic actuation were also desirable.

At the beginning of Phase I, valve preliminary requirements were established based upon steady-state and dynamic analysis of the TPA systems. The quality requirements were based upon two deliverable assemblies with one spare.

TP ASSY	N	D	L
LH_2	18	2.93 in. (7.44 cm)	6.0 in. (15.24 cm)
LO_2	7	1.71 in. (4.34 c[illegible]	6.0 in. (15.24 cm)

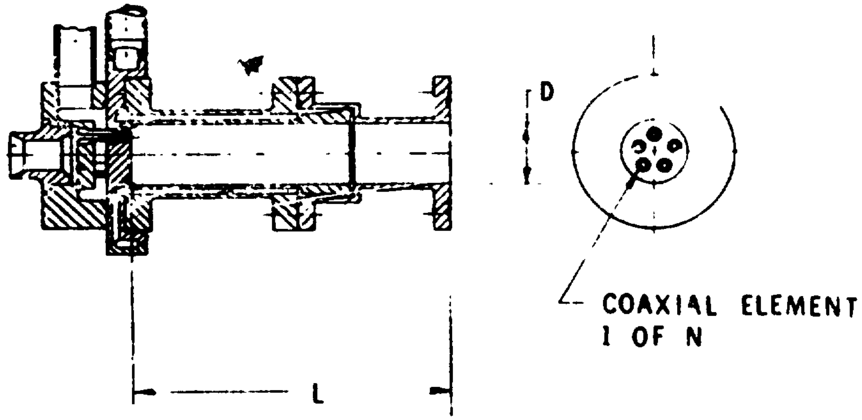

- COAXIAL INJECTOR
- DIRECT SPARK
- DUMP COOLED BODY
- BAFFLED COMBUSTOR

BASIC REASON FOR SELECTION

- EXPERIENCE

CONSIDERATIONS

- SCALING TO LH_2 SIZE (IGNITION)
- COLD PROPELLANT IGNITION

Figure 37. Gas Generator Configuration Selection

The pump inlet line size was specified as approximately four inches in diameter and 10 feet in length. A number of Rocketdyne flight-type valves and commercially available valves were evaluated. A four-inch diameter J-2 main fuel valve was selected based upon its ability to meet the ΔP and response requirements and its availability. However, based upon discussions during the Phase I oral presentation and consideration of the two-inch diameter line size from the propellant acquisition system currently under NASA contract, the line size and pump valve selection were reevaluated.

Pump discharge valves required as deliverable items on both the LO_2 and LH_2 TPA systems. Flight-type as well as facility type valves were evaluated and a J-2S idle mode ball valve was selected. The valve selected is a pneumatically actuated ball valve 3.048 cm (1.2 inch diameter passage through ball). It can be used without modification.

Gas generator propellant (on/off) valves are required. The LOX side and actuator portion of the MA-3 Atlas vernier valve was selected based upon its ability to meet the requirements and availability. The valve is a pneumatically actuated ball valve. The fuel side of the bipropellant valve will be removed (bolted assembly) and only the actuator and oxidizer side of the existing valve will be used. The oxidizer side (only) will be used because of its large capacity and cryogenic design features. This valve and actuator will be used for both the LO_2 and LH_2 gas generators on both the GO_2 and GH_2 propellant inlets. The only valve application requiring modification is the GH_2 valve on the LH_2 TPA (highest volumetric flowrate). This modification consists of enlarging the internal flow passage; however, the existing valve seals will be maintained.

SYSTEM ANALYSIS

System studies were conducted to analyze the system dynamics, identify failure modes and required safety features, and establish the systems operating conditions.

System Dynamics

Dynamic analyses were conducted to study start time, impact of bypass flow, and influence of inlet line inertia. Tank NPSP requirements were also studied.

The dynamic model utilized for the analyses is a lumped element digital model as shown in Fig. 38. When the accumulator reaches minimum pressure the GG operation is initiated and the turbopump begins rotation. When pump discharge pressure reaches operating pressure (1.103×10^7 N/m^2 or 1600 psia), the back pressure regulator opens to maintain rated low to the accumulator. For convenience, it was assumed that the liquid propellant flowing through the conditioner immediately turned to gas, thus eliminating the thermodynamic considerations from the process.

Utilizing the dynamic model, representative start transients were analyzed for time to the nominal operating condition and the inlet pressure drop corresponding to conditions of maximum flow acceleration. The start paths analyzed are shown on a typical head/flow pump map and correspond to normalized constant flow coefficient lines (ϕ/ϕ_{des}) in Fig. 39. The method of starting by achieving full discharge pressure and then reaching the required flow rate was dictated by the use of the back pressure regula or as specified by NASA.

The start time and acceleration NPSP for bypass flow condition corresponding to $\phi/\phi_{des} = 0.1$ resulted in instability in the dynamic model and were not pursued further. From the standpoint of the pump, operation within the specified head/flow range is preferrable. The NPSP values were determined based on an assumed sequence of the bypass valve and the back pressure regulator and therefore will require analysis based on the anticipated system response.

Failure Mode Analysis

A failure mode analysis was conducted and the failure modes identified are presented in Table 16 Methods of detecting the failures through instrumentation provided (Table 17) were also identified and the planned incorporation of specific safety features was established as outlined in Table 18.

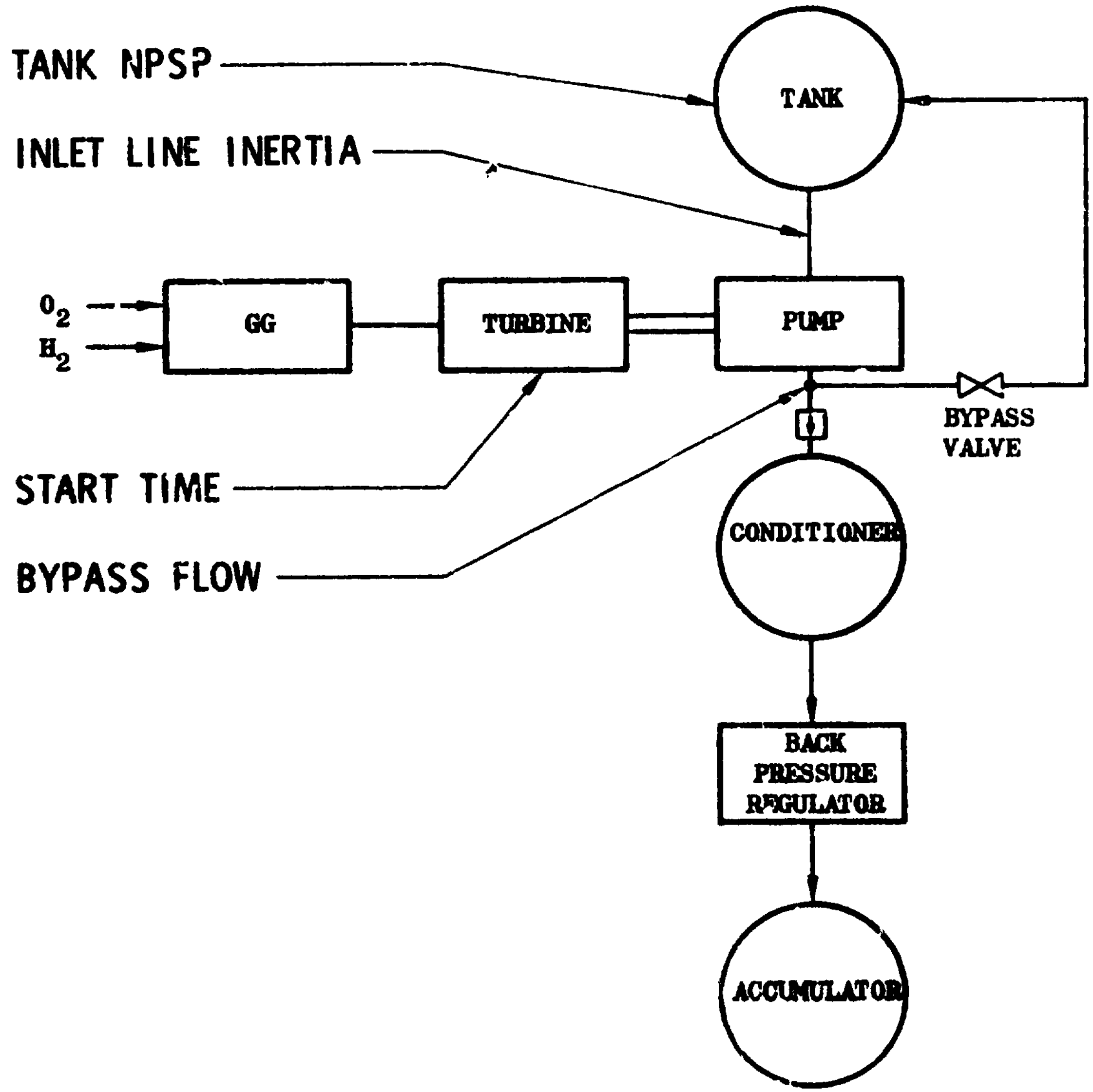

Figure 38. Dynamic Analyses

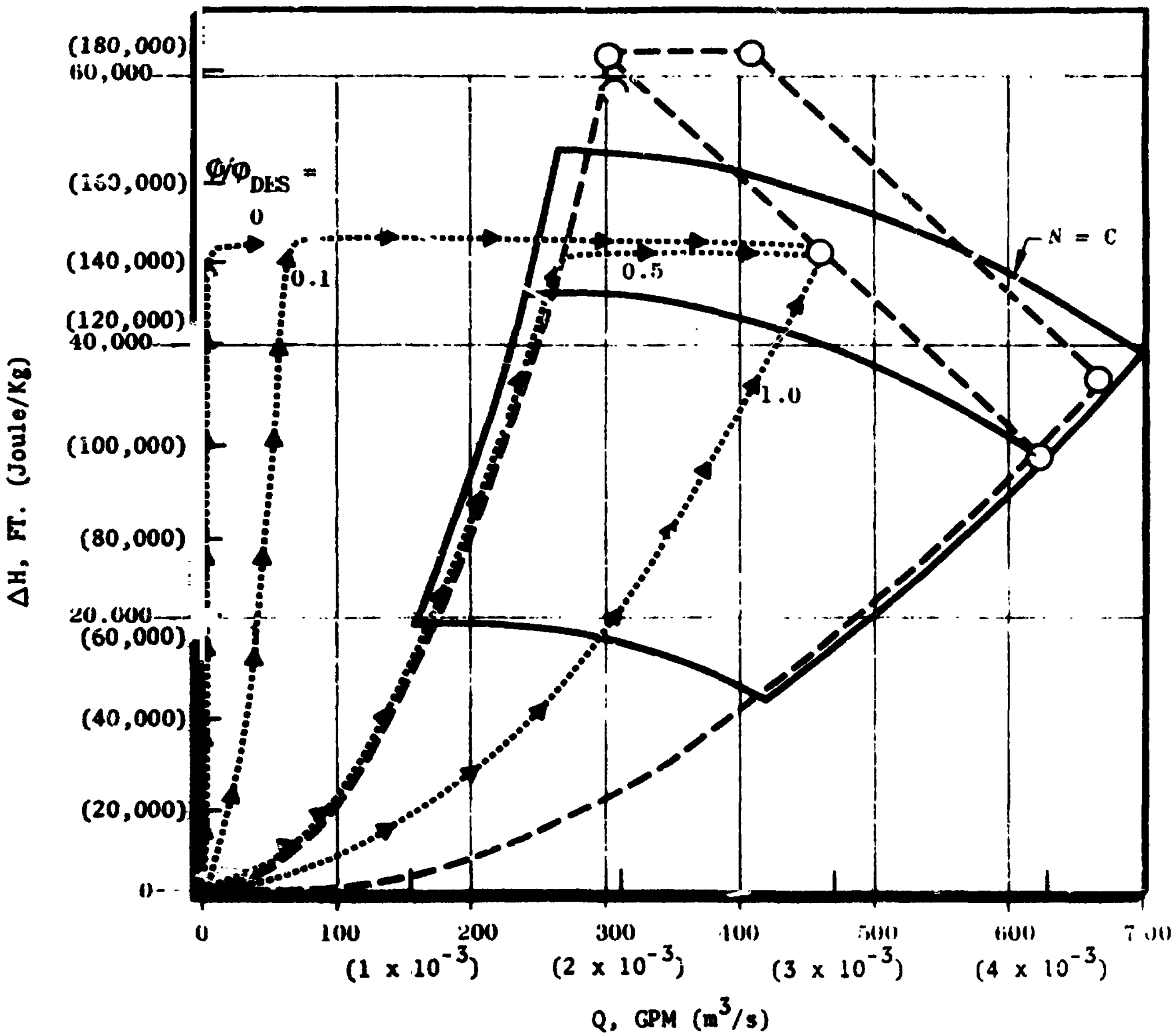

Figure 39. Alternate Start Conditions (Typical)

TABLE 16. CRITICAL FAILURE MODES

- Prestart Oxidizer Gas Generator Valve Leakage
- Failure to Ignite
    - Electrical Failure
    - Insufficient Oxidizer Flow
- High GG Mixture Ratio
    - Insufficient Fuel Flow
    - Excess Oxidizer Flow
- Turbopump Overspeed
    - Pump Cavitation
    - GG Overpressure
    - GG Overtemperature
- Gas Generator Inlet, or Discharge Valve Actuation Failure
- Bearing Failure
- Shaft Failure

System Operation

The system components and nominal operating conditions for the LO_2 and LH_2 turbopump assemblies were established and are presented schematically in Fig. 40.

TABLE 17. FAILURE MODE DETECTION

Mode	Related Measurement
Prestart Oxidizer GG Valve Leakage	Prestart Gas Generator Chamber Temperature and Pressure
Failure to Ignite	GG Chamber Pressure and Temperature at Start
High GG Mixture Ratio	GG Chamber Temperature and Pressure and T/P Speed
T/P Overspeed	T/P Speed and GG Chamber Pressure and Temperature
Valve Actuation Failure	Valve Position Indicators, Failure Effects
Bearing Failure	Bearing Race Temperature, T/P Speed, Accelerometers
Shaft Failure	T/P Speed, Pressure Measurements, Accelerometers

TABLE 18. APPLICATION OF SAFETY FEATURES

Active Overspeed	Incorporate in Both Breadboard and Flight Configurations
Passive Overspeed	Desirable Technology Area, Needs Development of Applicable Concept
Overtemperature	Incorporate on Initial Development Testing. Evaluate Need on Subsequent Testing and Flight Systems.
Turbine Blade Containment	Incorporate on Breadboard; Evaluate Additional Need of Flight Systems
Minimum Clearance Rubbing Protection (LO_2 Pump)	Incorporate on Breadboard and Flight Systems

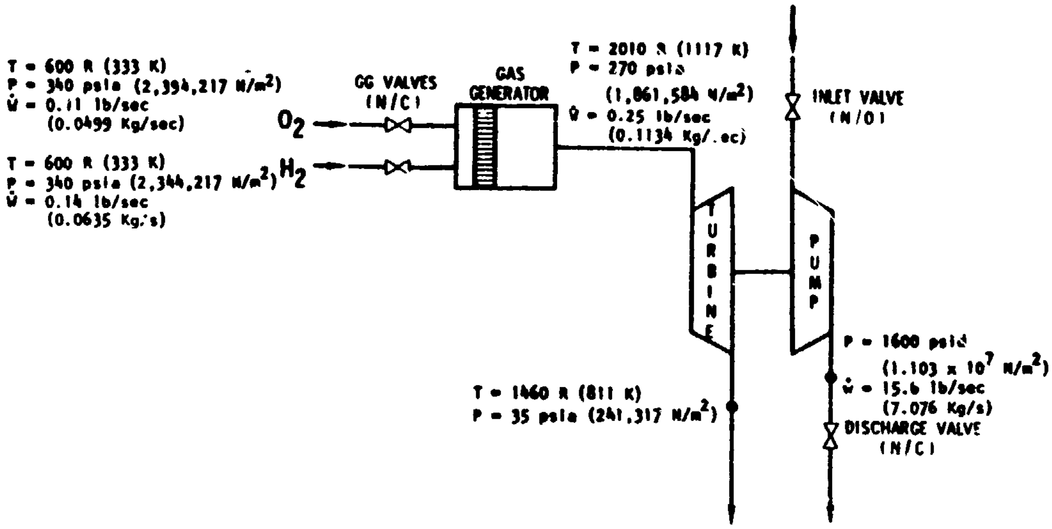

LO_2 System

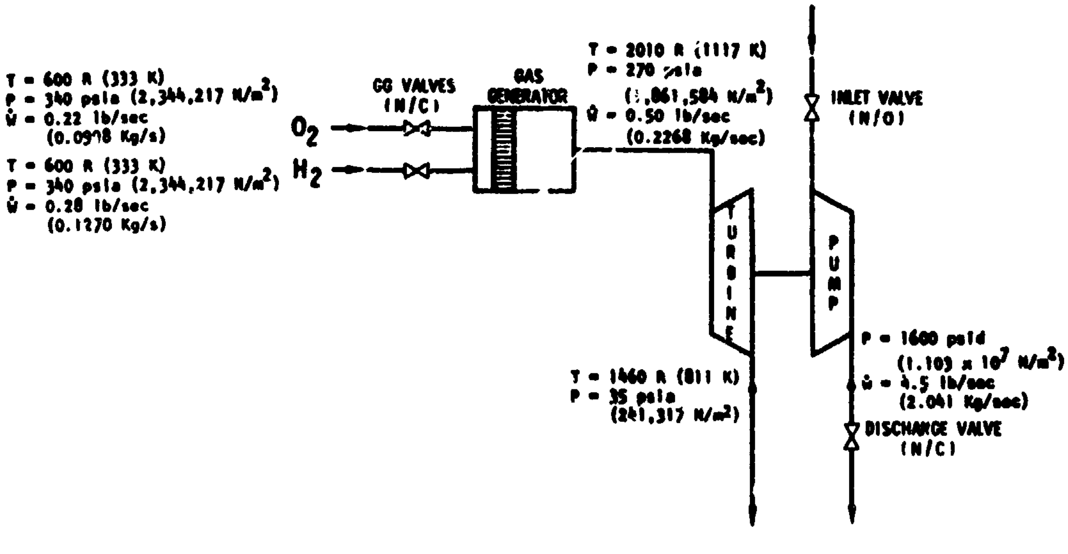

LH_2 System

Figure 40. LO_2 and LH_2 TPS System Schematics Nominal Operation

PHASE II - DETAILED ANALYSIS AND DESIGN

LIQUID OXYGEN TURBOPUMP

Design Requirements and Constraints

The performance and life requirements of the liquid oxygen turbopump are listed in Table 19. In addition, the pump is required to operate over the H-Q range indicated in Fig. 41a, with the liquid oxygen state at the inlet as defined in Fig. 41b.

As a result of the configuration studies conducted in Phase I, the oxidizer turbopump was defined as a single stage centrifugal pump and a single row, partial admission axial turbine with a shaft speed of 3142 rad/s (30,000 rpm). See Table 20.

LO_2 Turbopump Configuration

The configuration of the LOX turbopump which was designed to meet the foregoing requirements is presented in Fig. 42. The principal design parameters are summarized in Table 21.

The pumping elements consist of a variable lead helix inducer of constant outer diameter and tapered hub, and a centrifugal impeller containing four full and four partial vanes. The impeller vane discharge angle is 28 degrees. Additional detail information about the inducer and impeller is presented in Tables 22 and 23. Liquid oxygen from the impeller is discharged through a double tongue volute. The volute was machined into the inlet housing and closed out on the turbine side by the main pump housing. From the volute the liquid oxygen is delivered through a single discharge pipe of 3.023 cm (1.19 in.) internal diameter.

TABLE 19. APS OXIDIZER TURBOPUMP PERFORMANCE REQUIREMENTS

Pump:	Flow, m^3/sec (gpm)	6.309×10^{-4} (100)
	Inlet Pressure N/m^2 (psia)	137,895 - 344,738 (20-50)
	Developed Pressure, N/m^2 (psid)	1.103×10^7 (1600)
	Inlet Temperature, K (R)	92.8 - 103.9 (167-187)
Turbine:	Energy Source	O_2/H_2
	Exhause Pressure N/m^2 (psia)	24.317 (35)
Turbopump:	Life, tbo, hrs	10
	Operating Cycles	10,000
	Start Time, sec	1.5
	"ON" Time	2 sec. to 600 sec
	"OFF" Time	5 sec to 24 hrs
	Useful Life	10 years
	Seal Leakage	Minimized
	Maximum Surface Temperature	589 K (1060 R)
	Turbine to Pump Heat Flow	<52,752 Joule/hr (50 Btu/hr nonoperative) <158,256 Joule/hr (150 Btu/hr operative)

TABLE 20. APS OXIDIZER TURBOPUMP PHASE I RESULTS

Pump:	Single Stage Centrifugal
Turbine:	Single Row, Impulse, 49 percent admission Inlet pressure: 1,861,584 N/m^2 (270 psia) Inlet temperature: 1117 K (2010 R)
Nominal Shaft Speed:	3142 rad/sec (30,000 rpm)

FOLDOUT FRAME

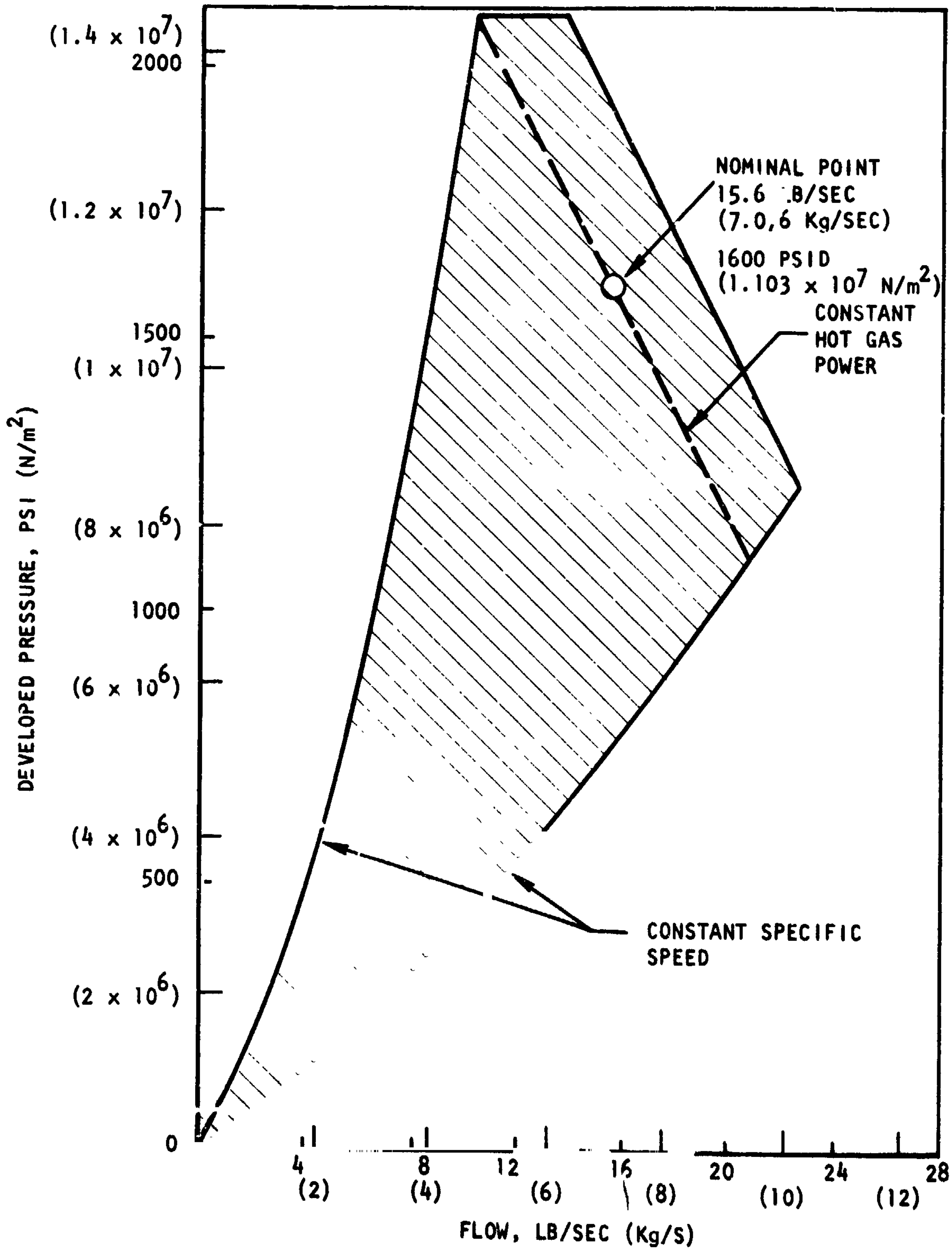

(a) Pressure - Flowrate - APS LOX Pump

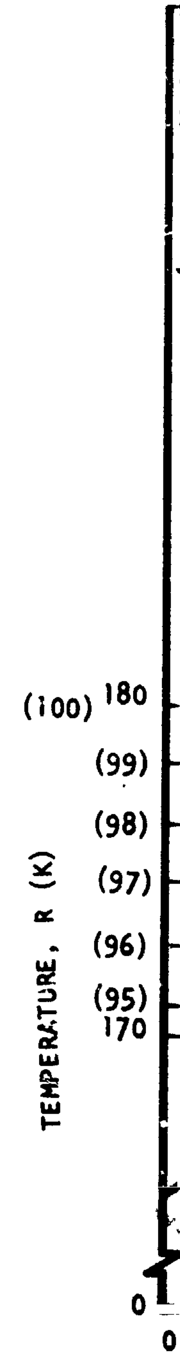

FOLDOUT FRAME

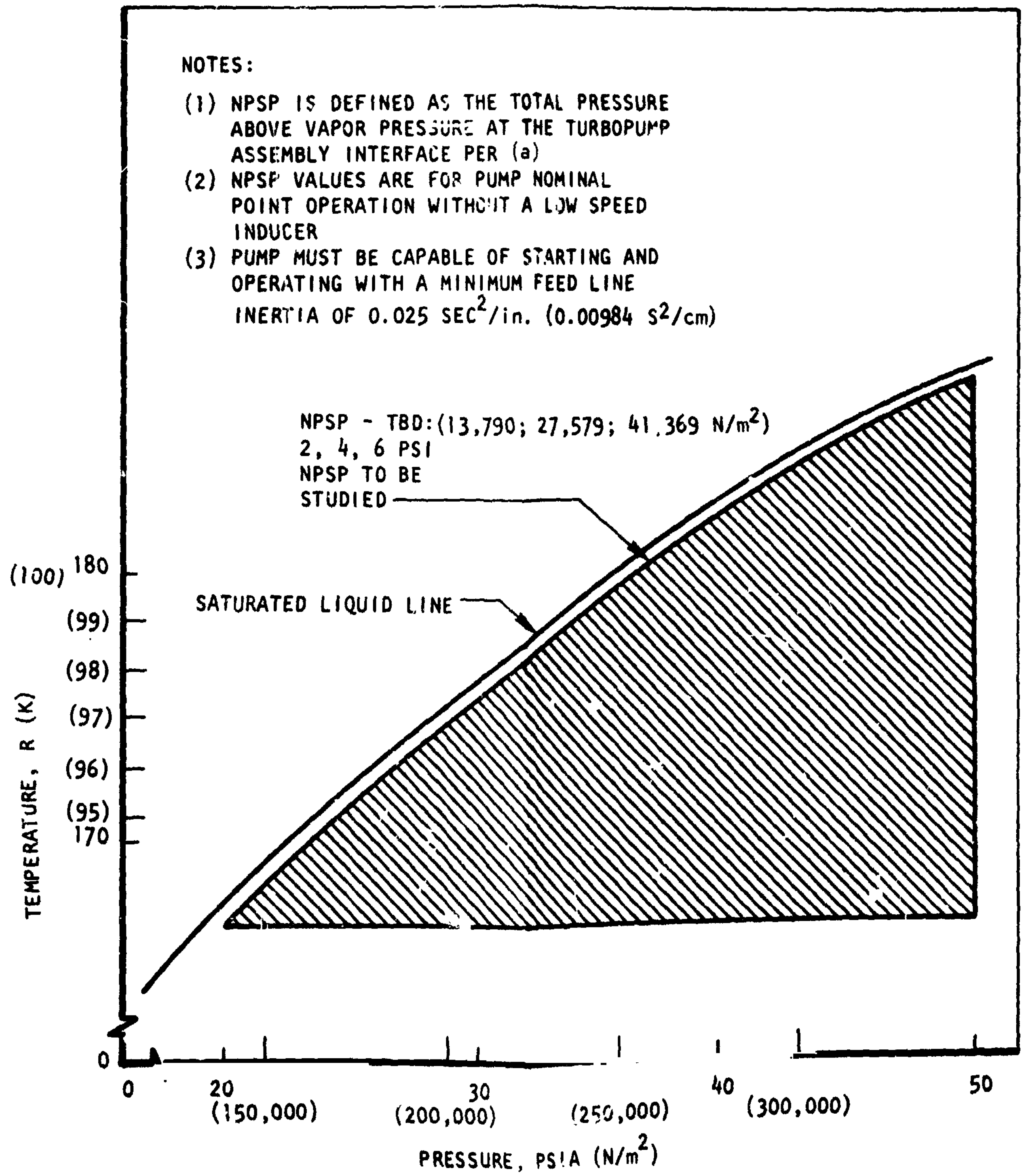

(b) APS Breadboard Oxygen Pump - Prestart and Run Box

Figure 41. Pump Operating Range and Inlet Conditions

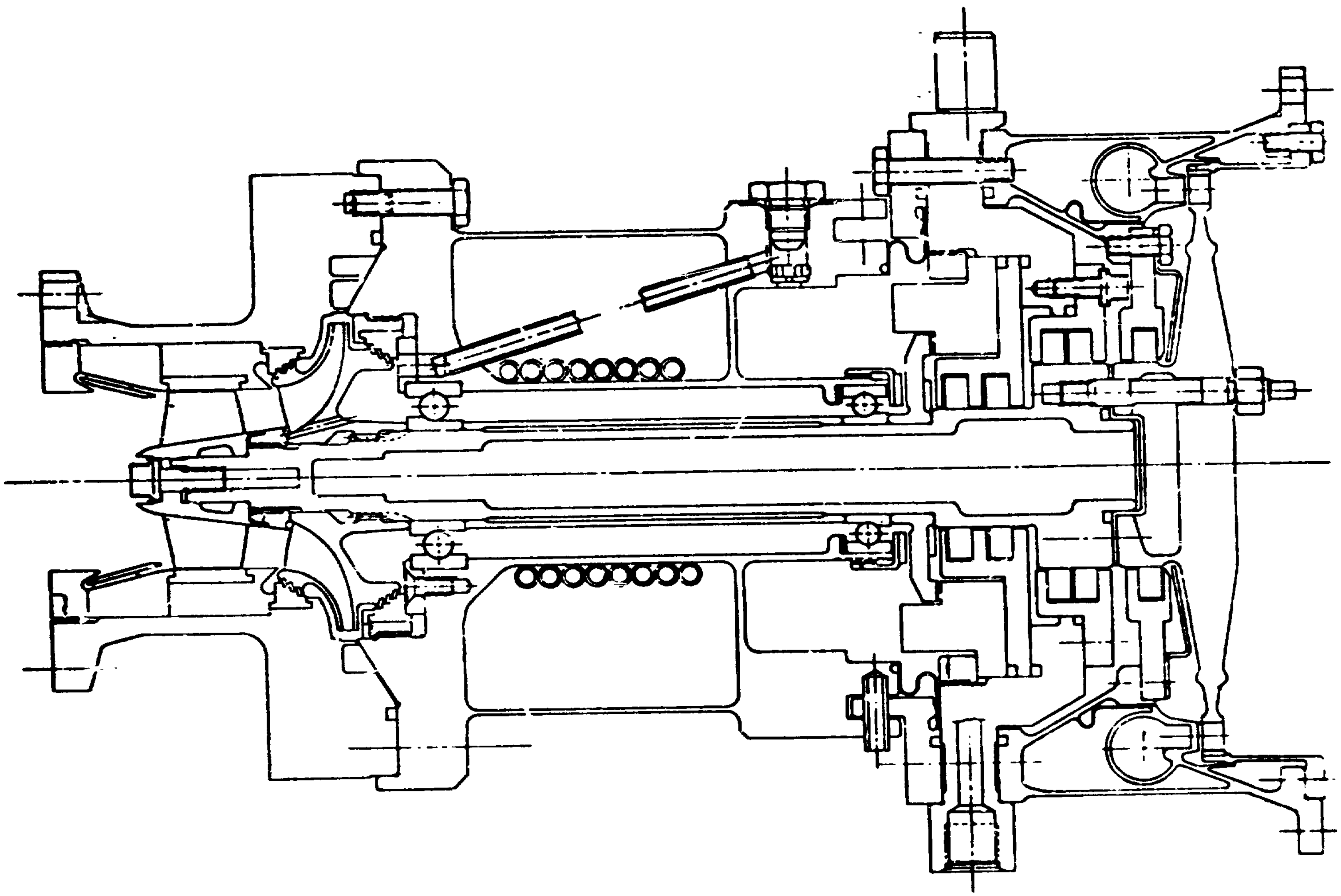

Figure 42. APS LO_2 Turbopump Layout

TABLE 21. APS OXIDIZER TURBOPUMP DESIGN DETAILS

Pump:	Inducer Diameter	4.953 cm (1.95 inches)
	Inducer Tip Speed	78.03 m/s (256 ft/sec)
	Impeller Diameter	8.509 cm (3.35 inches)
	Impeller Tip Speed	133.5 m/s (438 ft/sec)
	Efficiency Nominal	62 percent
	Developed Pressure (design)	1.105×10^{7} N/m^2 (1600 psia)
	Discharge Flowrate (design)	6.309×10^{-4} m^3/s (100 gpm)
Turbine:	Pitch Diameter	15.24 cm (6.00 inches) cm
	Blade Height	0.770 cm (0.303 inches) cm
	Pressure Ratio	7.72
	Power (design)	117,[illegible]1 W (158.0 HP)
	Efficiency (design)	24.3 percent
	Percent Admission	49
	Flowrate	0.1306 Kg/sec (0.288 lbs/sec)
Turbopump:	Bearing DN (design)	750,000
	Shaft Seal Rubbing Vel. (design)	89.9 m/s (295 ft/sec)
	Calculated Weight	31.297 Kg (69 lbs)*

*This is the "breadboard" turbopump weight including extra heavy inlet flanges and excess material in selected areas to reduce cost.

TABLE 22. MK-44-O INDUCER DESIGN PARAMETERS

	Oxidizer
Fluid	LOX
Type	Variable Lead Helix
Speed, rad/s (rpm)	3142 (30,000)
Flow, m^3/sec (gpm)	6.309 x 10^{-9} (100)
Head, Joule/Kg (ft)	1226 (410)
Inlet Tip Diameter cm (inches)	4.953 (1.950)
Inlet Hub Diameter cm (inches)	1.905 (0.750)
Discharge Hub Diameter cm (inches)	2.604 (1.025)
Blade Angle, inlet Tip (degree)	7.0
Blade Angle, Inlet rms (degree)	8.3
Blade Angle, discharge Tip (degree)	8.0
Tip Solidity	2.47
Inlet Flow Coefficient	0.049
Number of Vanes	3
Vane Thickness, Tip cm (inch)	0.0254 (0.010)
Vane Thickness, 1.00-inch diameter cm (inch)	0.1778 (0.070)
Cant Angle (degree)	10
Radial Tip Clear, mm (inch)	0.889 mm (0.0035)
Material	K-Monel

C-2

TABLE 23. MK-44-0 IMPELLER DESIGN

Type	Shrouded radial
Speed	3142 rad/s (30,000 rpm)
Through Flow	6.309×10^{-4} m^3/s (100 gpm)
Leakage Flow	1.861×10^{-4} m^3/s (29.5 gpm)
Pump Head	9655 Joule/Kg (3230 ft)
Specific Speed	0.2562 (700) Non-Dimensional
Blade Angle, Discharge	28 degrees
Blade Angle, Inlet Tip	10 degrees
Blade Angle, Inlet Hub	20.55 degrees
Inlet Flow Coefficient	0.063
Discharge Flow Coefficient	0.095
Number of Vanes	6 partial, 6 full
Eye Diameter	5.131 cm (2.020 inches)
Discharge Diameter	8.509 cm (3.350 inches)
Discharge Tip Width	0.277 cm (0.109 inches)

Recirculation around the impeller is minimized by step labyrinth wear rings on the front and rear shrouds. Each wear ring incorporates four steps, with a diametral clearance of 0.0127 cm (0.005 inch) between the stationary and rotating member. Kel-F is used for the liner to avoid an explosion hazard with the close clearances. Leakage past the rear wear ring is returned to the eye of the impeller through 12 holes of 0.127 cm (0.050 inch) diameter in the impeller hub.

To obtain a high suction performance, the inducer tip clearance is maintained at 0.0178 cm (0.007 inch) on the diameter. Since such small clearance inevitably leads to tip rubbing, a stationery Kel-F liner is included around the inducer. A back flow deflector is incorporated in front of the inducer to minimize the detrimental effect of reverse flow at the tip when operating at low flow rates. The back flow deflector captures the reverse flow and redirects it back into the inducer.

Power to the pump is provided by a single stage impulse turbine of 19 percent admission. To meet the bearing life requirements radial reaction loads from an unsymetrical nozzle pattern have to be avoided. Thus the nozzle segments of 90 degree span each are located diametrically opposed. A honeycomb seal is used at the tip of the rotor blades to maintain tip leakage at a low level. Torque is transmitted from the turbine disc to the shaft with body-bound studs.

To minimize the heat transfer from the turbine to the pump, these two areas are connected by thin cylindrical members. In addition, a high thermal resistance pin joint is included in the volute mounting flange and a titanium spacer is inserted between the turbine disc and shaft.

Cooling coils are wrapped around the cylindrical portion of the housing located between the two bearings. These are included to provide a backup cooling system for prestart conditioning, should a need be indicated based on heat transfer data.

The rotor is supported by a pair of 25 mm angular contact ball bearings, axially preloaded against each other by a Beleville spring to preclude ball skidding. Bearing lubrication is accomplished by circulating liquid oxygen through the bearings. The pressure gradient created by the pumping action of the back shroud of the impeller forces LOX into a lube passage located in the housing below the rear wear ring. From there, the coolant flows behind the turbine bearing, through both bearings into the impeller rear shroud cavity. Recirculation is enhanced by the use of an antivortex ring on the outboard side of the turbine bearing, which prevents reverse pumping by the liftoff seal mating ring. The recirculated coolant mixes with the fluid leaking past the impeller rear wear ring and by the resulting heat exchange its temperature is maintained at an acceptable equilibrium level.

Loss of propellant from the pump during coast periods and mixing of pump and turbine fluids is prevented by a seal package consisting of a liftoff seal and three shaft riding controlled gap seals. An overboard drain is provided on the downstream side of the pump and turbine seals, and the intermediate seal is pressurized to 344,738 N/m^2 (50 psig) with GHe purge gas to maintain absolute separation between the pump and turbine fluid regions.

The weight of the breadboard configuration of the turbopump including extra heavy inlet flanges and excess material in selected areas to reduce cost was calculated at 31.3 Kg (69 lb).

LO_2 Pump Predicted Performance

The overall performance of the selected pump design is shown in Fig. 43. Pump head rise is plotted versus delivered flowrate. The solid lines represent constant speed conditions and the dashed lines are points of constant efficiency. Superimposed on the pump performance, shown by the dotted lines, is a representation of the pump required operating envelope. Specific operating conditions defining the envelope are shown by the circles. The pump design point is also represented by a circle at the intersection of the 3142 rad/s (30,000 rpm), 6.309 x 10^{-4} m^3/s (100 gpm), and 62 percent efficiency lines.

The predicted pump NPSP requirements for the design point as well as for the specific operating points defining the overall operating envelope are shown in Fig. 44. NPSP requirements are based on the incorporation in the design of the back-flow deflector, which significantly improves the required NPSP at low flowrates as compared to a design without a backflow deflector.

An analysis was made to determine the static pressures at important points in the pump for the design point, the low flow point, and the high flow point. This analysis provides the basis for the selection of the bearing coolant flow system and also provides data to calculate the axial thrust loads which determines the location of the pump impeller aft wear ring. Static pressures at the design point are shown in Fig. 45.

The direction and amount of propellant flow through the pump, bearings and seals at the design point is shown in Fig. 46. Flow through the pump wear rings was calculated based on a wear ring radial clearance of 0.0127 cm (0.005 inch). Flow through the bearings is controlled by means of an orifice in the bearing coolant supply line (see turbopump layout drawing). Flow of 2.712 x 10^{-6} m^3/sec (0.43 gpm) through the primary LOX seal is calculated and based on empirical data on seals of similar design.

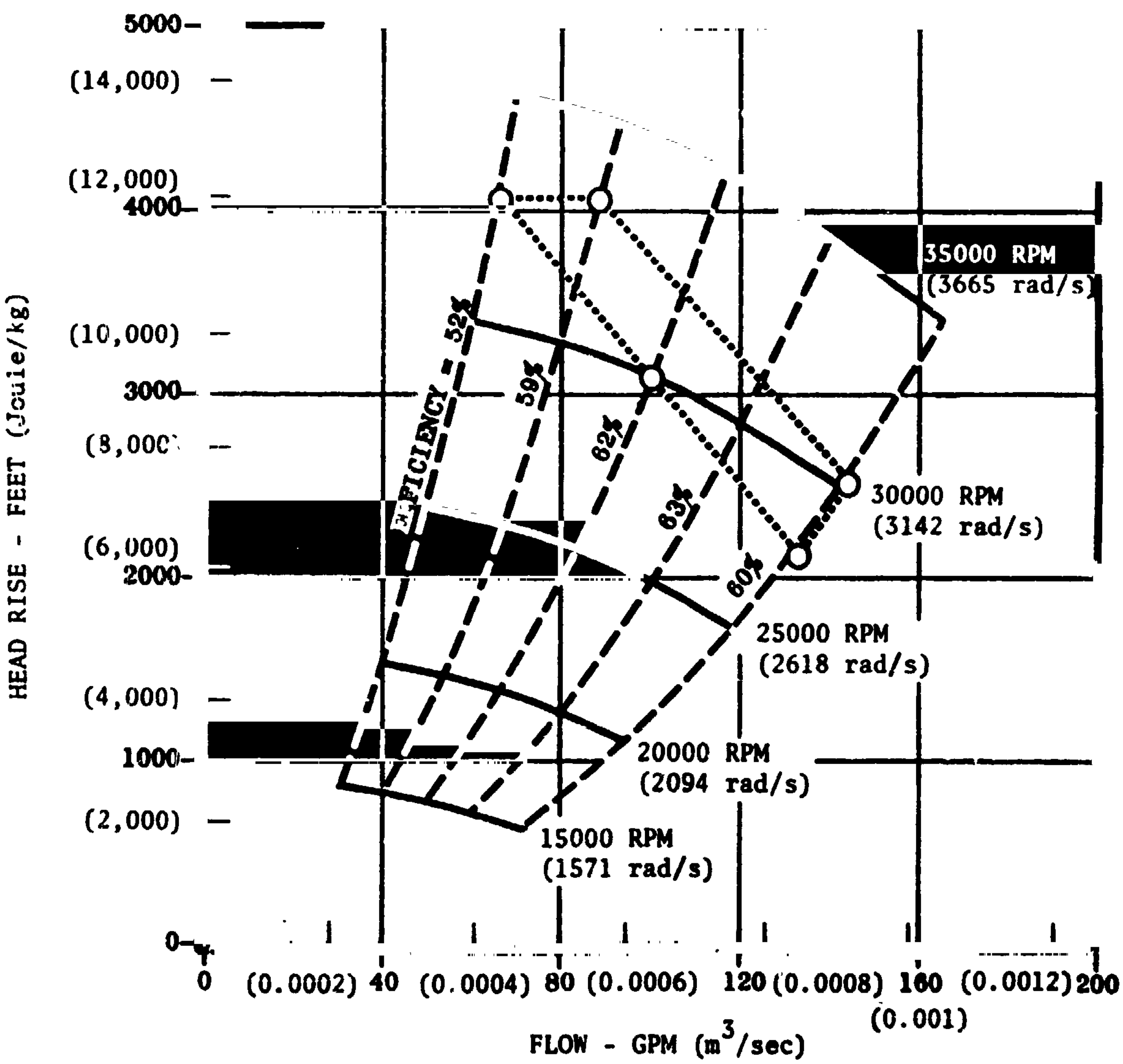

Figure 43. APS Oxidizer Pump Estimated Performance

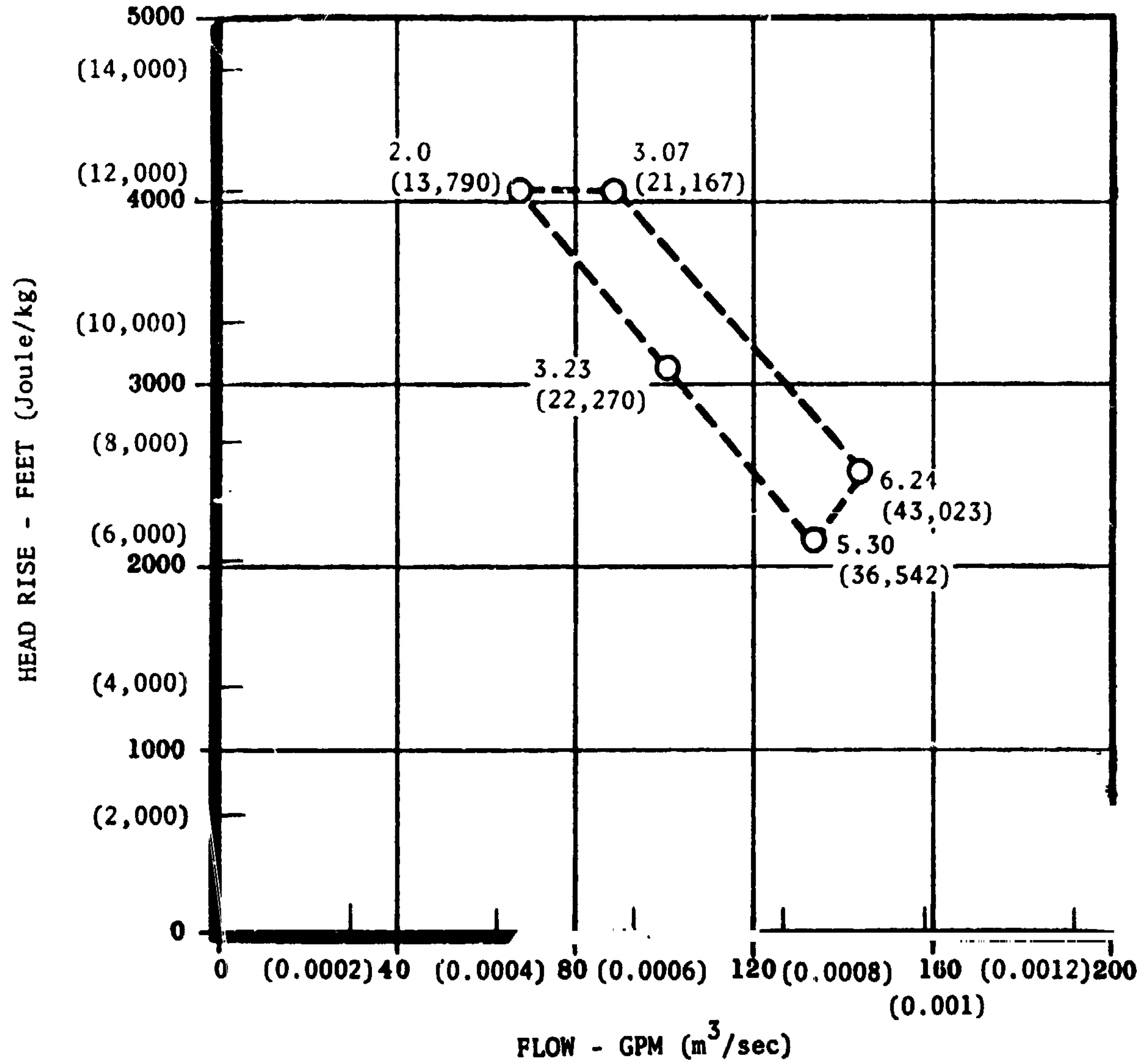

Figure 44. APS LOX Turbopump Required NPSP, psi (N/m^2)

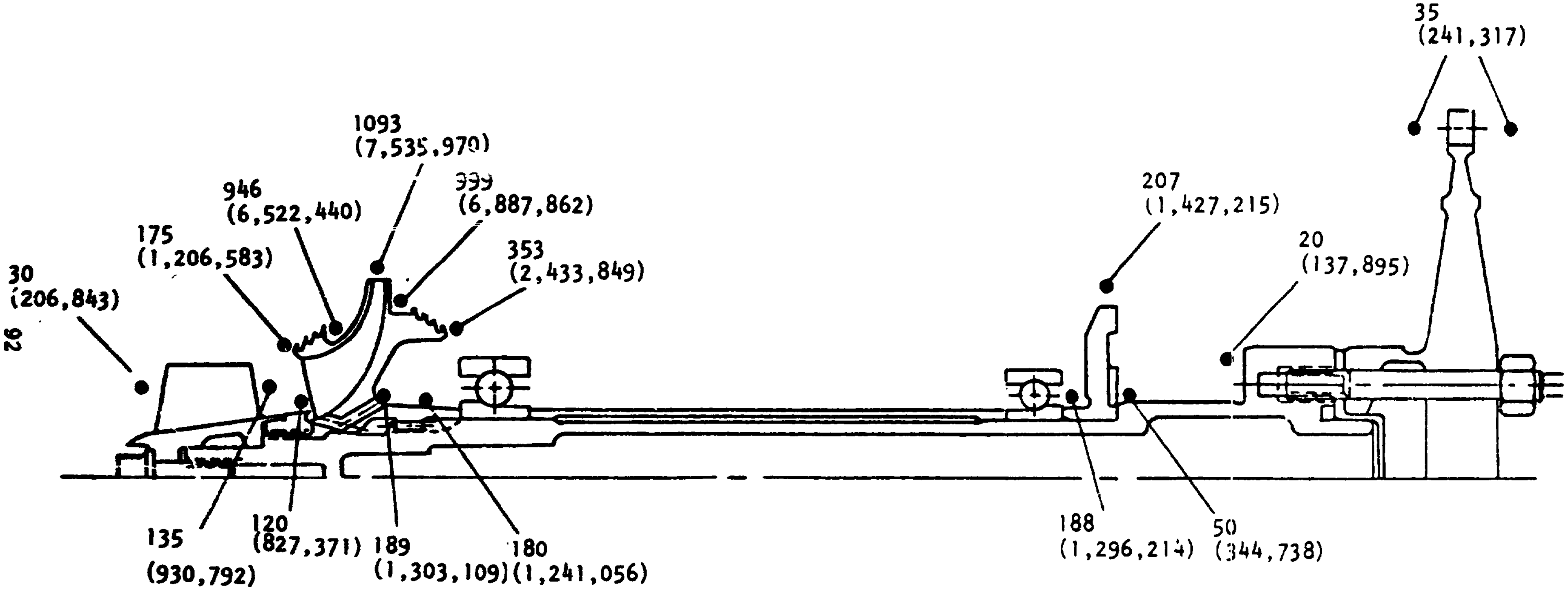

Figure 45. APS LOX Turbopump Static Pressures at Design Point, psia (N/m^2)

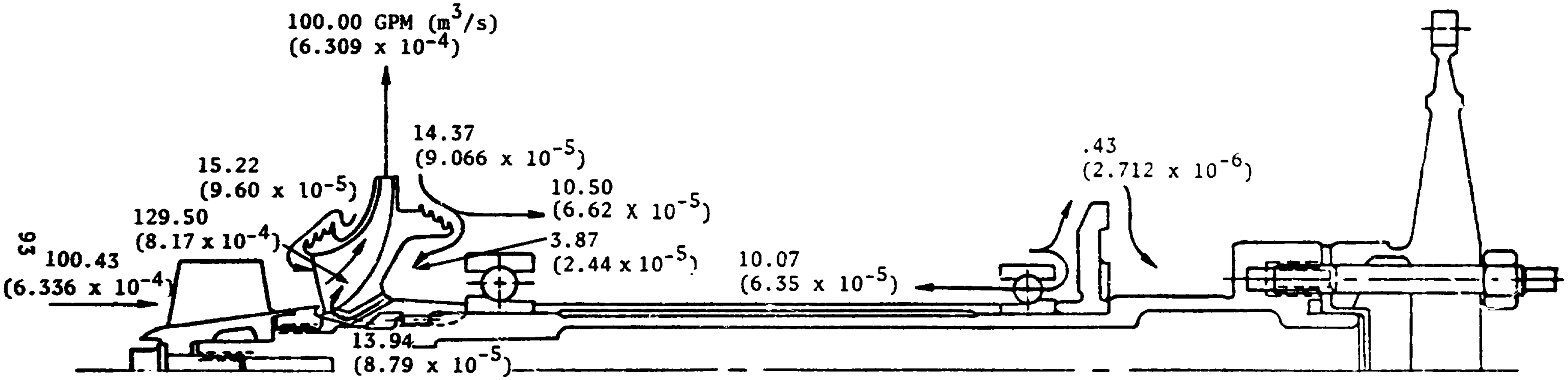

Fig. re 46. APS LOX Turbopump Flow Paths at Design Point, Flowing GPM (m^3/S)

Rotor axial thrust balance is accomplished by the radial location of the impeller rear wear ring. Based on a wide wear ring clearance tolerance, the radial location was established to provide a minimum axial thrust imbalance to maintain an unidirectional load over the entire operating envelope. Balance forces at the design point are illustrated in Fig. 47. At the design point the net imbalanced thrust is 1019 N (229 pounds) toward the turbine.

The effects of pump wear ring radial clearance on axial thrust and bearing coolant flowrate are shown in Fig. 48. Bearing thrust can be maintained unidirectional over a radial clearance range of zero to 0.0203 cm (0.008 inch) and at a maximum magnitude of approximately 1334 N (300 pounds). Over this same operating range, bearing coolant flow will vary from approximately 6.246×10^{-5} to 6.44×10^{-5} m^3/s (9.9 to 10.2 gpm).

LO_2 Turbine Design Performance

Developments in the field of rocketry have created a growing demand for small turbine driven power units using a high energy working fluid. The Mark 44 oxidizer turbine requires power in the order of 119,312 watt (160 horsepower), and gas pressures of several hundred pounds per square inch. For units at the lower end of the power scale. the combination of high energy propellant with low shaft horsepower output leads to a turbine design in which the nozzle arc is only a small fraction of the wheel circumference. Under these conditions of partial admission, the efficiency of the turbine is greatly reduced by pumping and mixing losses in the blading. For short duration units, the size and weight of the entire package rather than of the propellant alone are of primary importance. In addition, production considerations favor the use of the minimum possible number of stages. The designer is faced with the problem of obtaining the maximum possible energy extraction in one, or at most two turbine stages. Since it is rarely possible to utilize the kinetic energy of the fluid leaving the turbine, the figure employed to evaluate turbine performance is the so-called "total to static" efficiency. For a frictionless turbine the "total to static" efficiency is a function of the ratio u/c where the u is the blade speed, and c is called the equivalent velocity of the available energy. In practice the blade speed for contemporary machines is limited by the strength of available materials to approximately 487.7 m/s (1600 fps) at approximately 1089 K (1500 F).

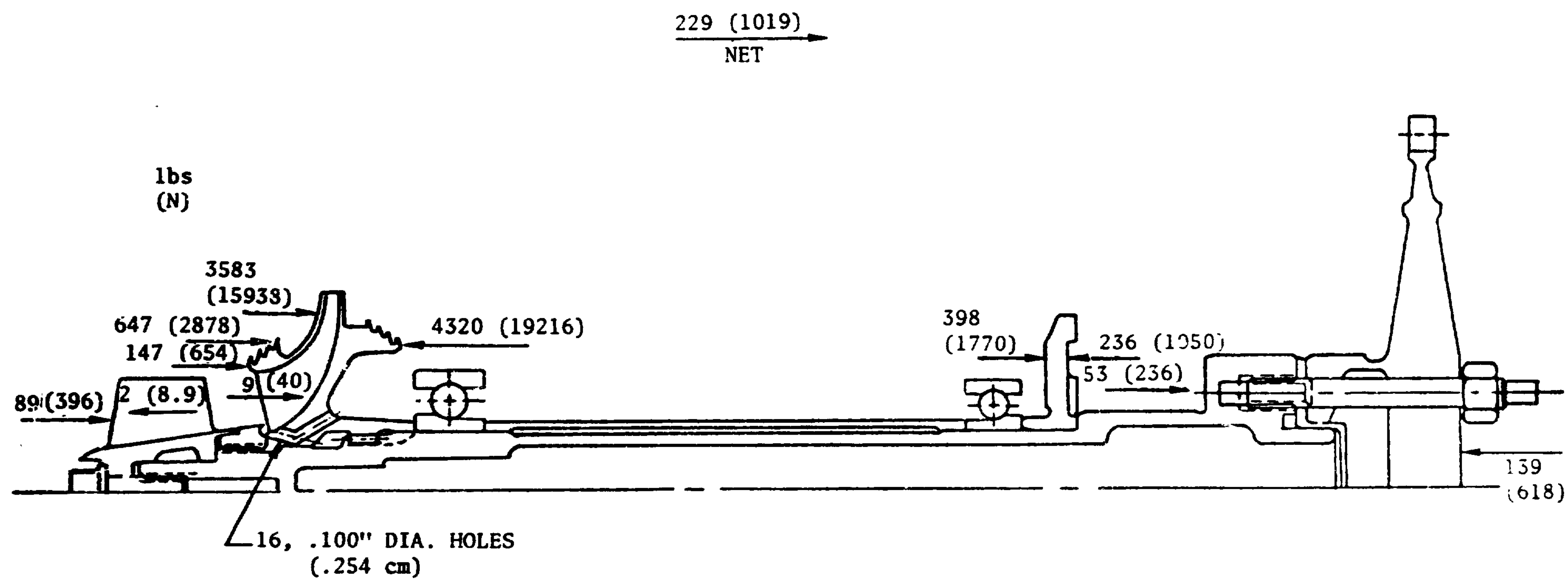

Figure 47. APS LOX Turbopump Axial Thrust at Design Point, Thrust in lbs (N)

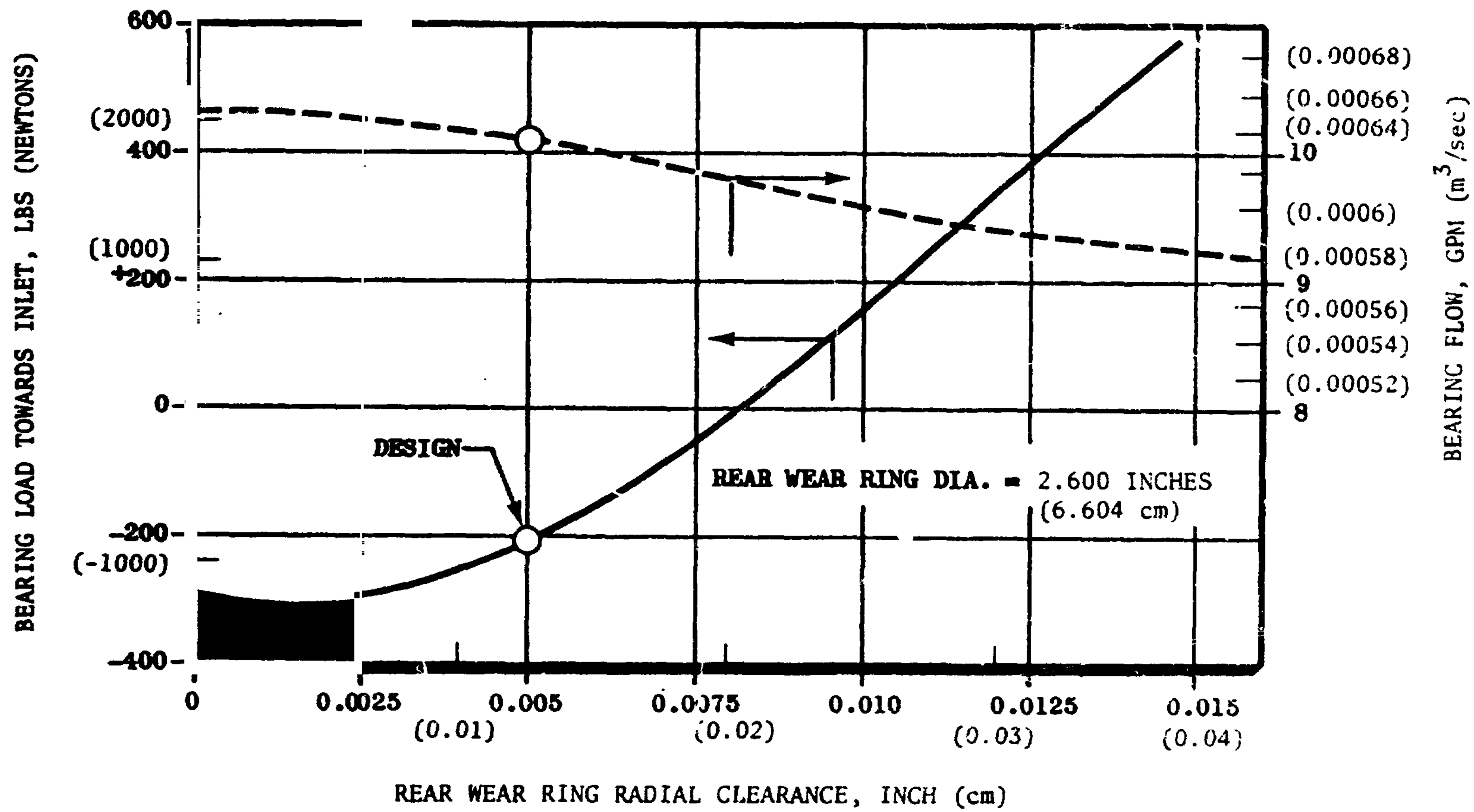

Figure 48. APS LOX Pump Clearance Effects on Axial Thrust

For low admission turbines it is impractical to use a reaction machine because a pressure difference cannot be maintained across the wheel unless very small axial clearances between wheel and nozzles can be ensured. Another important factor is blade temperature. The temperature of the gas leaving the nozzle of an impulse turbine is still lower than the temperature of the corresponding reaction turbine blading. Once the field was limited to impulse machines, a comparison of the 1-stage impulse turbine with the 2-stage impulse turbine for assumed values of nozzle efficiency and blade loss was made. The values used are those which experience indicates are valid for small full admission turbines. With losses included, the superiority of the 2-stage turbine over the 1-stage machine is less than for the ideal case, and at U/C = 0.20 it amounts to a difference of only 8 percent. In a partial admission turbine the improvement to be gained by staging is even smaller and may be nonexistent because windage and mixing losses in the second stage may exceed its work recovery.

The conclusion may be made that for a small axial turbine using a high energy fuel, the optimum turbine for many applications is a 1-stage impulse wheel. Where it is possible to use a full admission turbine, a 2-stage impulse turbine will give higher efficiency for very low velocity ratios.

Gas Properties. The gas driving the turbines is the combustion products from a parahydrogen-oxygen mixture ratio ~0.9:1. The effect of the pressure upon c_p and γ is neglected. Both c_p and γ are taken at the inlet temperature of 1117 K (1550 F). The gas properties used are:

c_p, Joule/kg/deg K = 8055
(Btu/lb/deg F = 1.924)
R, Joule/kg/deg K = 2093
(ft lb/deg R = 389)

Aerothermodynamic Design

Calculation Procedure. Using the given pump parameters, a series of pressure and energy distribution calculations through the turbine were made. This is a calculation procedure applied through the various rotor and stator elements in sequence. It employs the equation of continuity together with reasonable and consistent values of coefficients for nozzles and blades, two dimensional friction, and incidence losses. The particular procedure used is a systematic and rapidly convergent process, commencing at the turbine exhaust with assumed gas conditions and working back to the turbine inlet. Results of the detailed element-by-element calculation can be expressed in terms of diagram efficiency as a function of the isentropic velocity ratio. Diagram efficiencies computed as outlined above are basically two dimensional, in that they include only profile incidence, surface friction, and wake losses, the most important can be classified as follows:

1. End losses (annulus wall boundary layer and leakage losses)
2. Interstage seal leakage and leakage interference losses
3. Parasitic friction losses

End losses are primarily a function of nozzle and rotor blade height, configuration (shrouded or open-ended blades), operating tip clearances, and amount of reaction. Short nozzles contribute strongly to increased end losses.

Interstage seal losses are relatively high in a small high-pressure turbine. Special provisions have been made in the mechanical design of the unit to minimize effective clearance areas and resultant leakages.

The third category of losses, parasitic friction, is negligible since all stages are full admission and the ratio of power developed to stage size is high in the fuel turbine.

Once the desired pressure distribution was established, required flow areas at the throat of the various elements and resultant gas inlet and efflux angles were determined. The flow areas were sized to given an approximate design power split between nozzle-first rotor and stator-second rotor of 75 to 25 percent.

Loss Estimates. Two types of loss coefficient are used, one to determine the energy loss from blade inlet to blade exit, the other to estimate the flow loss from blade inlet to blade throat. The energy losses are used to determine stage and overall efficiency.

Performance. Based upon the loss estimation, the thermodynamic calculations were made and summarized. From these data the design parameters, velocity vector diagrams and estimated performance maps presented in Figs. 49 through 51 were generated. The required turbine flowrates over the operating range of the pump are presented in Fig. 52.

Cascade Design

Supersonic Nozzle Design. As a general rule, it is of no advantage to install converging-diverging nozzles if the theoretical Mach number at the nozzle exit does not exceed about 1.2 or similarly, if the theoretical area ratio of the exit to throat is less than about 1.02.

Because the flow across the nozzle of this turbine has a pressure ratio of 7.72 its theoretical Mach number is 1.6. Therefore, the nozzle should have convergent-divergent flow areas. Considerable after expansions would occur if converging nozzles were used. The critical pressure ratio for an isentropic expansion is 1.864. This could give an after expansion pressure ratio of 7.72/1.864 or 4.14. Using theoretical considerations, the above after expansion pressure ratios combined with a nozzle discharge angle of 71.5 degrees from the axial direction would cause a flow deflection of about 3.5 degrees. This would reduce the tangential velocity component and additional losses would occur from the entropy increase.

For this reason, convergent-divergent nozzles were used with an area ratio that requires a slight after expansion. The nozzle becomes shorter and the friction losses are reduced. A thick nose nozzle profile was selected to provide improved strength at this critical structural location and because it is adaptable aero-dynamically to the variant inlet velocity directions of the gas flowing into the nozzles from the manifold.

OXIDIZER

INLET TEMPERATURE, R (K)	T_{1t}	:	2010 (1117)
INLET PRESSURE, PSIA (N/m^2)	P_{1t}	:	270 (1,861,584)
EXHAUST PRESSURE, PSIA (N/m^2)	P_{2s}	:	35 (241,317)
PRESSURE RATIO	PR	:	7.72
SPEED, RPM (Rad/s)	N	:	30,000 (3142)
MEAN BLADE SPEED, F/S (M/s)	u_m	:	786 (239.6)
VELOCITY RATIO	u/c_o	:	.088
EFFICIENCY, %	η_{t-s}	:	24.3
FLOWRATE, LB/S (Kg/s)	$\dot{w}$	:	.288 (1306)
POWER, HP (Watt)	HP	:	158 (117,821)
ADMISSION, %	ϵ	:	49
STRESS X 10^9	N^2AA	:	5.15
SPECIFIC SPEED (NON DIMENSIONAL)	N_s	:	1.9 (.000695)

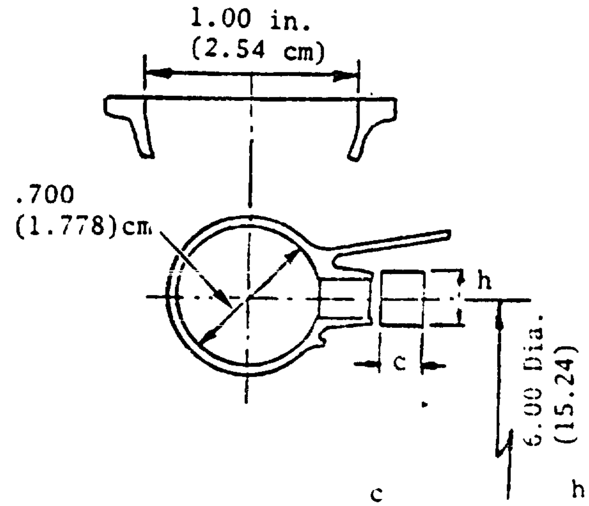

	c	h
Nozzle, in. (cm)	.300 (.762)	.258 (.655)
Rotor, in. (cm)	.220 (.559)	.303 (.770)

Figure 49. Mk-44-Oxidizer Turbine Design Parameters

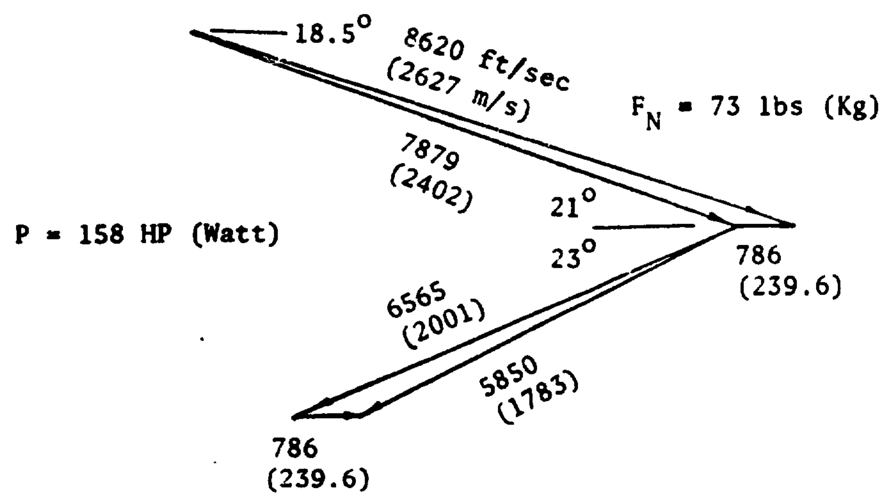

Power, HP (Watt)	HP	:	158 (117,821)
Speed, RPM (Rad/s)	N	:	30,000 (3142)
Gas Flow, lb/sec (Kg/sec)	$\dot{w}$	:	.288 (.1306)
Inlet Temp., F (K)	T_{1t}	:	1550 (1117)
Inlet Pressure, psia (N/m^2)	P_{1t}	:	270 (1,861,584)
Exhaust Pressure, psia (N/m^2)	P_{2s}	:	35 (241,317)
Pressure Ratio	PR	:	7.72
Efficiency, %	η_{ts}	:	24.3
Diagr. Correction	ϵd	:	.92
Admission, %	ϵ	:	49
Reynold's Number	Re	:	1.25×10^6

PRESSURE DISTRIBUTION:

Nozzle outlet: 35 psia (N/m^2) (241,317)

Rotor outlet: 35 psia (N/m^2) (241,317)

Figure 50. Mk-44 Oxidizer Turbine Velocity Vector Diagram (Nominal Operating Point)

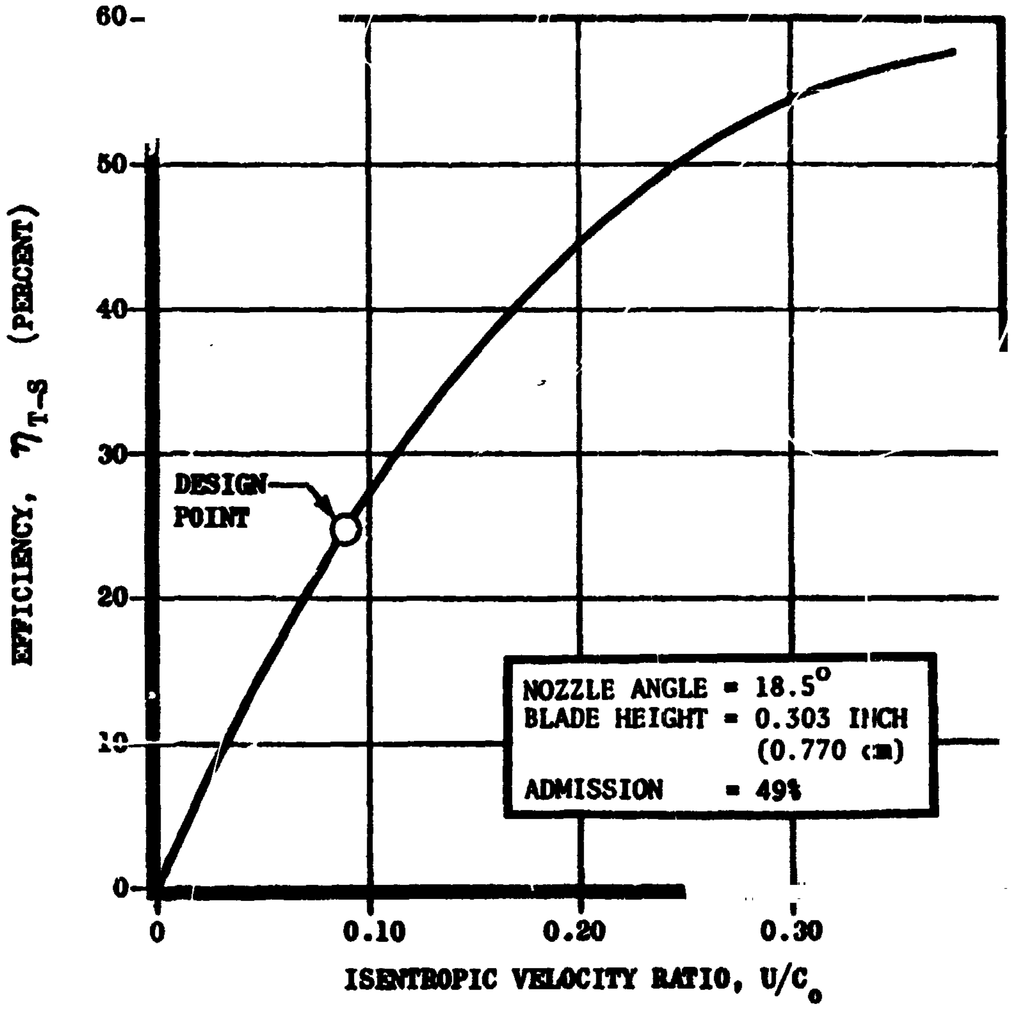

Figure 51. APS TPA MK-44 Oxidizer Turbine Estimated Efficiency

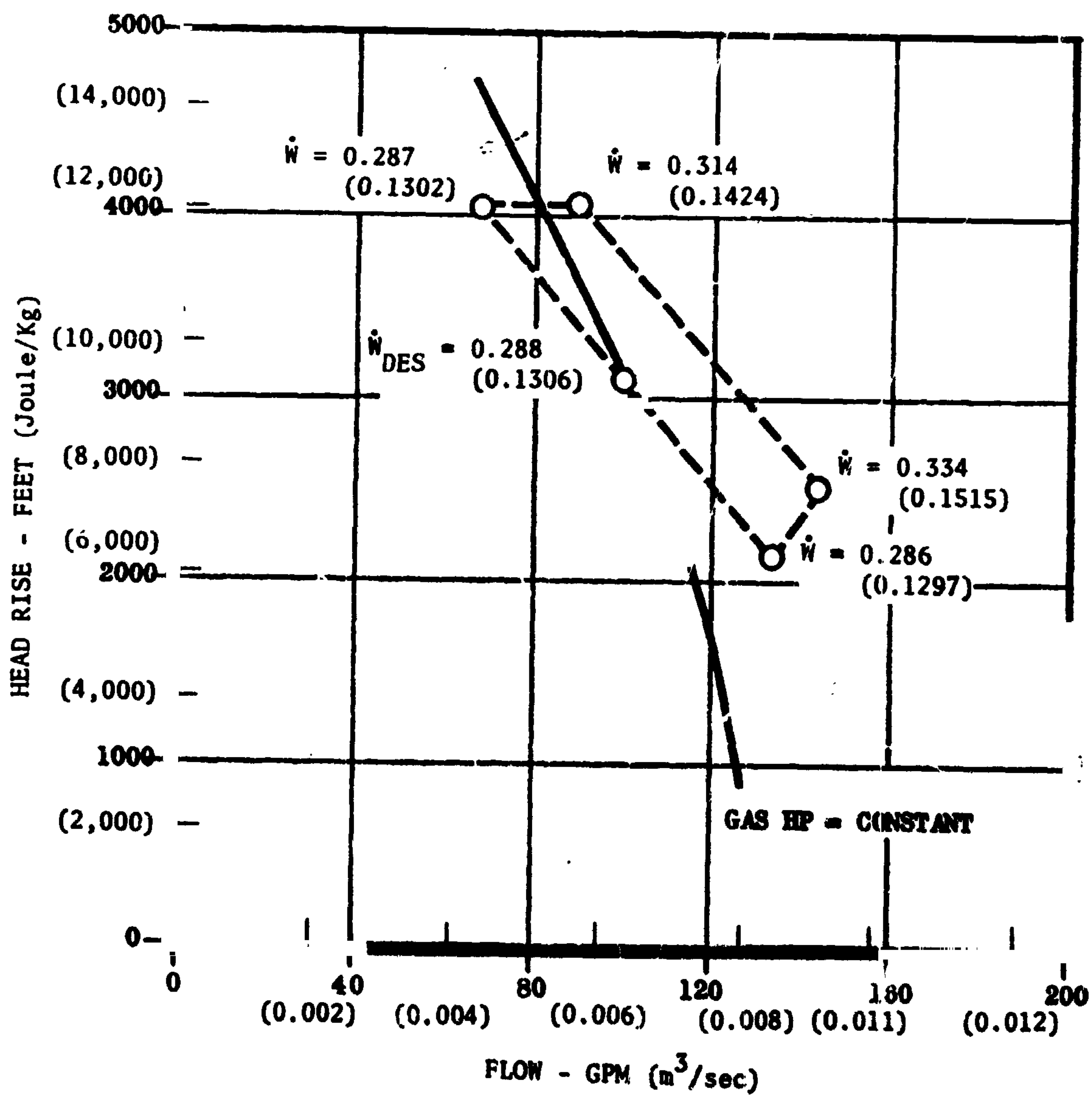

Figure 52. APS LOX Turbopump Turbine ẇ, lb/sec (Kg/sec)

Dangerous sustained resonant c nditions between nozzle excitation forces and blade variation frequencies must be avoided, particularly in the higher load range. The number of nozzles were therefore set so that at any nominal operating speed, the nozzle excitation frequency ZN (where Z equals number of nozzles and N equals RPS) and its second harmonic 2 ZN avoid close resonance with either the first or second tangential bending mode blade frequencies.

Blade Profiles and Solidities. It is usually advantageous to layout the different cascades with the smallest discharge angles that are possible. For the required discharge flow area, these angles are limited by the maximum blade heights that can be utilized, either because of the stress limitations, required overlaps, or the reasonable divergences of the meridional flow path.

Axial width of rotor blades were established by the following criteria:

1. Blade width in each stage must be such that basic gas bending stresses are sufficiently low and blade frequencies sufficiently high to avoid excessive vibratory stresses.
2. Blade width must be compatible with desired value of edge coeffifient, pitch-width ratio and opening coefficient

Trailing edge thicknesses are a reasonable minimum value consistent with adequate strength and fabrication ease. The edge coefficient of a blade row may be defined as $C_E = \frac{0}{0 + t}$ where C_E = edge coefficient, 0 = throat opening or width and t = trailing edge thickness or diamter.

Excessive wake losses may result if the edge coefficient falls much below 0.90. Leading and trailing edge divergence angles are as low as is consistent with edge strength and good flow area variation.

Trailing edge angles correspond closely to arc sin (0/p), where (0/p) is the opening coefficient or ratio of throat width to circumferential pitch. The gas efflux angle is controlled to a great extent by this ratio and a reasonable correspondence between trailing edge angle and arc sin (O/p) minimizes harmful separation losses along suction surface downstream from the throat.

The rotor blades have a supersonic relative velocity at the inlet. It has been shown through past experience with Curtis stages that rotor losses are not significantly increased. However, the blade profile must be thin with relatively sharp leading edges, and the blade inlet angle must correspond closely with the gas inlet angle. Ideally with small incidence angle a normal shock will occur at the rotor inlet. This increases the entropy and decreases the effective total pressure ahead of the cascade. The gas discharge angle of the rotor and stator blades are computed in accordance with the following relationship:

$$\mathrm{SIN}\ \beta_F = \frac{O}{p - \dfrac{t}{\mathrm{SIN}\ \beta_m}}$$

where:

β_F = discharge fluid angle measured from tangential direction

O = channel throat width normal to flow

p = pitch or blade spacing

t = blade trailing edge thickness

β_m = blade mean discharge angle measured from tangential direction

The solidities of the blading selected for this design and the number of blades in each cascade are shown in Fig. 53.

<u>Blade Profile Design</u>. The significant dimensions and angles used to control the profile design are illustrated in Fig. 54 through 57. The most important parameter is the opening coefficient, which is defined as the ratio of the minimum

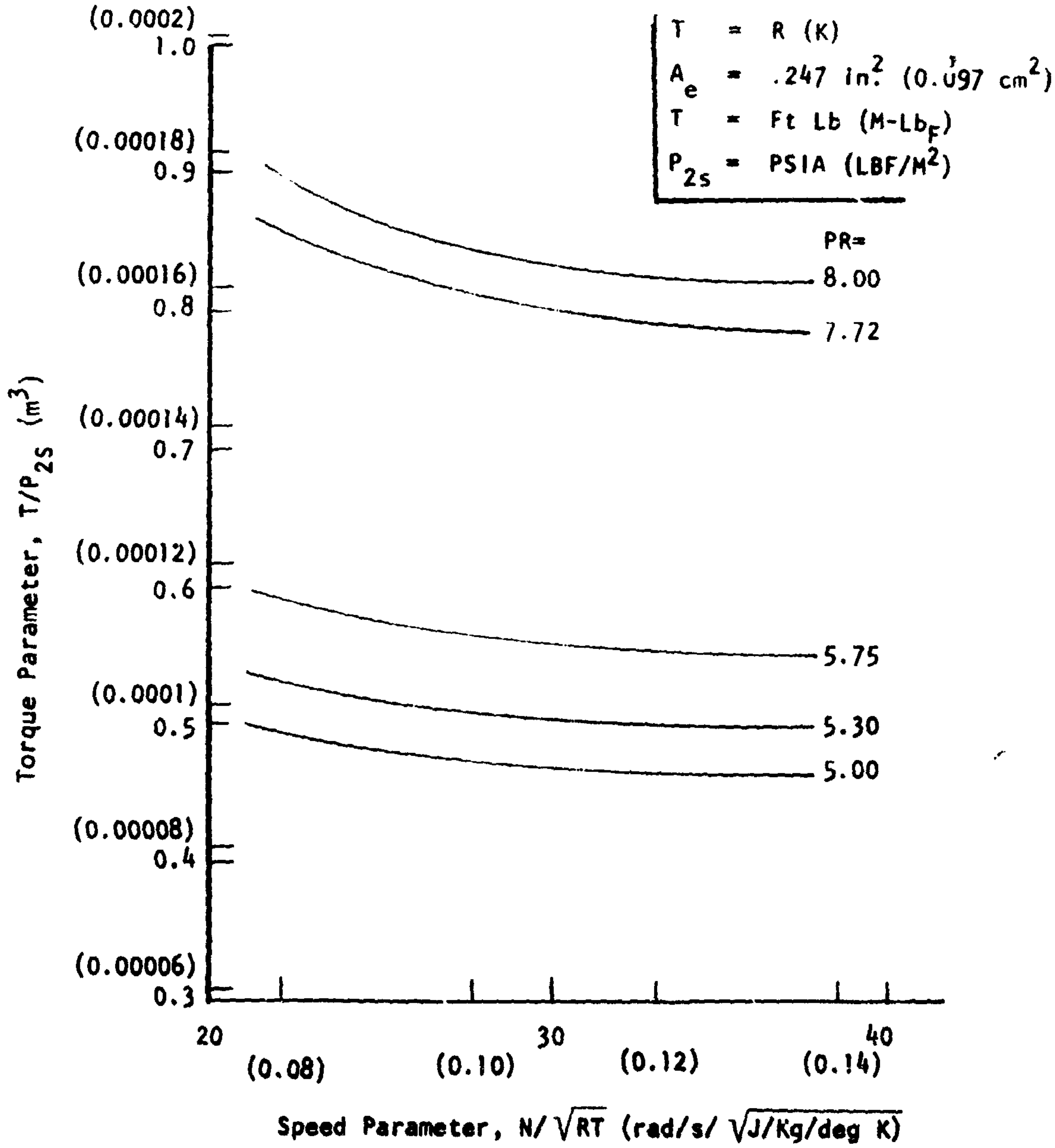

Figure 53. Mk-44 Oxidizer Turbine (Estimated Performance)

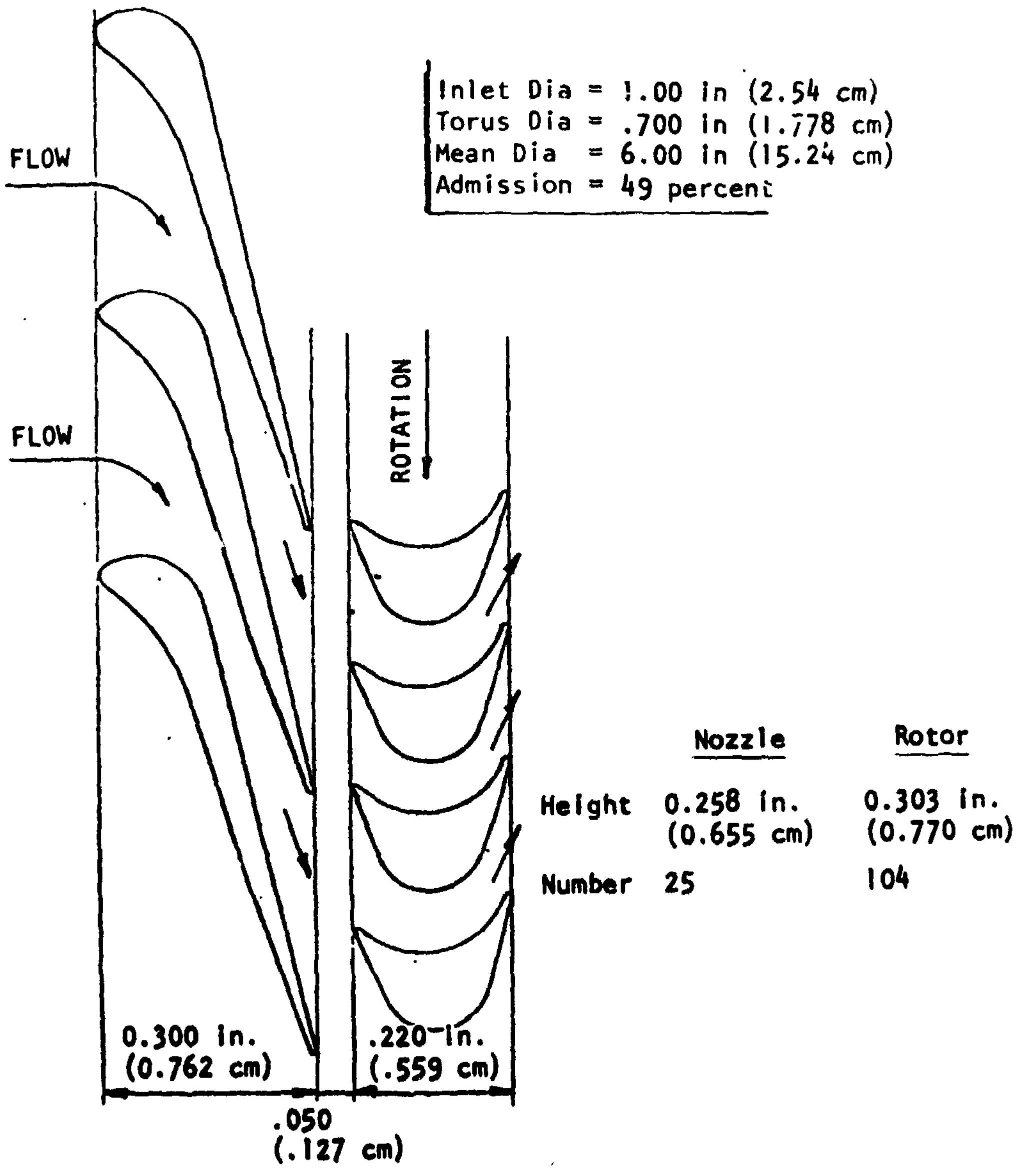

Figure 54. Mk-44 Oxidizer Turbine Gas Path Profile Sketch

Mean Dia	=	6.00 in (15.24 cm)
No. of Nozzles	=	51/25
Nozzle Height	=	.258 in (.655 cm)
Fillet Radii	=	.020 in (.051 cm)

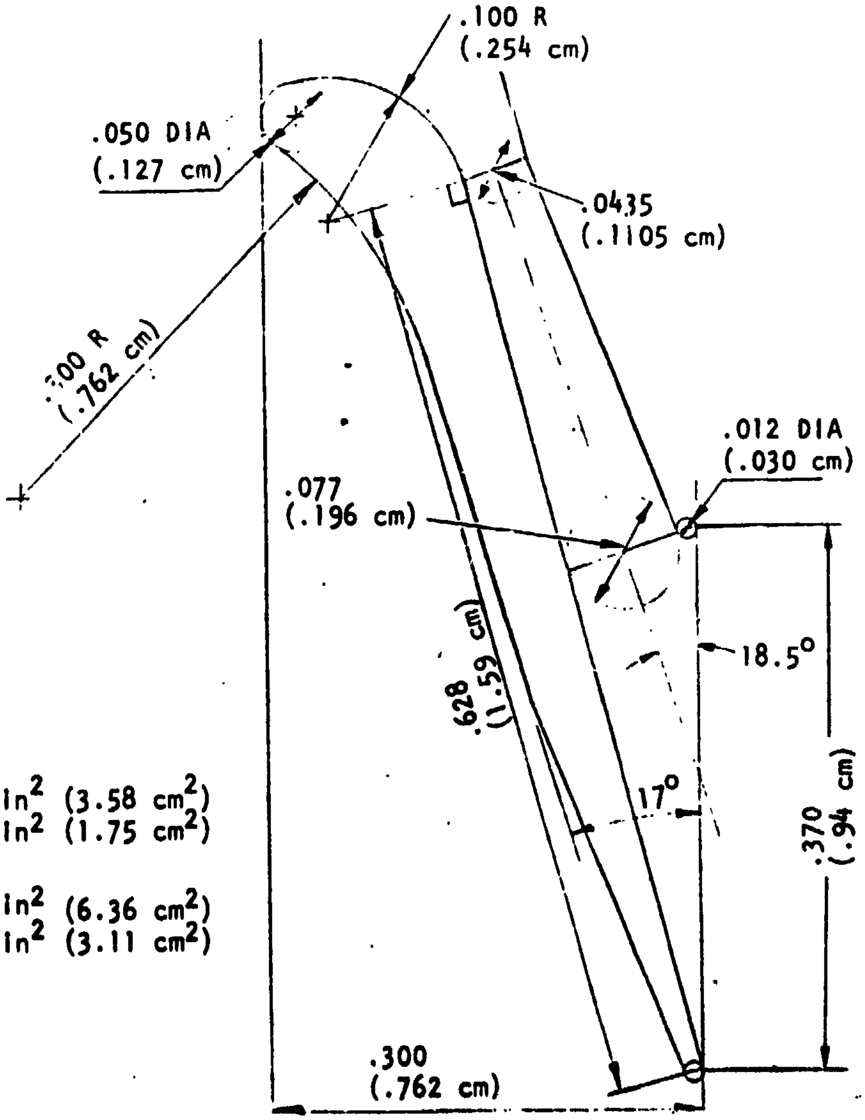

Area ± 5 percent

Throat:
- Fuel = .555 in^2 (3.58 cm^2)
- Lox = .271 in^2 (1.75 cm^2)

Exit:
- Fuel = .986 in^2 (6.36 cm^2)
- Lox = .482 in^2 (3.11 cm^2)

Figure 55. Nozzle Profile Sketch

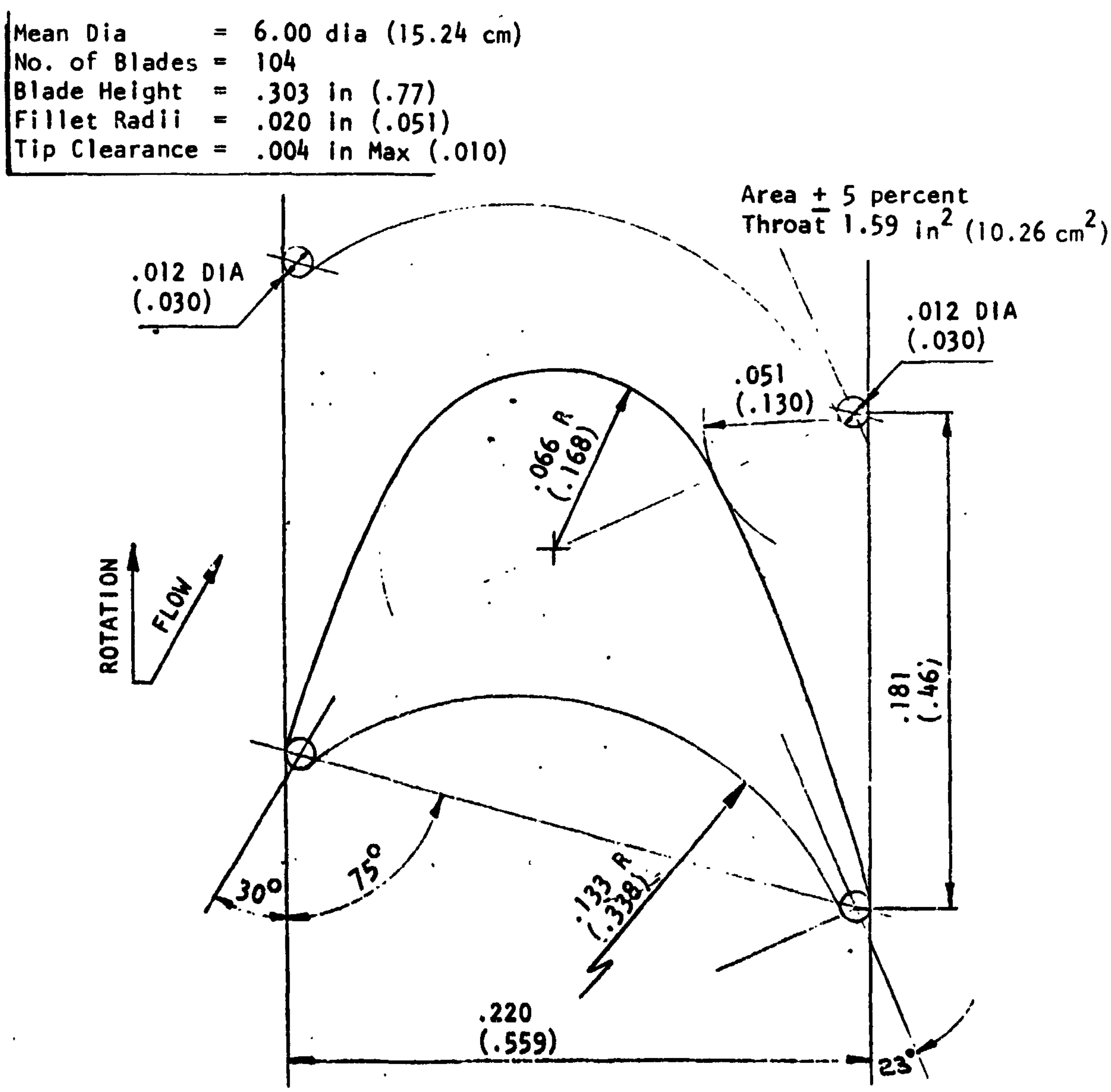

Figure 56. First Rotor Profile Sketch

Inlet Dia, in. (cm) D_I = 1.00 (2.54)

Torus Dia, in. (cm) D_t = 0.700 (1.78)

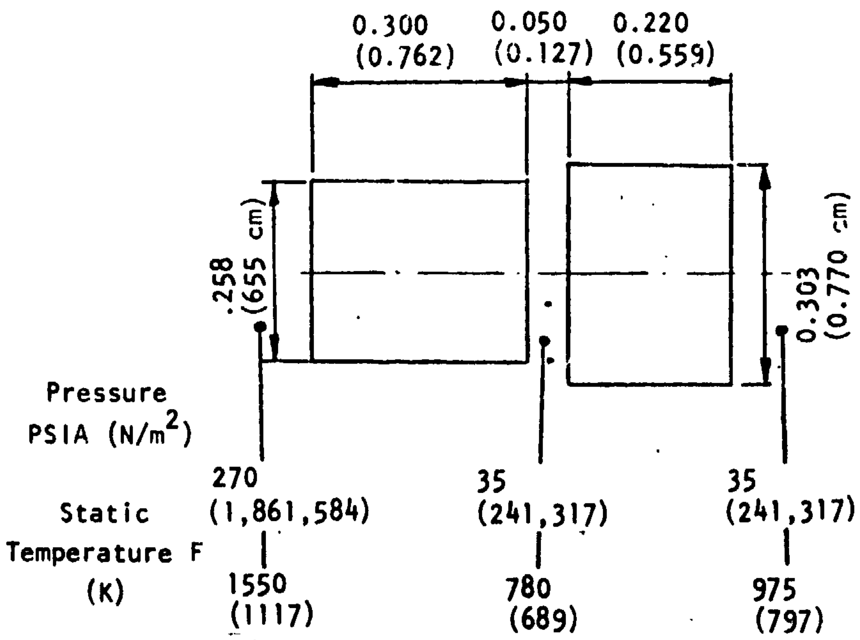

Design Parameter:

Inlet Temp, F (K)	T_{it}	=	1550 (1117)
Inlet Press, psia (N/m^2)	P_{it}	=	270 (1,861,584)
Press Ratio	PR	=	7.72
Speed, rpm (Rad/s)	N	=	30,000 (3142)
Mean Dia, in. (cm)	D_m	=	6.00 (15.24)
Flowrate, lb/s (Kg/s)	ω	=	.288 (.1306)
Horsepower (Watt)	HP	=	158 (117,821)
Efficiency, percent	η_{ts}	=	24.3
Admission, percent	ϵ	=	49

Figure 57. Oxidizer Turbine Gas Path

passage width or throat opening between adjacent blades to the circumferential pitch of the blades. Control of both flux angle and mass flow is exerted pr[illegible]y by means of the opening coeffi[illegible]. Since the integrated mean opening coefficient for a blade row also represent[illegible] the ratio of total throat area to annular area, mass flow through a bla[illegible] [illegible] height may be increased or decreased by corresponding changes in opening [illegible]ent.

Blading performance is affected [illegible] [illegible]ge extent by the aerodynamic loading on the profiles. The resultant for[illegible] [illegible]ing on a profile corresponds to the integrated pressure differences between the convex and concave surfaces. In closely pitched blades, these pressure differences and their accompanying turbulence losses are reduced. However, losses due to surface friction are thereby increased. Wide pitching decreases surface friction loss, but aerodynamic loading is increased. This may induce stalling with a rapid drop in performance.

Aerodynamic loading is a function of the cascade solidity on chord/pitch ratio. The permissible ranges of blading solidity for standard profiles have been fairly accurately established by test.

Blade Layout. Required blade pitches, throat opening and axial width or chords are established. Profiles are then laid out with the following considerations for guidance.

1. The stress in a blade due to centrifugal force is proportional to the blade volume. Profile thicknesses and cross sectional areas must therefore be closely controlled.
2. Geometric inlet and outlet angles are set at approximately the desired fluid angles. Exact correspondence is not necessary and is seldom obtained. Variations of up to three degrees are permitted for geometric outlet angles and as much as ten degrees for geometric inlet angles. (Closer tolerance for sup[illegible]rsonic)
3. Profile nose design depends upon stress conditions and fluid velocities

It is considered essential that the passage area between adjacent blades converge in the direction of flow at all points. In addition, the walls of the passage as formed by the blade surfaces are kept free of sharp changes in radius and curvature. The actual contours of the profiles are described by combination of circular arcs and parabolic arcs. Blade surface velocity distribution was computed using the stream filament method for compressible flow.

Flow Area Calculations. The determination of the correct flow areas is the most important step in the design of an efficient turbine. If these flow areas are wrong, the pressure downstream of the blade rows will differ from those used in the velocity diagram. This will cause the approach velocities of the following blade row to have fluid angles that deviate from the blade angle design and this will reduce the performance of the turbine.

Velocity Distribution and Blade Profile. The blade surface velocity distribution was computed using the Douglas-Neuman program, and local velocities relative to inlet and exit average velocities were determined on the suction and pressure side of the blade (Fig. 58).

LO_2 Turbopump Materials and Structural Analysis

The selection of materials for the LO_2 turbopump components is indicated in Fig. 59. The principal criteria for choosing the materials in the pump were. strength and ductility at cryogenic temperature, LOX compatibility, resistance to corrosion, thermal contraction coefficient and machineability. Similarly for the turbine components strength and ductility at the operating temperature, resistance to corrosion and ease of fabrication were weighed. Hydrogen embrittlement was not a factor in selecting turbine materials because the pressures were moderate 1,861,584 N/m^2 (270 psia) and the gas temperature 1128 K (2030 R inlet) was above the sensitive range. Thermal conductivity of the materials was considered in the pump and turbine materials to meet the heat soakback limitations.

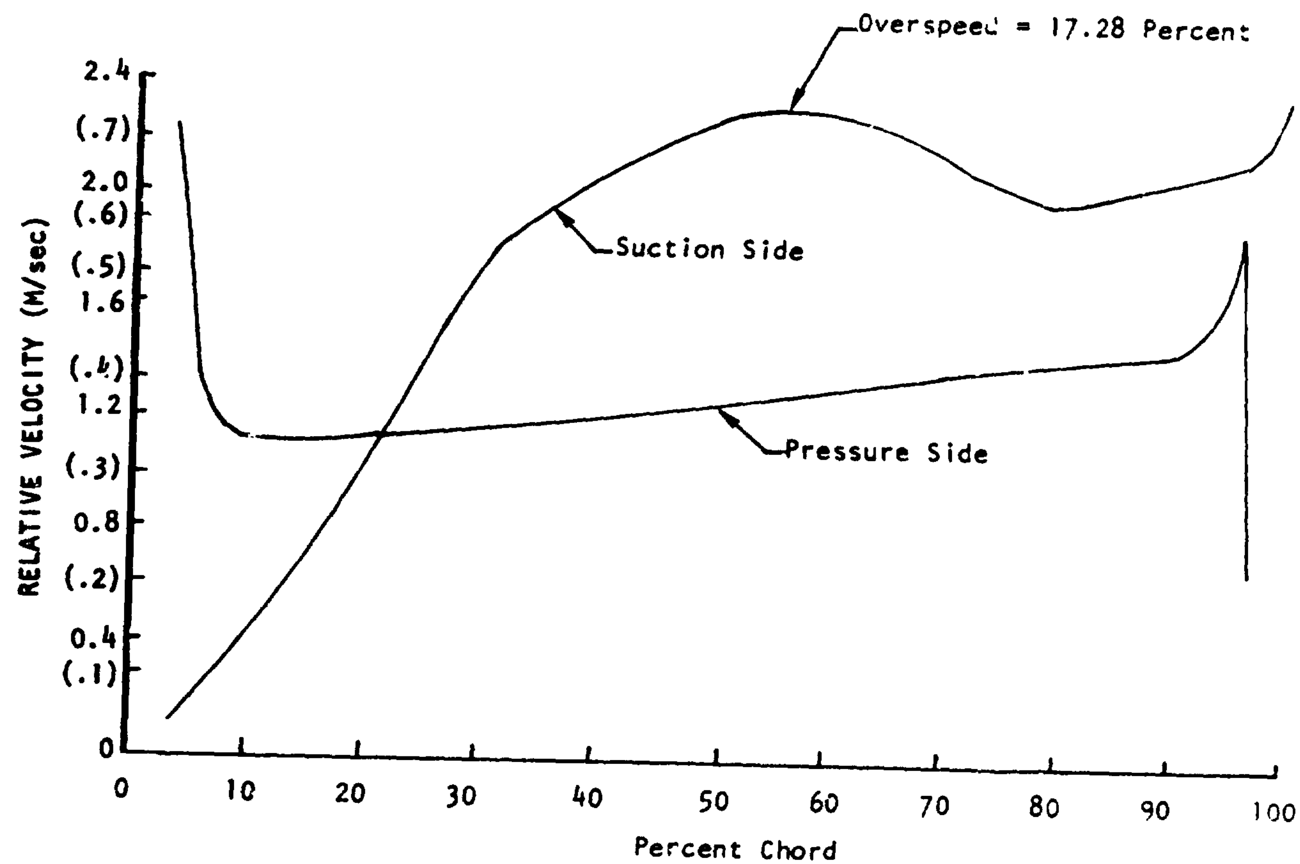

Figure 58. Blade Surface Velocity, First Rotor

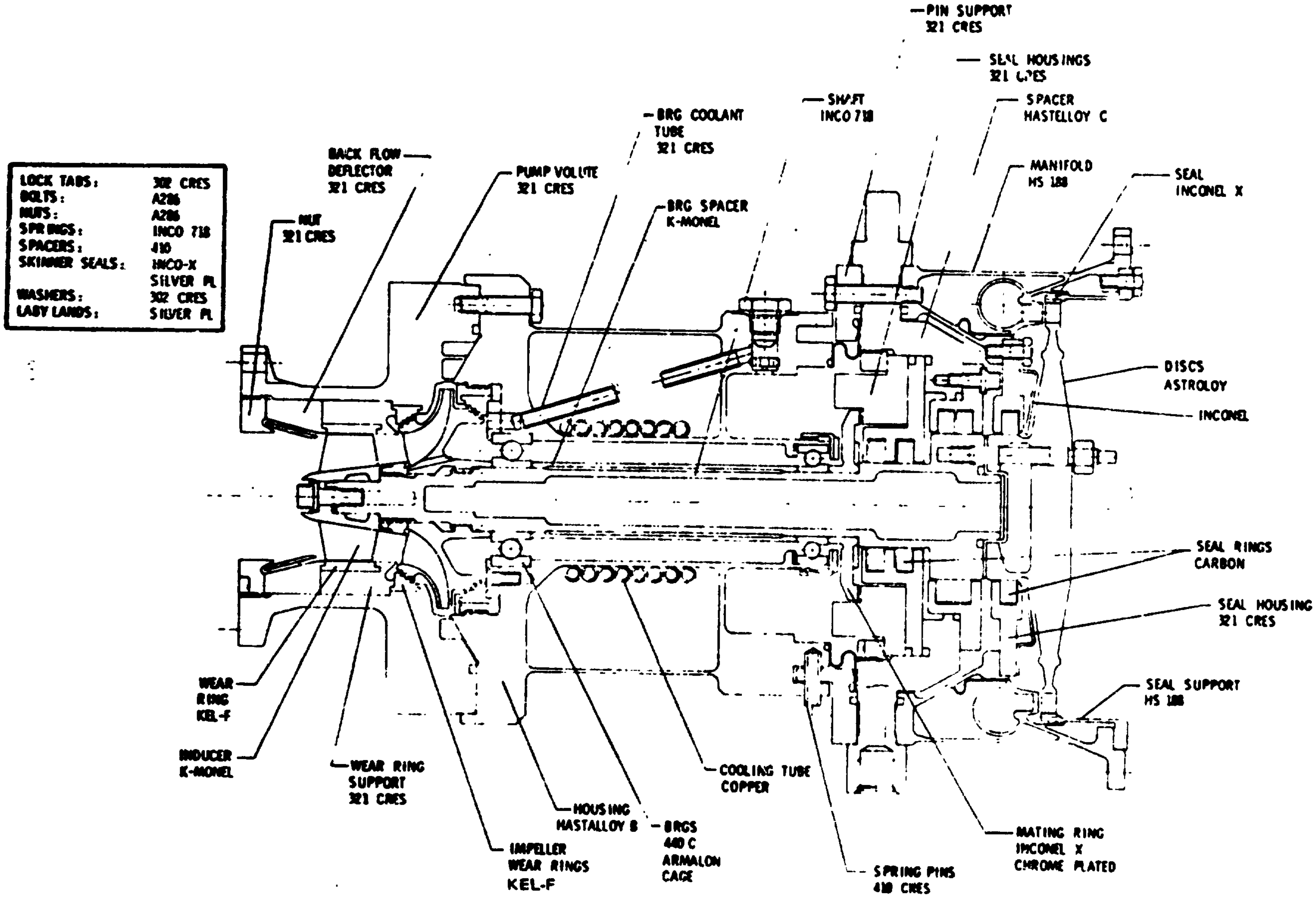

Figure 59. APS LO_2 Turbopump Materials

The combination of mean and alternating stresses for the inducer are shown in the Modified Goodman diagram presented in Fig. 60. The mean stress is the algebraic sum of the direct centrifugal, centrifugal bending, and pressure bending stresses. The alternating stress is assumed equal to 30 percent of the pressure bending stress based on Rocketdyne experience. The operating point indicated on the modified Goodman diagram is the highest stress location which occurs on the vane pressure side at the vane-hub junction at the wrap angle where the leading edge profile reaches full diameter. The blade is canted 10 degrees forward to partially cancel the pressure bending stress with centrifugal bending stress. The operating point lies within the allowable operating area.

Similarly, the Modified Goodman diagram for the impeller is presented in Fig. 61.

The vane was analyzed at three wrap-angle increments corresponding to the leading edge of the full vanes, the leading edge of the partial vanes, and the vane trailing edge. The highest mean stress occurs on the suction side of the vane at the vane-hub junction where the direct centrifugal and centrifugal bending stresses are tension and the pressure bending stress is compression. The stress values lie within the allowable area.

In Fig. 62 the allowable nozzle annulus area times speed squared limits for Astroloy as a function of temperature are presented, and the oxidizer turbine operating point is shown. The annulus area-speed squared parameter is a measured of the turbine blade direct centrifugal stress. Pressure bending stress, which results in alternating stress, subtracts from the allowable centrifugal stress as indicated on the curve. The blade weight factor of 1.0 indicates that the blade centrifugal weight is based on 100 percent of the stress area times the blade height. (The blade is not tapered or hollow.) At the higher temperatures, the allowable stress is limited by stress rupture rather than the short-time strength. The operating point lies well below the allowable curve.

In interference diagram shown in Fig. 63 the turbine blade natural frequency in cycles-per-second is plotted against turbopump speed. The dotted line closest to

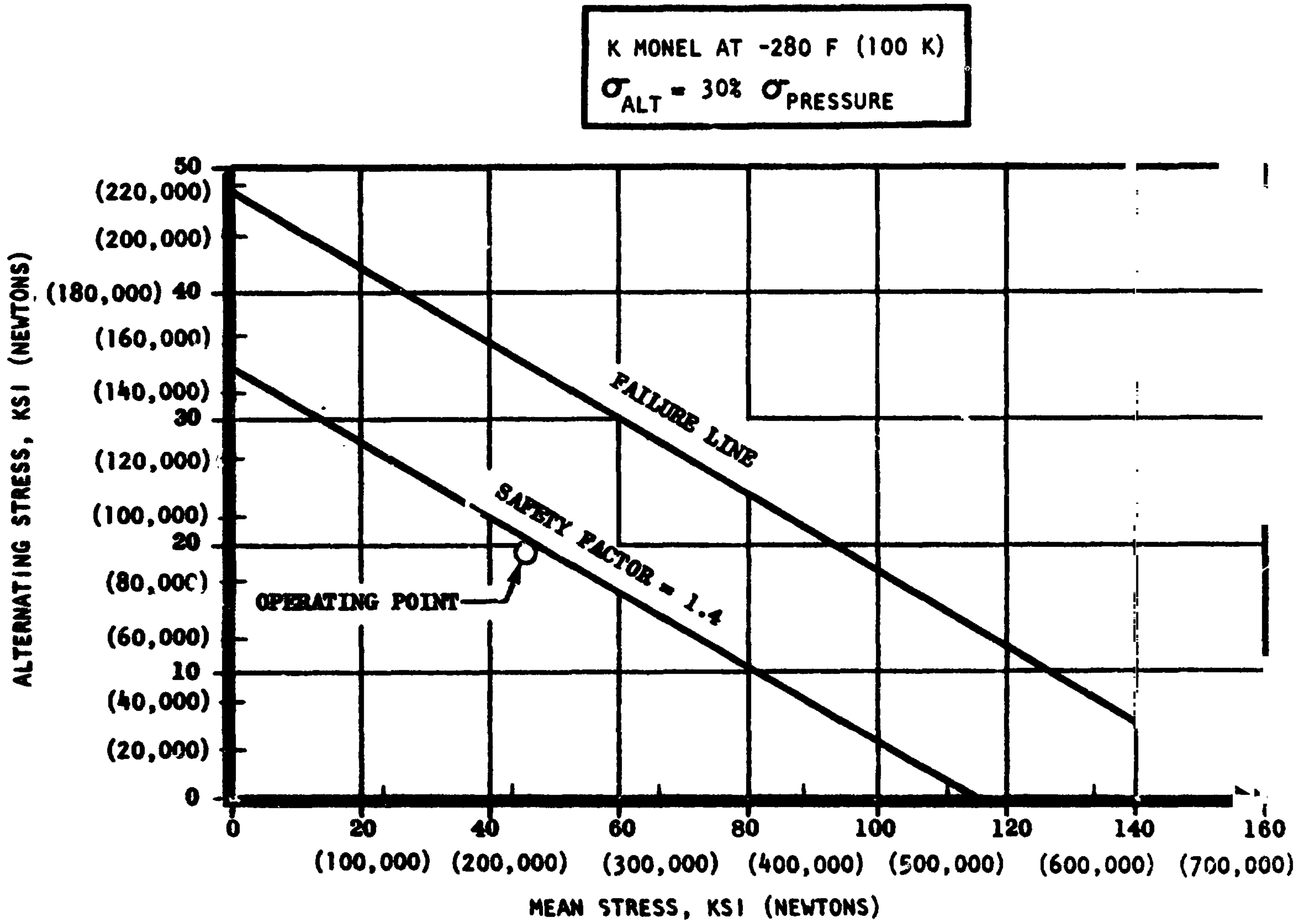

Figure 60. APS Oxidizer Inducer Blade Modified Goodman Diagram

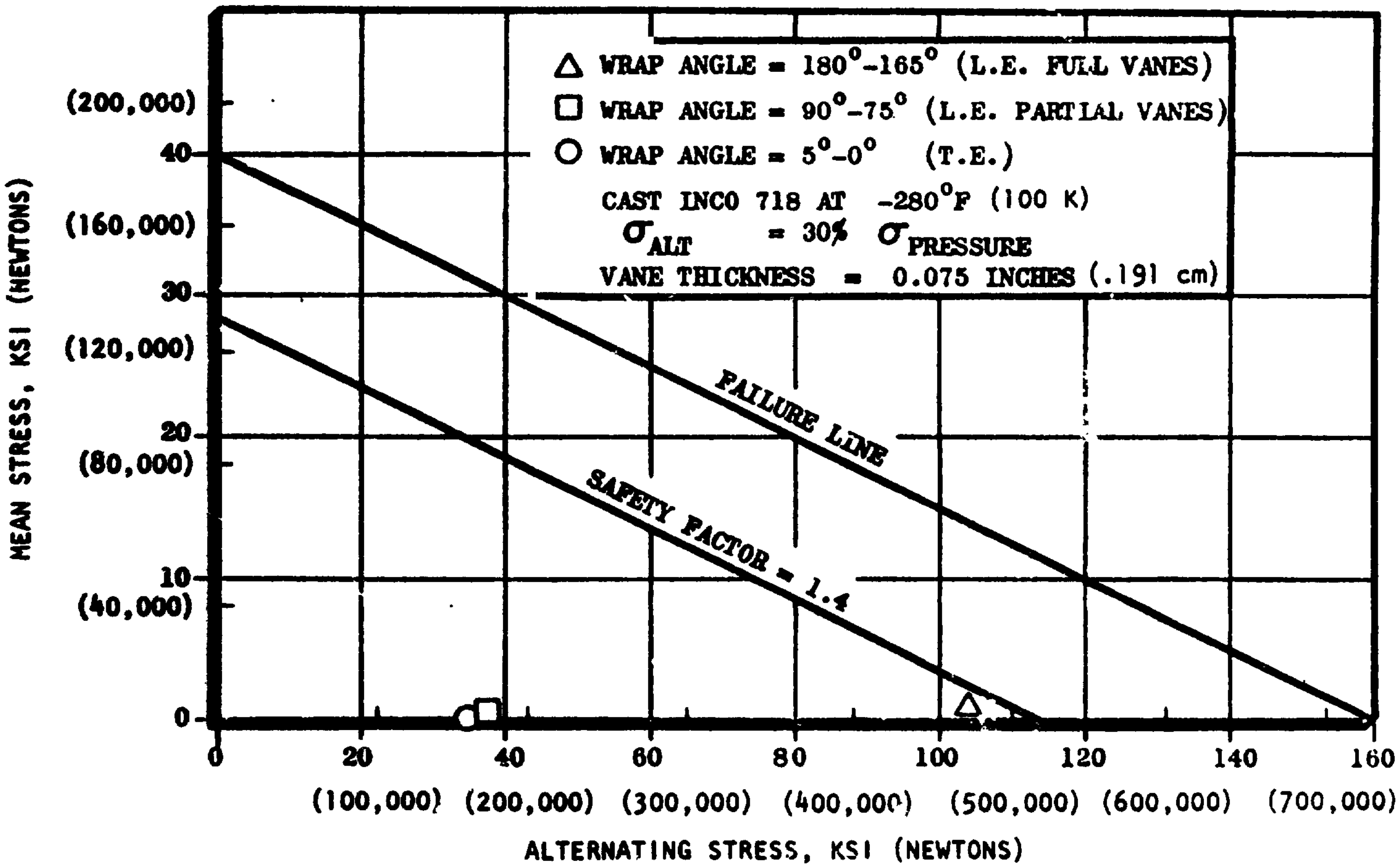

Figure 61. LOX Impeller Blade Analysis Modified Goodman Diagram

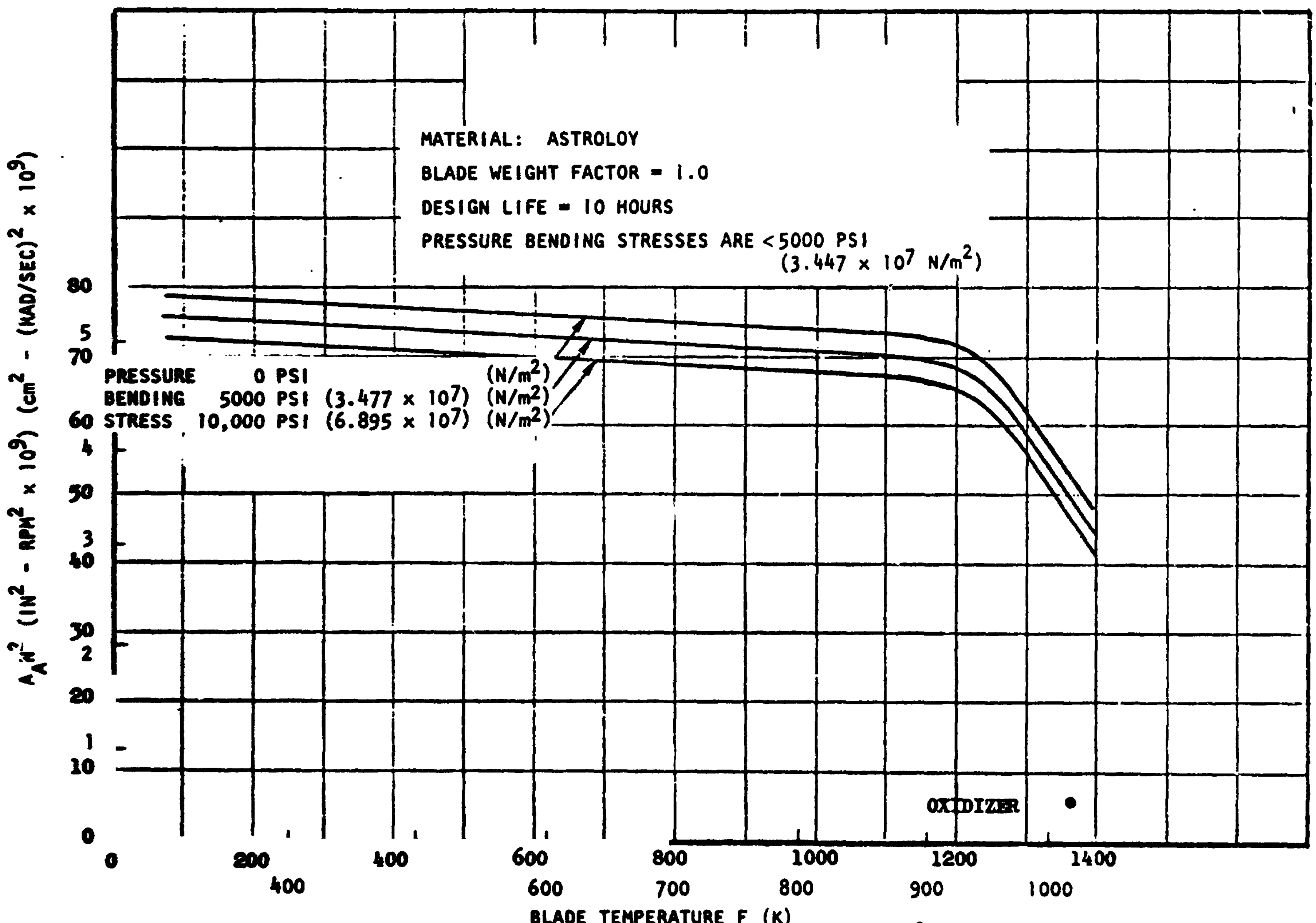

Figure 62. APS Oxidizer Turbine Blade Allowable $A_A N^2$ vs Temperature

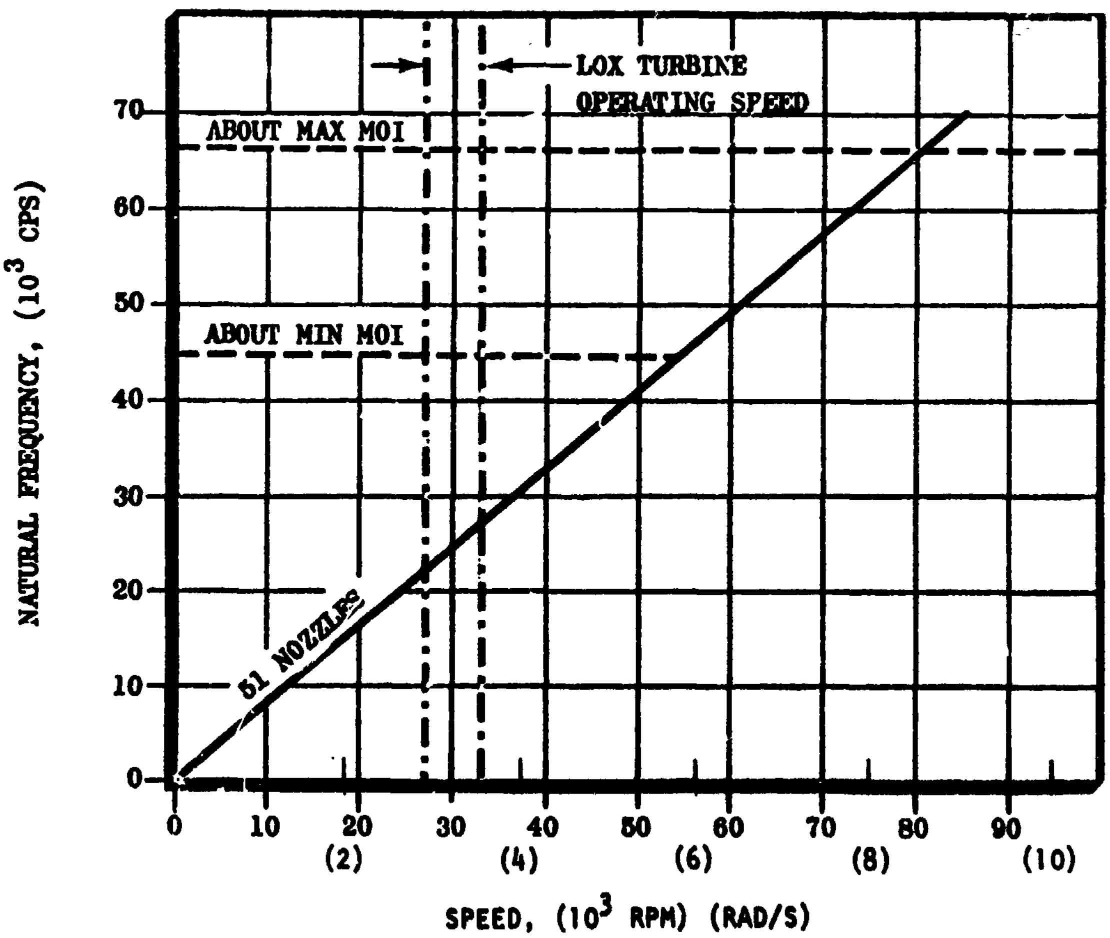

Figure 63. Oxidizer Turbine Interference Diagram
MK-44F First Stage Rotor

the top of the figure represents the blade natural frequency about the blade maximum moment of inertial (axial) and the lower dashed line the blade natural frequency about the minimum moment of inertial (tangential). The vertical dashed lines show the operating range of the turbopump in rpm and the solid line represents the nozzle forcing frequency. As can be seen, the nozzle forcing frequency is well below the natural frequencies of the blades in the operating range.

Rotordynamic Analysis

The critical speeds of the rotor were calculated using a finite element method. The shaft was approximated as a series of concentrated masses and inertias connected by elastic beam elements. Forward synchronous precision was assumed and the bearings were modeled as linear springs to ground. The gyroscopic effect of each rotating mass was included.

The first and second critical speeds are shown in Fig. 64. Critical speed is plotted against the turbine bearing spring rate for two different pump bearing spring rates; 0.35×10^6 N/cm (0.2×10^6 oz/in.) represented by the solid line and 0.876×10^6 N/cm (0.5×10^6 oz/in.) shown by the dashed line. The turbine bearing spring rate will be established at approximately 3.5×10^5 oz/in.), which is shown by the dotted line. The operating envelope of the turbopump is represented by the cross-hatched area and, as can be seen, turbopump operation is well out of the range of both the first and second critical speeds.

The shaft mode shape of the oxidizer turbopump at the first and second critical speed is shown in Fig. 65. Normalized radial deflection of the shaft is plotted as a function of axial location with the pump and turbine bearings located by the circles. As can be seen, there is some shaft bending present in both critical speeds-at the turbine end of the shaft at the first critical and at the pump end of the shaft at the second critical.

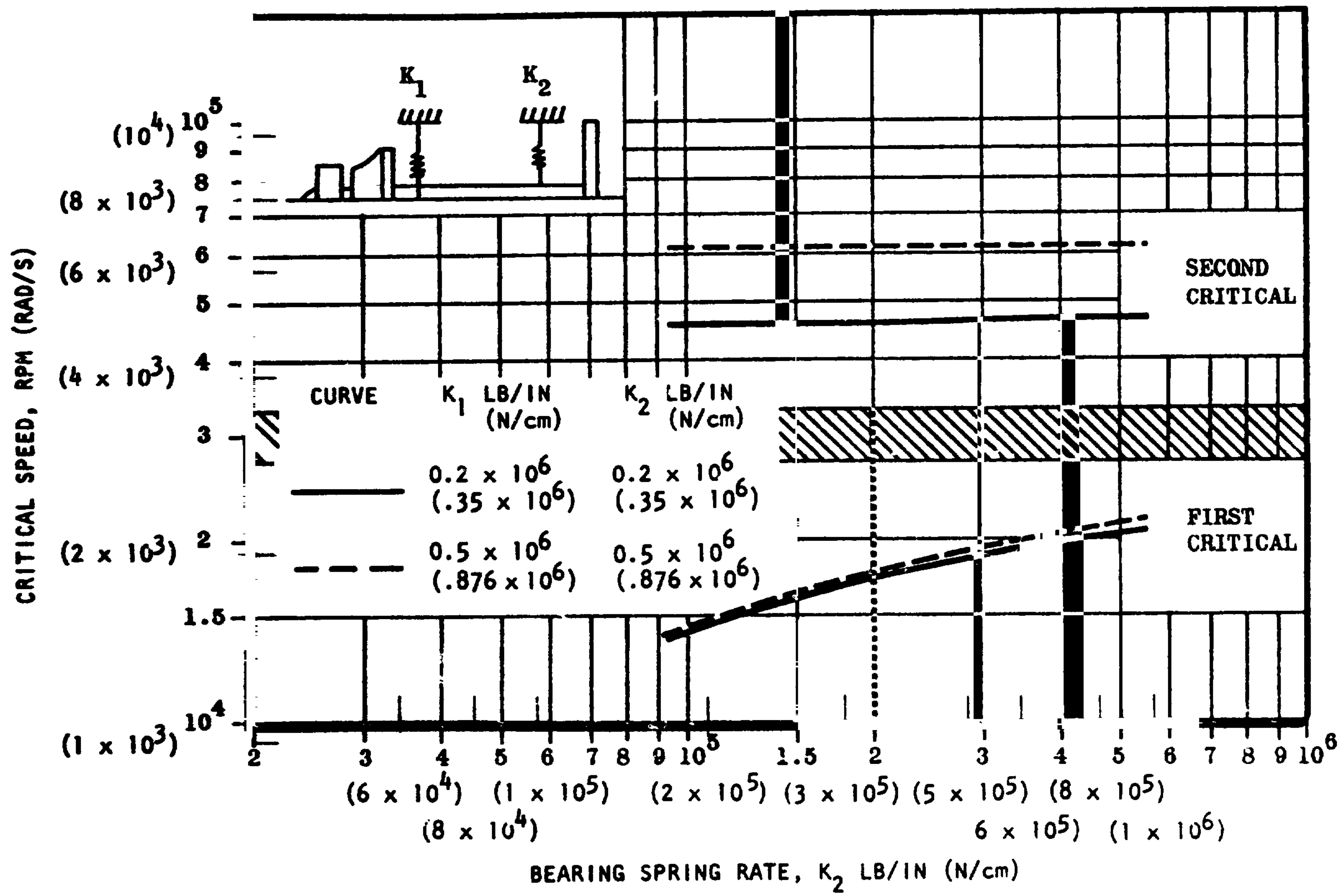

Figure 64. APS LOX Pump Critical Speeds

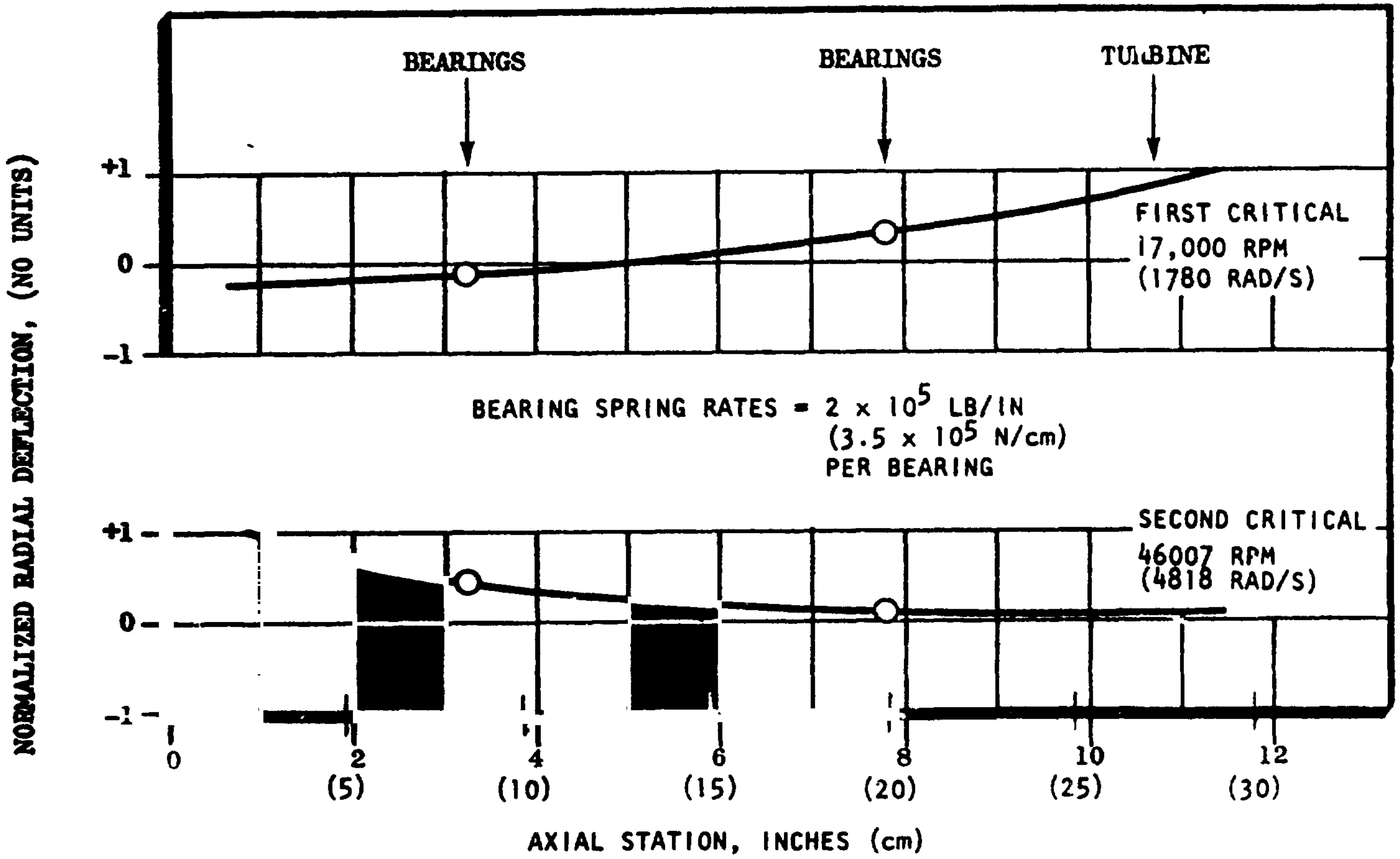

Figure 65. APS LOX Pump - Mode Snapes

Bearings and Seals

The oxidizer pump shaft is supported by two 25-mm ball bearings. The turbine end bearing is the extra light series (105) and the pump end bearing, which will take the turbopump unbalanced axial loads is a light series (205) which has a larger thrust capacity than the 105. Figure 66 shows the calculated B-1 life for the two types of bearings plotted against axial load. The maximum axial load in the 105 bearing is merely the locked-in pre-load of 89 to 222.4 N (20 to 50 pounds). As can be seen, B-1 calculated life is far in excess of the required 10 hours.

The cage material selected for the bearings of the oxidizer turbopump is Armalon, which is a glass fabric-supported teflon. This material has been successfully used for cages in the liquid oxygen and liquid hydrogen bearings for the J-2 and and J-2S turbopumps and in the liquid hydrogen nuclear turbopump. Several sets of bearings with Armalon cages have been operated for over 14 hours in liquid oxygen in a bearing and seal tester and exhibited very little wear and no deterioration. Figure 67 shows the tensile yield strength of the Armalon versus temperature, which shows that the material has quite adequate tensile strength over the range of turbopump operating temperatures.

Figure 68 shows the oxidizer turbopump seal package which consists of a liftoff seal, a primary LOX seal, a purged intermediate seal, and a turbine seal. Also shown schematically in the figure by the arrows are the paths of the leakage and purge flows during turbopump operation. At the left of the figure, liquid oxygen flows through the open liftoff seal and leaks through the primary LOX seal to a drain cavity from which it is purged by helium gas to a separate overboard drain. The purge gas pressure is kept at a level sufficient to assure flow and is always as shown by the arrows and thus the liquid oxygen is always kept separated from the hydrogen-rich turbine gases.

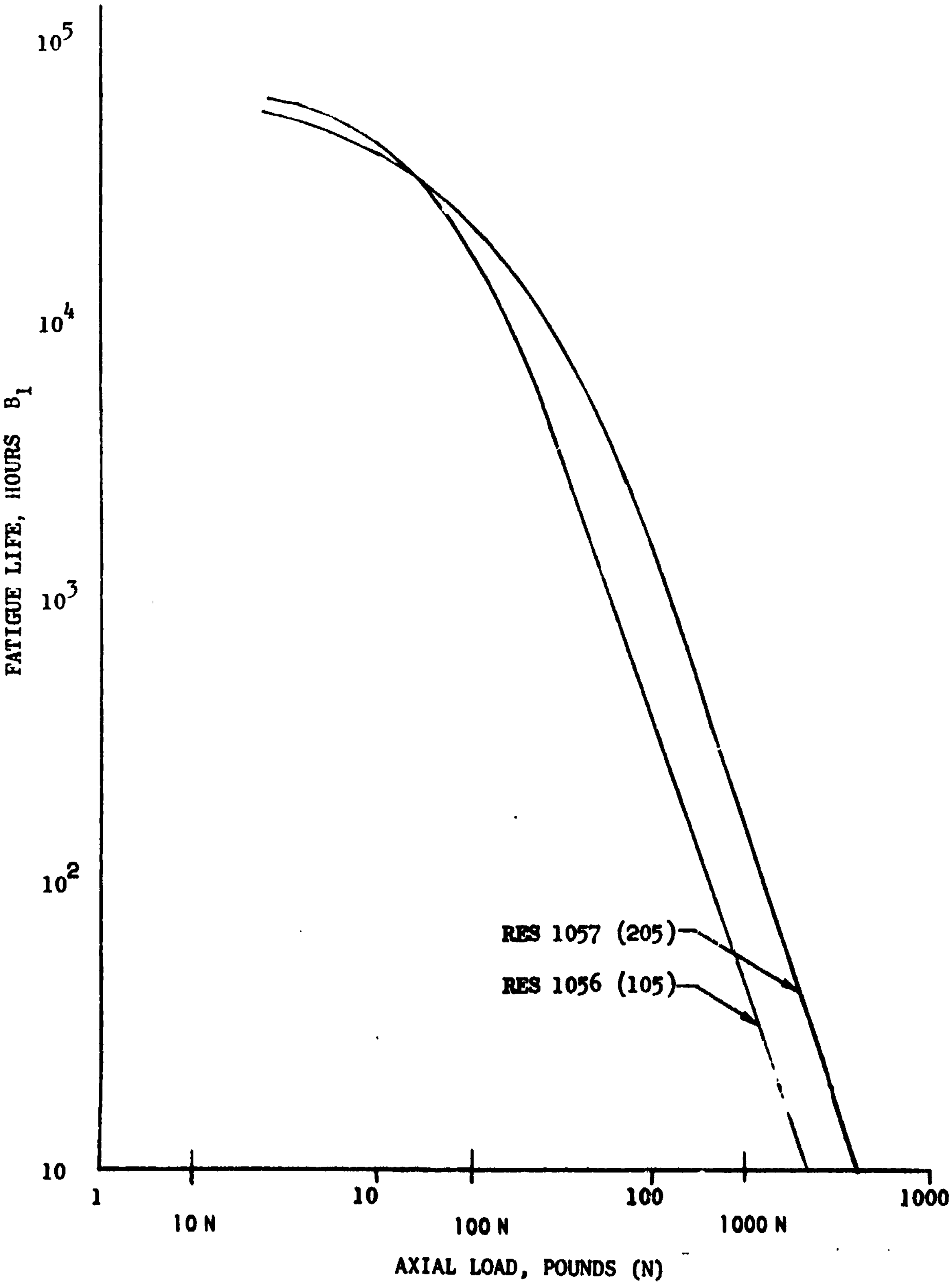

Figure 66. APS LO_2 Pump Bearings Life vs Load at 30,000 rpm (3142 Rad/s)

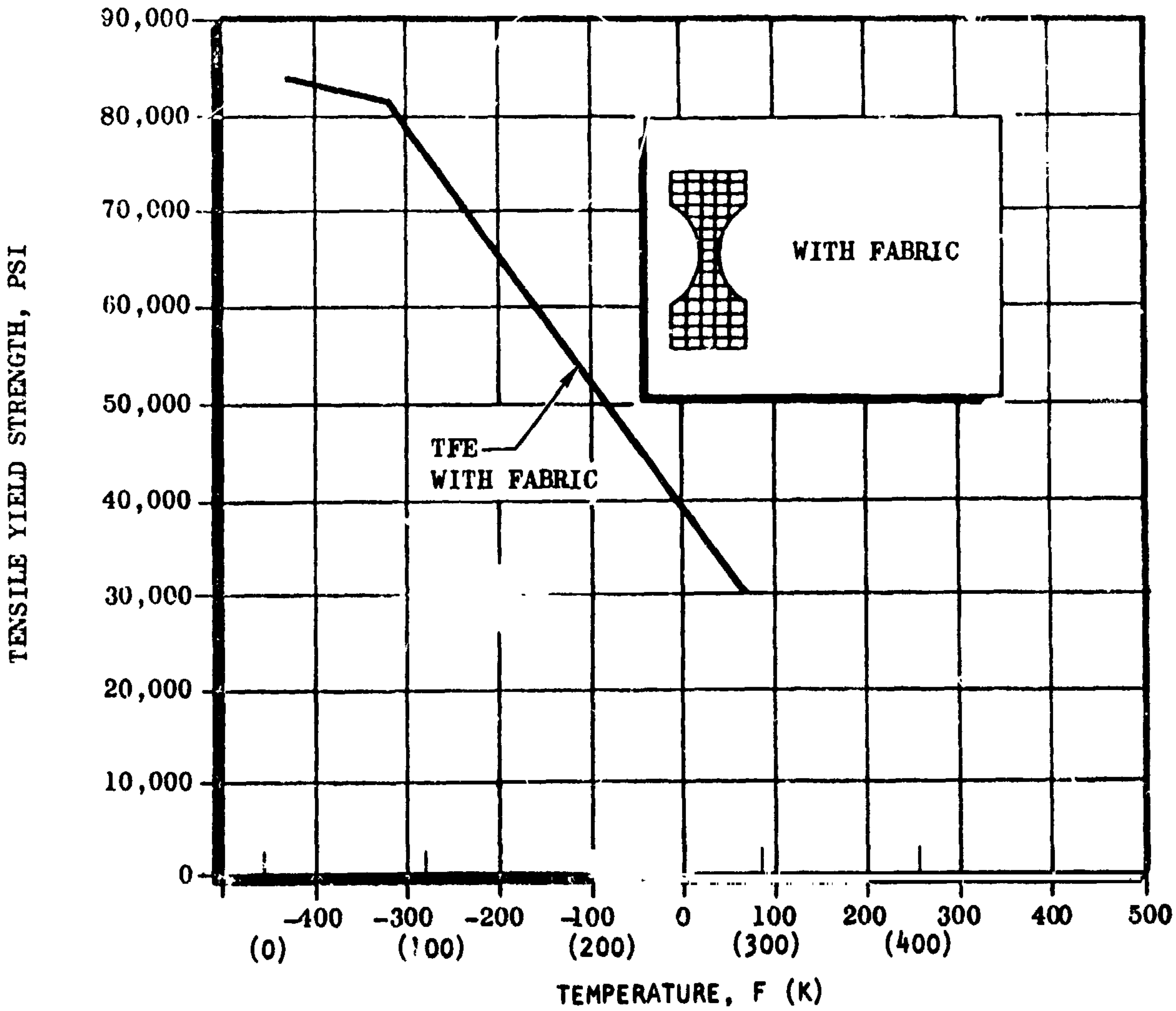

Figure 67. Effect of Temperature on the Tensile Yield Strength of Glass Fabric Reinforced Teflon

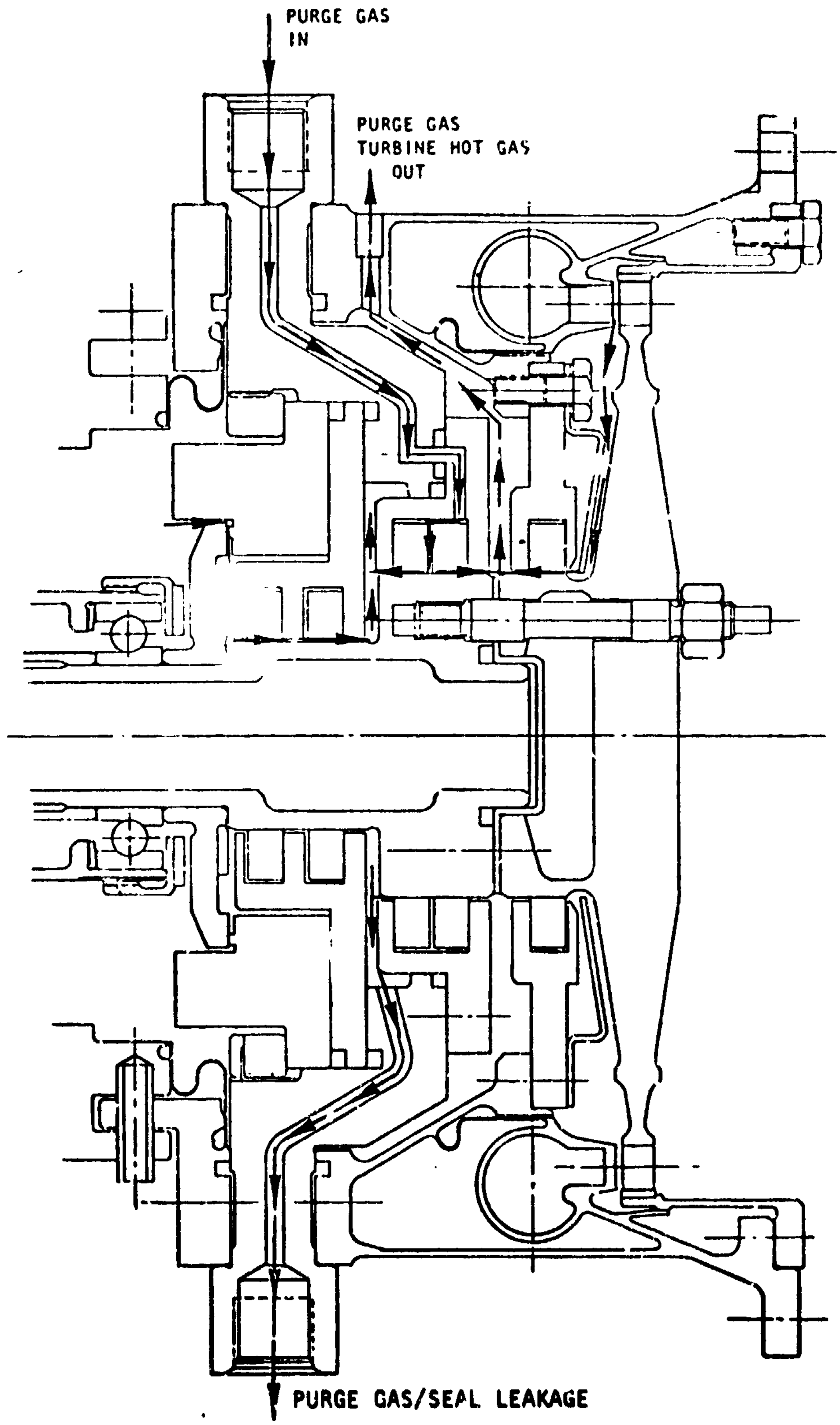

Figure 68. Oxidizer Turbopump Seal Package

Heat Transfer

The significant thermal features of the LOX turbopump design are:

1. Low conductivity material used for most parts (Hastelloy B, CRES 321
2. High thermal resistance joints used throughout
   a. Minimum contact area pump flange
   b. Pin joint and bellows between turbine flange and conical support
3. Ball joint TPA mount to vehicle
4. External cooling can be utilized in a number of ways
5. Heat leak to pump housing below 52,752 Joule/hr (50 Btu/hr) with zero external cooling

The lumped parameter thermal soakback model shown in Fig. 69 was used to evaluate the LO_2 turbopump designs. The model uses 15 modes to represent the turbopump and six flow nodes to represent the leakage flowrate. Solutions were obtained for the various designs using the Rocketdyne Differential Equation Analyzer Program (DEAP) to solve for the nodal temperatures and the quantity of energy reaching the pump body.

The major assumptions used in analyzing the turbopump design were:

1. TPA has been run to thermal equilibrium
2. Environment temperature is 300K (540 R)
3. Pump housing and cone are insulated with 1 inch of super insulation
4. Exhaust duct is also insulated and has a long L/D
5. Heat transfer coefficients for bleed and leakage flows based on hD/K = 2

These assumptions were made in conjunction with a long (10-hour) soakback period to evaluate various possible configurations for the turbopump. Although a 10-hour

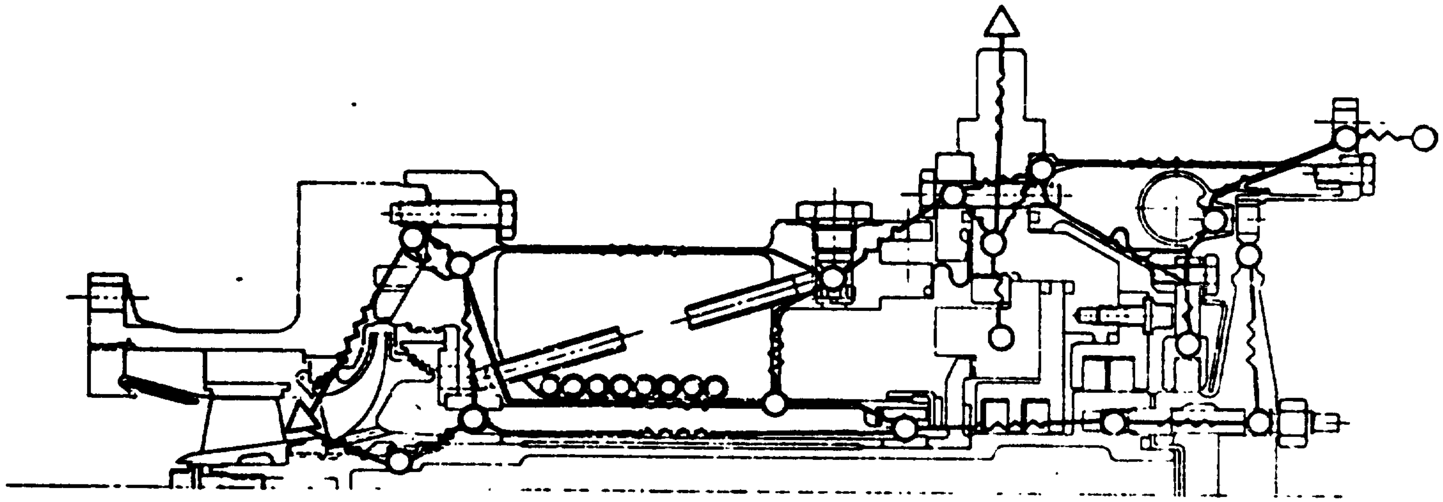

Figure 69. LO_2 TPA Thermal Model

soakback period is not likely to occur, the behavior of the turbopump under these conditions gives a worst case prediction for design since the 10-hour soakback period is long enough to reach the peak heat leak value for the designs. The cases analyzed included:

1. No external cooling -- 0.24 kg/hr (0.45 lb/hr) seal leakage assumed for O_2 pump
2. No external cooling -- no leakage
3. 0.113 kg/hr (0.25 lb/hr) H_2 coolant flow assumed for external cooling

The predicted soakback behavior of the LO_2 turbopump following a steady-state run for the case of nominal liftoff seal leakage and no external cooling is shown in Fig. 70. The predicted maximum heat leak of 49,587 Joule/hr (47 Btu/hr) occurs after 4 hours of soakback and the maximum turbine bearing temperature of 294 K (530 R) is satisfactory.

The predicted soakback behavior of the LO_2 turbopump following a steady-state run for the case of external cooling and nominal liftoff seal leakage using the bleed flow from the LH_2 turbopump as coolant is shown in Fig. 71. The predicted maximum heat leak is 29,541 Joule/hr (28 Btu/hr) and occurs after 3 hours of soakback and the maximum turbine bearing temperature is 178 K (320 R). As in the case of the LH_2 turbopump, the 0.113 kg/hr (0.25 lb/hr) flowrate could be reduced considerably.

The predicted soakback behavior of the LO_2 turbopump following a steady-state run for the case of no external cooling and no liftoff seal leakage is shown in Fig. 72. In this case, the maximum heat leak is 79,128 Joule/hr (75 Btu/hr) and occurs after 6 hours of soakback. Though the turbine bearing reaches 356 K (640 R), which is 61.1 K (110 R) hotter than the nominal leakage case, it is still within the safe operating temperature range.

Failure Mode Effects Analysis

During the design phase of the program, investigations were undertaken to establish all the possible failure modes such that design provisions could be made to eliminate and/or minimize potential hazards associated with the modes of failure. Potential failure modes, along with the provisions made to the design to eliminate or

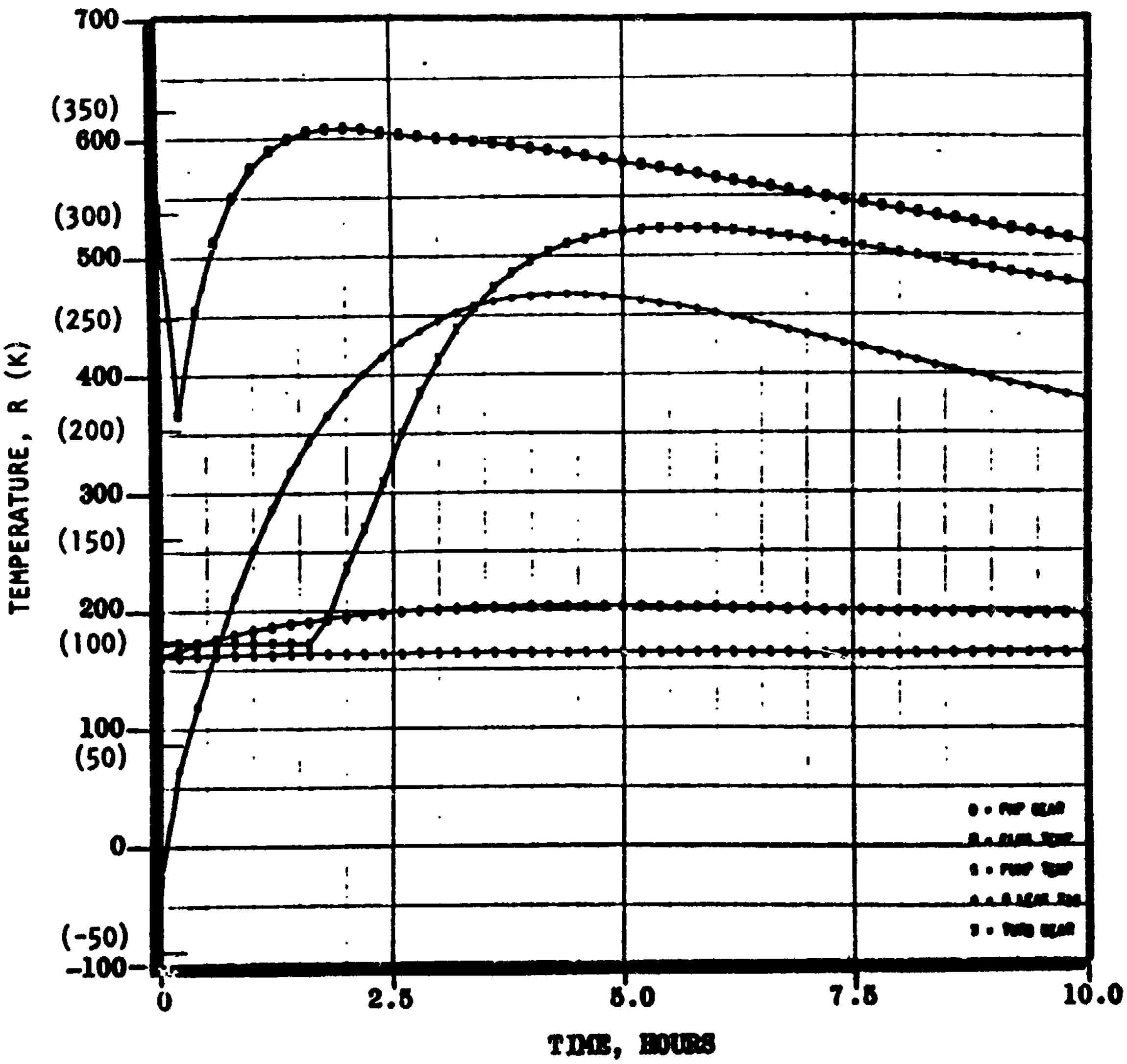

Figure 70. APS Turbopump Soakback Thermal Analysis
Sketch 204, No External Cooling

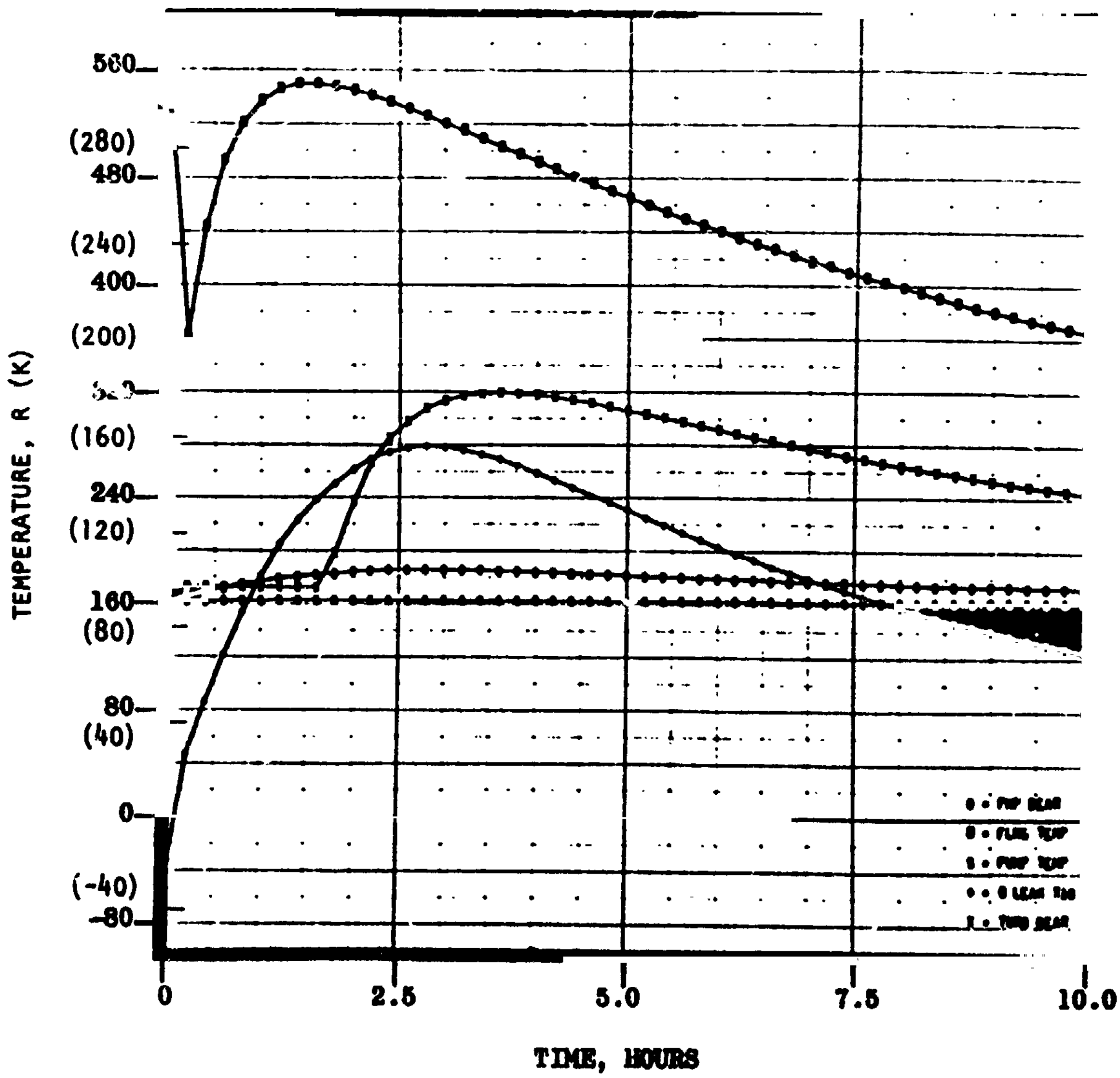

Figure 71. APS Turbopump Soakback Thermal Analysis Sketch 204, 0.25 lb/hr, (.113 Kg/hr), H_2 Cooling

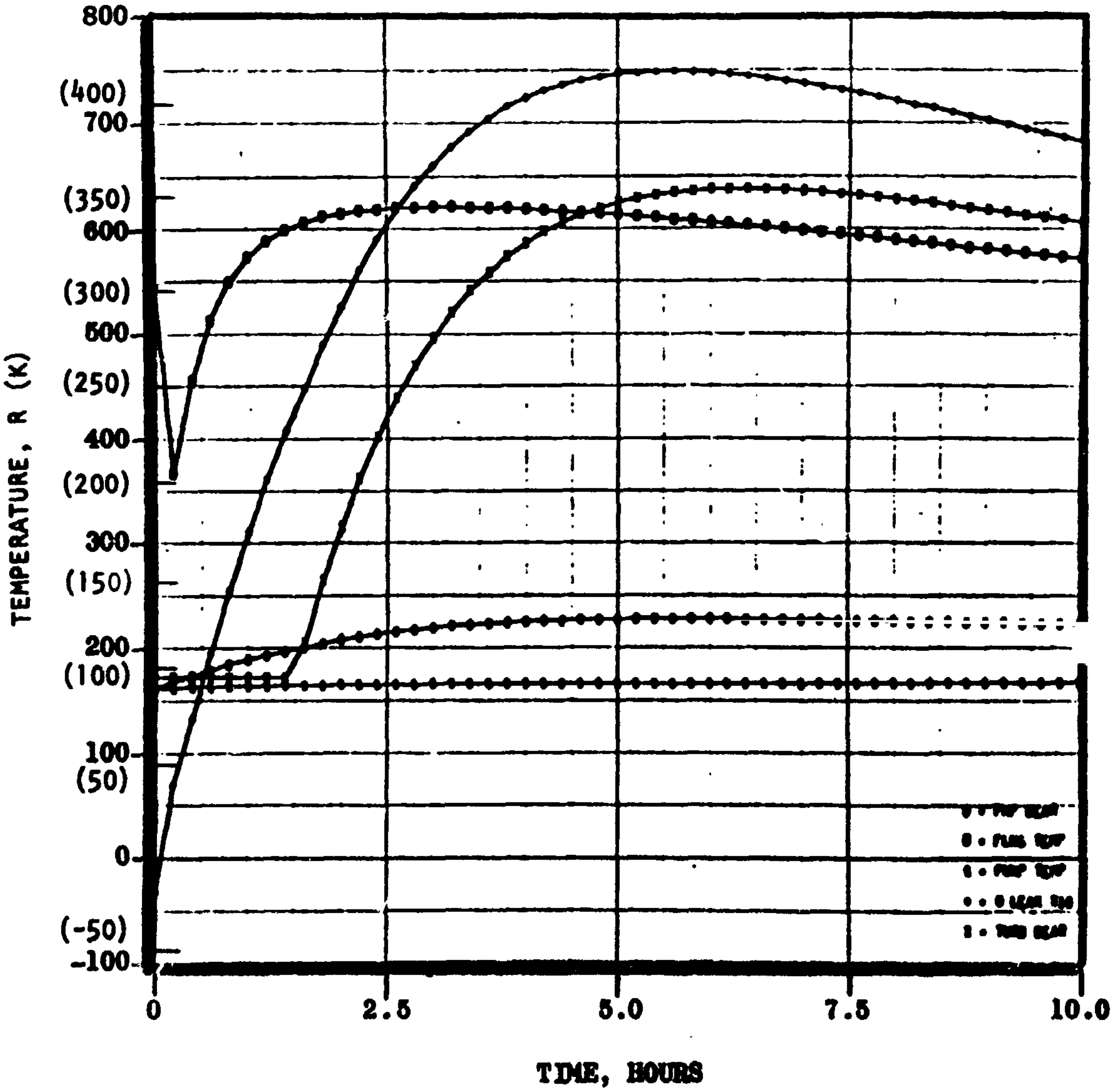

Figure 72. APS Turbopump Soakback Thermal Analysis
Sketch 204, No External Cooling, No Leak

minimize them, are shown in Table 24. Also shown is a list of instrumentation designed to detect and anticipate a failure situation developing as a result of the associated failure mode. The location of the instrumentation on the turbopump is identified in Fig. 73.

TABLE 24. APS OXIDIZER TURBOPUMP FAILURE MODE EFFECTS ANALYSIS

Potential Failure Mode	Design Provisions	Detection Instrumentation
• Bearings	Axially balanced rotor double tongue volute	Bearing temperature coolant flow pressure
• Liftoff Seal	Designed fail closed pressure balanced during operation back up seals, prevent loss of collant to bearings	Pressure, seal cavity
• Primary LOX Seal	Back up intermediate seal and turbine seal interseal, ambient drain with purge	Pressure, liftoff seal cavity
• Intermediate Seal	Back up primary seal and turbine seal interseal ambient drains	Seal drain flow (if loss of purge)
• Turbine Seal	Back up primary LOX seal and intermediate seal, ambient drain with purge	Seal drain temperature seal drain flow
• LOX Pump Explosion	Compatible material selection generous radial clearances adequate axial clearances silver wear rings Kel-F wear ring at inducer designed for no fretting	Pressure (indicate change in pump axial thrust), bearing temperature, coolant flow pressure, accelerometers to indicate excessive radial and axial displacements
• Excessive Axial Thrust	Capability of changing wear ring location on impeller back face.	Pressure on seal cavity
• Rotordynamics Problems	Operating speeds out of range of critical speeds. Balancing of rotor assembly	Accelerometers
• Bearing Coolant Stoppage	Capability of recirculating up to 80 percent through bearings	Bearing Temperature
• Overspeed	Overspeed trip pad on burst speed	Speed pick up electronic cut off device
• Turbine Over Temperature	Burn out elbow upstream of manifold use of high temperature material for blades, wheel and manifold	Turbine inlet temperature over temperature cut off
• Turbine Blade Failure	Turbine housing capable of containing blade	Accelerometers

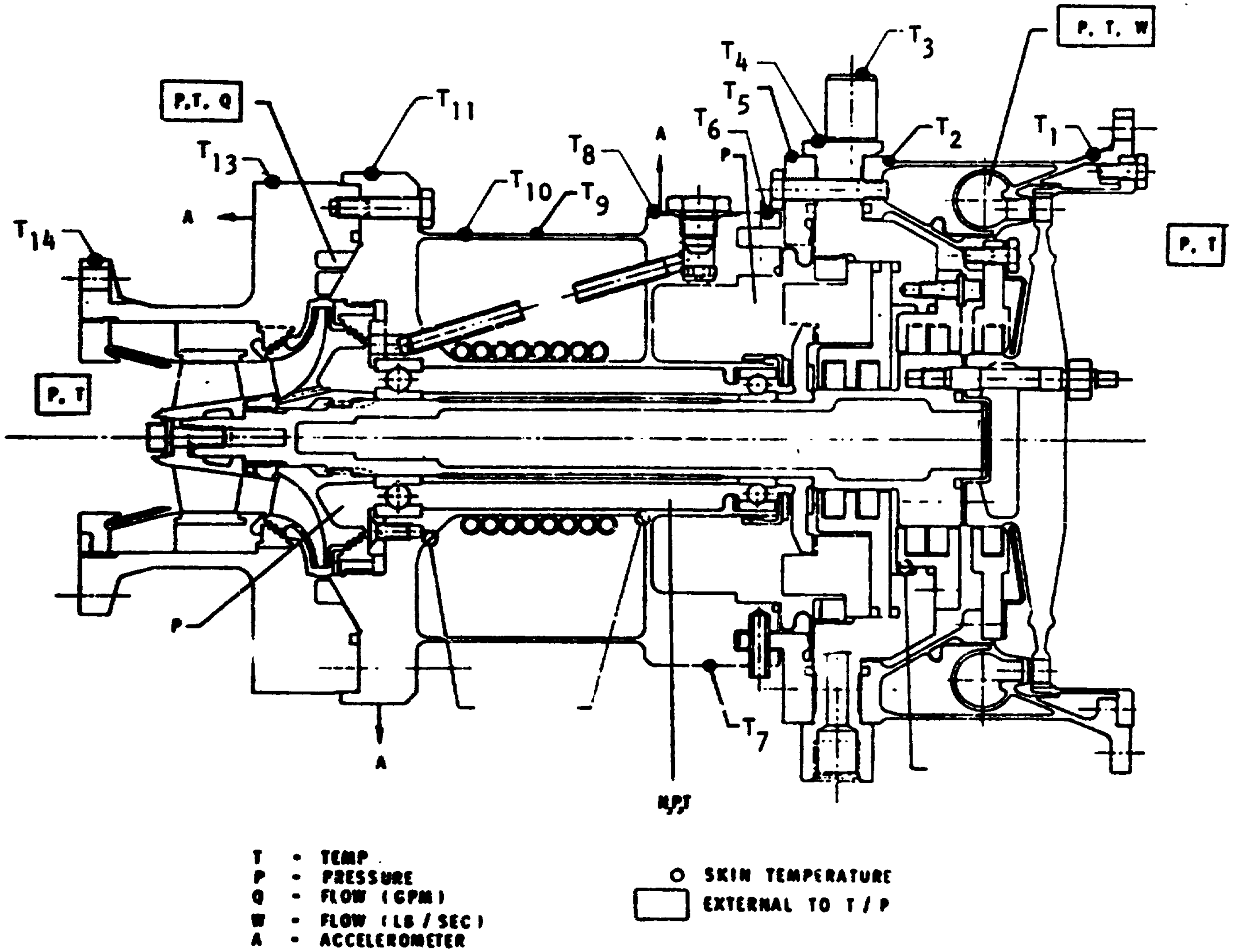

Figure 73. APS Oxidizer Turbopump Instrumentation Schematic

LIQUID HYDROGEN TURBOPUMP

Design Requirements and Constraints

The nominal performance and life requirements of the LH_2 turbopump are shown in Table 25. In addition to the nominal conditions, the pump is required to operate over the head-flow range enclosed by trapezoid shown in Fig 74. This includes flows ranging from 1.36 to 2.95 kg/sec (3.0 to 6.5 lb/sec), during which the developed pressures vary from 14,479,000 to 7,584,233 N/m^2 (2100 to 1100 psi). The state of the liquid hydrogen at the inlet of the pump is defined by Fig. 75.

LH_2 Turbopump Configuration

To select the turbopump configuration which best meets the requirements noted on Table 25, a study was conducted in Phase I of the program in which various turbopump types were evaluated and compared. The study included both transient and steady-state performance characteristics. The conclusions reached concerning the LH_2 turbopump configuration are shown on Table 26. Phase II was then initiated within the framework established by these parameters.

TABLE 25. SS-APS LH_2 TURBOPUMP PERFORMANCE REQUIREMENTS

Pump:	Flow	2.041 kg/s (4.5 lb/sec)
	Flow	0.02902 m^3/sec (460 gpm)
	Developed pressure	1.103 x 10^7 N/m^2 (1600 psia)
	Inlet pressure	124,106 - 344,738 N/m^2 (18 - 50 psia)
	Inlet temperature	20.8 - 25 K (37.5 - 45 R)
Turbine:	Energy source	O_2/H_2
	Exhaust pressure	2413.7 N/m^2 (35 psia)
Turbopump:	Life, tbo	10 hrs
	Operating cycles	10,000
	"ON" time	2 sec (minimum)
	"OFF" time	5 sec to 24 hrs
	Start Time	1.5 sec
	Turbine to pump heat flow	158,256 Joule/hr (50 Btu/hr static)
		52,752 Joule/hr (150 But/hr operating)

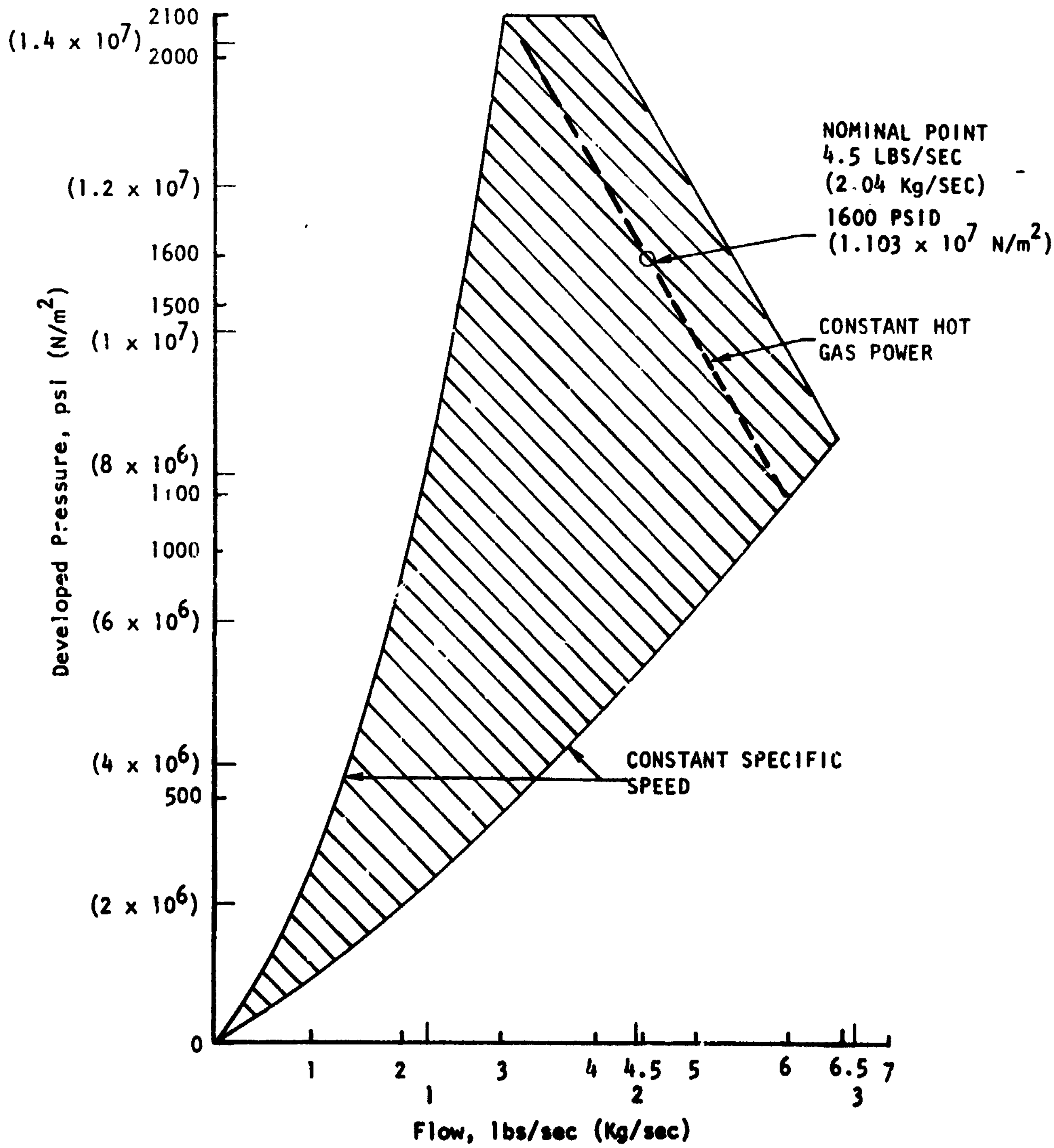

Figure 74. Pressure/Flowrate APS LH_2 Pump

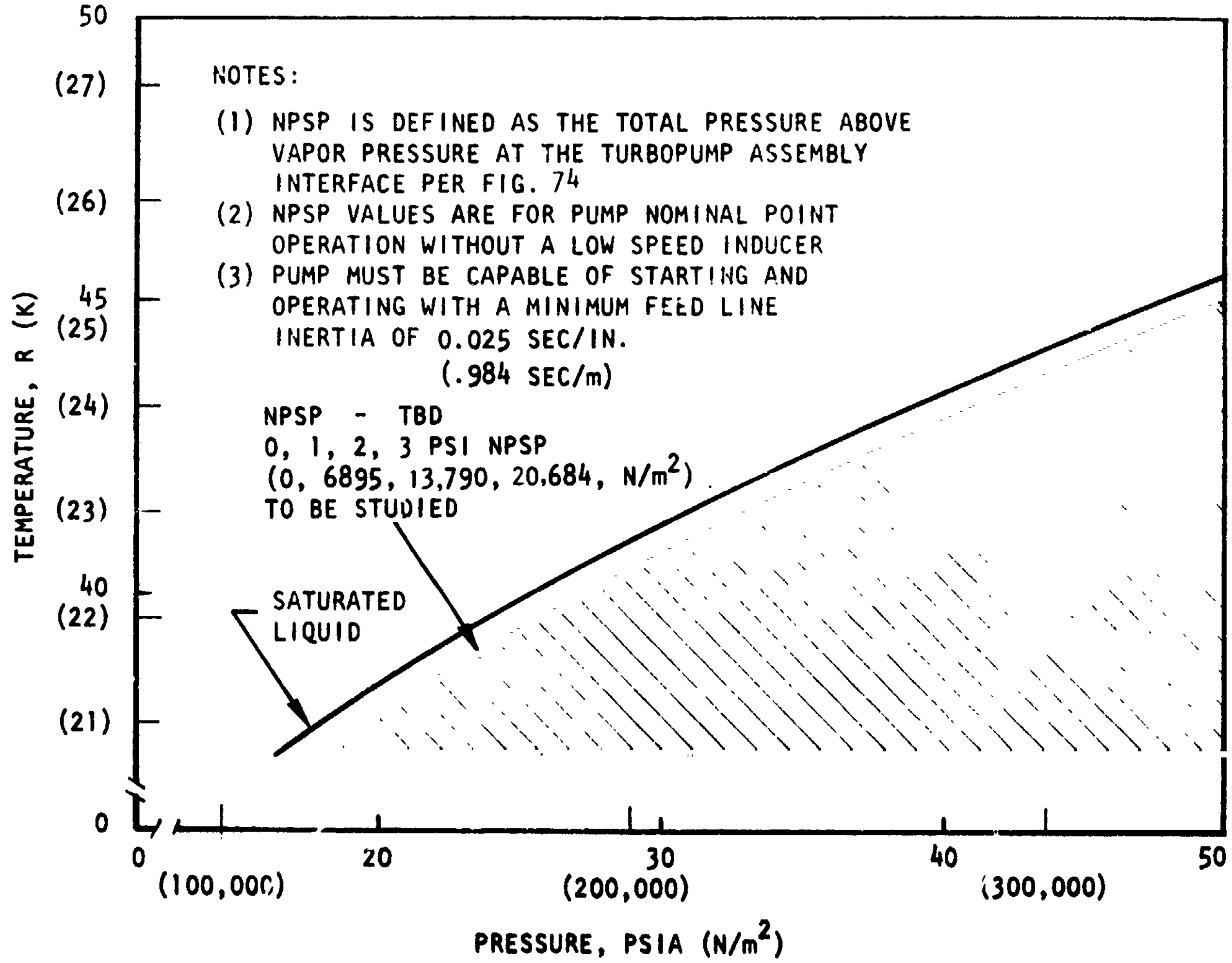

Figure 75. APS Breadboard Hydrogen Pump Start and Run Box Conditions

The final turbopump layout which emerged from the Phase II effort is shown in Fig. 76. The principal design parameters are summarized in Table 27.

TABLE 26. SS-APS LH_2 TURBOPUMP PHASE I RESULTS

• Pump:	Two stage centrifugal
• Turbine:	Two row
	Axial impulse
	100 percent admission
	Inlet pressure: 1,861,584 N/m^2 (270 psia)
	Inlet temperature: 1117 K (2010 R)
• Shaft speed:	6283 rad/s (60,000 rpm nominal)

The overall arrangement of the turbopump shows that the turbine-to-pump heat transfer limitations had a substantial influence on the turbopump design. The pump components are arranged in one group overhung on the left end of the rotor and the turbine components are grouped overhung outboard of the rear bearings on the other end of the rotor. The cryogenic regions and the hot turbine components are connected only by thin cylindrical or conical members which are most efficient from a combined thermal and structural consideration.

The pumping elements consist of a four bladed inducer (Ref. Table 28) with constant outer diameter and tapered hub, followed by a shrouded centrifugal impeller (Ref. Table 29) with five partial and five full vanes and a discharge angle of 35 degrees. The fluid from the first-stage impeller is discharged into a radial diffuser containing 11 guide vanes. This is followed by a vaneless turning passage and a radial inward flow diffusing section which directs the fluid to the eye of prewhirl into the fluid as the inducer, thus permitting the second-stage impeller to be hydrodynamically identical to the first stage impeller.

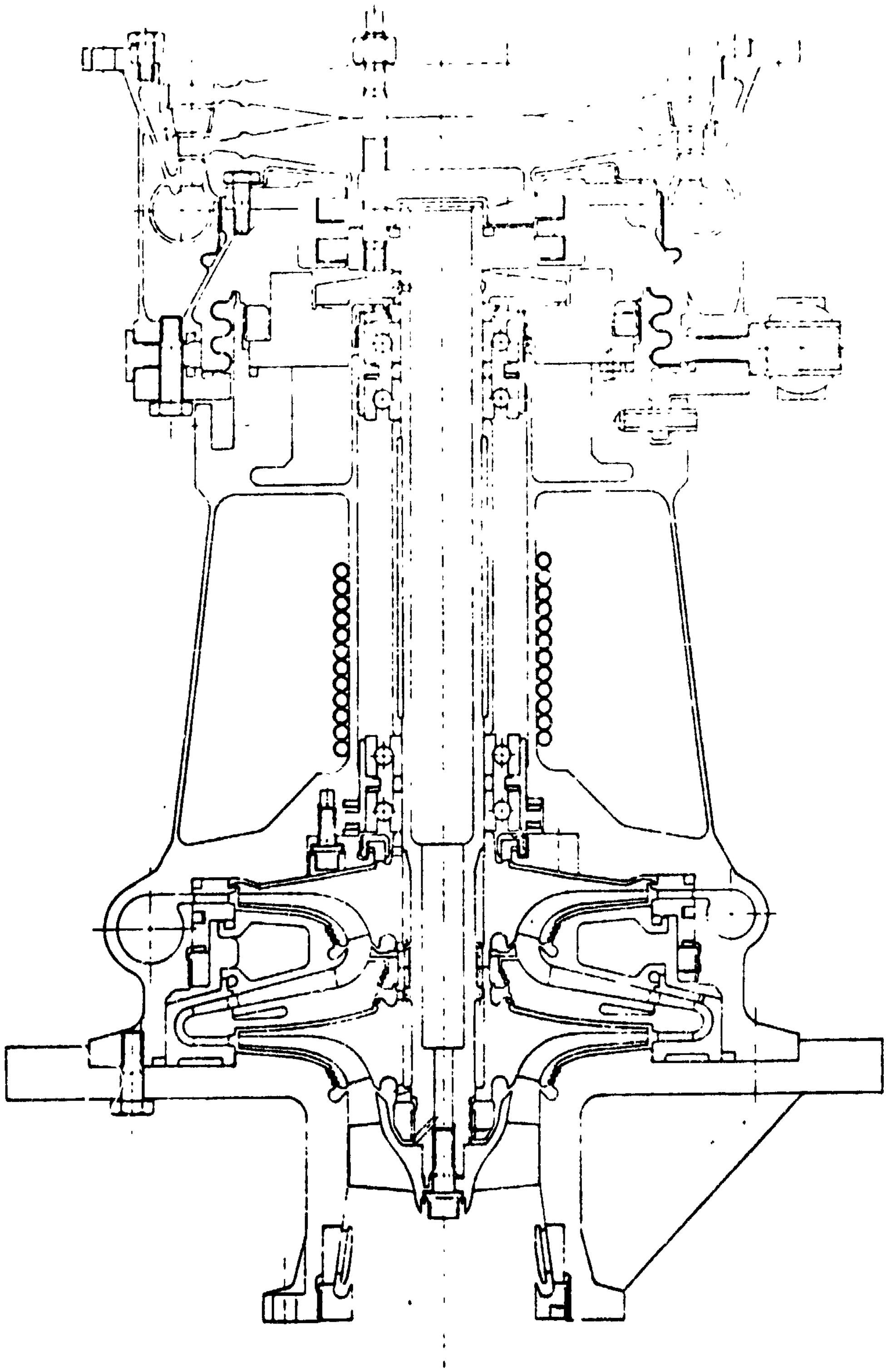

Figure 76. APS LH_2 Turbopump Layout

From the second-stage impeller, the fluid enters [illegible] dynamically identical to the first-stage diffuser. From there, the fluid is collected in a scroll-shaped volute and delivered to the system through a single discharge pipe.

TABLE 27. APS LH_2 TURBOPUMP NOMINAL DESIGN PARAMETERS

• Pump:	Inducer diameter	5.84 cm (2.300 inches)
	Inducer tip speed	182.9 m/s (600 fps)
	Impeller diameter	12.47 cm (4.910 inches)
	Impeller tip speed	390 m/s (1,280 fps)
	Total head rise	1.103×10^7 N/m^2 (1,600 psia)
	Flow rate	2.04 kg/s (4.5 lb/sec)
	Efficiency	52 percent
• Turbine:	Pitch diameter	15.24 cm (6.0 inches)
	Pitch line velocity	479 m/s (1,572 fps)
	First row blade height	0.770 cm (0.303 inches)
	Second row blade height	1.36 cm (0.536 inch)
	Percent admission	100
	Pressure ratio	7.72
	Efficiency	60.3 percent
	Power	607,000 Watt (814 hp)
• Turbopump:	Roto speed	6283 rad/s (60,000 rpm)
	Bearing dn	$.157 \times 10^6$ mm-rad/s (1.5×10^6 mm-rpm)
	Shaft Seal Surface speed	178.6 m/s (586 fps)
	Weight	38.1 kg (84 pounds)*

*This is the "breadboard" turbopump weight including extra heavy inlet flanges and excess material in selected areas to reduce cost

TABLE 28. MK-44-F INDUCER DESIGN PARAMETERS

	Fuel
Fluid	LH_2
Type	Variable lead helix
Speed rad/s (rpm)	6283 (60,000)
Flow m^3/s (gpm)	0.02908 (461)
Head m (ft)	685.8 (2250)
Inlet Tip Diameter cm (inches)	5.842 (2.300)
Inlet Hub Diameter cm (inches)	1.778 (0.700)
Discharge Hub Diameter cm (inches)	4.257 (1.676)
Blade Angle, Inlet Tip (degrees)	7.4
Blade Angle, Inlet rms (degrees)	9.96
Blade Angle, Discharge Tip (degrees)	9.65
Tip Solidity	2.24
Inlet Flow Coefficient	0.065
Number of Vanes	4
Vane Thickness, Tip cm (inches)	0.0254 (0.010)
Cant Angle (degrees)	10
Radial Tip Clear cm (inches)	0.0279 (0.011)
Material	Titanium

A back flow deflector is included in front of the diffuser. This feature had a double function. It minimizes reverse flow into the inlet duct which is highly desirable from a system standpoint, particularly if the turbopump is tank-mounted. An equally significant function of the back flow deflector is to reduce NPSP requirements at low Q/N conditions.

TABLE 29. MK-44-F IMPELLER DESIGN

Type	Shrouded centrifugal
Speed	6283 rad/s (60,000 rpm)
Through Flow	1,002,902 m^3/s (460 gpm)
Leakage Flow	.000164 m^3/s (26 gpm) (1st stage)
	.000328 m^3/s (52 gpm) (2nd stage)
Pump Head	149,454 Joule/kg (50,000 ft)
Stage Specific Speed	0.2372 (648) Non Dimensional
Blade Angle, Discharge	35 degrees
Blade Angle, Inlet Tip	14-1/2 degrees
Blade Angle, Inlet Hub	23-1/2 degrees
Inlet Flow Coefficient	0.117
Discharge Flow Coefficient	0.086
Number of Vanes	5 + 5
Eye Diameter	5.842 cm (2.300 inches)
Discharge Diameter	12.471 cm (4.910 inches)
Discharge Tip Width	0.254 cm (0.100 inch)

Internal recirculation in the pump is controlled by step labyrinth seals located at the impeller front shroud, first-stage impeller back shroud, and between the cross-over discharge and leakage return cavity. Axial thrust of the rotor is balanced by a self-compensating balance piston located in the rear shroud of the second-stage impeller. To operate the piston, fluid is bled from the discharge of the second-stage impeller, passed through a high-pressure orifice located at the impeller tip, then through a low-pressure orifice and returned to the second-stage inlet. Bearing lubrication is accomplished by allowing part of the balance piston flow to pass through both sets of bearings, through a step labyrinth control orifice, and through radial holes into the center of the shaft where it is returned to the main flow between the inducer and first-stage impeller.

The turbine is a typical Curtiss-type velocity compounded axial impulse machine. The gas is expanded fully through a convergent-divergent supersonic nozzle from the inlet pressure to the exhaust pressure. Approximately 75 percent of the gas power is absorbed by the first rotor and 25 percent by the second rotor. Rotor blades on both rows are of the impulse type. Stator vanes are included between the two rows to redirect the gas at the correct entrance angle for the second row.

Since the pump and turbine fluids are chemically compatible, an absolute separation between the two areas is not mandatory. A lift-off seal is incorporated in the design to prevent propellant loss during coast periods. During dynamic operation of the turbopump, the liftoff seal will be opened with pneumatic pressure, and leakage from the pump to the turbine will be controlled by a double-floating controlled gap shaft seal. No external drains between the two seals are provided.

Copper cooling-coils are wound around the bearing carrier to provide an optional alternate means of external cooling. A drain port is provided on the pump side of the liftoff seal to facilitate the evaluation of overboard bleeding during simulated coast periods.

LH_2 Pump Predicted Performance

Figure 77 shows the predicted performance characteristics of the LH_2 pump. Solid lines represent H-Q points at constant speed levels. Constant efficiency values are indicated by the long dashed lines and the required operating range of the pump is indicated by the box defined by the short dashed lines. The predicted efficiency of the pump at the nominal design condition was 52 percent.

Figure 78 shows the minimum required NPSP values at the significant points of the required pump operating range. The values noted are based on the inducer being able to operate without appreciable head loss at one inlet velocity head.

The static pressure levels at significant points of the pump were computed for the nominal design condition, and the internal flowrates were determined. These values

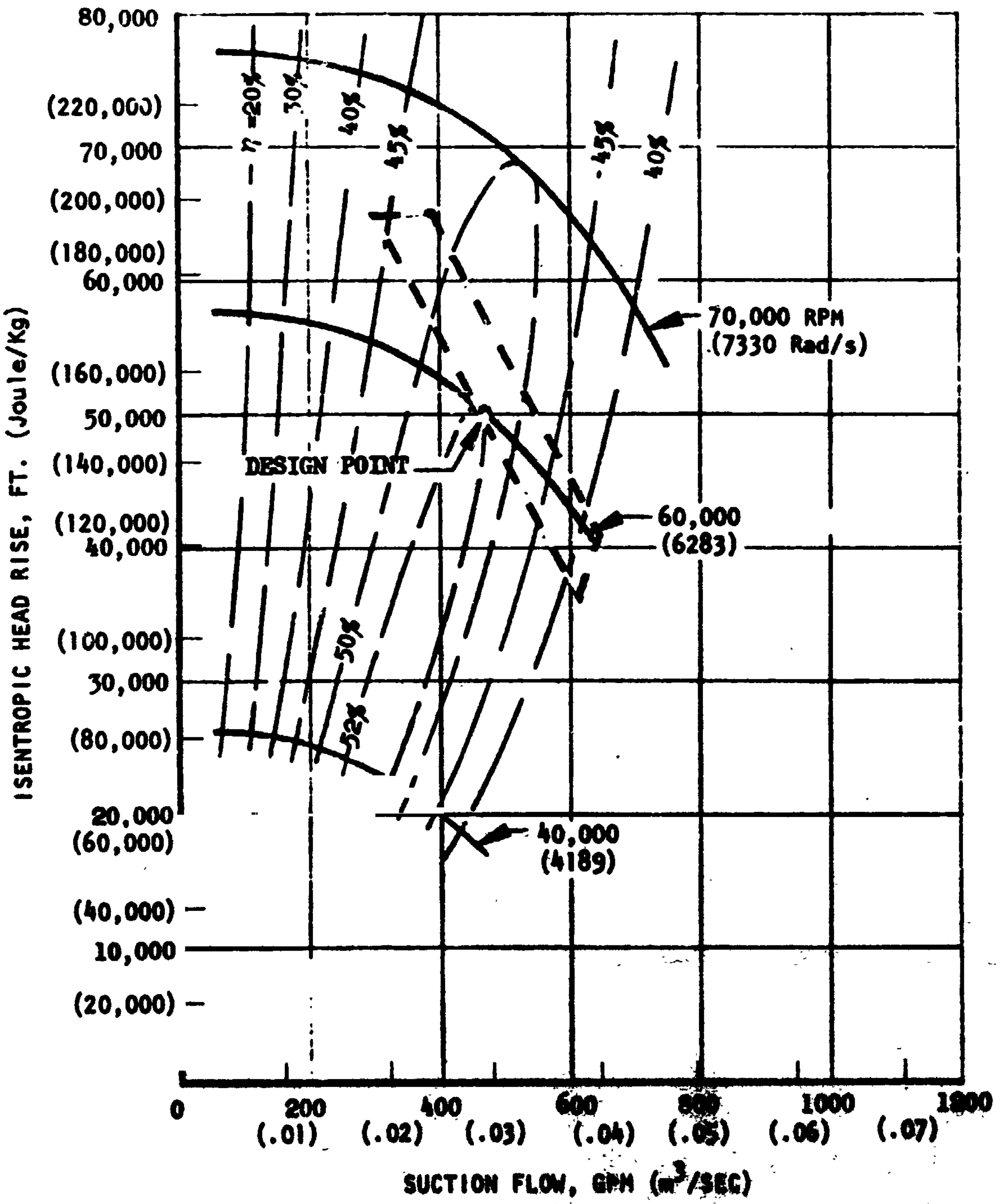

.igure 77. APS LH_2 Pump Predicted Performance Map

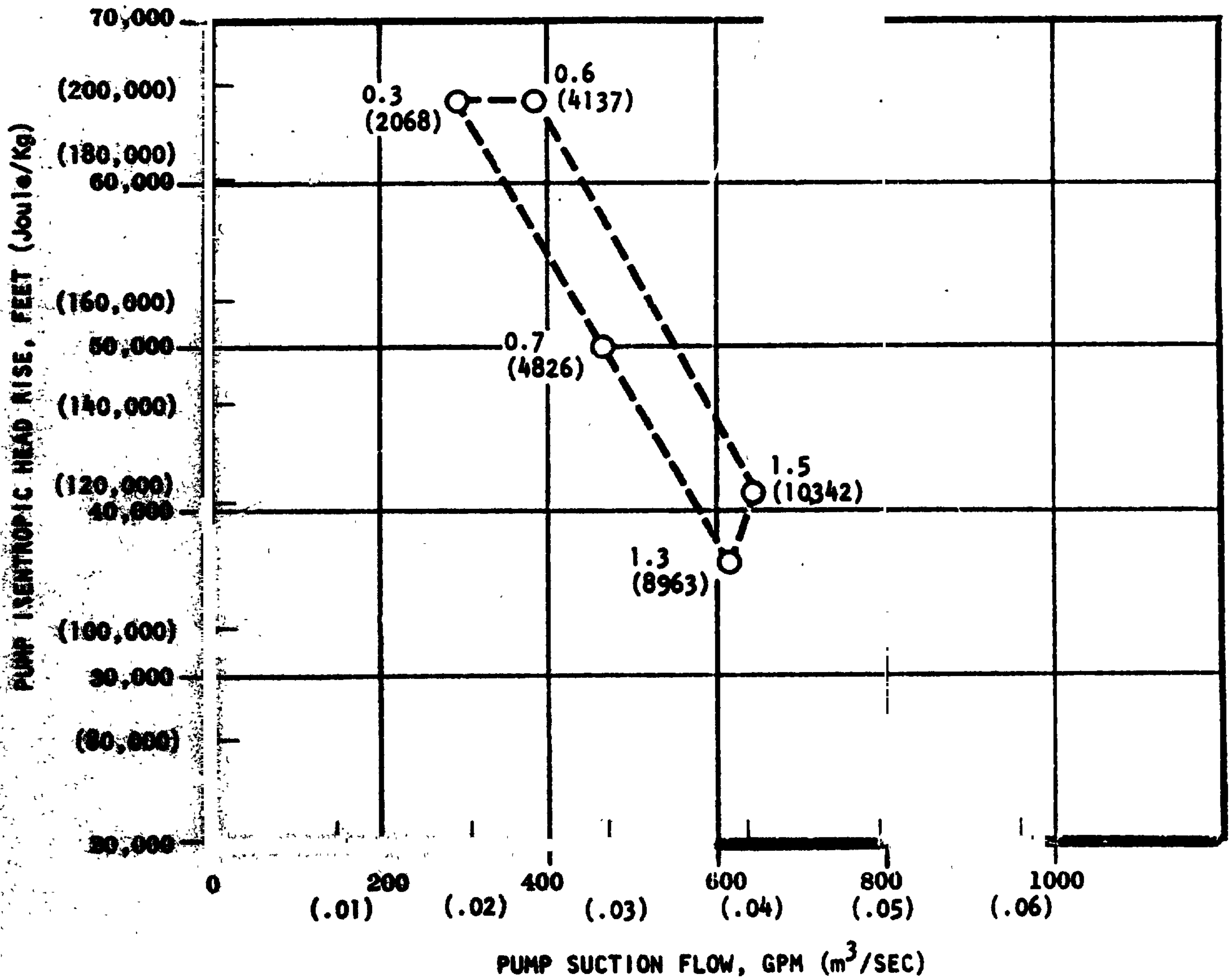

Figure 78. APS LH_2 Turbopump Required NPSP, psi (N/m^2)

are presented in Fig. 79 and 80. To determine the performance of the pump, internal heating effects had to be taken into consideration. The temperature of the fluid throughout the pump passages was mapped for this purpose. The temperatures obtained at significant points is illustrated in Fig. 81.

The performance of the LH_2 turbopump balance piston is shown in the figure. The thrust developed by the balance piston (pressure x area on the second-stage impeller rear shroud) is plotted as a function of the gap size at the high-pressure orifice. A total travel of 0.0254 cm (0.010 inch) is assumed. At the nominal design point, the balance piston develops a thrust of slightly over 97,861 N (22,000 pounds) and requires a flowrate of 0.127 kg/sec (0.28 lb/sec). The difference between the maximum and minimum thrust level indicated on the figure represents the compensating capability of the piston. The approximately 26,689 N (6,000 lbs) compensating capability indicated by the figure represents approximately 18 percent of the total shaft axial thrust load. While the balance piston is operating with a high-pressure orifice gap from zero to 0.0254 cm (0.010 inch), the bearings absorb only the axial load imposed by the preload springs.

Similar curves were generated for off-design conditions, which showed that the balance piston will neutralize the shaft axial thrust over the entire predicted operating range, including the low Q/N encountered during start.

LH_2 Turbine Performance

The Mark 44 fuel turbines must accomplish an isentropic enthalpy drop of 3,709,917 Joule/kg (1595 Btu/lb). The peripheral speed at the mean diameter was limited to 479.1 m/s (1572 fps). Impulse turbines are capable of obtaining operating efficiencies of about 75 percent without recovery of the leaving velocity head and about 80 percent with recovery of the leaving velocity head. This high performance implies an excessive number of stages for the large isentropic enthalpy drop, which is not desirable from considerations of weight and size. Outboard bearings are also not acceptable and the large overhang with the inboard bearing results in critical speed problems.

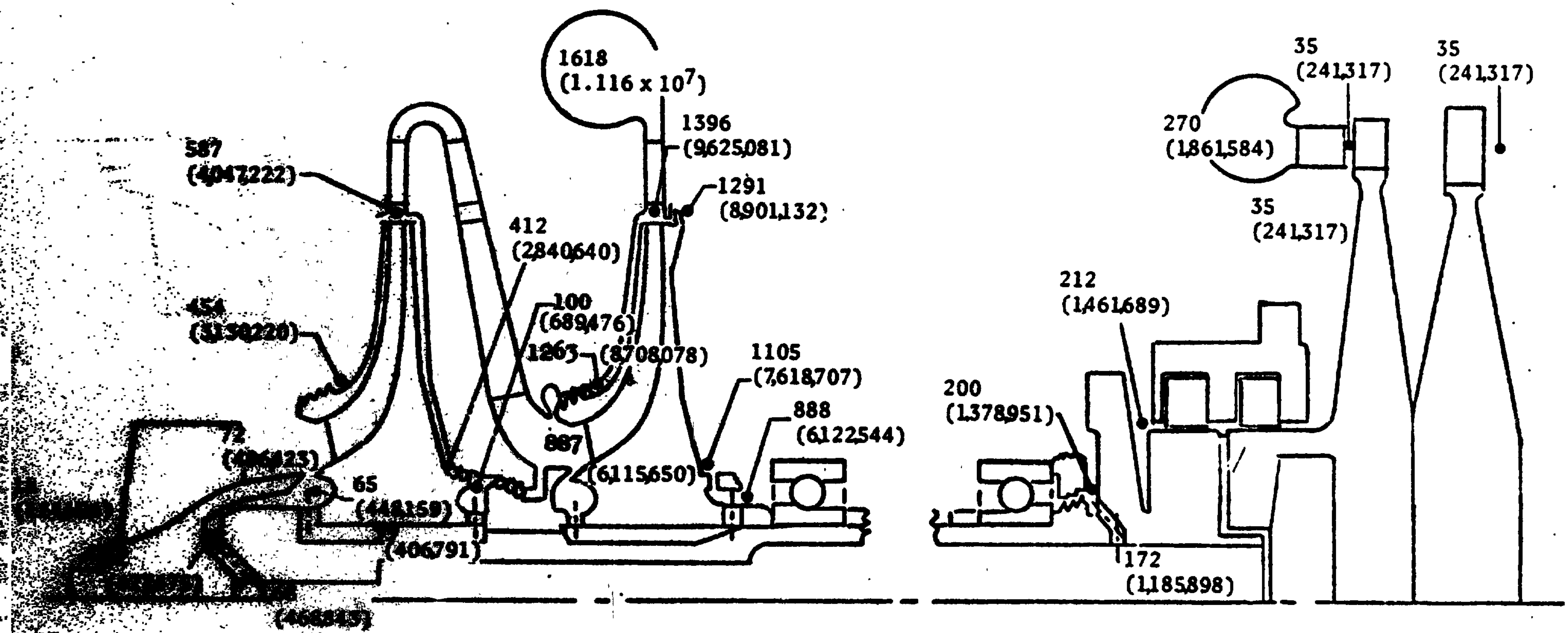

Figure 79. APS LH_2 Turbopump Static Pressures, psia (N/m^2)

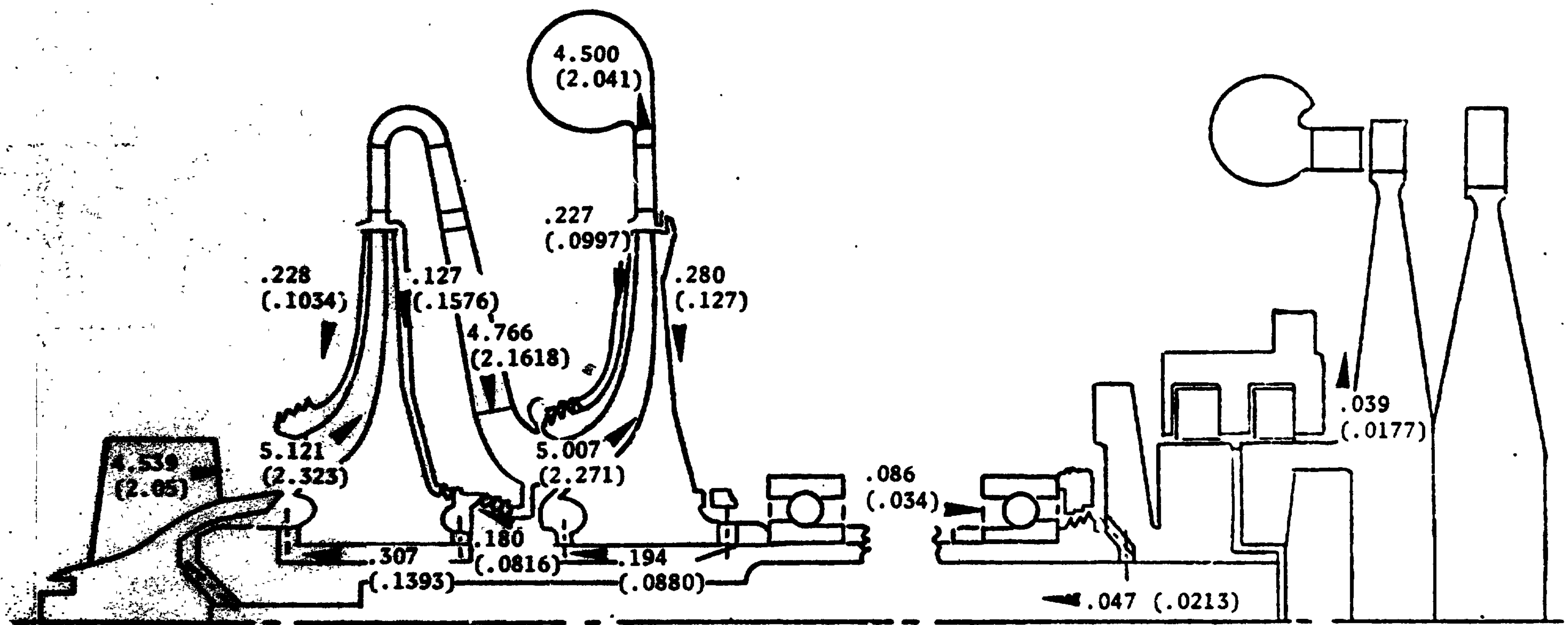

Figure 80. APS LH_2 Pump Internal Flows at Design Point, lb/sec (Kg/sec)

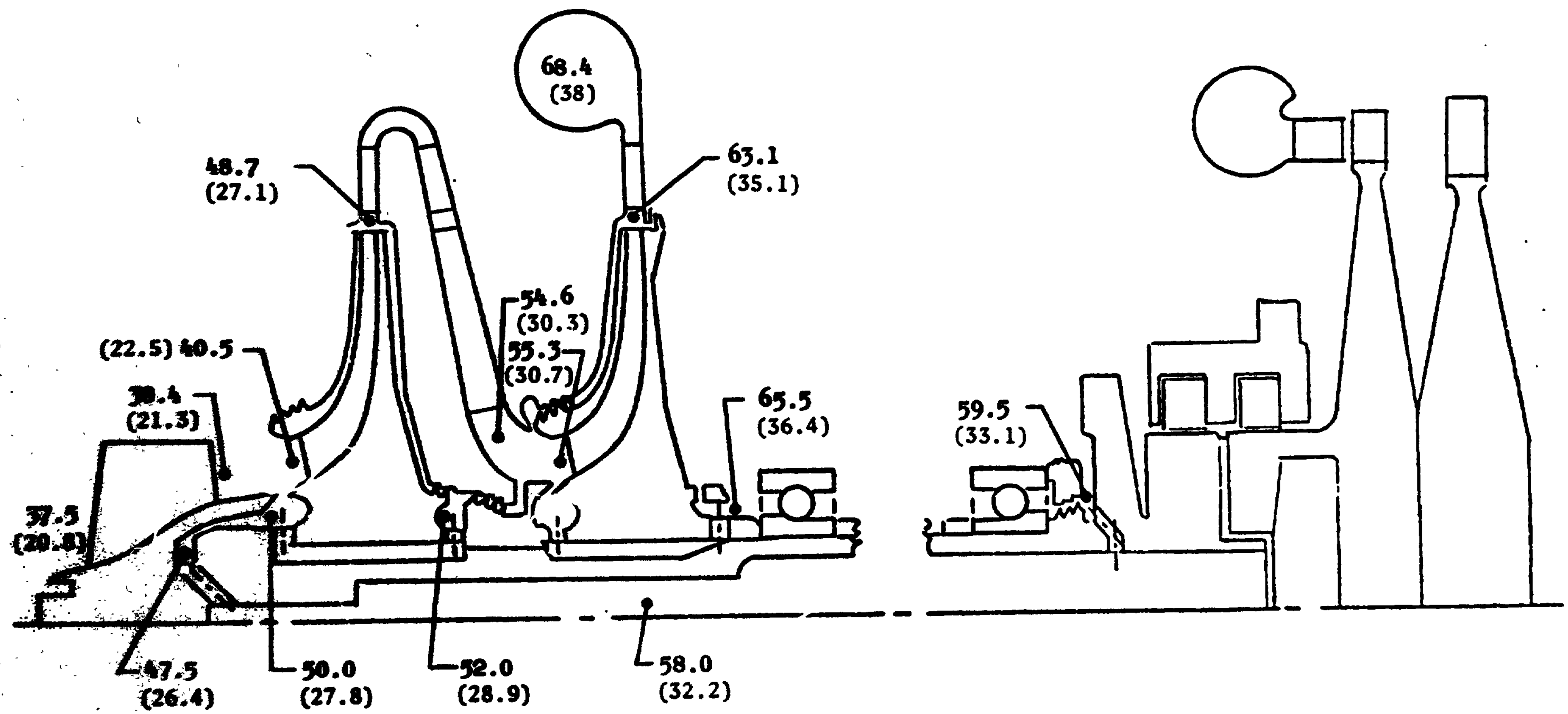

Figure 81. APS LH_2 Turbopump Fluid Total Temperatures, R (K)

The compromise selected between a multistage impulse turbine which operates at a high degree of efficiency and a single stage unit with a low degree of efficiency is the two-row Curtis turbine. Originally, Curtis stages were designed as pure velocity stages where the gas is expanded to the discharge pressure in the first nozzle. However, experience has shown that the performance of the turbine can be improved by applying a certain amount of reaction in the rotors and stators. The pressure drops accelerate the flow sufficiently to offset the decelerations from the frictional losses.

To minimize cost, certain features of the fuel and oxidizer turbines were made common. The inlet manifold, nozzle (except for the arc of admission) and the first row wheel are identical for both turbines. The advantages from the common approach include lower tooling and unit cost and savings on the turbine performance test costs.

Because of the common design approach, the discussion presented elsewhere in this report with respect to the oxidizer turbine calculation procedures, loss estimates cascade design and blade profile design are equally applicable for the fuel turbine.

The principal design parameters are summarized in Fig. 82. The vector diagram, predicted efficiency as a function of isentropic velocity ratio and torque parameter versus speed parameter are presented in Figs. 83 through 86.

The turbine flowrates required at various points of the specified operating range are indicated in Fig. 87. Detail information relative to blade profiles and general geometry is provided in Fig. 88 through 93.

The blade surface velocity distribution computed with the Douglas-Neuman program are shown in Figs. 94 through 96.

LH_2 Turbopump Materials and Structural Analysis

Figure 97 shows the materials which were selected for the LH_2 turbopump components. The pump components are mostly made of Inco 718. This material was selected

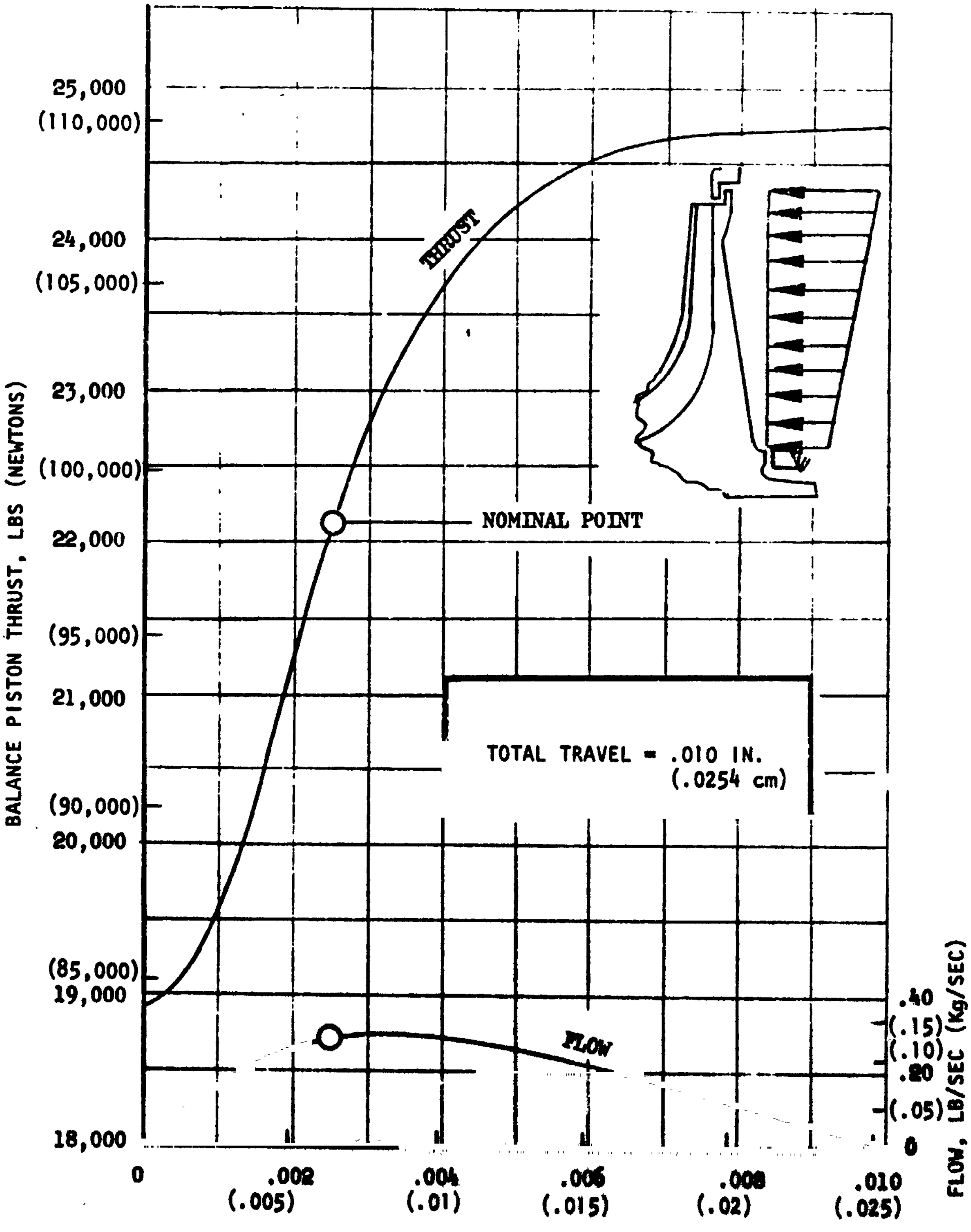

Figure 82. APS LH_2 Pump Balance Piston Performance

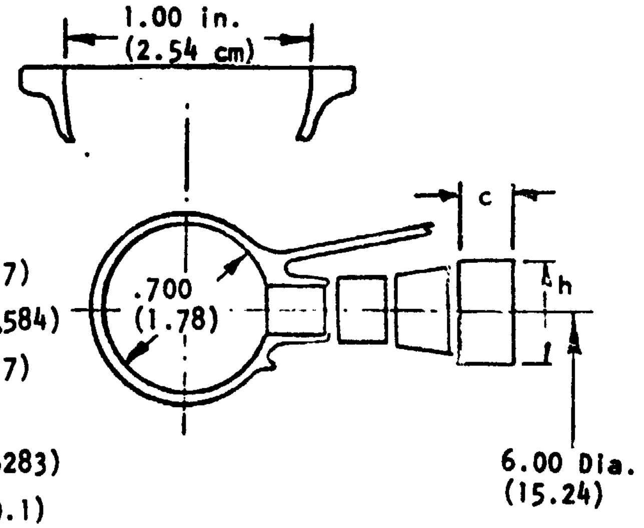

INLET TEMPERATURE, R (k)	T_{1t}	: 2010 (1117)
INLET PRESSURE, PSIA (N/m^2)	P_{1t}	: 270 (1,861,584)
EXHAUST PRESSURE, PSIA (N/m^2)	P_{2s}	: 35 (241,317)
PRESSURE RATIO	PR	: 7.72
SPEED, RPM (Rad/s)	N	: 60,000 (6283)
MEAN BLADE SPEED, F/S (M/s)	u_m	: 1572 (479.1)
VELOCITY RATIO	u/c0	: .175
EFFICIENCY, %	η_{t-s}	: 60.3
FLOWRATE, LB/S (Kg/s)	$\dot{w}$	: .598 (.2712)
HORSEPOWER (WATT)	HP	: 814 (607,000)
ADMISSION, %	ϵ	: 100
STRESS X 10^9 $(Rad/s)^2(cm)^2$	N^2AA	: 36.4 (.06187)
SPECIFIC SPEED (NON DIMENSIONAL)	N_s	: 5.8 (.00212)

	c	h
Nozzle	.300 (.762)	.258 (.655)
1st Rot.	.220 (.559)	.303 (.770)
Stator	.280 (.711)	.473 (1.2014)
2nd Rot.	.220 (.559)	.536 (1.361)

Figure 83. MK-44-Fuel Turbine Design Parameters

PRESSURE DISTRIBUTION:

NOZZLE OUTLET	35 PSIA ($241,317\ N/m^2$)
FIRST ROTOR OUTLET	35 PSIA ($241,317\ N/m^2$)
STATOR OUTLET	35 PSIA ($241,317\ N/m^2$)
SECOND ROTOR OUTLET	35 PSIA ($241,317\ N/m^2$)

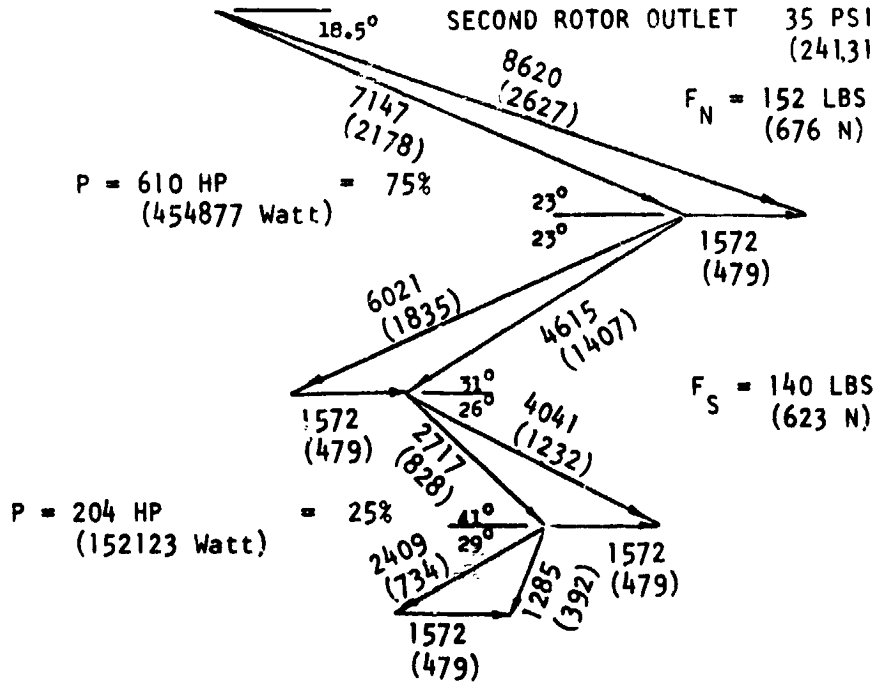

POWER, HP (WATT)	814 (607,000)
SPEED, RPM, N (RAD/S)	60,000 (6283)
GAS FLOW, LB/SEC, W (Kg/SEC)	.598 (.2712)
INLET TEMP, F, T_{1t} (K)	1550 (1117)
INLET PRESSURE, PSIA, P_{1t} (N/m^2)	270 (1,861,584)
EXHAUST PRESSURE, PSIA, P_{2s} (N/m^2)	35 (241,317)
PRESSURE RATIO, PR	7.72
EFFICIENCY, PERCENT, η_{t-s}	60.3
DIAGR. CORRECTION, ϵd	.94
ADMISSION, PERCENT, ϵ	100
REYNOLD'S NUMBER, RE	2.5×10^6

Figure 84. Velocity Vector Diagram (Nominal Operating Point)

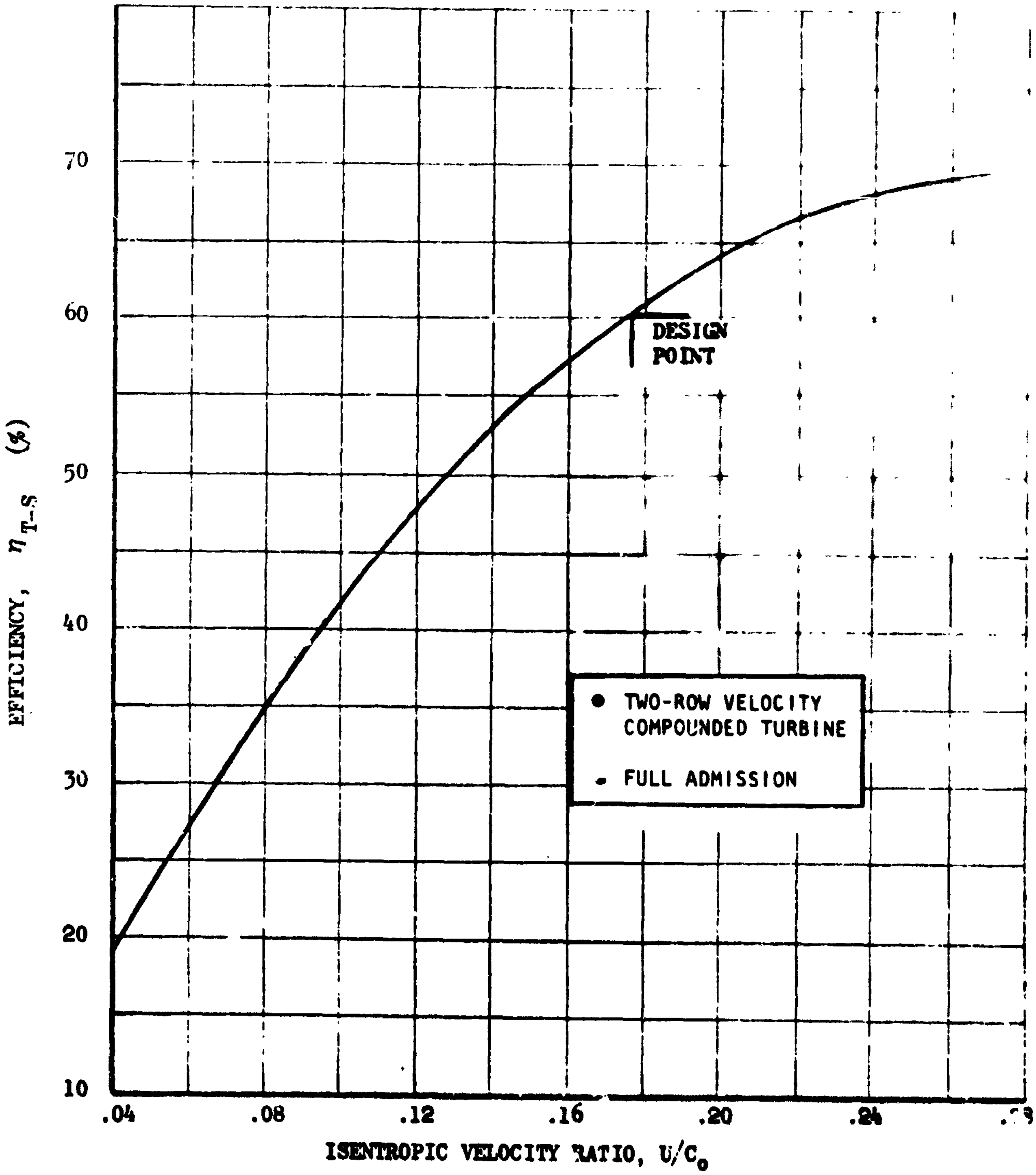

Figure 85. APS LH_2 Turbine Predicted Efficiency

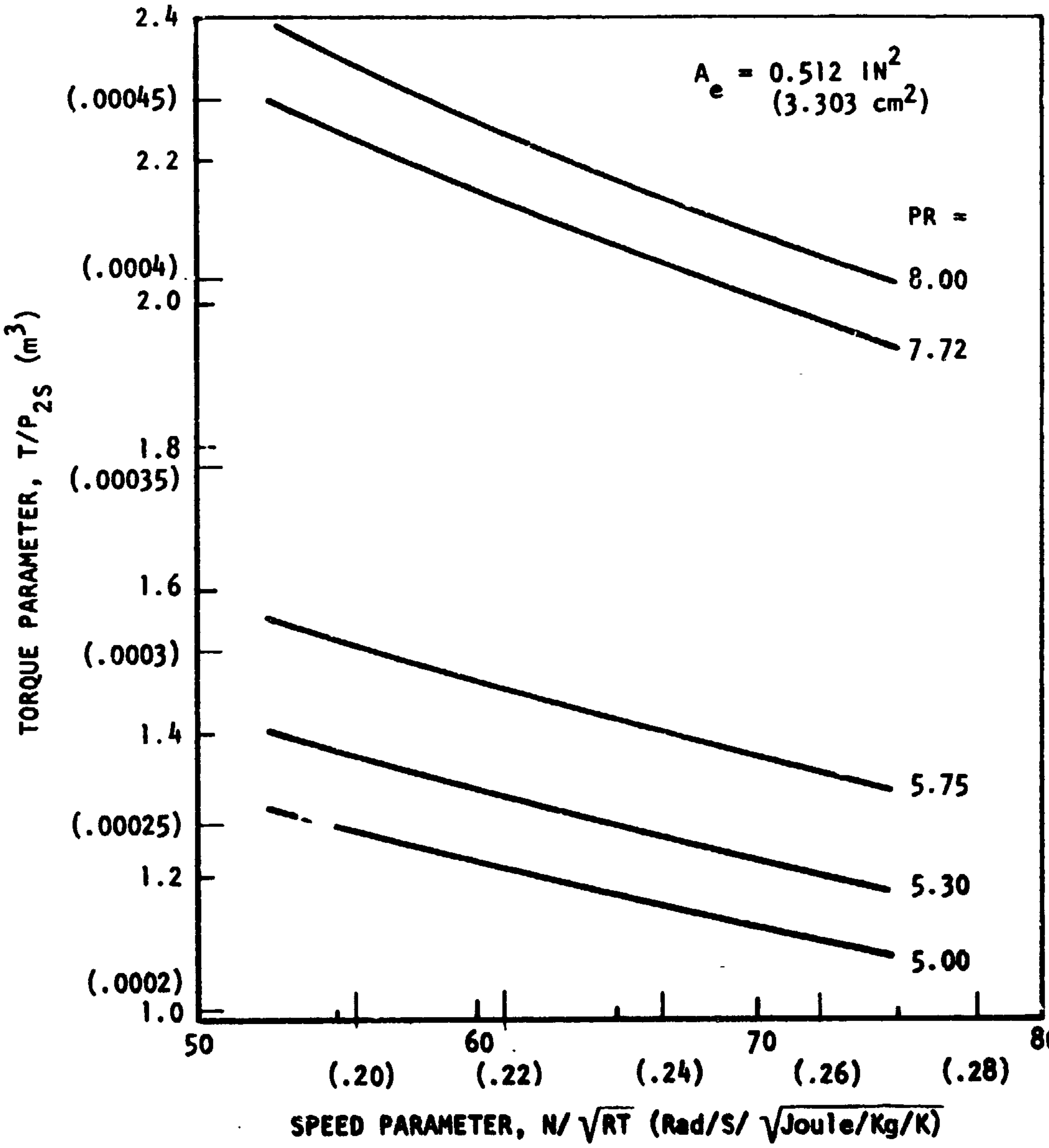

Figure 86. MK-44 Fuel Turbine - Estimated Performance

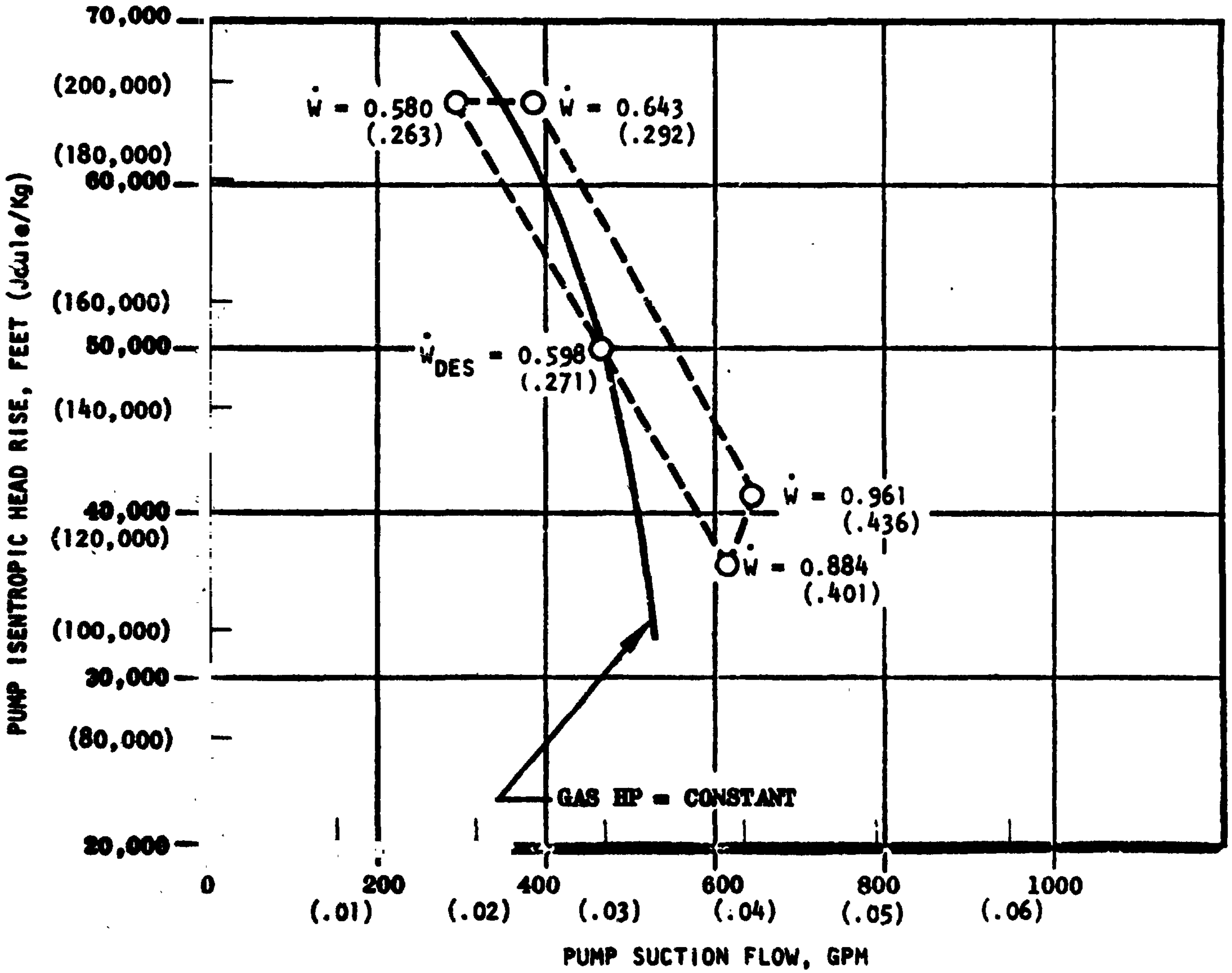

Figure 87. APS LH_2 Turbopump Turbine $\dot{w}$, lb/sec (Kg/sec)

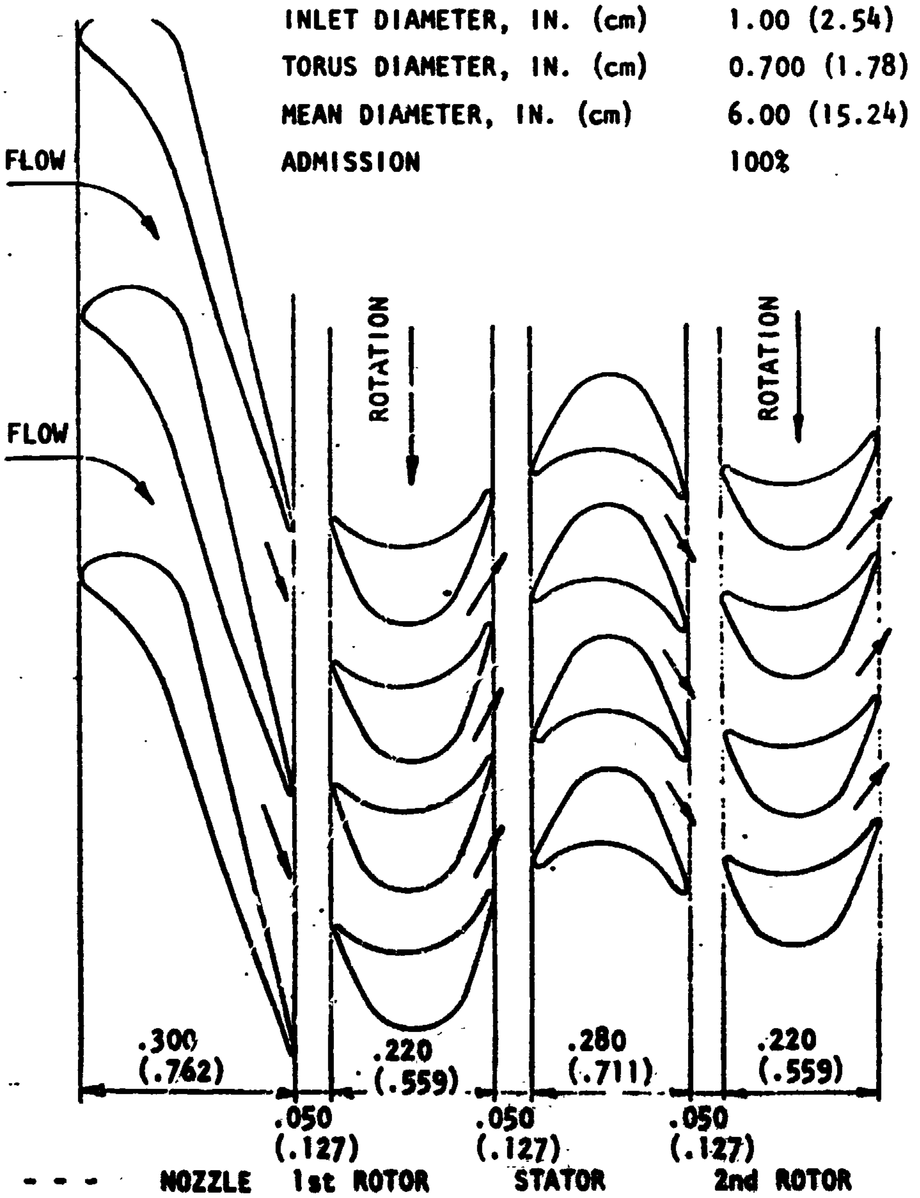

	NOZZLE	1st ROTOR	STATOR	2nd ROTOR
HEIGHT (cm)	0.258 (.655)	0.303 (.770)	0.390/0.473 (.991)/(1.201)	0.536 (1.361)
NUMBER	51	104	85	118

Figure 88. MK-44 Fuel Turbine - Gas Path Profile Sketch (Scale 5x)

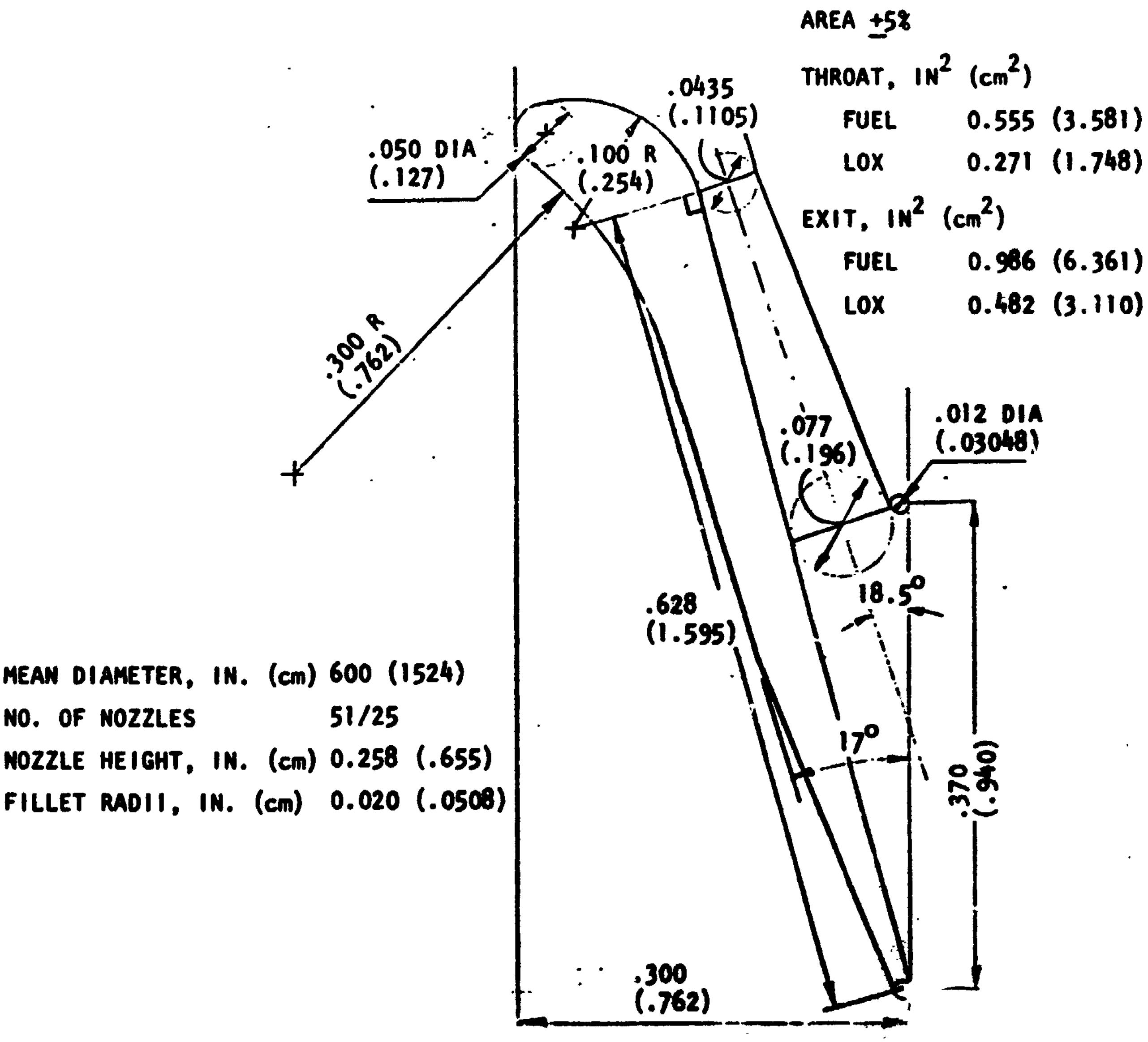

Figure 89. MK-44 Turbine - Profile Sketch
(Scale 10x)

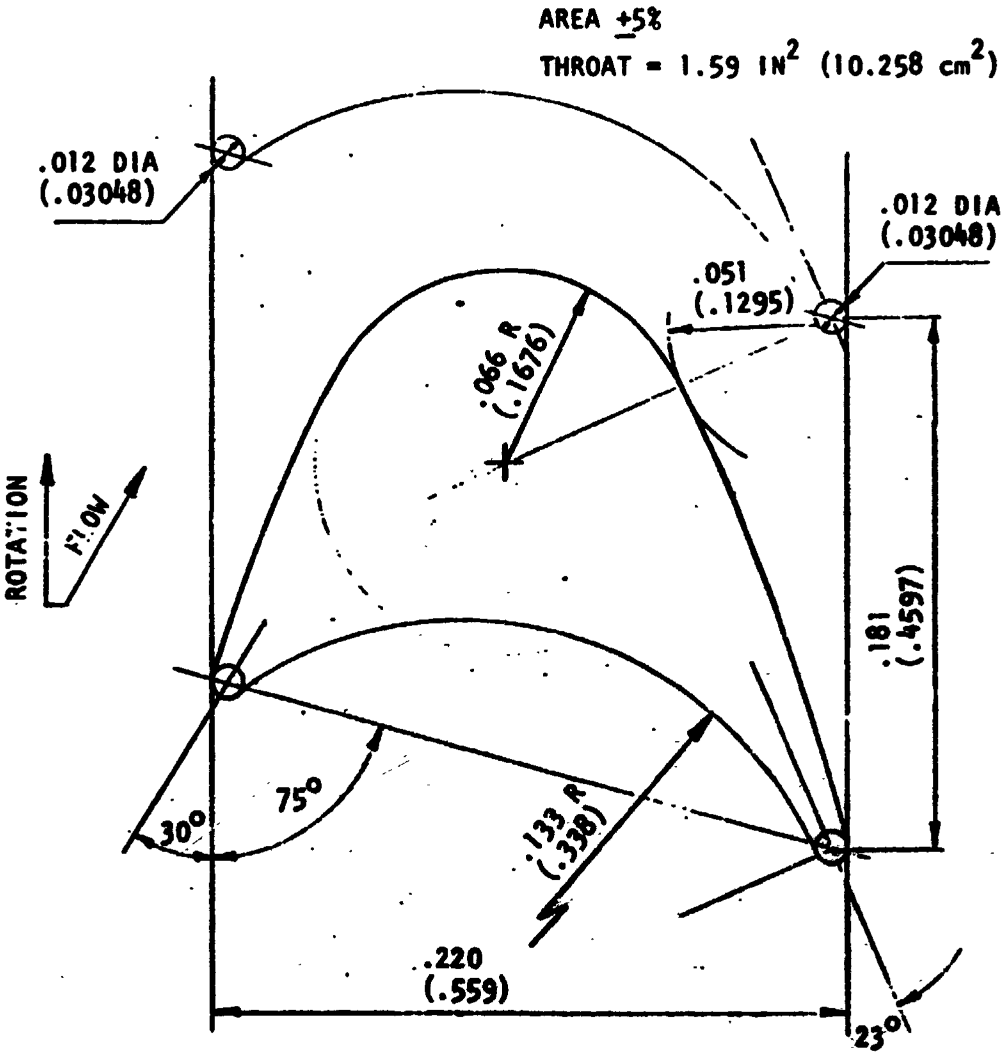

MEAN DIAMETER, IN. (cm)	6.00 (15.24)
NO. OF BLADES	104
BLADE HEIGHT, IN. (cm)	0.303 (.770)
FILLET RADII, IN. (cm)	0.020 (.051)
TIP CLEARANCE, IN. MAX (cm)	0.004 (.0102)

Figure 90. MK-44 Turbine Profile Sketch (Scale 20x)

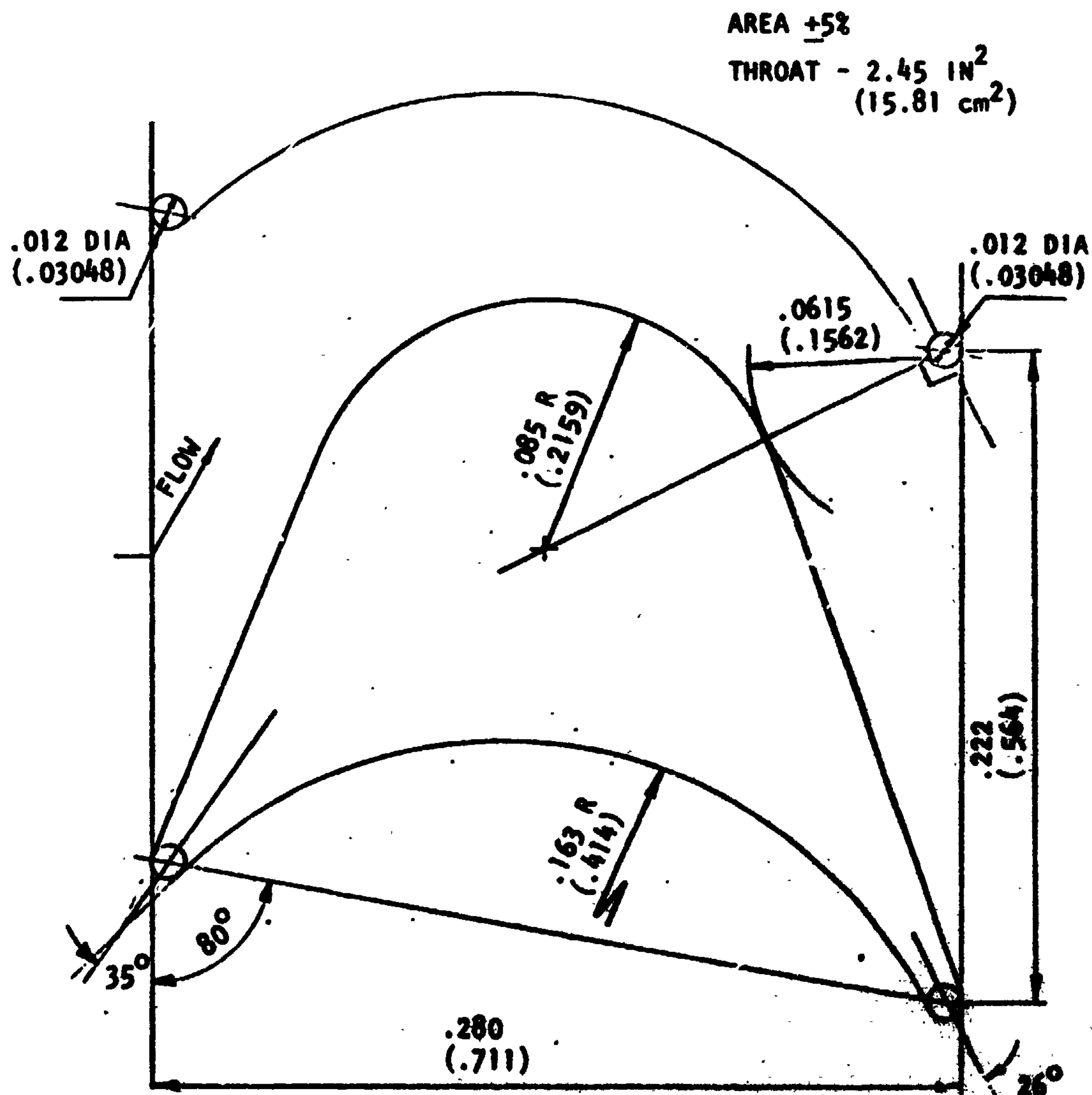

MEAN DIAMETER, IN. (cm)	6.00 (15.24)
NO. OF VANES	85
VANE HEIGHT, IN. (cm)	0.390/0.473 (.991/1.2014)
FILLET RADII, IN. (cm)	0.020 (.0508)

Figure 91. MK-44 Turbine Profile Sketch (Scale 20X)

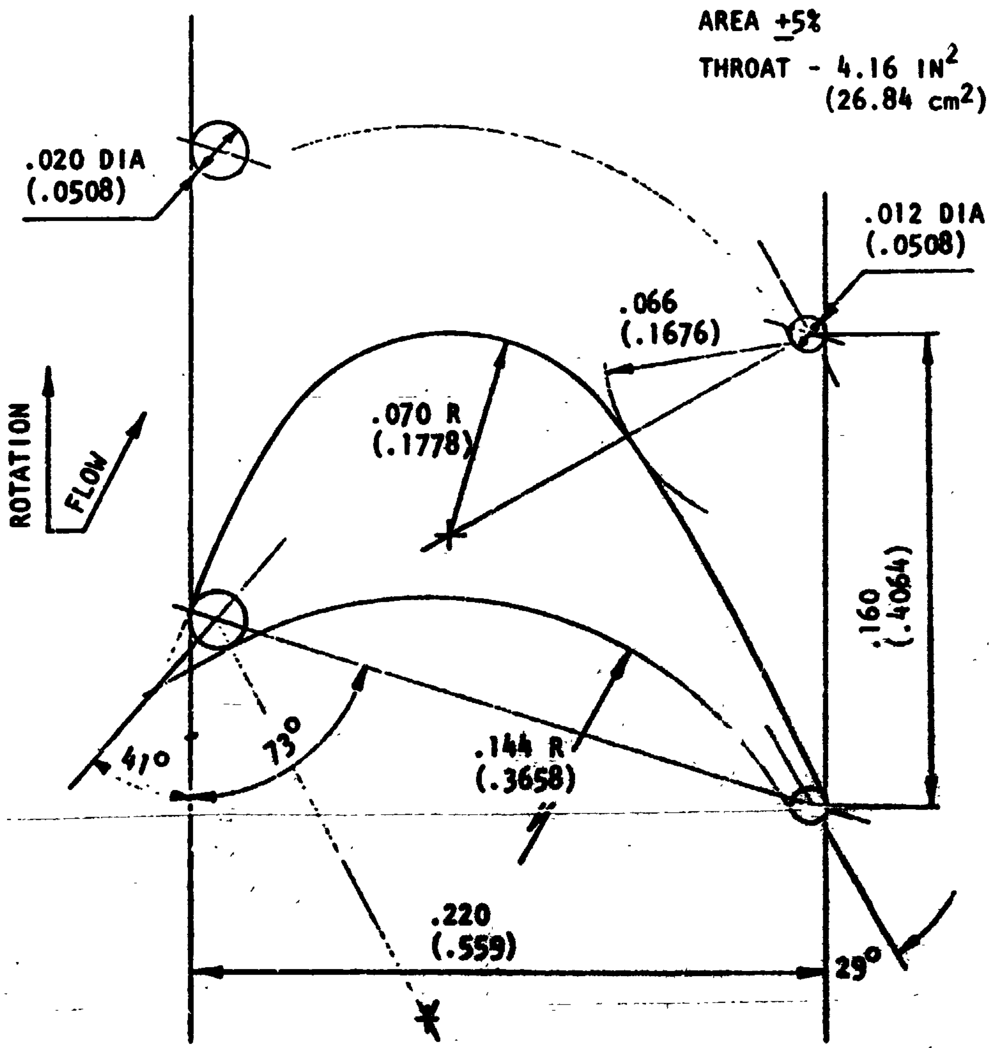

MEAN DIAMETER, IN. (cm)	6.00 (15.24)
NO. OF BLADES	118
BLADE HEIGHT, IN. (cm)	0.536 (1.3614)
FILLET RADII, IN. (cm)	0.020 (.0508)
TIP CLEARANCE, IN. (cm) MAX	0.007 (.0178)

Figure 92. MK-44 Turbine - Profile Sketch
(Scale 20x)

INLET DIAMETER, IN. (cm) D_i - 1.00 (2.54)

TORUS DIAMETER, IN, (cm) D_t - 0.700 (1.778)

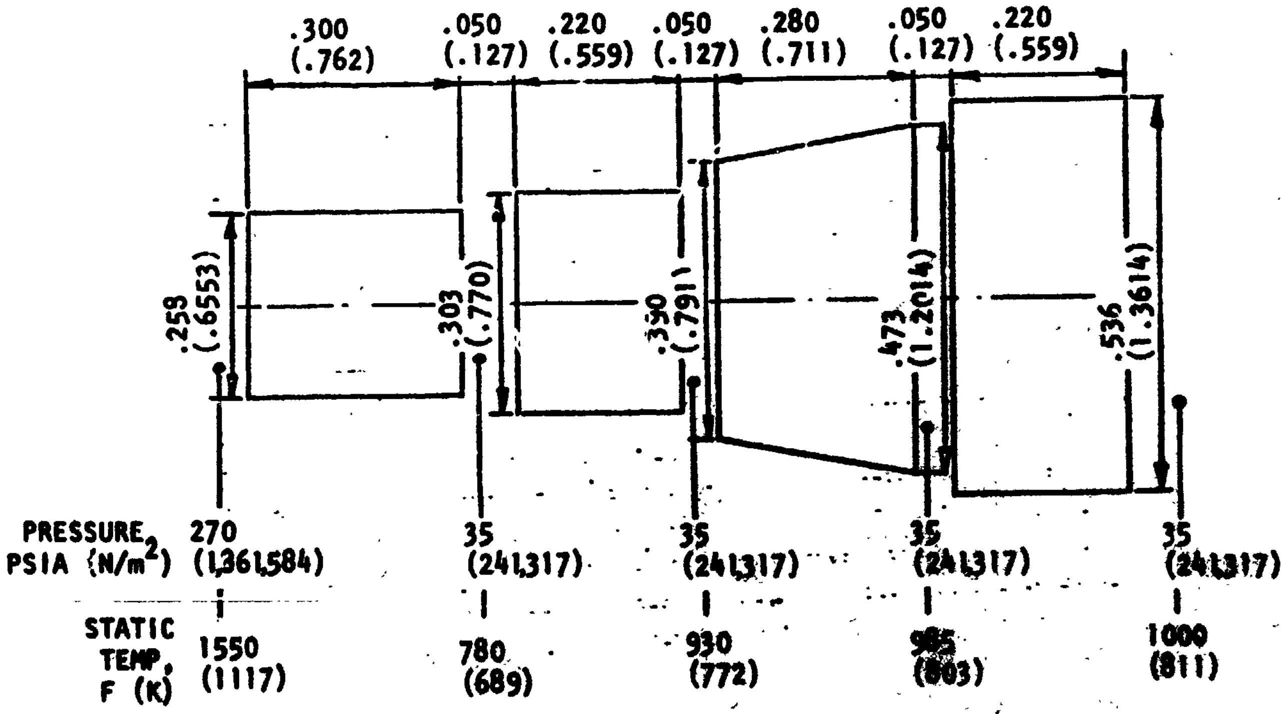

DESIGN PARAMETER:		
	INLET TEMPERATURE, F, T_{1t} °(K)	1550 (1117)
	INLET PRESSURE, PSIA, P_{1t} (N/m²)	270 (1861584)
	PRESSURE RATIO, PR	7.72
	SPEED, RPM, N (Rad/s)	60,000 ([illegible])
	MEAN DIAMETER, IN. D_m (cm)	6.00 (15.24)
	FLOW RATE, LB/SEC, W (kg/SEC)	0.5[illegible] (.2712)
	POWER, HP ([illegible])	[illegible]
	EFFICIENCY, %, η_{ts}	[illegible].3
	ADMISSION, %, ε	100

Figure 93, MK-44 Turbine - [illegible] Turbine Gas Path

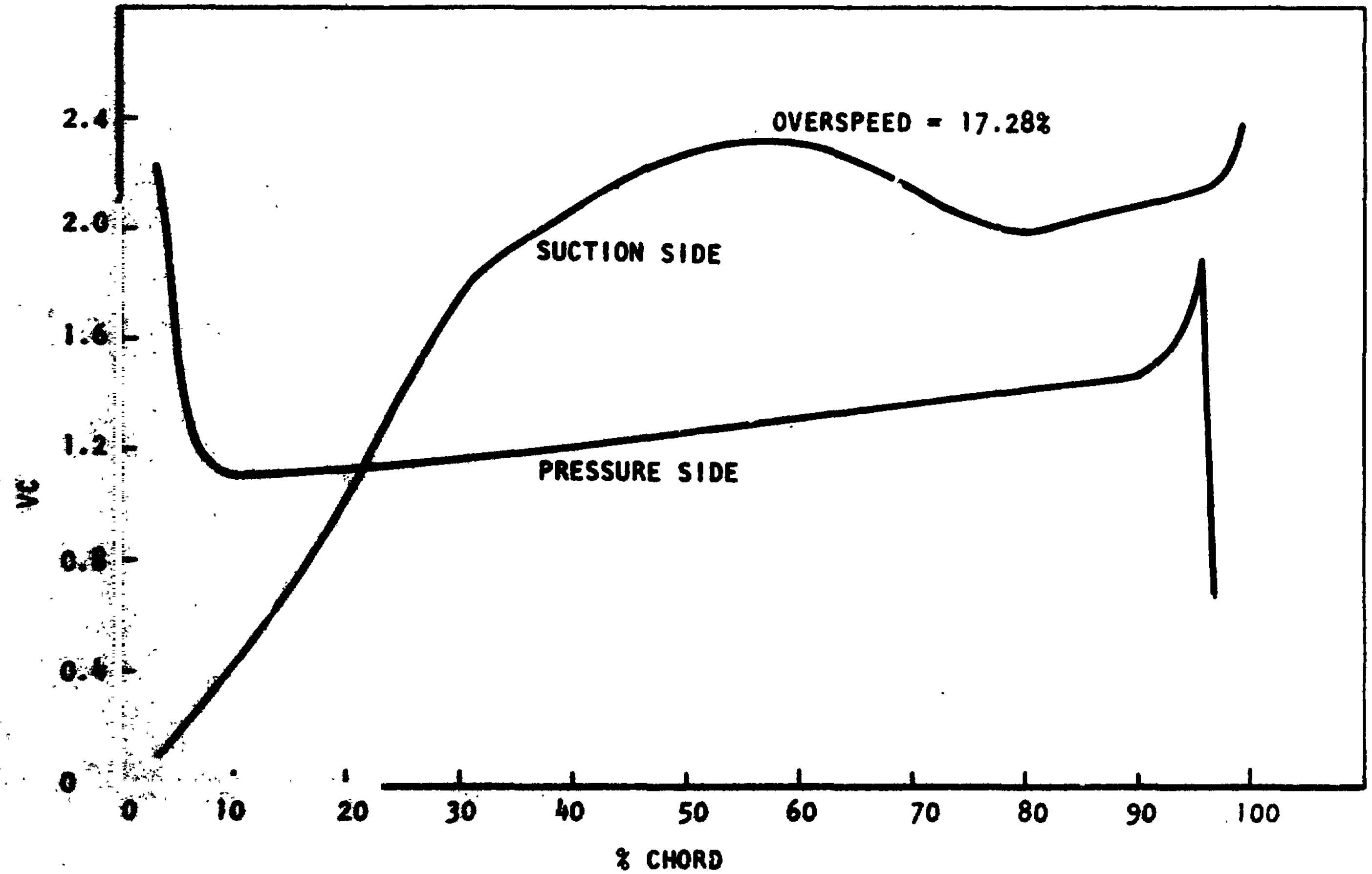

Figure 94. MK-44 Turbine - Blade Surface Velocity - 1st Rotor

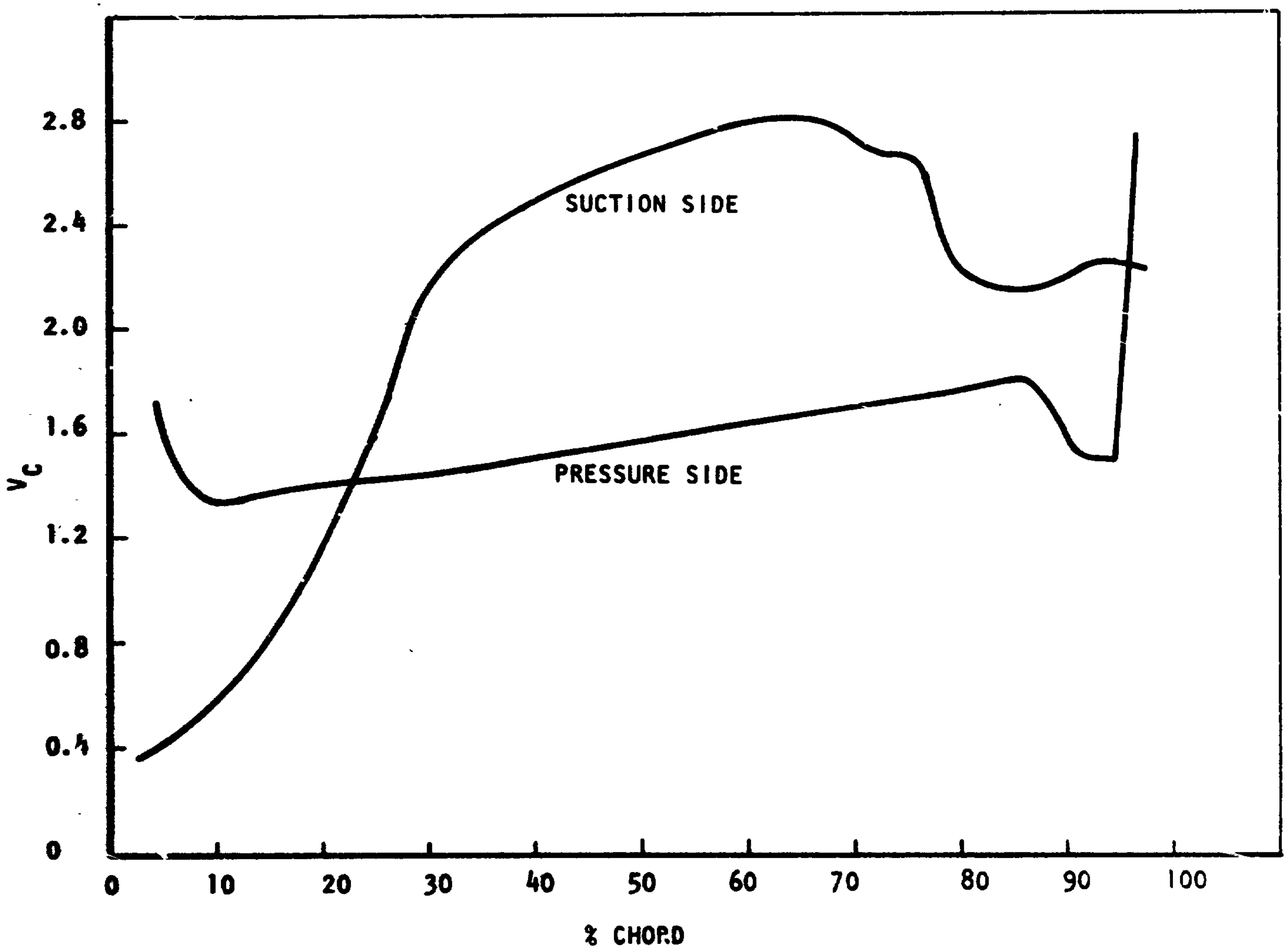

Figure 95. MK-44 Turbine - Blade Surface Velocity - Stator

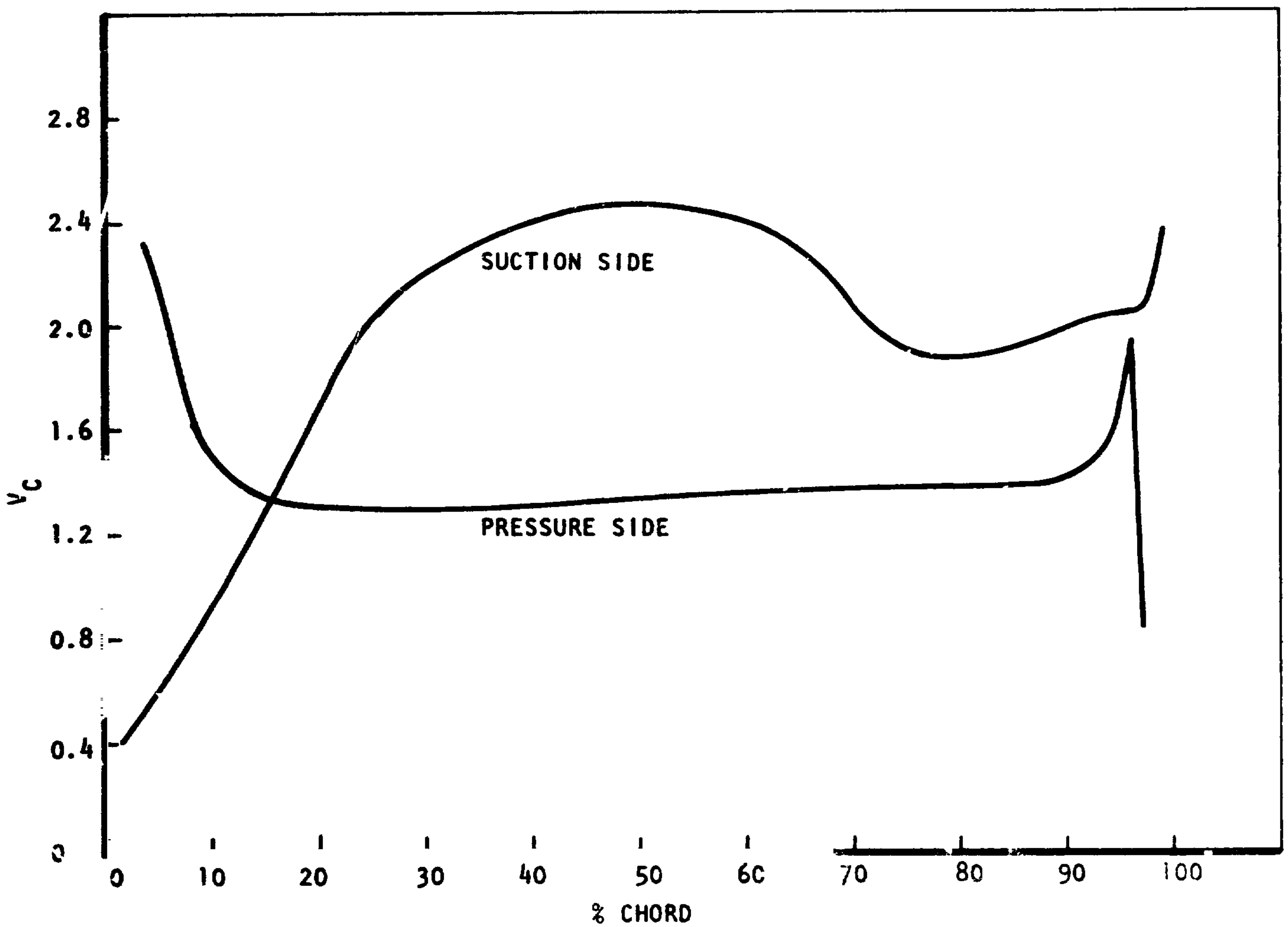

Figure 96. MK-44 Turbine - Blade Surface Velocity - 2nd Rotor

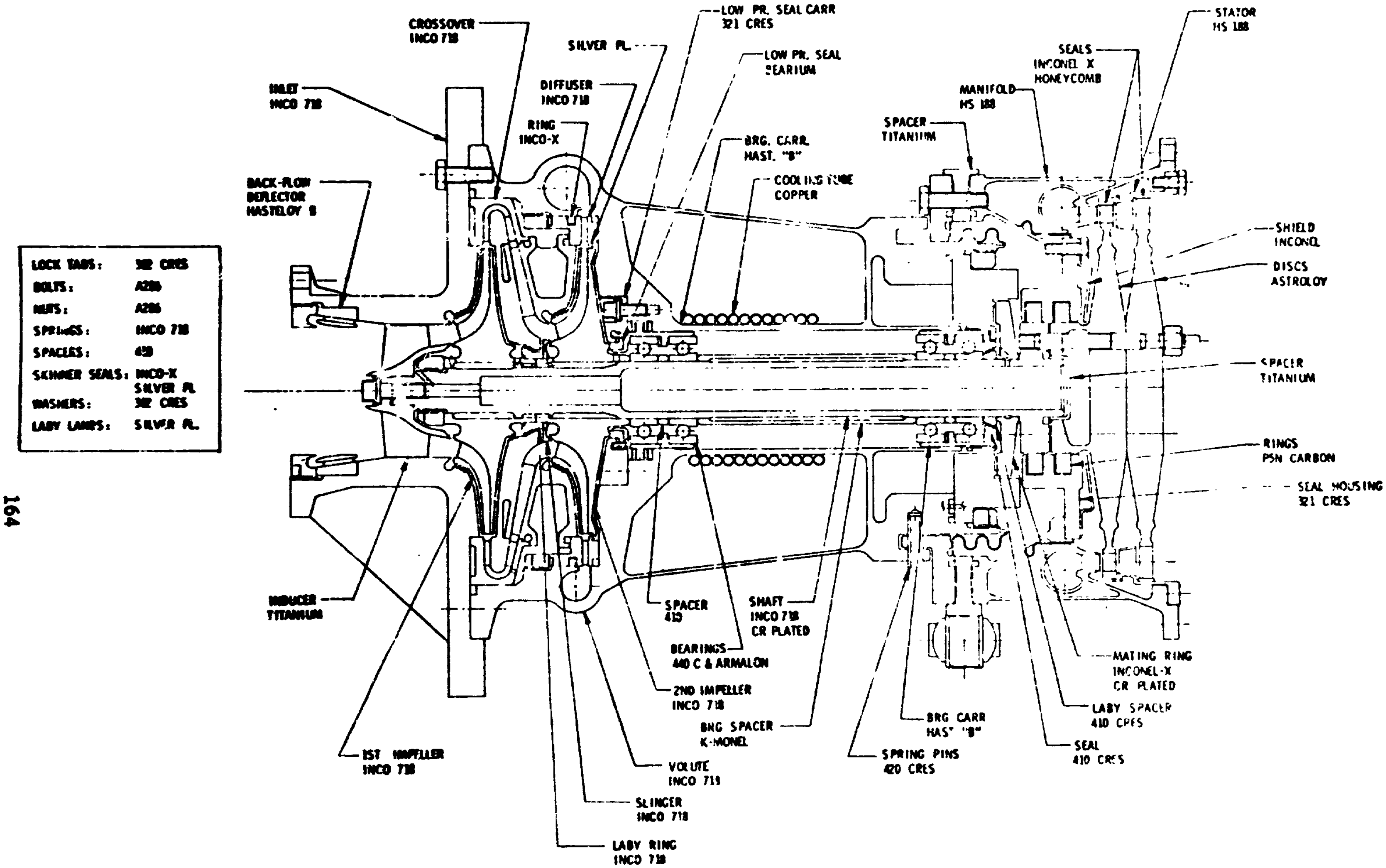

Figure 97. APS LH_2 Turbopump Materials

because it has excellent strength and elongation properties at LH_2 temperatures and, furthermore, it is a readily castable alloy which is important in a cost effective fabrication of the pump hydrodynamic surfaces. Since the inducer will be machined from a pancake forging, casting alloy will not be required for it. Titanium rather than steel was selected for the inducer to minimize the overhung mass. The impellers are being cast from Inco 718 by the lost wax process. The crossover is being cast from Inco 718 in two sections: the radial diffuser, turning passages and the first half of the inward flow passage are cast in one piece and the second half of the inward flow passage and the rib section are cast as a separate piece. The two castings are then joined by welding. The front part of the volute, including the hydrodynamic passages, is cast by the lost wax process, then the cylindrical members and the turbine end flanges are attached by welding. The shaft is machined from Inco 718 bar.

The turbine manifold is fabricated from HS 188. This material was selected because of its exceptional low-cycle fatigue properties and good weldability. To fabricate the manifold, the nozzle passages are eloxed from a ring forging, the external contour of the nozzle is machined, and the torus and supporting members are attached to the nozzle by welding. Both turbine disks are fabricated from Astroloy forgings with the blades machined integral with the disk. Turbine stator vanes are fabricated in a manner similar to the nozzle by eloxing the passages into solid ring forgings.

A modified Goodman diagram of the fuel inducer blade is shown in Fig. 98 . Failure line is defined at the ordinate intercept by the endurance strength and at the abscissa intercept by the ultimate strength. The operating point noted represents the highest anticipated blade loading at minimum flow and maximum speed. Based on past experience, the alternating stress is assumed to be 30 percent of the pressure stress. The mean stress is relatively low because the vanes are canted at 10 degrees so that the centrifugal bending stress tends to counteract the fluid bending stresses. For the most severe loading, a satisfactory factor of safety of 1.4 is maintained.

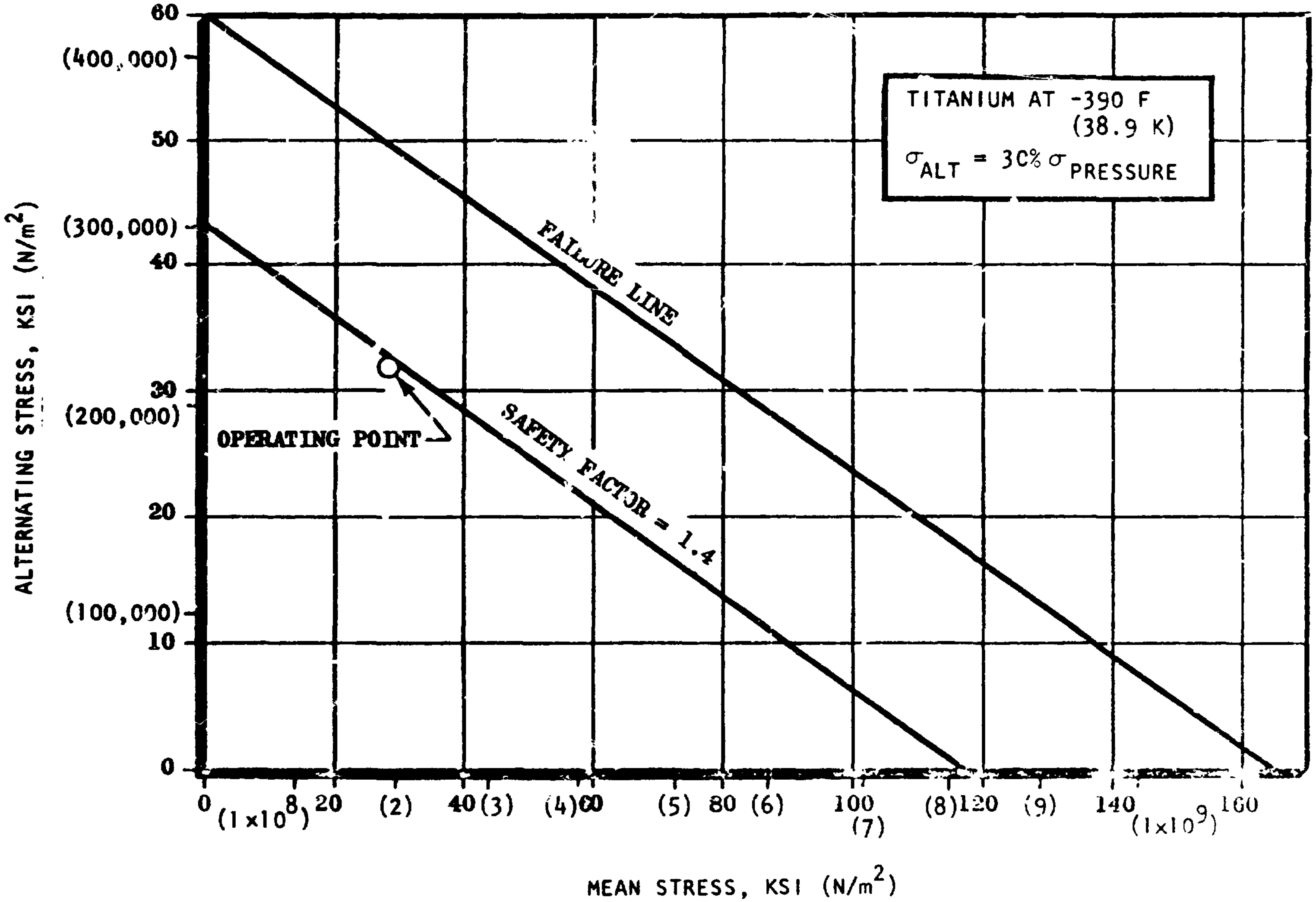

Figure 98. APS Fuel Inducer Blade Modified Goodman Diagram

Figure 99 presents the allowable turbine blade $A_A N^2$ parameter as a function of temperature. The ordinate is a product of blade annular area and rotor speed squared. This parameter is an indication of the centrifugal stresses to which the blades are exposed. Allowable stress levels as a function of temperature are indicated by the solid lines for Astroloy, with pressure-bending stress as a parameter. The pressure-bending stresses for both first- and second-row blades are less than $3{,}477 \times 10^7$ N/m^2 (5000 psi), thus the stress limit for fuel turbine blades is represented by the middle curve. The actual stress levels for both first- and second-stage blades are indicated in the figure. There is a substantial margin of safety for both blades.

An interference diagram for the fuel turbine first-row blades is presented in Fig. 100. The solid diagonal line correlates speed-to-blade passing frequency for the 51 nozzles. The natural frequency of the first-stage blades about the minimum moment of inertia, which is basically a tangential mode, falls below the operating range. The natural frequency about the maximum moment of inertia, an axial mode, falls above the operating range. No critical frequencies are excited in the operating speed range.

Similarly, Fig.101 presents the interference diagram for the fuel second-row blades. Because of the higher blade length, the natural frequencies about the minimum and maximum moments of the inertia are substantially lower than those of the first-stage blades. The natural frequency of Mode 2 about the minimum moment of inertia falls below the operating range. No natural frequencies are exited in the operating speed range.

Rotor Dynamics

Rotor critical speeds as a function of bearing radial spring rates are presented in Fig. 102. The first critical speed with the predicted spring rates is at approximately 1885 rad/s (18,000 rpm). The second critical speed is at 2932 rad/s (28,000 rpm), and the third critical speed 15,708 rad/s (150,000 rpm). The steady-state operating speed range falls between the second and third critical speeds, as shown in the figure. There is a more than satisfactory margin free of critical speeds, both below and above the steady-state operating range.

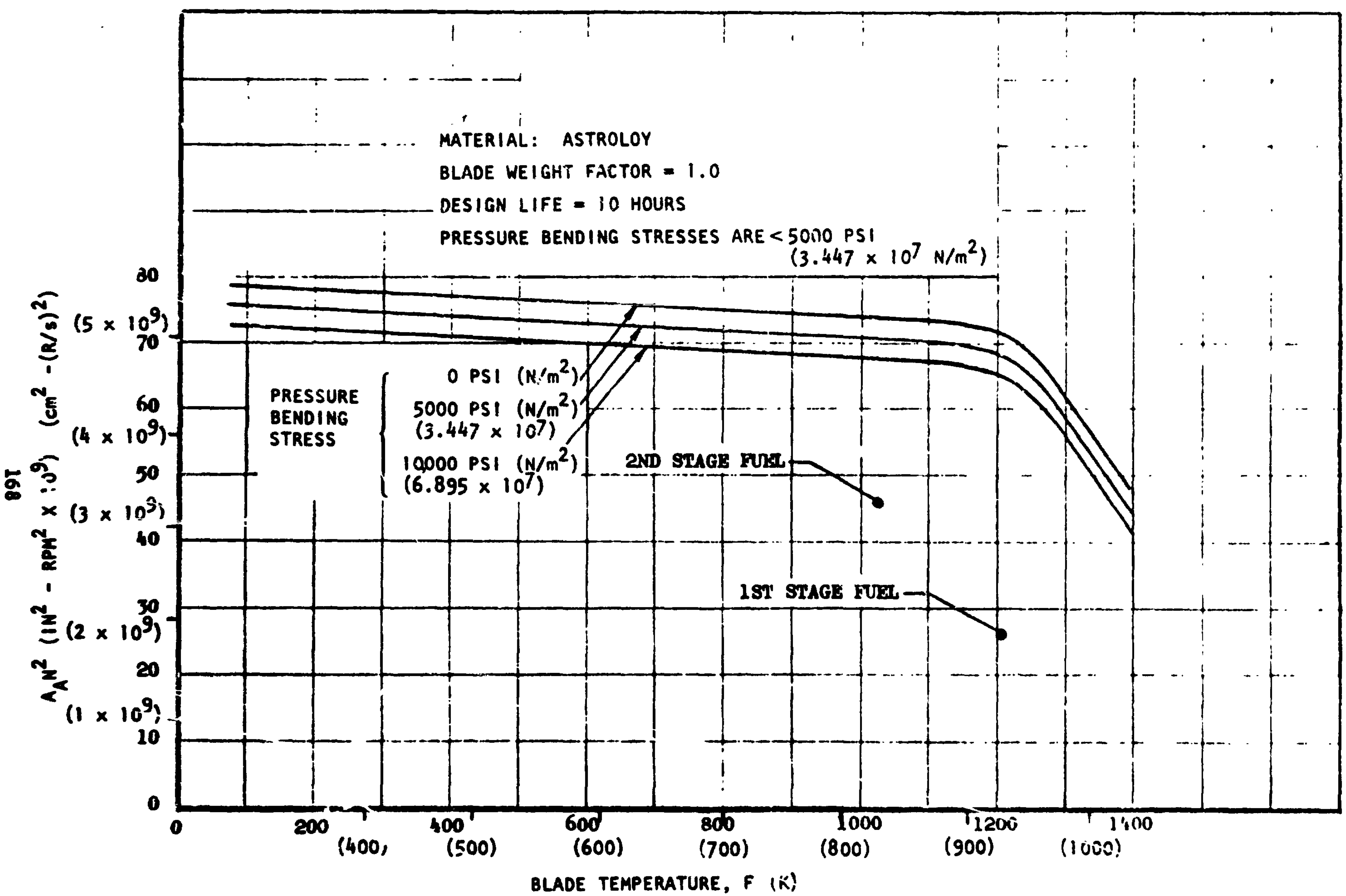

Figure 99. APS Fuel Turbine Blade Allowable $A_A N^2$ vs Temperature

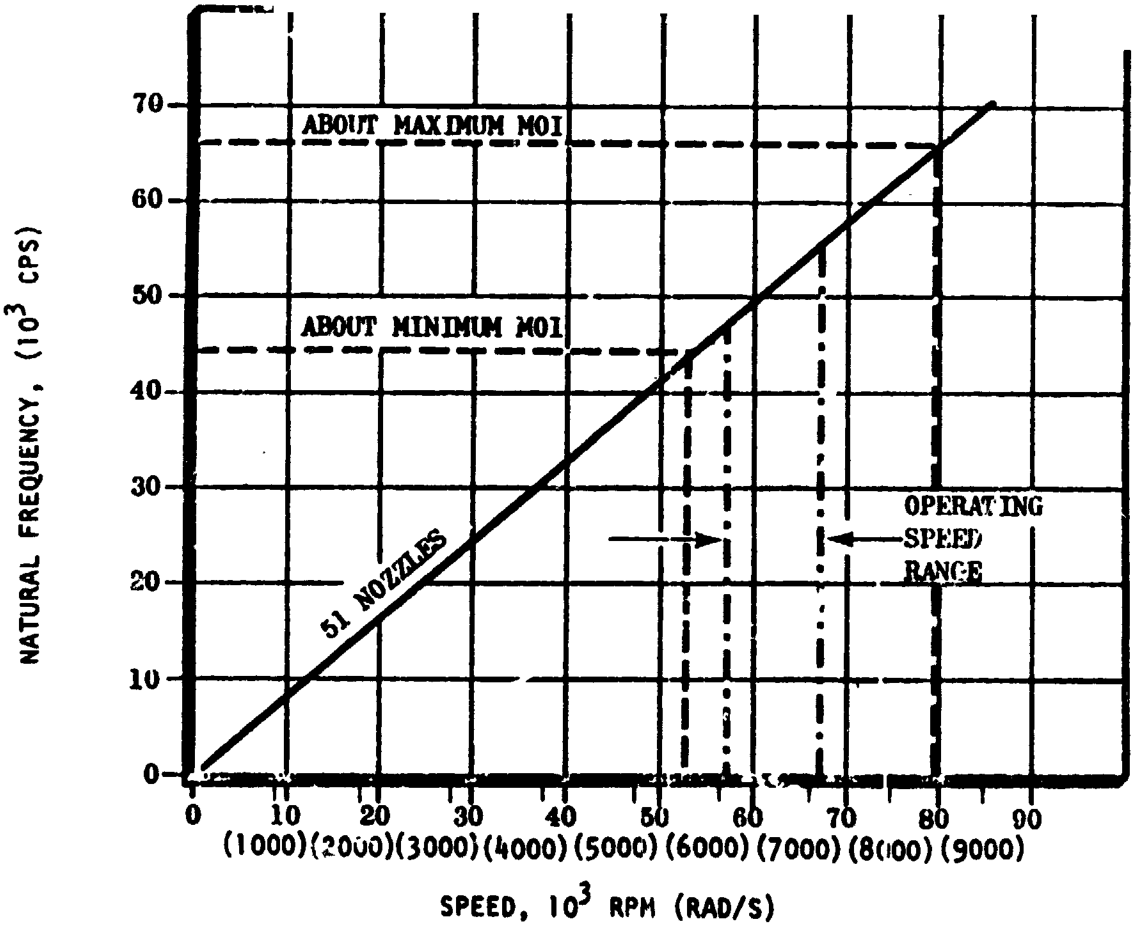

Figure 100. APS LH_2 Turbopump Turbine First Row Blade Interference Diagram

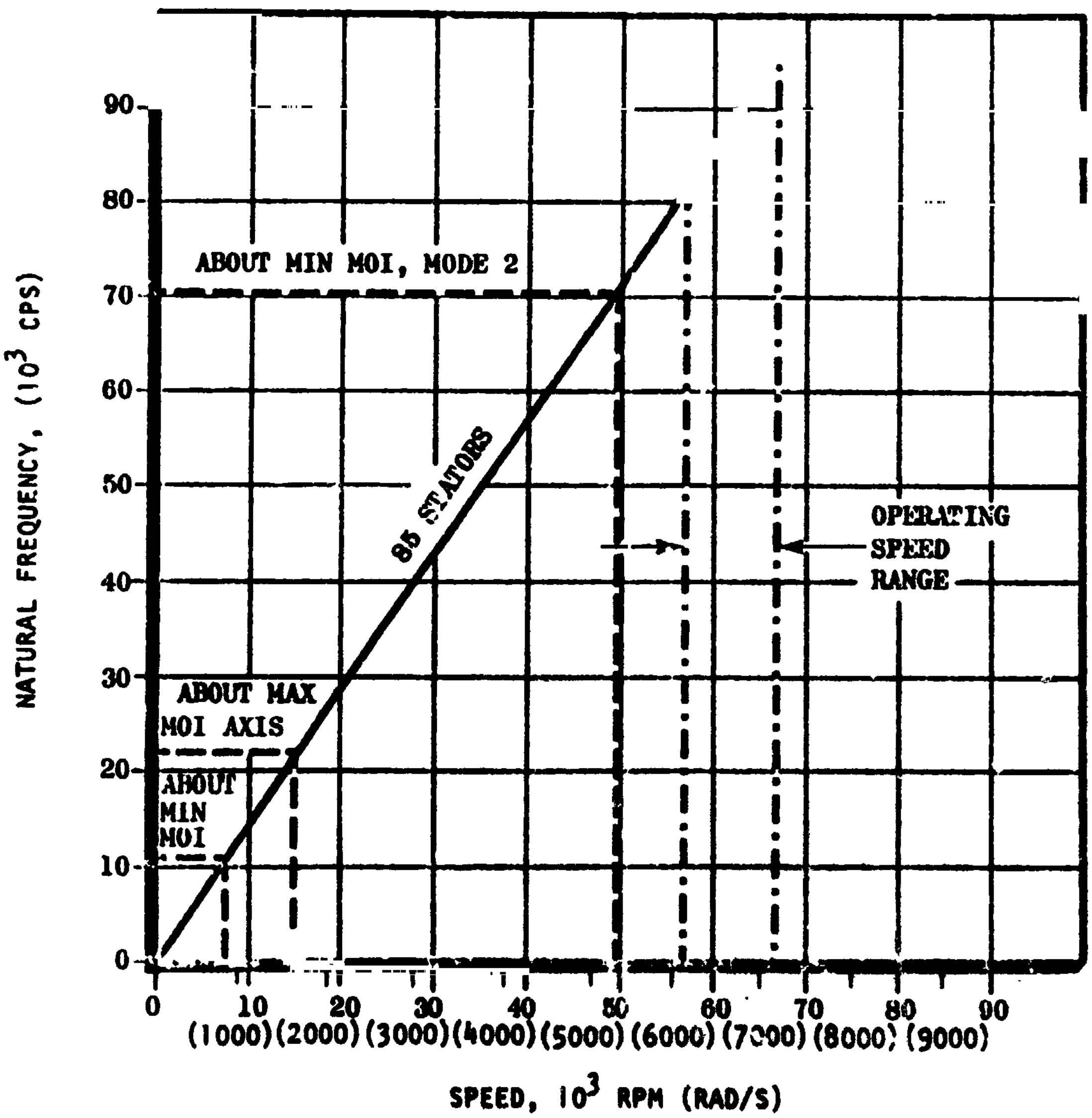

Figure 101. APS LH_2 Turbopump Turbine Second Row Blade Interference Diagram

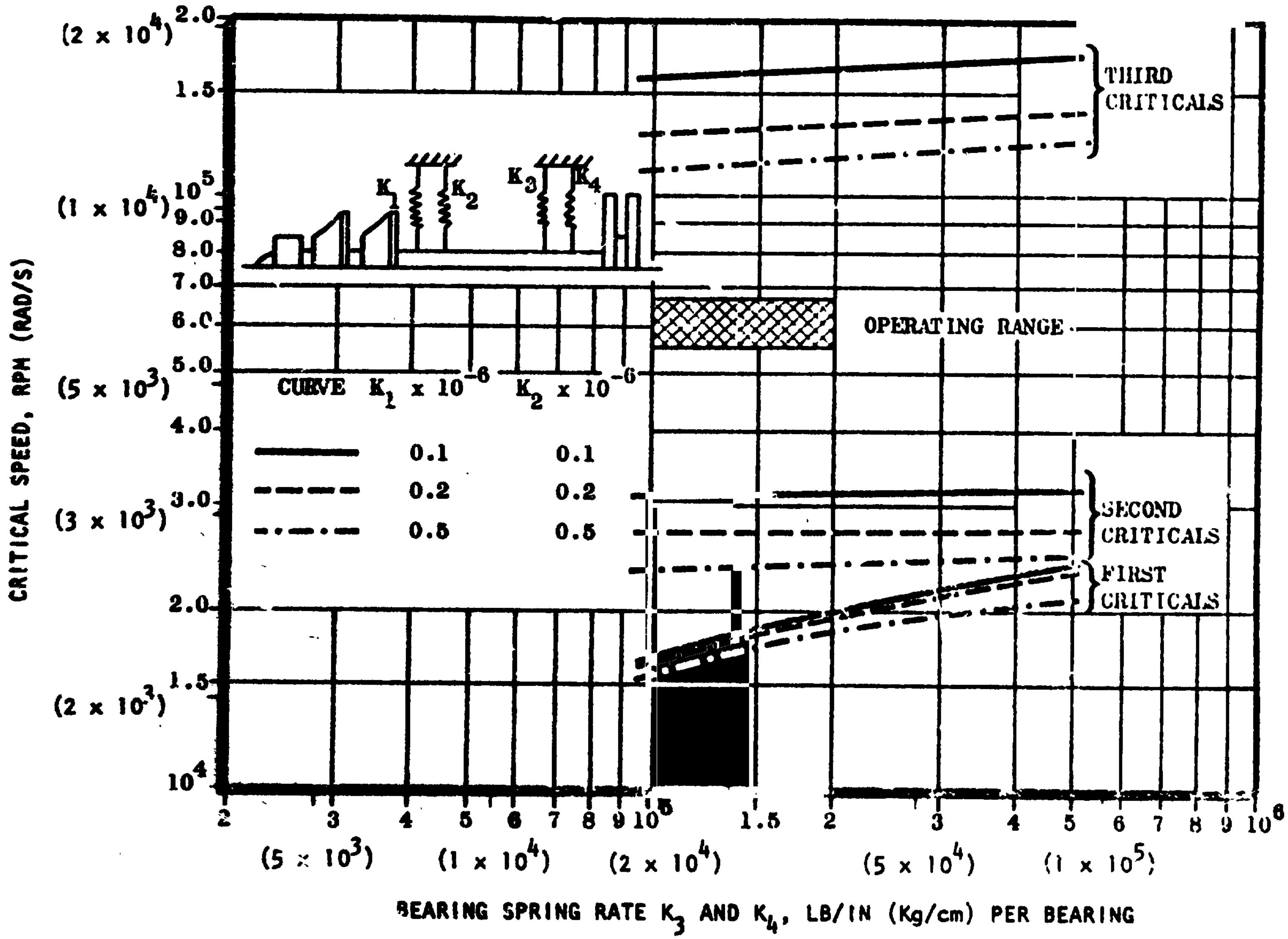

Figure 102. APS LH_2 Turbopump Rotor Critical Speeds

Figure 103 indicates the normalized rotor mode shapes at the various critical speeds. The first critical is substantially a stick mode with approximately equal deflections taking place at the pump and turbine end. The second critical is a bending mode with most of the deflections taking place at the pump end of the rotor. The third critical is also a bending mode with major deflections in the bearing area.

Bearing and Seals

Table 30 shows the significant design parameters for the 25 mm angular contact fuel bearing. On the basis of past experience, AISI 440-C consumable electrode vacuum melted steel was selected for race and ball material. Armalon was selected for the cage material because of its superior strength characteristics, and wide experience with it in cryogenic lubricated bearings. All bearings are preloaded to 65 pounds in the turbopump, with a resulting predicted B-1 fatigue life of 102 hours.

Figure 104 shows a schematic of the LH_2 turbopump lift-off seal. The seal design incorporates three bellows elements whose function it is to separate various fluid areas and to preload the carbon nose against the mating ring during static conditions. During coast, the actuation pressure is vented. There is 50 psia in the bearing cavity and zero psig on the turbine side of the liftoff seal. Under these conditions, the bellows preload the carbon nose against the mating ring. On a normal start, the actuation cavity is pressurized to 1,378,951 N/m^2 (200 psia) before rotation is initiated, causing the carbon nose to lift off.

Should the actuation pressure fail to materialize, rotation is started with the carbon nose in contact; when the bearing cavity pressure reaches the pressure level of 100 psia, the carbon nose is lifted off by hydraulic loading.

The shaft dynamic seal is a floating ring control gap shaft rider type, using two ring elements to reduce leakage and to provide redundancy. Each ring element is

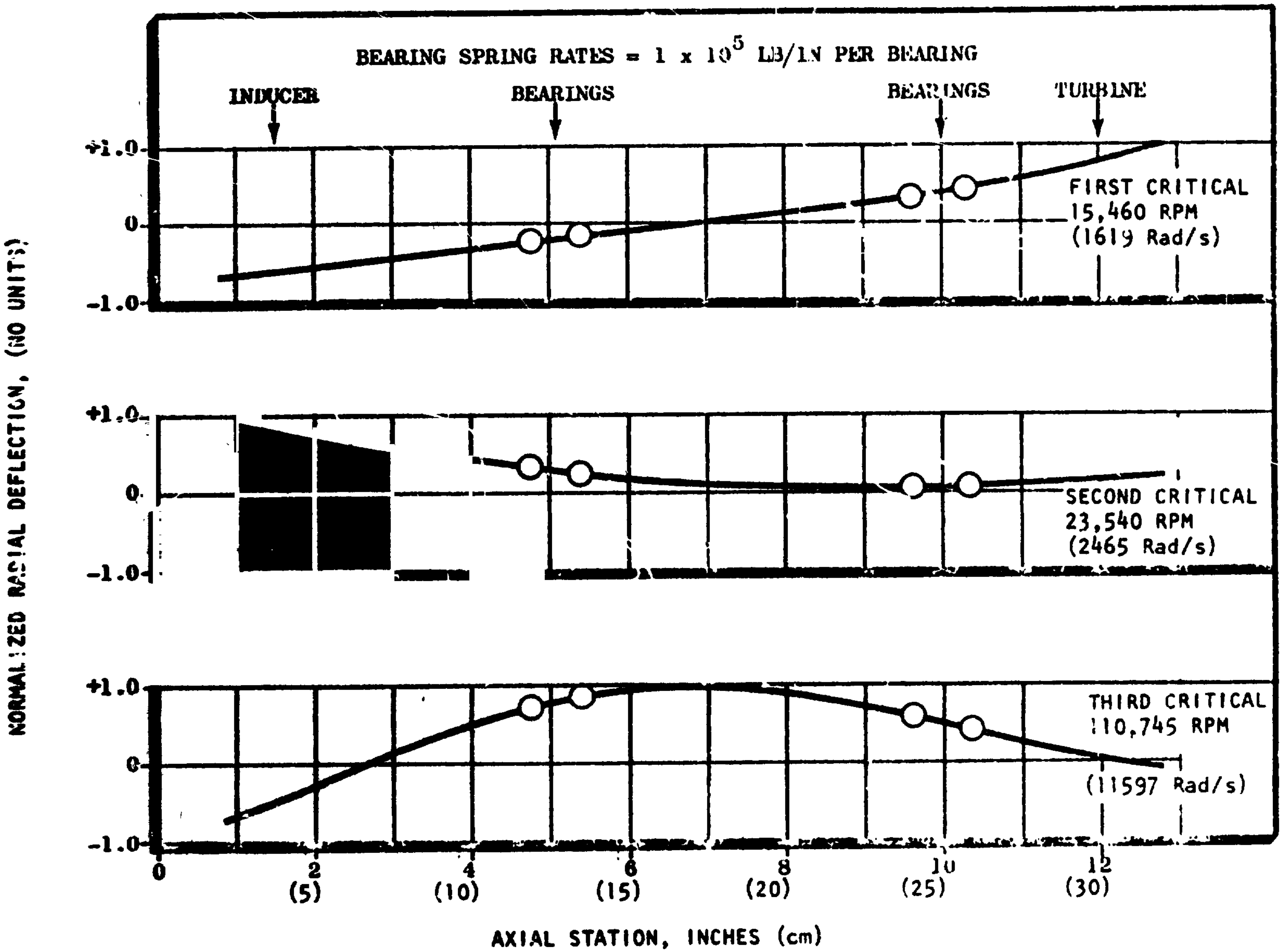

Figure 103. APS LH_2 Turbopump - Rotor Mode Shapes

TABLE 30. APS LH_2 TURBOPUMP BEARING DESIGN PARAMETERS

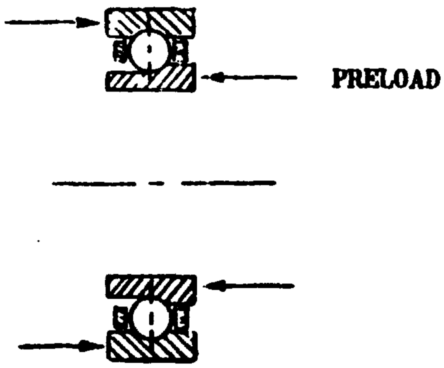

TYPE	:	Angular contact
BORE	:	25 mm
DN	:	1.5×10^6 mm rpm
PITCH DIAMETER	:	3.6068 cm (1.42 in.)
BALL DIAMETER	:	0.556 cm (7/32 in.)
NUMBER OF BALLS	:	11
RACE MATERIAL	:	A1S1 440C (CEVM)
BALL MATERIAL	:	A1S1 440C (CEVM)
CAGE MATERIAL	:	Armalon
AXIAL PRELOAD	:	448,159 N/m^2 (65 lb)
B_1 FATIGUE LIFE	:	192 hrs

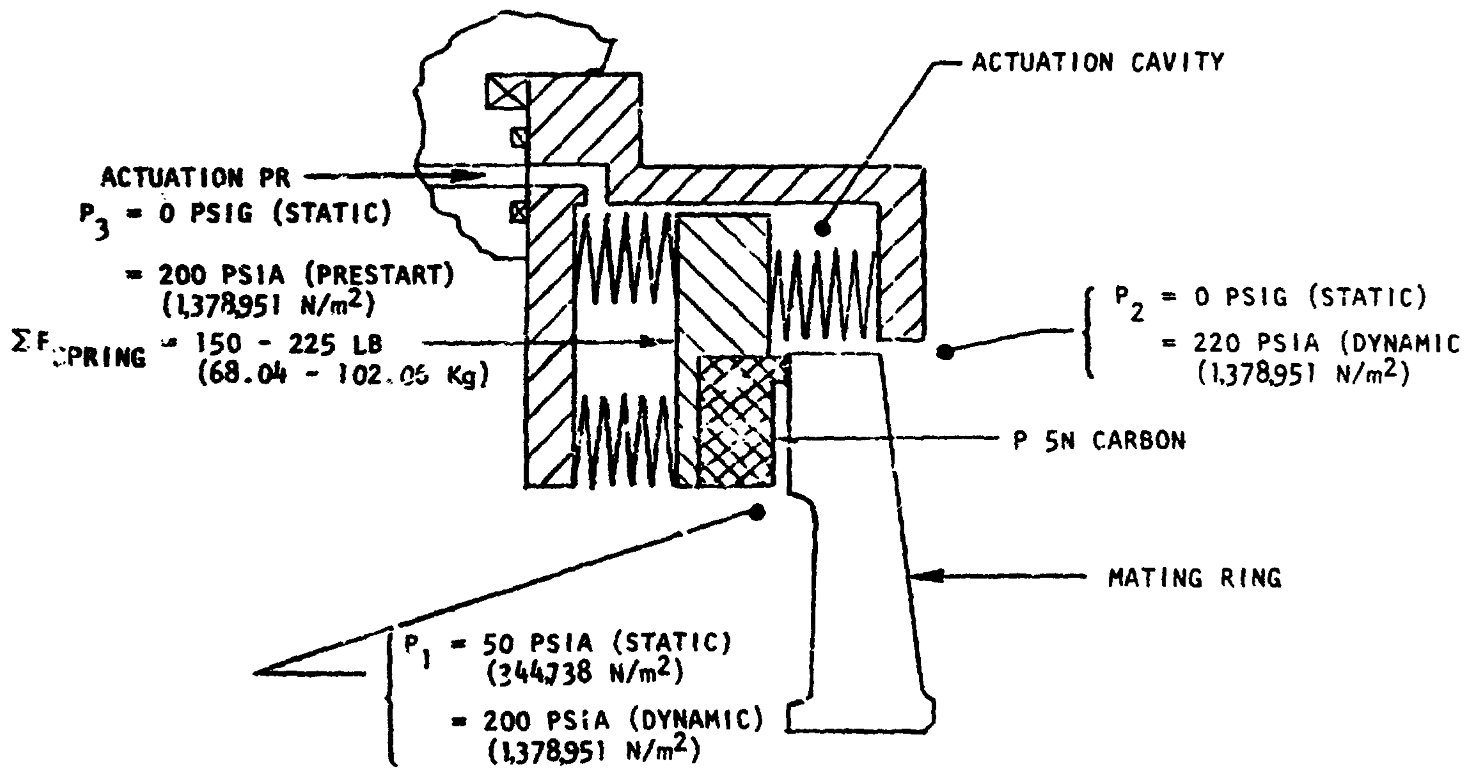

Figure 104. APS LH_2 Turbopump Lift-Off Seal Schematic

pressure balanced by relieving the contact surface except for a narrow sealing lip (Fig. 105). The sealing element is steel reinforced P5N carbon, and the housing is made from Inconel X. The shaft to seal ring diametral clearance is set at 0.003 inch.

Heat Transfer

The LH_2 turbopump design utilizes the low thermal conductivity of Inconel 718 in conjunction with minimum contact area flange designs (including a pin joint attachment and bellows at the turbine end) to thermally separate the pump and turbine. The turbopump is isolated from the vehicle by ball joint mounts to minimize energy transfer during long soakback periods. Cooling coils and a bleed port are included in the design to give flexibility in utilizing external cooling during testing of the turbopump.

A lumped parameter thermal model was used to evaluate the various design modifications under soakback conditions and consisted of 15 nodes representing the turbopump, (Fig. 106), with six fluid nodes (not shown) to represent the leakage (and bleed) flow through the shaft and bearings. This model also included a node representing the turbine exhaust duct to simulate the radiant heat input to the turbine blades during soakback. Solutions were obtained for the various designs using the Rocketdyne Differential Equation Analyzer Program (DEAP) to solve for the nodal temperatures and the quantity of energy reaching the pump body using variable conductivity and specific heats.

The following assumptions were used in analyzing the various turbopump designs:

1. TPA has been run to thermal equilibrium
2. Environment temperature is 300 K (540 R)
3. Pump housing and cone are insulated with 1 inch of super insulation
4. Exhaust duct is also insulated and has a long L/D
5. Heat transfer coefficients for bleed and leakage flows based on hD/K - 2

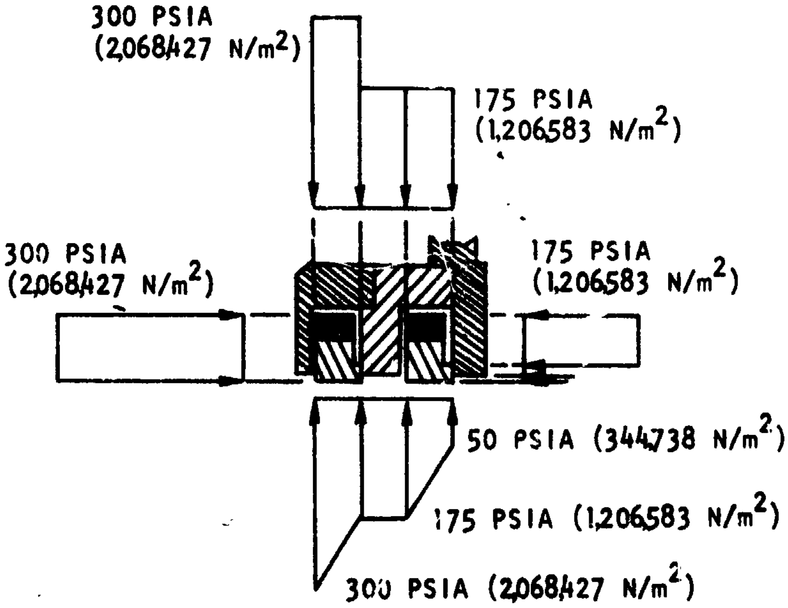

Figure 105. Shaft Seal Pressure Balance

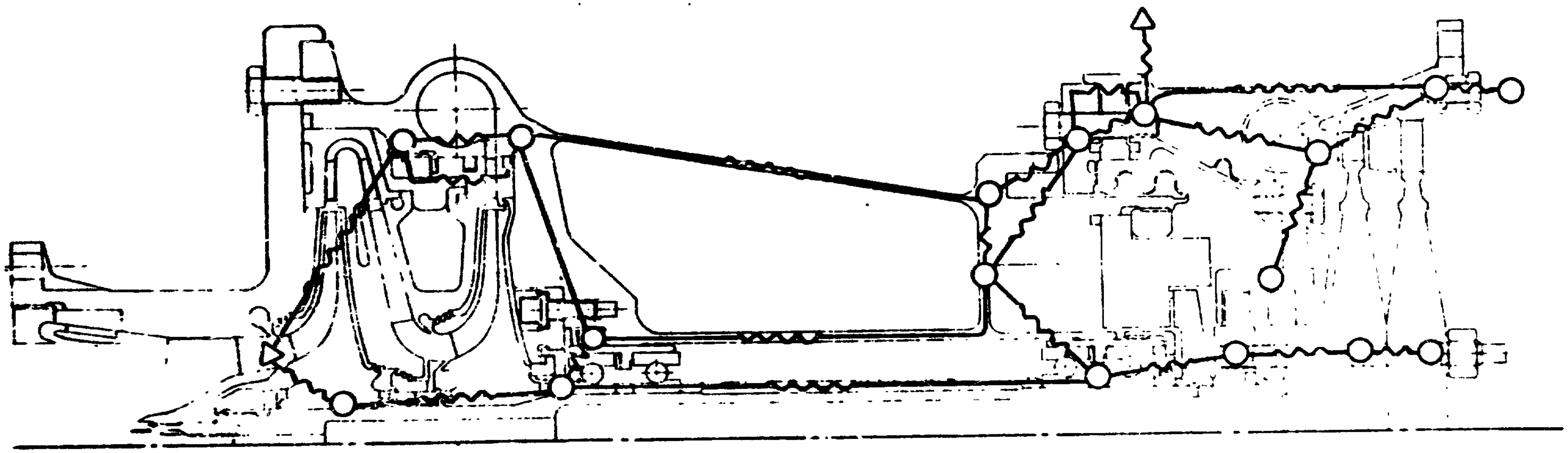

Figure 106. LH_2 TPA Heat Transfer Model

The preceding assumptions were used in conjunction with a long 10 hour soakback. Although a 10-hour soakback period is not likely to occur, the behavior of the turbopump under these conditions gives a worst case prediction for design since the 10-hour soakback period is long enough to reach the peak heat leak value for the designs.

The cases analyzed included:

1. No external cooling. Shaft seal leakage was assumed to be 0.0227 kg/hr (0.05 lb/hr)
2. No external cooling and no seal leakage
3. External cooling using 0.1134 kg/hr (0.25 lb/hr) of H_2 assumed

A comparison of the heat leak history to the pump body is shown in Fig. 107 for four of the designs that were evaluated. The upper curve for Sketch 102 represents the Phase I design using conventional flange designs. The curves for Sketches 103 and 104 show how incorporation of minimum contact area flanges can reduce the heat leak to below one half of conventional designs. However, the predicted turbine bearing temperature was felt to be marginal for these designs and the final design (Sketch 105) eliminated the pump housing flange to increase the heat leak and reduce the turbine bearing temperature. This design is felt to be the best compromise between the heat leak to the propellant and the turbine bearing temperature requirements

The predicted soakback behavior of the LH_2 turbopump design following a steady-state run under conditions of no external cooling and no leakage through the closed lift-off seal is shown in Fig. 108. This is an unlikely case because of the seal configuration and is presented to show that the heat leak to the propellant peaks after 7 hours at 83,348 Joule/hr (79 Btu/hr) and the turbine bearing temperature reaches 250 K (450 R) while the pump bearing and housing remain at essentially liquid temperature. Under these conditions, the heat leak rate exceeds the design goal of 52,752 Joule/hr (50 Btu/hr) after 3 hours of soakback and indicates that external cooling would be required to keep the turbopump ready for an instant start for off periods greater than 2 hours.

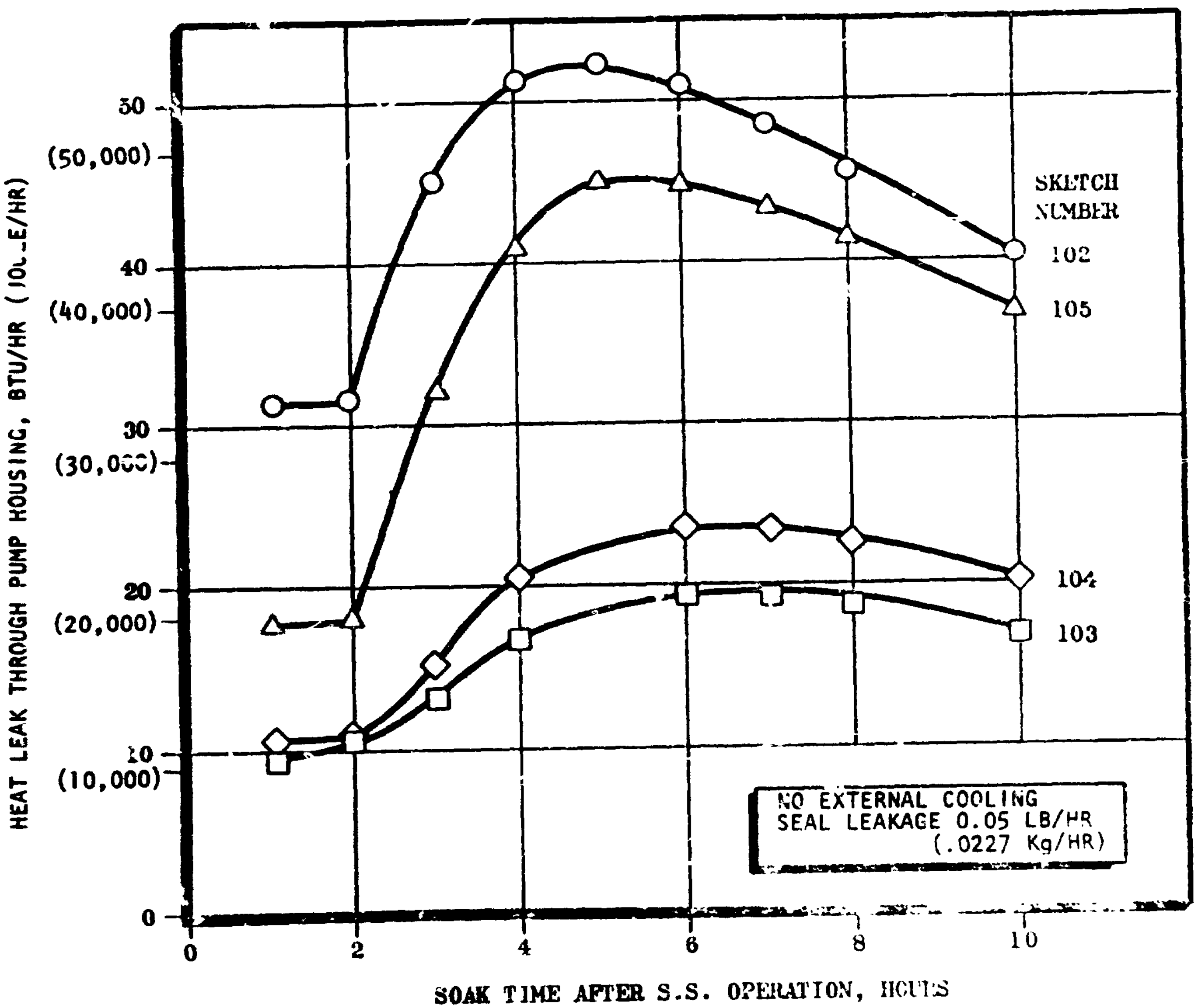

Figure 107. Comparison of Heat Leak for H_2 APS Turbopump Designs

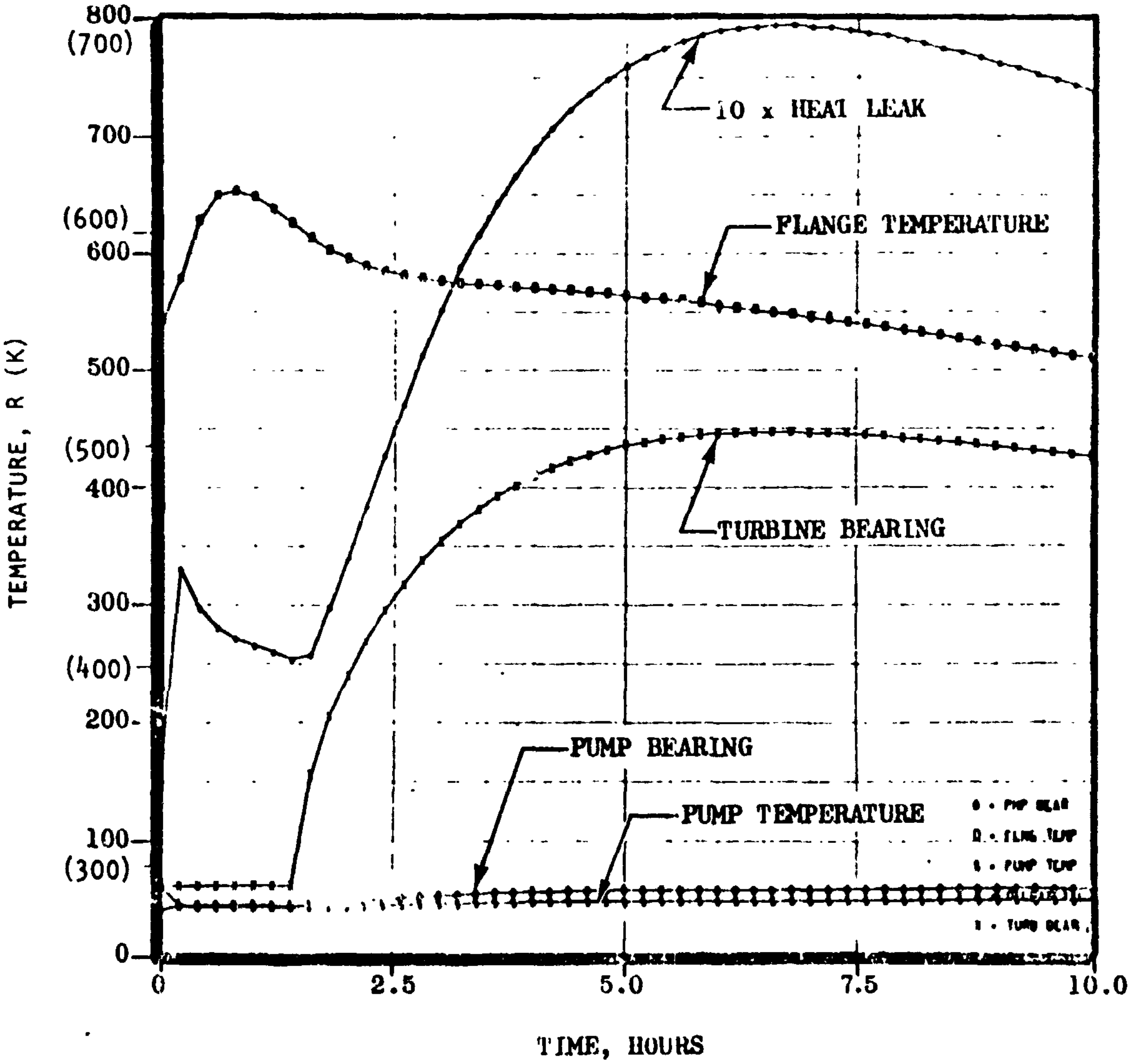

Figure 108. APS Turbopump Soakback Thermal Analysis
Sketch 105, No External Cooling, No Leak

Figure 109 shows the predicted soakback behavior of the LH_2 turbopump design following a steady-state run with a 0.1134 kg/hr (0.25 lb/hr) bleed flowrate (corresponding to a latent heat capability of 52,752 Joule/hr or (50 Btu/hr) through the shaft cavity. This type of external cooling was selected as the method most likely to maintain liquid in the pump itself as it provides a positive flowrate to remove any vapor generated around the pump impeller. The maximum heat leak in this case is 33,761 Joule/hr (32 Btu/hr) and the turbine bearing temperature never exceeds 69.4 K (125 R). These results indicate that the bleed flowrate could be reduced considerably and still maintain an ability for instant starts.

The predicted soakback behavior of the LH_2 turbopump design following a steady-state run for the case of nominal lift-off seal leakage and no external cooling is presented in Fig. 110 to illustrate that the design meets the requirement of a heat leakage rate no greater than 52,752 Joule/hr (50 Btu/hr). This figure presents the most probable behavior of the design and indicates a maximum heat leakage rate of 48,532 Joule/hr (46 Btu/hr) after 6 hours of soakback with a turbine bearing temperature of 177.8 K (320 R). While the turbopump would be capable of an instant start under these conditions, the life of the turbine bearing would probably be reduced (by overheating before adequate cooling could be provided) and external cooling should be provided.

The predicted soakback behavior of the LH_2 turbopump design is shown in Fig. 111 following a steady-state run for the case of nominal lift-off seal leakage and no external cooling as in the previous figure but with a methonal heat pipe added across the vehicle mount. This figure illustrates the influence of the mounting system on the soakback behavior of the design and shows that the thermal check-valve behavior of the heat pipe could reduce the peak heat leak from 48,532 Joule/hr (46 Btu/hr) to 37,981 Joule/hr (36 Btu/hr) and reduce the maximum turbine temperature by 22.2 K (40 R). Attachment of the heat pipe between the vehicle and the turbine exit flange would produce an even greater improvement if the vehicle could absorb the energy.

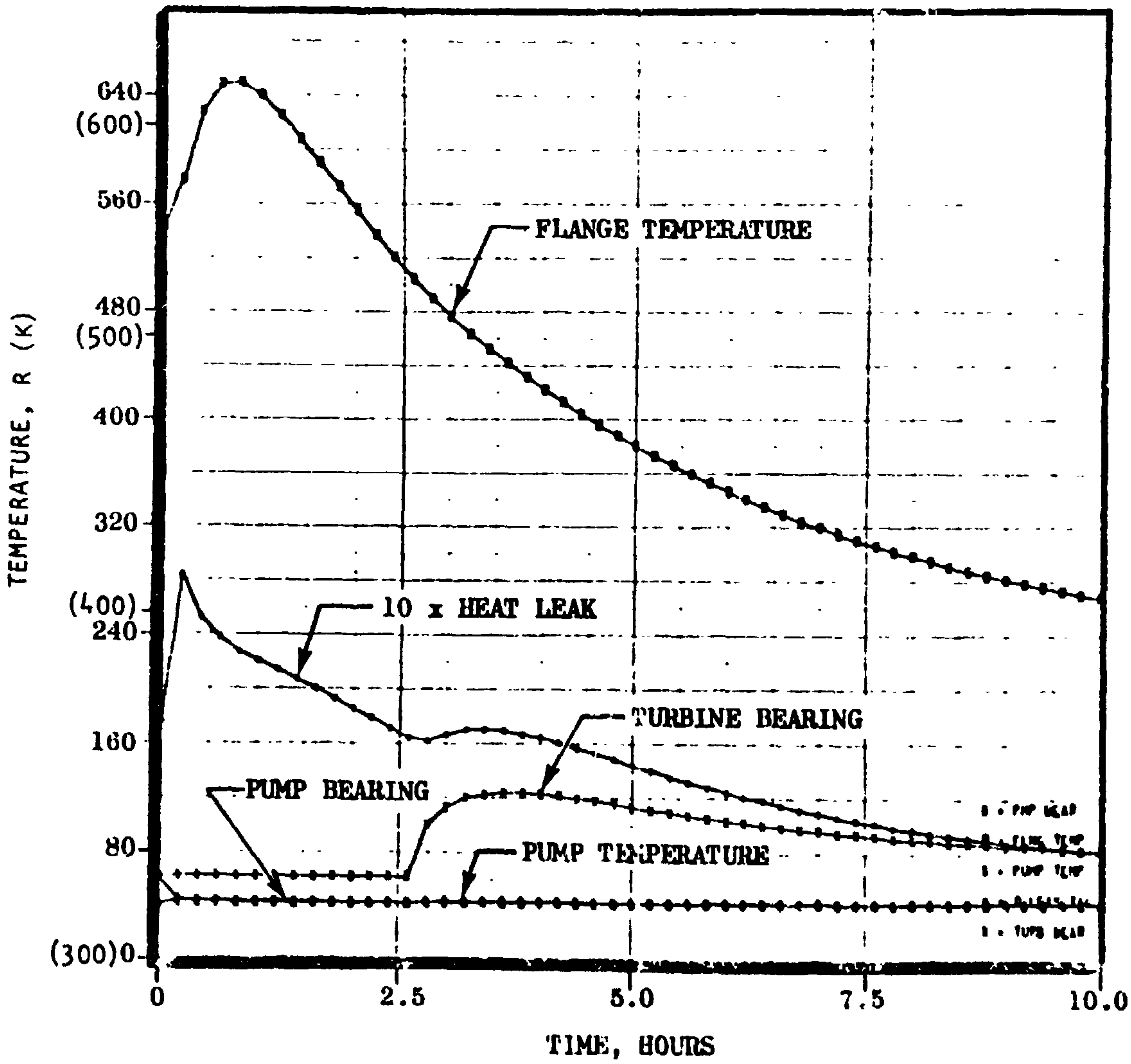

Figure 109. APS Turbopump Soakback Thermal Analysis
Sketch 105, 0.25 lb/hr Bleed Flow

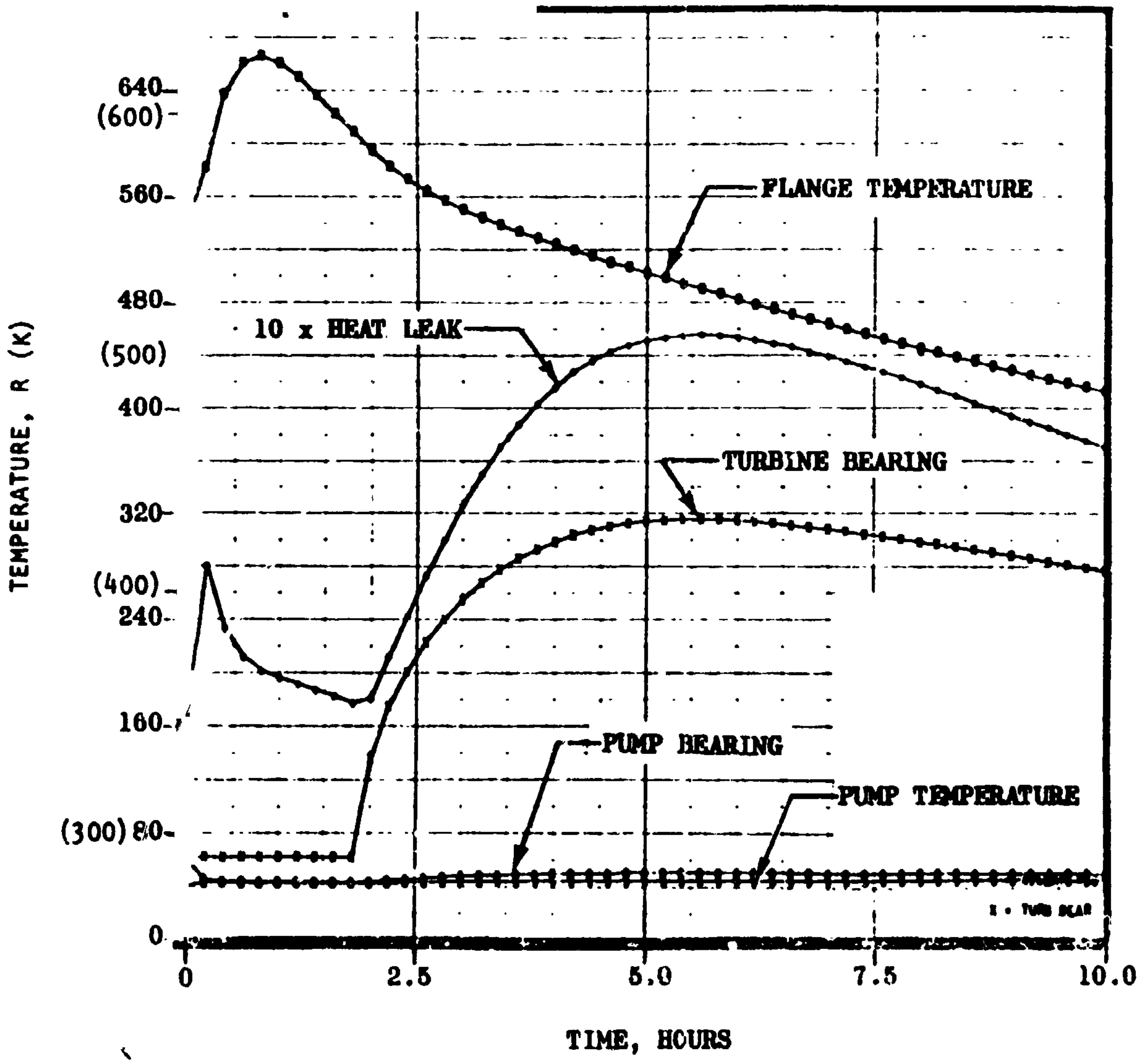

Figur› 110. APS Turbopump Soakback Thermal Analysis
Sketch 105, No External Cooling

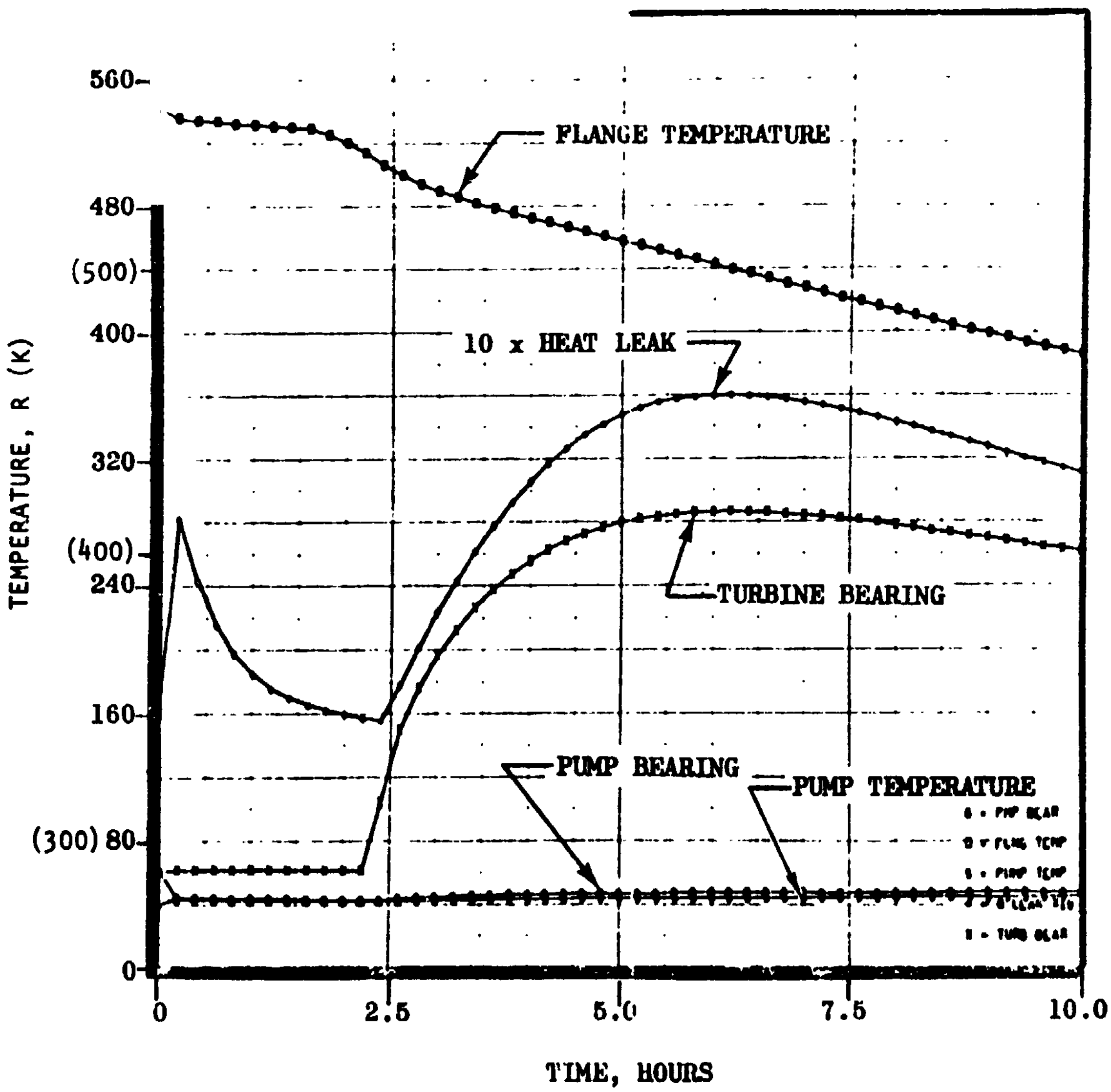

Figure 111. APS Turbopump Soakback Thermal Analysis, Sketch 105, Effect of Heat Pipe, No External Cooling

Failure Mode Effects Analysis

Potential failure modes for the liquid hydrogen turbopump were examined and design provisions have been made to minimize the possibility of these failures. In Table 31, the most likely failure modes are listed along with the preventative design provisions and the instrumentation which will be monitored to indicate an impending problem. The location of the instrumentation on the turbopump is identified in Fig. 112.

GAS GENERATORS

The LH_2 and LO_2 gas generators were designed to operate at a chamber pressure of 1,861,584 N/m^2 (270 psia) with a propellant inlet temperature of 333 K (600 R) and an inlet pressure of 2,344,217 N/m^2 (340 psia).

The hardware design parameters as shown in Figs. 113 and 114 are identical with the exception of the total flowrate, which is 0.1315 kg/s (0.29 lb/sec) for the LO_2 gas generator and 0.2722 kg/s (0.6 lb/sec) for the LH_2 gas generator.

The hydrogen TPA gas generator cross section is shown in Fig. 115. A 12-element coaxial injector is bolted to a GH_2 dump-cooled combustor body. The design incorporates provisions for either a side-mounted spark plug (direct spark igniter) mounted in the center of the injector. The turbine inlet elbow is shown and was test-fired with the gas generator as a component prior to welding the elbow to the turbine inlet manifold. The elbow is made from HS 188 material and has provisions for thermocouples at two planes to determine the exhaust gas temperature profile.

The coaxial injector element for the injector is shown in Fig. 116. The flowrate/element and nominal pressure drops are virtually identical to those tested successfully on a previous IR&D gas generator effort. The design provides adequate minimum pressure drops for the low temperature propellant operation.

TABLE 31. APS LH_2 TURBOPUMP FAILURE MODE ANALYSIS

Potential Failure Mode	Design Provisions	Instrumentation Provisions
Bearing	Balance piston	Axial Bently
	Double coolant service	Coolant temperature
	Bearings in high pressure LH_2	Balance cavity pressure accelerometers
Lift-off Seal	Fail closed design (static)	Actuation pressure
	Opened by operating pressure	Shaft seal cavity pressure
Shaft Seal	Floating ring design	Shaft seal cavity pressure
	Max leakage controlled by Laby.	
	Leakage no effect on BRG cool Q	
Excessive Axial Thrust	Balance piston absorbs up to 18 percent load change	Axial Bently
		Balance cavity pressure
Rotordynamic Instability	Operating speeds away from N_{CR}	Accelerometers
		Axial Bently
Overspeed	Rotor Mechanically OK for 70,000 rpm	Electronic overspeed trip
	Additional 18 percent safety factor	
GG over Temperature	Burnout elbow U/S manifold	Over temperature C/O
Turbine Blade Failure	Manifold retains individual blades Oper. range free of blade criticals	Accelerometers

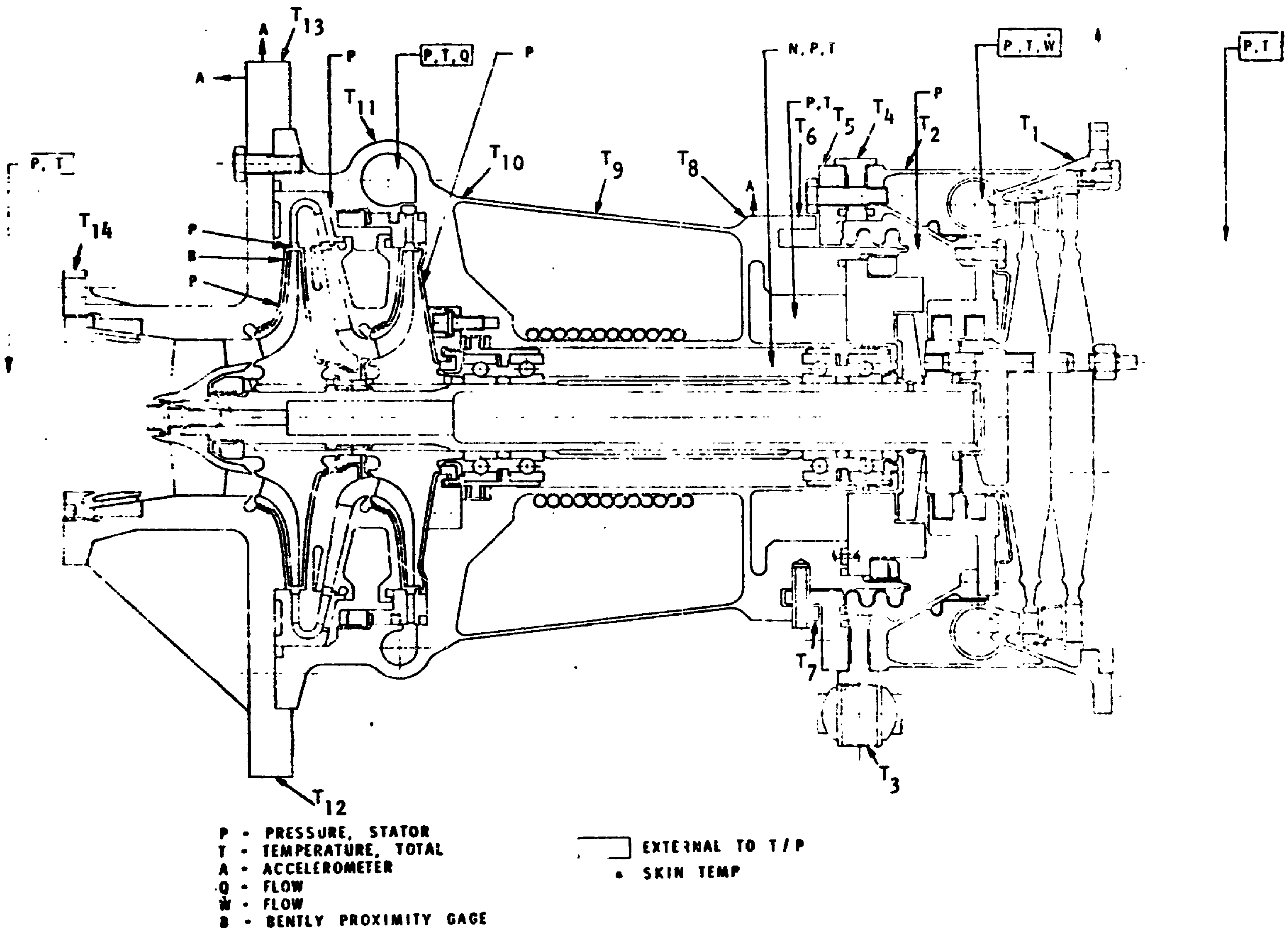

Figure 112. APS LH_2 Turbopump Instrumentation Schematic

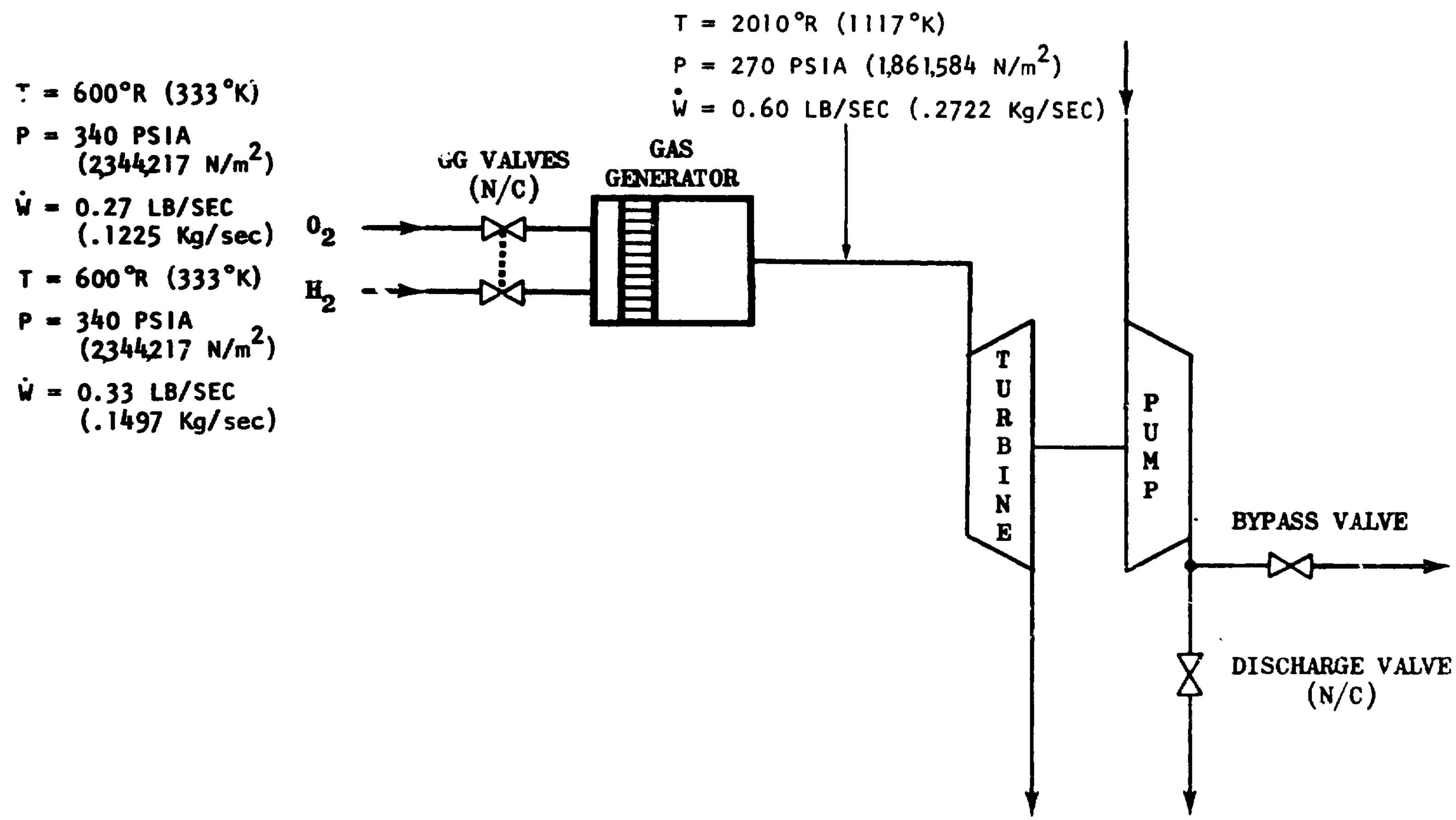

Figure 113. LH_2 TPA Gas Generator Nominal Operation

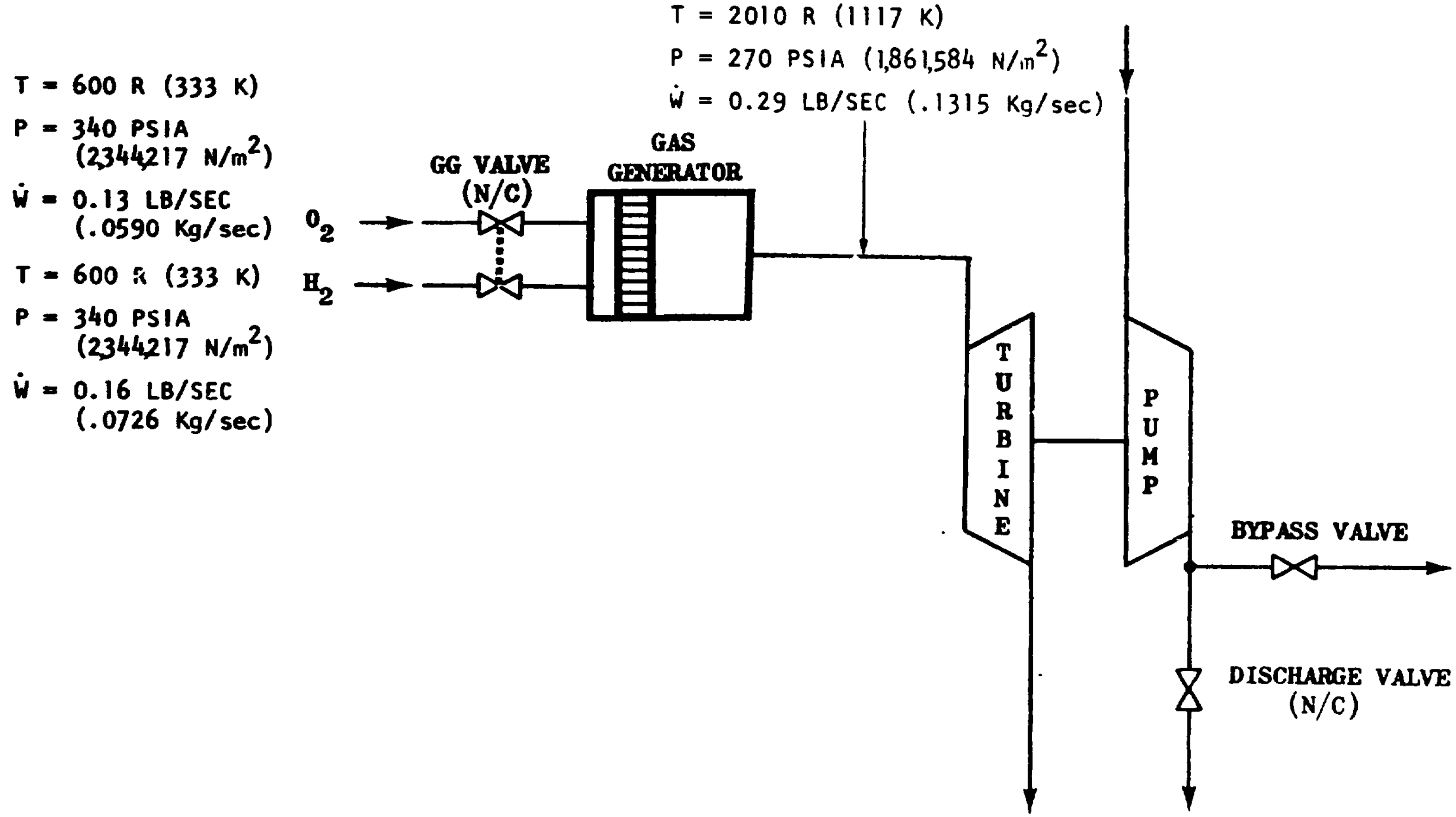

Figure 114. LO_2 TPA Gas Generator Nominal Operation

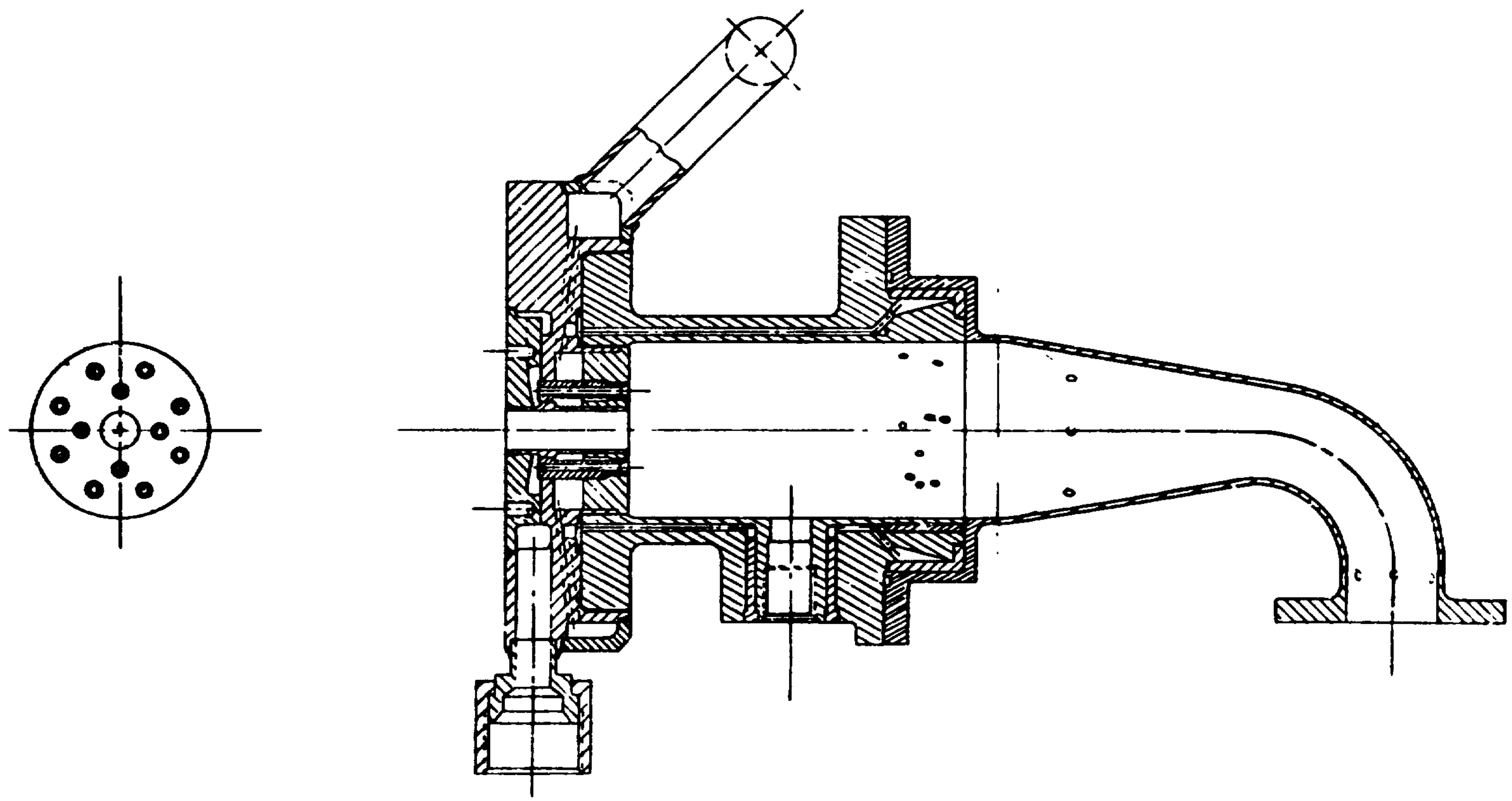

FEATURES

- COAXIAL INJECTOR (12 ELEMENTS)
- DIRECT SPARK IGNITER
- DUMP COOLED BODY
- PROVISION FOR INDIRECT SPARK IGNITER
- ELBOW AND TEMPERATURE RANGE FOR CHECKOUT TESTING

Figure 115. Hydrogen TPA Gas Generator Assembly

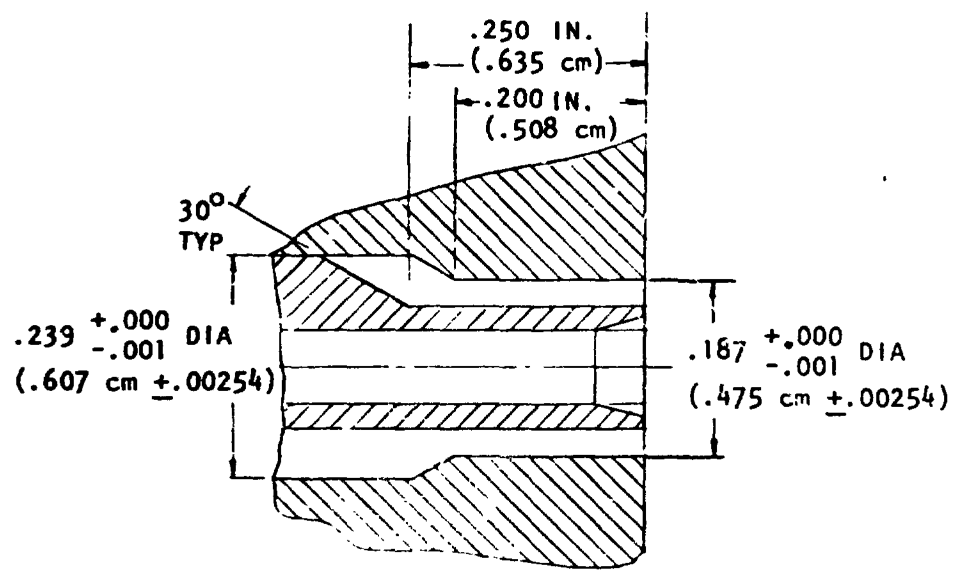

DESIGN PARAMETERS

$\dot{W}$/ELEMENT = 0.039 LB/SEC (.0177 Kg/SEC)

ΔP_F NOMINAL = 50 PSI (344,738 N/m^2)
MINIMUM = 20 PSI (137,895 N/m^2)

ΔP_O NOMINAL = 43 PSI (296,475 N/m^2)
MINIMUM = 36 PSI (248,211 N/m^2)

NOMINAL = 340 PSI INLET PRESSURE (2,344,217 N/m^2)
600 R INLET TEMPERATURE (333 K)

MINIMUM = 375 R GO_2 INLET TEMPERATURE
(2,585,534 N/m^2)
275 R GH_2 INLET TEMPERATURE (152.8 K)

Figure 116. Gas Generator Coaxial Injector Element

The gas generator body design is presented in Fig. 117. The view at the left shows the injector mounting flange. The injector operates at a mixture ratio of 1.3 o/f. The copper body is dump-cooled with 0.0576 kg/s ([illegible] lb/sec) of [illegible] which is injected into the combustor through 26 secondary hydrogen injection orifices. The 26 secondary hydrogen orifices are located on six planes and are drilled to provide impingement under each of the 12 injector elements and at the centerline of the combustor. Again, as with the injector design, this combustor design concept has been tested successfully on a previous Rocketdyne program and provides good C* performance and exhaust gas temperature characteristics.

A heat transfer analysis of the gas generator was conducted. The temperatures of the exhaust duct (HS 188 uncooled elbow), the gas generator flange (at the turbine inlet end), and the gas generator/injector flange during the start transient are presented in Fig. 118. The uncooled exhaust reaches essentially the exhaust gas temperature in about 10 seconds. (This duct and turbine inlet manifold are insulated to provide a maximum external temperature of 589 K or (600 F.) The cooled gas generator flange reaches a maximum temperature of approximately 506 K (450 F) and this will not be insulated. The injector flange temperature reaches approximately 339 K (150 F), which is approximately the propellant injection temperature for this worst case calculation:(T_{inlet} = 589 K (600 F).

The gas generator temperatures (the same portions of the gas generator as previous chart) are shown for the cutoff transient in Fig. 119. The gas generator body remains below the 589 K (600F) requirement during soak and, therefore, will require no external insulation. The cooled gas generator body provides a sink instead of a source (in uncooled) and helps thermally isolate the gas generator injector and valves.

The gas generator design has provision for either a direct spark and/or indirect spark igniter. Both configurations are presented in Fig. 120. All gas generator testing at Rocketdyne with the direct spark igniter has been conducted with ambient temperature GH_2/GO_2 propellants. Indirect spark igniters have been tested successfully with propellant temperatures below the requirements of this contract 152.8 K or

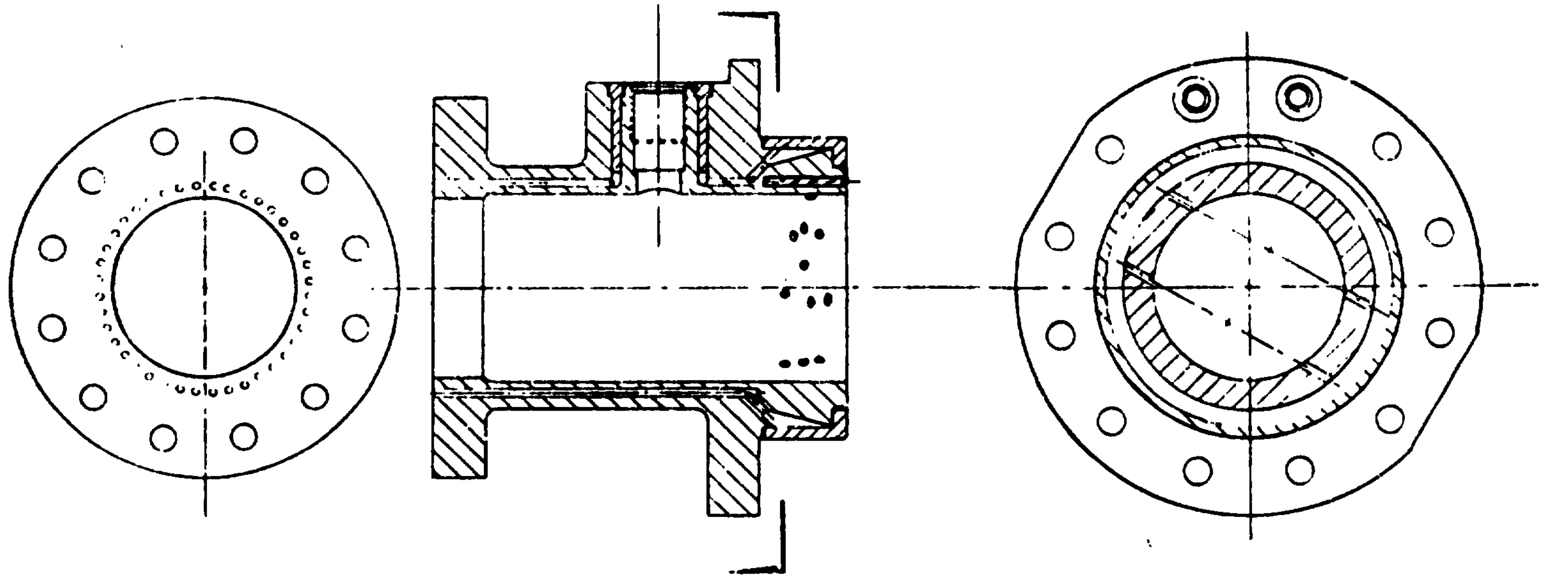

DESIGN PARAMETERS

$\dot{W}_{CORE}$	= 0.471 LB/SEC (.214 Kg/SEC)
MR_{CORE}	= 1.3
$\dot{W}_{DUMP}$	= 0.127 LB/SEC (.0576 Kg/SEC)
$\Delta P_{SECONDARY\ INJECTOR}$	= 45 PSI (310264 N/m^2)
INJECTION ORIFICE DIAMETER	= 0.078 INCHES (.1981 cm)
NUMBER OF INJECTION ORIFICES	= 26 (LOCATED ON 6 PLANES)
NUMBER OF COOLANT PASSAGES	= 40

Figure 117. Gas Generator Body Design

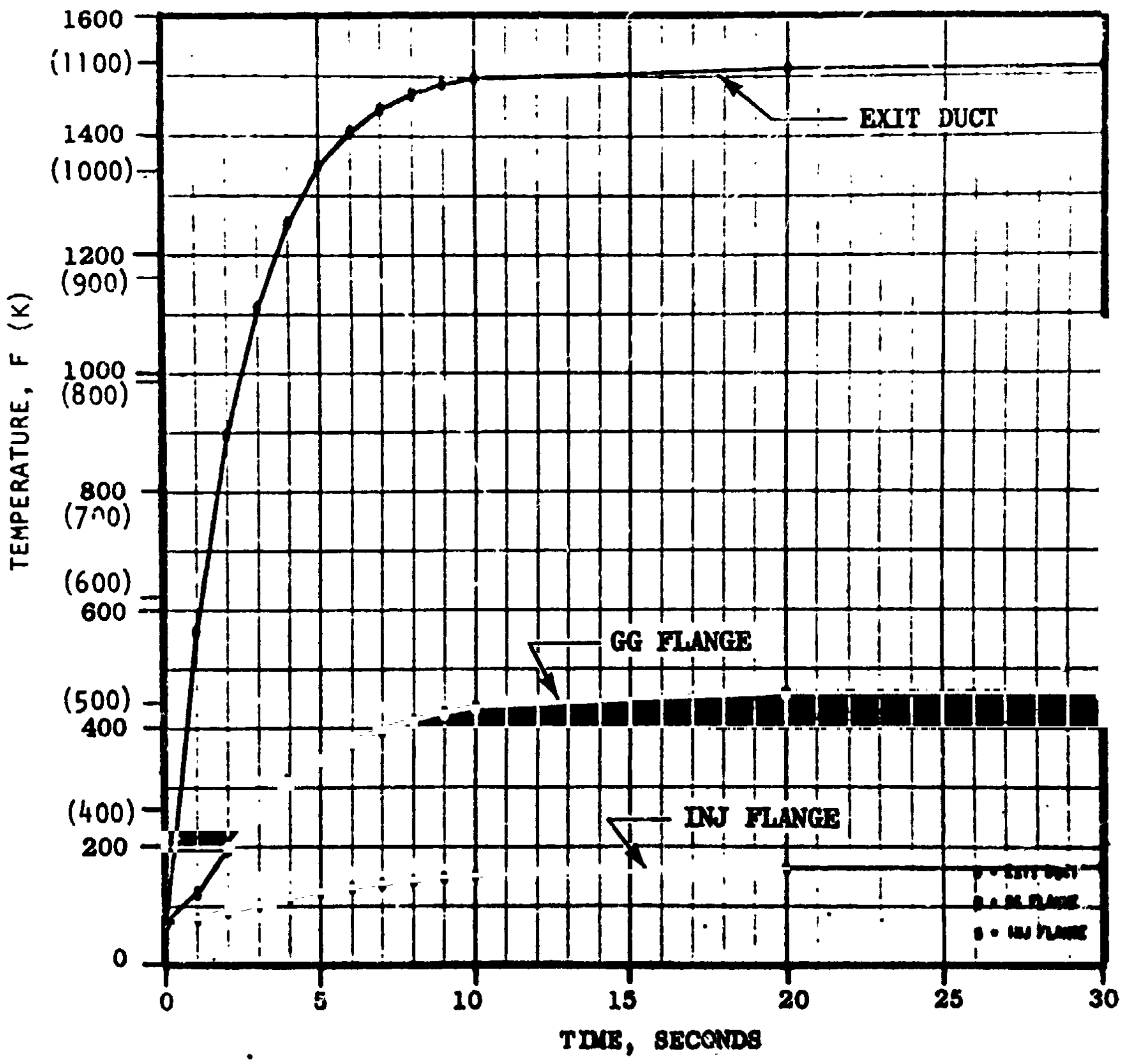

Figure 118. Gas Generator Start Transient

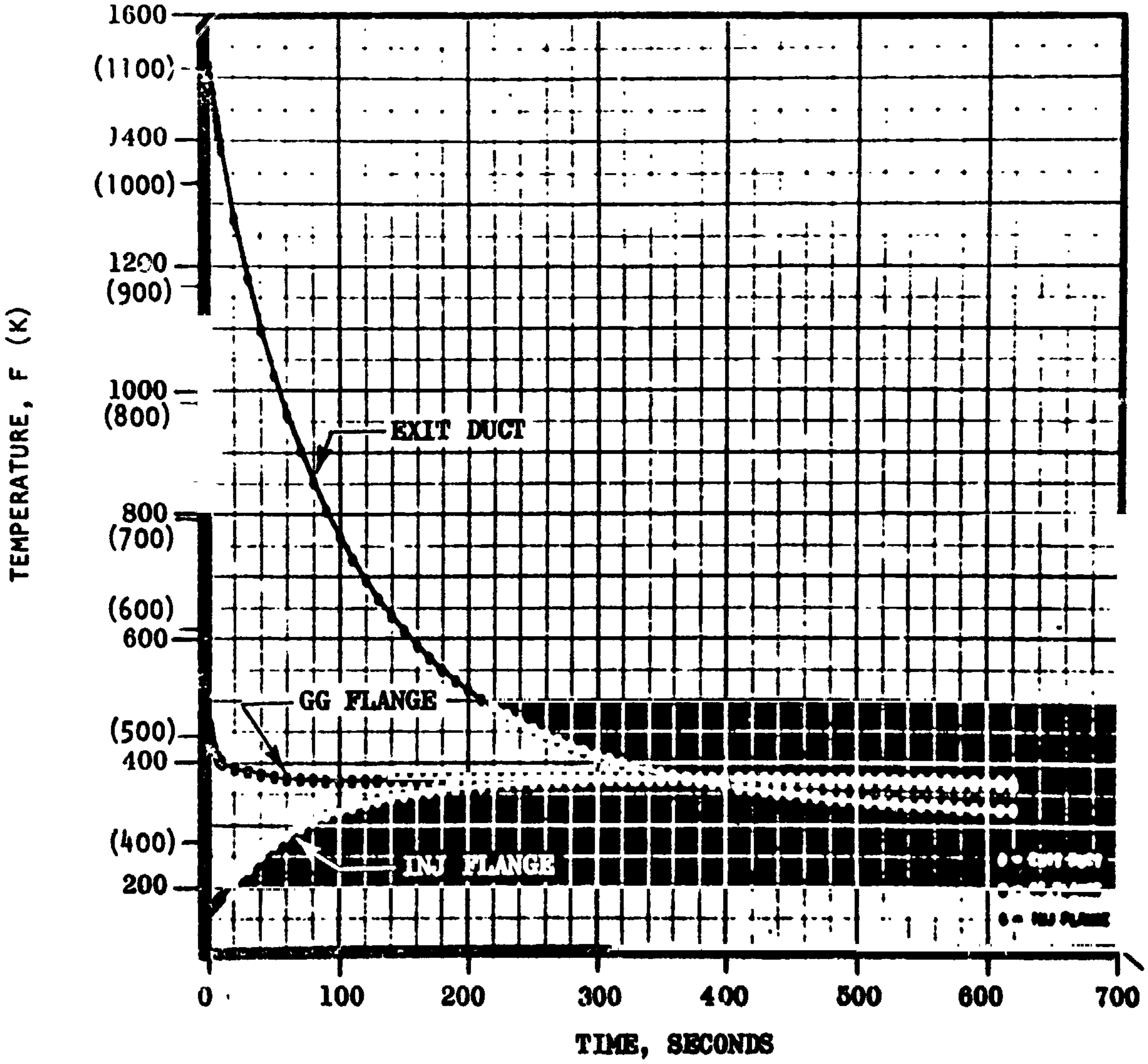

Figure 119. Gas Generator Cutoff Transient

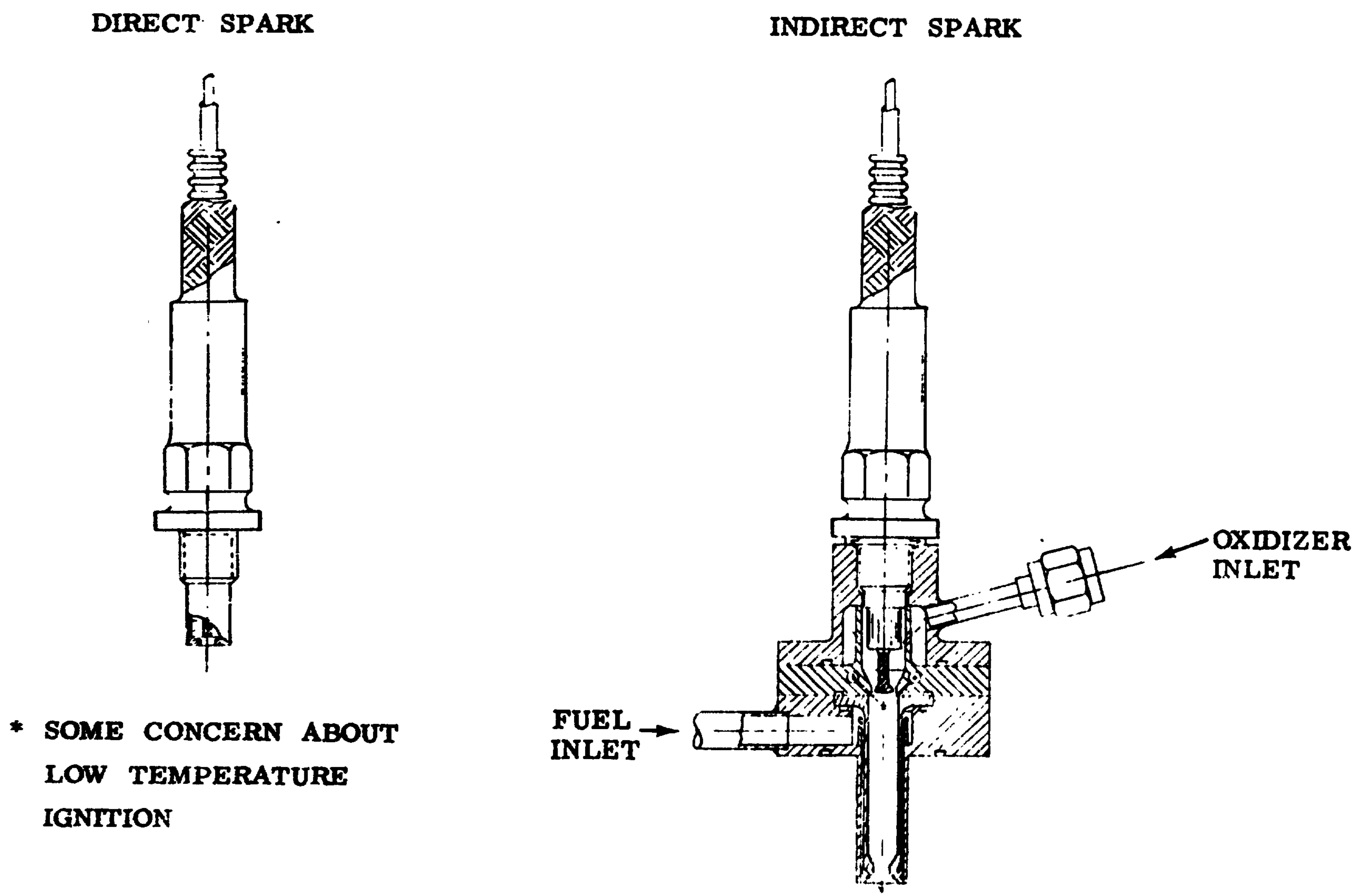

Figure 120. TPA Gas Generator Ignition

275 R GH_2 and 208.3 K or 375 R GO_2. However, since the direct spark ignition provides the less complex design (spark plug only), it will be evaluated first on gas generator component tests. If ignition problems are encountered utilizing cold temperature propellants, the more complicated but proven indirect spark igniter can be used.

The LO_2 TPA gas generator design is shown in Fig. 121 in the cross section. The design concept is identical to the LH_2 TPA gas generator just described. This gas generator is designed for a total nominal flowrate of 0.1315 kg/sec (0.29 lb/sec). A 5-element coaxial injector is bolted to a copper body which is GH_2 dump-cooled. Again, provisions are made for both direct and indirect spark ignition.

LO_2 TPA SYSTEM

The system schematic and nominal operating conditions are presented in Fig. 122. Pressures, temperatures, and flowrates are given at key points in the system. The gas generator propellant inlet conditions and pump discharge requirements were specified by NASA with the gas generator parameters selected to meet the operating requirements of the system.

The overall system schematic is shown in Fig. 123, including the pneumatically activated propellant valves and the solenoid valves. For the breadboard TPA system, the electrical interfaces include 9 control solenoids, a bearing coolant solenoid, an intermediate seal purge solenoid (LO_2 TPA only), a speed pickup, and the electrical supply to the gas generator spark igniter. The pneumatic interfaces include a single 310,264 N/m^2 (45 psi) helium source for control solenoids and a single 1,723,689 N/m^2 (250 psi) source for the liftoff seal. It should be emphasized that this valving arrangement was established based on the "breadboard" use of the assembly (maximum flexibility for control/system evaluation testing). Flight-type units would be simplified, including a single pneumatic interface and one electrical signal to the unit which is then passively sequenced (pressure ladder).

The TPA system sequencing including valve position prior to start, during the start transient, during the steady-state operation, and during the cutoff transient

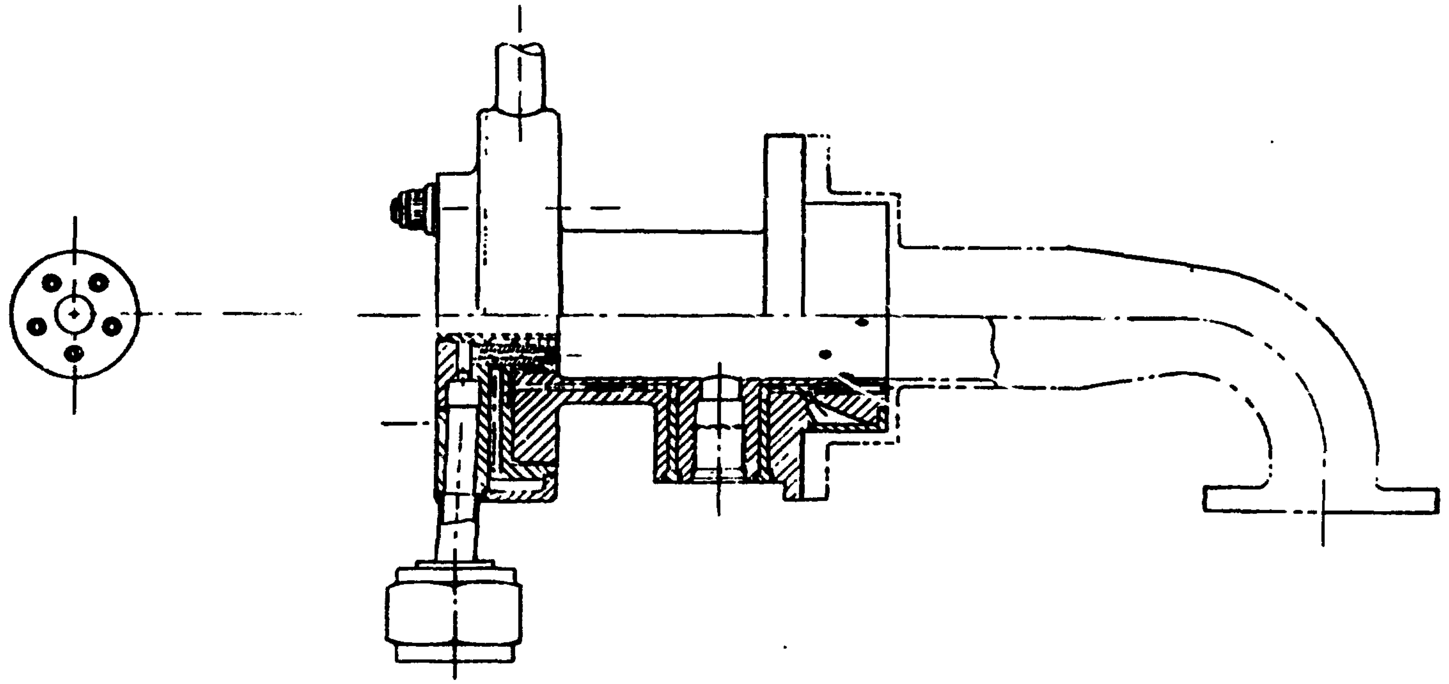

FEATURES

- COAXIAL INJECTOR (5 ELEMENTS)
- DIRECT SPARK IGNITER
- DUMP COOLED BODY
- PROVISION FOR INDIRECT SPARK IGNITER
- ELBOW AND TEMPERATURE RAKE FOR CHECKOUT TESTING

Figure 121. Oxygen TPA Gas Generator Assembly

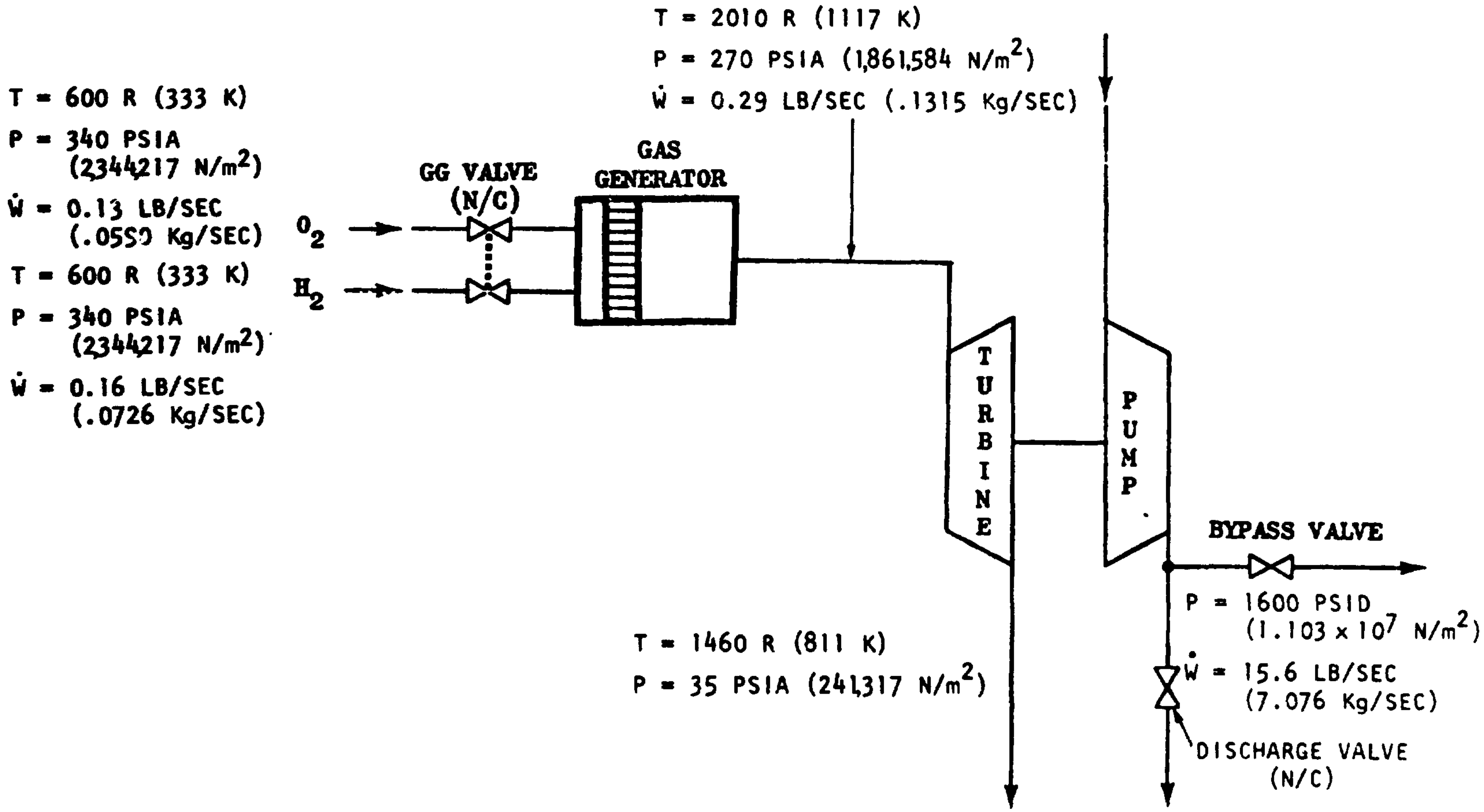

Figure 122. LO_2 TPA System Schematic Nominal Operation

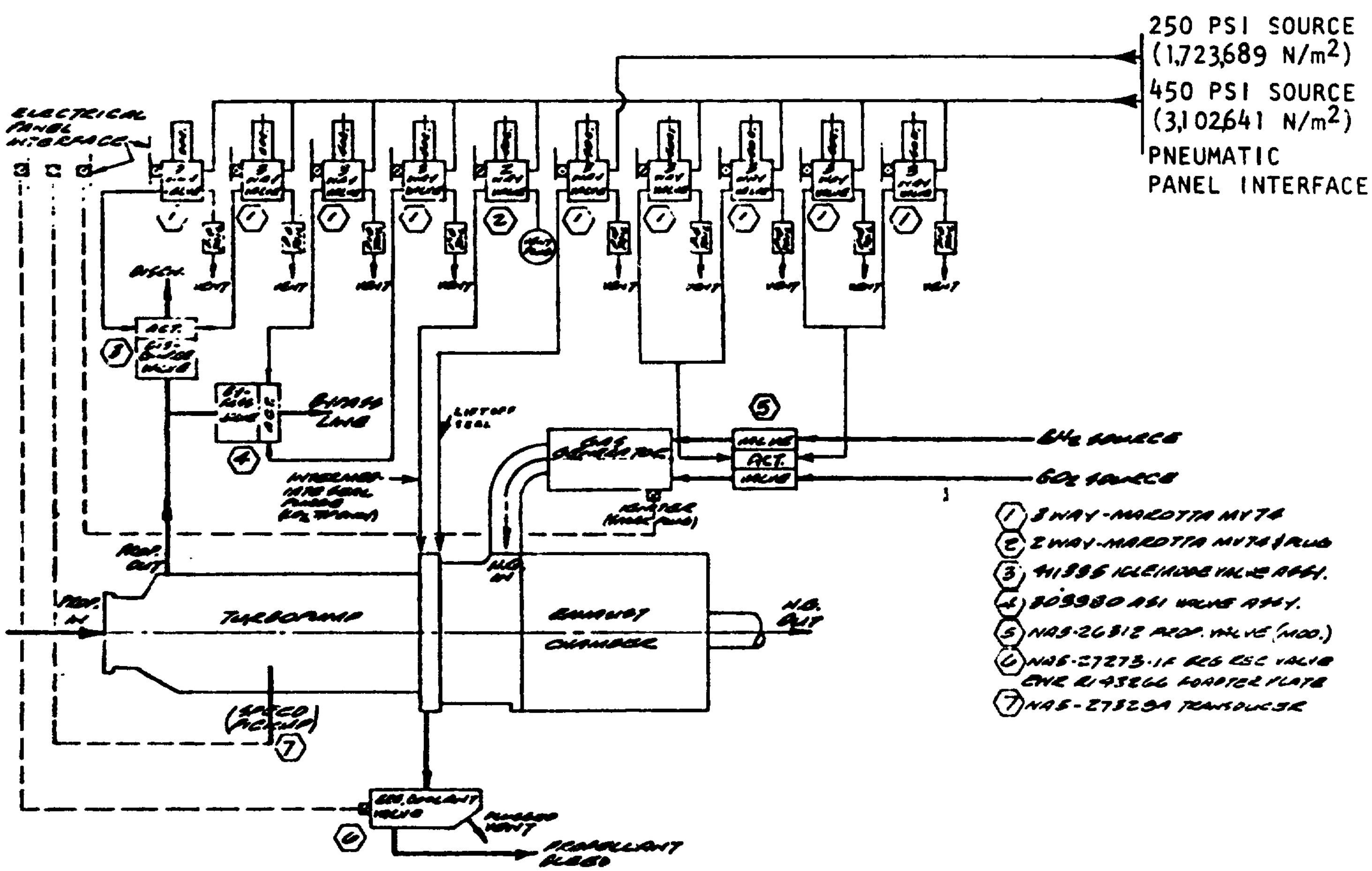

Figure 123. System Schematic APS Turbopump Test

is presented in Fig. 124. Prior to start, the pump discharge and gas generator bipropellant are in the closed position. The bypass and bearing coolant valves can be cycled open and closed; however, just prior to start, the bypass must be opened and the bearing coolant valve must be closed. The liftoff seal is pressurized open and for the oxidizer TPA only the intermediate seal purge is signaled On at all times when the liftoff seal is open.

At start, the gas generator spark is signaled On and the gas generator bipropellant valve is opened. The turbopump accelerates as propellant is pumped through the bypass valve. Approximately 0.5 second after start, when sufficient discharge pressure is obtained to pump through the system, the discharge valve is signaled Open as the bypass valve is signaled Closed.

At cutoff, the gas generator bipropellant is closed, which causes the pump to decelerate immediately (discharge pressure drops). As the discharge pressure drops, the discharge valve is closed and the bypass valve is simultaneously opened.

The LO_2 TPA side view layout shown in Fig. 125 shows the physical configuration, the arrangement of solenoid valves for control of valves and purges, and key dimensional relationships. The dual opening and closing solenoids are provided to insure reliable operation of the gas generator propellant valve. The orifice exhaust duct is utilized to maintain a constant turbine back pressure under seal level as well as vacuum conditions by maintaining choked turbine exhaust flow. The base configuration was selected to provide easy access for lifting or transporting the assembly.

The gas generator and propellant valves are mounted on the turbopump. The turbopump is supported on a thermally isolated 3-mount system with the pin joint mounting system permiting the required thermal expansion and contraction of the TPA components. The solenoid valves are mounted on the pneumatic accumulator manifold.

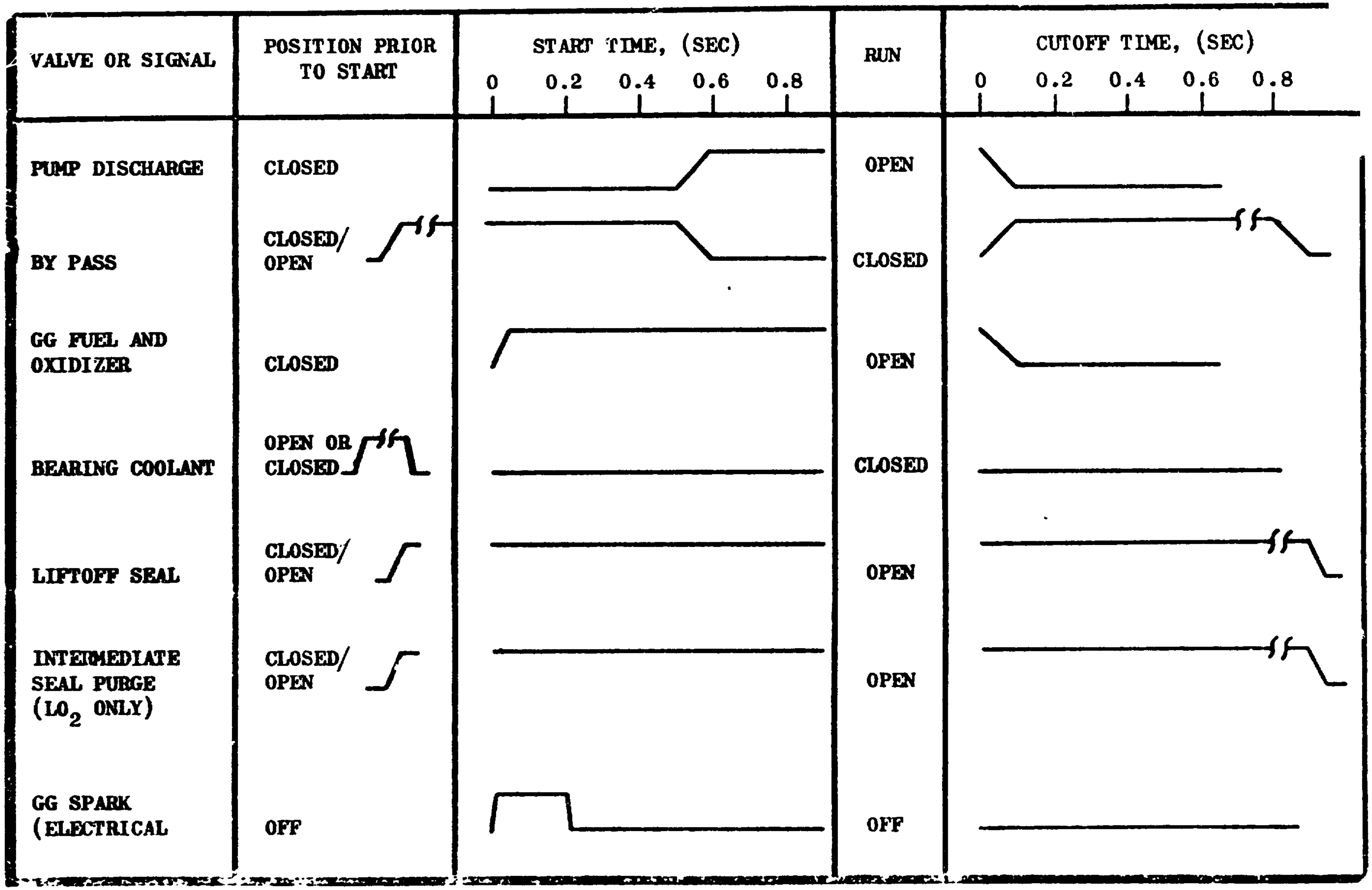

Figure 124. TPA System Sequence/Valve Position

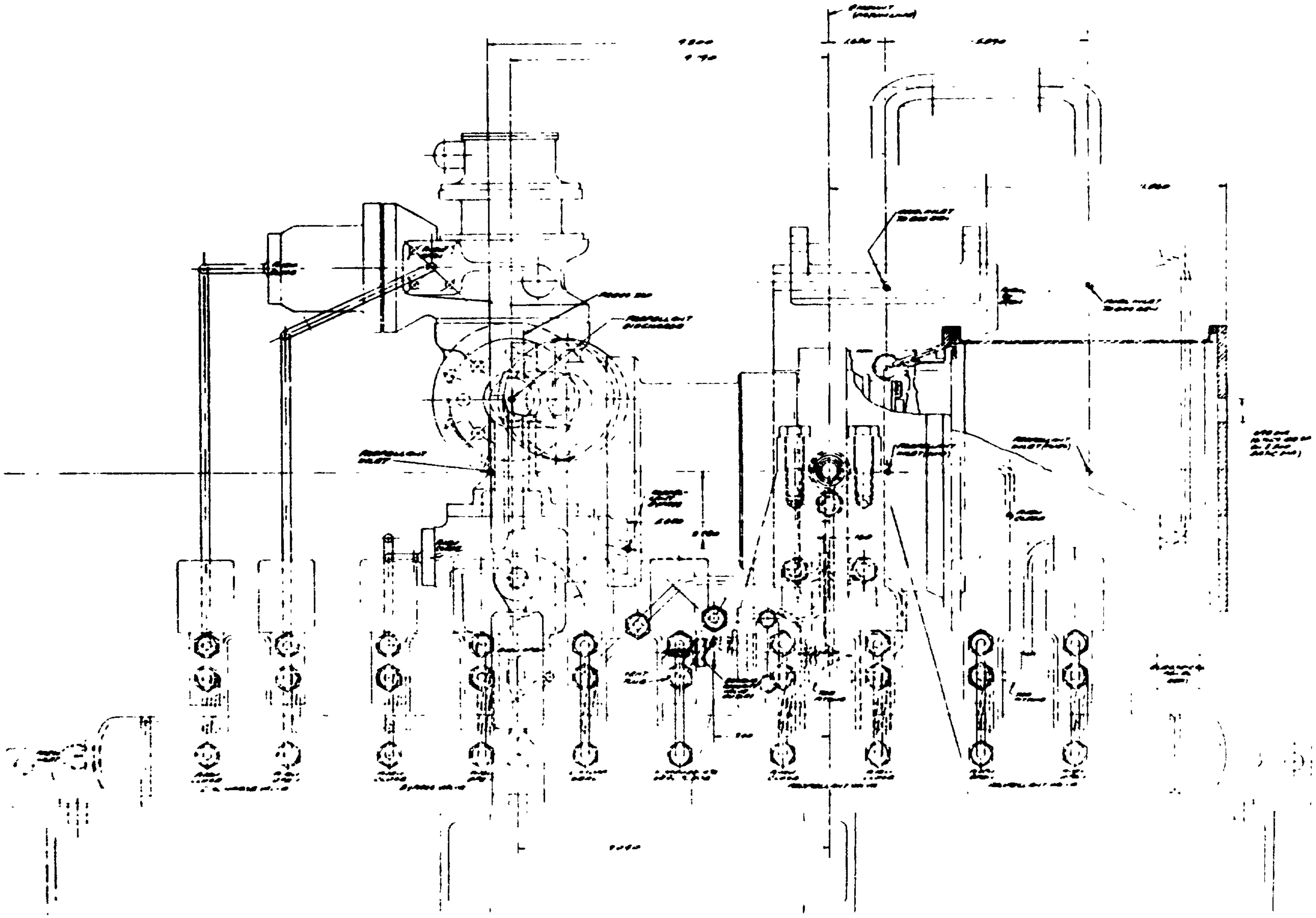

Figure 125. LO_2 TPA System Layout Side View

LH_2 TPA SYSTEM

The performance characteristics consisting of temperature, pressure and flowrate are schematically shown at key points in the system in Fig. 126. As in the LH_2 the gas generator inlet propellant conditions and the pump discharge requirements were specified by NASA while the gas generator parameters were selected to meet the operating requirements of the system.

The LH_2 TPA side view layout presented in Fig. 127, shows the same physical arrangement as the LO_2 TPA physical configuration.

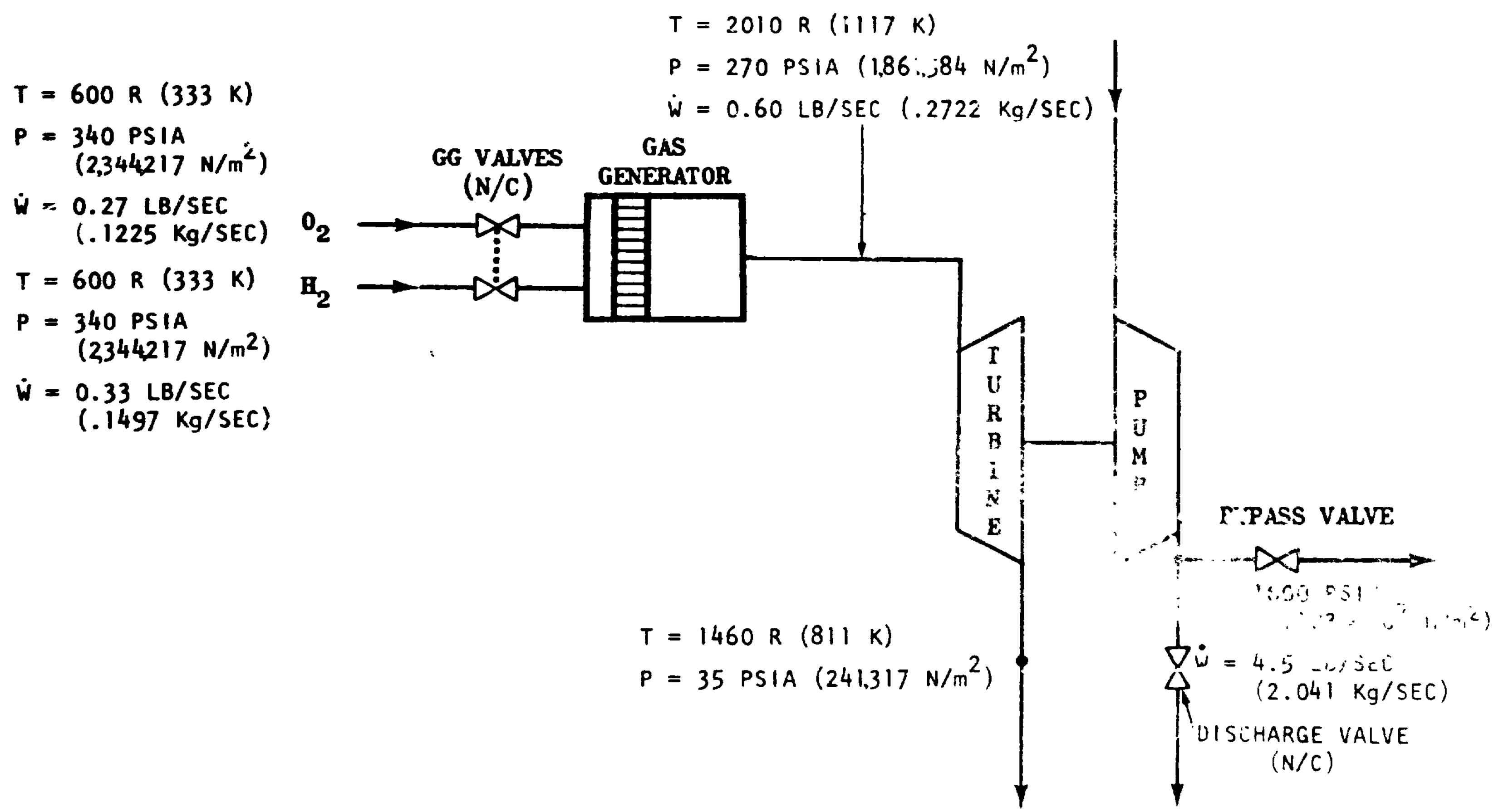

Figure 126. LH_2 TPA System Schematic Nominal Operation

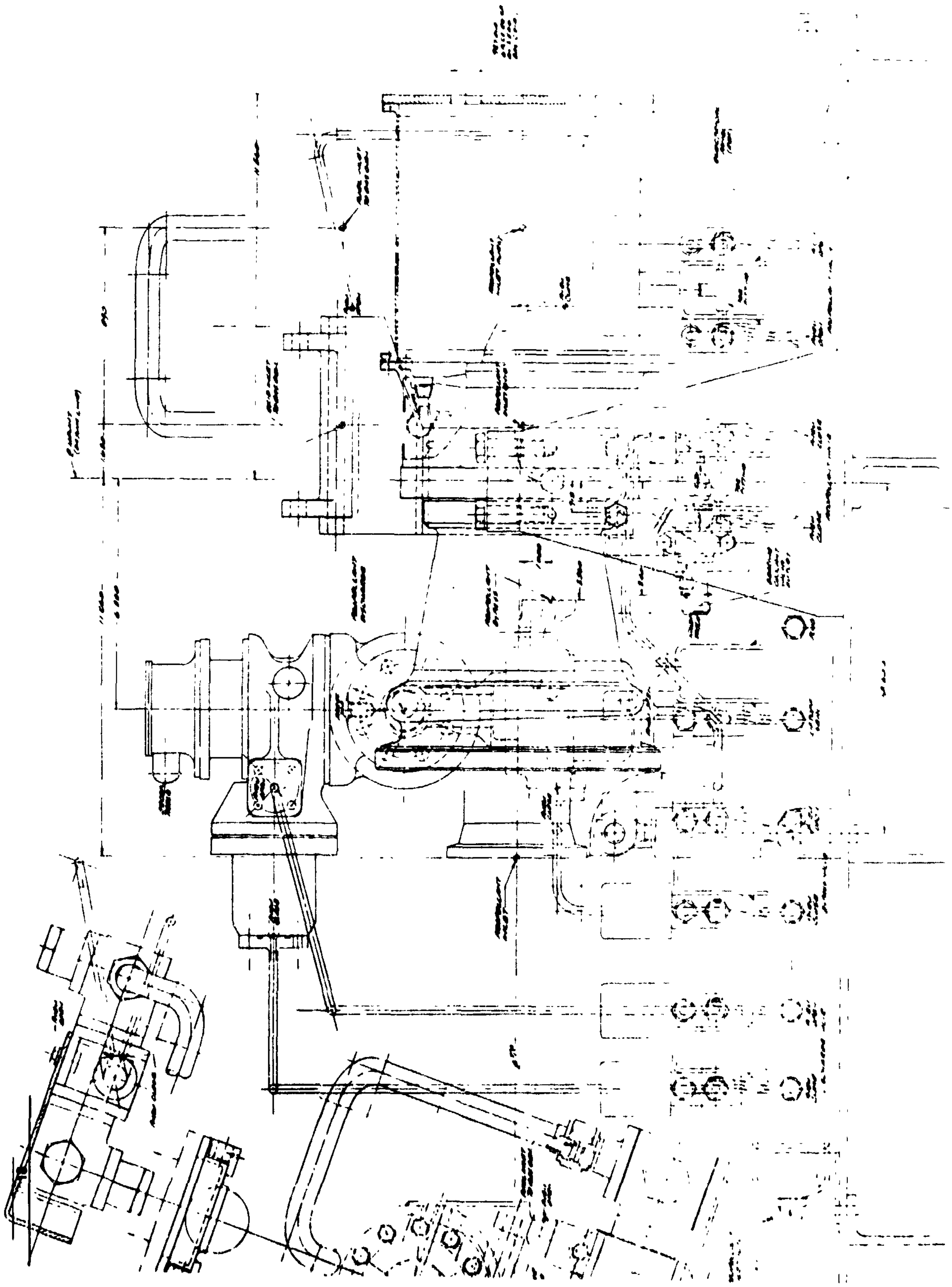

Figure 127. LH_2 TPA System Layout Side View

PHASE III FABRICATION AND ASSEMBLY

As specified in the contract, two LO_2 and two LH_2 turbopump assemblies were fabricated in support of the development test program and for subsequent acceptance and delivery to NASA-MSFC. Each unit consisted of the turbopump, solenoid control valves, and propellant valves located on a base. Interchangeability of components between the LH_2 and LO_2 units was incorporated wherever possible to take advantage of economies in fabrication. The fabrication and assembly processes are subsequently discussed.

LO_2 TURBOPUMP

Component Fabrication

The detail components of the oxidizer turbopump before assembly are shown in Fig. 128.

The inducer was fabricated from a K-Monel pancake forging. The vanes were generated on a five axis milling machine and hub features were produced by conventional machining techniques. The hydrodynamic passages of the impeller were generated by electrical discharge machining. The configuration of the impeller represents the approximate limit of present EDM capability: Because of the combination of small discharge tip width 0.2769 cm (0.109 inch) and discharge angle (28 degrees), blade wrap angle, and number of blades (4 partial and 4 full vanes), certain sections of the flow passages were very difficult to generate, resulting in high tool wear and very low material removal rates.

EDM process was also used to make the vaned flow passages of the antivortex ring. The volute was split along the turbine side of the hydrodynamic passage, so that the two passages resulting from the double tongue configuration were accessible for direct milling operation. The discharge pipe and flange were then joined to the volute by welding (Fig. 129).

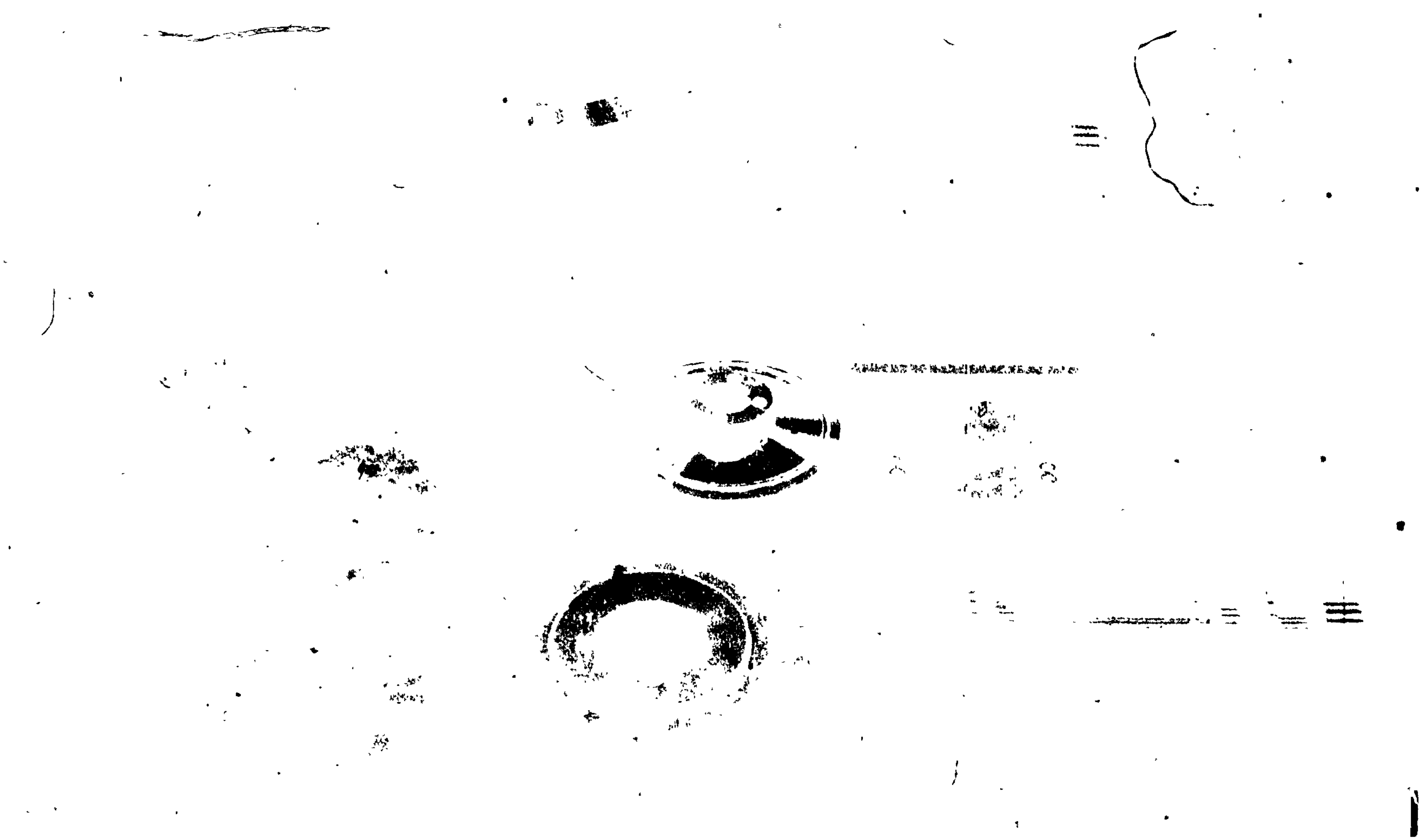

Figure 128. Liquid Oxygen Turbopump Components

Figure 129. Liquid Oxygen Turbopump

The pump housing (Fig. 130, center) was fabricated by rough machining from Hastelloy B forgings plus the pump end member as well as the two components which formed the primed joint on the turbine end. These pieces were then joined by welding to the inner cylindrical member and the radial plate on the turbine end. The bellows seal on the turbine end was added by welding and the entire welded structure was heat treated, after which the cooling tubes were added by hand brazing. The outer cylindrical member was attached by welding to the turbine and pump ends respectively, and these last two joints were left in the as-welded condition to preclude melting of the braze alloy used on the cooling tubes. The fabrication of the housing was then concluded by machining to drawing requirements.

Because the drain passages from the shaft seals required several bends to reach an external surface, the drain manifold located between the housing and turbine manifold was made an investment casting. The flow passages were cast by using cores; other features were machined by conventional methods.

The turbine wheel was machined from an Astroloy die forging with the blades integral to the disc. Blade surfaces were generated by electrical discharge machining. This presented no difficult problem, since the blades were unshrouded and as a result there was a straight radial access from the electrode to the outer diameter of the wheel.

The turbine nozzle passages were machined integral from an HS188 ring forging by electrical discharge machining. The passages were formed by entering with the electrode alternately from the inlet and discharge side, with the inner and outer shrouds remaining integral. The remainder of the manifold was a welded composite. Before the final closeout weld was accomplished by attaching the outside cylindrical component, insulation was incorporated around the manifold torus to reduce the heat transfer from the turbine to the pump. The insulation was Linde Opacified Insulation covered with a protective layer of foil.

The completed turbine components are shown in Fig. 131.

Figure 130. Liquid Oxygen Turbopump Housing

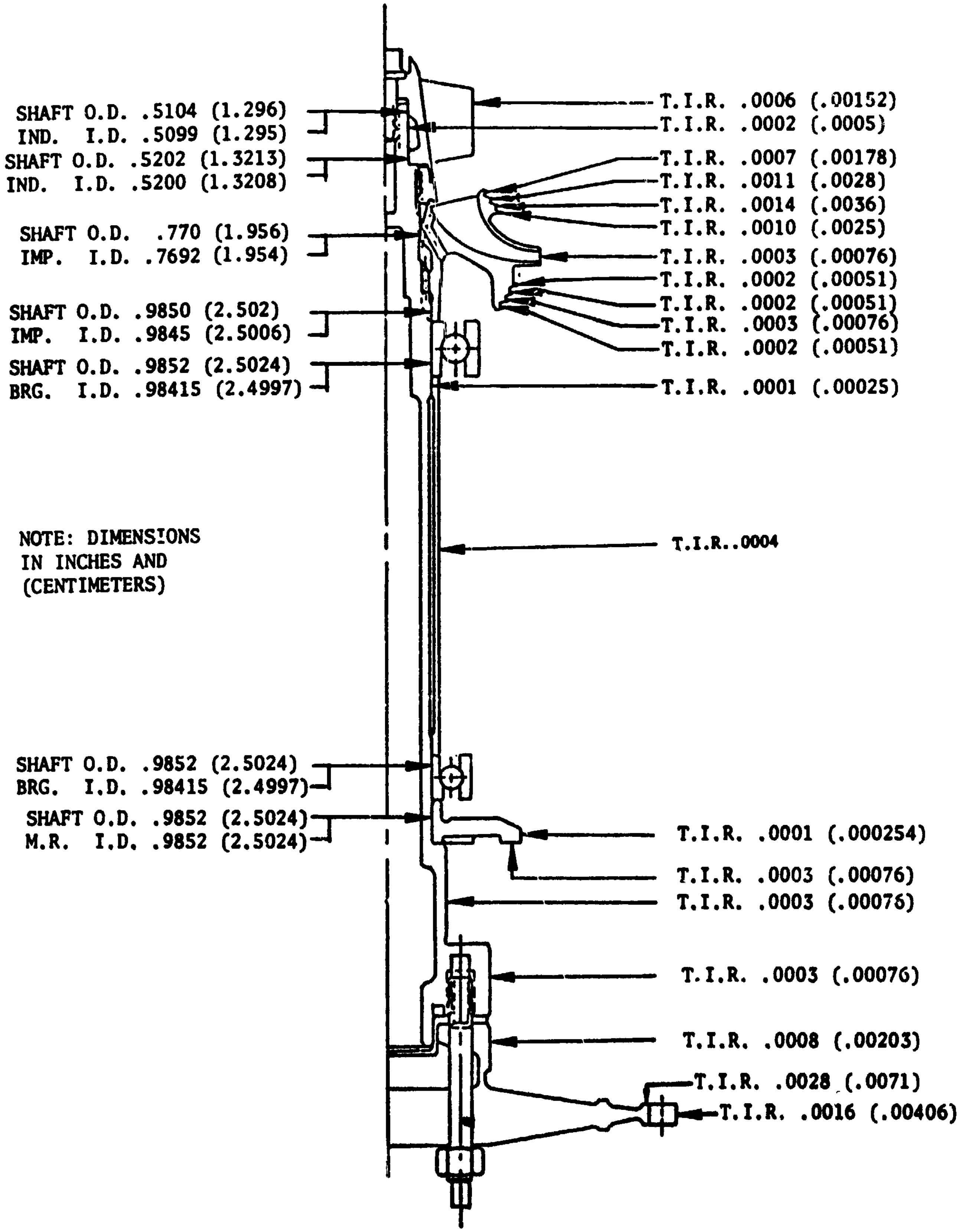

Figure 131. APS LOX Turbopump S/N 01 Rotor Runouts

Turbopump Assembly

Prior to assembly of the turbopump, the rotor components consisting of the shaft, inducer bolt, inducer, impeller nut, impeller, bearing spacer, mating ring, turbine wheel spacer, and turbine wheel were assembled with a pair of balance bearings (Fig. 132), and balanced to 0.0635 gr-cm (0.025 gr. in.) an 0.0889 gr-cm (0.035 gr. in.) unbalance in the plane of the impeller and turbine wheel, respectively.

Fits and eccentricities of the rotating parts were established. The results obtained are shown on Fig. 133 for T/P S/N 01 and Fig. 134 for T/P S/N 02.

The plan with the electrical-discharge machined surfaces of the nozzle and rotor blades was to remove the brittle remelt layer left on the generated surfaces after the EDM operation by shot-blasting. To establish the effectiveness of the shot-blasting technique, EDM samples were prepared of each material with various current intensities. The samples were submitted to the same shot-blasting procedure which was to be used subsequently on the turbine components. Metallographic analysis showed that the shot-blasting effectively removed the remelt layer on the samples where moderate or light current feed rates were used. Based on these results, the procedure for EDM was established. Examination of the turbine components revealed that in areas where the shot-blasting impact was not direct, as on the flat samples, the remelt layer was not completely removed. Other methods need to be explored to develop a technique for removing the remelt layer from EDM turbine passages.

Assembly of the turbopump was accomplished in the following sequence:

1. Measurements were taken to establish critical diametral and axial clearances (see Fig. 135 and 136).
2. All parts were LOX cleaned.
3. The impeller front wear ring, inducer liner carrier, inducer liner, back flow deflector spacer and the back flow deflector, its retaining nut lock, and nut were installed into the volute.

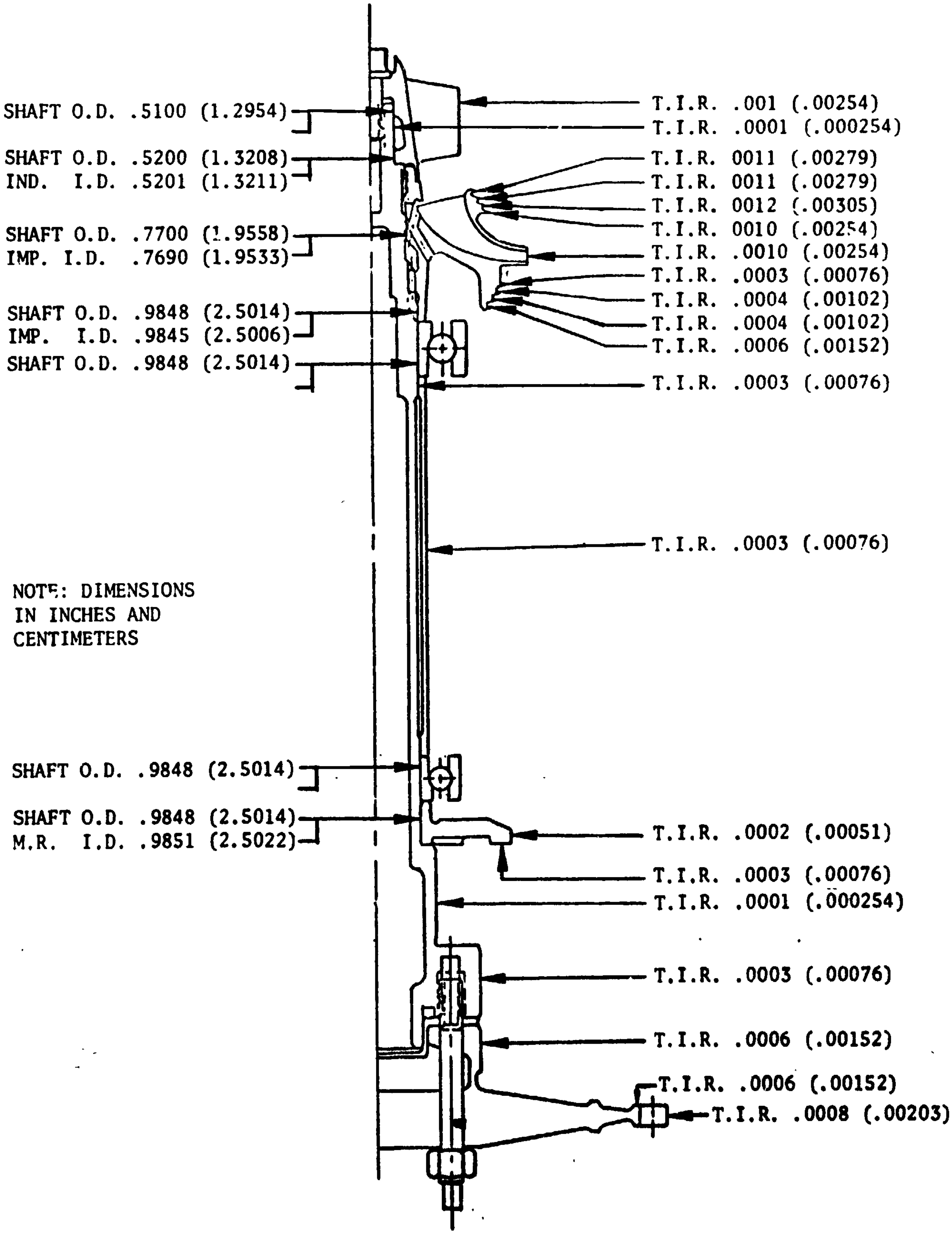

Figure 132. APS LOX Turbopump S/N 02 Rotor Runouts

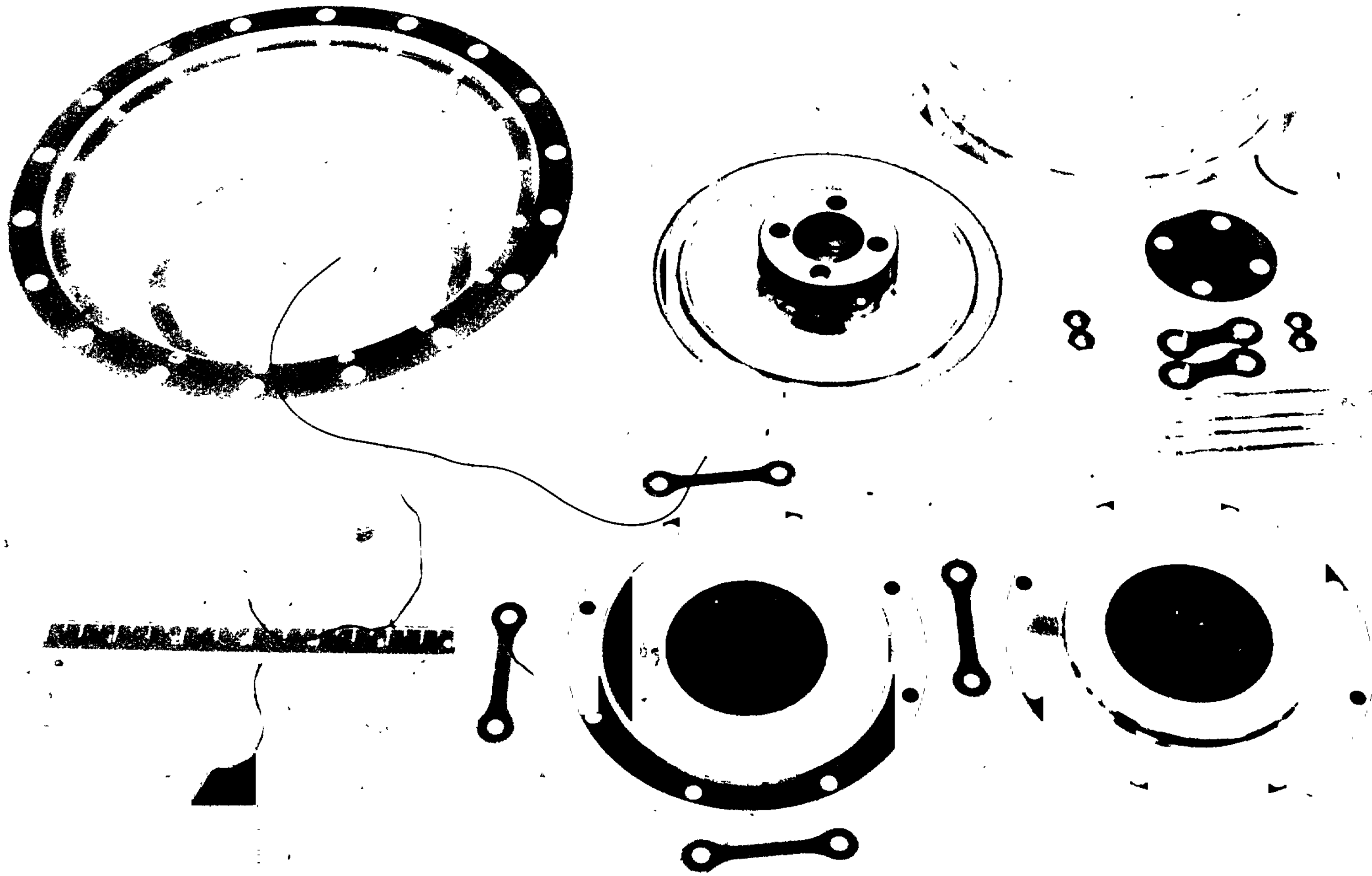

Figure 133. Liquid Oxygen Turbine Components

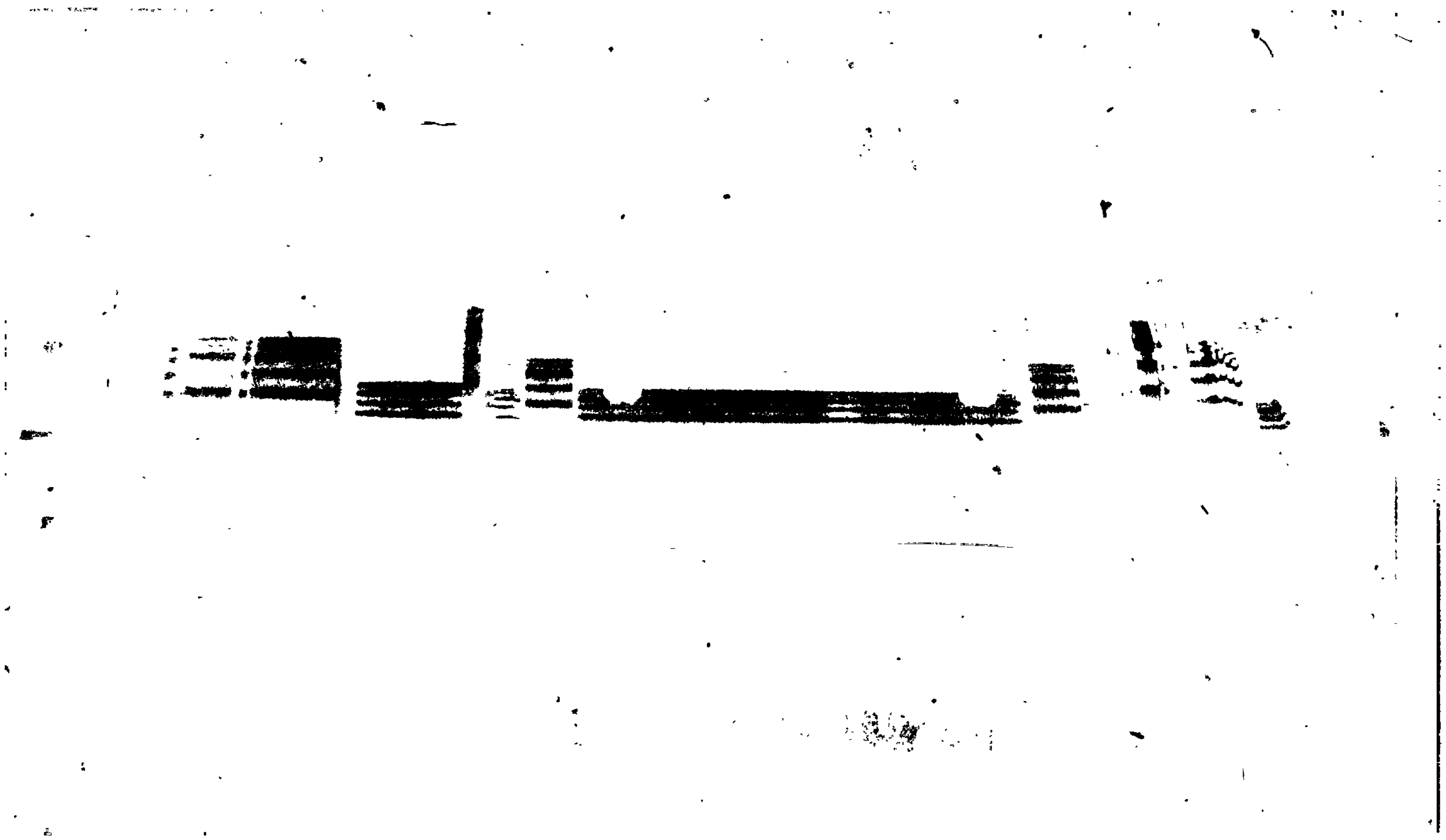

Figure 134. Liquid Oxygen Pump Rotor Assembly

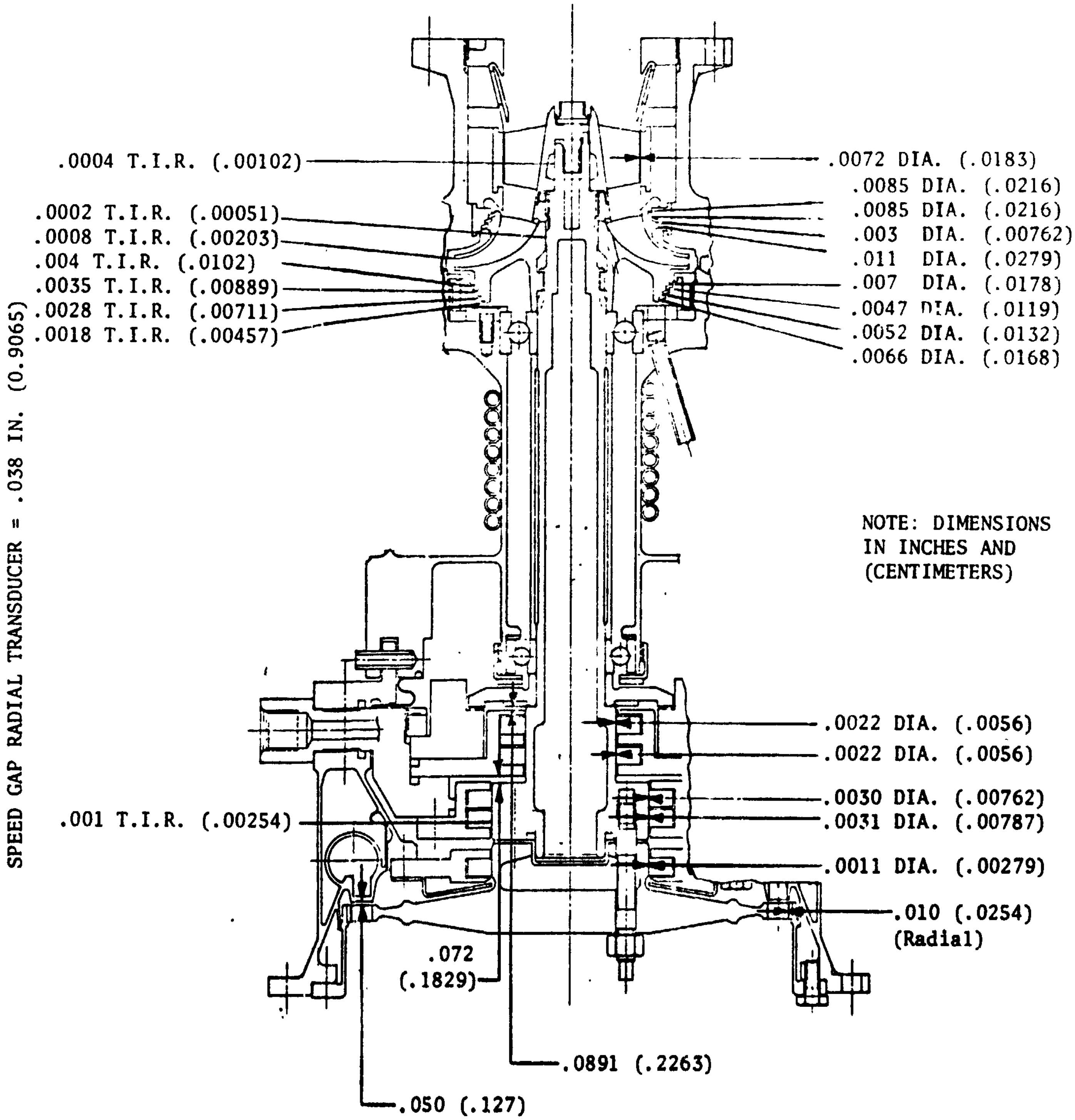

Figure 135. APS LO_2 Turbopump S/N 01 Ambient Clearances (Inches)

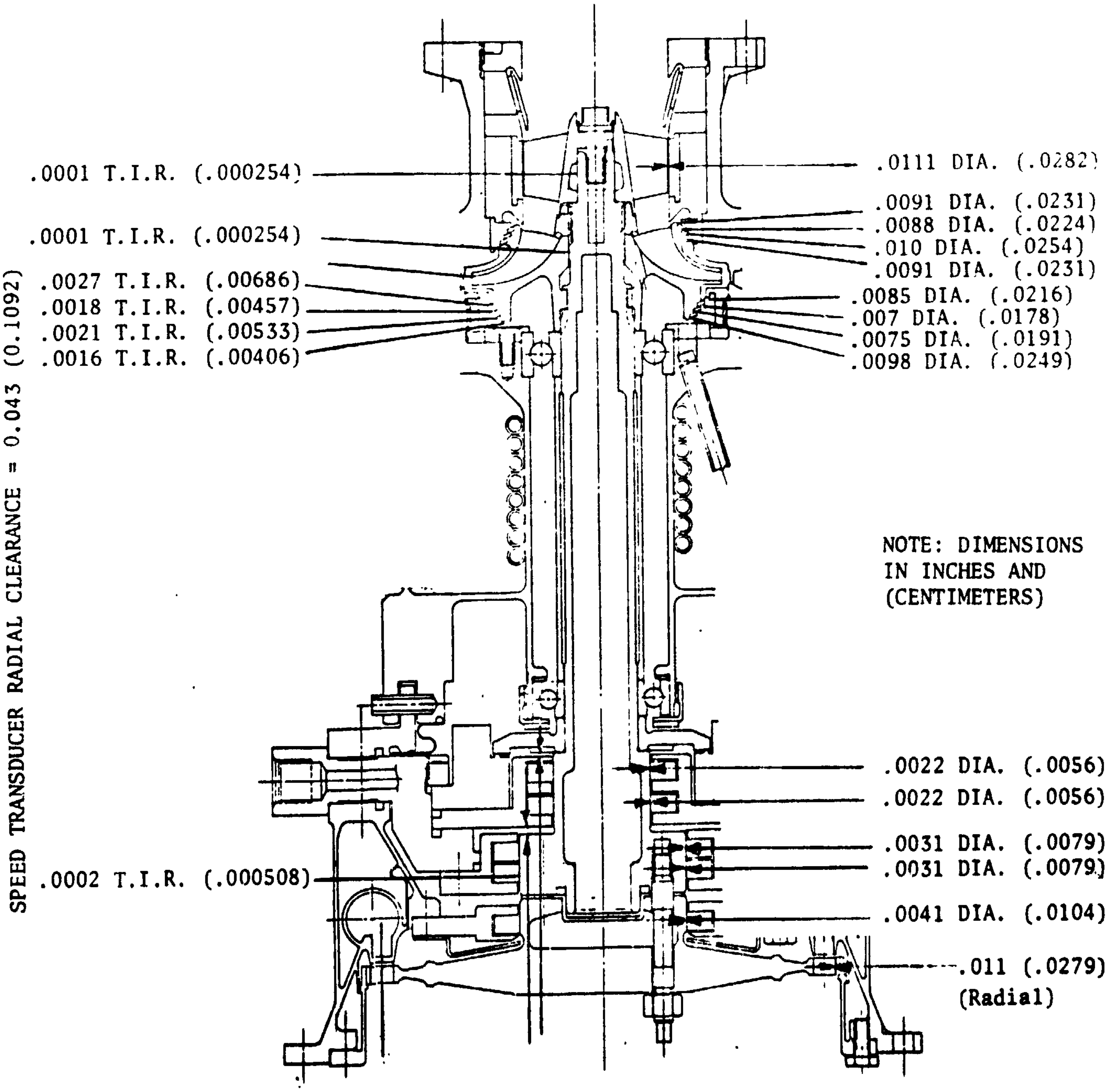

Figure 136. APS LO_2 Turbopump S/N 02 Ambient Clearances (Inches)

4. Rear bearing spring, rear bearing, bearing inner race spacer, front bearing and its outer race clamp and retaining screws were installed into volute. Rear bearing was retained with the antivortex ring, and the latter was secured with a locktab.

5. Mating ring spacer and mating ring were placed on rear bearing inner race. Earlier the spacer thickness was adjusted to provide the desired installed length for the lift-off seal.

6. The primary seal flange seal, lift-off actuation part seals on either side of the primary seal, the primary seal itself, lift-off seal and its retaining nut and lock were installed into the mounting ring.

7. A thin film of LOX compatible liquid teflon was applied to the mating ring surface which rests against the shaft shoulder. The mount ring subassembly created above was installed to the housing and the shaft chilled with LN_2 was inserted. To eliminate moisture from the shaft, the entire assembly was maintained under vacuum for 12 hours.

8. The impeller rear wear ring, its retaining ring and lock were installed and the impeller was pressed on the shaft with an arbor press. Impeller nut and retaining lock were added.

9. The inducer was installed by preheating to 450 K (350 F) and its retaining nut and lock were installed.

10. The volute and its flange seal were installed on the housing.

11. The intermediate seal was installed.

12. The turbine manifold and its flange seal was attached to the mount ring and the turbine shaft seal and turbine wheel tip seal were installed.

13. The wheel spacer, ground to provide 0.127 cm (0.050 inch) nozzle clearance was installed, along with the turbine wheel retaining studs and the turbine wheel.

14. The turbine wheel retaining nuts were tightened to obtain a 0.004 ±0.0005 inch stretch in the studs.

15. Functional checks (Table 32) were performed.

The assembled turbopump is shown in Fig. 137 and 138.

TABLE 32. MK-44 OXIDIZER TURBOPUMP ASSEMBLY FUNCTIONAL TESTS

	T/P S/N 01	T/P S/N 02
Lift-Off Seal Bellows Leakage at 1378951 N/m^2 (200 psig) GH_e	0	0
Lift-Off Seal Leakage at 241317 N/m^2 (35 psig) GH_e	0.2731 cm^3 [illegible] .55 scim)	1.639 cm^3/s (6 scim)
Lift-Off Seal Self Actuation Pressure	482,633 N/m^2 (70 psig)	468,843 N/m^2 (68 psig)
Primary Seal Leakage at 241317 N/m^2 (35 psig) GH_e	453 cm^3/s (1660 scim)	492 cm^3/s (1800 scim)
Interm. Seal Leakage at 241,317 N/m^2 (35 psif) GH_e, Pump Side	1912 cm^3/s (7000 scim)	2021 cm^3/s (7400 scim)
Iterm. Seal Leakage at 241,317 N/m^3 (35 psig) GH_e, Turbine Side	2185 cm^3/s (8000 scim)	1393 cm^3/s (5100 scim)
Rotor Torque, Lift-Off Seal Open	0.1412 Joule (20 in-oz)	0.0212 Joule (3 in-oz)
Rotor Torque, Lift-Off Seal Closed	3.84 Joule (34 in-lb)	--
Weight	--	31.75 Kg (70 lb)

Figure 137. Liquid Oxygen Turbopump (Turbine End)

Figure 138. Liquid Oxygen Turbopump (Pump End)

LH_2 TURBOPUMP

Component Fabrication

The detail components of the liquid hydrogen turbopump before assembly are shown in Fig. 139.

The inducer was machined from a titanium billet forging on a five-axis milling machine. The impeller was cast from Inco 718 by using a ceramic shell core as illustrated in Fig. 140. A small degree of difficulty was encountered in removing the core material from the internal flow passages of the casting. From the standpoint of core removal and capability of getting the ceramic slurry to flow through the hydrodynamic passages, the 0.254 cm (0.100 inch) discharge width, in combination with the 12.47 cm (4.91-inch) outer diameter came close to the limit of this casting method.

The crossover was initially planned to be fabricated in two cast sections as shown in Fig. 141 which were joined by welding. The lower part was a conventional investment casting of Inco 718. To cast the upper part, the ceramic shell core approach described for the impeller was used. However, more difficulty than anticipated was encountered in producing this part because the almost 180-degree bend made it difficult for the slurry to flow through and cover all the surfaces before local solidification and choking took place. This resulted in local imperfections in the flow passage wall surfaces. Furthermore, after the casting was poured, it was virtually impossible to remove the baked ceramic shell from the "bend" where it was not directly accessible for cleaning by hand. The problem was solved by machining part of the turning passage cover away, as shown in Fig. 142. This made the flow passage accessible to remove the core and to hand blend surface irregularities. Subsequently, a cover was machined from Inco 718 and welded to the crossover as shown in the figure.

The volute part of the housing (Fig. 143) was cast by using permanent injection mold dies and ceramic shells. The center cylinder, rear plate, and turbine-end mount ring were attached by welding. Subsequently, the cooling coils were

Figure 139. Liquid Hydrogen Turbopump Components

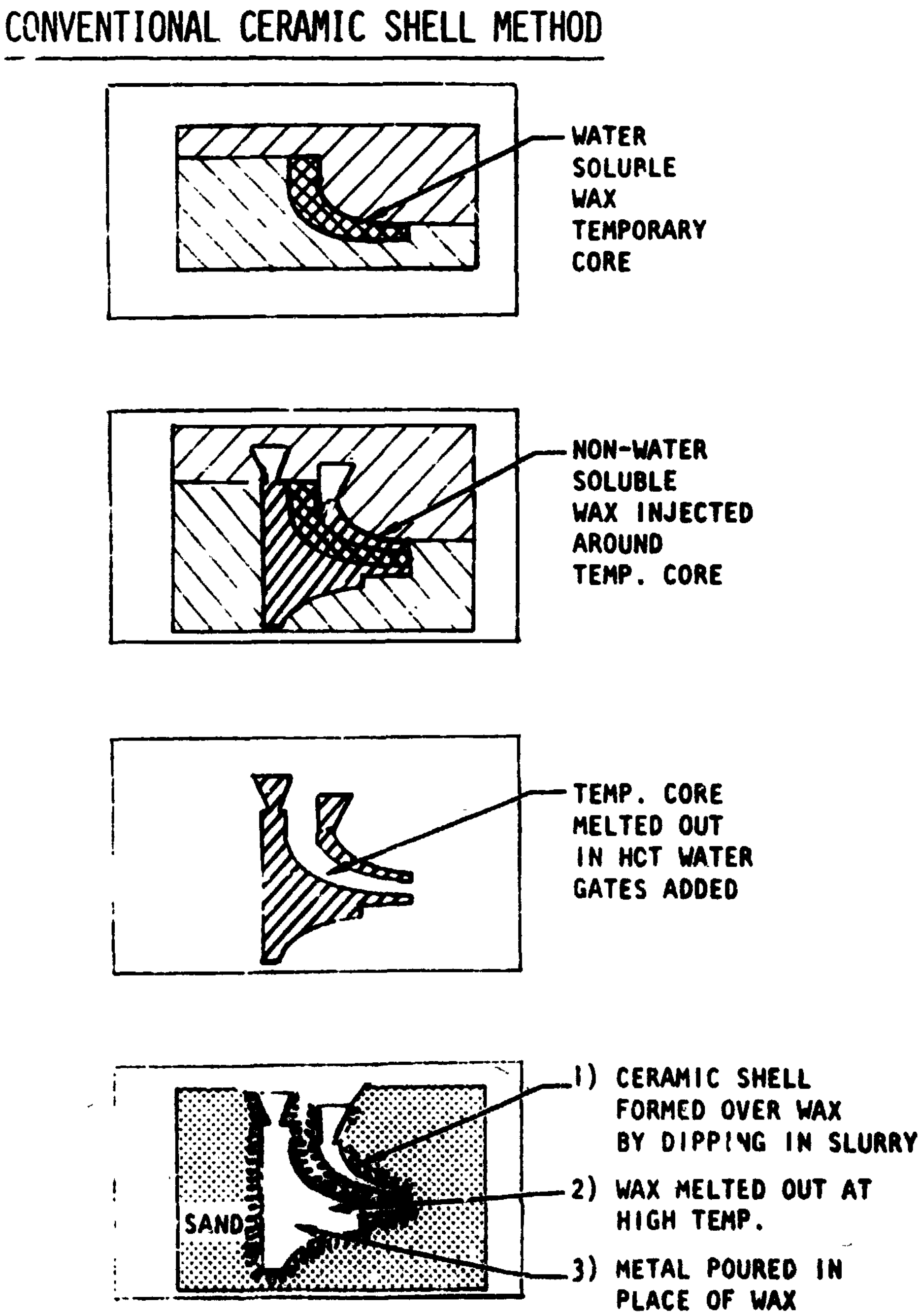

Figure 140. Impeller Casting

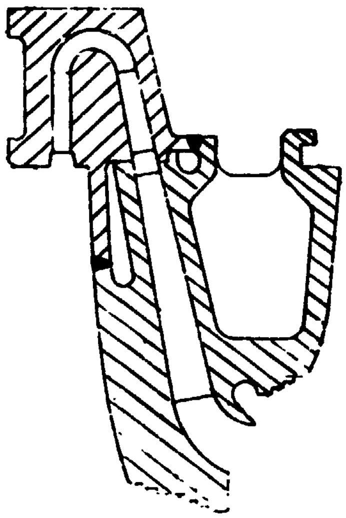

ORIGINAL DESIGN

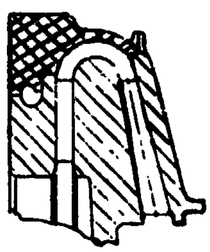

MODIFIED DESIGN

Figure 141. Crossover Fabrication

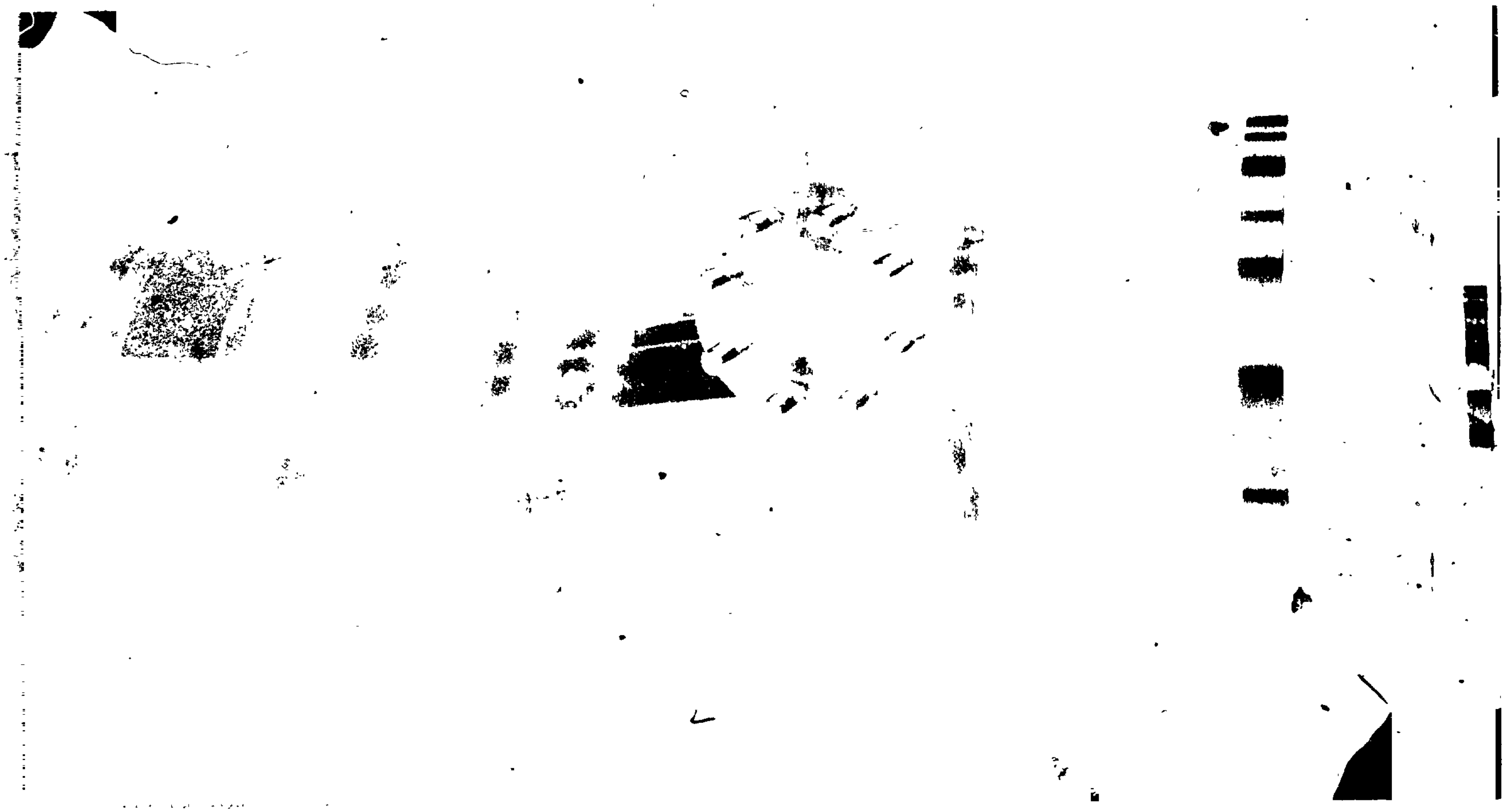

Figure 142. Liquid Hydrogen Turbopump Housing Components

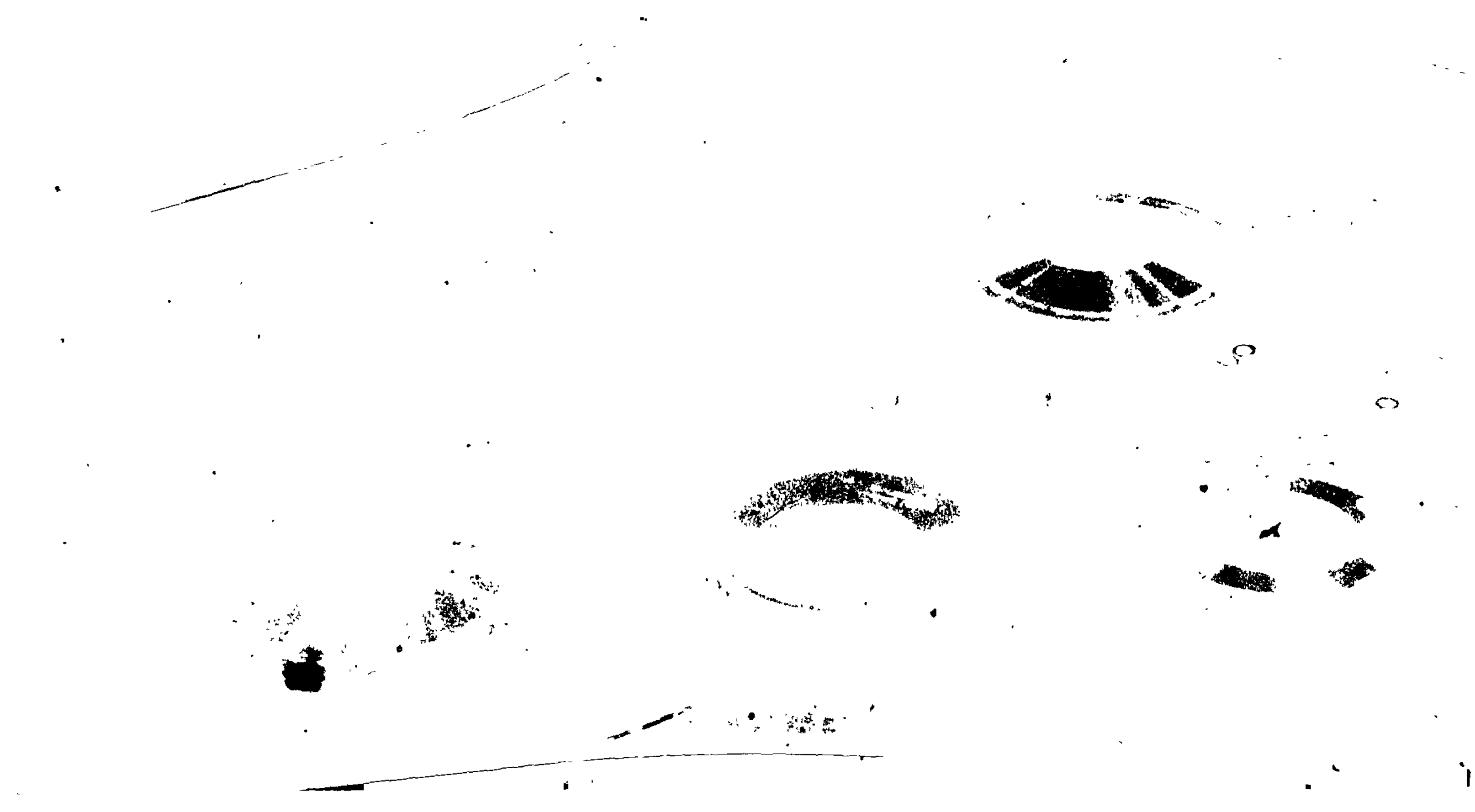

Figure 143. Liquid Hydrogen Turbine Components

installed on the center cylinder by hand brazing. On the initial attempt at brazing, apparently too much localized heat was applied to the welded structure. This caused many cracks not only in the center cylindrical part, but cracks also extended into the lower part of the casting. To effect a repair, the cracked sections were removed and replaced by sections machined from forged rings and the cooling tubes were installed by furnace brazing.

The turbine manifold and turbine first row wheel (Fig. 144) were identical, with the exception of the number of nozzle passages, to the corresponding parts of the LOX turbopump; therefore, their fabrication process followed the procedure described from LOX turbopump parts. Figure 144 shows the nozzle in the process of fabrication. A partially finished nozzle is shown on the left hand side, and the tool containing the electrodes used to form the inlet side of the nozzle is shown on the right. A nozzle being EDM is clamped in the machine.

A considerable degree of difficulty was encountered in generating the flow passages of the turbine stator. Since the vanes were shrouded at the inner as well as the outer diameter, access to the center of the passage with the electrode was limited. After an unsuccessful attempt to EDM axially from the inlet and discharge, this approach was abandoned and a 0.345-cm (0.136-inch) wide circumferential band was removed from the inner shroud to provide access for radial insertion of the electrode.

After the vane airfoil section was formed, the shroud was reinstated by brazing a band of Haynes 188 in place of the removed section.

The plan with the electrical discharge machined surface of the nozzle and rotor blades was to remove the brittle remelt layer left on the generated surfaces by shot-blasting after the EDM operation. To establish the effectiveness of the shot blasting technique, EDM samples were prepared of each material with various current intensities. The samples were submitted to the same shot-blasting procedure which was to be used subsequently on the turbine components.

Figure 144. Turbine Nozzle Fabrication

Metallographic analysis showed that the shot-blasting effectively removed the remelt layer on the samples where moderate or light current feed rates were used. Based on these results, the procedure for EDM was established. Examination of the turbine components revealed that in areas where the shot-blasting impact was not direct, as on the flat samples, the remelt layer was not completely removed. Other methods need to be explored to develop a technique for removing the remelt layer from EDM turbine passages.

Turbopump Assembly

Prior to buildup of the turbopump, the rotor components (shown in Fig. 145) were assembled into a balance assembly as shown in Fig. 146 and 147. Special balance bearings of small internal clearance were used, and one bearing at each end was replaced by an inner race to maintain the parts in their proper axial position. The rotor of turbopump S/N 01 was corrected to a residual unbalance of 0.025 gr. in. on the pump end and 0.3048 gr cm (0.12 gr. in.) on the turbine end. Similarly, the rotor of turbopump S/N 02 was corrected to a residual unbalance of 0.1524 gr cm (0.06 gr. in.) in the pump and turbine planes, respectively.

The radial runouts of the rotor critical surfaces were measured on the balance assembly (Fig. 148 and 149) and detail measurements were made to establish the radial fits (Fig. 150 and 151) and minimum axial clearances in critical areas.

The front and rear bearing packages, consisting of the two bearings, bearing cartridge, bearing outer race preload springs and inner race spacer were installed into a fixture and the axial preload was measured. The inner race spacer thickness was then adjusted until the desired preload of 334 N (75 pounds) was obtained.

The assembly of the LH_2 turbopump was performed as follows:

1. Front bearing package including the two bearings, outer race cartridge, outer race springs, inner race spacer and cartridge preloading springs and shims were installed into housing.

Figure 145. Liquid Hydrogen Turbopump Rotor Components

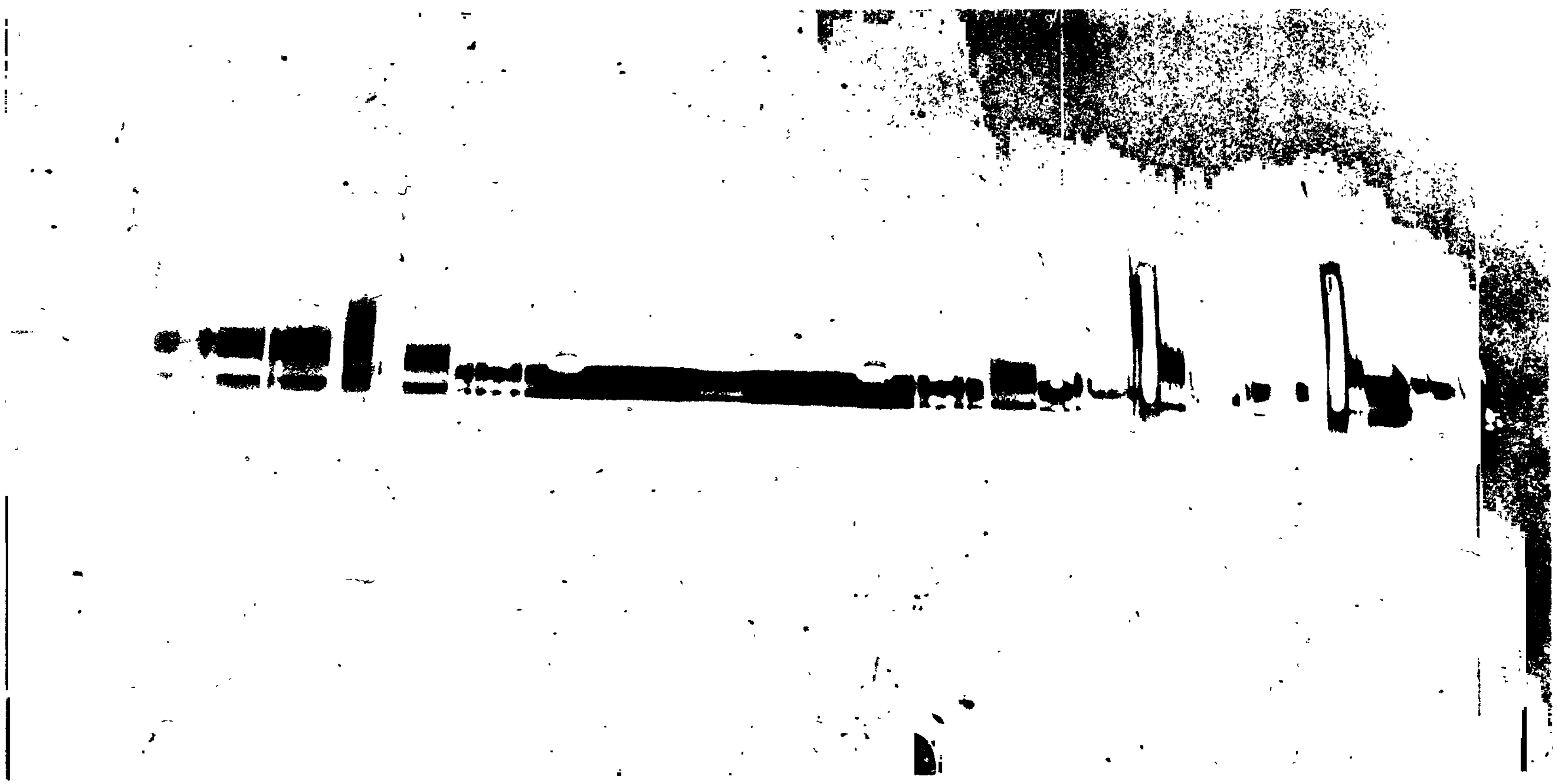

Figure 146. Liquid Hydrogen Rotor Assembly (Side View)

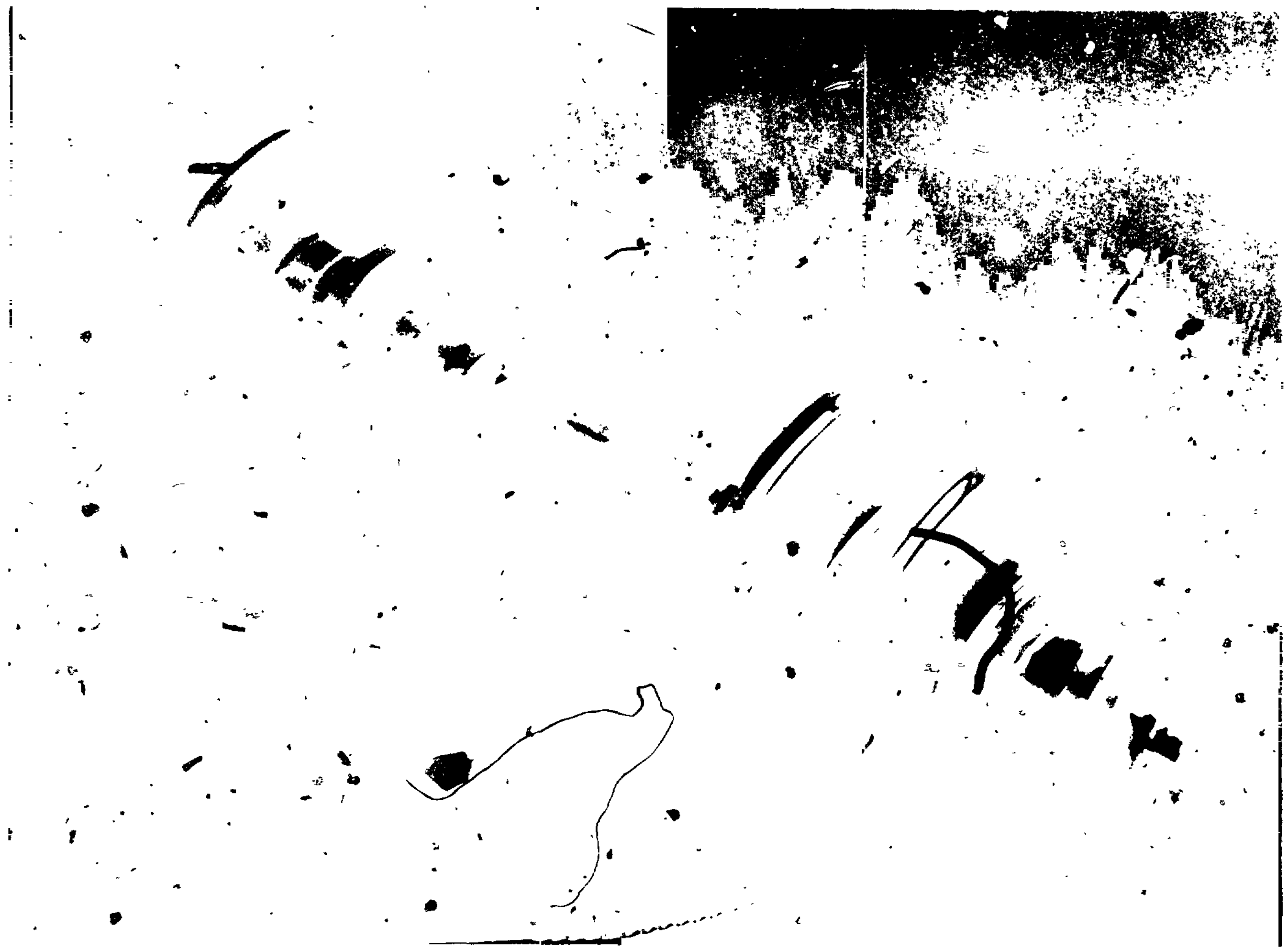

Figure 147. Liquid Hydrogen Rotor Assembly

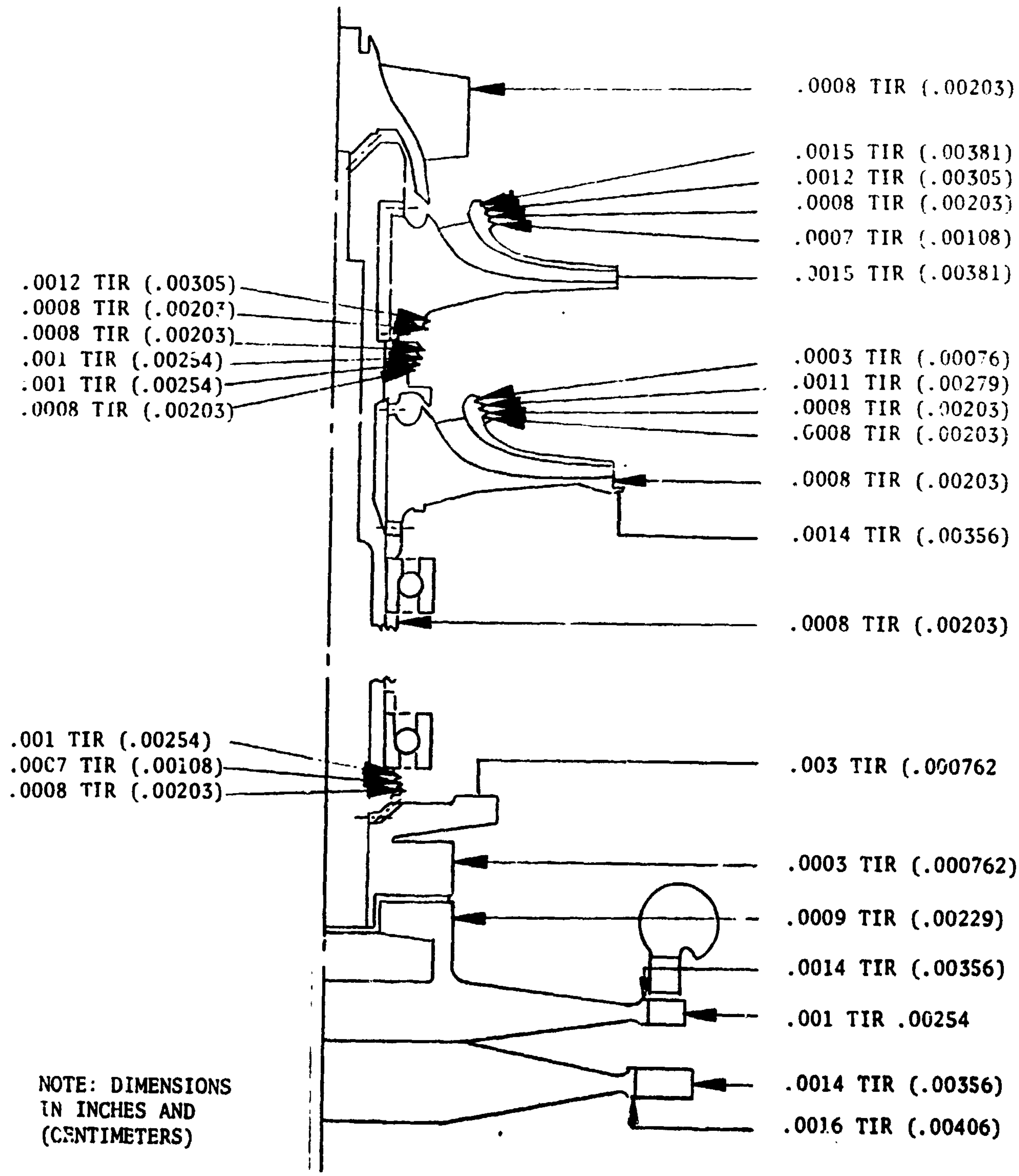

FIGURE 148. APS Fuel Turbopump S/N 01 Rotor Runouts

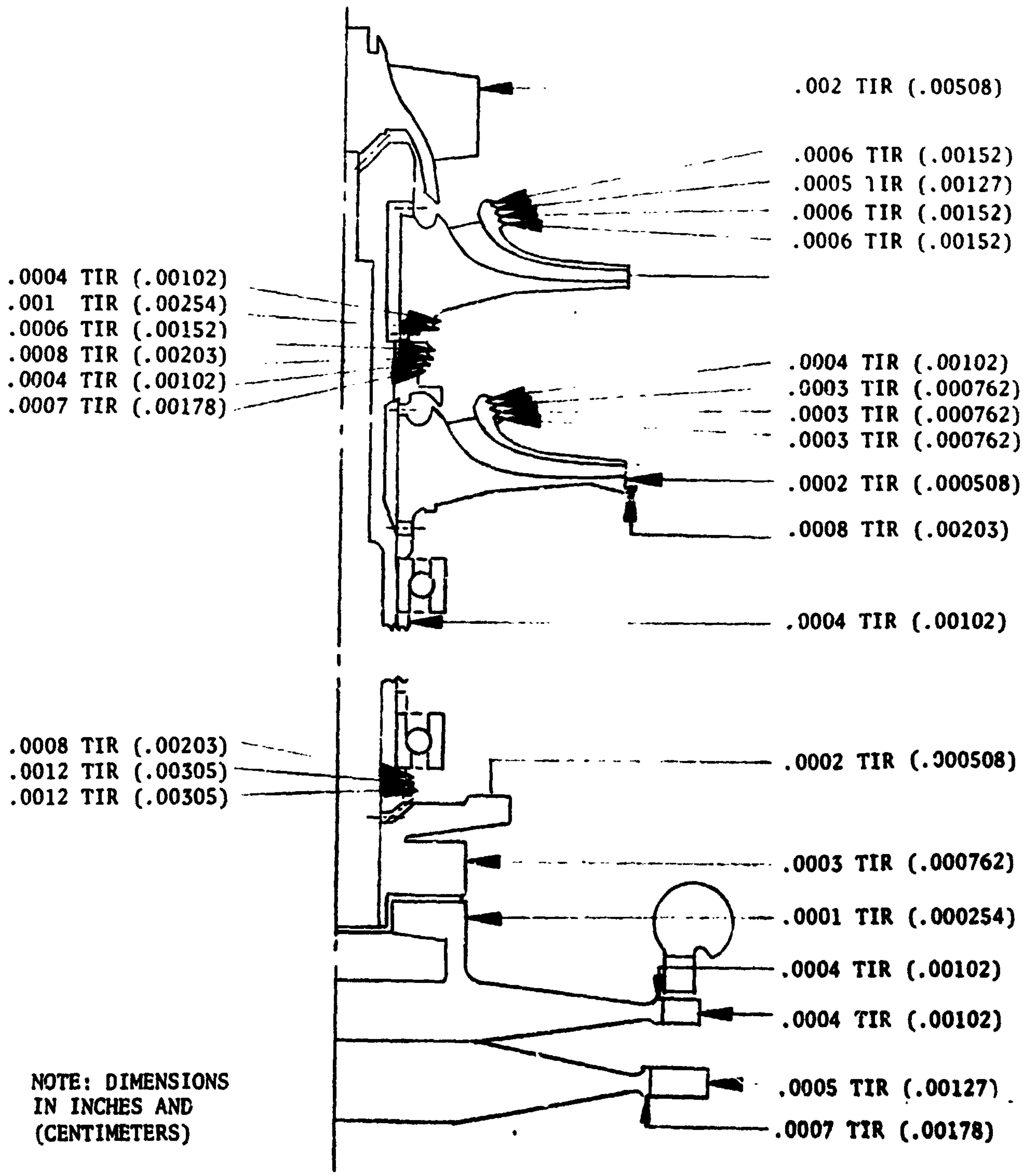

Figure 149. APS LH_2 Turbopump S/N 02 Rotor Runouts (Inches)

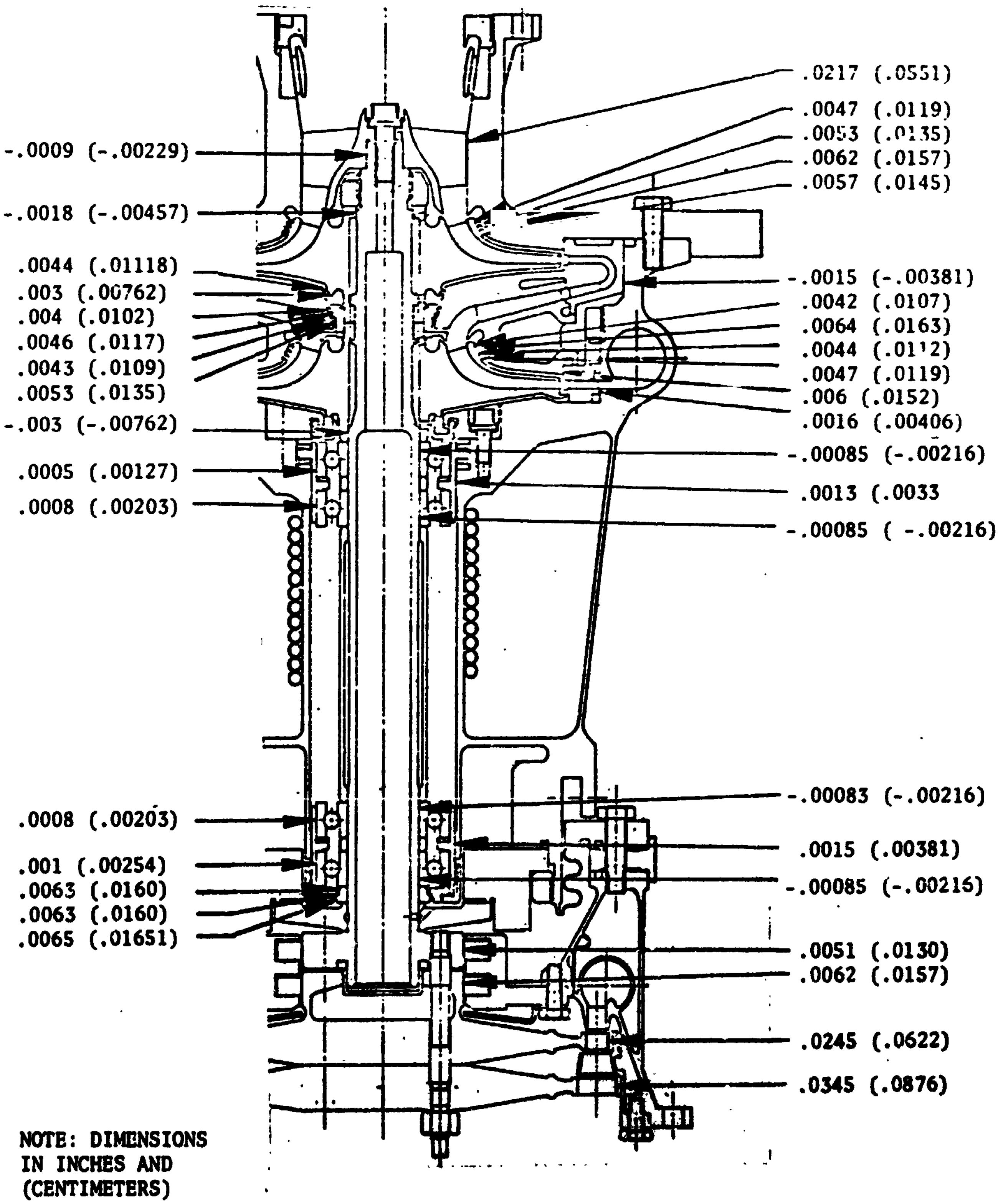

Figure 150. APS Fuel Turbopump S/N 01 Ambient Diametral Fits

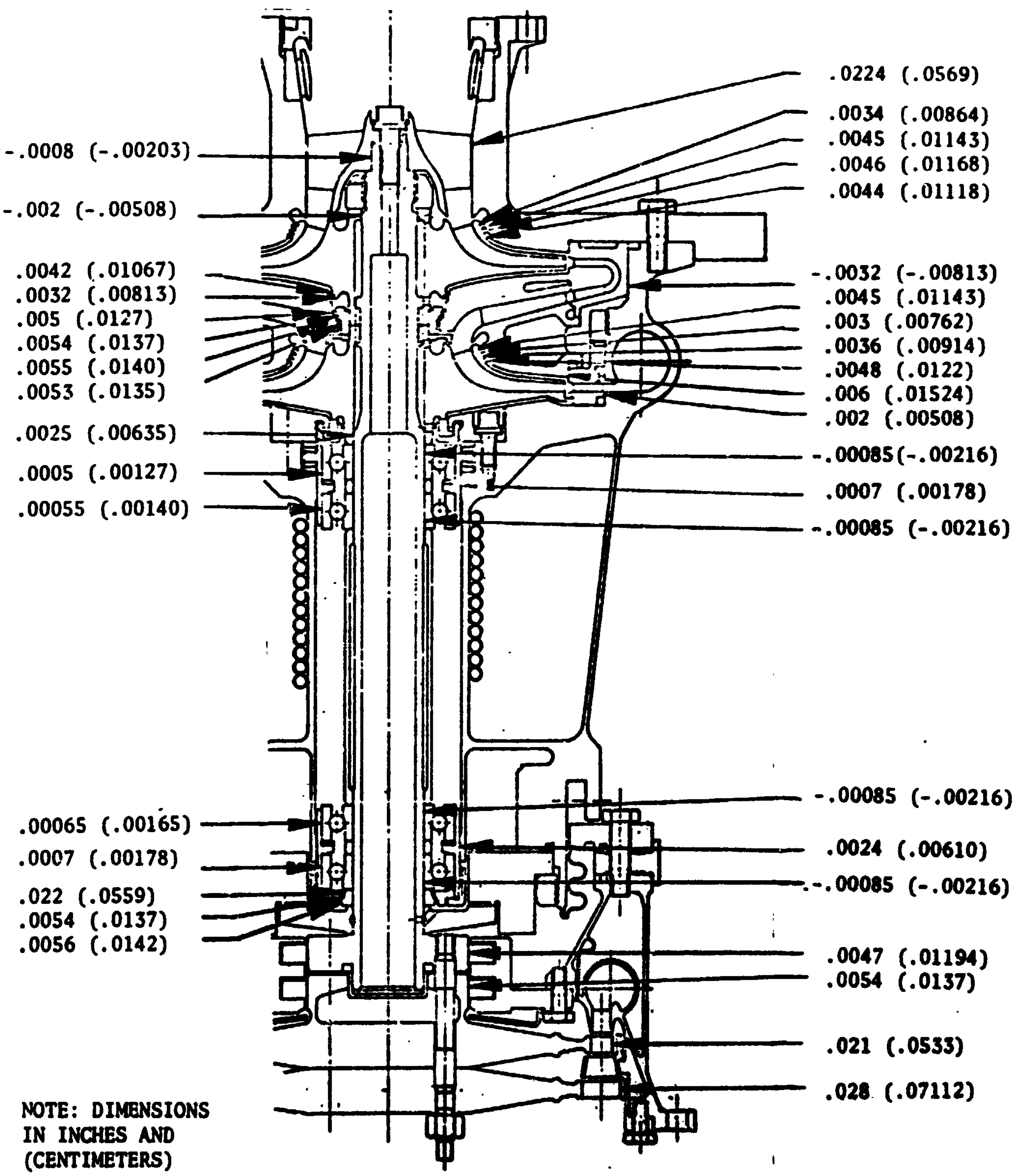

Figure 151. APS LH_2 Turbopump S/N 02 Ambient Diametral Fits

2. Balance piston low pressure orifice subassembly was installed into the housing.

3. A dummy shaft with a clearance radial fit at the bearings and second stage impeller was installed to aid in establishing the proper bearing loads at either end of the balance piston travel.

4. The second stage impeller and the diffuser containing the balance piston high pressure orifice were installed.

5. The total balance piston gap and the load absorbed by the bearings at the point where the balance piston high and low pressure seals contact was measured by alternately pushing the dummy shaft forward and aft with a loading mechanism. Adjustments were made in the thickness of the low pressure orifice shim and in the thickness of the bearing cartridge preloading spring shims until a total gap of 0.0254 ±0.00254 cm (0.010 ±0.001 inch), a rotor load of 1334 N (300 pounds) at the high pressure orifice and 2669 N (600 pounds) at the low pressure orifice was obtained.

6. The dummy shaft was removed and the lift-off seal was installed into the housing.

7. The lift-off seal mating ring, labyrinth spacer (thickness adjusted to provide proper lift-off seal operating length), rear bearing cartridge subassembly and the long bearing spacer were installed on the shaft.

8. The subassembly created above was installed into the housing, pushing shaft through front bearings and second stage impeller.

9. Pump crossover, first stage impeller, inducer and inlet were installed.

10. The pump was filled with LN_2 and the balance piston total gap and bearing load measurements were repeated at cryogenic temperature. Adjustments were made in the respective shims until the desired values were obtained.

11. To remove all moisture from the pump, it was placed in a vacuum oven at 0.254 cm (0.1 inch) Hg and 328 K (130 F) for 12 hours.

12. The back flow deflector was installed into the pump inlet.

13. The mount ring and the turbine manifold with the shaft seal attached were installed.

14. The turbine wheel spacer adjusted in thickness to provide 0.0127 cm (0.050 inch) nozzle clearance was installed, followed by wheel retaining studs and the first row wheel.

15. The stator ring spacer was ground to a thickness which would result approximately equal clearance before and after the stator; and the spacer, stator and second row wheel were installed. The wheel retaining nuts were tightened to obtain an elongation in the studs of 0.00127 cm (0.005 inch).

16. Functional checks were performed (Table 33).

The assembled turbopump is shown in Fig. 152.

GAS GENERATORS

Component Fabrication

The gas generator assemblies were fabricated as shown in Fig. 153 and 154. The injectors utilized a 304 CRES body, Nickel 200 posts, and an OFHC copper faceplate. The posts and faceplate were brazed into the body as a subassembly, and the manifold was closed out with a 304 CRES cover plate electron beam welded in place.

The body was fabricated from OFHC copper bar stock. The dump coolant holes through the walls of the body were drilled, as were the coolant injection holes, into the combustion zone. Injection holes were located in line with the injector posts. The body was milled to provide a coolant passage around the spark plug hole. The milled channel was subsequently capped with a spacer (electron-beam welded in place).

The cone was fabricated from HS188 to withstand the high temperature (1550 F) operating conditions.

TABLE 33. MK-44 LH_2 TURBOPUMP ASSEMBLY FUNCTIONAL TESTS

	T/P S/N 01	T/P S/N 02
Lift-Off Seal Bellows Leakage at 1,378,951 N/m^2 (200 psig) GH_e	0	0
Lift-Off Seal Leakage at 241,317 N/m^2 (35 psig) GH_e	6.4183 cm^3/s (23.5 scim)	1.0925 cm^3/s (4 scim)
Lift-Off Seal Self Actuation Pressure	965,266 N/m^2 (140 psig)	579,160 N/m^2 (84 psig)
Shaft Seal Leakage at 241,317 N/m^2 (35 psig) GH_e	--	1638 cm^3/s (6000 scim)
Rotor Torque, Lift-Off Seal Open	0.05649 Joule (8 in-oz)	0.07062 Joule (10 in-oz)
Weight	39.9 kg (88 lbs)	39.9 kg (88 lbs)

Figure 152. Liquid Hydrogen Turbopump (Turbine End)

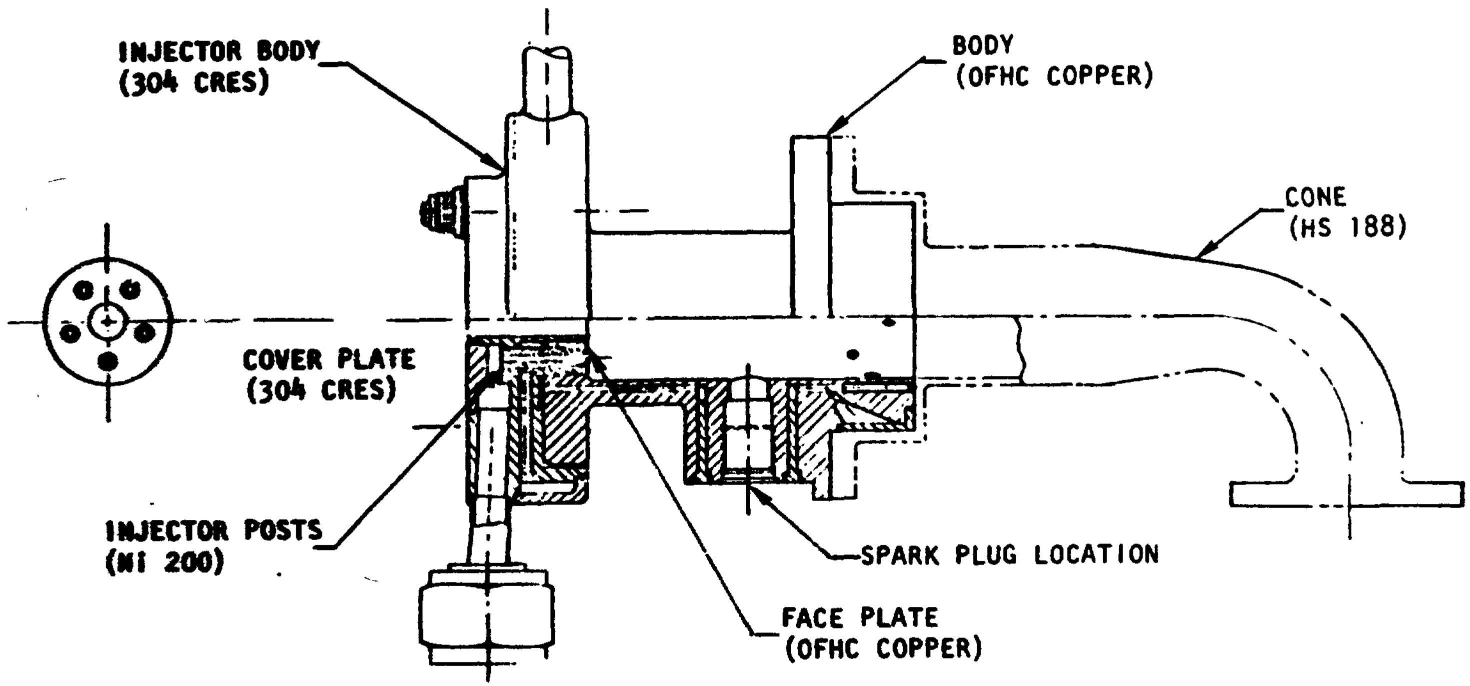

Figure 153. Oxygen TPA Gas Generator Assembly

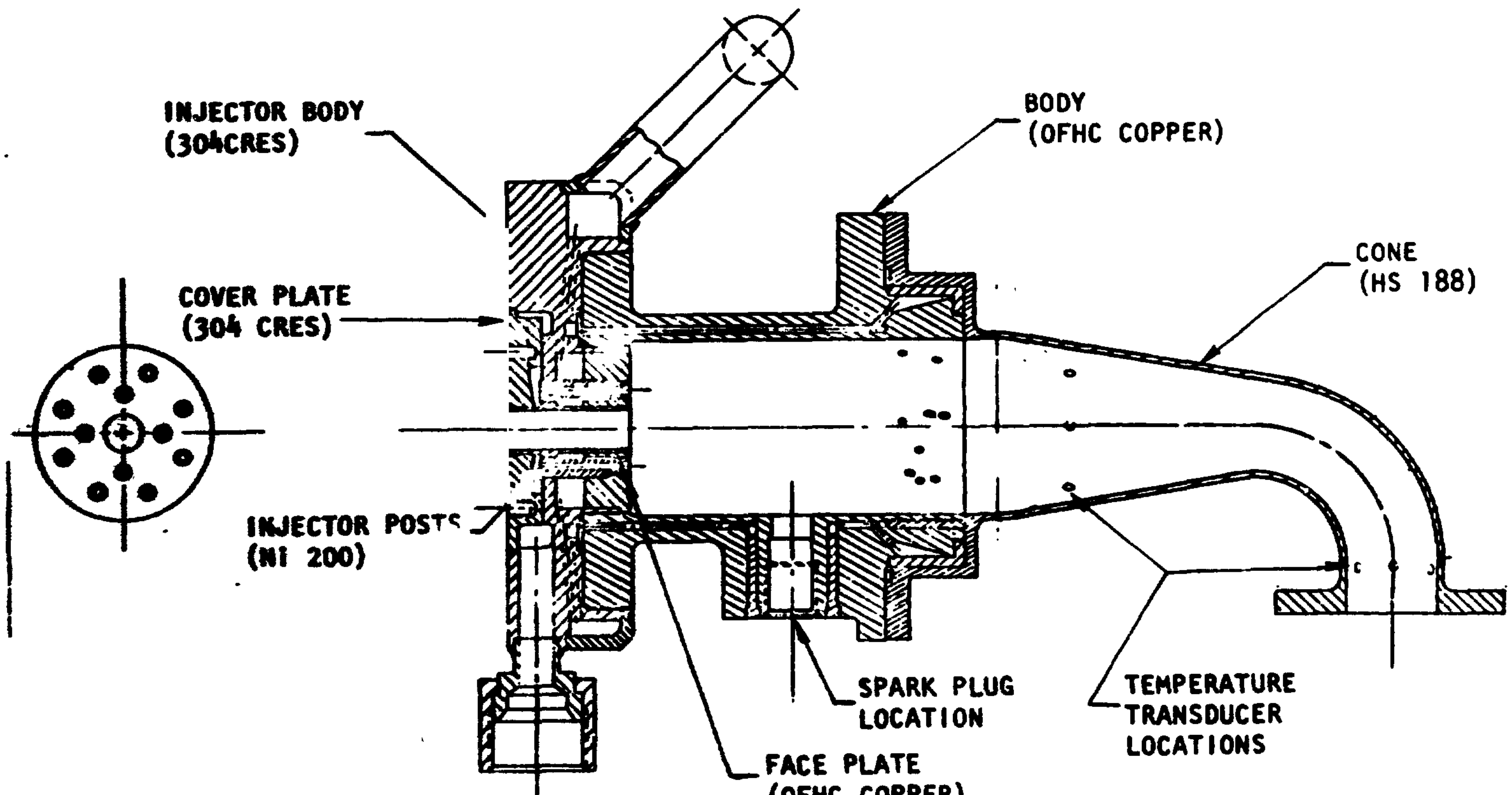

Figure 154. Hydrogen TPA Gas Generator Assembly

Assembly

The injectors, combustor bodies, and cones were assembled and incorporated into the complete subassembly by installing the bipropellant, mechanically linked ball valve, and manifold assembly as shown in Fig. 155. The interconnecting manifold was sized to assure a hydrogen lag during cutoff. In addition, a stub capped with a B-nut was provided in the fuel manifold to allow for subsequent adjustment should it prove necessary. The oxidizer manifold was minimized as much as possible to minimize the oxidizer to be purged during cutoff.

The only significant fabrication problem encountered was not discovered until the checkout test of the first LO_2 gas generator was in progress. As shown in Fig. 156, the thermocouple weld in the HS188 cone failed during the hot-fire test.

An electron microprobe analysis of the failure zone revealed the presence of a 300 CRES weld rod application, resulting in diffusion of carbon into the HS188 which consequently provided an embrittled zone. The major portion of the weld had been conducted using Hastelloy W weld rod as is required. It was hypothesized that the welder picked up the wrong weld rod, began the weld, and then switched to the proper weld rod. The part was repaired by replacing the cylindrical section and the assembly was returned to service.

No other problems were encountered throughout all hot-fire testing conducted with the gas generator assemblies.

LO_2 TURBOPUMP ASSEMBLY

The LO_2 turbopump assembly includes the turbopump, gas generator, pneumatic and electrically controlled valves, unit base, and associated interconnective plumbing and electrical connections. The unit is shown in Fig. 157 and 158, respectively. The gas generator was welded to the turbine manifold and the turbopump/gas generator was mounted on the base at three points to allow for thermal growth of the components without imposing a bending load on the turbopump. The

Figure 155. Gas Generator Assembly

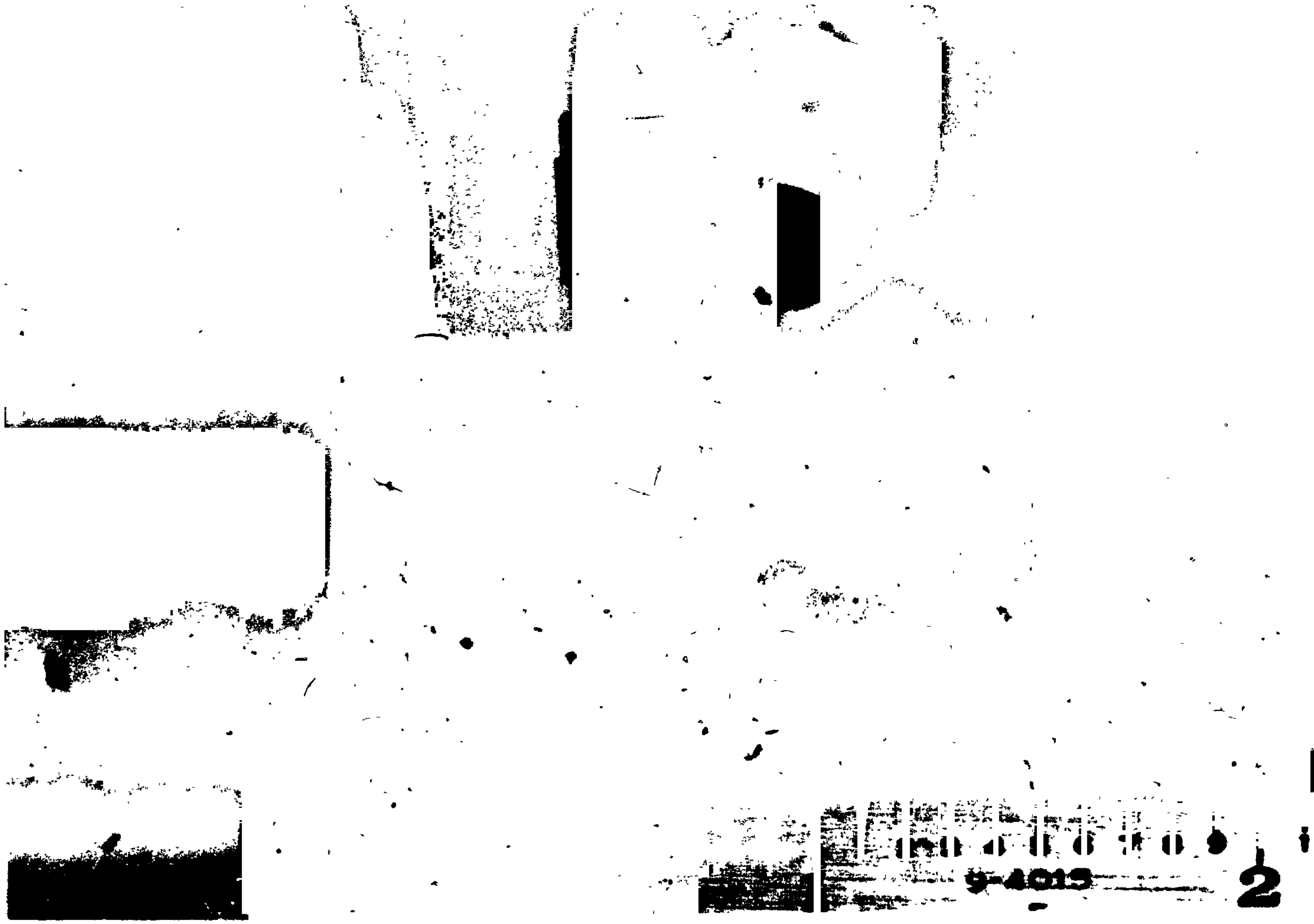

Figure 156. Gas Generator Weld Failure

Figure 157. Liquid Oxygen Turbopump Assembly (Pump End)

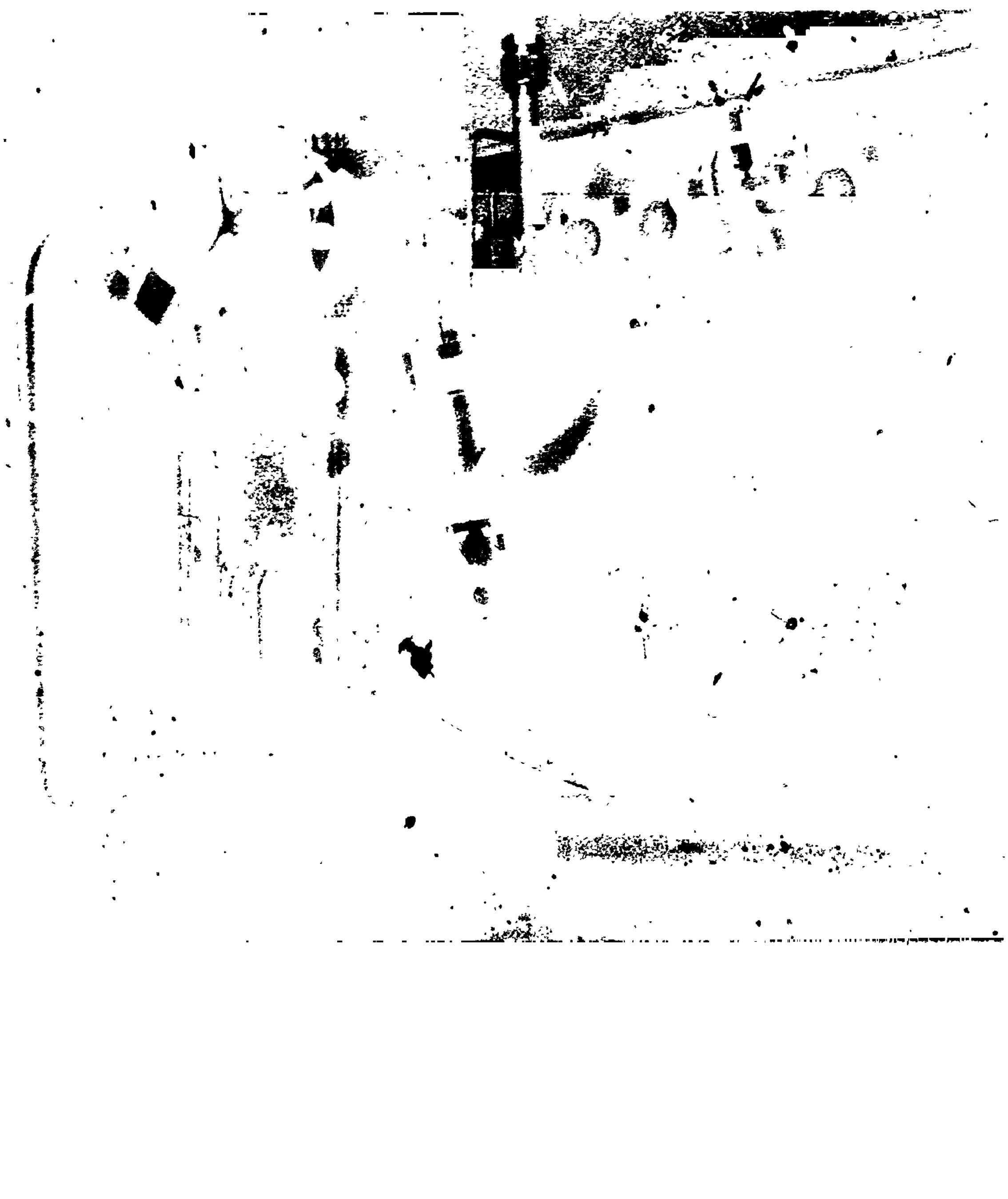

Figure 158. Liquid Oxygen Turbopump Assembly (Turbine End)

gas generator was separately supported by a clevis arrangement which allowed thermal growth while supporting the weight in the vertical direction. The control valves were close-coupled to provide a minimum of priming volume and were attached to a common manifold for ease of manifolding. The base was designed to provide easy lifting capability as well as rigid support to the components and was fabricated from plate with bends for stiffening. For thermal insulation, the turbine assembly and gas generator were wrapped with quartz cloth, and polyurethane foam was applied to the pump portion of the assembly. The compact packaging of the unit allowed for its efficient transportation to and from the test facility without damage. Two LO_2 units were assembled and delivered for test.

LH_2 TURBOPUMP ASSEMBLY

The LH_2 turbopump assembly is shown in Fig. 159 and 160. The same base, valve and interconnective line arrangement was utilized on the LH_2 units. This commonality provided significant flexibility and economy of the fabrication process. Two LH_2 units were assembled and delivered for test.

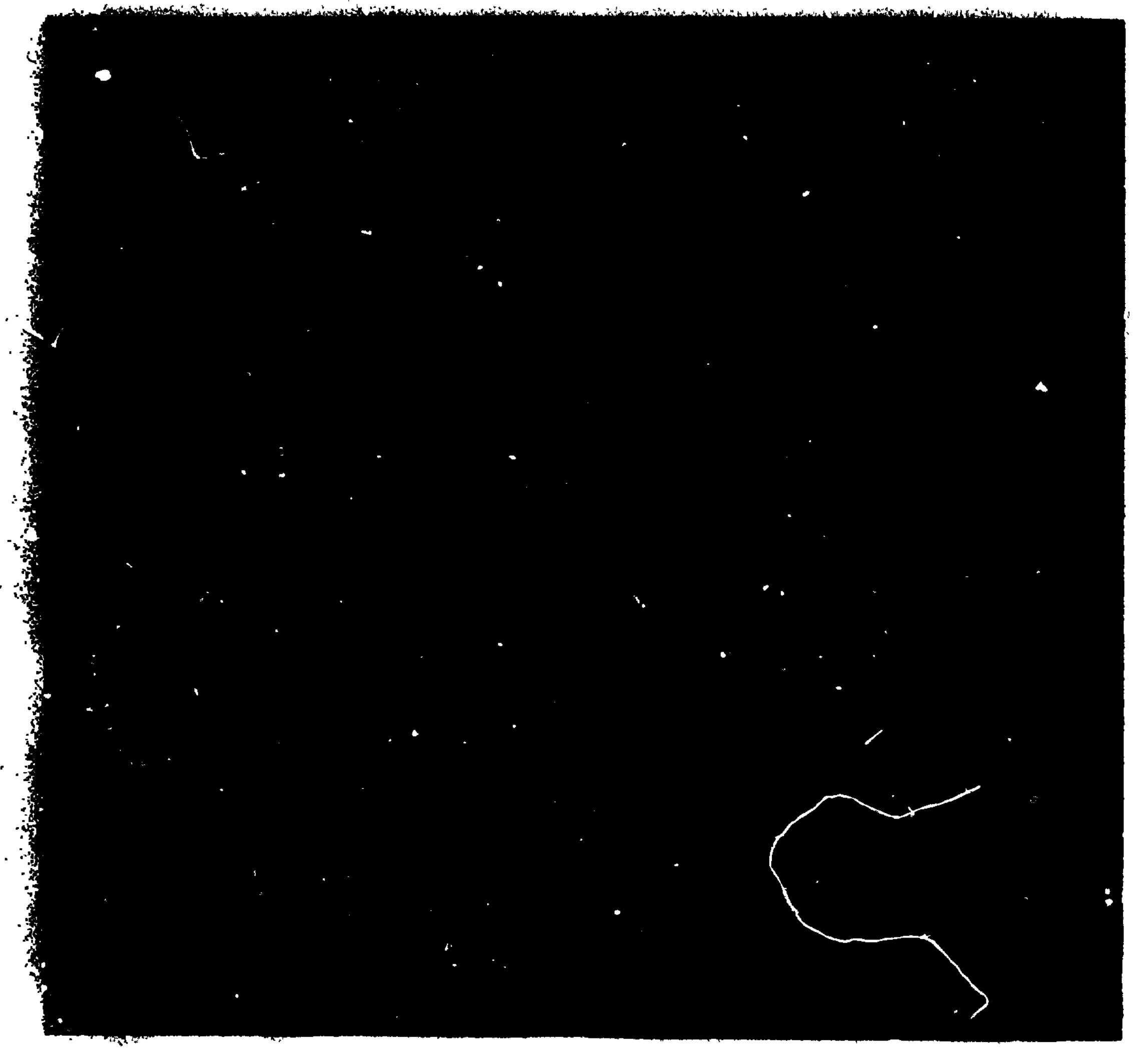

Figure 159. Liquid Hydrogen Turbopump Assembly (Pump End)

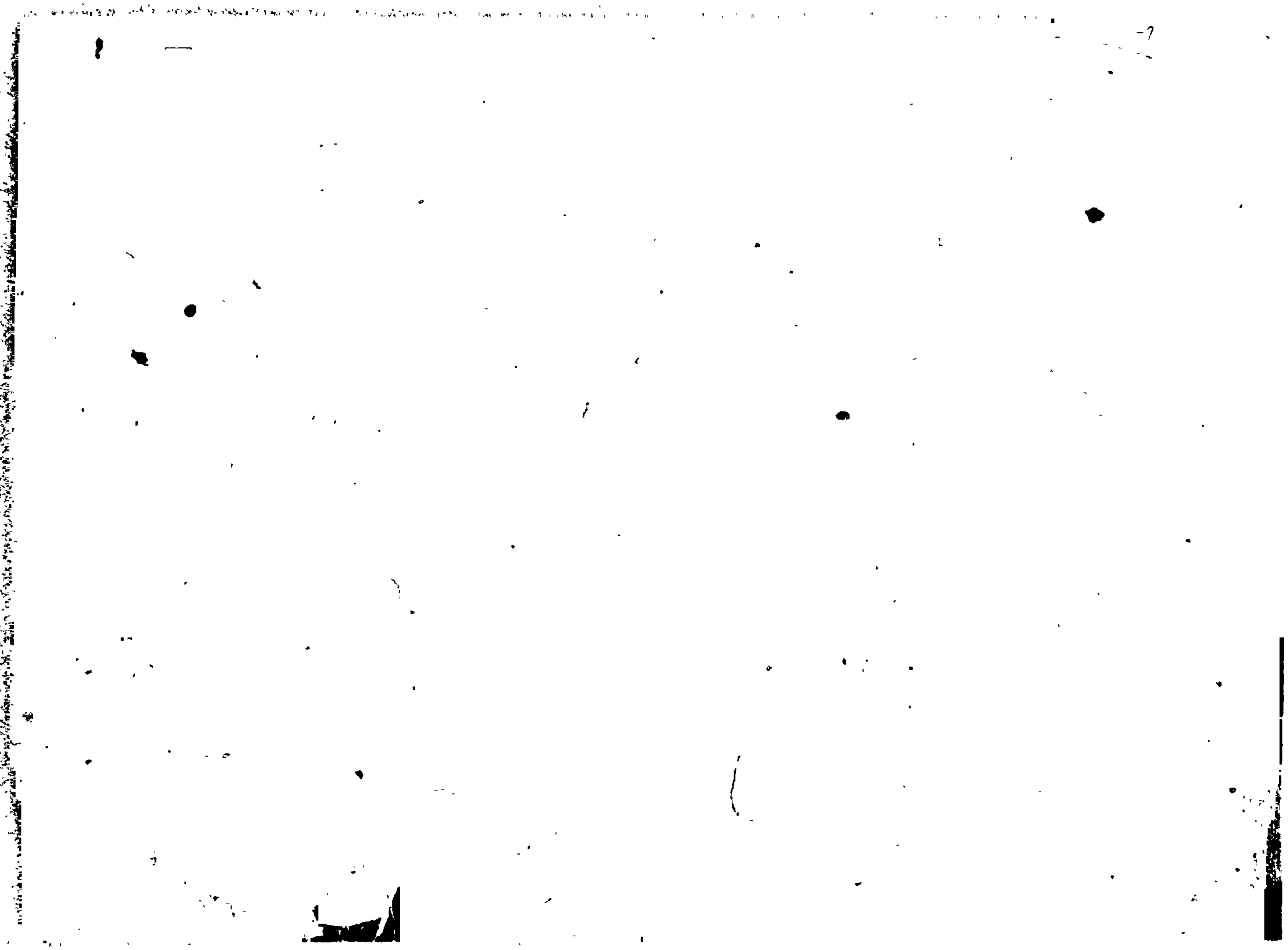

Figure 160. Liquid Hydrogen Turbopump Assembly (Turbine End)

PHASE IV - DEVELOPMENT TEST

To demonstrate the capabilities of the LO_2 and LH_2 turbopump assemblies, a development test program was conducted. Discussion of the facilities utilized the specific tests conducted and the analysis of results is subsequently presented.

FACILITY DESCRIPTION

This test program was conducted at the CTL-4 test facility of the Santa Susana Field Laboratory. Test cells 26A and 26B were specifically designed for testing of oxygen and hydrogen turbopumps and components, and the position of these cells is shown in the plan of module 2 of CTL-4. Presented is a description of the turbopump facility capability and operation including propellant feed systems, controls, instrumentation, and data reduction procedures (Fig. 161).

Propellant Systems

The pumped liquid propellant is supplied to the test positions from elevated vacuum jacketed storage tanks through insulated lines. Liquid oxygen is supplied to cell 26A as shown in Fig. 162, and liquid hydrogen is supplied to cell 26B as shown in Fig. 163. The facility inlet line shown in Fig. 164 provides a smooth transition to the pump inlet with a pieze ring for accurate measurement of the inlet static pressure and redundent temperature transudcers for measurement of the inlet temperature. Downstream of the turbopump assembly discharge valve ia a position controlled facility throttle valve. This throttle valve could be preset and varied during a test to obtain specified values of pump discharge resistance (Q/N).

The gas generator propellant feed system is shown in Fig. 165 and has a common propellant supply and control system for the two test positions. This system was designed to provide gaseous oxygen and hydrogen at specified pressures and temperatures. Liquid propellant and ambient temperature gaseous propellant were mixed by pressure and temperature controlled servo valves to provide oxygen from 208 K (375 R) to ambient temperature (approximately 294 K or 530 R) and hydrogen from

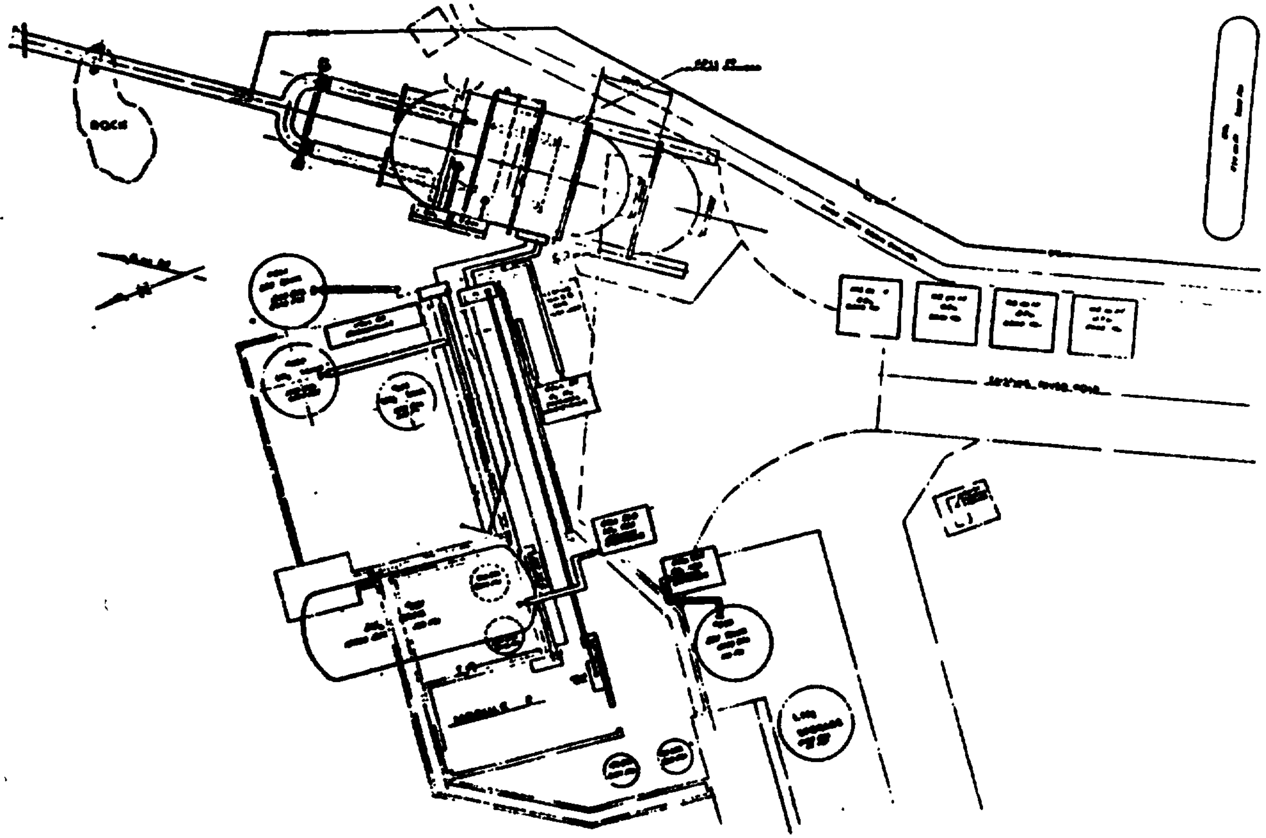

Figure 161. Module 2, CTL-4, APS Facility System

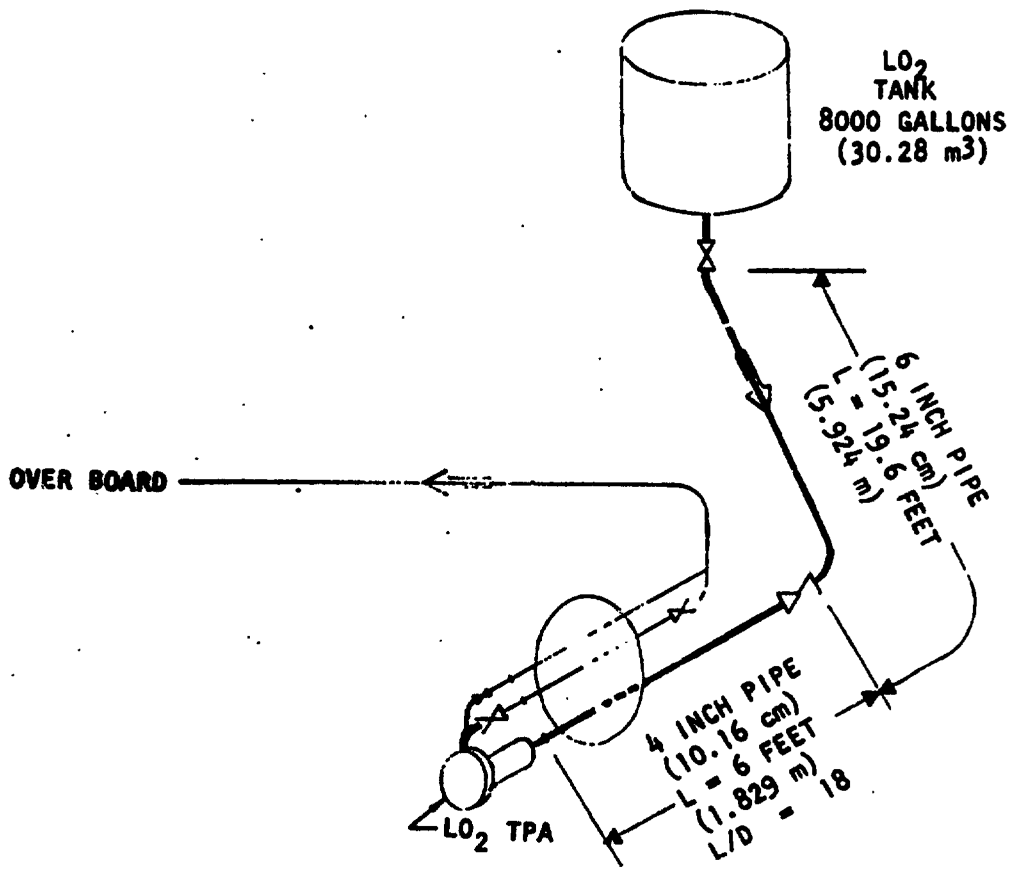

Figure 162. 26A - LO_2 TPA Facility

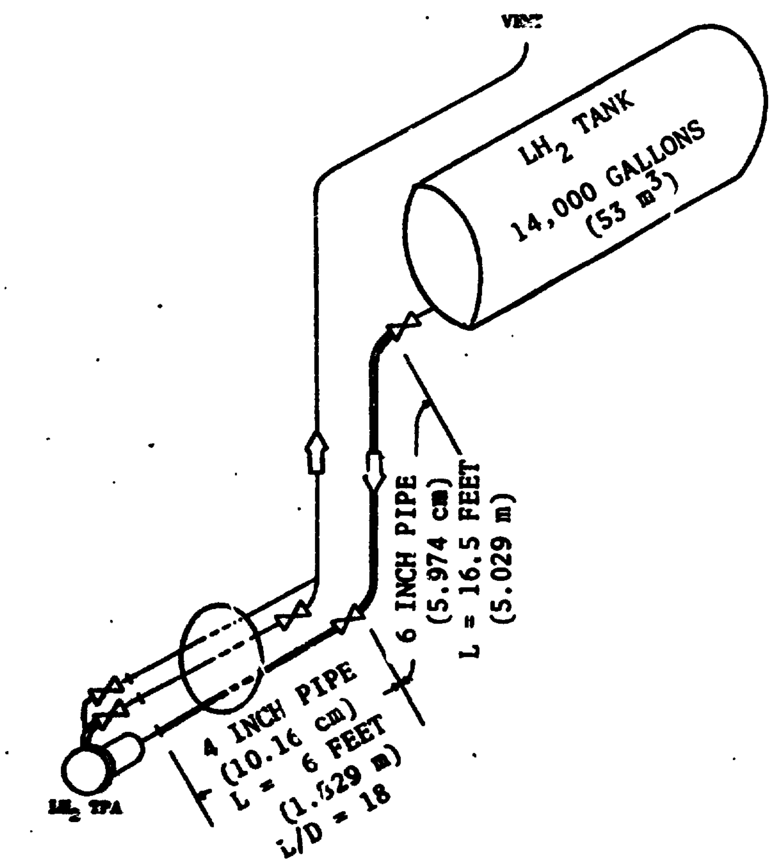

Figure 163. Cell 26B-LH_2 TPA Facility
(Hydrogen Feed System)

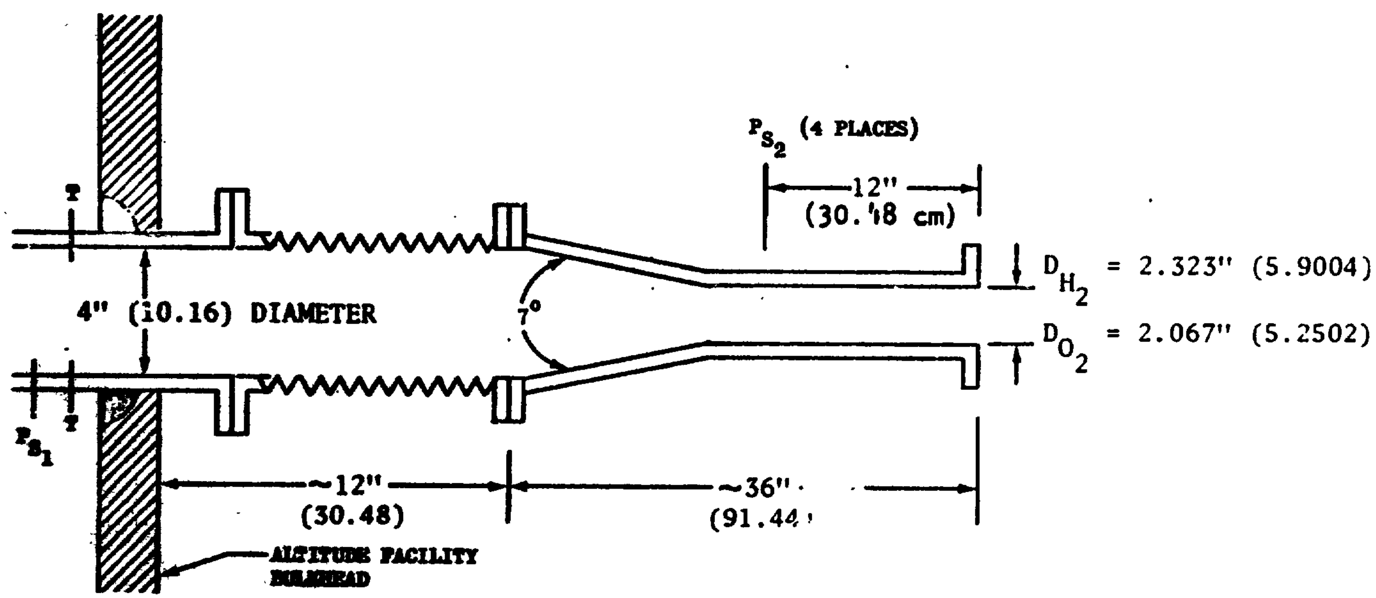

Figure 164. Turbopump Inlet Line Configuration

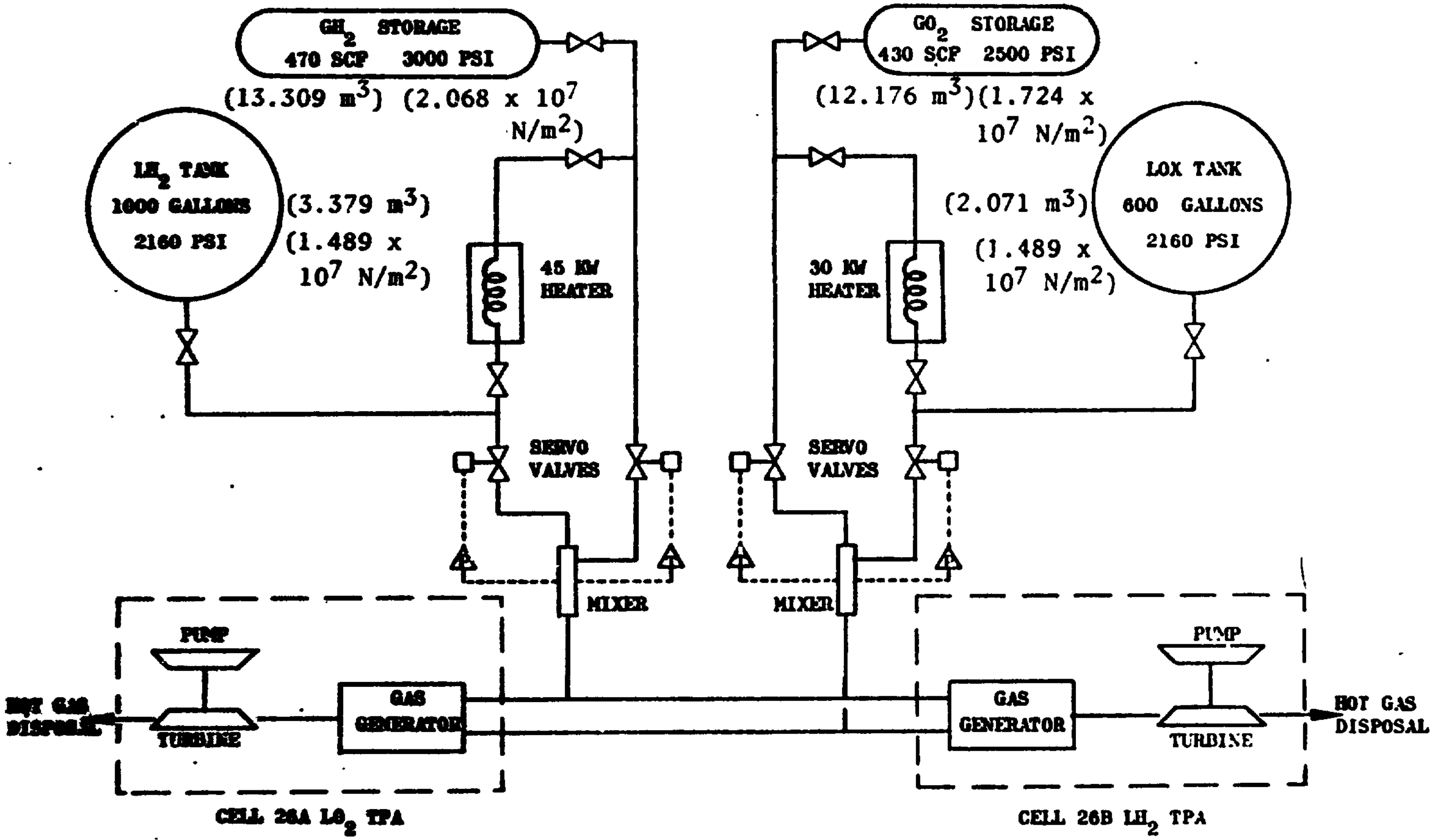

Figure 165. Gas Generator Propellant Feed System

153 K (275 R) to ambient temperature. Heated and ambient temperature propellant were mixed to provide propellant up to 333 K (600 R). Nominal total propellant flowrate was 0.1315 kg/s (0.29 lb_m/sec) to the oxygen pump position and 0.272 kg/s (0.6 lb_m/sec) to the hydrogen pump position at a mixture ratio of 0.8:1 (o/f).

Ambient temperature gaseous hydrogen turbine drive was used during initial check-out and evaluation phases of turbopump testing. This required a gaseous hydrogen flowrate approximately 2.6 times the nominal hydrogen flowrate required for hot gas 1117 K (1550 F) operation. To provide additional hydrogen flowrate capacity for gaseous hydrogen turbine drive tests, both legs of the propellant mixer system (Fig. 165) were used, and both servo valves were used as pressure controlled valves.

During cold gas drive tests on the LO_2 TPA, the hydrogen was supplied through the gas generator through the normal flow path. No modification of the gas generator was required other than removing and capping the gaseous oxygen facility line at the bipropellant valve to prevent backflow of hydrogen into the oxygen system. The bipropellant valve was used to control flowrate, and the pressure at the valve inlet was approximately 4,826,330 N/m^2 (700 psig) for nominal pump operation.

During cold gas drive test on the LH_2 TPA, the gas generator assembly was modified to pass the required flowrate without excessive inlet pressures. The gas generator bipropellant valve was bypassed, and the hydrogen was supplied to a fitting on the hydrogen gas generator feed line between the valve and injector plus hydrogen was supplied through the spark plug port. The gas generator upstream pressure for nominal pump operation was approximately 4,481,592 N/m^2 (650 psig). Without the gas generator modification and with the hydrogen supplied through the normal flow circuit, the pump could be operated at nominal Q/N and 6074 rad/s (58,000 rpm) with a valve upstream pressure of approximately 6,205,281 N/m^2 (900 psig).

Altitude Simulation

An altitude chamber was used to determine the thermal characteristics of the turbopump assemblies during operation and cost periods. The assemblies were installed on a platform cantilevered from a bulkhead as shown in Fig. 166, and all propellant lines, controls and instrumentation passed through the bulkhead with the exception of the turbine discharge duct. During thermal data tests, the vacuum chamber shown in Fig. 166 was rolled in place against the bulkhead, and the turbine discharge duct was installed through the chamber and sealed. A vacuum pump maintained a pressure of approximately 2758 N/m^2 (0.4 psia) during testing and post test soak periods (3 to 4 hours).

Controls

Proper pretest facility preparation was automatically assured by preparation complete circuits. Sequencing of the turbopump assembly components were controlled by an electronic sequencer capable of being preset in increments of 1 millisecond. This sequencer was used for spark ignition system, gas generator bipropellant valve, ignition detection circuit, and pump discharge and bypass valves.

The gas generator chamber pressure level was used to assure successful ignition. For given gas generator inlet conditions, the ignited chamber pressure was reliably predictable in advance, and the unignited pressure level is significantly lower. Therefore, if a minimum pressure level was not achieved in a specified time after signal to the gas generator (typically 0.3 seconds), the test was terminated.

Critical operating parameters were automatically monitored by voltage comparator cutoff devices with a response of 1 millisecond. Safe shutdown of the turbopump was automatically achieved if any of the critical parameters exceeded a specified value. These parameters were pump inlet pressure and temperature, pump discharged pressure, pump speed, liftoff seal actuation pressure, and intermediate seal purge inlet pressure (LO_2 TPA). A vibration safety cutoff unit monitored vibration in the range synchronous to pump speed. An electrical interlock circuit assured that the pumpdischarge and bypass valves were not both closed anytime during a test.

Figure 166. Altitude Simulation Chamber

Instrumentation

To monitor turbopump operation, approximately 75 parameters were recorded from the turbopump assembly and facility systems. These parameters were recorded on several types of devices, each selected for a specific purpose.

All parameters, except high frequency transducers (i.e., accelerometers) were recorded on the digital data acquisition system to be available for subsequent computer processing. The digital system was used to obtain steady state data, and data was typically recorded at a sample rate of 10 KC (approximately 100 channels) during tests. A sample rate of 0.6 KC was used during the extended periods of 3 to 4 hours used to obtain thermal soak data. Parameters required for setting up and operating the facility and turbopump were also recorded on direct inking graphic recorders (DIGR) which have a 1 cps response. Parameters required to monitor turbopump operation during the test and to assess test results immediately after the test were recorded on 4 channel Brush strip recorders. Approximately 32 parameters were recorded and displayed in a location convenient to the development engineer who was in direct contact with the conducting test engineer. The Brush recorder has a response of 30 cps plus an IRIG "B" time signal and can be conveniently used for reduction of test data. A direct write 12 inch oscillograph was used for high response (240 cps) recording of key parameters and was available immediately after a test to evaluate turbopump operation. A frequency modulated analog tape recorder (F/M tape) was used for high frequency parameters such as accelerometers and proximity probes with a response up to 20 KC.

Standard facility type transducers were used to measure pressure and temperature. Strain gage type pressure transducers with an appropriately selected ranges were used for pressure measurements. Resistant temperature bulbs were used for cryogenic propellant temperature measurements. Thermocouples were used for gas and skin temperature measurements. Subsonic venturis were used for the gas generator propellants flows and the pumped fluid flow. Pressure differential transducers were used to accurately measure the upstream to throat pressure difference. The venturis were typically selected for a pressure difference of 137,895 N/m^2 (20 psid) at nominal flowrate, and the pressure transducer had a range of 0 to 344,738 N/m^2 (50 psid).

Systems were also set up to measure the leakage and bleed flowrates. On the LO_2 TPA, the intermediate seal purge, and pump and turbine leakage were measured. The intermediate seal purge (GHe) was measured and controlled by a sonic nozzle on the assembly placed between the 3,102,641 N/m^2 (450 psig) supply manifold and the purge inlet 24,317 to 379,212 N/m^2 (35 to 55 psig). Turbine leakage was passed through a water bath heat exchanger to stabilize the temperature to approximately ambient temperature and discharged to atmosphere through an orifice. The pressure drop across the orifice and the gas temperature was used to measure flowrate. The pump leakage was similarly pass through a water bath heat exchanger except a pitot tube was used to measure gas velocity with a 0 to 13790 N/m^2 (2 psid) pressure transducer. (An orifice was not used in order to minimize backpressure.) The bearing cavity bleed flowrate on both turbopumps could be measured by passing the flow through a water bath heat exchanger and discharging to atmosphere through an orifice.

Data Processing

During gas generator component testing, data was processed using the digital system computer and a time-share computer system. For turbopump assembly testing, the digital data tape was processed by IBM System 370 computer.

The data reduction requirements of the gas generator component test program were relatively modest, and the time-share computer system approach proved to be an expedient method to process the data. Each test setup included approximately 30 parameters, and only one to two data slices were typically selected for each test. The use of the digital system computer and a time-share terminal allowed the data to be reduced at the test site immediately after conclusion of the test period. After a test series, data slices were selected, and the digital system computer was used to read the magnetic data tape and reduce digital counts to engineering units. Output was in the form of a typed page and a punched paper tape. The paper tape was then read into a time-share terminal located at the test site, and the data was processed by a program which calculated flowrates and gas generator performance. The output was measured and calculated data in the convenient format shown in Fig. 167.

```
                    L02 TPA G-G TEST DATA

TEST NØ.   18   SL NØ.  3   DUR TØ SL =  99.40 SEC   TØT DUR= 163.20 SEC

LØNG DURATIØN DURABILITY DEMØNSTRATIØN

GGPERF, 1-71   RED. DATE    15:50     MAY. 26, 1972

CALCULATED FLØWS:
   G.G. ØXIDIZER  =   0.1299  LBM/SEC
   G.G. FUEL      =   0.1658  LBM/SEC

   GG TØT FLØW     =    0.296  LBM/SEC
   G.G. M.R.      =   0.783  LBM/SEC


PERFØRMANCE PARAMETERS:
   CSTAR MEAS.     = 7609.530  FT/SEC
   CSTAR THEØR.    = 7661.934  FT/SEC

   CSTAR EFF.     =   99.316  PERCENT


MEASURED INPUT DATA --- PRES=PSIA,   TEMP=DEG-R
GG ØXIDIZER:
US V PR   318.12  VENT T    540.60  VEN DP     23.79  GG PIØ   305.56
VAL PR    312.42  VALVE T   543.86

GG FUEL:
US V PR   366.86  VENT T    523.72  VENT DP     5.56  GG PIF   323.66
VAL PR    354.12  VALVE T   524.09
CØØL P    312.21  CØØL T    653.48

CHAMBER PRESSURE:
PC        264.34  PC-1      268.56  PC-2      261.78  PC-CØR   268.77

CØMBUSTIØN TEMPS:
TC1      2076.87  TC2      2160.61  TC3      2091.64  TC4      1975.68
TC5      2021.81  TC6      2035.87

SKIN TEMPS:
TS1       901.28  TS2      1034.49  TS3      1841.08  TS4      1967.56
TS5      1100.92
```

Figure 167. Data Reduction Format--Gas Generator Component Test

Turbopump assembly testing has a more extensive processing requirement, and the digital magnetic tape was processed on the 370 system. A program written for this test effort calculated propellant flowrates, leakages flows, and turbopump actual and scaled performance parameters. These measured and calculated data (approximately 125 items) for all slices were outputed in a 14 page format. Figure 168 presentes a sample of the reduced data.

GAS GENERATOR COMPONENT TESTING

The effort included the development and checkout of the gas generators of the LH_2 TPA (nominal flowrate of 0.272 KG/s (0.6 lb_m/sec) and LO_2 TPA (nominal flowrate of 0.0907 Kg/s (0.20 lb_m/sec). Each of the two units of LH_2 and two units of LO_2 gas generators were tested to verify operation and integrity. Ignition, performance, stability, effluent gas quality, and duration capability were demonstrated. Satisfactory operation was demonstrated over a range of mixture ratios. flowrates, and propellant inlet temperatures. This test effort consisted of (1) company-funded gas generator development, (2) LO_2 TPA gas generator checkout, and (3) LH_2 TPA gas generator checkout.

Gas Generator Development Test Program

The gas generator hardware used during this effort as designed met the requirements of the LH_2 TPA. The unit operated at a nominal chamber pressure of 1,861,584 N/m^2 (270 psia), combustion gas temperature of 1117 K (1550 F), and flowrate of 0.272 Kg/sec (0.6 lb_m/sec). The design was scaled up from a concept previously developed under company-funded IR&D. The unit had provision for direct spark ignition and indirect ignition using an air gap igniter located in the injector. Excellent operation was demonstrated using direct spark ignition over the range of conditions required by the TPA. At the conclusion of testing, this design with direct spark ignition was selected for the LH_2 TPA, and a scaled design was selected for the LO_2 TPA.

Facility. Testing was conducted at Cell 29A, CTL-4. (Subsequent component and turbopump assembly tests were conducted at Cells 26A and 26B which were being

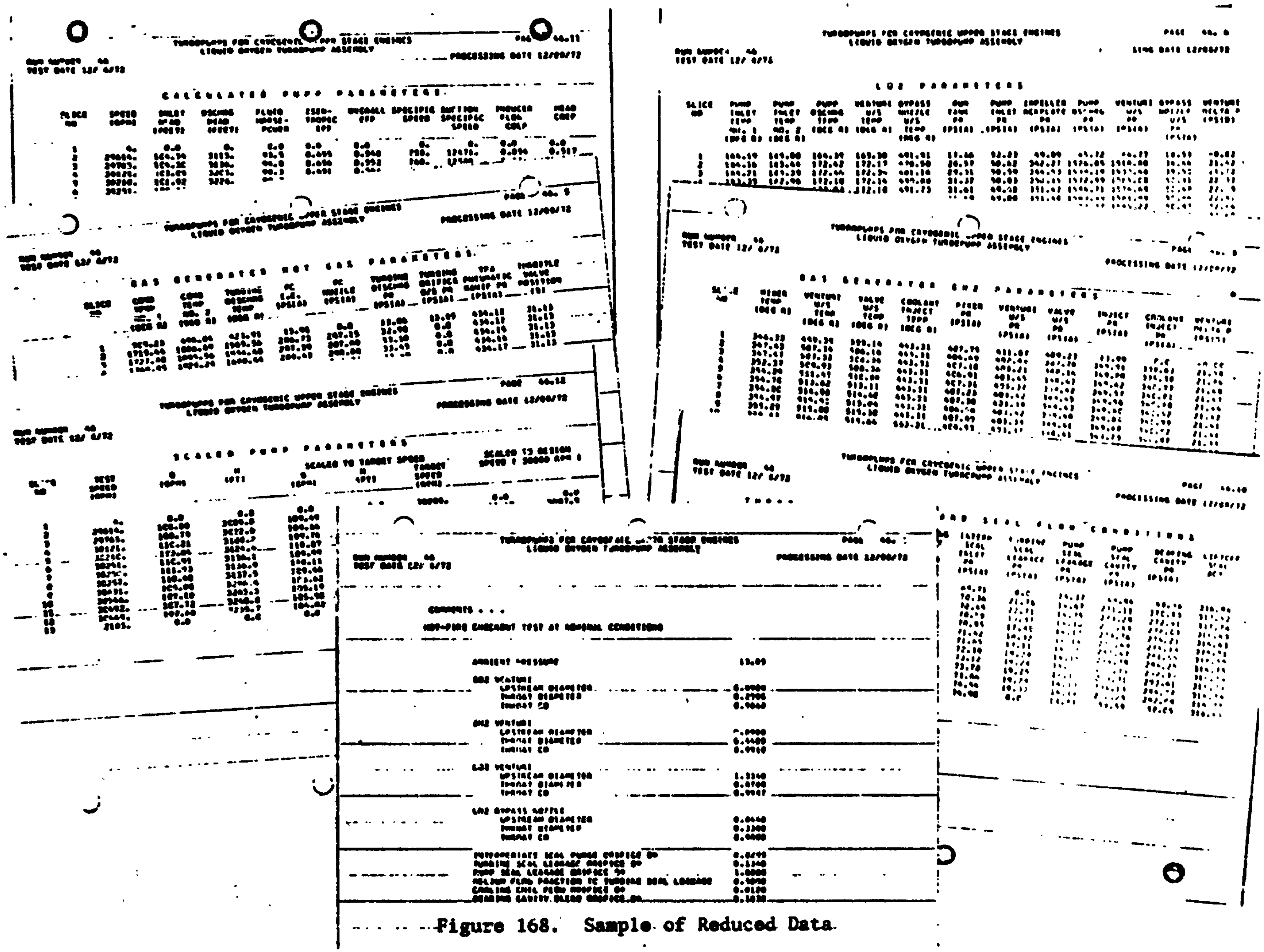

Figure 168. Sample of Reduced Data

constructed at the time of this effort.) Propellant was supplied by the existing facility oxygen and hydrogen systems, and pressure to the test hardware was controlled by servo systems located upstream. Heat exchangers located upstream of the servo valves were used to temperature-condition the propellants. A bipropellant valve (Fig. 169) was used as part of the gas generator assembly. The initial installation did not include the indirect spark torch igniter and associated control valves. Installation of these was not required due to success obtained with the direct spark igniters, and all tests were conducted using direct spark ignition. A GLA variable energy exciter unit was used for most tests, and a J-2 spark exciter was also evaluated. Instrumentation was similar to that used in subsequent turbopump assembly testing except additional combustion and skin temperatures were used to define the gas generator combustion and thermal characteristics.

Test Program. A summary of the test program is presented in Table 34 . The program was initiated on 25 January 1972 with propellant blowdowns of each propellant system to calibrate the facility/hardware, establish valve response and determine pressure response. The initial series of hot-firing tests were conducted to evaluate ignition and gradually increase duration to obtain steady-state data. Some problems of temperature spiking at start and cutoff were corrected by modifications to the facility hydrogen servo system. On tests 41 and 45, igniter energy was systematically reduced to the minimum value obtainable with the GLA exciter. Successful ignitions were obtained on all tests. Test 46 was conducted with the exciter off ("0" energy) to verify that auto-ignitions were not being obtained. Tests 47 to 54 were conducted to evaluate off nominal operation. Satisfactory operation was obtained on all tests including ±10 percent in mixture ratio and ±50 percent in total flowrate. Tests 55 through 58 were conducted to evaluate operation with cold propellants (152.8 K or 275 R GH_2 and 208.3K or 375 R GO_2). Tests 59 through 61 was conducted with the J-2 exciter (360 mJ stored energy at rate of 60 cps) to evaluate the effect of spark rate on ignition. Hard starts were obtained due to propellant accumulation (about 16 msec between sparks) in the gas generator. Therefore, a higher spark rate (200 cps) was recommended for future applications.

At this point in the test program, the basic objectives had been met. However, two additional areas of investigation were undertaken. The first was to improve

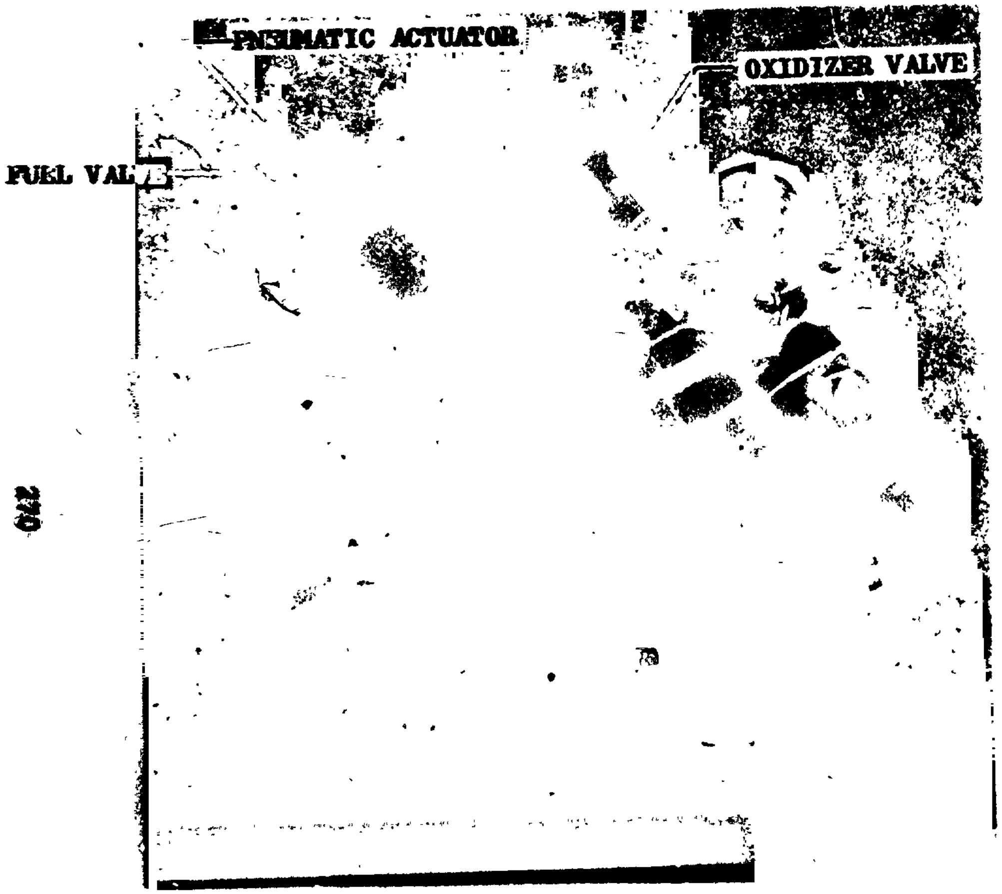

- DESCRIPTION
  - MA-3 VERNIER PROPELLANT VALVE
  - BALL VALVE
  - 3/4 INCH TUBE FITTINGS
  - PNEUMATIC ACTUATION
- MODIFICATIONS REQUIRED
  - REMOVE FUEL SIDE VALVE AND REPLACE WITH ANOTHER OXIDIZER SIDE
  - INCREASE FLOW AREA FOR H_2 TPA H_2 VALVE
- CHARACTERISTICS (LH_2 TPA)
  - 14 ΔP AT 0.419 LB/SEC GH_2
  - 3 ΔP AT 0.406 LB/SEC GO_2
  - 30 MSEC RESPONSE

Figure 169. Gas Generator Propellant Valve LH_2 and LO_2 TPA

TABLE 34. GAS GENERATOR DEVELOPMENT TEST SUMMARY

TEST NO.	DATE	CONDITION	DURATION sec.	PROPEL. TEMP. T_f/T_o (°R)	ENERGY* SET (J)	OBJECTIVE	COMMENTS
GO_2 B/D	1/25/72	-	-	Ambient	-	Determine ΔP's.	Data at .1, .2, .3, .4 m/sec
GH_2 B/D		-	-	Ambient	-		
037	1/27/72	Nominal	.4	Ambient	.5	Checkout operation.	Temp. spike at cutoff.
038			.9		.5	Extend duration	
039			5.9		.5		Perf., Stability & h.t. - good.
040			2		.4	Lower spark energy.	Seq. malfunction, P_c cut.
041			11.8		.4		Good ignition.
042			11.8		.3		
043			11.9		.2		
044			11.5		.1		
045			.2		.05		Seq. malfunction, P_c cut.
046			.2		Off	Check for auto-ignition.	No ignition, P_c cut.
047	2/1/72	Nominal	3.4	Ambient	.1	Mixture ratio variations.	Satisfactory operation.
048		-10% MR	11.7				
049		+10% MR	11.8				
050		Nominal	121.2			Duration capability.	
051		Nominal	11.7			Check after duration test.	
052		50% flow	11.7			Flowrate variations.	
053		50% flow	25.4				
054		150% flow	11.6				
055	2/3/72	Nominal	11.3	275/375	.1	Evaluate cold prop. ign.	Good ignition & operation.
056		Nominal	11.7		.05		
057		-10% MR	11.3		.1		
058		+10% MR	11.6		.1		
059		Nomin.	11.0		J-2 Exciter	Evaluate lower spark rate. (60 cps, all other tests 200 cps)	Hard start, 12 ms delay.
060		-10% MR	11.5				7 ms delay.
061		+10% MR	[illegible].5				
H_2/N_2 B/D	2-9-72	-	-	-	-	Eval. response w/valve mods.	Closing response 140 ms
062-065	2/11/72	H_2/N_2 B/D	-	-	-	Eval. 1/2" solenoids	Closing response 200 ms
066		Nominal	11.2	Ambient	.1	Eval. turbine blade heat	No streaking indicated.
067-068			11.5/11.5			Evaluate cycling.	Satisfactory operation.
069-070			54.7/11.3			Eval. start/cutoff on hot turbine blade	
071-0[illegible]	2/16/72	H_2/N_2 B/D	-	-	-	Eval. sequencing w/modified facility electrical	Start time 4 [illegible] Cutoff time [illegible] sec

[*Stored energy (delivered = 0.25 stored energy)] the start and cutoff response and demonstrate transient times applicable to proposed future applications. Larger solenoid valves (1/2 inch instead of 1/4 inch Marotta valves) were installed to decrease the pneumatic fill time of the bipropellant valve. Blowdowns were conducted and an actual increase in response time was realized. After considerable analysis, the problem was traced to the facility electrical power supply to the solenoid valves which was limiting the current and thus limiting solenoid energize and de-energize times. With the facility electrical system modified and the 1/4-inch Marotta solenoids re-installed, start times (0 to 98 percent P_c) of 57 msec and cutoff times (100 to 10 percent P_c) of 55 msec were obtained.

The second area of additional investigation involved a more vivid demonstration of gas generator exhaust gas quality and pulsing operation of the gas generator. A small turbine blade (Mark 4) was installed in the gas generator exhaust immediately downstream of the exhaust elbow and orifice. Test 066 was the checkout test. Tests 067 and 068 were conducted in pulse mode (valve shut and immediately reopened). Test 069 was of a long duration to insure steady-state turbine blade temperature 1089 K (1500 F) and then Test 070 was immediately conducted. The results indicated completely satisfactory operation (no blade overheating, indicating no streaking and no detrimental temperature spike at start or cutoff).

Another phase of this investigation was to verify the operation of the redundant control valves. A schematic of this system is shown in Fig. 170, the redundancy was incorporated to assure safe shutdown of the system in event that a control solenoid (Marotta MV-74) failed. By orificing the pair of vents to an equivalent flowrate of one solenoid, and single solenoid valve failure would not prevent the gas generator valve from opening or closing through at a slower rate. A series of checkouts were conducted in which various combinations of the control valves were "failed" (simulated by disconnecting the electrical connector) while the gas generator valve was closed and open. In all cases the bipropellant valve operated in the expected manner.

<u>Summary</u>. Forty-four tests were conducted to evaluate ignition performance, stability, and exhaust gas temperature with ambient and cold temperature propellants

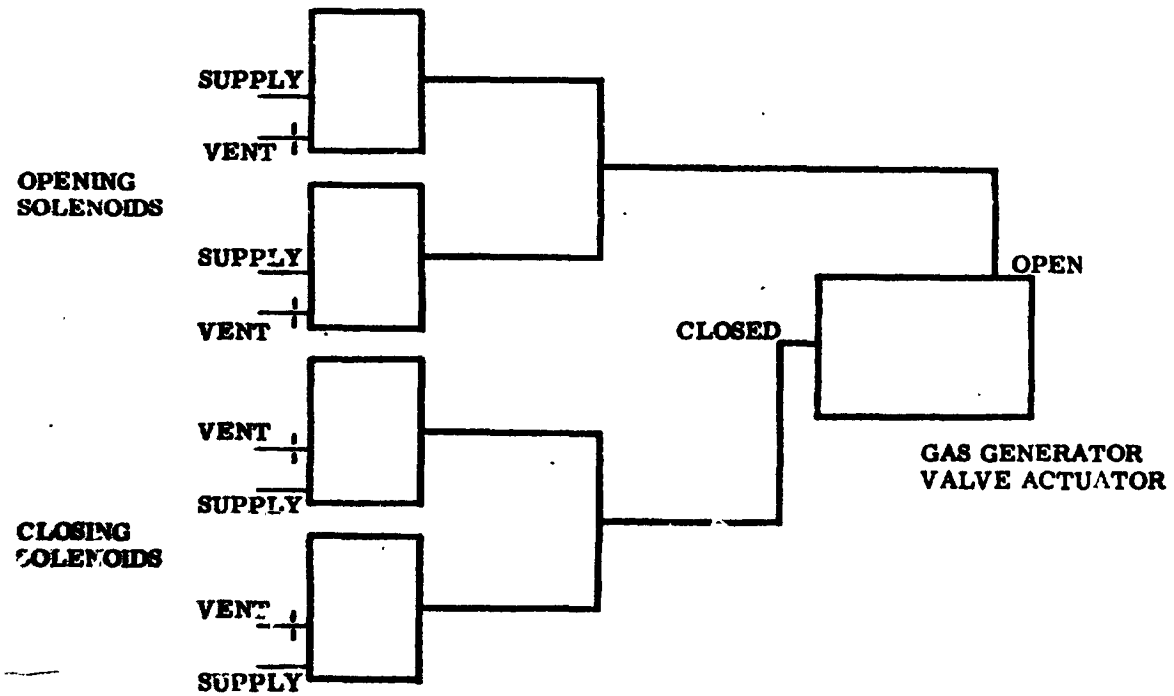

Figure 170. Gas Generator Valve Redundant Control

at nominal and off nominal mixture ratio and flowrate conditions. The results showed reliable ignitions at all conditions tested including tests with propellant temperature of 153 K (275 R) GH_2 and 208 K (375 R) GO_2. Ignition was obtained with direct spark ignition, and the more complex indirect ignition system (torch ignition with separate propellant valves) was not required nor tested. A summary of the conclusions is shown in Table 35 including a combustion efficiency of greater than 99 percent, good stability, and a uniform exhaust gas temperature profile.

TABLE 35. GAS GENERATOR TEST DATA SUMMAR

η_{c*}	- 99 percent
Stability	- Excellent
Temperature Profile	- ±208 K (±374 R) upstream of elbow ±21 K (±38 R) downstream of elbow
+10 percent MR	- No effect
-10 percent MR	- No effect
+50 percent Flow	- No effect
-50 percent Flow	- No effort
Start Time	- 57 msec signal to 90 percent P_c
Cutoff Time	- 55 msec signal to 10 percent P_c
Ignition	
Spark Rate	- 200
Energy	- 50 mj stored (~12 mj delivered)

LO_2 TPA Gas Generator Checkout Test Program

The LO_2 gas generator units No. 1 and No. 2 was a flowrate scaled design off the design developed during the previous company-funded effort. The unit operated at a nominal chamber pressure of 1,861,584 N/m^2 (270 psia), combustion gas temperature of 1117 K (1550 F), and flowrate of 0.1315 kg/sec (0.29 lb_m/sec). Ignition was achieved by direct spark. Each unit was tested to verify gas generator operation and integrity. Tests were conducted over a range of operating conditions with flowrates from 50 to 120 percent of nominal, mixture ratio from -10 to +10 percent of nominal, and propellant inlet temperatures from 153 to 333 K (275 to 600 R) fuel and 208 to 333 K (375 to 600 R) oxidizer. Both units demonstrated successful operation with reliable ignition, good start and cutoff response, stable performance, combustion efficiencies over 99 percent, and uniform exhaust gas temperature distribution (±17.8 K or 32 F) at the gas generator exist.

Facility: Testing was conducted at the cell 26A test position of CTL-4 which was constructed for testing of the LO_2 TPA. The gas generator was installed with the same position and propellant feed system as to be used for the turbopump assembly testing. Thus, this component testing also checkout and verified operation of the propellant feed systems to be used for subsequent turbopump assembly testing (Fig. 171). The gas generator was install on a mock turbopump which provided the correct orientation for the gas generator and was an exhaust duct for the exhaust gases. Instrumentation was the same (Fig. 172) as that to be used on assembly testing except additional combustion gas and skin temperature measurements were used to further characterize the gas generator operation. A GLA variable energy spark unit was used for all tests.

Test Program. A summary of the test program is presented in Table 36 for both gas generator units. Testing was initiated on 24 May 1972 with propellant blowdowns of each propellant system to calibrate the facility/hardware, and establish valve and pressure response.

Hot fire testing was initiated with the unit No. 1 using ambient temperature propellants. During the initial tests, facility problems were encountered with a duration timer and the gaseous oxygen servo-system response. This situation was corrected, and testing proceeded with the planned objectives. Tests 10 through 16 were conducted with durations to 30 seconds, off-design mixture ratio of ±10 percent, and flowrates from 50 and 120 percent of nominal. Test 18 demonstrated the capability of operating for extended duration and was conducted for a duration of 163 seconds. This test had been scheduled for 600 seconds but was terminated prematurely when radiation heating from the mock turbopump/discharge duct damaged control wiring. This was corrected for subsequent testing by rerouting the control wiring.

TABLE 36. LO_2 GAS GENERATOR TEST SUMMARY

Test No.	Unit	P_c N/m^2 (psia)	MR (o/f)	W Kg/sec (lb_m/sec)	T_c K (R)	Duration (sec)	Propellant Temperature	Objective	Comments
1-9	1	-	-	-	-	-	Amb.	Facility calibration	
10		1875374 (272)	0.79	.133 (0.294)	1100 (1980)	6.9	Amb.[1]	Check-out	Sequence malfunction, manual cut.
11		1882269 (273)	0.79	.134 (0.296)	1117 (2010)	10.0		Nominal MR	
12		1854690 (269)	0.76	.132 (0.292)	1078 (1940)	10.0		-10% MR	
13		1889163 (274)	0.96	.1315 (0.290)	1272 (2290)	10.0		+10% MR	
14		1882269 (273)	0.85	.132 (0.292)	1183 (2130)	30.0		30 sec duration	
15		990740 (145)	1.03	.0694 (0.153)	1351 (2432)	10.0		50% flow	
16		1013529 (147)	0.92	.0717 (0.158)	1260 (2270)	30.0		50% flow	
17		2185638 (317)	0.77	.158 (0.348)	1106 (1990)	10.0		Maximum flow	
18		1847795 (268)	0.78	.1347 (0.297)	1122 (2020)	163.2		Durability	Cut due to facility heating problem
19a		1640952 (238)	0.75	.1234 (0.272)	945 (1701)	6.4	Cold	Check-out	Minimum MR } Sequence and GO_2 servo-system malfunction. Manual cut.
19b		1875374 (272)	1.41	.1295 (0.285)	1503 (2706)	6.4		Check-out	Maximum }
20		1730584 (251)	1.05	.1229 (0.271)	1167 (2100)	1.6		Check-out	
21		1751268 (254)	0.83	.1279 (0.282)	1017 (1830)	10.0		Nominal MR	
22		1716795 (249)	0.77	.1288 (0.284)	978 (1760)	10.0		-10% MR	
23a		1778847 (258)	0.96	.1293 (0.285)	1131 (2036)	8.9		+10% MR	Prior to duct failure
23b	1	1461689 (212)	0.93	.166 (0.366)	1050 (1890)	8.9		+10% MR	Post-duct failure
24	2	1847795 (268)	0.85	.1306 (0.288)	-	0.5	Amb.	Check-out	
25		1896058 (275)	0.78	.1306 (0.288)	1085 (1953)	5.0		Check-out	
26		1896058 (275)	0.78	.1306 (0.288)	1090 (1962)	10.0		Nominal MR	
27		1875374 (272)	0.78	.1342 (0.296)	1117 (2010)	229.0		Duration	
28		1861584 (270)	0.75	.1288 (0.284)	1064 (1916)	8.5	Hot	Nominal MR	
29		1854690 (269)	0.75	.1302 (0.287)	1078 (1941)	10.0		Nominal MR	
30-34	2	-	-	-	-	-	Amb.	Calibration	GH_2 turbine drive.

(1) Ambient temperature propellants are approximately 294 K (530 R). Cold temperature propellants are 144 K (260 R) fuel and 234 K (530 R) oxidizer. Hot temperature propellants are 328 K (591 R) fuel and [illegible] (588 R) oxidizer.

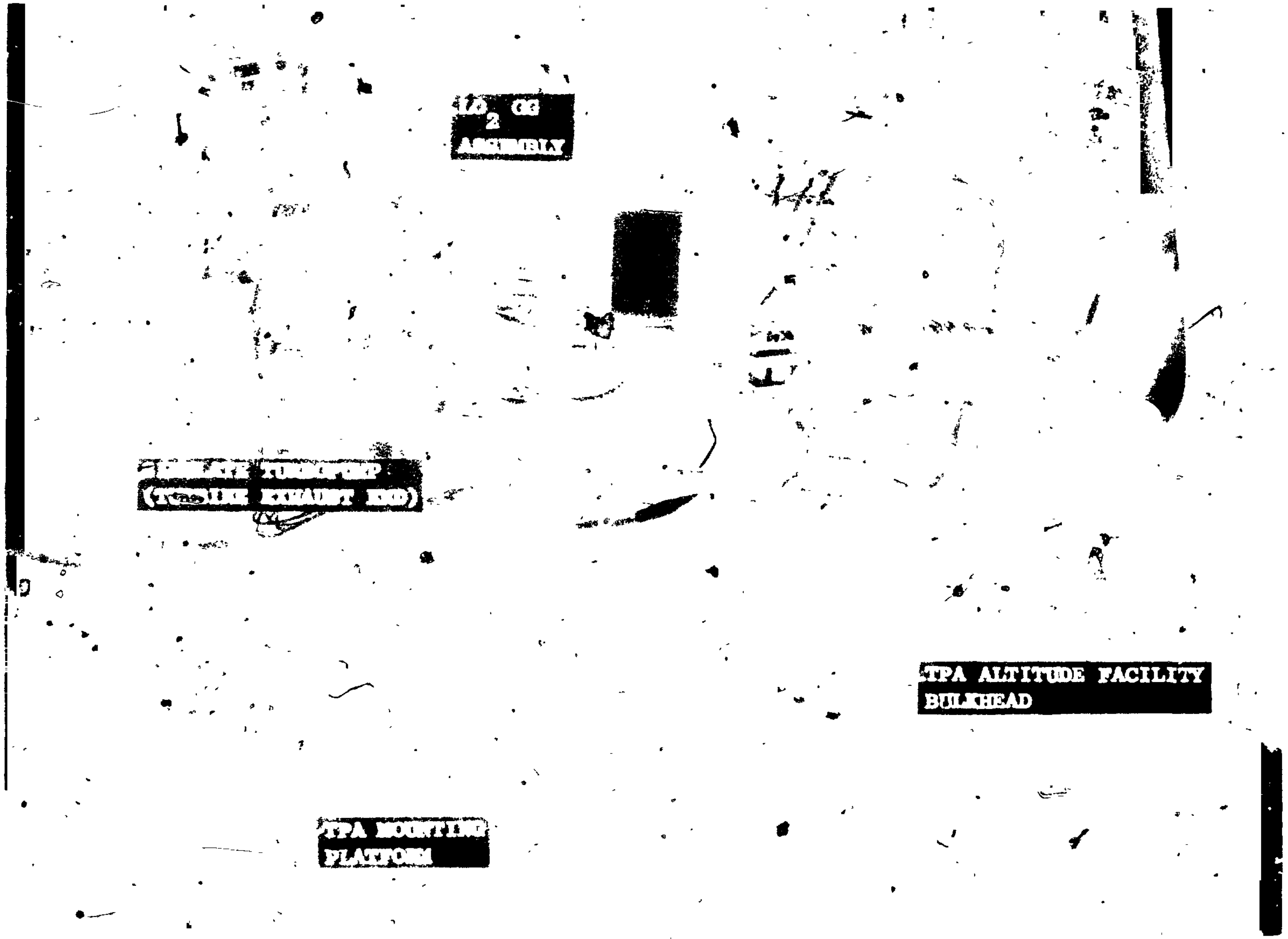

1ST61-5/19/72-S1B

Figure 171. LO_2 TPA Test Facility

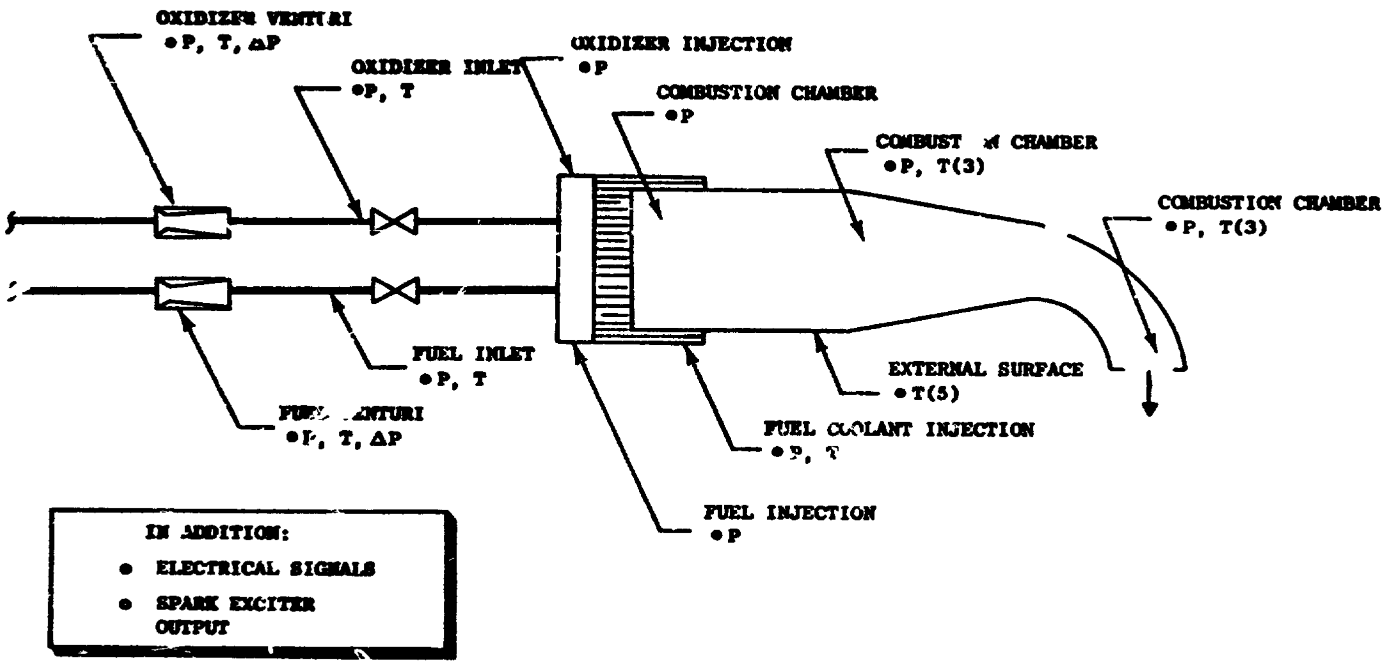

Figure 172. Gas Generator Instrumentation Schematic

Tests 19 through 23 were conducted with cold temperature propellants with a fuel temperature of approximately 153 K (275 R) and an oxidizer temperature of approximately 208 K (375 R). On the first test (19), the oxidizer servo-control failed causing the oxidizer inlet pressure to vary considerably, and the combustion temperature varied from 1117 K (1550 F) down to 944 K (1240 F) and up to 1500 K (2240 F) when the test was terminated. There was no apparent damage to the gas generator. The remainder of the tests were conducted with duration increasing to 10 seconds, and a off design mixture ratio of ±10 percent. On the last scheduled test on unit No. 1 (23), a thermocouple instrumentation port on the uncooled HS-188 gas generator exhaust duct failed resulting in a 0.762 cm (0.3 inch) diameter hole around the affected zone. No other erosion or overheating was apparent. The failure was an isolated problem of the initial welded installation of the instrumentation port aggravated by the momentary high flame temperature experienced on test 19 when the oxidizer servo-control malfunctioned.

Metallurgical analysis of the instrumentation port that failed showed that the failure was due to the use of the wrong weld rod (stainless steel instead of Hastelloy W or Haynes 188) during welding on this particular port by the vendor. This resulted in brittleness due to the insolubility of impurities. All other weld joints was penetrant inspected, and use of the improper weld rod was limited to the one failed joint. The No. 1 unit was repaired by welding in a new HS-188 cylindrical section, and no further problems of this nature was experienced during the remainder of testing.

Gas generator unit No. 2 was tested on tests 24 through 27 to verify operation and integrity. Tests were conducted at nominal conditions with ambient temperature propellants with increasing test durations. On the last test, duration capability was demonstrated by operating for a duration of 229 seconds, but the test was terminated before its scheduled 600 seconds when the facility mock turbopump/exhaust duct failed. (Air aspirating into the facility duct mixed with the fuel rich hot exhaust gas resulting in a higher gas temperature.)

Tests 28 and 29 were conducted on unit No. 2 with 333 K (600 R) propellant inlet temperature to verify operation at the upper limit of the propellant inlet temperature requirement.

Summary. Twenty tests were conducted on unit No. 1 and No. 2 of the LO_2 gas generators which verified the integrity of the design to operate over the required range of propellant inlet conditions. These units were subsequently installed on the turbopump assemblies.

LH_2 TPA Gas Generator Checkout Test Program

The unit No. 2 LH_2 gas generator was of the same design as the unit No. 1 gas generator previously evaluated during the gas generator development test program. The unit operated at a nominal chamber pressure of 1,861,584 N/m^2 (270 psia), combustion gas temperature of 1117 K (1550 F), flowrate of 0.272 kg/s (0.6 lb_m/sec), and direct spark ignition. This checkout test series demonstrated the integrity and successful operation of unit No. 2.

Facility. Testing was conducted at the Cell 26B test position of CTL-4 which was constructed for testing of the LH_2 TPA. The gas generator was installed on a mock turbopump/exhaust duct with the same position and propellant feed system as to be used for turbopump assembly testing. Thus, this component testing also checkout operation of the propellant feed system used for turbopump assembly testing. Instrumentation was the same as that used on assembly testing except additional combustion gas and skin temperature measurements were used to further characterize the gas generator operation. An EGG spark unit was used for ignition. This unit had been designed and procured to assure positive ignition of the turbopump gas generators, and the unit had a spark rate of 200 cps with a minimum delivered spark energy of 100 mJ.

Test Program. The objective of this test series was to checkout unit No. 2 gas generator. (all development experimental objectives had been evaluated during previous test efforts). A summary of this test program is presented in Table 37. A series of tests were conducted at nominal conditions with ambient temperature propellants in increasing durations from 0.5 to 343 seconds. The last scheduled test had a scheduled duration of 600 seconds but was terminated at 343 seconds when a hydrogen leak from an instrumentation port ignited and overheated the bipropellant actuator body. The actuator body failed and the valve closed terminating the test.

TABLE 37. LH_2 UNIT NO. 2 GAS GENERATOR TEST SUMMARY

Test No.	P_c, N/m^2 (psia)	MR (o/f)	w, kg/s (lb_m/sec)	T_c, K (R)	Duration, second	Objective	Comments
1	1,875,374 (272)	1.08	.2644 (0.583)	1150 (2070)	0.5	Checkout Nominal	
2	1,978,795 (287)	0.84	.2853 (0.629)	1078 (1940)	1.0	Checkout Nominal	
3	2,033,953 (295)	0.82	.2903 (0.640)	1117 (2010)	5.0	Checkout Nominal	
4		0.83	.2871 (0.633)	1133 (2040)	10.0	Nominal	
5	2,040,848 (296)	0.85	.2849 (0.628)	1117 (2010)	343.1	Durability	GH_2 leak-valve failure

Tests conducted with ambient temperature propellants. EGG spark exciter unit used for all tests.

Summary. A series of five tests were conducted which verified successful operation of the unit No. 2. The operating characteristics were per design and the same as unit No. 1. The bipropellant valve was repaired and the unit was installed on a LH_2 turbopump assembly.

Gas Generator Operating Characteristics

The gas generator concept as shown in Figs. 173 and 174 features a multi-element coaxial injector, a cooled copper body, and an uncooled discharge duct. Salient features are scalability, reliable ignition by direct spark, nominal temperature requirements for seals and spark plug, high combustion efficiency, and controlled start and cutoff transients. This design was developed and tested on a company-funded program with a unit operating with 0.0907 kg/s (0.2 lb_m/sec). The concept was scaled to operating requirements of the TPA's with a flowrate of 0.1315 and 0.2722 kg/s (0.29 and 0.6 lb_m/sec).

The multi-element coaxial injector (Fig. 175), is designed for stable combustion and high combustion efficiency of greater thatn 99 percent. Twelve injector elements are used for the LH_2 gas generator and five injector elements are used for the LO_2 gas generator. All of the oxidizer and approximately 60 percent of the fuel are mixed by the injector to produce a higher temperature core (approximately 1533 K or 2300 F) at a mixture ratio of 1.3:1 o/f or greater. This mixture ratio is very ignitable by spark ignition over a wide range of propellant temperatures and pressures. The remainder of the fuel is used to cool the copper body with a typical bulk temperature rise of 350 K (170 F) (Fig. 176). This fuel is injected into the core flow by injection holes at the downstream portion of the body. The coolant injection pattern is designed to penetrate the various zones of the core to produce a uniform mixture ratio of 0.82:1 o/f with a combustion temperature of 1550 F. The spark plug is located in the side of cooled copper body where the operating temperature is approximately 339 K (150 F). Thus, the spark plug to body seal, and the spark plug internal sealing is not subjected to high temperatures. Because of the cooled body, the injector to body seal and the body to uncooled duct seal are in cooled regions eliminating the problems associated with high temperature sealing.

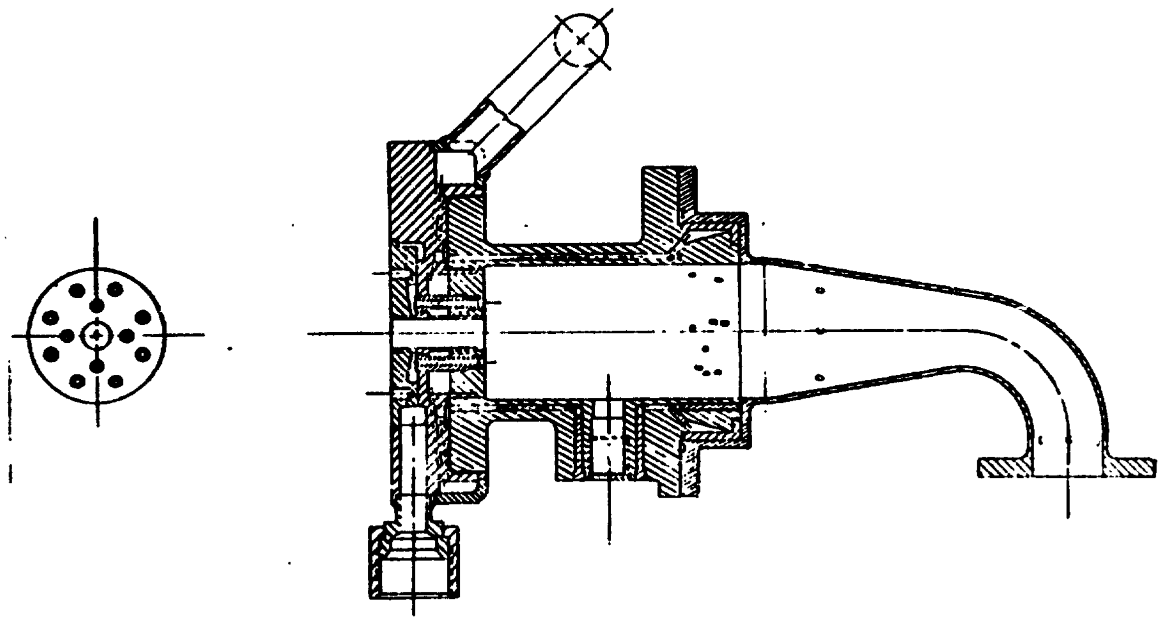

FEATURES

- COAXIAL INJECTOR (12 ELEMENTS)
- DIRECT SPARK IGNITER
- DUMP COOLED BODY
- PROVISION FOR INDIRECT SPARK IGNITER
- ELBOW AND TEMPERATURE RANGE FOR CHECKOUT TESTING

Figure 173. Gas Generator Concept

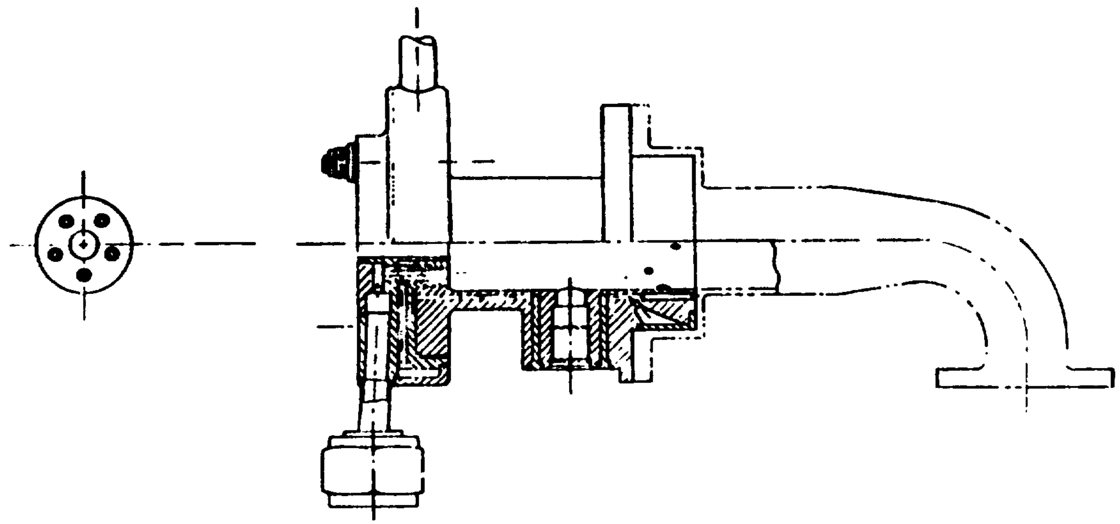

FEATURES

- COAXIAL INJECTOR (5 ELEMENTS)
- DIRECT SPARK IGNITER
- DUMP COOLED BODY
- PROVISION FOR INDIRECT SPARK IGNITER
- ELBOW AND TEMPERATURE RAKE FOR CHECKOUT TESTING

Figure 174. Oxygen TPA Gas Generator Assembly

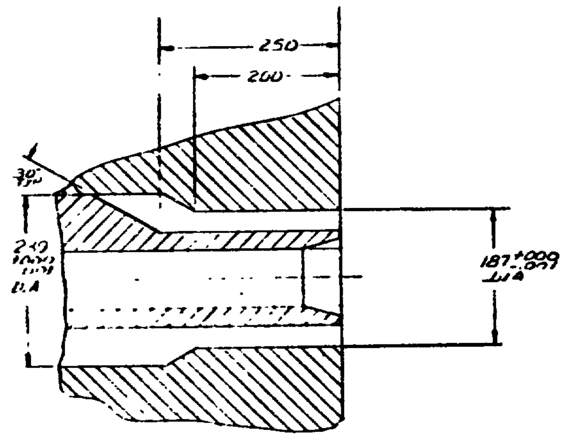

DESIGN PARAMETERS *

$\dot{W}$/ELEMENT = 0.039 LB/SEC (0.0177 kg/sec)

ΔP_F NOMINAL = 50 PSI (344,738 N/m^2)
MINIMUM = 20 PSI (137,895 N/m^2)

ΔP_O NOMINAL = 43 PSI (296,475 N/m^2)
MINIMUM = 36 PSI (248,211 N/m^2)

NOMINAL = 340 PSI INLET PRESSURE (2,344,217 N/m^2)
600 R INLET TEMPERATURE (333 K)

MINIMUM = 375 R GO_2 INLET TEMPERATURE (208 K)
275 R GH_2 INLET TEMPERATURE (153 K)

* Element dimensions given for LH_2 gas gemerator

Figure 175. Gas Generator Coaxial Injector Element

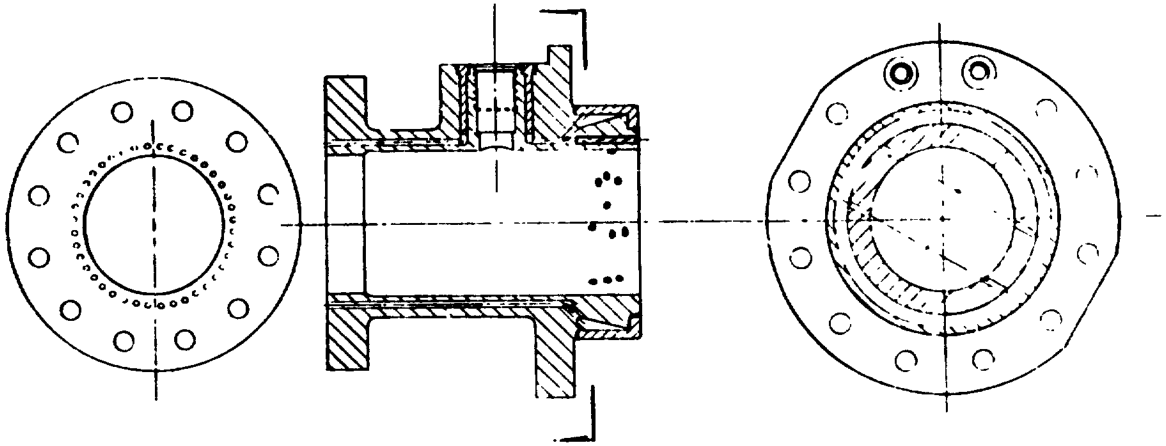

DESIGN PARAMETERS

$\dot{W}_{CORE}$	= 0.471 LB/SEC (0.2136 kg/s)
MR_{CORE}	= 1.3
$\dot{W}_{DUMP}$	= 0.127 LB/SEC (0.0576 kg/s)
$\Delta P_{SECONDARY\ INJECTOR}$	= 45 PSI (310,264 N/m^2)
INJECTION ORIFICE DIAMETER	= 0.078 INCHES (0.198 m)
NUMBER OF INJECTION ORIFICES	= 26 (LOCATED ON 6 PLANES)
NUMBER OF COOLANT PASSAGES	= 40

Figure 176. Gas Generator Body Design

The injector feed is volumetrically balanced to control of start and cutoff transients. The volume from the valve downstream seal to the injection elements is balanced to produce a fuel to oxidizer volume ratio of 17:1 which corresponds to a mixture ratio of approximately 0.9:1 o/f or combustion temperature of 1600 F. This achieves even priming and draining of the manifold during start and shutdown eliminating the requirement for purges or sequencing of the propellant valves. Response is good with a measured pressure rise to 90 percent chamber pressure of approximately 10 milliseconds and cutoff to 10 percent chamber pressure of approximately 20 milliseconds. There were no high temperature spikes at start or cutoff. The feed system can be seen in Fig. 177. The oxidizer valve is mounted close to the injector, and an aluminum spacer is inserted into the downstream portion of the valve body and the inlet line to further minimize oxidizer volume. To achieve the relatively large volume required for the fuel feed system, an extra large line size is used between the valve and injector which provided most of the required volume. Another tube is "teed" into the line to provide the remainder of the volume. (This section could be used to tune the volume if required by inserting a spacer or additing a section of line.)

The uncooled duct contained a number of instrumentation ports located downstream of the cooled body flange and at the exit of the chamber. During component testing, a flange was welded to the exit which contained a nozzle to simulate the area of the turbine manifold. During operation, the downstream portion of the duct reaches combustion temperature of 1117 K (1550 F) radiation heat to the surrounding areas, and a refrasil cloth wrapped around this duct was used to eliminated radiation heating of the adjacent assembly and wiring.

The temperature profile of the combustion gases were measured during component testing by a rake of three thermocouples at the two instrumentation locations on the duct. The upstream location where is located near the point of secondary injection, and the typical temperature profile indicated a high temperature core with a temperature distribution of ±464 K (±375 F). At the exit of the gas generator downstream of the elbow complete mixing has taken place, and the measured temperatures agreed with the expected theoretical temperature with a distribution of less than 278 K (40 F).

Figure 177. Gas Generator Assembly

LO_2 TURBOPUMP ASSEMBLY TEST

The liquid oxygen turbopump development test program was successfully conducted on the unit No. 1 TPA. This unit was removed from the facility, inspected, and returned for acceptance testing. Both units were then acceptanced tested. During acceptance testing, additional tests were conducted under company-funding to evaluate pump performance at high flowrates. A total of 78 tests with an accumulated duration of 8,579 seconds was conducted during these test efforts. The LO_2 TPA installed on the test facility is shown in Fig. 178 .

LO_2 TPA Development Test

The development test program was initiated on 6 November 1972, and all tests were conducted on the unit No. 1. A total of 53 tests were conducted with an accumulated duration of 6580 seconds of which 44 tests were conducted by hot-firing the gas generator (A minimum of 50 starts and 6,000 seconds duration was scheduled.) The test program is summarized in Table 38, and all the scheduled test objectives were conducted including constant speed pump performance, critical speed, cavitation performance, constant power pump performance, low Q/N start, duration demonstration, and thermal tests.

The first test was planned to be a low speed checkout test by slowly ramping to 1257 rad/s (12,000 rpm); however, the pump failed to maintain speed. The pump would repeatedly cycle to 209 to 52.4 rad/s (2000 to 500 rpm) and stop. After the test, the pump was inspected by removing the LO_2 inlet housing. The inspection revealed that the inducer tips were rubbing on the Kel-F inducer tunnel. The pump was reassembled and the second test was attempted with the same result. Because of suspected liftoff seal rubbing, the liftoff seal actuation pressure was increased to 2,068,427 N/m^2 (300 psig), and a successful 200 second test was conducted at 1257 rad/s (12,000 rpm) over a range of developed head and flowrate.

Following the initial checkout of the assembly, tests were conducted to locate the critical speed (test 4) and map pump constant speed hydrodynamic performance (test 5 and 6).. Tests 7, 8, 9, and 10 were conducted to evaluate the cavitation

Figure 178. LO_2 Turbopump Test Installation

TABLE 38. SUMMARY OF TEST ON LO_2 UNIT NO. 1

Test No.	Duration (sec)	Turbine Drive	Results	Comments
1	-	GH_2	Cycled to ~5,000 rpm and stopped.	Inspected inlet housing.
2	-	GH_2	Cycled to ~5,000 rpm and stopped.	Increased liftoff seal pressure for Test 3.
3	200.2	GH_2	Pump performance at 1257 rad/s (12,000 rpm)	OBJECTIVES ACHIEVED
4	5.0	GH_2	Ramp to 2932 rad/s (28,000 rpm). Locate critical speed.	
5	315.5	GH_2	Pump performance at 2356 rad/s (22,500 rpm).	
6	360.7	GH_2	Pump performance at 3142 rad/s (30,000 rpm).	
7	122.2	GH_2	Cavitation performance at 0.00379 m^3/s (60 gpm) and 3142 rad/s (30,000 rpm).	Cavitation not achieved. OBJECTIVES ACHIEVED
8	331.7	GH_2	Cavitation performance at 0.00379 m^3/s (60 gpm) and 3142 rad/s (30,000 rpm).	
9	285.9	GH_2	Cavitation performance at 0.00631 m^3/s (100 gpm) and 3142 rad/s (30,000 rpm).	
10	182.8	GH_2	Cavitation performance at 0.00883 m^3/s (140 gpm) and 3142 rad/s (30,000 rpm).	
11	3.7	Hot Gas	Checkout at 0.00631 m^3/s (100 gpm) and 3142 rad/s (30,000 rpm).	
12	200.7	Hot Gas	Checkout at 0.00631 m^3/s (100 gpm) and 3142 rad/s (30,000 rpm).	

TABLE 38 (Continued)

Test No.	Duration (sec)	Turbine Drive	Results	Comments
--	-	--	Turbine inspection	Excellent condition.
13	300.8	Hot Gas	Checkout at 0.00631 m^3/s (100 gpm) and 3142 rad/s (30,000 rpm). R/S	OBJECTIVES ACHIEVED
14	301.5	Hot Gas	Constant power map. Initial Q of 0.00789 m^3/s (125 gpm)	
15	146.5	Hot Gas	Constant power map. Initial Q of 0.00681 m^3/s	Terminated due to facility malfunction.
16	250.3	Hot Gas	Constant power map. Initial Q of 0.00681 m^3/s (108 gpm).	Completed power map.
17	401.9	Hot Gas	Constant power map. Initial Q of 0.00517 m^3/s (82 gpm).	OBJECTIVES ACHIEVED
18	500.9	Hot Gas	Constant power map. Initial Q of 0.00915 m^3/s (145 gpm).	
19	10.5	Hot Gas	50% Q/N start.	
20	600.5	Hot Gas	Duration demonstration.	
21	0.7	Hot Gas	25% Q/N start.	
22	0.6	Hot Gas	Dead-head start.	
23	600.5	Hot Gas	Duration demonstration	
24	-	-	Altitude facility, reference thermal data test. Four-hour soak.	
25	200.5	GH_2	Altitude facility, Four-hour post-test thermal soak.	

TABLE 38. (Concluded)

Test No.	Duration (sec)	Turbine Drive	Results	Comments
26	200.5	Hot Gas	Altitude facility. Four-hour post-test thermal soak.	OBJECTIVES ACHIEVED
27	199.8	Hot Gas	Altitude facility. Nominal test at 0.00631 m^3/s (100 gpm) and 3142 rad/s (30,000 rpm). Restart after 23-minute soak and no pre-chill. Restart after 41-minute soak and no prechill. 100-minute thermal soak.	
28	200.2	Hot Gas		
29	200.3	Hot Gas		
30-56	55.6	Hot Gas	Altitude facility. Pulsing at 0.00631 m^3/s (100 gpm) and 3142 rad/s (30,000 rpm). Two seconds on-time and 5 seconds off-time. Cooling coils used with 4-hour post-test thermal soak.	
	6580.0 Accumulated Duration			

performance of the LO_2 pump. The tests were conducted with the tank pressurized to a nominal value and an orifice in the pump inlet line to compensate for tank liquid level elevation during steady-state flow conditions. During the test, the tank was vented slowly until the pump discharge pressure dropped off. Tests 11 and 12 were conducted with the turbine drive gas provided by hot firing the gas generator to fully check out the system. The tests were a complete success and a planned turbine inspection was conducted. The turbine wheel was removed for inspection which showed that the turbine wheel and turbine nozzles were in excellent condition. The unit was reassembled, and a 300-second hot gas checkout test was conducted (Test 13).

During the early test effort, data indicated a possible marginal condition in the proper lubrication of the bearings. To investigate this condition, the bearing lubrication flow was diverted overboard rather than returning it to the eye of the impeller and special measurements were taken. The overboard lubrication system was used on Tests 7 through 13, and the data indicated that adequate lubrication flow was being provided through the normal circuit. The original bearing lubrication system with the flow returned to the eye of the impeller was installed for Test 14 and subsequent tests.

Pump performance was determined over a range of Q/N values for four different levels of turbine drive power (test 14 through 18). Turbine power was provided by hot firing the gas generator. Each test was initiated by operating at 3142 rad/s (30,000 rpm) and a selected value of liquid oxygen flowrate, and pump performance was measured while system resistance (Q/N) was varied over the range of interest.

Low Q/N start capability was successfully demonstrated during Tests 19, 21, and 22 when the pump was started at 50 percent of Q/N, 25 percent of Q/N, and a dead-head start. Extended duration capability was demonstrated by two tests (20 and 23) conducted at nominal flow conditions of 0.00631 m^3/s (100 gpm) and 3142 rad/s (30,000 rpm) for a duration of 10 minutes each.

The concluding test effort was directed toward measurement of thermal soakback, restart without reconditioning, and on/off pulsing under simulated altitude conditions.

The effort was initiated with a long reference soakback period. Soakback data was then taken after a cold gas drive test (25) and hot gas turbine drive (26). To evaluate restart capability, a hot fire test was conducted at nominal conditions, and the turbopump was restarted after 23 minutes and 41 minutes respectively without prechilling between tests. The final test series of 27 tests consisted of 2 seconds on/5 seconds off cycle testing. Having completed the LO_2 turbopump development test effort during which all objectives were met or exceeded, the No. 1 LO_2 was removed from the test facility and shipped to the Rocketdyne Engineering Development Laboratory for inspection.

LO_2 TPA Data Analysis

The head-flow characteristics and overall efficiency obtained with the initial LOX pump are presented in Fig. 179. The data shown was obtained with turbopump S/N 01, but the performance of turbopump S/N 02 was very similar, therefore the presented data can be considered as typical. Both the H-Q and efficiency characteristics of the pump matched the predicted values very well. The actual head generated at design flow was slightly higher than predicted; the slope of the H-Q curve reflected the predicted slope very accurately. The overall efficiency of the pump, based on the output of the calibrated turbine, was exactly as predicted, 62 percent at design flow.

The suction performance of the pump was established at three flowrates: 0.00341 m^3/s (54 GPM), 0.00650 m^3/s (103 GPM), and 0.00915 m^3/s (145 GPM). The obtained characteristics are presented in Fig. 180. The critical NPSH levels, defined at a 2 percent head drop-off, for the above flowrates were at 19.4 and 23.9 Joule/kg (6.5 ft., zero ft., and 8 ft.), respectively. At the approximate design flow 0.00650 m^3/s (103 GPM) the critical NPSH was actually below zero; the data indicated that the inducer was capable of pumping a substantial amount of vapor fraction.

The net axial thrust on the rotor was computed based on measured pressure levels. The obtained values were lower than the 890 N (200 lb.) predicted toward the turbine end. Nominally the thrust values were around zero; in some instances small thrust levels toward the pump were calculated. The magnitudes were too small to establish positively whether a reverse thrust condition actually existed. In any case, there was no detrimental effect in evidence either in rotordynamic behavior or bearing performance.

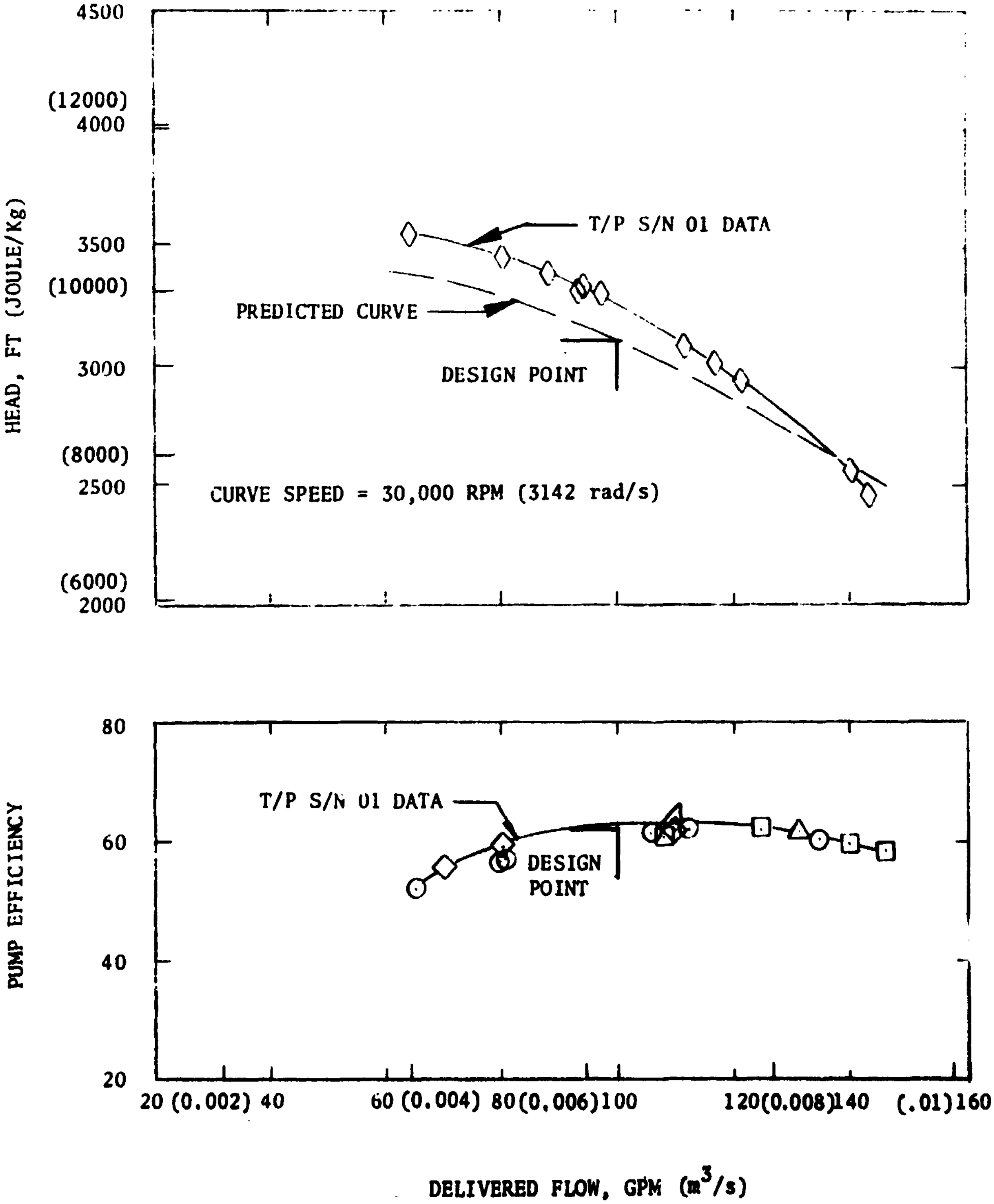

Figure 179. APS LOX Pump

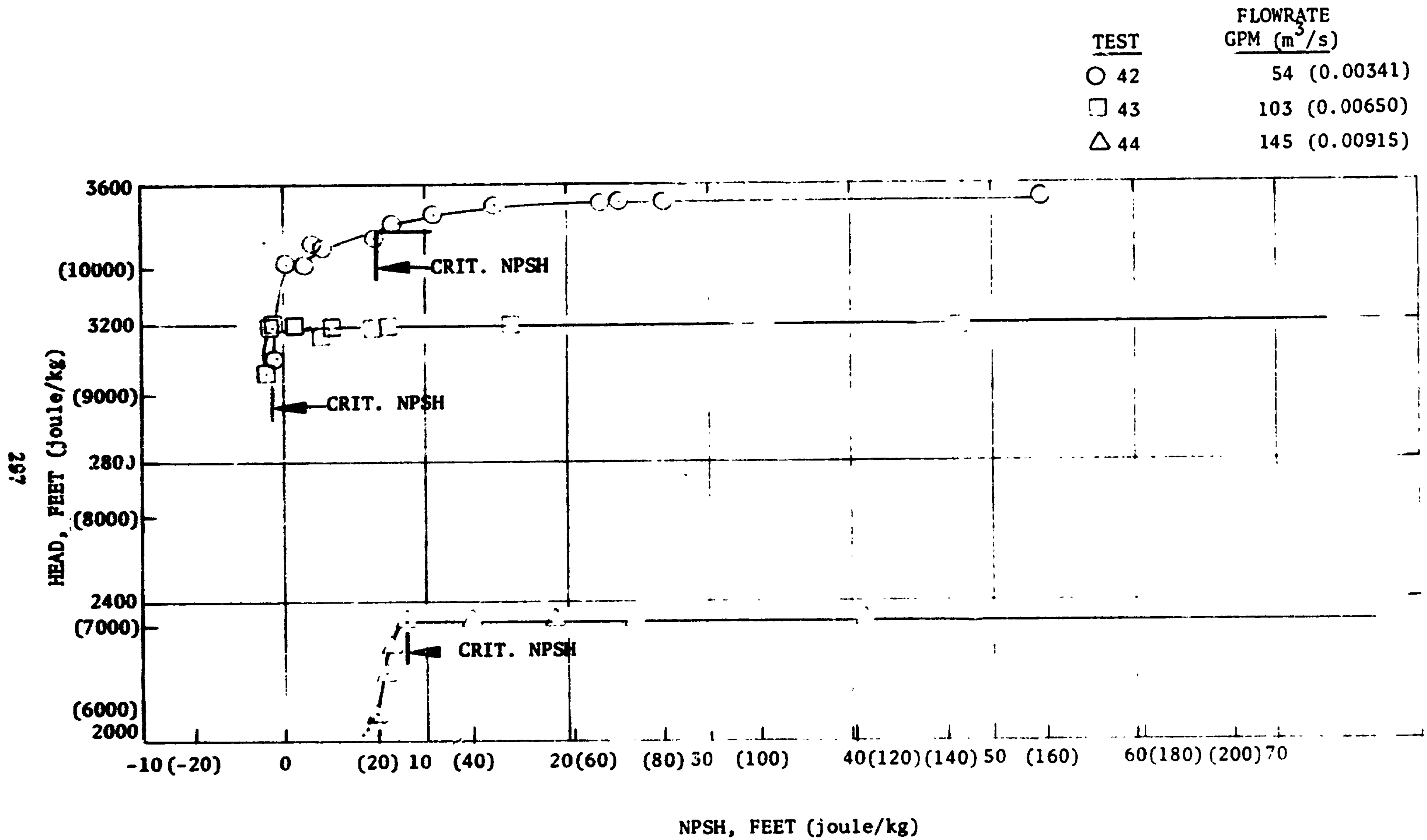

Figure 180. Mark 44 (APS) Oxidizer Pump Suction Performance (T/P S/N 01; Pump Speed 30,000 RPM (3142 rad/s)

The performance characteristics of the oxidizer turbine were established during calibration tests using ambient gaseous nitrogen as propellant. The test speed was set at 572.8 rad/s (5,470 rpm) to obtain the same blade-to-gas spouting velocity ratio (u/c_o) as with hot hydrogen-oxygen combustion gases at 3142 rad/s (30,000 rpm). The resulting efficiency obtained are shown in Fig. 181. At the design pressure ratio of 7.72 and u/c_o of 0.09 the efficiency was 22 percent, close to the predicted value of 24.3 percent.

LO_2 Turbopump Mechanical Performance

Throughout the development and acceptance testing of both LOX turbopumps, no mechanical failures were encountered. The first unit (S/N 01) completed the entire planned development test series, accumulating 55 starts and 6220 seconds without the necessity of removing the turbopump from the test stand for mechanical modifications or correction. Subsequently, the second unit successfully passed acceptance tests, bringing the total operating time to 78 starts and 8579 seconds. The test series encompassed a complete range of anticipated operating conditions including long durations up to 600 seconds, short cycling (2 seconds on 5 seconds off), dead head starts, simulated altitude and operation at flows ranging from 0.00315 to 0.0126 m^3/s (50 GPM to 200 GPM) and speeds in excess of 3560 rad/s (34,000 RPM).

Both turbopumps were partially disassembled after the test series by removing the inlet housing, which facilitated visual inspection of the inducer, impeller, back flow deflector and the Kel-F inducer liner and impeller front wear ring. The partially disassembled pump S/N 02 is shown in Fig.182. None of the parts exhibited any evidence of degradation. The inducer and impeller front wear ring labyrinth teeth rubbed on the stationary Kel-F mating parts, as anticipated.

The exhaust duct and turbine wheel were removed from Turbopump S/N 01 after 12 starts and 2052 seconds of testing. No axial rubbing had taken place between the rotor blades and the nozzle. As planned, the rotor blades rubbed a path into the honeycomb tip seal. Spalling of the chrome plated sealing surface was evident on the wheel under the turbine seal ring. This was apparently a result of attempting

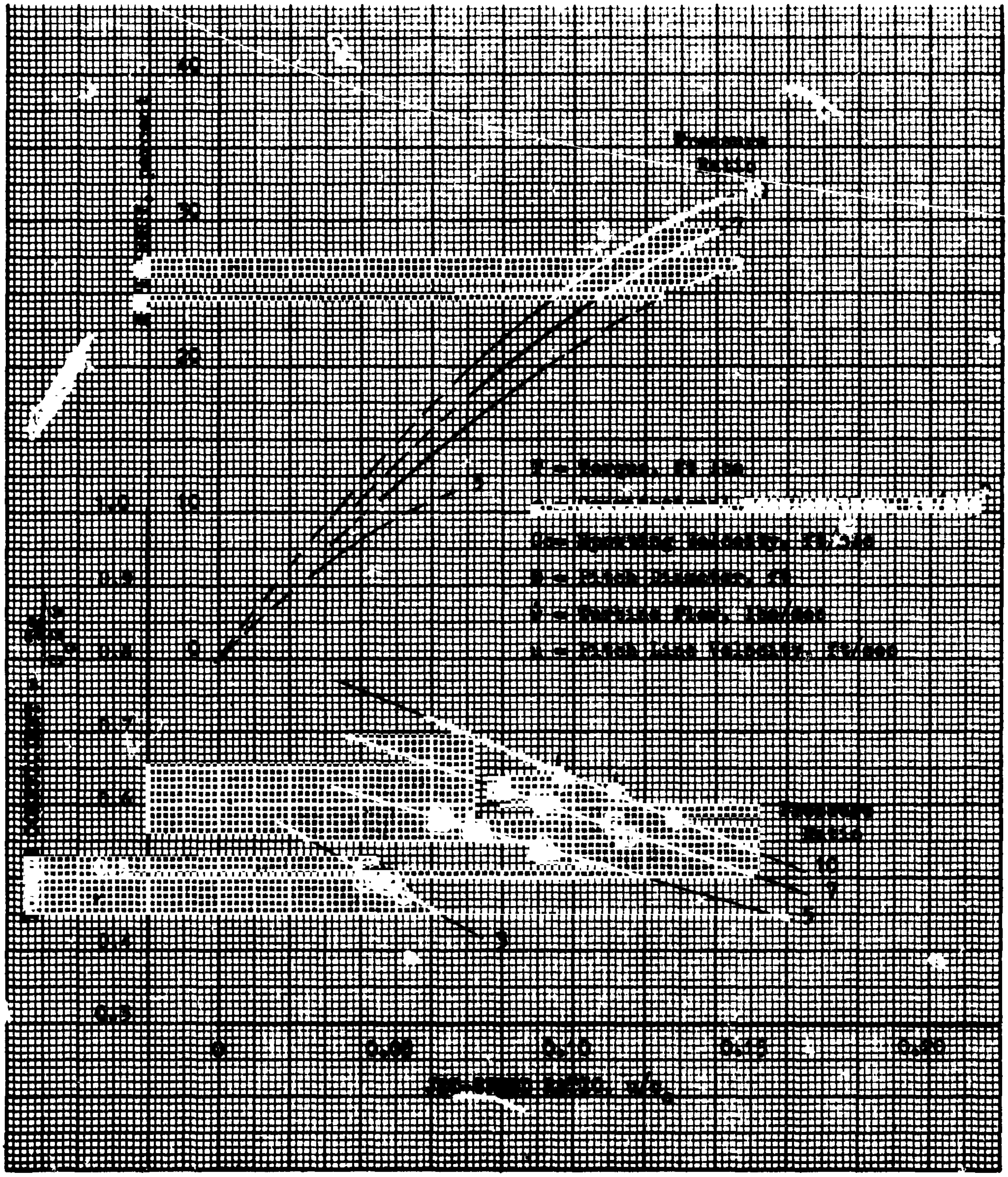

Figure 181. APS LOX Turbine Performance (51% Admission Single Row GN_2 Calibration Data)

(a) LO_2 Pump

(b) LO_2 Turbine

Figure 182. LO_2 Pump and Turbine S/N 02 (Post Accept)

to hold too tight of a radial clearance 0.002794 cm (0.0011 inch diametral) between the seal ring and the wheel. The problem was resolved on the second unit and on the LH_2 turbopumps by opening up the radial clearance to 0.00508 cm (0.002 inch) minimum.

From a rotordynamic standpoint, the behavior of the turbopump was satisfactory. Accelerometers located on the pump volute and turbine manifold showed vibration levels of 5 g peak-to-peak at nominal speed. Increased synchronous vibration amplitudes were evident at 1885 rad/s or 18,000 rpm (20 g p/p max) and at 2618 rad/s or 25,000 rpm (40 g p/p max). An analysis of the turbopump installation revealed that valve masses mounted on the turbopump had critical frequencies which approached the above values, and when these frequencies were changed by adding mass to the valve, the high amplitudes were either reduced or completely eliminated.

LH_2 TURBOPUMP ASSEMBLY TEST

The liquid hydrogen turbopump development test program was conducted on units No. 1 and No. 2. Development testing was initiated on unit No. 1, and testing was terminated when weld cracks appeared on the turbine housing. The remainder of the development test objectives and the acceptance test requirements were successfully completed on unit No. 2. Additional testing was conducted under company-funding to evaluate pump operation at speeds up to 7121 rad/s (68,000 rpm). A total of 70 tests with an accumulated duration of 6,351 seconds was conducted during these test efforts.

Unit No. 1 LH_2 TPA Test

Development testing was initiated on 7 May 1973. A total of 57 tests were conducted with an accumulated duration of 5,091 seconds of which 45 tests were conducted by hot-firing the gas generator. Testing on this unit was terminated when weld failure occurred on the turbine manifold housing, and the remainder of the development tests were conducted on unit No. 2. The unit No. 1 test effort is summarized in Table 39, and the completed test objectives were constant speed pump performance, critical speed, cavitation performance, constant power pump performance, low Q/N start, duration demonstration, and thermal data tests. All development requirements and evaluations had been completed (including the required number of starts) except the scheduled 6,000 seconds of operation.

TABLE 39. SUMMARY OF TESTS ON LH_2 UNIT NO. 1

Test No.	Duration, seconds	Turbine Drive	Objectives	Comments
1	86.8	GH_2	Low speed (1257 rad/s or 12,000 rpm) checkout test	Objectives Achieved
2	0.9		Ramp to 4712 rad/s (45,000 rpm) located critical speed	
3	276.6		Pump performance at 4712 rad/s (45,000 rpm)	
4	106.0		Pump performance at 5498 rad/s (52,500 rpm)	
5	351.0		Pump performance at 5498 rad/s (52,500 rpm)	
6	251.1		Pump performance at 6283 rad/s (60,000 rpm)	
7	201.0		Pump performance at 6283 rad/s (60,000 rpm)	
8	213.2		Cavitation performance at 6283 rad/s (60,000 rpm) and 0.0284 m^3/s (450 gpm)	
9	31.4		Cavitation performance at 6283 rad/s (60,000 rpm) and 0.0189 m^3/s (300 gpm)	Cavitation not achieved
10	180.8	GH_2	Cavitation performance at 6283 rad/s (60,000 rpm) and 0.0189 m^3/s (300 gpm)	Objectives achieved
11	5.0	Hot Gas	Checkout at nominal Q/N and 5236 rad/s (50,000 rpm)	
12	340.6		Checkout at nominal Q/N and 5236 rad/s (50,000 rpm)	
13	7.6		Nominal Q/N and 6283 rad/s (60,000 rpm)	Facility cutoff
14	0.6	Hot Gas	Nominal Q/N and 6283 rad/s (60,000 rpm)	Pump locked (~15 sec)
15	64.7	GH_2	Checkout, ramp to 6074 rad/s (58,000 rpm)	Verified normal operation
16	50.4	GH_2	Checkout, ramp to 6074 rad/s (58,000 rpm)	Verified normal operation
17	400.0	Hot Gas	Nominal operation at 6283 rad/s (60,000 rpm) and 0.0284 m^3/s (450 gpm)	Objectives achieved

TABLE 39. (Concluded)

Test No.	Duration, seconds	Turbine Drive	Objectives	Comments
18	0.3	Hot Gas	Altitude facility, nominal conditions	Facility cutoff
19	400.0	Hot Gas	Altitude facility, nominal conditions followed by 4 hour wet pump thermal soak	Objectives achieved
--	--	--	Inspection of LH_2 inlet and turbine discharge	Installed modified LH_2 housing
20	336.9	GH_2	Checkout and pump performance at 5498 rad/s (52,500 rpm)	Objectives achieved
21	261.9	Hot Gas	Constant power map. Initial Q of 0.0284 m^3/s (450 gpm) and N of 6283 rad/s (60,000 rpm)	Objectives achieved
22	299.2		Constant power map. Initial Q of 0.0284 m^3/s (450 gpm) and N of 6283 rad/s (60,000 rpm)	
23	600.0		Duration capability-nominal conditions	
24-25	10.3		Cycle tests, 10 sec on, 5 sec off	Facility malfunction
26-50	252.5		Cycle tests 10.1 sec on, 5 sec off	Objectives achieved
51	1.0		Low Q/N start, 75 percent nominal Q/N	
52	0.9		Low Q/N start, 50 percent nominal Q/N	
53	0.9		Low Q/N start, 25 percent nominal Q/N	
54	0.8		Low Q/N start, deadhead	(Pump stalled)
55	321.3		Nominal conditions	
56	21.1		Nominal conditions	Facility malfunction
57	1.5		Nominal conditions	H_2 leak, test terminated
58	9.3	Hot Gas	Nominal conditions	H_2 leak, test terminated
--	--	--	Inspection	Turbine housing leak
			57 tests and 5091.0 seconds accumulated duration	

Testing was initiated using gaseous hydrogen ... ie drive. The first test was a low spe... ...ckout test conducted by slowly ram... and operating at 0.257 rad/s (12,000 rpm). The next test verified critical ...ed locations by ramping to 4712 rad/s (45,000 rpm).

After these initial checkout tests, the ... hydrodynamic performance was mapped (test 3 through ...) at three speed le... ... 4712, 5498 and 6283 rad/s (45,000, 52,500 and 60,000 rpm). During these ...s, it was noted that the developed head was below the predicted values particularly in the high flow range of the operating map.

On test 3 an oscillation in all the pump pressures occurred of approximately 137,895 N/m^3 (20 psi) at a frequency of 8 cps. The test was automatically terminated by the inlet pressure redline. This repeated on the following test. From the data it was postulated that a vapor pocket had existed in the pump, and these gases were being expelled by the hydrogen lubrication flow to the impeller inlet. On test 5, the automatic redline was replaced by an engineering observer. The oscillation occurred again, but the test was allowed to continue to observe the nature of the oscillation. After approximately five seconds the oscillation dampened and the pump operated normally (indicating the gas pocket had been expelled). The pretest chilldown procedure was modified to assure a more complete chilldown of the lubrication circuit by bleeding through the bearing cavity bleed circuit. The bearing cavity bleed was closed during pump operation. The revised prechill procedure almost completely eliminated the occurrence on subsequent tests.

Cavitation performance was evaluated on tests 8, 9, and 10. The pump was started to 6283 rad/s (60,000 rpm) and a selected Q/N, and the run tank was slowly vented until the pump developed pressure decreased by approximately 5 percent. A 5 second checkout test (11) was conducted at nominal Q/N and 5236 rad/s (50,000 rpm) by not firing the gas generator to fully checkout the system. This test was repeated (12) for a long duration, and the turbopump system operated very satisfactorily. Test 13 was conducted at 6283 rad/s (60,000 rpm), however, the gas generator gaseous oxygen servo-control malfunctioned increasing the gaseous oxygen flowrate to the gas generator. The test was automatically terminated by the turbine inlet, temperature reline. An adjustment was made to the set conditions to compensate for the servo system problem, and the test was repeated a short time later. On this repeat test (14), the gas generator operated satisfactorily at a power level corresponding to 60,000 for 14.9 second before the pump started. The cutoff signal was given at approximately the same time that the pump started. A probable cause of the pump binding was attributed to normal wearing between the turbine wheel tip and the turbine housing wear surface. On the preceeding short hot fire, the turbine wheel approached its operating temperature faster than the housing. When the test was repeated approximately ten minutes later, the wheel was warmer than the housing and had grown thermally against the wear ring. After fifteen seconds of hot-gas operation, the wheel and housing were heated to operating temperature and the pump started. To verify that this was the cause, a cold gas turbine drive test (GH_2) was conducted by slowly increasing the turbine pressure from zero. The pump started with an inlet pressure of approximately 413685 N/m^2 (60 psig). The pump was ramped to 6074 rad/s (58,000 rpm), where the pump operated normally. This cold gas spin was repeated, and the pump started immediately and operated normally as it was ramped to and operated at 6074 rad/s (58,000 rpm). A hot gas test was conducted (17) at nominal conditions for 400 seconds, and the pump operated very satisfactorily. An inspection was made of the second stage turbine wheel which verified that normal wearing of the wear surface had occurred.

The next test effort was directed toward measurement of thermal soakback. Tests 18 and 19 were conducted in the vacuum chamber. A high combustion temperature occurred on the start of test 18 and the test was terminated. The test was repeated (19) at nominal conditions for a duration of 400 seconds followed by a four hour soak period.

An on-site inspection was conducted on the second stage turbine by removing the inlet housing. The pump inducer and first stage impeller were in excellent condition. The 0.0254 cm (0.010 inch) thick silver plating on the first stage labyrinth had spalled almost completely due to poor bonding of the plating. This could have been a cause of the low pump performance. Another possible cause was internal leakage from the pump discharge past the piston seals to the pump inlet. The inlet housing was replaced with a housing (from unit No. 2) which had been modified by installing a seal to prevent the suspected internal leakage. This housing also contained a properly silver plated labyrinth seal.

Testing resumed with a gaseous hydrogen turbine drive checkout test at nominal conditions. Pump operation was normal and some increase in performance was noted.

The remainder of the tests were conducted with hot gas turbine drive. Constant power performance was mapped through the nominal conditions of 0.0284 m^3/s (450 gpm) and 6283 rad/s (60,000 rpm). Duration capability was demonstrated with a 600 second test, at nominal conditions and cycle tests were conducted with 10 seconds of operation and 5 seconds off. Tests 51 through 54 evaluated low Q/N start by starting the pump with nominal power with various values of system resistance (Q/N), and terminating the test when speed reached 5236 rad/s (50,000 rpm). The pump started at 75 percent, 50 percent, and 25 percent of nominal Q/N. The pump stalled with a deadhead start.

Tests 56 through 58 were attempted at nominal conditions but were prematurely terminated. Test 56 was terminated due to an improper speed indication while tests 57 and 58 were terminated because of hydrogen leakage. Post test inspection revealed that severe weld cracks had occurred in the turbine manifold housing. The assembly was removed and shipped to the Rocketdyne Development Laboratory for disassembly and inspection. The pump and bearings were found to be in excellent condition. Cracks were found in the turbine housing weld and in the turbine manifold. Some damage had occurred on the turbine wheels as a result of the failure of the housing The turbopump could not be easily repaired nor acceptance tested. A description of the assembly condition is presented in a later section.

Unit No. 2 LH_2 TPA Test

Testing was conducted for acceptance of the unit No. 2 with a minimum of 10 starts and 500 seconds of operation and completion of the remaining development program objectives of 6,000 seconds of operation. An additional test was conducted (company-funded with customer approval) to evaluate pump operation at speeds up to 7121 rad/s (68,000 rpm) near nominal Q/N. A summary of test effort is presented in Table 40, a total of 13 tests were conducted with an accumulated duration of 1260 seconds.

TABLE 40. SUMMARY OF TESTS ON LH_2 UNIT NO. 2

Test No.	Duration, seconds	Turbine Drive	Objectives	Comments
59	110.0	GH_2	Checkout, ramp to 5498 rad/s (52,500 rpm)	Objectives achieved
60	2.0	Hot Gas	Checkout at nominal conditions	
61	5.0		Checkout at nominal conditions	
62	400.1		Nominal conditions and constant power performance map	
63-69	70.0		Cycle tests (6283 rad/s or 60,000 rpm), 10 seconds on and 5 seconds off	
70	600.0		Constant power map from 0.0252 m^3/s (400 gpm) and 5498 rad/s (52,500 rpm)	
71	73.2	Hot Gas	High rpm performance (6493 to 7121 rad/s or 62,000 to 68,000 rpm)	

13 tests and 1,260.3 seconds accumulated duration

The scheduled acceptance tests were conducted on tests 59 and 69, and the acceptance tests series was similar to the LO_2 TPA acceptance test program. The initial test was a gaseous hydrogen turbine drive where the pump was slowly ramped to 5498 rad/s (52,500 rpm) at nominal Q/N. Subsequent tests were conducted by hot-firing the gas generator. Test 60 was a checkout test hot-firing the gas generator, and the pump started to 6807 rad/s (65,000 rpm). The power level was adjusted, and the checkout test was repeated where the pump started to and operated at 6283 rad/s (60,000 rpm). A 400 second test (62) was conducted at nominal conditions and constant power performance was evaluated. A series of 7 cycle tests was conducted at nominal conditions with an operating time of 10 seconds and an off time of 5 seconds.

To further map the pump performance of unit No. 2, a 600 second test (70) was conducted at nominal Q/N and 5498 rad/s (52,500 rpm) and a constant power performance map was determined. An additional test was conducted where data was obtained at a higher than nominal speed from 6283 to 7121 rad/s (60,000 to 68,000 rpm).

During pretest checkouts, a small hydrogen leak was detected at the pump to turbine support shell. This leak occurred with the pump prechilled to liquid hydrogen temperature, and a leak could not be detected at ambient temperature with gaseous helium. Hydrogen was apparently leaking from the pump internal into the normally inert and vented support shell. To prevent leakage from occurring during the planned hot-fire tests, a vent port was installed on the shell prior to test 60, and the leakage was vented to a safe area.

LH_2 Turbopump Data Analysis

The pump performance data obtained on the initial series of test with turbopump S/N 01 is shown in Fig. 183. Isentropic head is obtained by establishing the isentropic enthalpy change from inlet temperature and pressure to discharge pressure and converting it to a mechanical equivalent by multiplying by 778. Isentropic efficiency is equal to the ratio isentropic head to polytropic head based on measured discharge temperature and pressure.

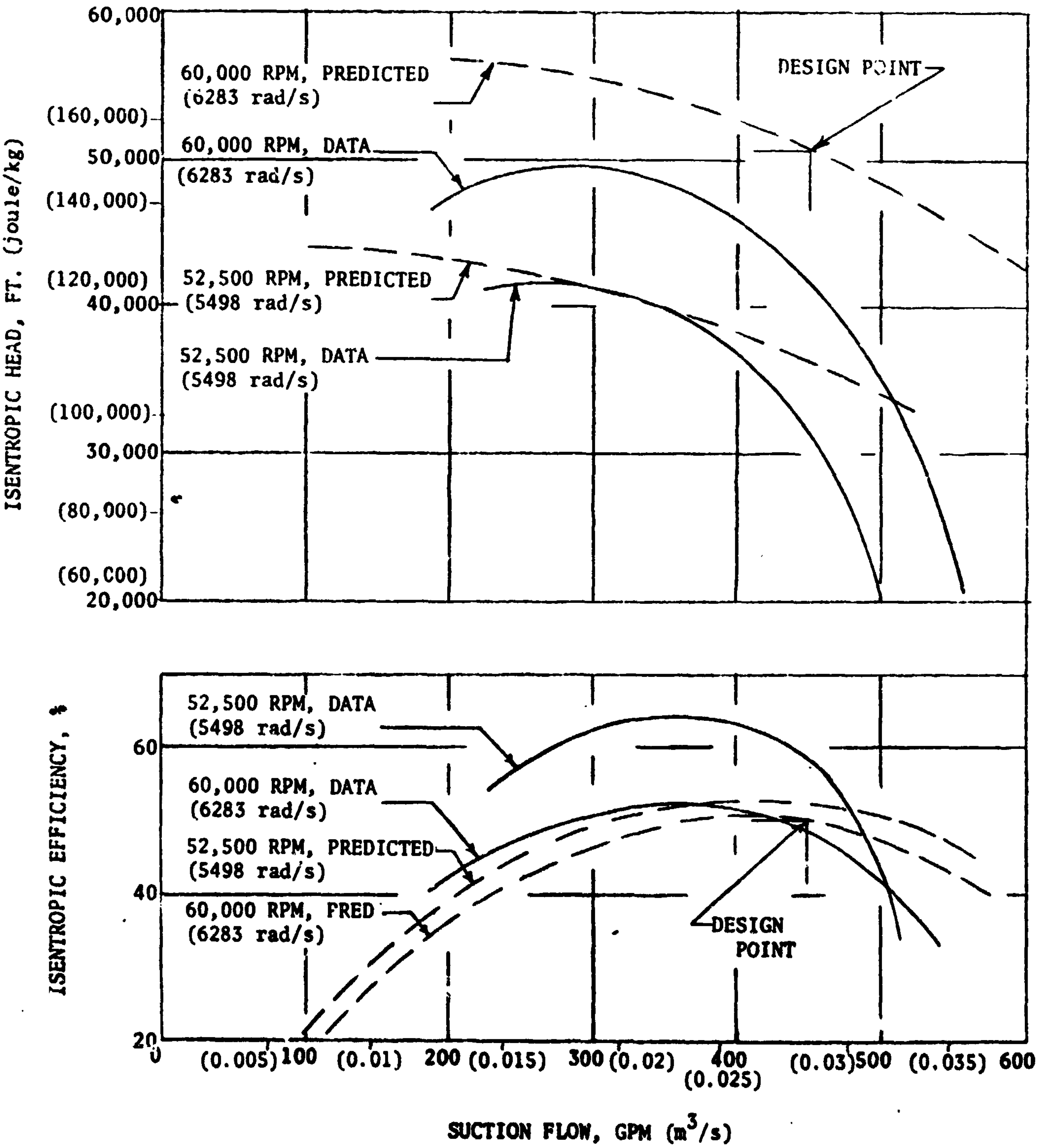

Figure 183. APS Fuel Pump Performance (T/P S/N 01 Before 1st Stage Wear Ring was Restored and Before Front Internal Leak Path was Sealed)

The data obtained at 5498 rad/s (52,500 rpm) in the initial tests series matched the predicted H-Q characteristics closely at design Q/N although the developed heat fell off sharply at higher flowrates. The efficiency obtained at 5498 rad/s (52,500 rpm) was substantially higher than predicted. Because of compressibility effects, the performance was poorer at 6283 rad/s (60,000 rpm). Although the actual efficiency exceeded the prediction at low flowrates, the developed head fell short of the predicted over the entire flow range.

After the initial test series an analysis was made to determine the cause for the low developed head. It was concluded that part of the problem was internal recirculation in the area of the rear bearings and around the crossover from the second stage discharge to the first stage discharge. The latter leak path was sealed by adding a spring seal between the inlet housing and the crossover as shown in Fig. 184. In the process of incorporating the seal it was noted that the silver plating on the inlet housing opposite the first stage impeller front wear ring had come off. Thus, instead of 0.0127 cm (0.005 inch) diametral wear ring clearance per design, the pump was tested with approximately 0.0635 cm (0.025 inch) clearance. The inlet was replaced by one with a good quality silver plate on the wear ring land.

Figure 185 shows the performance characteristics of turbopump S/N 01, after the first stage wear ring was repaired and the front internal leak path was sealed. A substantial improvement in performance was realized: The head was closer to predicted and the efficiency was substantially higher than predicted over a wider flow range.

The performance of turbopump S/N 02, presented in Fig. 186, was lower, both in the head developed and the efficiency attained, even though the configuration of the pumps was the same.

The suction performance evaluation was conducted on turbopump S/N 01, on the first test series, before the front leak path was sealed and the first stage front wear ring was restored. The results are shown in Fig. 187. Two percent head decrease occurred at 299 Joule/kg (100 ft) NPSH at the lower flowrate, while at the approximate design flow the 2 percent head decrease was at 254 Joule/kg (85 ft) NPSH. The

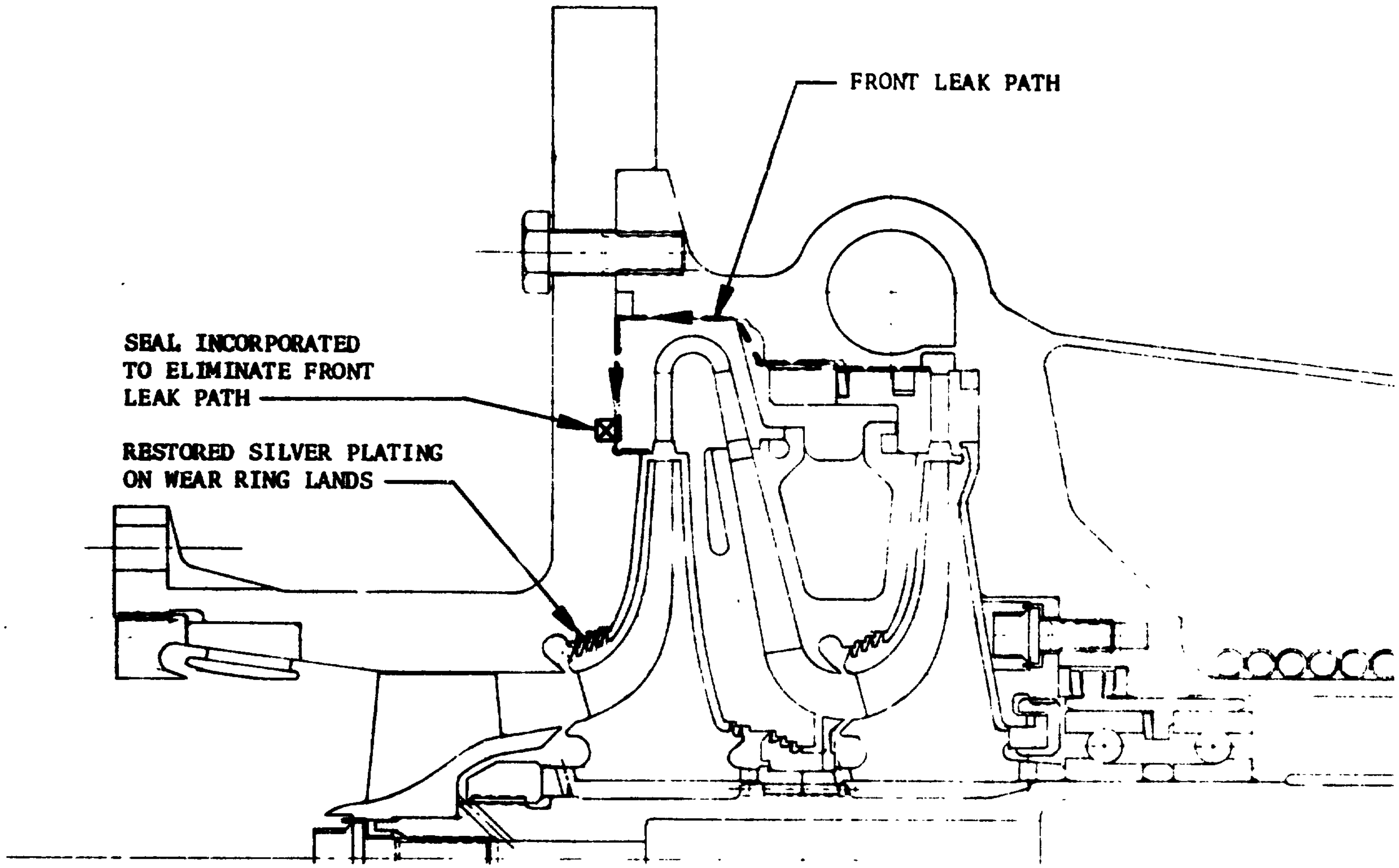

Figure 184. Mk-44 Fuel Pump Modifications After Initial Tests With T/P S/N 01

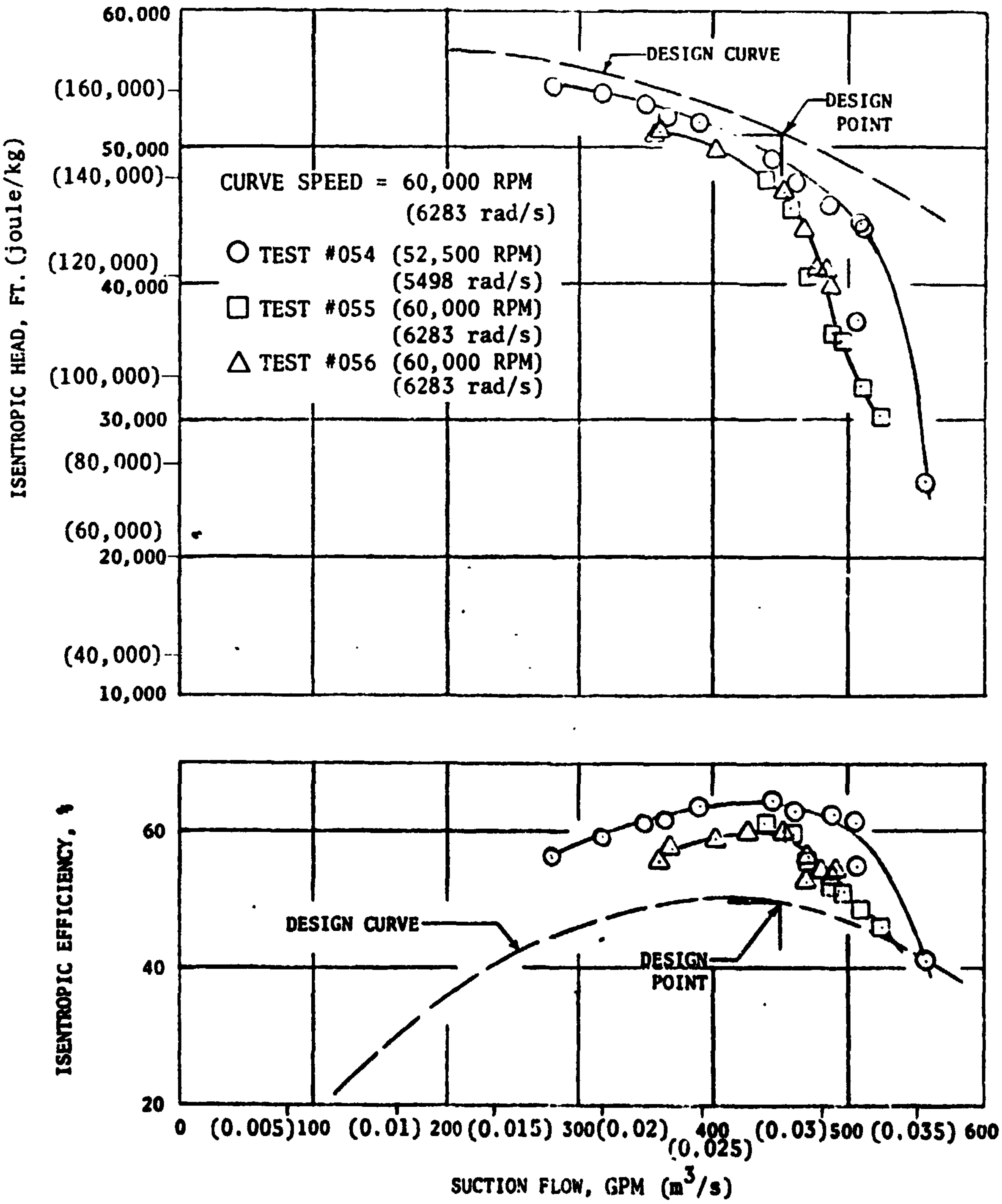

Figure 185. APS Fuel Pump Performance (T/P S/N 01 1st Stage Wear Ring Restored and Front Internal Leak Path Sealed)

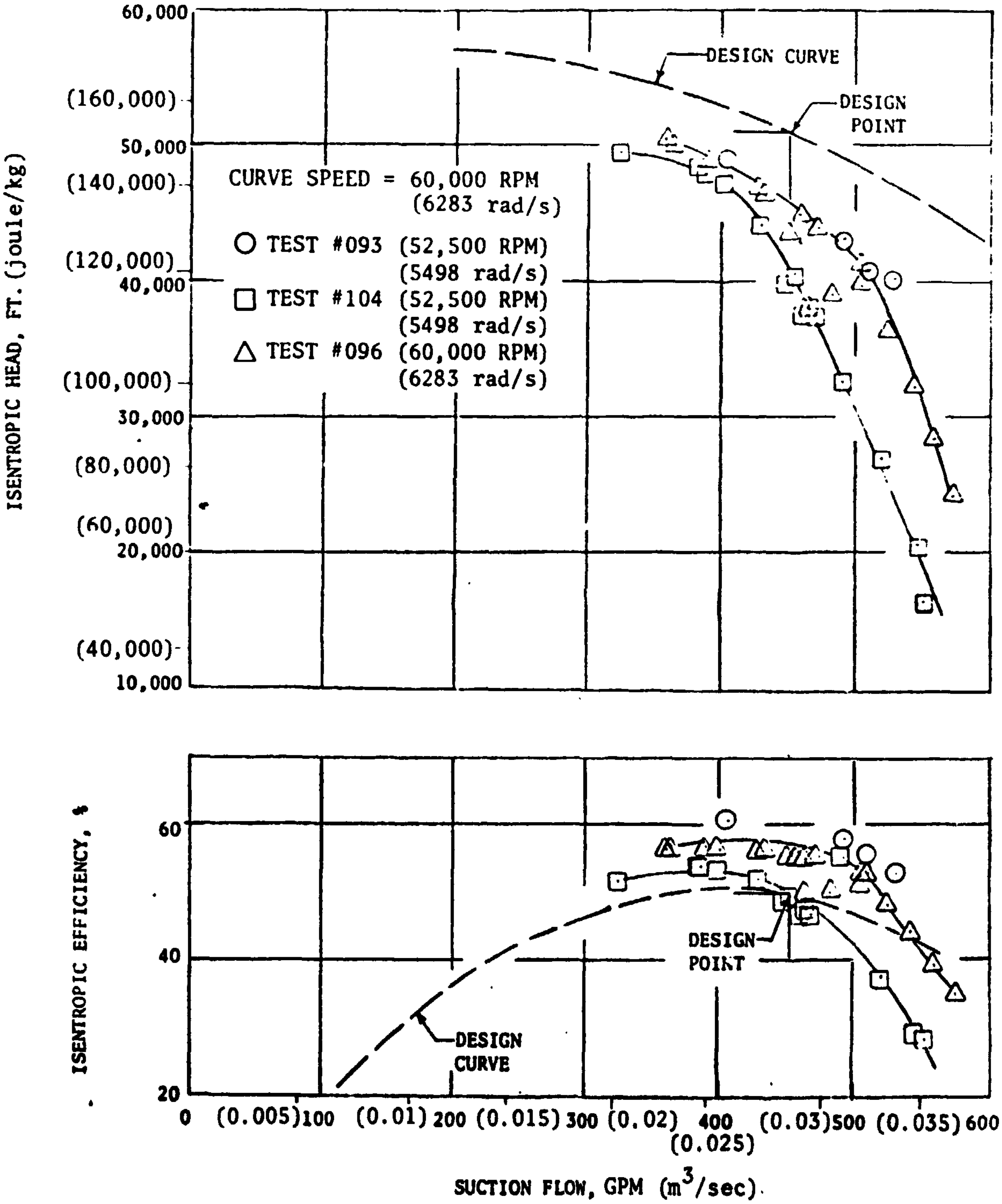

Figure 186. APS Fuel Pump Performance (T/P S/N 02 With Front Internal Leak Path Sealed)

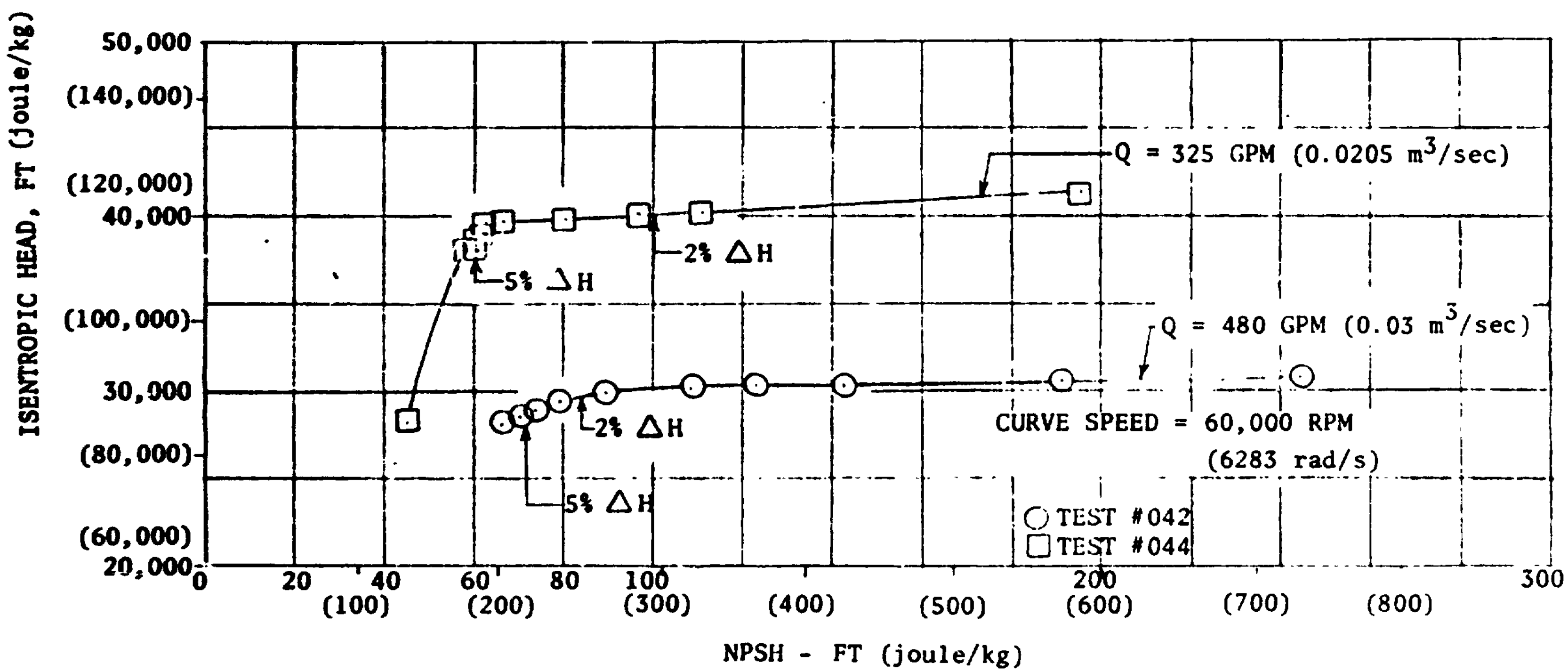

Figure 187. APS Fuel Pump Suction Performance (T/P S/N 01 Before 1st Stage Wear Ring was Restored Before Front Internal Leak Path was Sealed)

corresponding NPSH values for the 5 percent head change were 179 Joule/kg (60 ft) and 209 Joule/kg (70 ft), respectively. It is surmised that the large first stage front wear ring leakage due to the failed silver plating had a degrading effect on suction performance, but the suction performance tests were not repeated to assess the degree of improvement after the wear ring was restored.

The output criteria of the MK-44 liquid hydrogen pump required design parameters and features in certain areas for which little or no empirical data was available and as a result analytical techniques and extended extrapolation had to be applied. In the subsequent discussion, significant hydrodynamic results are summarized and analyzed for probable causes for deviation from predicted values.

The balance piston operated successfully thereby demonstrating that the analytical techniques for axial thrust prediction, criteria for thrust force margin and balance piston design procedures are satisfactory. Inspection of the bearings after testing showed that only light bearing radial loads were experienced. This verifies the capability of the selected vaned diffuser crossover system to produce low radial forces on the shrouded impellers over a wide flow range. The losses in the vaned-diffuser cross-over system calculated from test results were lower than predicted.

At the design point flow rate of 0.029 m^3/s (460 gpm) and 6283 rad/s (60,000 rpm), the test head was lower than initially predicted and the test efficiency was higher than predicted. The test head rise dropped more rapidly at flow rates above the design point than was predicted. In an effort to evaluate the differences between predicted and test performance, the performance was again calculated using actual build clearances and hardware dimensions but with increased estimates of boundary layer thickness.

This resulted in a predicted design point head approximately 10 percent lower than test values with good agreement in efficiency. The predicted head flow slope was still flatter than test values.

The difference between predicted and test performance may have been caused by blockage due to the return of hot two-phase hydrogen to the inlet through the impeller seals and balance piston flow passages. The process of mixing and condensing these flows is not well defined and this effect is much more pronounced for low specific speed pumps such as the APS fuel pump.

The number of impeller blades possible to produce was limited to ten, which in turn dictated a lower impeller discharge blade angle.

Typically the lower the impeller blade angle, the greater is the tendancy for boundary layer fluid to collect on the suction surfaces of the blades rather than leaving along the impeller side walls. The impeller exit passage aspect ratio (peripheral spacing/tip width) was very high (13.37) for the APS compared to conventional size pump (≈2.50). The further the design had to deviate from optimum geometry to accommodate fabrication constraints for small low specific speed pumps, the less predictable the performance became.

The value of blade and vane thicknesses and flow passage boundary layer allowances, expressed as percentage of free area, used in the performance prediction analyses are presented in Table 41.

Figure 188 compares the performance predicted with increased passage blockage and build clearance values for turbopump S/N-1 with test results for turbopump Serial No.'s 1 and 2. The efficiency was more correctly predicted with the increased material and boundary layer blockage values. However, the predicted head vs flow characteristic is flatter than determined by test.

Figure 189 compares the performance of the first stage of the APS pump based on test results with the predicted performance for the two sets of material and boundary layer blockage values listed in Table 41. The increased blockage allowances reduced the head rise while only slightly influencing the head vs flow characteristic slope. The head flow characteristic slop was largely determined by the impeller both for the test and analytical results. Possible reasons for differences between test and analytical characteristics could have been increased impeller inlet blockage due to blockage by two-phase fluid entering from the impeller wear ring or greater housing internal leakage flows than allowed for. As the pump

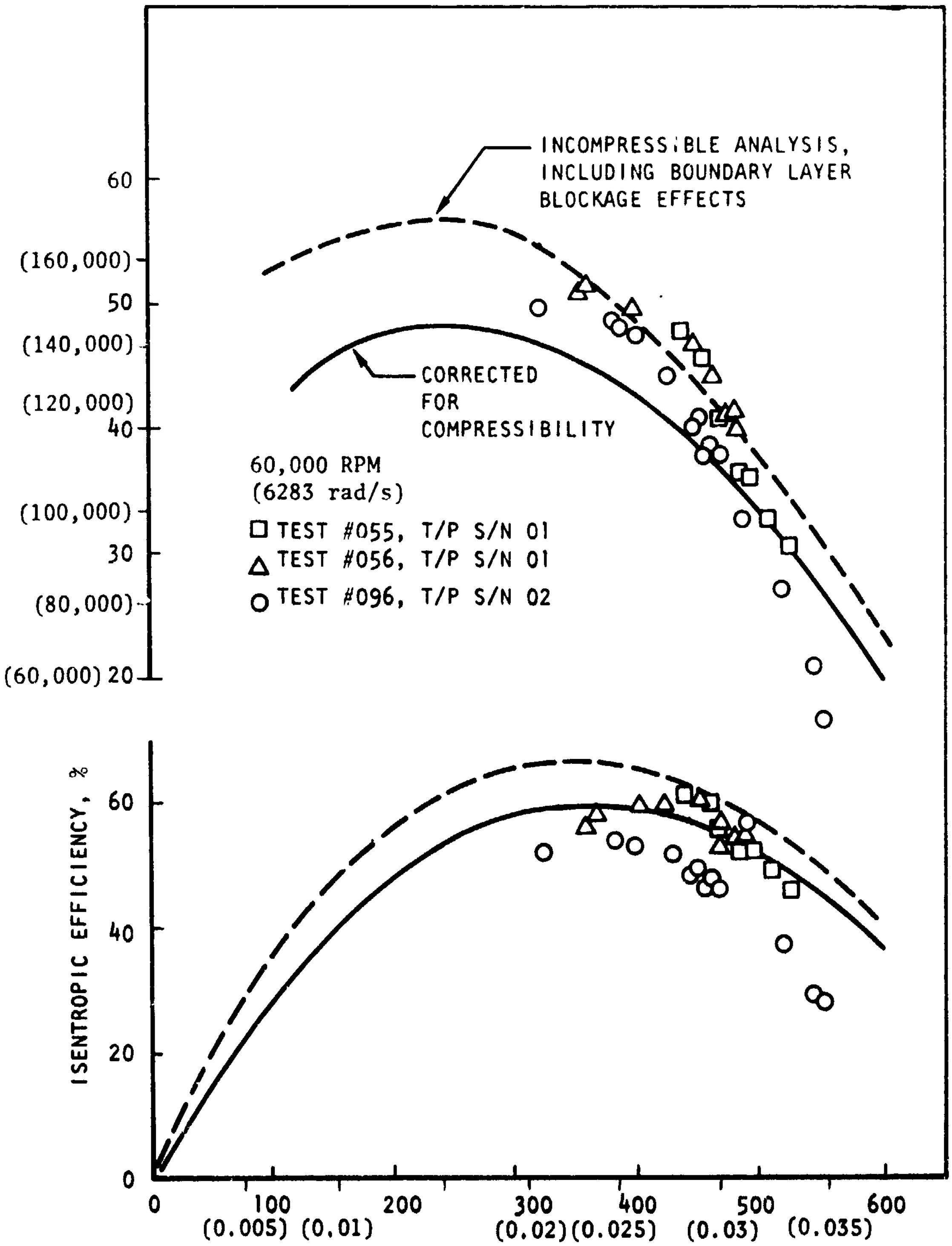

Figure 188. APS Fuel Pump Performance

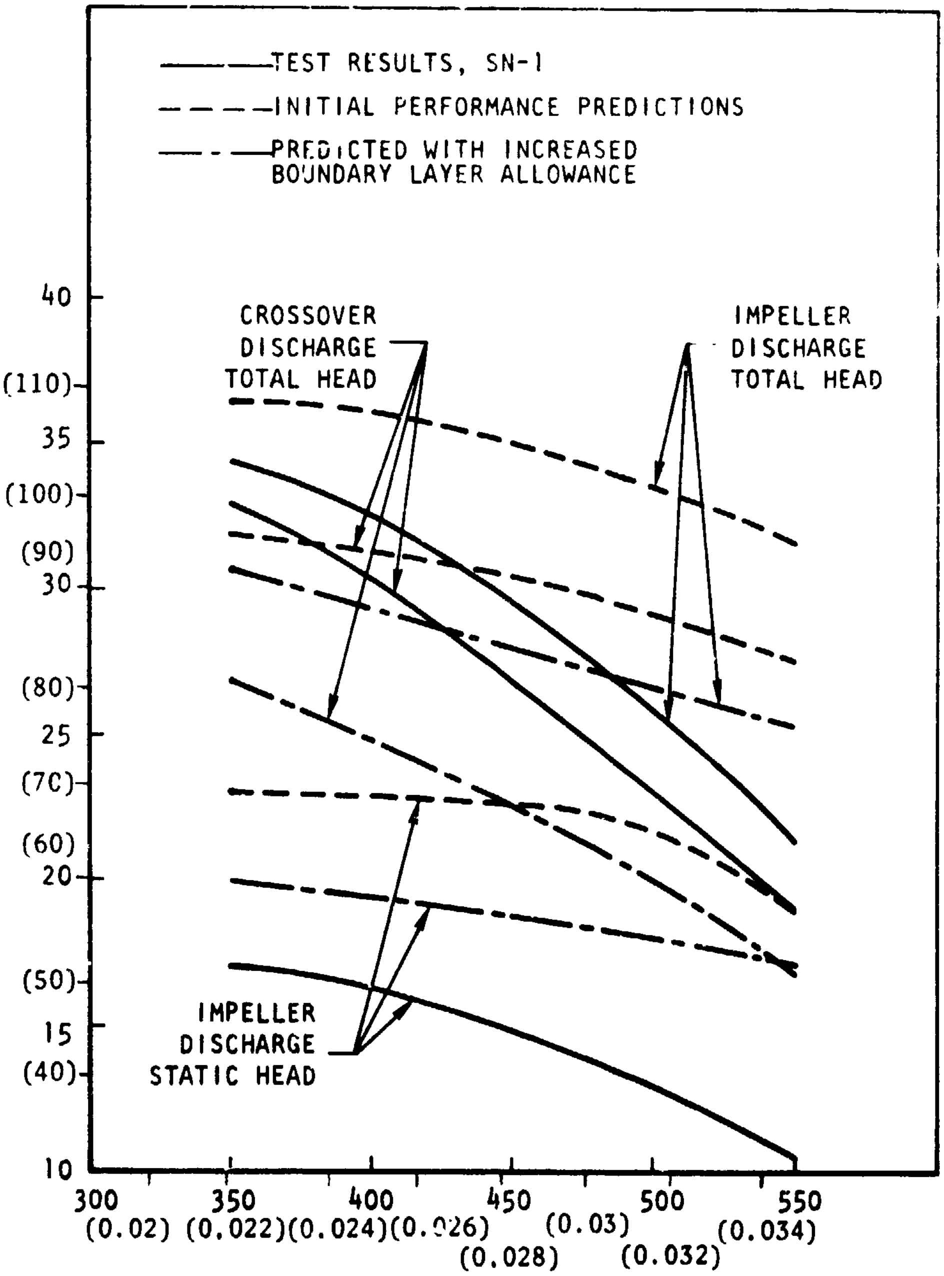

Figure 189. APS Hydrogen Pump First Stage Performance

specific speed is increased the influences which result in poorer predictability become less important. Vaned diffuser discharge pressure and cross-over discharge pressure are nearly identical based on calculations and vaned diffuser pressures are therefore not plotted.

TABLE 41. APS FUEL PUMP COMPUTER PROGRAM INPUT BLOCKAGE VALUES

	Original Calculation	Increased Blockage
Impeller Inlet		
Blade normal thickness, cm (inch)	0	0.127 (0.050)
Boundary layer area reduction, percent	10	10
Impeller Discharge		
Blade normal thickness, cm (inch)	0	0.297 (0.117)
Boundary layer area reduction, percent	10	40
Diffuser Inlet		
Vane normal thickness, cm (inch)	0	0.0762 (0.030)
Boundary layer area reduction, percent	10	10
Diffuser Exit		
Vane normal thickness, cm (inch)	0	0.0762 (0.030)
Boundary layer area reduction, percent	10	40
Crossover Exit		
Vane normal thickness, cm (inch)	0	0.0762 (0.030)
Boundary layer area reduction, percent	20	20
Volute		
Boundary layer area reduction, percent	20	20

The turbine performance characteristics, as established by GN_2 calibration using a torquemeter and a power absorbing device are presented in Fig. 190. The measured efficiency at the design jet speed ratio of 0.178 and pressure ratio of 7.72 was 49.5 percent, compared to a predicted value of 60 percent. The lower efficiency obtained was attributed primarily to three factors: The rotor blade surface finish and the surface finish of the interstage stator was poorer than anticipated, actual rotor tip radial clearance was higher than the value used in

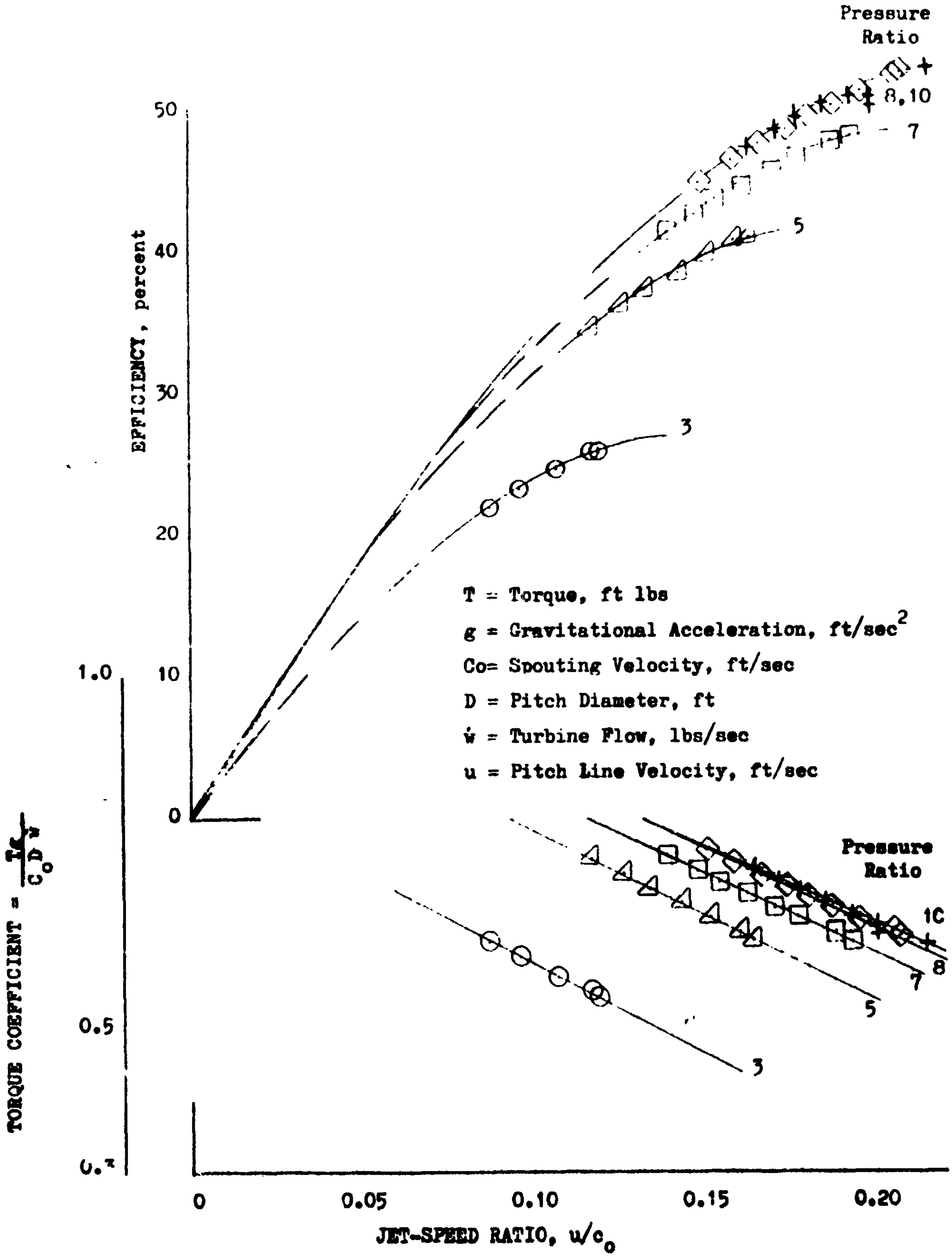

Figure 190. APS Fuel Turbine Performance (Full Admission Two Row GN_2 Calibration Data)

the design analysis, and finally the cell size used in the honeycomb tip seal was coarse compared to the small blade tip surface area.

LH_2 TPA Mechanical Performance

All development testing was performed with the initial build of turbopump S/N 01. A total of 58 tests and 5091 seconds of operation was accomplished, of which 45 tests for an accummulated 2940 seconds were conducted using hot gas for turbine propellant. On the remainder of the tests, ambient gaseous hydrogen was used to drive the turbine.

From a rotordynamic standpoint, the operation of the turbopump was excellent. The rotor operated smoothly at all speed levels where steady state dwell was attempted and ramps through the entire speed range did not result in noticeable increase in the vibration level when passing through the first and second criticals. Wear patterns on the rotor and mating parts did not disclose any signs of rotordynamic instability.

A review of the initial pump performance data revealed that the developed head was lower than predicted. To determine the cause, a partial inspection of the pump was made after the 14th test, and it was found that the silver plating on the stationary land opposite the first stage impeller inlet labyrinth was missing. The mechanics of the bond failure indicated improper cleaning of the base surface prior to plating. The inlet was replaced, and the discrepant part was replaced. No further problems were encountered with the silver plated wear rings.

On the 58th and 59th tests of the development test series, hot gas leakage was observed emanating from the turbine manifold and as a result testing was terminated and the turbopump was disassembled for inspection. An overview of the principal detail parts after disassembly is presented in Fig. 191. A detailed account of the condition of the parts is given in the following:

Pump: The posttest condition of the pump components was excellent, without any sign of degradation as a result of testing. The inducer, impellers, crossover

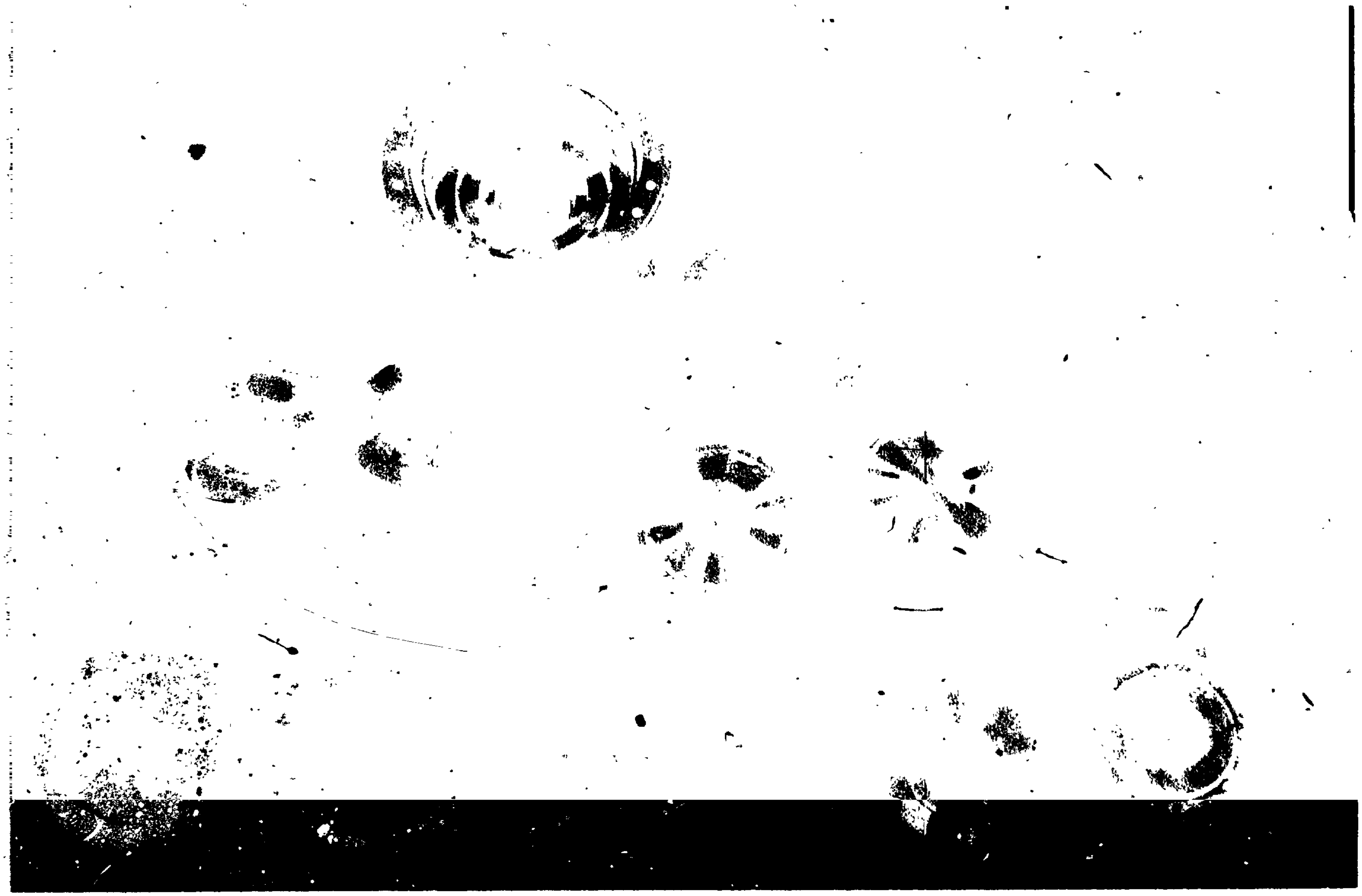

Figure 191. LH_2 Turbopump Components S/N 01 (Posttest)

and diffuser ring are shown in Fig. 192 after testing. No inducer rubbing had taken place with the radial tip clearance at 0.0254 cm (0.010 inch). Each impeller wear ring labyrinth tooth rubbed a shallow groove in the silver plated land, as expected. No galling or fretting had taken place on any mating surfaces.

Both balance piston orifices were in excellent condition, the only contact evident between the stationary lands and the impeller surfaces was that which occurred during assembly load checks. The stationary high pressure and low pressure orifice surfaces as well as the rotating low pressure orifice surface are illustrated in Fig. 193 after testing.

Seals and Bearings: The control gap shaft seal was in excellent condition after development testing (Fig. 194). No measurable clearance change had occurred and the mating chrome plated surface on the shaft, as well as the flame sprayed surface an the first stage disc showed no evidence of wear or spalling. No degradation in the liftoff seal (Fig. 195) sealing surface had taken place and the three seal internal bellows were intact.

All four bearings (Fig. 194) appeared in good condition after the development test series on T/P S/N 01. There was no evidence of surface distress either on the balls or on the races.

Turbine. The development testing with turbopump S/N 01 was stopped because of hot gas leakage from the turbine manifold. Leak checks and partial disection of the manifold revealed two cracks in the areas indicated in Fig. 196 and 197. The structural weld crack in the external cylindrical member resulted from a poor fitup, i.e., the two members which were joined were not properly aligned over part of the circumference. Metallurgical examination of the crack in the torus revealed the presence of porosity and lack of weld penetration. Both welds were of Class I type; both passed X-ray tests. Apparently, the difficulty in properly evaluating the soundness of the welds lay in the fact that the X-rays had to be shot through multiple layers of metal which tends to give poorer resolution. The misaligned condition of the external weld went unnoticed during visual inspection due to human error.

Figure 192. LH_2 Inducer, Impellers, and Crossover S/N 01 (Posttest)

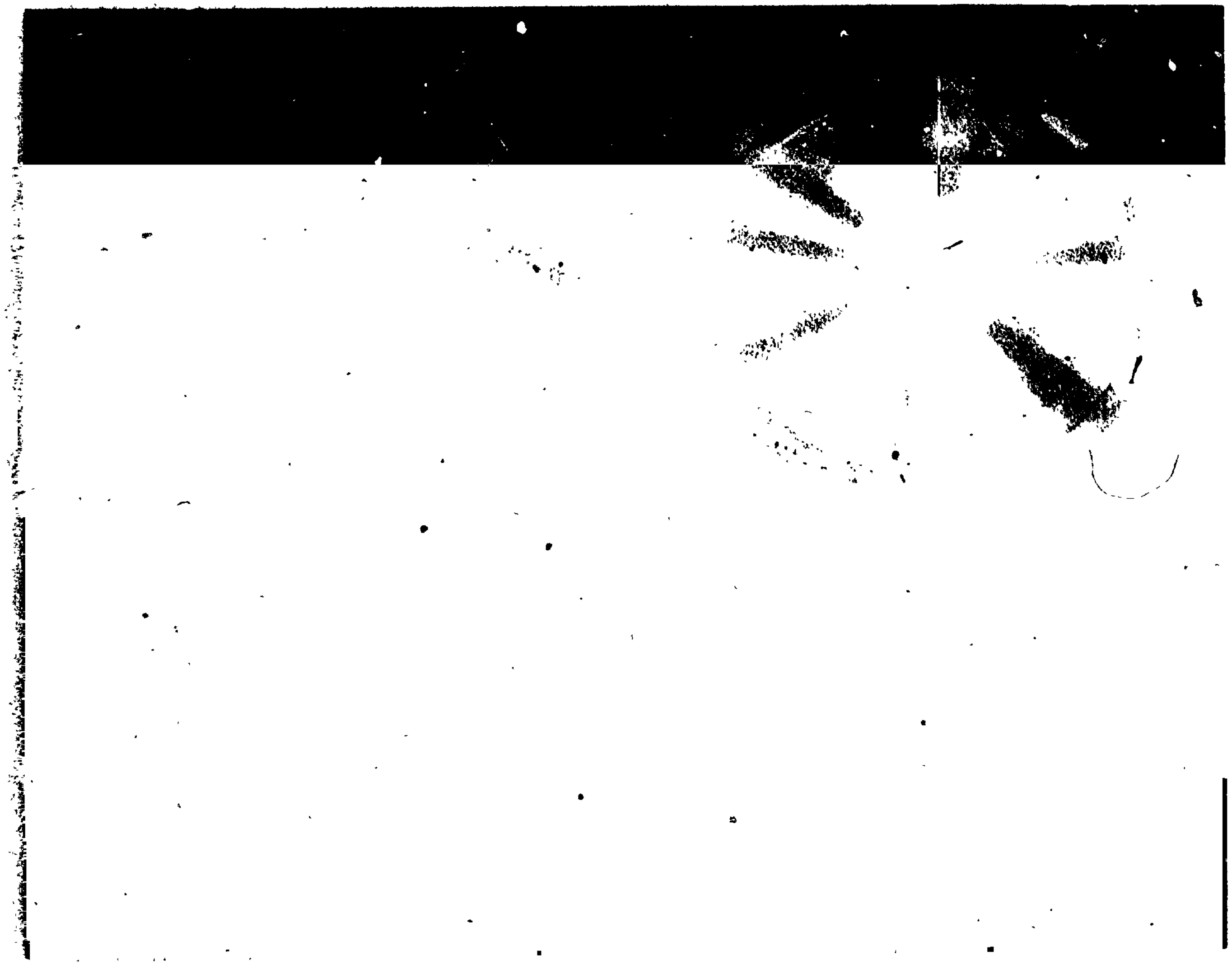

Figure 193. LH_2 Balance Piston Components
S/N 01 (Posttest)

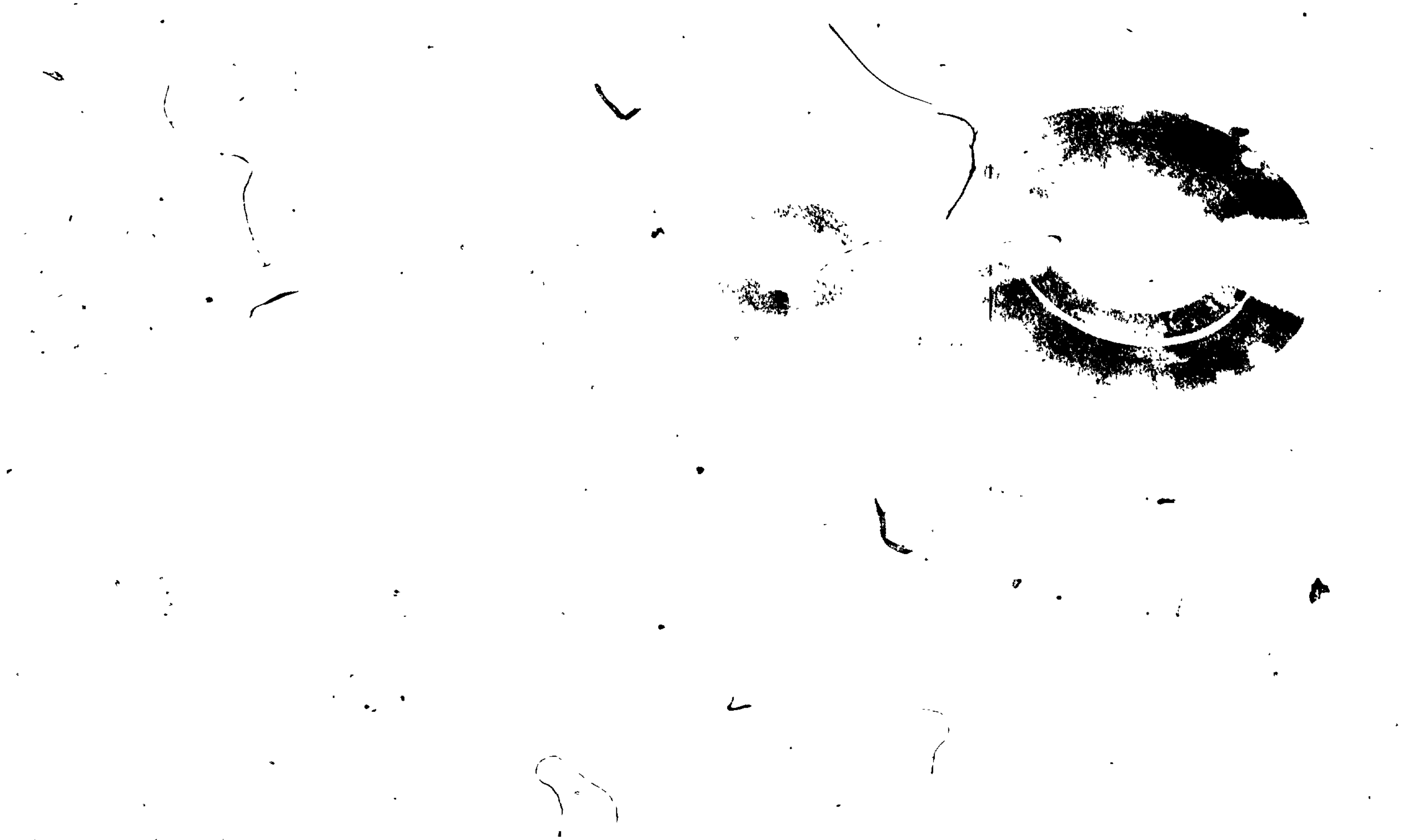

Figure 194. LH_2 Bearings and Control Gap Seals S/N 01 (Posttest)

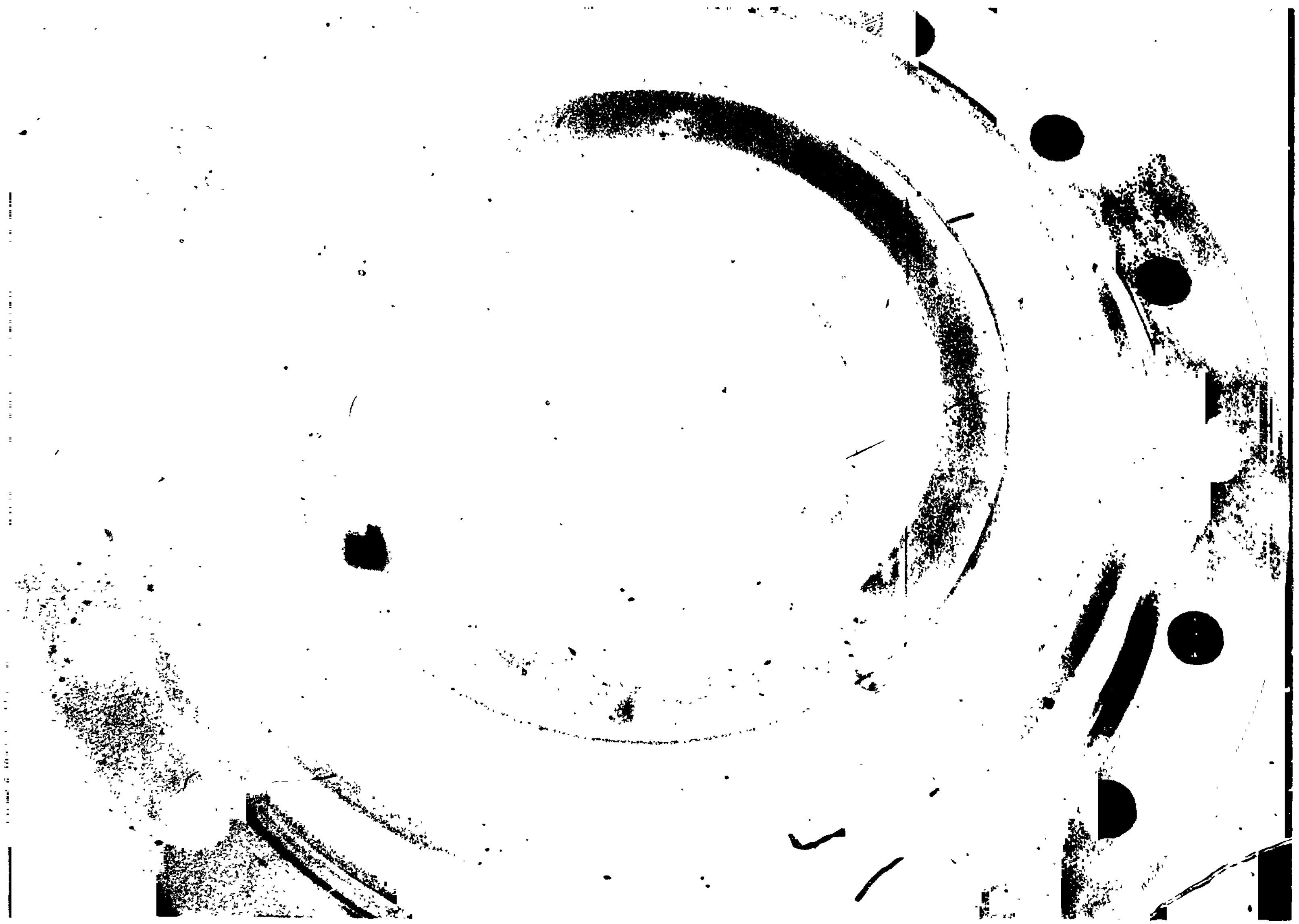

Figure 195. LH_2 Turbine Manifold Crack (Internal Crack)

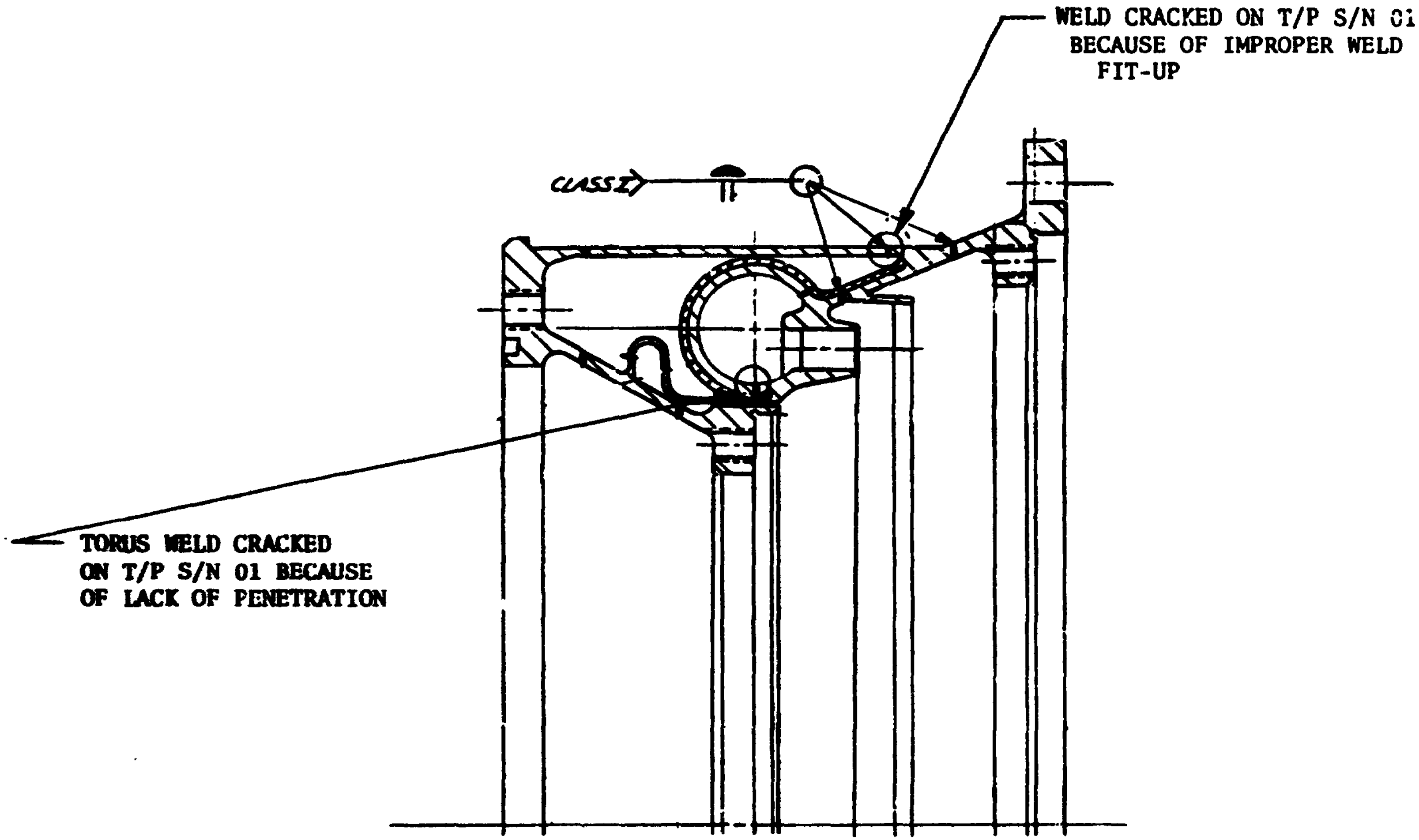

Figure 196. APS Fuel Turbine Manifold

Figure 197. LH_2 Turbine Manifold Crack (External Crack)

At the time of the manifold failure, turbopump S/N 01 had accumulated 58 starts and 5091 seconds, of which 45 starts and 2940 seconds were with hot propellant gas. The conclusion that the failure resulted from faulty fabrication and quality control and not from a basic weakness in the design is supported by the fact that three other structurally identical manifolds (one fuel, two oxidizer) have accumulated a total of 92 starts and 9479 seconds testing under the same or more severe conditions without failure.

The cracks in the structural members of the manifold resulted in axial displacement of the nozzle and stator, causing rubbing at the leading edges of the first and second row rotor blades (Figs. 198 and 199). Small hairline cracks were evident at the blade roots of both wheels and two of the second row blades were missing. The blade cracking was attributed to a combination of the following:

1. Excessive exictation caused by rubbing
2. Brittle re-melt layer after electrical discharge machining of the blades not completely removed by the shot blasting technique used

Although it was surmised that the primary cause was rubbing, surface brittleness may have contributed to the problem and in future applications other methods for removing the remelt layer such as electro chemical milling should be explored.

THERMAL ANALYSIS

The thermal isolation of the pump from the turbine is necessary to minimize the total energy transferred during transients of the turbopumps. Since the structural requirements dictate to a great extent the physical dimensions of the various turbopump components, the thermal isolation had to be obtained through: (1) an appropriate material selection, (2) use of high thermal resistance joints connecting the components, and (3) minimizing the energy transferred by radiation from the hot turbine components to the colder pump components.

Thermal isolation was obtained in the design of both the LH_2 and LO_2 pumps by a close coordination between the mechanical and thermal analysis of the

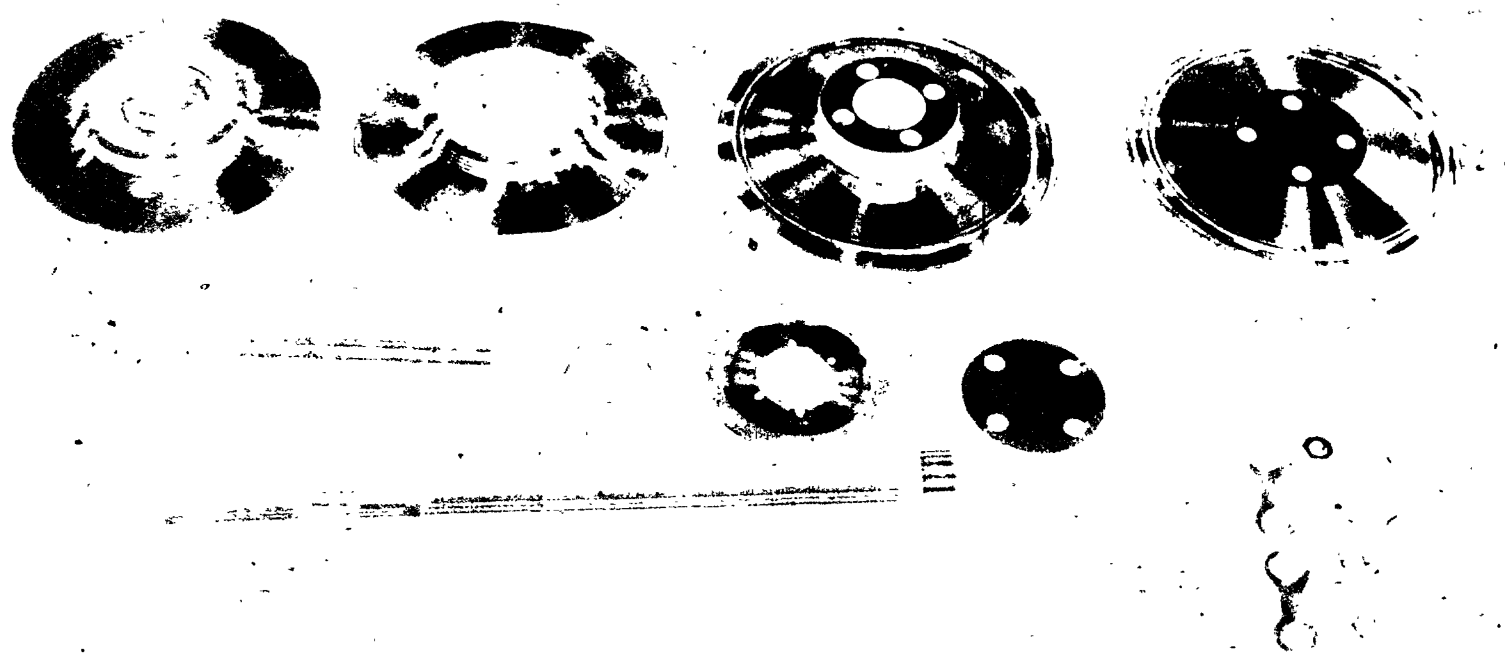

Figure 198. LH_2 Turbopump Rotating Assembly S/N 01 (Posttest)

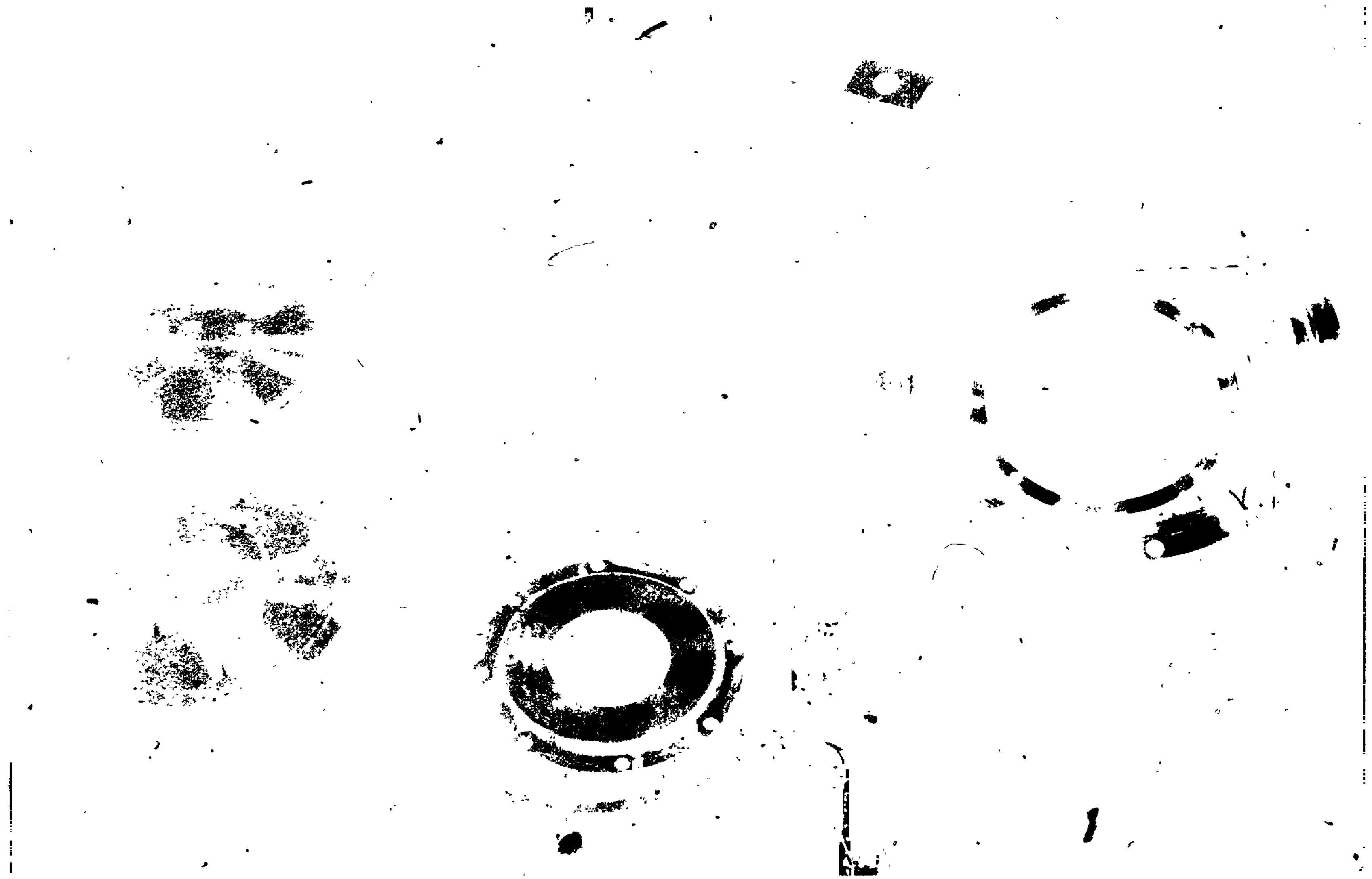

Figure 199. LH_2 Turbine Components S/N 01 (Posttest)

turbopump using a discrete nodal model of the turbopumps to predict the effect of each design change on thermal behavior.

The turbopump designs used low thermal conductivity low thermal capacitance materials throughout, combined with minimum contact area joints at the mounting point, and junction of the pump and turbine. The minimum contact area principle for attachment design ensured a good reproducibility of the overall thermal behavior of the joint since the high loading pressure/low contact area minimized the uncertainties in predicting the contact resistance effect in the joint. Radiation interchange between the turbine manifold and the turbopump housing was minimized through use of a "super-insulation" blanket (alternate nickel/quartz layers) around the manifold. The blanket was very effective in reducing energy interchange from the turbine manifold to the colder components based on the altitude simulation tests conducted on the LO_2 turbopump even though a hard vacuum was not established during the test.

The analysis of the chilldown and soakback of a turbopump was strongly dependent on the ability to predict the fluid conditions throughout the turbopump. The procedure used at Rocketdyne for this type of analysis is to use the general purpose Differential Equation Analyzer Program (DEAP) for a combined flow and thermal analysis of the turbopump. Besides solving the general second-order, partial-differential equation:

$$\nabla \cdot (K\nabla\phi) + \vec{W} \cdot \nabla\phi + q = \rho C \frac{\partial\phi}{\partial t}$$

the program also solves the one-dimensional energy equation using the fluid enthalpy as the dependent variable:

$$\dot{W} \frac{\partial H}{\partial x} + \rho C A \frac{\partial H}{\partial t} = \sum qp$$

This allowed two-phase flow aspects of the problem to be incorporated directly in the analysis using bivariate tables to establish the H-P-T relationships of the fluid.

ANALYSIS MODEL

The analytical model used to predict the thermal behavior of the both turbopumps used 32 discrete nodes to represent the various parts of the turbopump, as shown in Fig. 200, and a series of 15 fluid nodes to describe the flow circuit which was analyzed using the fluid enthalpy to account for two-phase flow effects on the thermal behavior of the turbopump.

Figures 201 and 202 show the original prediction for the turbopump soakback behavior without and external refrigeration source and will be compared later with predictions made after modifying the model to match the test data.

ANALYSIS OF LO_2 TURBOPUMP TEST DATA

The thermal test data for soakback obtained from the first three altitudes APS LO_2 turbopump tests is summarized in Table 42 and represents soakback under three different conditions as well as childown at an approximately constant flowrate. Other childown tests were attempted but only one set of valid data was obtained (Test 003).

The chilldown behavior of the APS LO_2 turbopump is compared with predictions in Fig. 203 for several of the test points on the turbopump. Figure 204 shows the computed quality of the discharge fluid during the two-phase portion of the test. The flowrate was not measured during this portion of the test and was computed based on the bypass nozzle area and pump discharge pressure to be about 0.1361 kg/s (0.3 lb/sec) during the chilldown. The pressure measurements indicated that the pump itself did not offer any significant resistance to this flow.

The large mass of the pump housing took about 10 minutes to cool to approximately liquid temperature, as shown in Fig. 203, while the other components remained essentially at ambient temperature. The flow at the pump outlet became two-phase after 2 seconds but required almost 9 minutes to become entirely liquid. The LO_2 heat transfer coefficient in the pump cavity was varied empirically to match the overall response of the pump housing and the value used to obtain the curves,

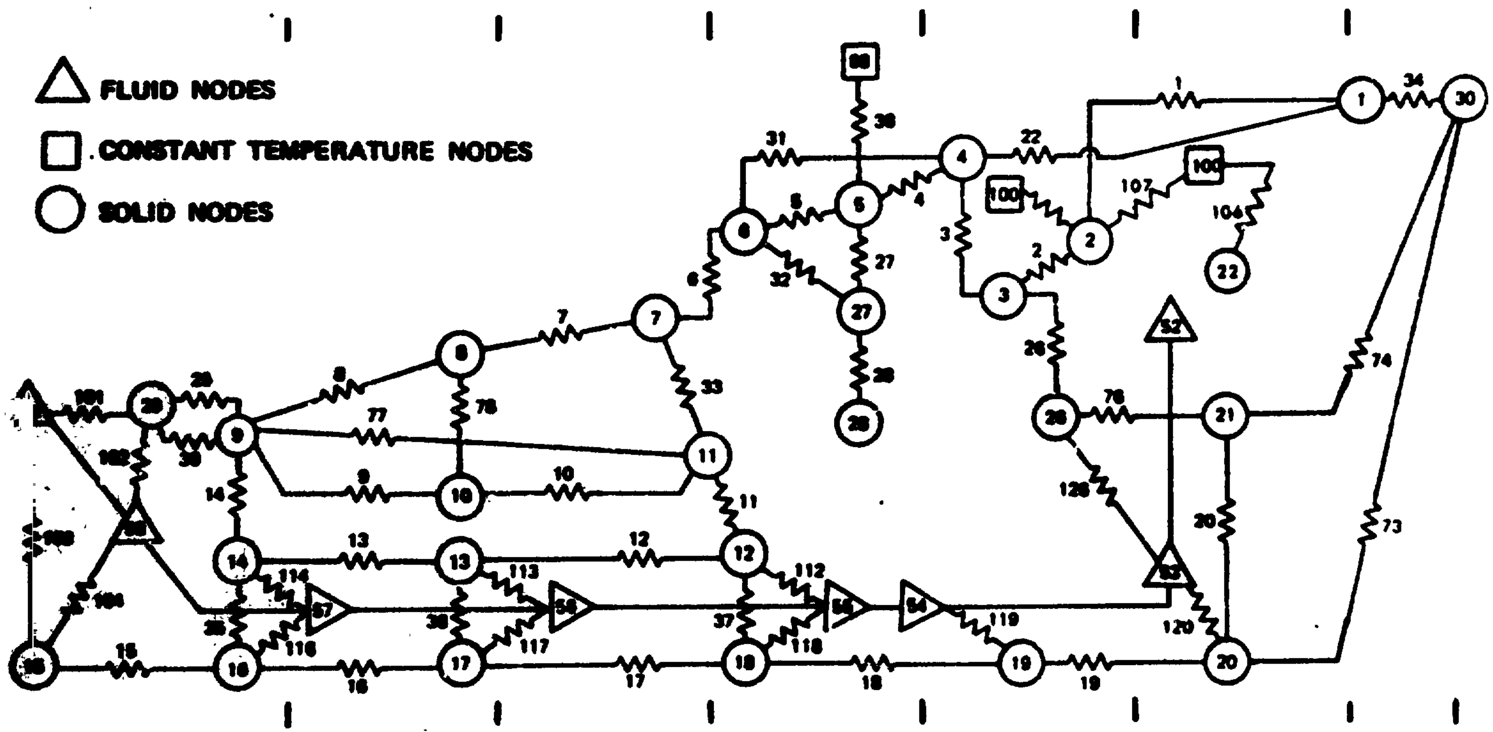

Figure 200. APS Turbopump System Model

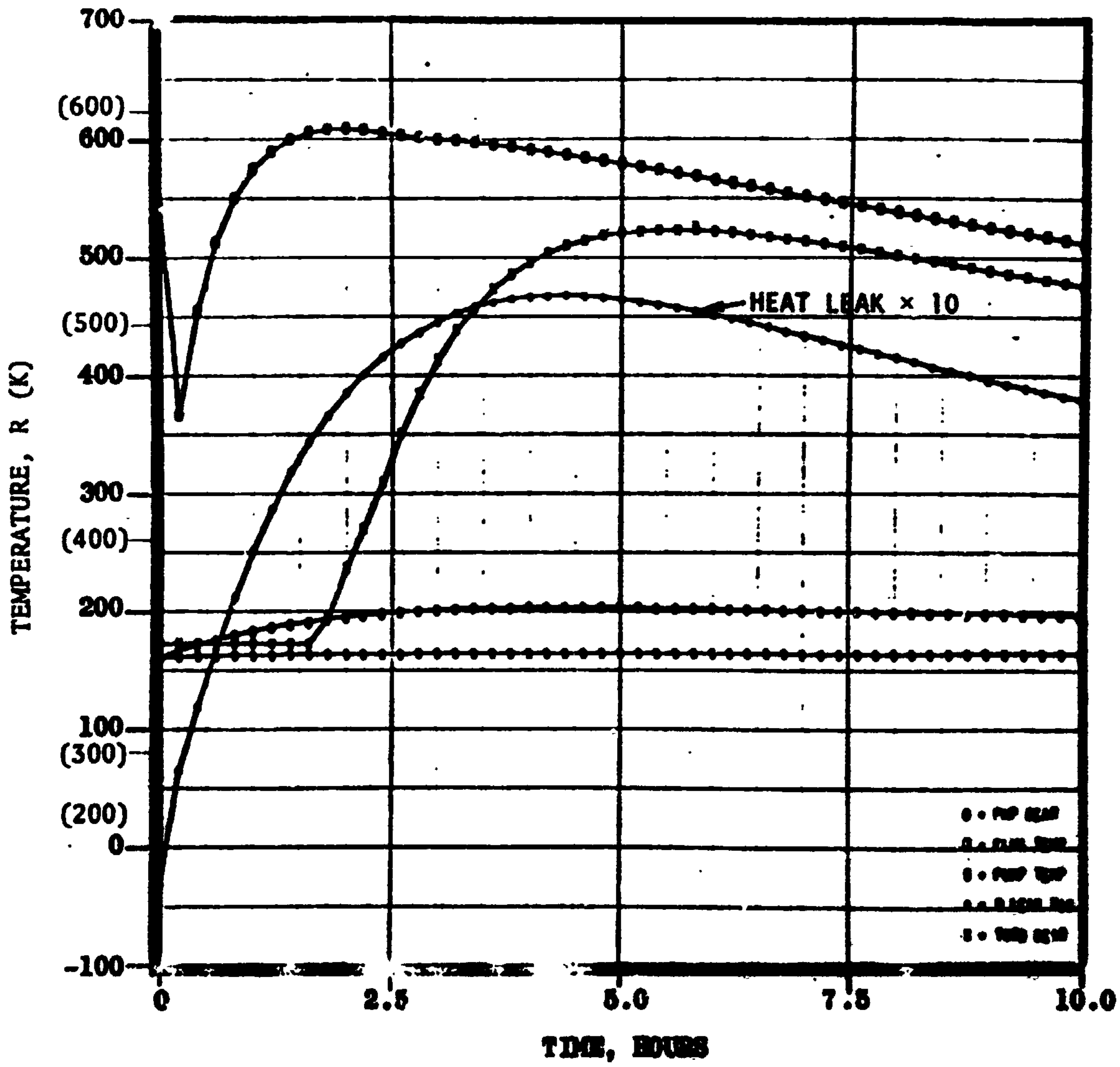

Figure 201. APS Turbopump Soakback Thermal Analysis
Sketch 204, No External Cooling

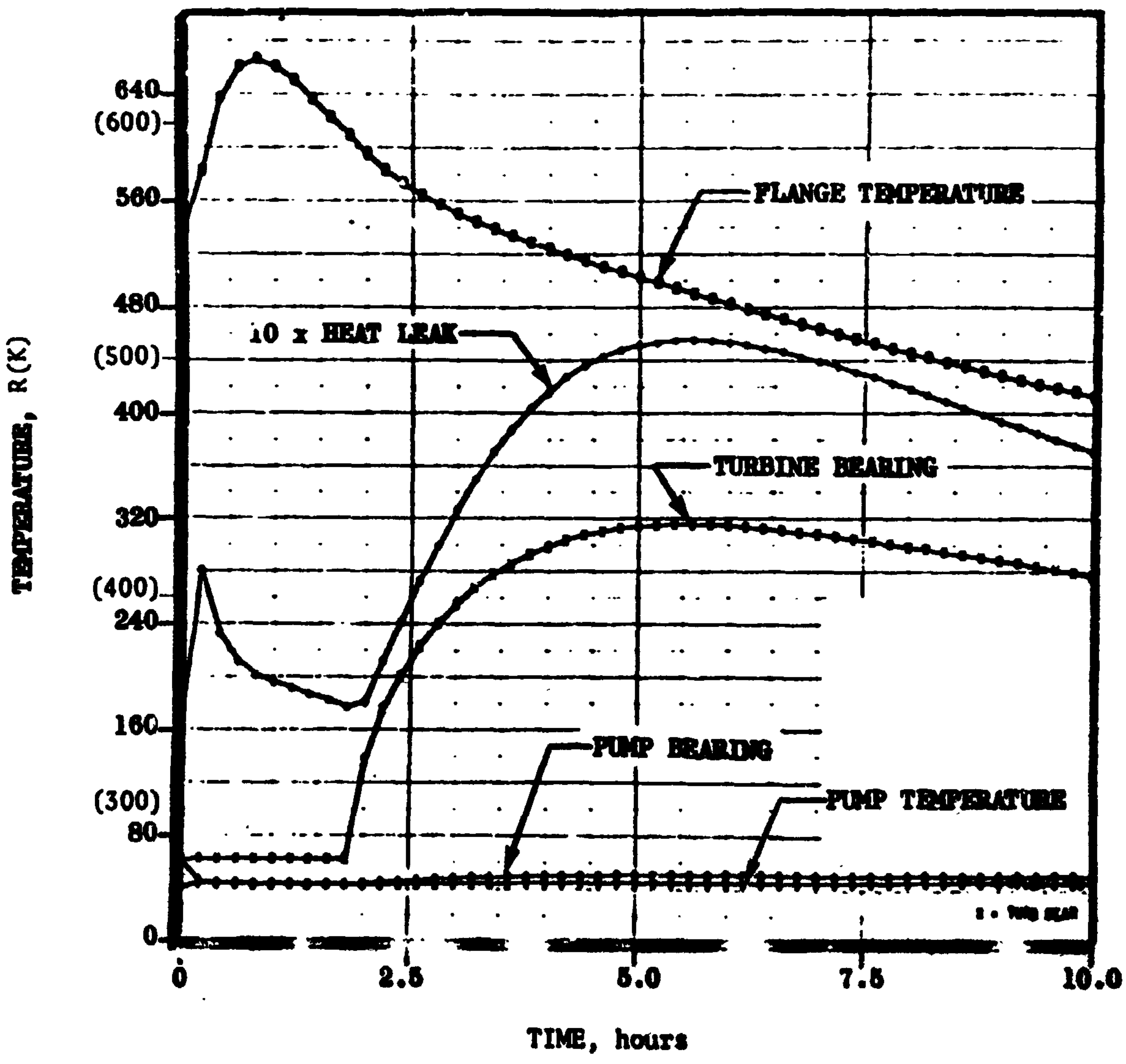

Figure 202. APS Turbopump Soakback Thermal Analysis
Sketch 105, No External Cooling

TABLE 42. LO_2 SOAKBACK DATA*

Temperature in degrees k and (R)

Test	Time (min.)	T/P 1	T/P 2	T/P 4	T/P 5	T/P 6-8	T/P 9	T/P 10-11	T/P 11-14
Prechill and Soak (Dry)									
1	0	223 (401)	135 (243)	220 (220)	121 (218)	111 (200)	98 (176)	92 (165)	92 (165)
	30	232 (417)	183 (330)	178 (320)	176 (316)	144 (260)	119 (215)	96 (173)	106 (190)
	51	240 (432)	196 (352)	191 (344)	189 (341)	161 (290)	136 (245)	114 (205)	122 (220)
	81	248 (446)	209 (376)	206 (370)	203 (365)	181 (325)	158 (284)	136 (245)	139 (250)
	101	252 (453)	216 (388)	212 (382)	211 (380)	200 (360)	183 (330)	164 (296)	172 (310)
	131	256 (461)	225 (405)	222 (400)	222 (400)	204 (367)	183 (330)	167 (300)	172 (310)
	149	259 (466)	230 (414)	227 (409)	226 (407)	211 (380)	191 (344)	174 (314)	178 (320)
	179	263 (473)	237 (426)	234 (422)	233 (420)	222 (400)	202 (364)	189 (340)	194 (350)
Ambient Gas and Soak (Wet)									
2	0	260 (468)	187 (337)	166 (299)	154 (278)	122 (220)	87 (156)	94 (170)	92 (165)
	30	244 (440)	183 (329)	176 (317)	173 (312)	144 (260)	122 (220)	103 (186)	106 (190)
	55	253 (437)	192 (345)	186 (335)	184 (331)	156 (280)	129 (232)	106 (190)	111 (200)
	85	243 (437)	201 (361)	196 (352)	194 (350)	168 (302)	135 (243)	108 (195)	117 (210)

TABLE 42. (Continued)

Temperature in degrees k and (R)

Test	Time (min.)	T/P 1	T/P 2	T/P 4	T/P 5	T/P 6-8	T/P 9	T/P 10-11	T/P 12-14
Ambient	**Gas and Soak (Wet) (Continued)**								
	104	244 (439)	206 (370)	201 (362)	200 (360)	172 (310)	139 (250)	109 (196)	117 (210)
	134	246 (443)	211 (380)	207 (373)	206 (371)	178 (320)	142 (256)	109 (196)	117 (210)
	154	247 (445)	214 (385)	210 (378)	209 (376)	183 (330)	144 (260)	109 (197)	119 (215)
	206	250 (450)	221 (398)	217 (391)	216 (389)	189 (340)	149 (268)	109 (196)	119 (215)
Good Chill Data									
3	0	992 (1786)	371 (668)	257 (451)	197 (355)	125 (225)	87 (156)	94 (170)	92 (165)
	34	536 (965)	383 (690)	364 (655)	354 (637)	239 (430)	161 (290)	107 (193)	100 (180)
	45	467 (840)	364 (655)	351 (631)	344 (620)	256 (460)	173 (311)	109 (197)	108 (195)
	75	393 (707)	327 (589)	319 (575)	256 (460)	175 (315)	109 (197)	111 (200)	
	94	366 (659)	308 (554)	301 (541)	297 (534)	244 (440)	171 (307)	109 (197)	111 (200)
	124	339 (610)	282 (507)	274 (494)	272 (490)	226 (407)	161 (289)	108 (195)	111 (200)
	150	323 (582)	263 (473)	256 (460)	253 (455)	211 (380)	153 (276)	107 (193)	111 (200)
	180	309 (556)	244 (439)	236 (425)	233 (420)	197 (355)	146 (263)	106 (190)	111 (200)

TABLE 42. (Concluded)

Temperature in degrees k and (R)

Time (min.)	Pump Disch	T/P 1	T/P 2	T/P 4	T/P 5	T/P 6-8	T/P 9	T/P 10-11	T/P 12-14
Test 3 Childown Data									
0	287 (517)	285 (513)	284 (512)	284 (511)	284 (512)	284 (511)	284 (511)	284 (511)	284 (511)
0.2	104 (188)	286 (514)	286 (514)	285 (513)	285 (513)	284 (511)	279 (503)	239 (430)	254 (457)
4.4	101 (182)	286 (514)	286 (514)	285 (513)	286 (514)	283 (509)	274 (494)	217 (390)	237 (426)
8.4	102 (184)	287 (516)	286 (515)	284 (512)	285 (513)	281 (506)	248 (446)	161 (290)	153 (275)
10.4	96 (173)	287 (516)	287 (516)	284 (512)	284 (512)	278 (500)	234 (422)	142 (255)	123 (221)
12.4	94 (170)	287 (516)	287 (516)	281 (505)	281 (505)	272 (490)	221 (398)	126 (227)	112 (202)

*See figure 73 for thermocouple locations

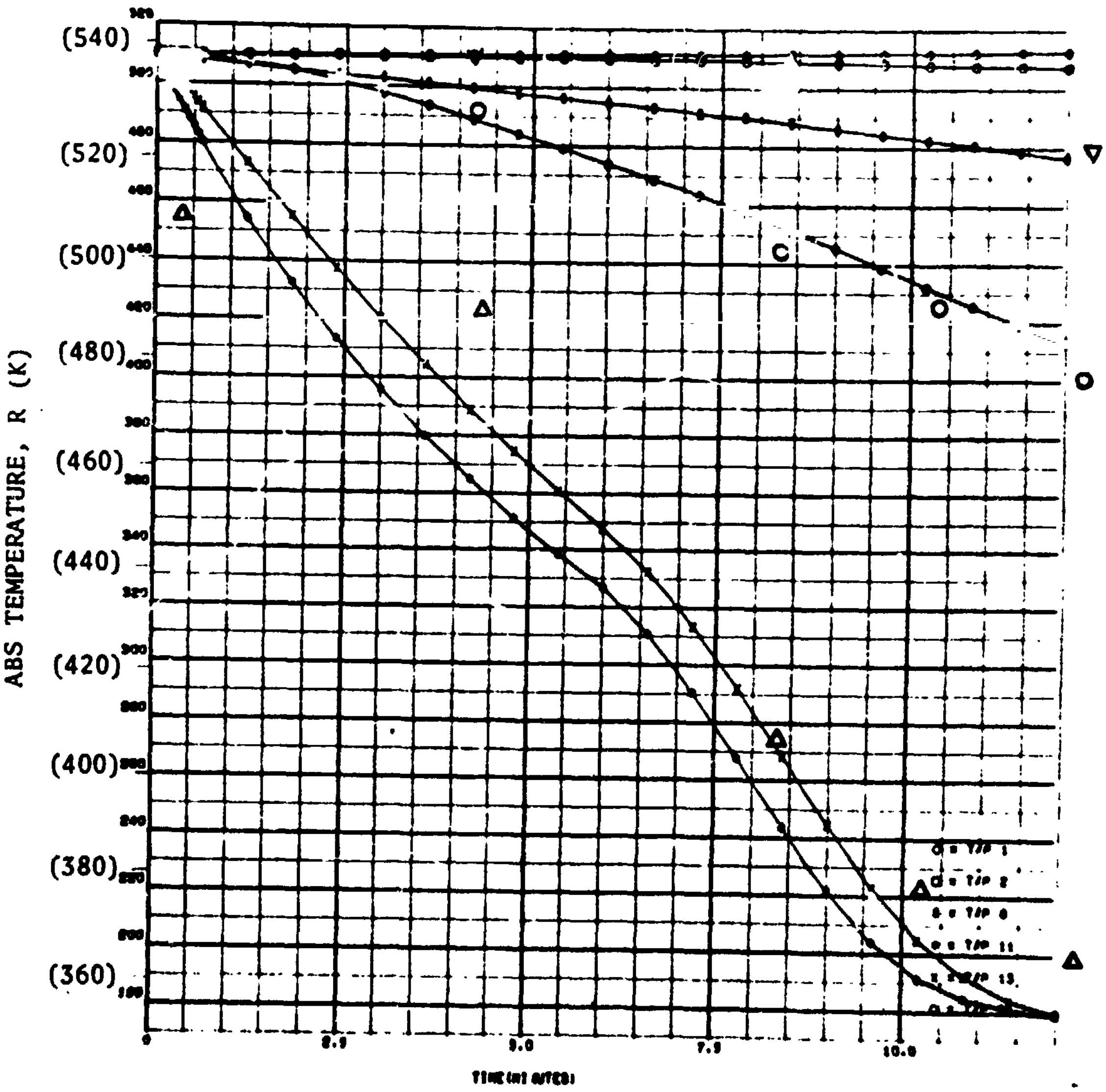

LEGEND - TEST DATA
▽ T/P 8
○ T/P 9
△ T/P 13

Figure 203. Comparison of Experimental and Predicted Childown Temperatures

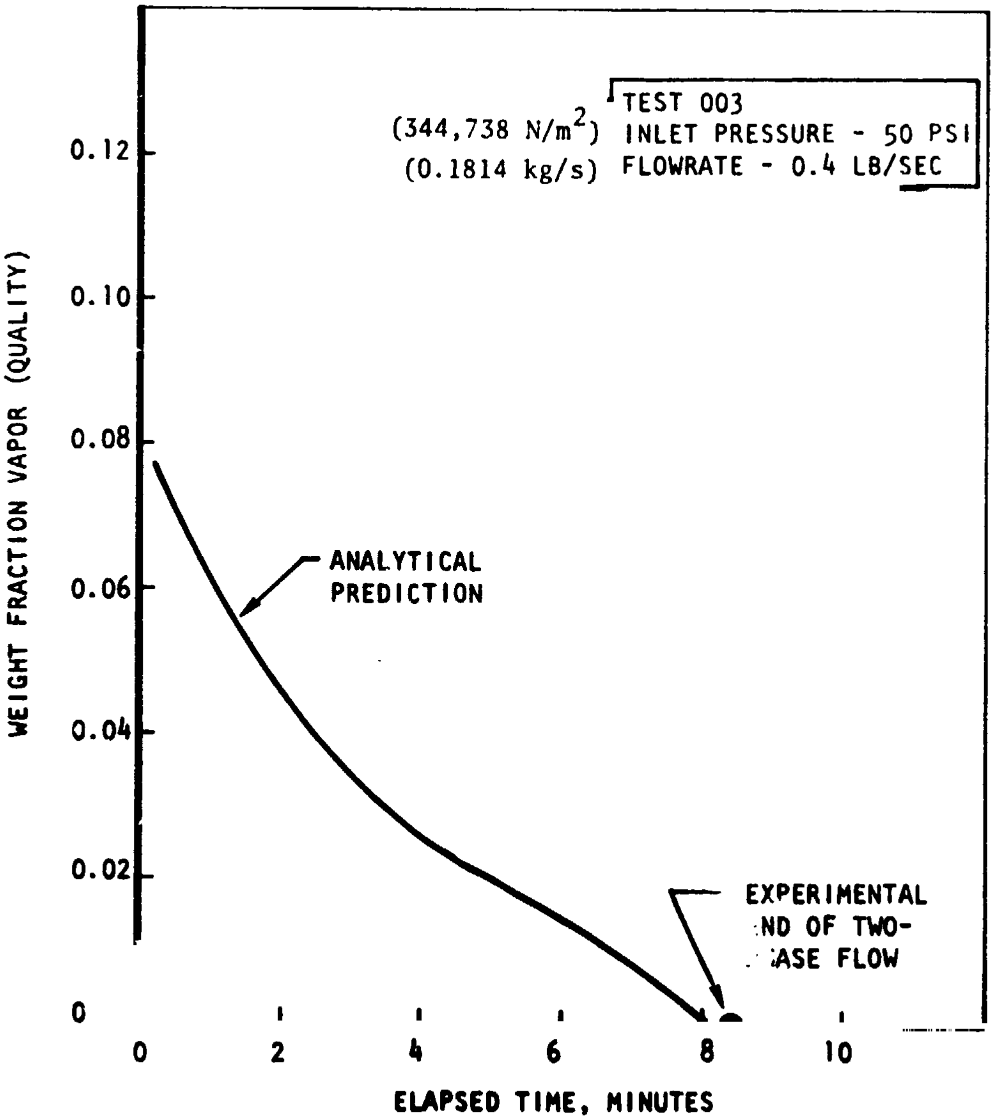

Figure 204. APS Pump Discharge Fluid Quality vs Time

shown in Fig. 202, was about equal to the value reported for low flowrates (corresponding to an initial heat transfer rate of 2 watts/cm^2). Because of the poor heat transfer conditions in the pump housing and uncertainties in flow distribution through the pump, this is felt to be excellent agreement. This agreement between the measured pump housing temperatures and predictions, shown in Fig. 203, indicates that the predictions also give the correct amount of energy transferred to the fluid during childown so that the transition time from two-phase to liquid at the pump discharge, as shown in Fig. 204, also substantiates the LO_2 flowrate used in the analysis.

The soakback data for the APS LO_2 TPA was obtained for three different thermal conditions at the start of soakback:

1. Complete childown without turbine drive gas and a dry pump during soakback
2. Steady-state operation with ambient temperature drive gas and a wet pump during soakback
3. Steady-state operation with hot turbine drive gas with a wet pump during soakback

The data from the first soakback condition was used to derive a value for the foamed-in-place insulation and is compared with predictions in Fig. 205. The effective thickness was found to be approximately 2.54 cm (1 inch), which was considerably thinner than the actual insulation. Heat leaks from the pump inlet and discharge flanges were probably responsible for the discrepancy.

Figures 206 and 207 compare the experimental and predicted soakback temperatures following steady state runs with ambient temperature and gas generator turbine drive gases and indicates reasonable agreement between the prediction and test data. The major difference between these predictions and the earlier calculations (shown in Fig. 201) was the absence of any boiloff period which was predicted in the earlier calculations. The measured temperatures were somewhat lower than the originally predicted values because of lower conductance through the flange attachment structure than predicted.

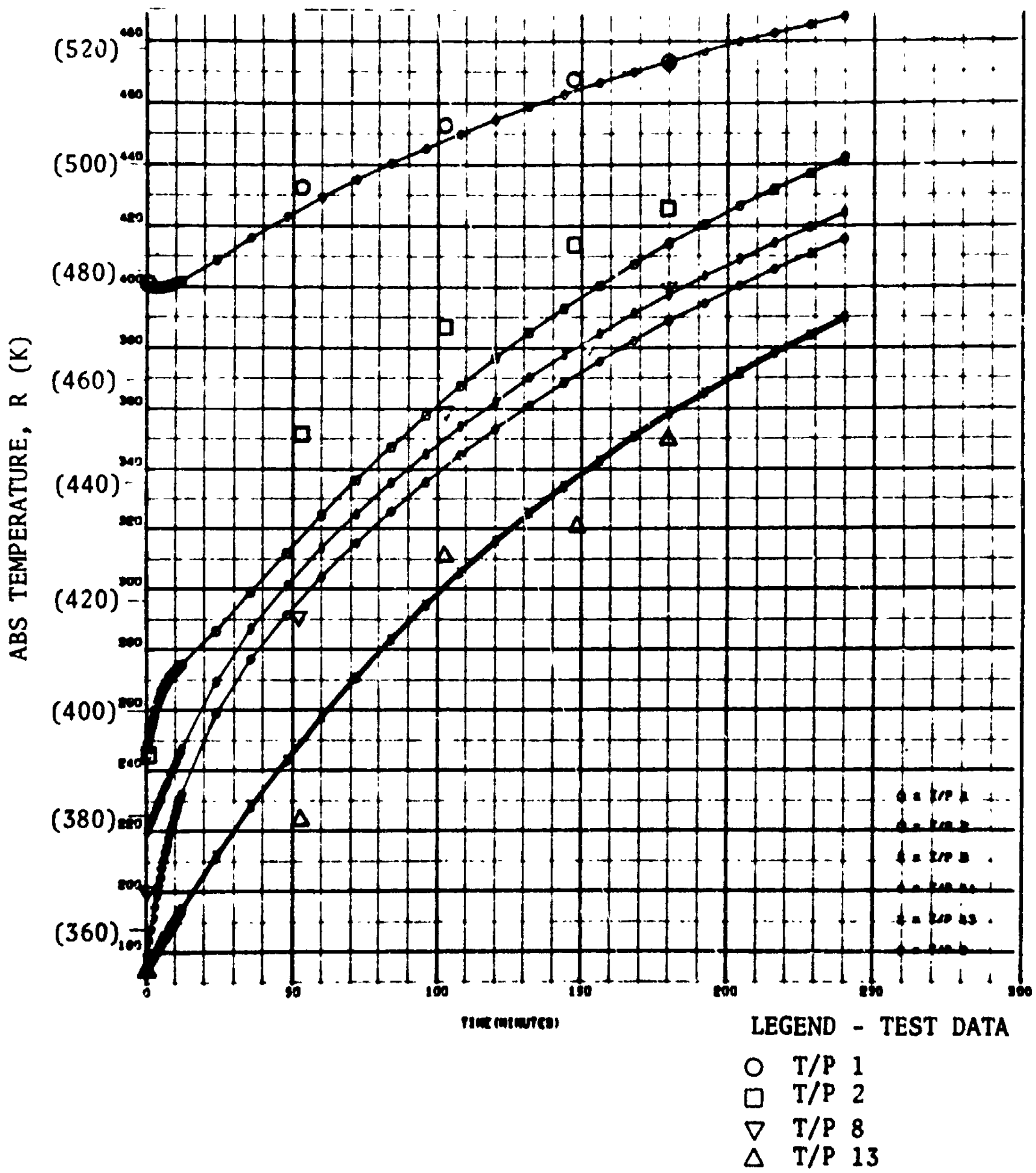

Figure 205. Comparison of Predicted and Experimental Dry Pump Soakback Temperatures

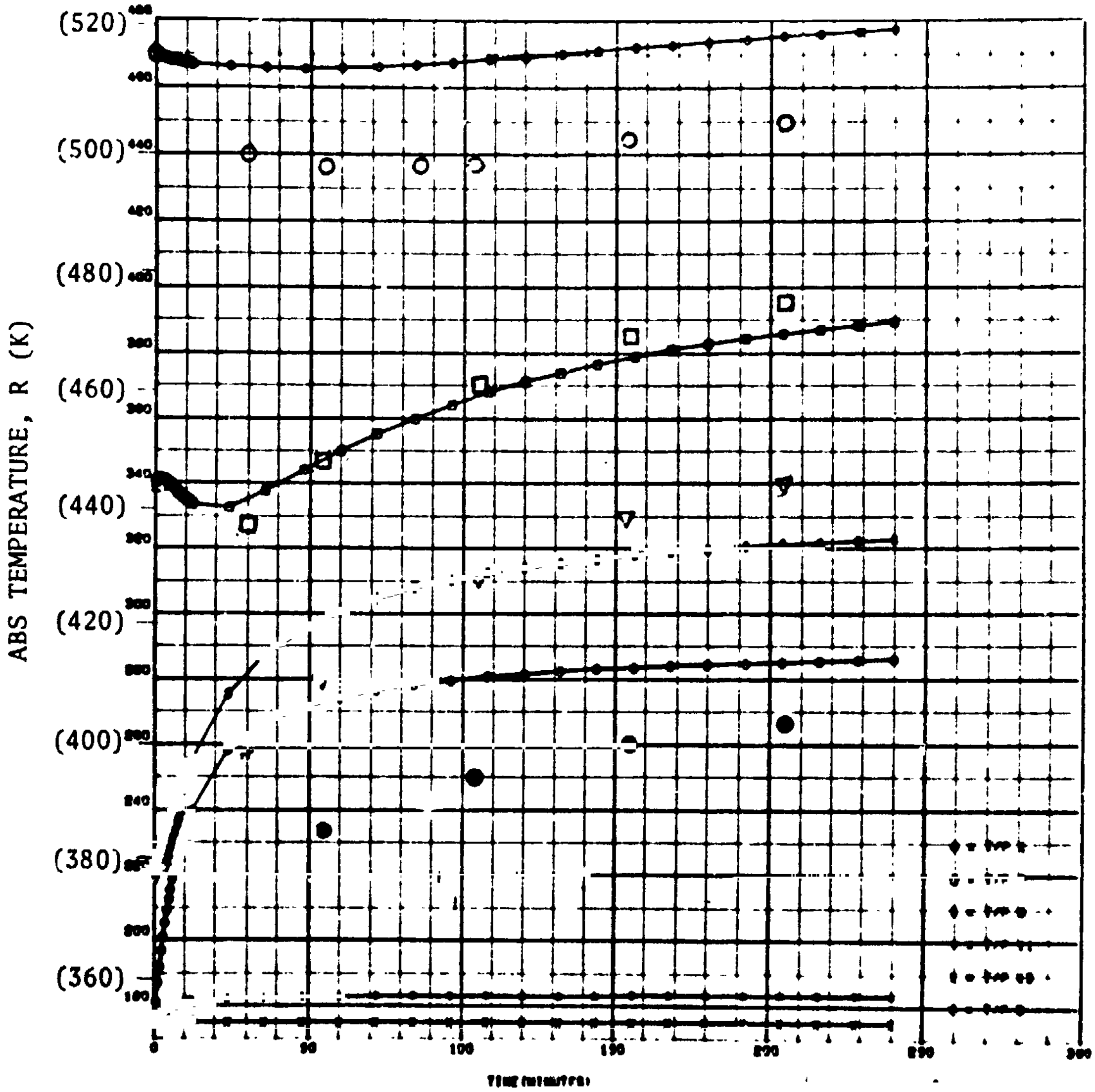

LEGEND - TEST DATA

○ T/P 1
□ T/P 2
▽ T/P 8
● T/P 9

Figure 206. Comparison of Predicted and Experimental Ambient Drive Gas Soakback Temperatures

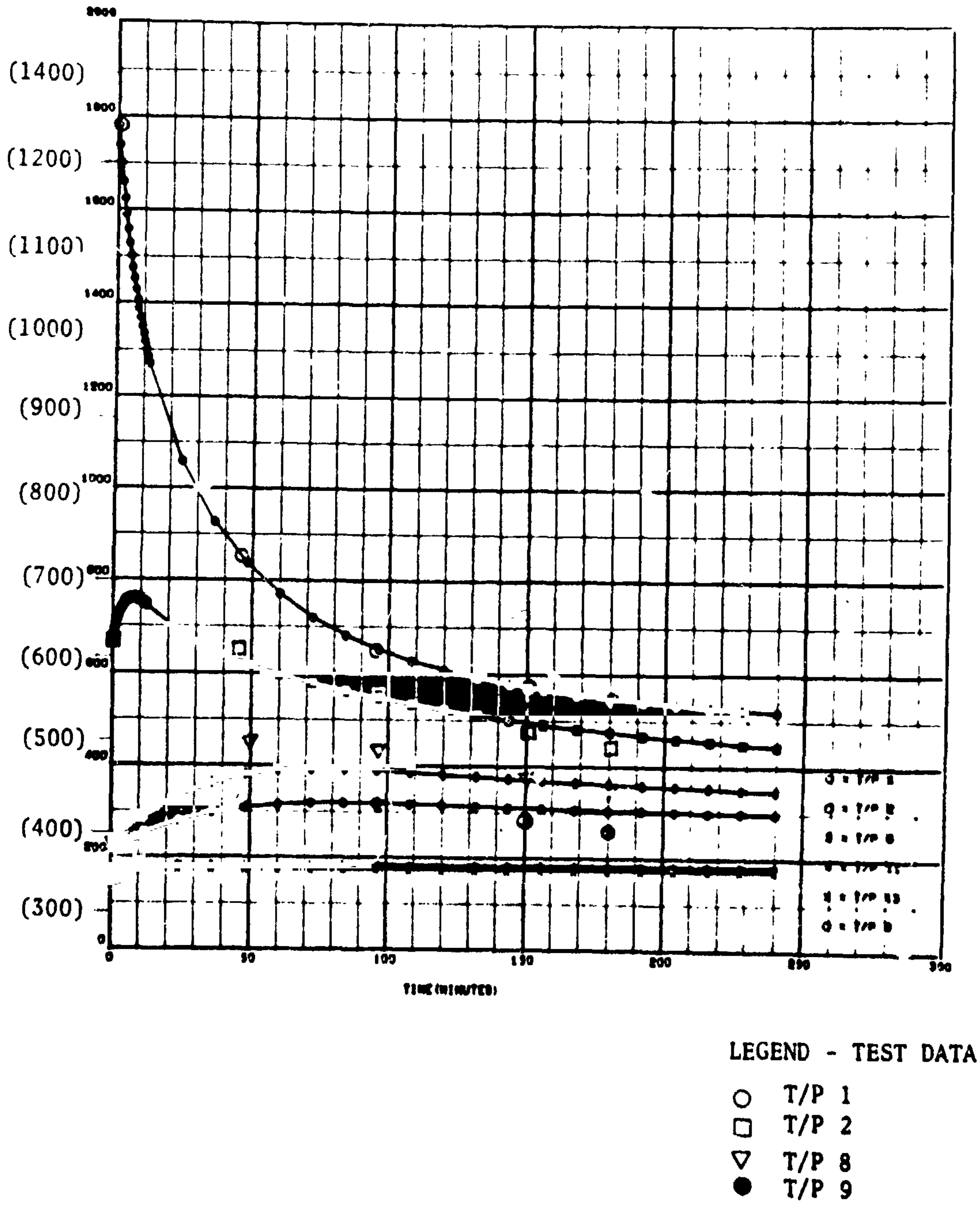

Figure 207. Comparison of Experimental and Predicted Soakback Temperatures for LO_2 Turbopump

The heat leak into the pump fluid was not measured but predicted by the computer model. The maximum heat leak with no external cooling was predicted to be 94,954 Joule/hr (90 Btu/hour) and to occur 100 minutes after shutdown. This corresponded to the time of greatest temperature difference between the pump housing and T/P9 as shown in Fig. 207. This maximum was larger than the goal of 52,752 Joule/hr (50 Btu/hr), but for an extended soakout period of 10 hours or greater, the average heat leak would have met the design goal.

ANALYSIS OF LH_2 TURBOPUMP TEST DATA

Soakback data for the LH_2 turbopump was obtained following test 53 and is listed in Table 43. Figure 208 compares the predicted and experimental soakback temperatures including the turbine bearing temperature. This data shows evidence of cooling by the seal leakage (estimated at 0.0136 kg/hr or 0.03 lb/hr based on the bearing temperature) as it flowed past the turbine. The test data for T/P 1 (turbine flange) was considerably below the prediction which did not include any cooling of the housing by the leakage. The flange attachment structure for the LH_2 pump appeared to provide better insulation than the LO_2 design as indicated by the lower than predicted temperatures for T/P 8 shown in Fig. 208.

The maximum heat leak into the LH_2 pump fluid with no external cooling was predicted to be 126,605 Joule/hr (120 Btu/hr) and to occur 2 hours after shutdown.

Comparing Figs. 201 and 208 indicates again that the absence of boiloff cooling after shutdown was the biggest difference with the turbine bearing temperature following close to the predicted value and the turbine flange temperatures falling faster than predicted.

Both turbopump assemblies exhibited satisfactory soakback behavior and with the allowable external cooling would meet the design goal of 52,752 Joule/hr (50 Btu/hr) heat leak into the wetted pump fluid and also exhibit and average long turn heat leak considerably below 52,752 Joule/hr (50 Btu/hr).

TABLE 43. LH_2 SOAKBACK DATA*

Temperature in degrees k and (R)

Time (min.)	T/P 1	T/P 2	T/P 4	T/P 5	T/P 7-8	T/P 10-11	T/P 12-14	T_{Bear}
0								
5	338 (608)	221 (398)	250 (450)	247 (445)	53 (95)	22 (39)	44 (80)	23 (42)
25	238 (429)	221 (398)	--	--	102 (184)	32 (58)	32 (58)	61 (109)
50	214 (385)	232 (418)	124 (223)	154 (277)	122 (220)	35 (63)	28 (51)	84 (152)
100	212 (381)	244 (439)	164 (295)	178 (321)	151 (271)	38 (69)	33 (60)	115 (207)
150	224 (404)	252 (453)	191 (344)	195 (351)	169 (304)	42 (75)	34 (61)	132 (238)
175	227 (409)	253 (456)	198 (356)	199 (359)	176 (316)	42 (76)	34 (62)	138 (248)
212	232 (418)	256 (460)	207 (373)	206 (371)	182 (328)	44 (80)	35 (63)	146 (262)
217**	233 (420)	256 (461)	209 (376)	207 (373)	182 (327)	44 (79)	35 (63)	109 (196)
222	234 (421)	311 (560)	209 (377)	207 (373)	178 (320)	43 (77)	34 (62)	89 (161)
227	234 (421)	254 (457)	209 (376)	207 (373)	172 (310)	42 (75)	34 (62)	73 (132)
245	233 (419)	245 (441)	201 (362)	201 (361)	159 (287)	40 (72)	34 (62)	46 (82)

* See figure 112 for thermocouple locations
** Bleed initiated

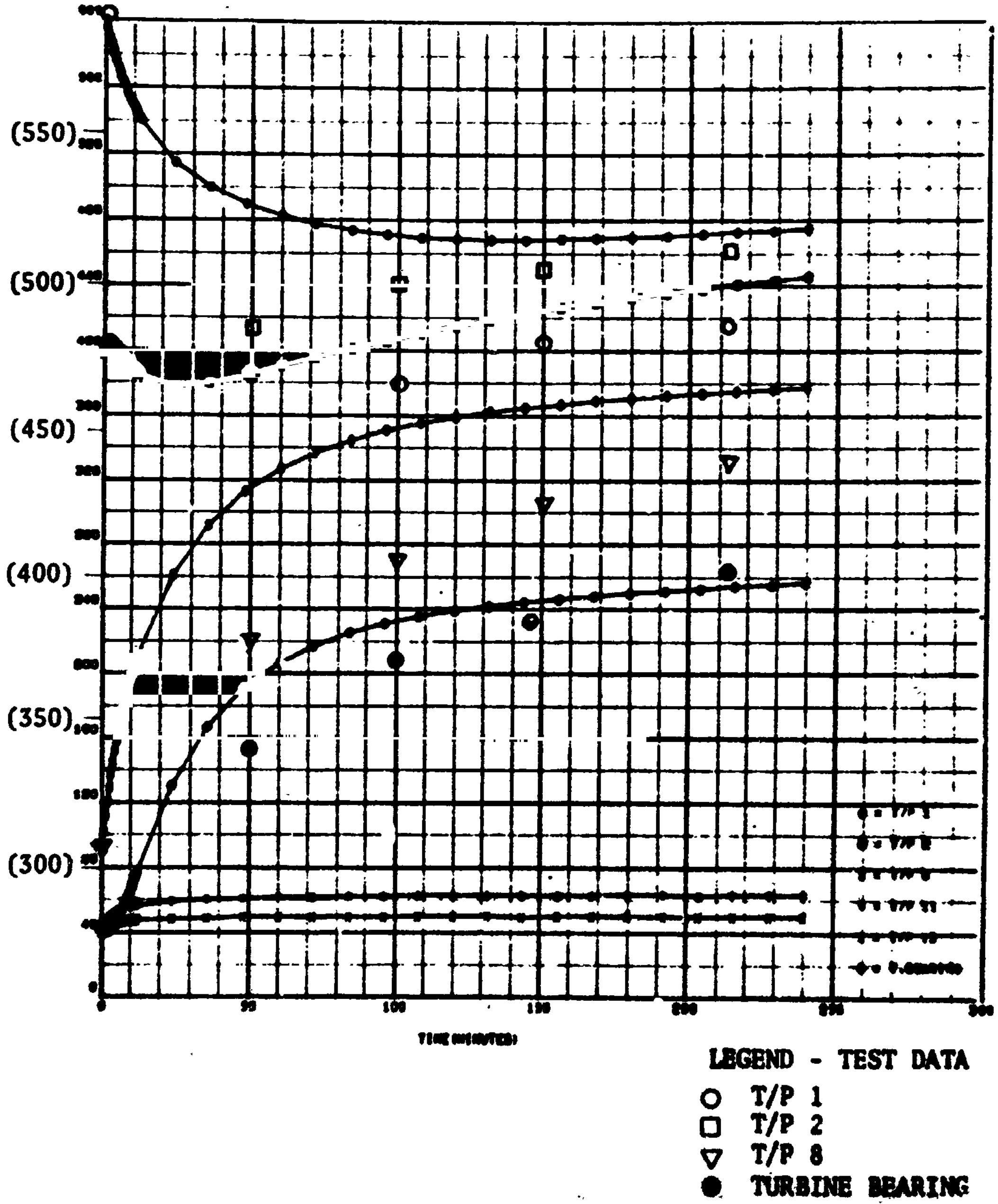

Figure 208. Comparison of Experimental and Predicted Soakback Temperatures for LH_2 Turbopump

PHASE V - ACCEPTANCE TEST

As specified in the Program Plan a test series was to be conducted to verify the acceptability of each unit prior to delivery to NASA-MSFC. The planned acceptance test series was to consist of 10 tests for a minimum of 500 seconds of accumulated duration.

The first test of the acceptance series was a checkout test with gaseous hydrogen turbine drive of approximately 100 to 150 seconds duration. The pump was slowly ramped to nominal operating speed (3142 rad/s or 30,000 rpm for LO_2 and 5498 rad/s or 52,500 rpm for LH_2) and conditions adjusted to nominal Q/N. This test established the operating conditions of the individual assembly which was used for setup of initial hot-firing of the gas generator. The remainder of the acceptance tests were conducted with hot gas turbine drive. A 5 second hot gas checkout test was conducted at nominal conditions. If required, the gas generator inlet conditions were adjusted, and a 400 seconds duration test was conducted for verification of performance at nominal conditions, and Q/N was varied to establish constant power performance. (Data from constant power operation was corrected to also obtain constant speed performance at the design speed.) The final test series consisted of 7 cycles with 10 seconds on time and 5 seconds off time at nominal conditions.

A summary of the tests conducted on each turbopump assembly is presented in Table 44. A detail description of all testing was previously presented under the discussion of the Phase IV Development Test Program. Successful operation was verified on the Unit No. 2 LO_2 and LH_2 turbopump assemblies after completion of assembly and on Unit No. 1 LO_2 turbopump assembly after detail inspection and reassembly. The Unit No. 1 LH_2 TPA which had been damaged as a result of weld failure on the turbine manifold during development testing could not be conveniently repaired for acceptance test. At the conclusion of the acceptance testing, external inspection of the units was conducted and the assemblies were found to be in excellent condition.

TABLE 44. SUMMARY OF ACCEPTANCE TESTS

Test	Turbine Drive	Objectives	LO_2 Unit No. 1		LO_2 Unit No. 2		LH_2 Unit No. 1		LH_2 Unit No. 2	
			Test No.	Duration seconds	Test No.	Duration seconds	Test No.	Duration seconds	Test No.	Duration seconds
1	GH_2	Slowly ramp to speed 3142 rad/s (30,000 rpm) for LO_2 5498 rad/s (52,500 rpm) for LH_2 and adjust to nominal Q/N. Establish pump operating characteristics	69	146.0	58	147.3	--	--	59	110.0
2	Hot Gas	Checkout test of hot gas conditions. Adjust conditions if required.	71	5.0	59	5.0	--	--	61	5.0
3	Hot Gas	Operate at nominal N and Q. Establish constant power map. (To be corrected for constant speed performance.)	72	400.0	60	400.0	--	--	62	400.1
4	Hot Gas	Cycle tests to nominal N and Q. 10 seconds on and 5 seconds off	73 to 79	70.0	61 to 67	70.0	--	--	63 to 69	70.0
				621.0		622.3				585.0

*Nominal conditions for LO_2 TPA are 3142 rad/s (30,000 rpm) on 0.00631 m^3/s (100 gpm).
Nominal conditions for LH_2 TPA are 6283 rad/s (60,000 rpm) and 0.0284 m^3/s (450 gpm).

APPENDIX A

TURBOPUMP ASSEMBLY OPERATION

Presented is a description of the installation and operation of the LO_2 and LH_2 turbopump assemblies. The operation is typical of that used during development and acceptance testing. All the detailed information required to install and operate the assembly is provided including interfaces, valve control, pretest preparation, operating conditions and sequencing.

Installation

Installation includes the propellant lines, pneumatic control, electrical controls, and instrumentation. To facilitate installation and changing of assemblies, many of the interfaces are located at an interface panel.

The interface requirements which are not contained on the interface panel are tabulated in Table 45 for the LO_2 and LH_2 assemblies. These include the propellant lines, turbine exhaust, valve electrical controls (solenoid valves), and special instrumentation. Valve identifications are shown in the assembly propellant and control schematic presented in Fig. 209.

An interface panel (Fig. 210) simplified initial installation, removal, and reinstallation of assemblies. The bleed, purge, and pressure tap ports are identified in Table 46 for the LO_2 TPA and Table 47 for the LH_2 TPA. Thermocouple leads were wired to terminal boards on the panel, and these are identified in Table 48 for both LO_2 and LH_2 assemblies. Turbopump surface temperatures and cooling coil temperatures used for thermal tests were installed on the Unit No. 1 assemblies only.

Pretest Operation

Critical parameters may be monitored to assure proper set conditions, gas generator ignition, and turbopump operation. Suggested redline parameters are those used

TABLE 45. TURBOPUMP ASSEMBLY INTERFACES

Type	Interface	Description
Propellant	Pump Inlet LO_2	5.08 cm (2.0 in.) ID, 0.635 cm (1/4 in.) diameter bolts on 10.478 cm (4.125 in.) diameter bolt circle, 12 places. NAFLEX double flange seal. Facility flange flat with 32c finish
	Pump Inlet LH_2	5.969 cm (2.35 in.) ID, 0.635 cm (1/4 in.) diameter bolts on 9.652 cm (3.80 in.) diameter bolt circle, 8 places. NAFLEX double flange seal. Facility flange flat with 32c finish.
	Pump Discharge (J-2S idle mode valve) No. 12	3.632 cm (1.430 in.) ID, 0.953 cm (3/8 in.) diameter bolts on 9.682 cm (3.812 in.) diameter bolt circle, 8 places. NAFLEX double flange seal. Facility flange flat with 32c finish.
	GG Fuel Inlet No.14	1.905 cm (3/4 in.) AN
	GG Oxidizer Inlet No. 14	1.905 cm (3/4 in.) AN
	Pump Bypass (J-2 ASI valve) No. 13	2.54 cm (1 in.) AN
Hot Gas	Turbine Exhaust	19.05 cm (7.5 in.) ID., 0.635 cm (1/4 in.) diameter bolts on 20.57 cm (8.1 in.) diameter bolt circle, 18 places.
Electrical Control	Discharge Valve Close	NC-Marotta MV-74P valve-2 pin connector P/N 3106E-10SL-4
	Discharge Valve Open No. 2	NO
	Bypass Valve Close No. 3	NO
	Bypass Valve Open No. 4	NC
	Intermediate Seal Purge No. 5 (LO_2 TPA only)	NC
	Liftoff Seal Purge No. 6	NC
	Gas Generator Close No. 7 and No. 8	NC
	Gas Generator Open No. 9 and No. 10	NO
	Bearing Cavity Bleed No. 11	NC-Weston Valve, NAS-27273-4 pin connector P/N MS 3106E-14S-25

TABLE 45. (Concluded)

Type	Interface	Description
Instrumentation	Speed Pickup	Rosemount P/N 148L
	Bear Cavity Temperature	Rosemount P/N 134LU
	Discharge Valve Position	6 pin connector, P/N NAS 27466T1198S
	Bypass Valve Close Position	2 pin connector, P/N MS 3106E10SL-4S

Valve numbers are identified in plumbing schematic.
NO - normally open

NC - normally close

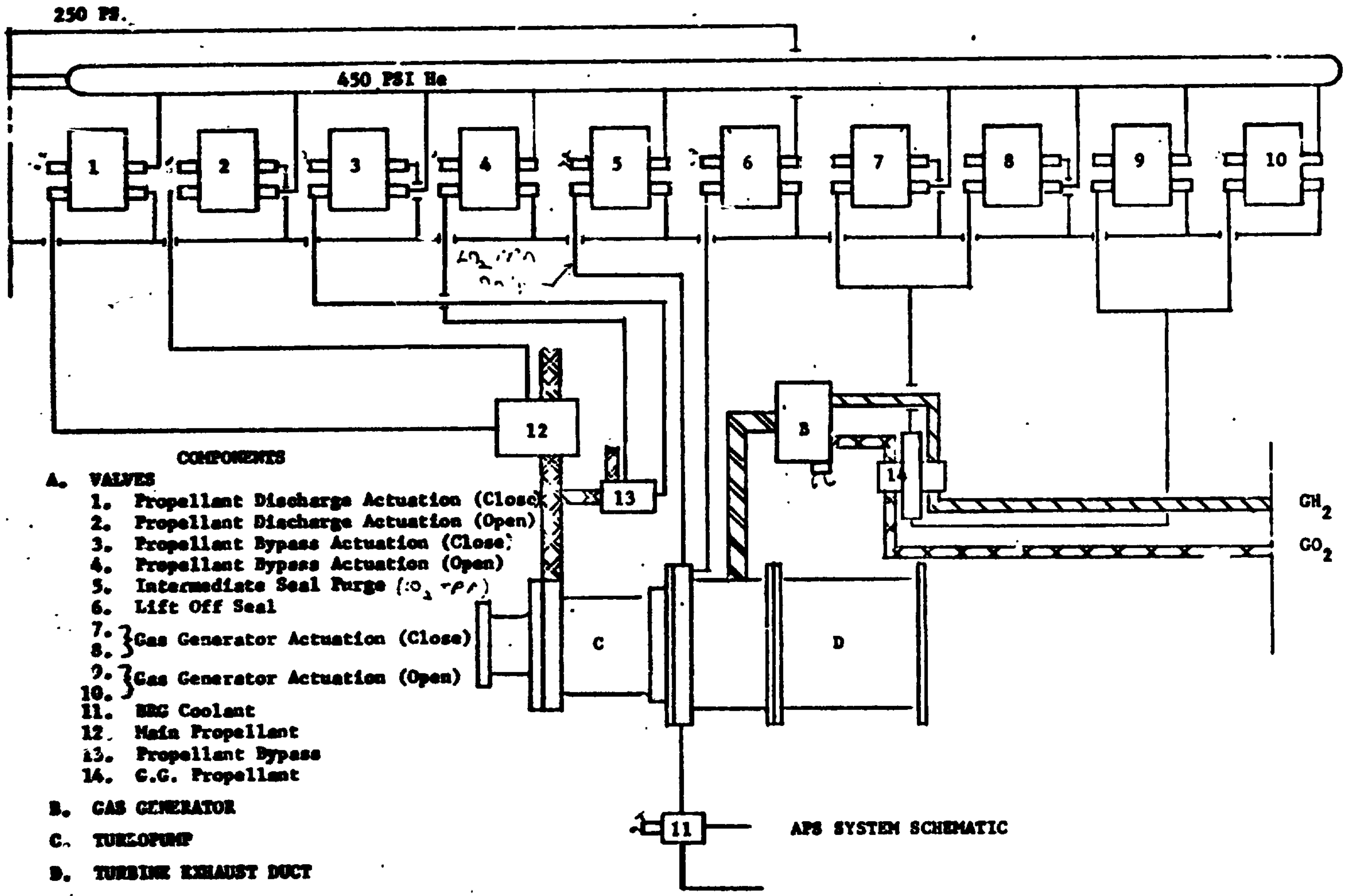

Figure 209. Propellant Schematic

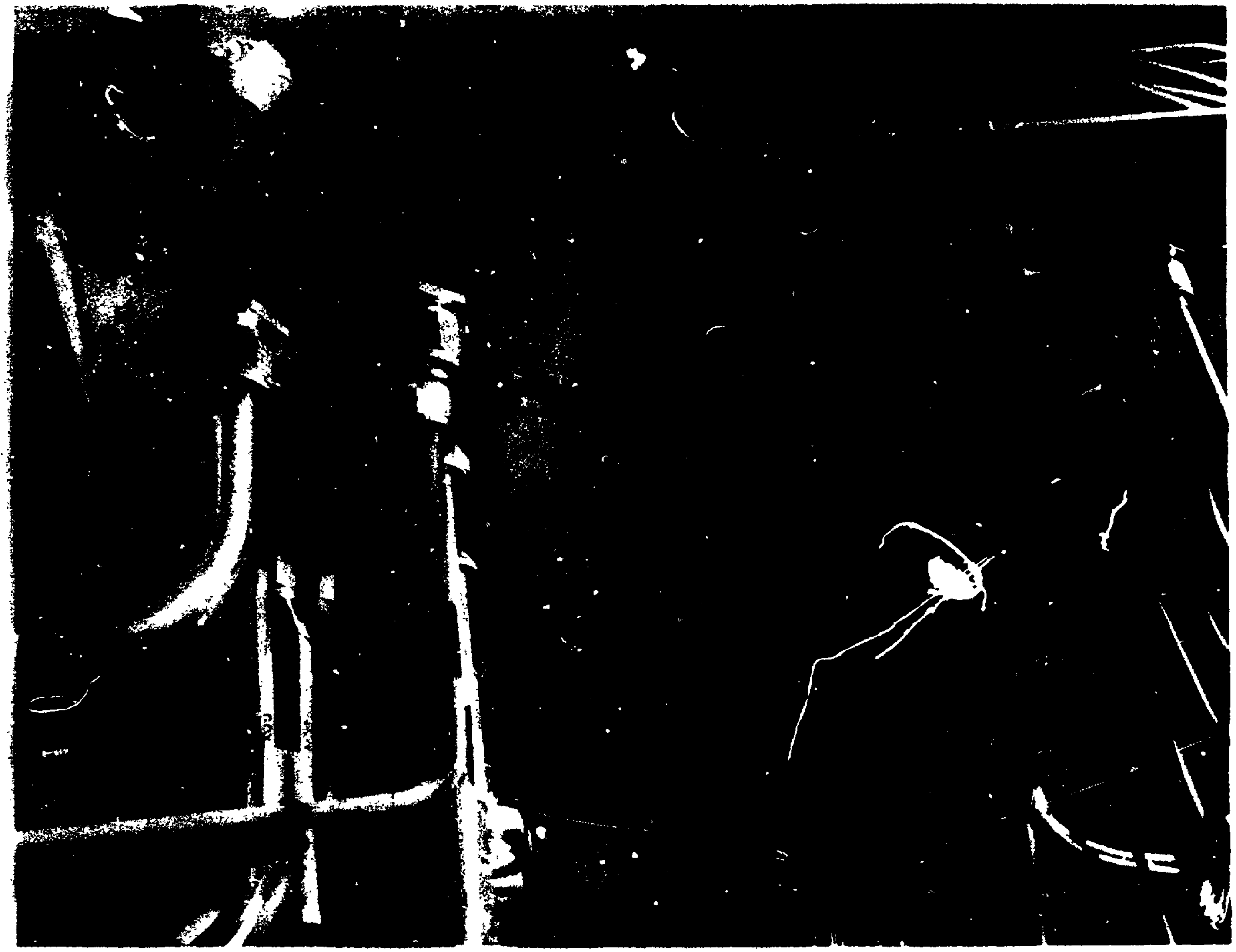

Figure 210. Interface Panel on LO_2 TPA

TABLE 46. LO_2 TPA INTERFACE PANEL BLEEDS, PURGES, AND PRESSURE TAPS

No.	Size AN Fitting	Name	Remarks
1	1/2	GH_2 Gas Generator Valve Bleed	Located upstream of valve
2	1/4	Coiling Coil Out	(1)
3	3/4	Pump Seal Drain	GO_2 and He gases
4	1/4	Liftoff Seal Supply Pr	300 psig He
5	1/2	450 psig He Manifold	Valve control
6	1/2	He Vent-Control Valves	
7	1/4	Gas Generator Purge	(1)-Located downstream side of GH_2 valve
8	1/4	He Vent-Bearing Cavity Bleed Valve	
9	1/4	Coiling Coil In	(1)
10	1/4	Bearing Cavity Bleed	GO_2 gases
11	1/2	GO_2 Gas Generator Valve Bleed	Located upstream of valve
11a	1/2	Turbine Seal Drain	He and turbine drive gases
12	1/8	GG GH_2 Injection Pr	(2)
13	1/8	GG GO_2 Injection Pr	(2)
14	1/8	Turbine Discharge Pr	(2)
15	1/8	Intermediate Seal Inlet Pr	(2) Located downstream of control nozzle
16	1/8	Impeller Back Plate Pr	(2)
17	1/8	Pneumatic Manifold Pr	(2)
18	1/8	Liftoff Seal Actuation Pr	(2)
19	1/8	Pump Discharge Pr	(2)
20	1/8	GG Injector End Chamber Pr	(2)
			(2)

TABLE 46. (Concluded)

No.	Size AN Fitting	Name	Remarks
21	1/8	Bearing Cavity Pr	(2)
22	1/8	GG Chamber Pr	(2)
23	1/8	Seal Cavity Pr	(2)
24	1/8	GG GH_2 Coolant Injection Pr	(2)
25	1/4	Intermediate Seal Relief	To facility He relief valve set to 55 psig

(1) Not required for turbopump operation

(2) Instrumentation port

TABLE 47. LH_2 TPA INTERFACE PANEL BLEEDS, PURGES, AND PRESSURE TAPS

No.	Size AN Fitting	Name	Remarks
1	1/2	450 psig He Manifold	Valve control
2	1/4	Coiling Coil In	(1)
3	1/4	Coiling Coil Out	(1)
4	1/4	Liftoff Seal Supply Pr	300 psig He
5	1/4	Bearing Cavity Bleed	GH_2 gases
7	1/2	GH_2 Gas Generator Valve Bleed	Located upstream of valve
8	1/2	GO_2 Gas Generator Valve Bleed	Located upstream of valve
9	1/2	He Vent-Control Valves	
10	1/4	He Vent-Bearing Cavity Bleed Valve	
11	1/8	GG GH_2 Injection Pr	(2)
12	1/8	GG Coolant Injection Pr	(2)
13	1/8	GG GO_2 Injection Pr	(2)
14	1/8	GG Injector End Chamber Pr	(2)
15	1/8	GG Chamber Pr	(2)
16	1/8	Turbine Discharge Pr	(2)
17	1/8	Impeller Near Ring Pr	(2)
18	1/8	Impeller Tip Pr	(2)
19	1/8	2nd Stage Inlet Pr	(2)
20	1/8	Pump Discharge Pr	(2)
21	1/8	Balanced Piston Cavity Pr	(2)
22	1/8	Bearing Cavity Pr	(2)
23	1/8	Pump Seal Cavity Pr	(2)
24	1/8	Liftoff Seal Actuation Pr	(2) Located downstream of control valve
25	1/8	Pneumatic Manifold Pr	(2)

(1) Not required for turbopump operation
(2) Instrumentation port

TABLE 48. TPA INTERFACE PANEL THERMOCOUPLES

Panel No.	Name	Location	Thermocouple Type	Remarks
1A	Turbine Discharge T	T/C Panel	C/A	2.54-1.27 cm (1-1/2 in.) Emersion
2A	GG Flange T	↓	↓	
3A	GG Duct T	↓	↓	
5A	Bearing Cavity, Bleed T	↓	I/C	
6A	Cooling Coil In T	↓	↓	
7A	Cooling Coil ΔT (In)	↓	↓	(1)
8A	Cooling Coil ΔT (Out)	↓	↓	(1)
1B	Surface T (1)	↓	C/A	(1)
2B	Surface (2)	↓	↓	(1)
3B	Surface (3)	↓	↓	(1)
4B	Surface (4)	↓	↓	
5B	Surface (5)	↓	I/C	(1)
6B	Surface (6)	↓	↓	(1)
7B	Surface (7)	↓	↓	(1)
8B	Surface (8)	↓	↓	(1)
9B	Surface (9)	↓	↓	(1)
10B	Surface (10)	↓	↓	(1)
1C	Surface (11)	↓	↓	(1)
2C	Surface (12)	↓	↓	(1)
3C	Surface (13)	↓	↓	(1)
4C	Surface (14)	↓	↓	(1)
5C	GG Tc #1	↓	C/A	Duct upstream location. .254 cm (0.1 in. emersion
6C	GG Tc #2	↓	↓	Duct downstream location. 1.016 cm (~0.4 in.) emersion
7C	Intermediate Seal	↓	↓	LO_2 TPS only

during development and acceptance testing, and typical values are tabulated in Table 49. These minimum and maximum values will assure that during pump operation the intermediate seal purge is on and flowing (LO_2 TPA only), the liftoff seal has been actuated, pump inlet conditions are in the liquid propellant region, pump is operating normally, gas generator has ignited and is operating normally, and turbine inlet temperature is within safe operating limits. The gas generator chamber pressure level is used to detect ignition. The unignited chamber pressure is approximately one half of the normal pressure; therefore, the chamber pressure should achieve a minimum of 75 percent of normal chamber pressure within in 0.3 seconds after electrical signal to the gas generator valve.

To assure that the gas generator system is primed to the bipropellant valve, bleed points have been located at the valve body and terminated at the interface panel. No purges downstream of the valves were required nor used during development or acceptance testing.

The turbopump is prechilled by flowing liquid propellant through the pump through the bypass (or discharge) valve under tank head pressure until liquid propellant temperatures are obtained at the pump inlet and discharge. (During development testing on the LO_2 TPA, the pump was restarted after a 20 and 40 minute period where the discharge and bypass valves were closed and the inlet exposed to tank head conditions.) Insulation on the pump assembly will reduce the time required for prechill although insulation is not required for either the LO_2 or LH_2 TPA. Actuating the liftoff seal was found to further aid in prechilling the bearing cavity region. On the LH_2 TPA, the bearing cavity bleed was used during prechill to achieve a more complete chill of the bearing cavity and eliminate a gas pocket. This gas pocket will cause a momentary oscillation in pump pressures when the gas is discharged by the lubrication flow into the impeller as previously discussed.

Gas generator inlet pressures are presented in Table 50 for ambient temperature propellants and a nominal chamber pressure of 1,861,584 N/m^2 (270 psia). The inlet pressures vary proportionally with chamber pressure for other power levels (chamber pressure). Inlet conditions are presented for both hot gas and cold gas (gaseous hydrogen) turbine drive. (A description of the cold gas feed system and requirements

TABLE 49. TPA REDLINE PARAMETERS

Parameter	LO_2 TPA	LH_2 TPA
Pump Inlet Pressure, N/m^2 (psig) min.	144,790 (21)	179,264 (26)
Pump Inlet Temperature, K (F) max.	+97 (-285)	+24.4 (-416)
Pump Discharge Pressure, N/m^2 (psig) max.	1.45×10^7 (2100)	1.45×10^7 (2100)
Gas Generator Chamber Pressure, N/m^2 (psig) min.(1)	75 percent operating Pc	
Combustion Temperature, K (F) max.	1167 (1640)	1167 (1640)
Speed, rad/s (rpm) max.	35,000	68,000
Liftoff Seal Pressure, N/m^2 (psig) min.	1,723,690 (250)	1,723,690 (250)
Radial Acceleration g rms(1)	10	10
Intermedial Seal Pressure N/m^2 (psig) min.	206,843 (30)	--

(1) Used for ignition detection. Not required for cold gas drive.

(2) 100 to 1500 cps.

TABLE 50. GAS GENERATOR INLET PRESSURES

	LO_2 TPA		LH_2 TPA	
	Unit No. 1	Unit No. 2	Unit No. 2	Unit No. 2
Hot Gas (T_c = 1117 K or 1500 F)				
Chamber Pressure	1,860,584 (270)	1,861,584 (270)	1,861,584 (270)	1 861,584 (270)
GO_2 Valve Upstream Pressure	2,144,269 (311)	2,206,322 (320)	2,040,848 (296)	1,985,690 (288)
GH_2 Valve Upstream Pressure	2,475,218 (359)	2,330,428 (338)	2,364,902 (343)	2,158,059 (313)
Cold Gas GH_2				
Chamber Pressure	1,861,584 (270)	1,861,584 (270)	1,861,584 (270)	1,861,584 (270)
GH_2 Valve Upstream Pressure	5,102,120 (740)	4,467,803 (648)	3 054,377 (443)	
GH_2 Upstream Pressure Modified Feed	--	--	4,516,066 (655)	3,599,063 (522)

Static pressures in N/m^2 and (psia) with ambient temperature propellants (~294°K or 530 R)

Valve upstream pressures vary linearly with chamber pressure static pressures measured in 1 in. AN fitting.

is presented in Gas Generator Operation.) The gas generator chamber pressure (turbine manifold inlet pressure) is given in Table 51 for operation at nominal pump speed and flowrate with the supplied turbine discharge orifice plate. This plate was designed to provide an approximately 241,317 N/m^2 (35 psia) turbine backpressure when the gas generator is operating with hot gas. This turbine manifold pressure is approximately the same for cold gas as well as hot gas operation although the cold gas (gaseous hydrogen) flowrate is 145 percent of the nominal hot gas flowrate.

Operation

Sequencing for the turbopump assembly is shown in Fig. 211 . During pretest setup, the bearing coolant valve may have been used and is closed, the liftoff seal has been actuated, and the intermediate seal purge is on. The spark on and gas generator on signal may be given simultaneously, and typically the first spark will occur at 15 to 20 milliseconds while the propellant valve opens at 55 milliseconds. Successful ignition is verified at 75 milliseconds. An alternate simplified sequence was used during most development and acceptance test where discharge valve was open and the bypass valve closed throughout the test operation.

TABLE 51. TYPICAL TURBINE MANIFOLD INLET PRESSURE

	LO_2 TPA		LH_2 TPA	
	Unit No. 1	Unit No. 2	Unit No. 1	Unit No. 2
Pump Speed, rad/s (rpm)	3142 (30,000)	3142 (30,000)	6283 (60,000)	6283 (60,000)
Pump Flow, m^3/s (gpm)	0.00631 (100)	0.00631 (100)	0.0284 (450)	0.0284 (450)
Discharge Orifice Cd A, cm^2 ($in.^2$)	53.34 (21)	53.34 (21)	83.82 (33)	83.82 (33)
Turbine Manifold Pressure, N/m^2 (psia)(1)	1,930,532 (280)	2,344,217 (340)	2,585,534 (375)(2)	2,654,482 (385)(2)

(1) Turbine manifold inlet pressure varies approximately with speed according to:

$P \propto N^2$

(2) Average value for LH_2 TPA since some variation occurred.

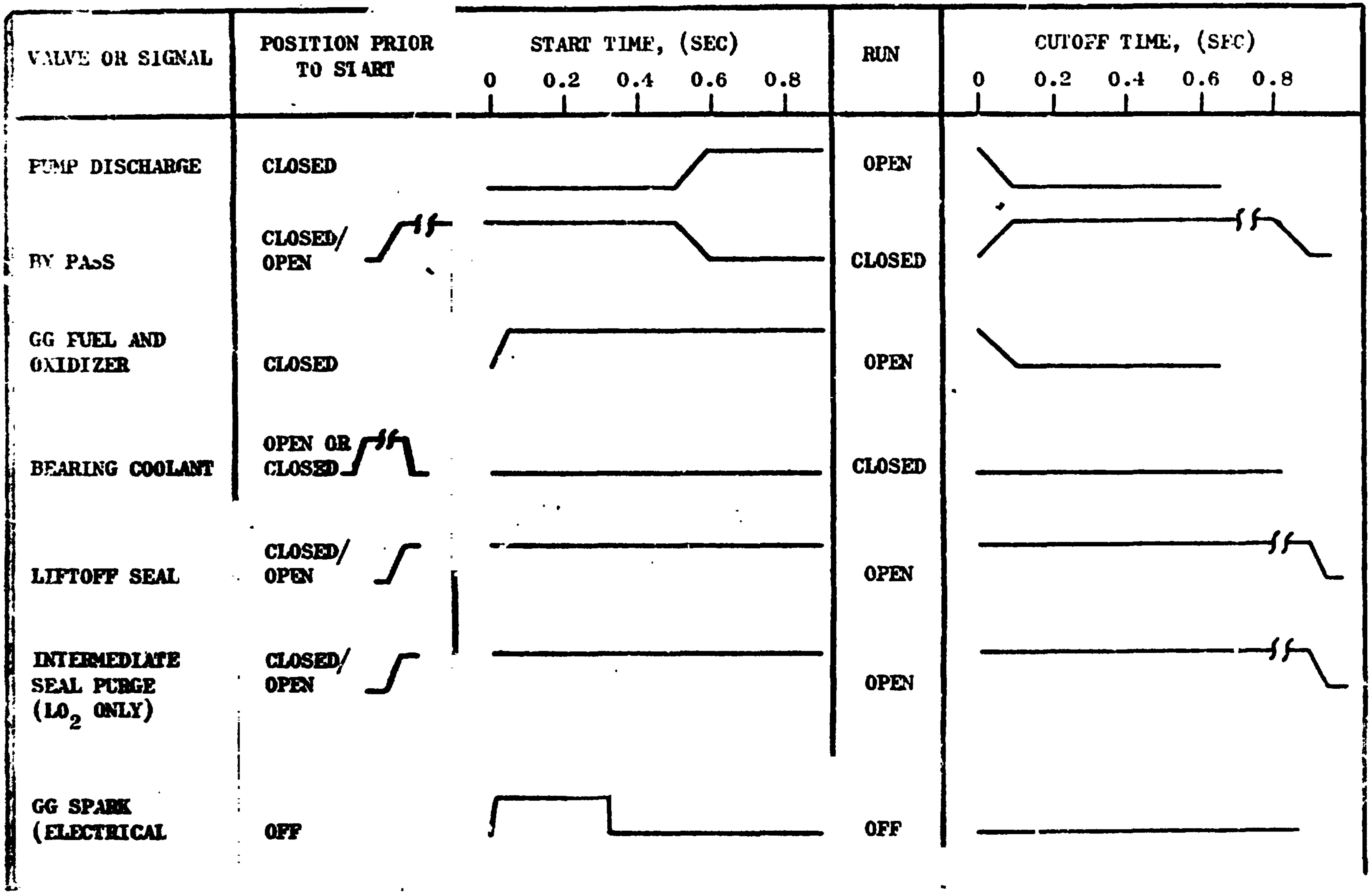

Figure 211. TPA System Sequence/Valve Position